

LECH PAWLOWSKI

THE SCIENCE AND ENGINEERING OF  
**THERMAL SPRAY  
COATINGS**



SECOND EDITION

WILEY

# The Science and Engineering of Thermal Spray Coatings

Second Edition

# The Science and Engineering of Thermal Spray Coatings

Second Edition

Lech Pawłowski

*Ecole Nationale Supérieure de Chimie de Lille,  
Villeneuve d'Ascq, France*



John Wiley & Sons, Ltd

Copyright © 2008

John Wiley & Sons Ltd, The Atrium, Southern Gate, Chichester,  
West Sussex PO19 8SQ, England  
Telephone (+44) 1243 779777

Email (for orders and customer service enquiries): cs-books@wiley.co.uk  
Visit our Home Page on [www.wiley.com](http://www.wiley.com)

All Rights Reserved. No part of this publication may be reproduced, stored in a retrieval system or transmitted in any form or by any means, electronic, mechanical, photocopying, recording, scanning or otherwise, except under the terms of the Copyright, Designs and Patents Act 1988 or under the terms of a licence issued by the Copyright Licensing Agency Ltd, 90 Tottenham Court Road, London W1T 4LP, UK, without the permission in writing of the Publisher. Requests to the Publisher should be addressed to the Permissions Department, John Wiley & Sons Ltd, The Atrium, Southern Gate, Chichester, West Sussex PO19 8SQ, England, or emailed to [permreq@wiley.co.uk](mailto:permreq@wiley.co.uk), or faxed to (+44) 1243 770620.

Designations used by companies to distinguish their products are often claimed as trademarks. All brand names and product names used in this book are trade names, service marks, trademarks or registered trademarks of their respective owners. The Publisher is not associated with any product or vendor mentioned in this book.

This publication is designed to provide accurate and authoritative information in regard to the subject matter covered. It is sold on the understanding that the Publisher is not engaged in rendering professional services. If professional advice or other expert assistance is required, the services of a competent professional should be sought.

The Publisher and the Author make no representations or warranties with respect to the accuracy or completeness of the contents of this work and specifically disclaim all warranties, including without limitation any implied warranties of fitness for a particular purpose. The advice and strategies contained herein may not be suitable for every situation. In view of ongoing research, equipment modifications, changes in governmental regulations, and the constant flow of information relating to the use of experimental reagents, equipment, and devices, the reader is urged to review and evaluate the information provided in the package insert or instructions for each chemical, piece of equipment, reagent, or device for, among other things, any changes in the instructions or indication of usage and for added warnings and precautions. The fact that an organization or Website is referred to in this work as a citation and/or potential source of further information does not mean that the author or the publisher endorses the information the organization or Website may provide or recommendations it may make. Further, readers should be aware that Internet Websites listed in this work may have changed or disappeared between when this work was written and when it is read. No warranty may be created or extended by any promotional statements for this work. Neither the Publisher nor the Author shall be liable for any damages arising herefrom.

#### *Other Wiley Editorial Offices*

John Wiley & Sons Inc., 111 River Street, Hoboken, NJ 07030, USA

Jossey-Bass, 989 Market Street, San Francisco, CA 94103-1741, USA

Wiley-VCH Verlag GmbH, Boschstr. 12, D-69469 Weinheim, Germany

John Wiley & Sons Australia Ltd, 42 McDougall Street, Milton, Queensland 4064, Australia

John Wiley & Sons (Asia) Pte Ltd, 2 Clementi Loop #02-01, Jin Xing Distripark, Singapore 129809

John Wiley & Sons Ltd, 6045 Freemont Blvd, Mississauga, Ontario L5R 4J3, Canada

Wiley also publishes its books in a variety of electronic formats. Some content that appears in print may not be available in electronic books.

#### *British Library Cataloguing in Publication Data*

A catalogue record for this book is available from the British Library

ISBN 978-0-471-49049-4

Typeset in 10.5/13pt Sabon by Integra Software Services Pvt. Ltd, Pondicherry, India  
Printed and bound in Great Britain by TJ International, Padstow, Cornwall  
This book is printed on acid-free paper.

*To my wife Muryel and to my children Irene and David*

# Contents

<i>Preface to the Second Edition</i>	xv
<i>Preface to the First Edition</i>	xvii
<i>Acronyms, Abbreviations and Symbols</i>	xxi
<b>1 Materials Used for Spraying</b>	<b>1</b>
1.1 Methods of Powders Production	3
1.1.1 Atomization	5
1.1.2 Sintering or Fusion	8
1.1.3 Spray Drying (Agglomeration)	11
1.1.4 Cladding	20
1.1.5 Mechanical Alloying (Mechanofusion)	26
1.1.6 Self-propagating High-temperature Synthesis (SHS)	28
1.1.7 Other Methods	32
1.2 Methods of Powders Characterization	35
1.2.1 Grain Size	35
1.2.2 Chemical and Phase Composition	38
1.2.3 Internal and External Morphology	39
1.2.4 High-temperature Behaviour	41
1.2.5 Apparent Density and Flowability	42
1.3 Feeding, Transport and Injection of Powders	42
1.3.1 Powder Feeders	43
1.3.2 Transport of Powders	44
1.3.3 Injection of Powders	44
References	47

<b>2 Pre-Spray Treatment</b>	<b>53</b>
2.1 Introduction	53
2.2 Surface Cleaning	54
2.3 Substrate Shaping	55
2.4 Surface Activation	56
2.5 Masking	64
References	66
<b>3 Thermal Spraying Techniques</b>	<b>67</b>
3.1 Introduction	67
3.2 Flame Spraying (FS)	69
3.2.1 History	69
3.2.2 Principles	70
3.2.3 Process Parameters	71
3.2.4 Coating Properties	74
3.3 Atmospheric Plasma Spraying (APS)	74
3.3.1 History	74
3.3.2 Principles	74
3.3.3 Process Parameters	75
3.3.4 Coating Properties	79
3.4 Arc Spraying (AS)	79
3.4.1 Principles	79
3.4.2 Process Parameters	80
3.4.3 Coating Properties	81
3.5 Detonation-Gun Spraying (D-GUN)	82
3.5.1 History	82
3.5.2 Principles	82
3.5.3 Process Parameters	83
3.5.4 Coating Properties	84
3.6 High-Velocity Oxy-Fuel (HVOF) Spraying	85
3.6.1 History	85
3.6.2 Principles	85
3.6.3 Process Parameters	86
3.6.4 Coating Properties	89
3.7 Vacuum Plasma Spraying (VPS)	89
3.7.1 History	89
3.7.2 Principles	89
3.7.3 Process Parameters	91
3.7.4 Coating Properties	92
3.8 Controlled-Atmosphere Plasma Spraying (CAPS)	93
3.8.1 History	93
3.8.2 Principles	93

3.8.3	Process Parameters	94
3.8.4	Coating Properties	96
3.9	Cold-Gas Spraying Method (CGSM)	96
3.9.1	History	96
3.9.2	Principles	97
3.9.3	Process Parameters	97
3.9.4	Coating Properties	100
3.10	New Developments in Thermal Spray Techniques	100
	References	107
<b>4</b>	<b>Post-Spray Treatment</b>	<b>115</b>
4.1	Heat Treatment	115
4.1.1	Electromagnetic Treatment	116
4.1.2	Furnace Treatment	149
4.1.3	Hot Isostatic Pressing (HIP)	150
4.1.4	Combustion Flame Re-melting	152
4.2	Impregnation	154
4.2.1	Inorganic Sealants	154
4.2.2	Organic Sealants	157
4.3	Finishing	158
4.3.1	Grinding	158
4.3.2	Polishing and Lapping	159
	References	159
<b>5</b>	<b>Physics and Chemistry of Thermal Spraying</b>	<b>167</b>
5.1	Jets and Flames	168
5.1.1	Properties of Jets and Flames	169
5.2	Momentum Transfer between Jets or Flames and Sprayed Particles	180
5.2.1	Theoretical Description	181
5.2.2	Experimental Determination of Sprayed Particles' Velocities	186
5.2.3	Examples of Experimental Determination of Particles Velocities	190
5.3	Heat Transfer between Jets or Flames and Sprayed Particles	192
5.3.1	Theoretical Description	193
5.3.2	Methods of Particles' Temperature Measurements	208
5.4	Chemical Modification at Flight of Sprayed Particles	210
	References	214

<b>6 Coating Build-Up</b>	<b>221</b>
6.1 Impact of Particles	222
6.1.1 Particle Deformation	223
6.1.2 Particle Temperature at Impact	236
6.1.3 Nucleation, Solidification and Crystal Growth	241
6.1.4 Mechanisms of Adhesion	246
6.2 Coating Growth	249
6.2.1 Mechanism of Coating Growth	249
6.2.2 Temperature of Coatings at Spraying	251
6.2.3 Generation of Thermal Stresses at Spraying	255
6.2.4 Coatings Surfaces	264
6.3 Microstructure of the Coatings	264
6.3.1 Crystal Phase Composition	264
6.3.2 Coatings' Inhomogeneity	278
6.3.3 Final Microstructure of Sprayed Coatings	280
6.4 Thermally Sprayed Composites	281
6.4.1 Classification of Sprayed Composites	282
6.4.2 Composite Coating Manufacturing	282
References	284
<b>7 Methods of Coatings' Characterization</b>	<b>291</b>
7.1 Methods of Microstructure Characterization	292
7.1.1 Methods of Chemical Analysis	297
7.1.2 Crystallographic Analyses	303
7.1.3 Microstructure Analyses	307
7.1.4 Other Applied Methods	315
7.2 Mechanical Properties of Coatings	317
7.2.1 Adhesion Determination	318
7.2.2 Hardness and Microhardness	324
7.2.3 Elastic Moduli, Strength and Ductility	325
7.2.4 Properties Related to Mechanics of Coating Fracture	332
7.2.5 Friction and Wear	334
7.2.6 Residual Stresses	339
7.3 Physical Properties of Coatings	340
7.3.1 Thickness, Porosity and Density	341
7.3.2 Thermophysical Properties	342
7.3.3 Thermal Shock Resistance	348
7.4 Electrical Properties of Coatings	350
7.4.1 Electrical Conductivity	350

7.4.2 Properties of Dielectrics	353
7.4.3 Electron Emission from Surfaces	357
7.5 Magnetic Properties of Coatings	357
7.6 Chemical Properties of Coatings	359
7.6.1 Aqueous Corrosion	359
7.6.2 Hot-gas Corrosion	363
7.7 Characterization of Coatings' Quality	364
7.7.1 Acoustical Methods	365
7.7.2 Thermal Methods	368
References	370
<b>8 Properties of Coatings</b>	<b>383</b>
8.1 Design of Experiments	384
8.2 Mechanical Properties	389
8.2.1 Hardness and Microhardness	389
8.2.2 Tensile Adhesion Strength	403
8.2.3 Elastic Moduli, Strengths and Fracture Toughness	412
8.2.4 Friction and Wear	434
8.3 Thermophysical Properties	452
8.3.1 Thermal Conductivity and Diffusivity	454
8.3.2 Specific Heat	471
8.3.3 Thermal Expansion	472
8.3.4 Emissivity	479
8.3.5 Thermal Shock Resistance	480
8.4 Electric Properties	484
8.4.1 Properties of Conductors	484
8.4.2 Properties of Resistors	492
8.4.3 Properties of Dielectrics	493
8.4.4 Electric Field Emitters	500
8.4.5 Properties of Superconductors	501
8.5 Magnetic Properties	502
8.5.1 Soft Magnets	502
8.5.2 Hard Magnets	504
8.6 Optical Properties	504
8.6.1 Decorative Coatings	505
8.6.2 Optically Functional Coatings	505
8.7 Corrosion Resistance	507
8.7.1 Aqueous Corrosion	507
8.7.2 Hot-medium Corrosion	518
References	521

<b>9 Applications of Coatings</b>	<b>543</b>
9.1 Aeronautical and Space Industries	545
9.1.1 Aero-engines	545
9.1.2 Landing-gear Components	549
9.1.3 Rocket Thrust-chamber Liners	550
9.2 Agroalimentary Industry	551
9.3 Automobile Industry	551
9.4 Ceramics Industry	554
9.4.1 Free-standing Samples	554
9.4.2 Brick–Clay Extruders	555
9.4.3 Crucibles to Melt Oxide Ceramics	557
9.4.4 Ceramic Membranes	557
9.5 Chemical Industry	557
9.5.1 Photocatalytic Surfaces	557
9.5.2 Tools in Petrol Search Installations	559
9.5.3 Vessels in Chemical Refineries	560
9.5.4 Gas-well Tubing	560
9.5.5 Polymeric Coatings on Pipeline Components	560
9.5.6 Ozonizer Tubes	561
9.6 Civil Engineering	562
9.7 Decorative Coatings	563
9.8 Electronics Industry	563
9.8.1 Heaters	564
9.8.2 Sources for Sputtering	565
9.8.3 Substrates for Hybrid Microelectronics	565
9.8.4 Capacitor Electrodes	566
9.8.5 Conductor Paths for Hybrid Electronics	566
9.8.6 Microwave Integrated Circuits	566
9.9 Energy Generation and Transport	567
9.9.1 Solid-oxide Fuel Cell (SOFCs)	567
9.9.2 Thermopile Devices for Thermoelectric Generators	569
9.9.3 Boilers in Power-generation Plants	571
9.9.4 Stationary Gas Turbines	571
9.9.5 Hydropower Stations	572
9.9.6 MHD Generators	572
9.10 Iron and Steel Industries	572
9.10.1 Continuous Annealing Line (CAL)	573
9.10.2 Continuous Galvanizing Section	574
9.10.3 Stave Cooling Pipes	574
9.11 Machine Building Industry	574

9.12	Medicine	575
9.13	Mining Industry	577
9.14	Non-ferrous Metal Industry	577
9.14.1	Hot-extrusion Dies	577
9.14.2	Protective Coatings against Liquid Copper	578
9.14.3	Protective Coatings against Liquid Zirconium	578
9.15	Nuclear Industry	579
9.15.1	Components of Tokamak Device	579
9.15.2	Magnetic-fusion Energy Device	579
9.16	Paper Industry	580
9.16.1	Dryers	580
9.16.2	Gloss Calender Rolls	582
9.16.3	Tubing in Boilers	582
9.17	Printing and Packaging Industries	583
9.17.1	Corona Rolls	583
9.17.2	Anilox Rolls	585
9.18	Shipbuinding and Naval Industries	588
9.18.1	Marine Gas-turbine Engines	588
9.18.2	Steam Valve Stems	588
9.18.3	Non-skid Helicopter Flight Deck	588
	References	588
	<i>Index</i>	597

# Preface to the Second Edition

Since the first edition of *The Science and Engineering of Thermal Spray Coatings* was published in 1995, thermal spray technology has continued its scientific, technical and economic growth. The major laboratories have been equipped with diagnostic tools, enabling observation of individual particles and an intelligent optimization of spray processes. The modelling of the processes has progressed with the dissemination of sophisticated software and rapid computers. Nanotechnologies were introduced by an appropriate manufacturing of spray powders or by using powder suspensions. Finally, an understanding of the environmental impact of the technology has progressed considerably.

Technical progress is related mainly to the development of new spray techniques, such as, among others, the cold gas spray method, which enables obtaining many metal and alloy coatings with reduced oxidation and plasma spraying with axial injection of powders, which increases considerably the productivity of deposition. Many sophisticated methods of pre- and post-spray treatments and the coatings' characterization were introduced into industry in a routine way.

Economic progress is related to the new areas of coatings' applications. The sprayed coatings have gained a recognized place in the biomedical, chemical, printing and automobile industries. New applications will hopefully introduce the deposits into the electronics industry.

The first edition of the book was very well received and many people involved in the technology have used the book. More than 400 citations of this book in bibliographies are witness to its popularity and usefulness. The second edition is entirely rewritten by taking into account new developments, maturing of the technology and the author's views. Discussions with many colleagues have enabled me to refine the book's

content. Consequently, the chapter about the ‘organization of a spray workshop’ has been removed from this present edition.

I wish to thank the many students who have encouraged me to finish this second edition. My gratitude also goes to my Ph.D., graduate and undergraduate students, who have helped me in the realization of my scientific ideas; many of them being considered in the present book. In addition, many thanks also go to the copyright holders for their permission to re-use a number of figures. Last but not least, let me thank my family for supporting me during the writing of this book.

Lech Pawlowski  
Lille, France  
December, 2007

# Preface to the First Edition

My contact with thermal spraying started in the autumn of 1973 when I was asked to choose the subject for an M.Sc. thesis. As were most of my fellow students at the Electronic Technology Institute of the Technical University of Wroclaw (Poland), I was attracted more by the technology of semiconductors. My tutor, Professor Licznerski, then changed my mind, by showing me very thick coatings and explaining the deposition technique of plasma spraying.

This deposition method is just one from the 'family' of thermal spraying techniques. Thermal spraying is now used in the research laboratories of many universities and also in industry. The laboratories will soon complete an understanding of the physical and chemical phenomena of spraying. Industry is exploring new applications of these coatings. The expansion of thermal spraying in the laboratories and in industry has created the need for this volume.

This book is therefore addressed to professionals at different educational levels. Highly trained researchers and engineers can find a physical background of thermal spraying processes, a description of coatings characterization techniques and an up-to-date review of the coatings properties.

The sales officers and technicians will hopefully appreciate the basic information concerning the consumables used in thermal spraying and the methods of pre- and post-spraying techniques.

Finally, the entrepreneur, who wishes to invest in thermal spray techniques will find a description of thermal spraying technology and remarks concerning the organization of a thermal spray workshop.

This book gives a complete description of the technology of thermal spraying, starting with a discussion of powder manufacturing and testing

techniques and the methods of pre-spray treatment. The most important techniques of thermal spraying in present use, as well as those in the research and development stage, are discussed. Finally, the techniques of post-spraying treatment, such as mechanical finishing, high-pressure and high-temperature treatments and laser treatment are outlined.

The book also explains the physics of thermal spraying and the phenomenon of acceleration of heating the solid particles in the flames. The problems related to the coatings build-up, which starts with the 'splash' of an individual particle through to the generation of thermal stresses in the coating, are also discussed. Special attention is given to the methods of coating characterization, including microstructure investigation, as well as the testing of mechanical and physical properties and non-destructive methods enabling control of their quality. The coatings' properties, determined by the methods discussed, their relation to the coatings' microstructure and processing parameters are systematically reviewed. Similarly, coating applications in such important branches of modern industry as aeronautics, printing, electronics and others are presented.

A chapter related to the creation and organization of a modern thermal spray workshop concludes the text.

Many people have contributed in a more or less direct way to the book's creation.

I wish to acknowledge the friendly support of Professor P. Fauchais, of the University of Limoges (France). I am equally grateful to Professor S. Sturlese who, together with other scientists of Centro Sviluppo Materiali in Rome (Italy), revised the reviews of thermal and electrical properties of the coatings, which are incorporated in this book.

Dr R.C. Tucker, Jr of Praxair ST in Indianapolis (IN, USA) kindly revised the chapter concerning the D-gun™ technique, while Dr K. Kirner from Gerlingen (Germany) contributed to the corrections of the proof-pages.

Ing. F. Kilp of Cermet Vertrieb OHG. in Düsseldorf (Germany) and Dr D. Lombard of Pechiney in Voreppe (France) made available their papers about the powder production methods. Professor A. Vardelle of the University of Limoges (France) provided the papers about the impact of sprayed particles, while Dr J. Tekeuchi of Tocalo in Kobe (Japan) made available the photographs of the coated rollers applied in the paper and steel industries.

I want to express my gratitude to the following colleagues and organizations who sent me the requested photographs and permitted me to use them as the figures in the book: Mr J. Andresen, Dr Ing.

Z. Babiak, Batelle Columbus Laboratories, Dipl. Ing. P. Bork, Dr T. Cosack, Mr F.J. Driller, Professor H. Herman, Mr B. Kushner, Mrs and Mr Lemmens, Dr E.H. Lutz, Dr M. Marchese, Dr A. Mascanzoni, Matrasur, Dr Monerie-Moulin, Ms B. Ottesen, Dipl. Ing. E. Prinz and Mr G. Slaughter, Sherritt Inc.

Many thanks to my wife Muryel for drawing many of the figures and her support and patience during the last months of the book's writing.

Lech Pawlowski  
Nozay, France  
August 1994

# Acronyms, Abbreviations and Symbols

## ACRONYMS/ABBREVIATIONS

1SLD	One-step laser deposition
2SLD	Two-step laser deposition
2-D	Two dimensional
3-D	Three dimensional
AA	Average roughness (see $R_a$ )
AC	Alternating current
AEA	Acoustic emission analysis
AFM	Atomic force microscopy
AHF	Ability-of-heating factor (defined in Equation (5.32))
APS	Atmospheric plasma spraying
ARCI	Advanced Research Centre for Powder Metallurgy and New Materials, International (Hyderabad, India)
AS	Arc spraying
AZO	Aluminium zinc oxide
b.c.c.	Body-centred cubic
BET	Brunauer–Emmett–Teller (technique of porosity evaluation (see Table 7.7))
BIC	Bunsen ice calorimeter
BSE	Backscattered electron
c	Cubic
CAPS	Controlled-atmosphere plasma spraying
CaSZ	Calcia-stabilized zirconia
CBN	Cubic boron nitride

CCD	Charge-coupled device
CeSZ	Ceria-stabilized zirconia
CFD	Computational fluid dynamics
CGSM	Cold-gas spraying method
CLA	Central-line average (see $R_a$ )
CP	Continuous pulse
CVD	Chemical vapour deposition
CW	Continuous wave
DC	Direct current
DCB	Double-cantilever beam
D-GUN	Detonation-gun spraying
DIC	Differential interference contrast
DMF	Difficulty-of-melting factor (defined in Equation (5.32))
DOE	Design of experiment
DSC	Differential scanning calorimetry
DT	Double torsion
DTA	Differential thermal analysis
e	Base of normal logarithm ( $\approx 2.718$ )
e-beam	Electron beam
EBPVD	Electron-beam physical vapour deposition
EDS	Energy-dispersive spectroscopy
EELS	Electron energy-loss spectroscopy
EMPA	Electron microprobe analysis
EXAFS	Extended X-ray absorption fine structure
f	Focus
F	Fuel
f.c.c.	Face-centred cubic
FS	Flame spraying
FS-powder	Flame spraying using a powder
FS-wire	Flame spraying using a wire
FTIR	Fourier transform infrared spectroscopy
FWHM	Full width at half maximum
HA	Hydroxyapatite ( $\text{Ca}_{10}(\text{PO}_4)_6(\text{OH})_2$ )
HAZ	Heat-affected zone
HBSS	Hank's balanced salt solution
h.c.p.	Hexagonal close-packed
HF	High frequency
HIP	Hot isostatic pressing
HOSP	Homogenous oven spherical powder
HPPS	High-power plasma spraying

HVAF	high-velocity air-fuel
HVOF	High-velocity oxy-fuel
HYPREPOC	Hydrogen-pressure-reducing powder coating
ICP	Inductively coupled plasma
ICPES	Inductively coupled plasma-emission spectroscopy
ID	Internal diameter
IPS	Inert plasma spraying
ir	Infrared
IRS	Infrared absorption spectroscopy
ITO	Indium tin oxide
L	Liquid
L2F	Laser Two Focus
LCVD	Laser-assisted chemical vapour deposition
LD	Line density
LDV	Laser Doppler velocimetry
LF	Laser-flash method of thermal diffusivity determination
LPPS	Low-pressure plasma spraying (see VPS)
LSP	Laser-shock processing
LTE	Local thermodynamic equilibrium
LV	Laser velocimetry
Mag	Magnification
MB	Modulated-beam method of thermal diffusivity determination
MF	Mechanofusion
MgSZ	Magnesia-stabilized zirconia
MIP	Mercury-intrusion porosimetry
MMC	Metal-matrix composite
MOCVD	Metal-organic chemical vapour deposition
NDT	Non-destructive testing
NIC	Nomarski interference contrast
OM	Optical microscopy
PECVD	Plasma-enhanced chemical vapour deposition
PLD	Pulsed-laser deposition
PVD	Physical vapour deposition
PTA	Plasma-transferred arc
PZT	Lead-zirconate-titanate
R	Alkyl group, $C_nH_{2n+1}$ , e.g. $CH_3$ or $C_2H_5$
RF	Radiofrequency
rpm	Rotations per minute

RS	Raman spectroscopy
RT	Room temperature
SAD	Selected area diffraction
SAW	Surface acoustic wave
SBF	Simulated body fluid
SCE	Standard calomel electrode
ScSZ	Scandia-stabilized zirconia
SE	Secondary electron
SEM	Scanning electron microscopy
SHS	Self-propagating high-temperature synthesis
SIMS	Secondary-ion mass spectrometry
slpm	Standard litre per minute
SOFC	Solid-oxide fuel cell
SPS	Shrouded plasma spraying
STM	Scanning tunnelling microscopy
t	Tetragonal
t'	Tetragonal non-transferable phase of sprayed stabilized ZrO <sub>2</sub>
TAT	Tensile adhesion test
TBC	Thermal-barrier coating
TCP	Tricalcium phosphate (Ca <sub>3</sub> (PO <sub>4</sub> ) <sub>2</sub> )
TEM	Transverse electromagnetic (wave); transmission electron microscopy
TGA	Thermogravimetric analysis
TGO	Thermally grown oxide
TSC	Thermally sprayed composite
TSR	Thermal shock resistance
TTBC	Thick thermal-barrier coating
TTCP	Tetracalcium phosphate (Ca <sub>4</sub> P <sub>2</sub> O <sub>9</sub> )
UPS	Underwater plasma spraying
uv	Ultraviolet
VPS	Vacuum plasma spraying (see LPPS)
WDS	Wavelength-dispersive spectroscopy
WSP	Water-stabilized plasma
XPS	X-ray photoelectron spectroscopy
XRD	X-ray diffraction
XRF	X-ray fluorescence
YAG	Yttrium aluminum garnet
YBCO	YBa <sub>2</sub> Cu <sub>3</sub> O <sub>7-x</sub>
YSZ	Yttria-stabilized zirconia

## TRADE NAMES

Amdry™	Powder(s), manufactured by Sulzer Metco, Wohlen, Switzerland
Amperit™	Powder(s), manufactured by HC Starck, Goslar, Germany
Axial III™	Plasma torch, commercialized by Northwestern Mettech, Richmond, BC, Canada
D-gun™	Detonation spray technique, used by Praxair ST, Appleton, WI, USA
DPV-2000™	Diagnostic tool enabling temperature and velocity to be determined, commercialized by Tecnar, St-Bruno, QU, Canada
JetStar™	HVAF spray technique, used and commercialized by Praxair ST, Appleton, WI, USA
Laserblast™	Laser installation, for cleaning and activation of surfaces, Quantel, Les Ulis, France
Plazjet™	High-enthalpy spray torch, commercialized by TAFA, Concord, NH, USA
PROTAL™	Surface activation by laser ablation, Sulzer Metco, Wohlen, Switzerland and the University of Belfort-Montbéliard, France
Rokide™	Flame spraying of ceramic rods, Saint Gobain, La Défense, France
RotaPlasma™	Plasma spraying of the internal parts of cylinder bores with a jet rotating around the cylinder axis, developed and commercialized by Sulzer Metco, Wohlen, Switzerland
Sonarc™	Spray technique (a combination of AS and HVOF), developed at the University of Dortmund, Germany
SprayWatch™	Diagnostic tool enabling temperature and velocity to be determined, commercialized by Oseir, Tampere, Finland
Super D-gun™	Spray technique (a further development of D-gun™), used by Praxair ST, Appleton, WI, USA
Triplex™	Plasma spray torch, developed by Professor K Landes, Munich, Germany and used by Sulzer Metco, Wohlen, Switzerland

## SYMBOLS<sup>1,2</sup>

$\Delta_f H^\circ$	Standard enthalpy of formation
$\Delta x$	Variation of variable $x$
$a$	Fraction of absorbed energy (see Equation (4.4)) or diffusivity (see Equation (4.5))
$A$	Constant
$B$	Magnetic induction
$Bi$	Biot number (defined in Equation (5.30))
$c$	Velocity of sound or velocity of light (see Equation (5.46))
$c_p$	Specific heat under constant pressure (defined in Equation (7.21))
$c_v$	Specific heat at constant volume
$C$	Capacity
$C_D$	Drag coefficient (see Equation (5.13))
$d$	Diameter or thickness (see Equation (7.29))
$div(\vec{v})$	$\frac{\partial v_x}{\partial x} + \frac{\partial v_y}{\partial y} + \frac{\partial v_z}{\partial z}$
$e$	Charge on an electron ( $1.602 \times 10^{-19}$ C)
$\vec{e}_x, \vec{e}_y, \vec{e}_z$	Unitary vectors in $x$ -, $y$ -, $z$ -directions
$E$	Energy; elastic modulus (see Equation (6.18)); electric field
$f$	Frequency
$F$	Force
$Fro$	Frouard number (defined in Equation (1.9))
$g$	Gravitation constant ( $9.81 \text{ m/s}^2$ )
$\overrightarrow{grad}(v)$	$\frac{\partial v \vec{e}_x}{\partial x} + \frac{\partial v \vec{e}_y}{\partial y} + \frac{\partial v \vec{e}_z}{\partial z}$
$G_i$	Interfacial fracture energy
$G_{1c}$	Critical energy per unit area at crack propagation for mode-1 fracture
$h$	Static enthalpy; heat transfer coefficient (see Equation (5.28)); Planck constant ( $6.6262 \times 10^{-34}$ J s); thickness of lamella
$H$	Total enthalpy; hardness (see Equations (7.11) and (7.12)); magnetic field intensity

<sup>1</sup> Symbols with arrows above – vectors; symbols without arrows above – scalar quantities.

<sup>2</sup> In some cases, symbols are also explained in the text and/or figures.

$H_{\text{ev}}$	Enthalpy of evaporation
$H_{\text{m}}$	Enthalpy of melting
$HK$	Knoop hardness
$HRC$	Rockwell hardness
$HV_c$	Vickers microhardness, under a load of $c$ Newtons
$i$	Integer number
$I$	Electric current; intensity of radiation
$j$	Current density
$k$	Kinetic energy of turbulent flow; reaction constant (see Equation (5.8)); Boltzmann constant ( $1.38 \times 10^{-23}$ J/K)
$K$	Quality of laser beam (see Equation (4.3)); toughness
$K_{1c}$	Critical stress intensity factor (fracture toughness) at mode 1 of fracture
$Kn$	Knudsen number (defined in Equation (5.20))
$l$	Length; distance; path
$L$	Optical absorption depth at which the power density decreases by a factor of 1/e (see Equation (4.4))
$m$	Mass
$M$	Mach number ( $v/c$ )
$n$	Integer number
$N$	Integer number; concentration
$Nu$	Nusselt number (defined in Equation (5.28))
$p$	Pressure
$p^*$	Vapour pressure
$P$	Porosity; power
$Pr$	Prandtl number (defined in Equation (5.29))
$q$	Feed rate; flow rate; power density (see Equation 4.5)); heat flux (see Equations (5.12) and (7.24))
$r$	Radius; variable in cylindrical and spherical systems of coordinates
$R$	Reflectivity; radius; universal gas constant ( $\approx 8.314$ J/(mol K)); resistance
$R_a$	Average roughness, defined as the arithmetical average of the absolute values of the amplitudes of the surface with regard to a mean line along the measured distance
$R_i$	Rate of generation of the chemical species per unit volume (see Equation (5.1))
$R_{\max}$	Maximum roughness, defined as the ‘deepest valley’ in the surface inside the measured distance
$R_s$	Sheet resistance

$R_z$	Average roughness – a mean of the absolute values of five greatest heights and five greatest cavities on a surface
$Re$	Reynolds number (defined in Equation (5.18))
$S$	Area; source of energy (see Equation (5.4))
$t$	Time
$T$	Temperature
$TCR$	Thermal coefficient of resistivity; thermal contact resistance
$TEC$	Thermal expansion coefficient (defined in Equation (7.23))
$U$	Root of transcendental equation (Equations (6.7)–(6.9))
$v$	Velocity
$\vec{v} \times \vec{v}$	Vectorial product, resulting in a vector
$\vec{v} \cdot \vec{v}$	Scalar product, resulting in a scalar
$V$	Voltage
$w$	Weight
$x$	Variable in Cartesian system of coordinates
$X$	Variable in Cartesian system of coordinates
$y$	Variable in Cartesian system of coordinates
$Y$	Variable in Cartesian system of coordinates
$z$	Variable in Cartesian system of coordinates
$Z$	Variable in Cartesian system of coordinates; atomic number
$\alpha$	Angle; root of transcendental equation (Equations (6.12)–(6.16))
$\beta$	Temperature exponent in Arrhenius equation (Equation (5.8)); dimensionless velocity of vaporization (see Equation (5.39)); width of a diffracted peak on a diagram at half maximum, corrected for instrument contribution (see Equation (7.4)); enhancement of electrical-field factor (see Equation (7.31))
$\gamma$	Ratio of specific heats ( $c_p/c_v$ ) (see Equation (7.17))
$\varepsilon$	Dielectric constant; dissipation rate of kinetic energy of turbulent flow ( $k$ ); radiative emission coefficient (see Equation (5.31)); strain (see Equation (7.13))
$\varepsilon_0$	Dielectric constant of vacuum ( $8.854 \times 10^{-12} \text{ F/m}$ )
$\eta$	Dynamic viscosity
$\theta$	Wetting angle; angle of diffraction (see Equation (7.3)); parameter relative to feed rate of a composite (see Equation (8.3))
$\lambda$	Thermal conductivity; wavelength
$\mu$	Molar mass; friction coefficient (see Equation (7.10))
$\mu_r$	Relative magnetic permeability

- $\nu$  Poisson modulus/ratio  
 $\xi$  Flattening parameter of splat with regard to initial parameter (see Equation (6.2))  
 $\pi$  Constant ( $= 3.1415\ldots$ )  
 $\rho$  Density; resistivity  
 $\sigma$  Stefan–Bolzmann constant ( $\approx 5.670\ 51 \times 10^{-8}\ \text{W}/(\text{m}^2\text{K}^4)$ ; surface tension (see Equation (6.4)); stress (see Equation (6.18)), Figures 7.13 and 7.25); electrical conductivity (see Equation (7.26))  
 $\tau$  Duration of pulse; lapse of time  
 $\phi$  Equivalence ratio (see Equation (3.2)); work function  
 $\chi$  Ratio of specific heats under constant pressure and constant volume (5/3 for monatomic gases)

## INDEXES

- |      |   |
|------|---|
| 0    | Initial   |
| I    | Mode of fracture (see Section 7.2.4)  |
| II   | Mode of fracture (see Section 7.2.4)  |
| III  | Mode of fracture (see Section 7.2.4)  |
| a    | Activation  |
| app  | Apparent  |
| bb   | Black body  |
| c    | Combustion; critical; contact (see Equation (6.12)); convective (see Equation (6.17)); coercive (see Figure 7.32) |
| co   | Coating   |
| corr | Corrosion   |
| cr   | Crystal   |
| d    | Deposition  |
| D    | Doppler; drag   |
| def  | Deformation   |
| e    | Electron  |
| eff  | Effective   |
| ev   | Evaporation   |
| f    | Formation; fracture (see Equations (7.13) and (7.25))   |
| fi   | Film  |
| fr   | Fringe  |
| g    | Gas   |
| h    | Miller symbol   |

i	Integer number; impact (see Equation (6.1))
in	Injector
ind	Indenter
ion	Ionization
j	Integer number
k	Miller symbol; kinetic; integer number (see Equation (8.2))
l	Miller symbol
L	Liquid
m	Melting; matrix (see Equation (7.16))
M	Median
max	Maximum
mf	Mean free (see Equation (5.20))
min	Minimum
mol	Molecular
n	Integer number
p	Particle; powder
pass	Passivation
pi	Pipeline
pitt	Pitting
q	Quenching
r	Relative; radiative (see Equation (5.31)); residual (see Figure 7.32)
s	Spot; saturated (see Equation (5.39) and the following); solid (see Figure 5.22, plus associated text and Equation (6.5)); substrate (see Equations (6.13) and (6.17)); solidification (see Equation (6.7))
st	Stoichiometric
th	Thermal
VS	Volume–surface
x	Direction of $x$ -axis
y	Direction of $y$ -axis
z	Direction of $z$ -axis

## EXONENTS

- 0 Atom in ground state
- 1 First ionization level
- 2 Second ionization level
  
- D Dissociation

# 1

## Materials Used for Spraying

The materials used in thermal spraying are principally powders, rods and wires. The wires are made of metals or alloys and are used mainly in flame-spraying (FS-wire) and arc-spraying processes (AS). The methods of wire manufacturing are part of the metals and alloys mechanical working and forming technology that is described in textbooks on metals technology (e.g. Callister, 1994). The wires can be made of:

- metals, such as Al or Zn;
- alloys, such as Ni + 5 wt%Al (e.g. wire type Sulzer Metco 8400) or Ni + 18 wt% Cr + 6 wt%Al (e.g. wire type Sulzer Metco 8443);
- composites that are cored wires, shown in Figure 1.1, which contain a metallic sheath (Co or FeCr) and a filler made of a hard material such as WC (Drzeniek and Steffens, 1987) or Cr<sub>3</sub>C<sub>2</sub> (Sikorski *et al.*, 1996).

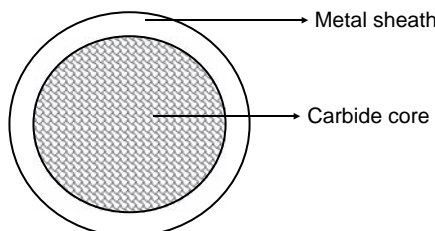


**Figure 1.1** Cored wire containing an outer sheath of a metal and a core of tungsten carbide

A typical wire has an outer diameter ranging between 2.4 and 5 mm. Two diameters are used very frequently, namely 3.18 mm (1/8 in) and 4.76 mm (3/16 in). Ceramic rods are sometimes used in spraying by using a combustion torch. One well-known flame-spraying rod process is Rokide™ (Saint Gobain, La Defense, France) which allows oxide ceramics to be deposited (Gartner and Walker, 1980). Sometimes, short rods are placed inside a long polyethylene sheath. In this way, the deposition process becomes nearly continuous, with a short interruption when a rod is ‘sprayed out’. This is useful for deposition of thick coatings on large pieces with processing that requires many rods. An important advantage of wire and rod spraying is that the molten particles are nearly single-sized. Consequently, the lamellae inside the coatings are more homogeneous than that sprayed with powders. However, the deposition techniques of AS or FS-wire produce rather porous coatings which considerably reduce this advantage. At the present time, powders are used mainly in thermal spraying and thus this discussion will focus on powder manufacturing methods.

A sprayed coating can be characterized by a set of specified parameters related to its future applications, such as wear resistance, heat isolation, electric resistivity, etc. These parameters are strongly dependent on the powder material and the spray process. The process may modify the properties of the initial material during the powder particle flight in a jet or a flame and at its ‘splash’ on a substrate. The modifications can result from material reduction, oxidation, rapid solidification, cooling and other phenomena. A wise choice of powder should include consideration of all of the possible modifications. Even ‘smarter’, is to take advantage of the deposition process to create an added value, i.e. coatings with particularly good properties. An example, from the area of thin film deposition, is the idea of *nanocomposites* proposed by Veprek (1999) which consists of deposition by Plasma-enhanced chemical vapour deposition (PECVD) of films with nano-dimensional reinforcements (e.g. TiN) inside an amorphous matrix (e.g. Si<sub>3</sub>N<sub>4</sub>). The hardness of the films was shown to be greater than that of any nitrides, carbides or diamond-like coatings synthesized as films or coatings (Pawlowski, 2003). An example of such a ‘smart design’ in the area of thermal spraying is deposition of a *self-bonding coating* with the use of a powder that reacts exothermally at high temperatures. Such a reaction contributes by heating the interface between the sprayed lamellae and substrate and promotes good coating adhesion. An example of a powder that reacts exothermally is a mixture of Ni and Al (Dittrich, 1965). Research into new smart materials is one of the tasks of engineers in powder manufacturing companies.

As the properties of powders considerably influence the quality of the coatings, they should be characterized very carefully. These properties can be roughly divided into physical and chemical ones. The physical characteristics include the following:

- granulometry;
- internal and external morphology;
- apparent density and flowability;
- thermal properties, including the use of differential thermal analysis (DTA) and thermogravimetric analysis (TGA).

The most important fundamental chemical property is the *chemical bond*. The type of bond determines many important properties of materials that films and coatings are made from (Holleck and Schier, 1995):

- *ionic bonds* are found in chemically stable and inert materials, such as  $\text{Al}_2\text{O}_3$  and  $\text{ZrO}_2$ ;
- *covalent bonds* are found in strong and tough materials, such as diamond,  $\text{SiC}$  and  $\text{Si}_3\text{N}_4$ ;
- *metallic bonds* are found in well-adhering and tough materials, such as many metals (e.g. Ti and Ta) and also some carbides (e.g. WC and TiC) and nitrides (TaN and CrN).

The following chemical properties determine the quality of the coatings:

- chemical composition;
- phase content;
- element distribution.

Materials for thermal spraying also include masking tapes and coatings sealants (epoxy or silicone resins). These materials will be discussed in the chapters covering pre- and post-spray treatments.

## 1.1 METHODS OF POWDERS PRODUCTION

The following types of powders are currently used in thermal spraying:

- metals, e.g. molybdenum or nickel;
- alloys, e.g. a *self-fluxing alloy* of  $\text{Ni} + 16 \text{ wt\% Cr} + 3.5 \text{ wt\% B} + 3.5 \text{ wt\% Si} + 4.5 \text{ wt\% Fe} + 1 \text{ wt\% C}$ ;

- oxide ceramics, e.g.  $\text{Al}_2\text{O}_3$ ;
- oxide alloys, e.g.  $\text{ZrO}_2 + 8 \text{ wt\% Y}_2\text{O}_3$ ;
- *cermet<sup>1</sup> clads*,<sup>2</sup> e.g. graphite + 20 wt% Ni;
- *cermet agglomerates*,<sup>3</sup> e.g. WC + 12 wt% Co;
- carbides, e.g.  $\text{Cr}_2\text{C}_3$ ;
- *composite<sup>4</sup> clads*, e.g. AlSi + 47 wt% polyimide and 6 wt% organic binder.

The powders can be injected into a jet or a flame either as a suspension in a carrier gas or as a suspension in a liquid. The latter allows processing of very small particles and is useful to obtain *nanostructured<sup>5</sup> coatings*.

The industrial methods of powder manufacturing depend mainly on the types of materials used. The methods of powder manufacturing discussed in this present book are presented in Table 1.1. The powder-preparation methods shown in this table does not pretend to be complete but is rather a mixture of methods already in industrial use with those that are about to gain in popularity. The interested reader may found further information in more specialized surveys such as, e.g. Johnson (1987) or Kushner *et al.* (1988).

**Table 1.1** Methods of powders manufacturing from different kinds of materials

Metals and alloys	Ceramics	Composite clads	Composite agglomerates
Atomization in vacuum, inert gas, air or water	Fusing or sintering and crushing	Chemical cladding	Spray drying
Fusing or sintering and crushing	Spray drying	Porous cladding	SHS <sup>a</sup>
MF <sup>b</sup>	SHS <sup>a</sup> Sol-gel Gas-phase methods	MF <sup>b</sup>	MF <sup>b</sup>

<sup>a</sup> SHS, self-propagating high-temperature synthesis.

<sup>b</sup> MF, mechanofusion.

<sup>1</sup> A cermet is defined as an association between a ceramic and a metal.

<sup>2</sup> A clad is defined as a layer of a material.

<sup>3</sup> An agglomerate is defined as an association between materials in the form of particulates.

<sup>4</sup> A composite is defined as an association between two different kinds of materials, e.g. a metal with polymers, a ceramic with polymers or a ceramic with a metal.

<sup>5</sup> A nanostructure has, by definition, a size smaller than 100 nm.

The most versatile powder preparation method is spray drying, which allows any kind of small material particulates to be kept together with an organic binder in a large spherical agglomerate. However, spray drying is not a cheap method for powder development. This is because the purchase of an appropriate installation, together with optimization of processing parameters or ‘renting’ the service of a specialized company to develop a desired powder, are expensive. To save time and money, one can easily modify the composition by blending different powders. The blend should be mixed carefully and additional attention should be paid in order to avoid the separation of powders at injection to a jet or a torch.

### 1.1.1 ATOMIZATION

Atomization is applied mainly to the manufacture of metal and alloy powders. A typical process (Figure 1.2) consists of melting the metal in an inductive heater (1, 2), the melt (3) is then poured into the previously

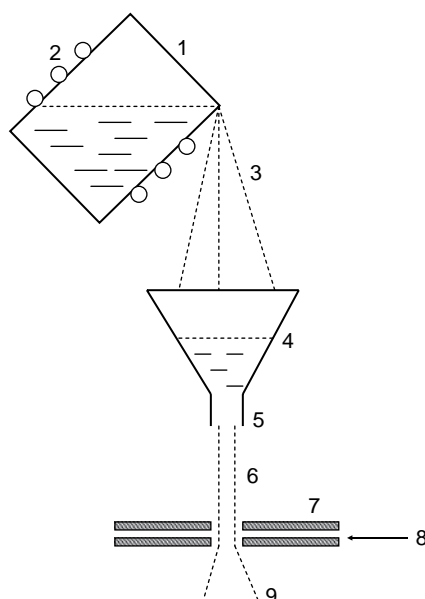


**Figure 1.2** Illustration of the metal atomization process: (1) heater; (2) induction heating coils; (3) molten metal; (4) funnel; (5) calibrated outlet; (6) liquid metal; (7) nozzle; (8) atomizing gas or liquid; (9) metal particles

heated funnel (4) having a calibrated outlet (5) and drops down as a liquid jet (6) onto the nozzle (7). Inside the nozzle is introduced, under high pressure, the atomizing medium which is usually a gas or water (8). The metal solidifies during the ‘free-fall’ forming small powder particles (9). The most important processing parameters influencing the atomization process are collected in Table 1.2.

**Table 1.2** The most important parameters influencing the atomization process of powder manufacturing (Meinhardt *et al.*, 1990)

Process element	Parameters
Atmosphere	Inside the heater Inside the atomization tower
Molten metal or alloy	Chemical composition Physical parameters, such as viscosity, surface tension and difference between boiling and melting point Funnel outlet diameter Melt velocity
Atomization medium	Gas or liquid Pressure Flow rate Velocity Viscosity
Nozzle	Diameter Angle
Atomization tower	Melt falling height from funnel to nozzle Height Cooling medium

Certain applications demand powders that are virtually oxygen-free. The oxygen content depends on the following process parameters (after Meinhardt *et al.*, 1990) which give the purest powder (top of the list) or the least pure one (bottom of the list):

- atmosphere inside the melting chamber:
  - vacuum;
  - inert gas;
  - air atmosphere.

- atomization medium:
  - gas;
  - water.
- cooling medium in the atomization tower:
  - gas;
  - water.

The inert gas and vacuum atomization are frequently used to produce high-purity intermetallic powders, such as Ni<sub>3</sub>Al, Ti<sub>3</sub>Al or FeAl (Gorham Advanced Materials Institute, 1990). The cooling medium influences the geometrical shape of the atomized particles. Water-atomized powder particles are often irregular, while gas-atomized powder particles could be ideal spheres (Figure 1.3), spheres with small satellites or spherical in shape.

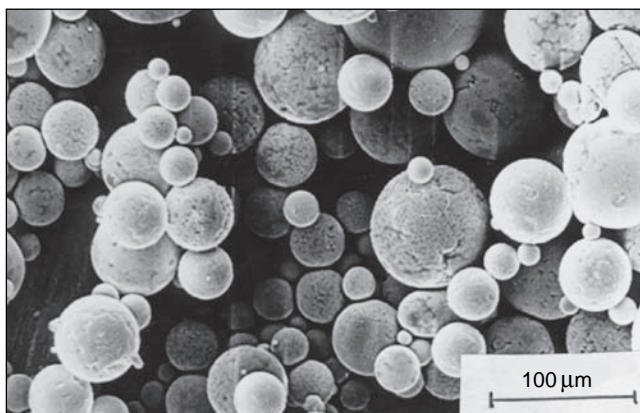


Figure 1.3 Scanning electron micrograph (secondary electrons) of a gas-atomized powder of a self-fluxing alloy having a composition (in wt%) of Ni + 16Cr + 4.5Fe + 3.5B + 3.5Si + 1C (magnification  $\times 240$ ). Reproduced by permission of Dr Zenon Babiak, retired from The University of Dortmund, Germany

The cooling medium determines, to a degree, the phase composition of the powder particles. Gas cooling results in relatively low cooling rates of  $10^{-1}$ – $10^2$  K/s. Water cooling leads to much greater liquid material cooling rates of  $10$ – $10^4$  K/s, which may result in the formation of metastable phases or precipitates. Some commercially available powders produced by atomization are presented in Table 1.3. The powders

**Table 1.3** Typical commercial powders produced by inert gas, gas and water atomization

Powder type	Chemical composition (wt%)	Application <sup>a</sup>	Atomization medium	Grain size ( $\mu\text{m}$ )	Trade name
Cobalt alloy	Co + 32Ni + 21Cr + 8Al + 0.5Y	Hot-temperature corrosion; TBC's bond coat	Inert gas	-45 + 10	CO-210-24
Nickel alloy	Ni + 22Cr + 10Al + 1Y Ni + (18–21)Cr	Bond coat	Gas Water	-106 + 56 -45 + 22	Amdry 962 <sup>b</sup> Amperit 250.1 <sup>c</sup>

<sup>a</sup> TBC, thermal-barrier coating.

<sup>b</sup> Amdry, powders manufactured by Sulzer Metco, Wohlen, Switzerland.

<sup>c</sup> Amperit, powders manufactured by HC Starck, Goslar, Germany.

produced by atomization have small internal porosities and excellent flowability properties which result from their spherical shapes.

### 1.1.2 SINTERING OR FUSION

Oxides, carbides and cermets powders can be manufactured by sintering or fusion. The resulting powder particles are ‘blocky’ and irregular, which renders their flowability to be relatively poor. To improve this parameter, they can be submitted to *spheroidization* in flame or in plasma. The spheroidization conditions need, however, to be optimized carefully in order to avoid (if not desired) a formation of internal porosity (Klima and Kotalik, 1997).

The manufacturing of typical powders prepared by fusion or sintering is discussing by using the examples of chromium oxide and tungsten carbide with cobalt.

#### Chromium Oxide

The raw material for the production of  $\text{Cr}_2\text{O}_3$  powder is a fine green pigment obtained chemically from the chromic iron ore. The pigment contains submicron particles. The pigment can be fused in an arc furnace (Kushner *et al.*, 1988; Beczkowiak and Mundinger, 1989) for 10–20 h.

Thereafter, a block of chromium oxide is broken after removing an outer shell. Finally, jaw crushers and double-roll mills crush the remaining block into smaller particles. Fusion occurs above the melting point of the material ( $T_m = 2710\text{ K}$  for  $\text{Cr}_2\text{O}_3$ ). Sintering takes place at a temperature which is usually about  $0.7 \times T_m$ . A typical, commercially available fused and crushed chromium oxide powder is shown in Figure 1.4.

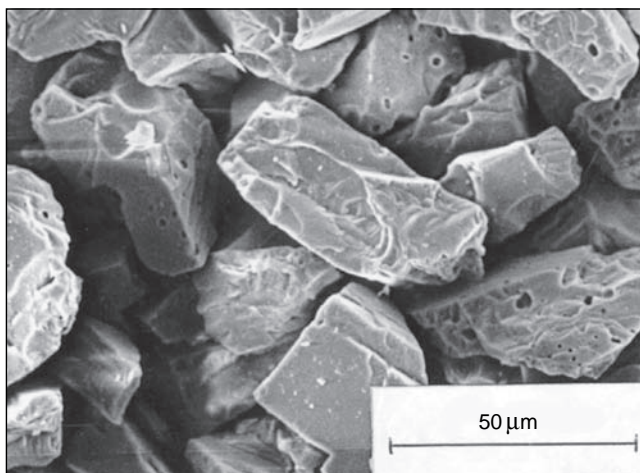


**Figure 1.4** Scanning electron micrograph (secondary electrons) of a commercially available fused and crushed chromium oxide powder (Pawlowski *et al.*, 1993). Reproduced from Pawlowski *et al.*, 1993, in *TS93, DVS-Berichte Band 152*, DVS, Düsseldorf, Germany, pp. 132–138. Copyright (1993), with permission from DVS

The powders prepared in this way are mostly dense and blocky. Chromium oxide powder can also be prepared by sintering or spray drying. The latter route is recommended, if the sprayed coating should not contain metallic chromium inclusions. The high-temperature treatment that occurs at sintering or fusion of chromium oxide may lead to reduction to suboxides or to metallic chromium:

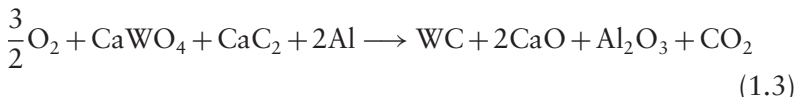


The metallic chromium should be washed away with acids. Chromium oxide powder can be prepared by an appropriate heat treatment in crystalline form, i.e. the powder particles are small crystals. Such a powder was developed by Praxair ST, Indianapolis, IN, USA.

### Cermet of Tungsten Carbide with Cobalt

Tungsten carbide can be prepared by carburizing tungsten in the following way (Eschnauer and Kilp, 1977; Houck, 1981):

- A solid-state reaction at  $T = 1673\text{--}1973\text{ K}$  between fine tungsten and carbon powders. The powders produced by this technique are too fine for thermal spraying.
- A *Thermite reaction*, also called the *Menstruum process*, for producing tungsten monocarbide utilizes the exothermic reaction generated by alumino-thermite reactions to convert tungsten ores, such as  $\text{CaWO}_4$ ,  $\text{FeWO}_4$  or  $\text{Fe}(\text{Mn})\text{WO}_4$ , into crystalline tungsten carbide that contains 6.13 wt% carbon. Examples of the reactions involved are as follows:



- The first reaction starts at about 1070 K while the second one takes place in the temperature range 2720–3270 K. After cooling, the crystal mass contains about 65 wt% WC and the balance is iron and excess aluminium. Leaching with acids leaves pure WC with less than 0.2 wt% Fe.
- Carbon-resistance melting of tungsten-bearing materials (powders, wires, etc.) in a graphite crucible to form cast tungsten carbide  $\text{WC}-\text{W}_2\text{C}$  containing about 3.9 wt% carbon.
- The next stage of carbide manufacturing is product crushing and powder screening to get the desired grain size.
- The last step is mixing with an organic binder and cobalt in quantities of 12–20 wt% with regard to carbide and sintering under an inert or reducing atmosphere (Schwier, 1985; Simm and Steine, 1985).

Figure 1.5 shows a cermet powder of  $\text{WC}-\text{CoCr}$  produced by sintering and crushing. The powder has an important internal porosity.

Typical commercial powders manufactured by sintering, fusing and crushing are shown in Table 1.4.

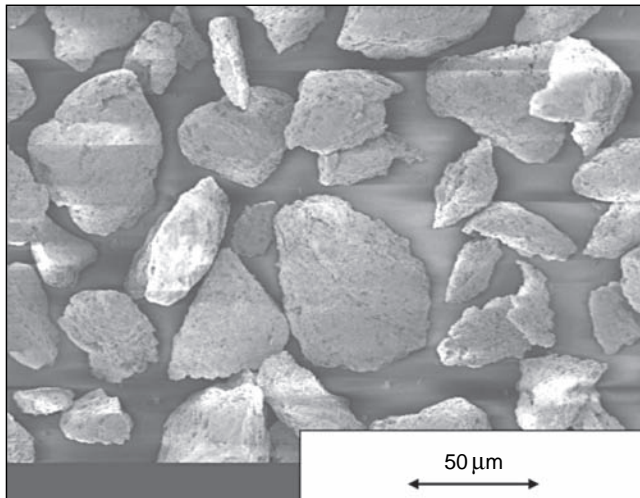


**Figure 1.5** Scanning electron micrograph (secondary electrons) of a WC–CoCr commercial cermet powder described in Table 1.4 (Colin *et al.*, 2001)

**Table 1.4** Typical commercial powders prepared by using sintering, fusing and crushing

Powder type	Chemical composition (wt%)	Application	Production method	Grain size (μm)	Trade name
Pure oxide	99.5 Cr <sub>2</sub> O <sub>3</sub>	Wear resistance	Fusing and crushing	–45 + 22	Amperit 704.0
Alloy of oxides	Al <sub>2</sub> O <sub>3</sub> + (12–14) TiO <sub>2</sub> + 0.5SiO <sub>2</sub>			–30 + 5	Amdry 6224
Cermet	WC + 10Co + 4Cr		Sintering and crushing	–45 + 11	Amdry 5843

### 1.1.3 SPRAY DRYING (AGGLOMERATION)

The spray-drying technique, sometimes called *agglomeration*, allows many kinds of materials to be agglomerated. Spray drying has been applied to manufacture powders of:

- metals, e.g. molybdenum (Cheney *et al.*, 1975; Houck, 1981);
- oxides and oxide alloys, e.g. Cr<sub>2</sub>O<sub>3</sub> + TiO<sub>2</sub> (Kim *et al.*, 2001) or ZnO + Al<sub>2</sub>O<sub>3</sub> (Tului *et al.*, 2003);

- nitrides and mixtures of nitrides with oxides, e.g.  $\text{Si}_3\text{N}_4 + \text{Al}_2\text{O}_3 + \text{Y}_2\text{O}_3$  (Thiel *et al.*, 1996);
- cermets, e.g.  $\text{TiC} + \text{Ni}$  or  $\text{WC} + \text{Co}$  (Vuoristo *et al.*, 1996).

More recently, spray drying has been applied to agglomerate extremely fine precursors that are expected to result in sprayed *nanostructured coatings* with superior mechanical properties (Kear, 1997).

### Principle of Spray Drying

The spray-drying process (Figure 1.6) consists of introducing a slurry containing finely dispersed precursors to be agglomerated, organic binder and water. The pump (2) feeds the slurry into a centrifugal atomizer (1a) or a nozzle atomizer (1b). The atomized slurry is dried in the stream of cleaned (3) and heated (4) gas (mostly air) and the moisture

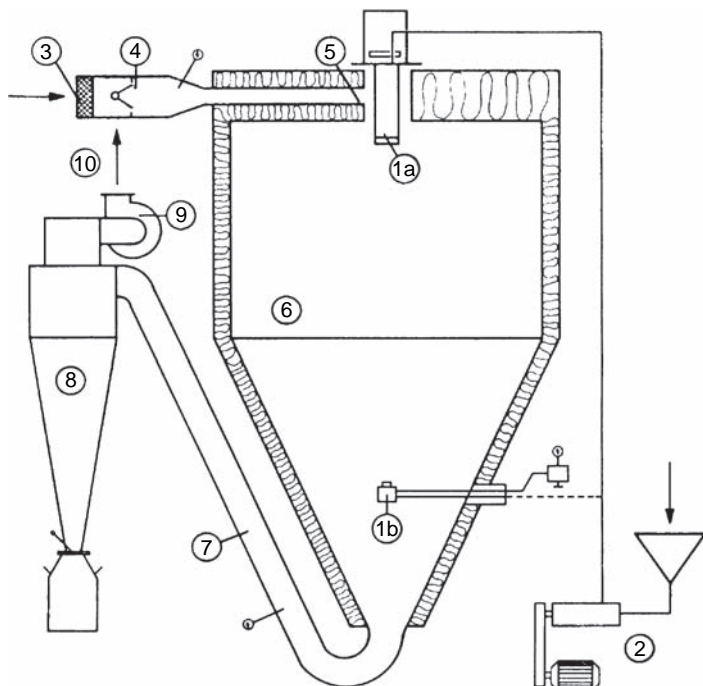


**Figure 1.6** Illustration of a spray drier: (1a) centrifugal atomizer; (1b) nozzle atomizer; (2) feed pump; (3) gas-cleaning filter; (4) gas heater; (5) gas distributor; (6) drying chamber; (7) duct; (8) powder separator; (9) exhaust fan; (10) outlet gas duct

contained in the droplets evaporates during flight in the chamber (6). The gas is cleaned out in the cyclone (9) and recycled again to the heater (10). The solid particles are collected in the powder collector (8).

A typical industrial spray dryer is shown in Figure 1.7.



**Figure 1.7** A typical industrial spray drier. Reproduced by permission of Ole Poulsen, APV A/S, Copenhagen, Denmark

The preparation of powders by spray drying can be divided into the following process stages (Masters, 1985):

- preparation of slurry;
- atomization of slurry into spray;
- spray-air contact (mixing and flow);
- drying of spray (evaporation of moisture and volatiles);
- separation of dried product (beyond the scope of this present book);
- densification of powder (optional process realized after spray drying).

### Preparation of Slurries

The majority of spray-dried powders are generated from water-based slurries; the others are discussed by Masters (1985). The preparation of

a slurry starts with the dispersion of fine precursors in water. A *binder* is added to agglomerate them after drying. This must be soluble or dispersible in the liquid to form a slurry and when dried it must form a coating which adheres to the agglomerated materials. The organic binders used (with mass fractions in the dried powders varying between 2 and 5 wt%) are frequently as follows (Lukasiewicz, 1989; Keller *et al.*, 2001):

- poly(vinyl alcohol);
- methyl cellulose or carboxymethyl cellulose;
- poly(ethylene glycol);
- acrylic ester–styrene copolymer.

Other components of a slurry have the following functions:

- *Plasticizers*, such as glycerine, which prevent the cracking of brittle binders.
- *Deflocculating agents*, such as sodium molybdate, which help in preventing the agglomeration of precursors.
- *Wetting agents* (soaps) and *suspending agents* (sodium carboxymethyl cellulose) which are useful to maintain the precursors in suspension. An important property of the slurry is the content of solid. A high percentage of solid means less water to evaporate during drying and more powder output. Typical values vary from 50 to 80 wt%.

The following properties of a slurry should be characterized (Lukasiewicz, 1989):

- *Density of the slurry and foam content*. The density is defined as the net weight divided by the actual volume. The foam content is the difference between the actual and theoretical density.
- *Weight percent solids* is determined by heating the slurry to a temperature sufficient to eliminate water and organics.
- *Viscosity of a slurry*, determined by using a viscometer, is typically in the range of  $\eta = 0.002\text{--}0.5 \text{ Pa s}$ .

## Atomization

*Atomization*, as stressed by Masters (1985), has *nothing in common* with atoms or molecules but rather describes a process of liquid bulk

break-up into millions of individual droplets, forming a spray. A cubic metre of a liquid contains about  $2 \times 10^{12}$  uniform 100  $\mu\text{m}$  droplets. The energy necessary for this process can be supplied by centrifugal, pressure, kinetic or sonic effects. There are the following types of industrial atomizers (Masters, 1985; Bork, 2001):

- *Fountain or pressure nozzle atomizer* (utilization of pressure energy) in which a slurry, under a pressure up to 680 atm, is sprayed from a nozzle from the bottom of a drying chamber, is used for the production of coarse spherical granules with a mean particle size of 150–300  $\mu\text{m}$ . The drying chamber is tall with a small diameter (*high body*).
- *Two-fluid nozzle atomizer* (utilization of kinetic energy) in which a slurry, under a pressure up to 7 atm, and an atomizing gas are passed through a nozzle head placed in the bottom of a drying chamber. This type of atomizer is used to produce fine and medium coarse powders. The drying chamber has a large diameter and is short (*wide body*).
- *Centrifugal or rotary atomizer* (utilization of centrifugal energy) in which a slurry is sprayed from a rapidly rotating plate (up to 35 000 rpm and a peripheral velocity up to 300 m/s) placed in the top of a drying chamber under the action of a centrifugal force. This atomizer is used to manufacture medium coarse particles of size 30–100  $\mu\text{m}$ .

### Spray–Air Contact

Droplet–air mixing determines the drying time and degree of moisture removal from the droplets. This removal occurs in a hot gas that can be injected into a drying chamber in two ways:

- *Co-current airflow* occurs when the gas inlet is located near the atomizing device and the direction of hot gas is the same as the direction of the spray. In this configuration, any spray droplets enter into contact with the gas having the highest temperature and drying is rapid at the beginning of its trajectory. Consequently, the evaporation time is short but the particles can be porous due to the evaporation intensity (Figures 1.8 and 1.9). (also see Table 1.5). A rotary atomizer is commonly used in co-current airflow dryers.

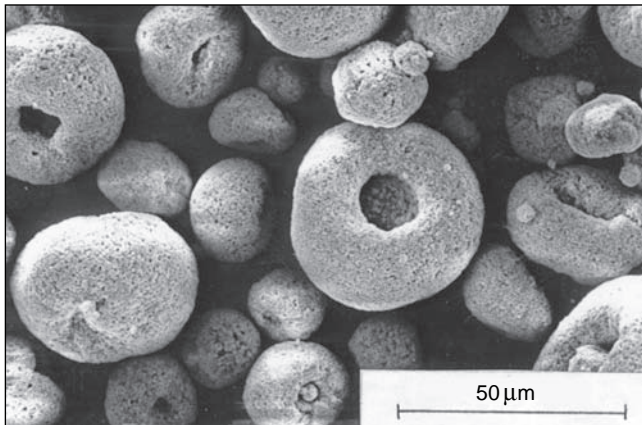


**Figure 1.8** Scanning electron micrograph (secondary electrons) of a spray-dried powder of  $\text{Cr}_2\text{O}_3 + \text{SiO}_2$ . Further details about the processing parameters are given in Table 1.5 (Bartnik *et al.*, 1992)

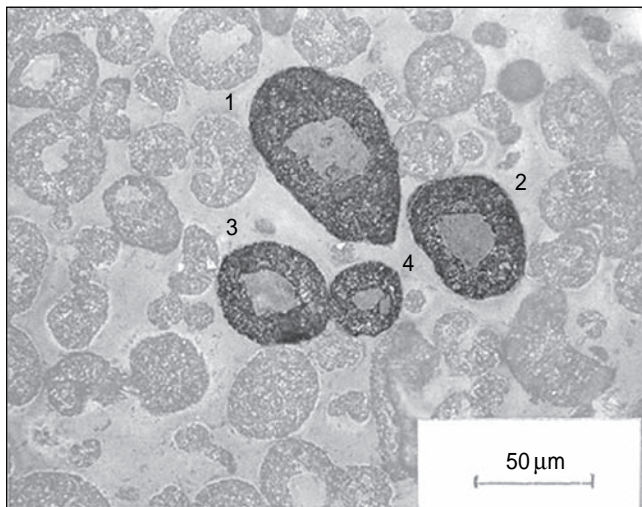


**Figure 1.9** Optical micrograph of a metallographic cross-section of the powder shown in Figure 1.8. The numbered particles have the following internal porosities (%): (1) 22.8; (2) 26.6; (3) 26.7; (4) 21.5. Further details about the processing parameters are given in Table 1.5 (Bartnik *et al.*, 1992)

- The *counter-current airflow* configuration has a gas inlet on the opposite side of the drying chamber. In this case, the sprayed particles meet cool, humid air at the beginning of their trajectory and the hottest air at the end. As high temperatures of particle surfaces can be realized, the organic binder should not be heat sensitive. Counter-current flow is used mainly with nozzle atomizers.
- Mixed airflow* is the combination of both of the above. It is commonly used in *fountain atomizers* with a nozzle located at the base of the drying chamber (see (1 b) in Figure 1.6) while the drying air inlet is placed at the top of the chamber. The spray is initially directed against the airflow (*counter-current* condition), then stops and starts to fall down the chamber (*co-current* condition). Mixed flow conditions are used in small laboratory installations or in pilot line ones (Lukasiewicz, 1989).

The choice of an atomizer and of airflow conditions has a major influence on spray-dried powder particle sizes and morphology. Examples of the processing conditions of new powders used in the development of *wear-resistant* and *optical functional coatings* are shown in Table 1.5.

Table 1.5 Parameters used in the development of new powders using spray drying

Chemical composition of powder (wt%)	$\text{Cr}_2\text{O}_3 + 5\text{SiO}_2$	$\text{ZnO} + (3 \text{ or } 22)\text{Al}_2\text{O}_3$
Application Composition of slurry	Wear-resistant coatings Water + $\text{Cr}_2\text{O}_3$ pigment + $\text{SiO}_2$ + binder (poly(vinyl alcohol))	Optical functional coatings Water + $\text{ZnO}$ + $\text{Al}_2\text{O}_3$ + dispersive medium + binder <sup>a</sup>
Atomization method	Disc rotating at 31 000 rpm	Nozzle
Spray-air contact	Co-current airflow Inlet temperature, 513 K Outlet temperature, 393 K	Inlet temperature, 523 K Outlet temperature, 423 K
Densification of powder particles	Arc plasma	Heat treatment at 1573 K for 6 h
Reference	Bartnik <i>et al.</i> , 1992	Tului <i>et al.</i> , 2003

<sup>a</sup>  $\text{ZnO}$  and  $\text{Al}_2\text{O}_3$  precursors have sizes of 0.5–1.0  $\mu\text{m}$ .

## Drying of Sprays (Evaporation of Moisture)

Evaporation from a droplet takes place in two stages (Masters, 1985):

- Initially, there is sufficient moisture within the droplet to replenish that lost at the surface. Diffusion of the moisture from inside the droplet maintains the conditions and the evaporation rate is constant. This stage is often called the *constant-rate period*. When the moisture level becomes too low, a dried shell forms on the outer surface of the droplet.
- Finally, evaporation depends on the rate of moisture diffusion through the dried shell. This stage of evaporation is called the *falling-rate period*.

One of the mechanisms of hollow particle formation (see Figure 1.9) can be related to the moisture evaporation rate which is faster than the diffusion of solid back to the droplet interior. Voids are present on completion of the evaporation.

## Densification of Particles

As spray-dried powder particles are more or less porous, this influences the conditions of heating in flames or flumes (Hurevich *et al.*, 2002). In industrial practice, such powders need to be sprayed using more power input with regard to dense powders, meaning:

- a greater flow rate of fuel gas and oxygen while spraying using flame-spraying (FS) or high-velocity oxy-fuel (HVOF) techniques;
- more electrical power while spraying using arc-spraying (AS) or atmospheric-plasma-spraying (APS) techniques.

Such an economic consideration can justify the additional step in spray-drying powder processing known as *high-temperature densification*. This densification can be carried out by:

- sintering;
- arc plasma;
- radio frequency (RF) plasma.

Spray-dried powders melted (in an oven) on their surfaces and being porous inside are sometimes called *homogenous oven spherical powders* (HOSPs). The morphology of chromium oxide–silicium oxide after arc-plasma densification is shown in Figures 1.10 and 1.11.

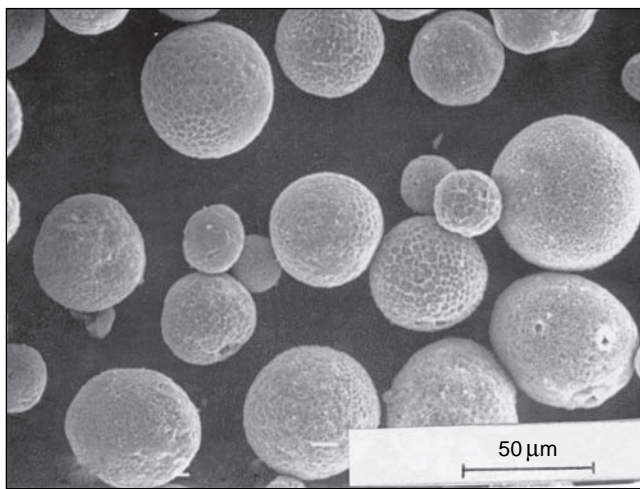


**Figure 1.10** Scanning electron micrograph (secondary electrons) of an arc-plasma-densified  $\text{Cr}_2\text{O}_3 + 5 \text{ wt\% SiO}_2$  powder (the initial powder is shown in Figure 1.8). Further details about the processing parameters are given in Table 1.4

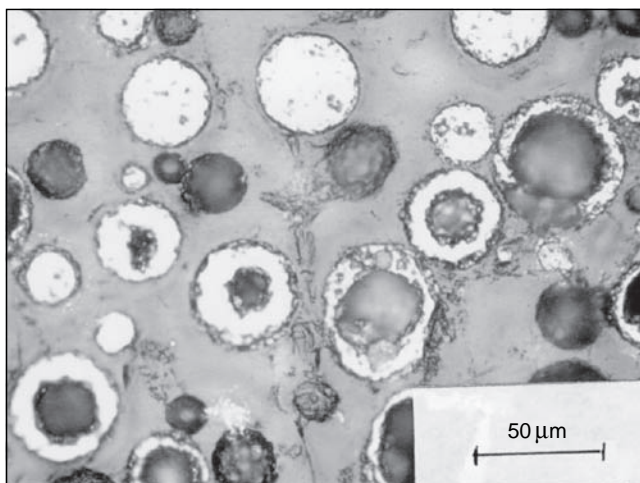


**Figure 1.11** Optical micrograph (in bright field) of a cross-section of the arc-plasma-densified  $\text{Cr}_2\text{O}_3 + 5 \text{ wt\% SiO}_2$  powder shown in Figure 1.10 (the cross-section of the initial powder is shown in Figure 1.9)

*High-temperature densification* modifies not only the powder particle morphology but may result in the formation of new phases. For example, the experimental spray-dried powder, including ZnO and Al<sub>2</sub>O<sub>3</sub> precursors, submitted to heat treatment at 1573 K for 6 h (see Table 1.5), revealed the formation of spinel ZnAl<sub>2</sub>O<sub>4</sub>. Some typical, commercially available powders prepared by spray-drying are shown in Table 1.6. The development of advanced coatings sometimes necessitates new materials to be sprayed. The powders of such materials can be manufactured by spray-drying. This can be done by using laboratory-scale spray-drying equipment that allows the manufacture of small batches of powders. Although any new powder development needs time to master the spray-drying procedure and optimization of the composition of the slurry, this effort is often justified. A good example is the development of *optical functional coatings* on a basis of ZnO + Al<sub>2</sub>O<sub>3</sub> undertaken by Tului *et al.* (2003), as shown in Table 1.5.

**Table 1.6** Typical commercial powders produced by spray drying

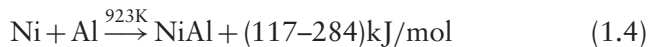
Powder type	Application	Chemical composition (wt%)	Production method	Grain size (μm)	Trade name	Manufacturer
Oxide	Bioactive coating	Ca <sub>5</sub> (PO <sub>4</sub> ) <sub>3</sub> OH	Spray drying	See Figure 1.22	—	Tomita, Japan
Cermet	Wear resistance	WC + 12Co	Spray drying, plasma densification	—53 + 10	JK 7112	Deloro Stellite, Germany
		Cr <sub>3</sub> C <sub>2</sub> + 25NiCr	Spray drying, densification	—53 + 10	JK 7184	

### 1.1.4 CLADDING

Cladding offers another possibility of preparing cermet and composite powders. The concept of clad coating of the core is useful in the following situations:

- Core material has to be protected against chemical modification at spraying, such as oxidation or decarburization. An example of such cladding is cobalt on a tungsten carbide core or nickel on a graphite core.

- Enhancement of adhesion by an exothermic reaction. An example of such a powder is an aluminium core coated with nickel. These components react in following way (Clegg *et al.*, 1973):



- The wettability and flowability of ceramic powders improve after cladding ceramic cores with metallic layers (Lugscheider *et al.*, 1991).

A representation of a cladded particle is shown in Figure 1.12.

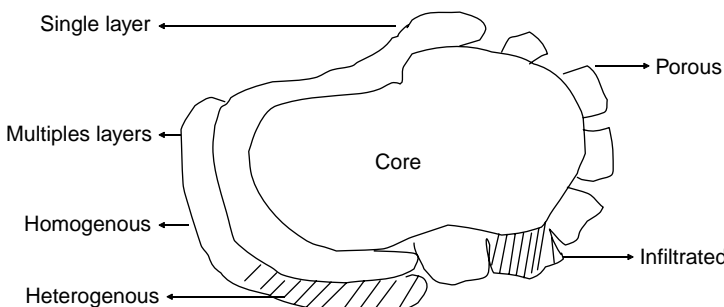


**Figure 1.12** Illustration of a powder particle showing possible cladding (after Lugscheider *et al.*, 1991). Reproduced by permission of E. Lugscheider, Terolab Surface Group, Lausanne, Switzerland

The technologies of powder preparation can be divided following the phase in which the process is carried out, as follows:

- solid-phase cladding;
- liquid-phase cladding;
- gas-phase cladding.

On the other hand, one can categorize this process following the morphology of the obtained layer as:

- dense cladding that includes most of the previously shown processes;
- porous cladding.

### Solid-Phase Cladding

Solid-phase cladding includes *mechanical alloying* which is described in detail in Section 1.1.5. The following aspects must be considered (Lugscheider *et al.*, 1991):

- Core particles must be mechanically strong during alloying which is mainly an *attritor* process. This excludes, for example, a graphite core.
- The ratio of core particles and coating material should be calculated precisely. If there is not enough layer material, the core material will be crushed. Too much layer material will prevent cladding.

This type of cladding is used to obtain layers on aluminium or on iron oxide and chromium oxide. The coated oxide powders are used for magnetic recording.

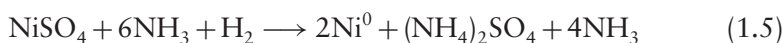
### Liquid-Phase Cladding

Liquid-phase cladding processes are popular and allow many core materials to be coated. The most important liquid-cladding processes are as follows (Lugscheider *et al.*, 1992):

- chemical precipitation;
- electrolytic coating;
- painting (porous cladding).

***Chemical Precipitation*** The most important process of chemical precipitation based on the electrode-less reduction of metal salt solution is the *hydrogen-pressure-reducing powder-coating* (HYPREPOC) process. In this, the core powder is suspended by mechanical agitation in an aqueous metal salt solution and the metal is reduced by application of hydrogen ( $p \approx 4 \text{ MPa}$ ) at a high temperature (up to  $T = 523 \text{ K}$ ). An exception is a molybdenum clad in which salt is reduced at as high a temperature as  $1270 \text{ K}$ .

The precipitation takes place in an autoclave. Sometimes, ammonia is added to the reactants and the final reaction, using the example of nickel sulfate, may be as follows:



From a technological point of view, metal layers on different core materials are the most important. Some metals form coatings easier than others (Figure 1.13).

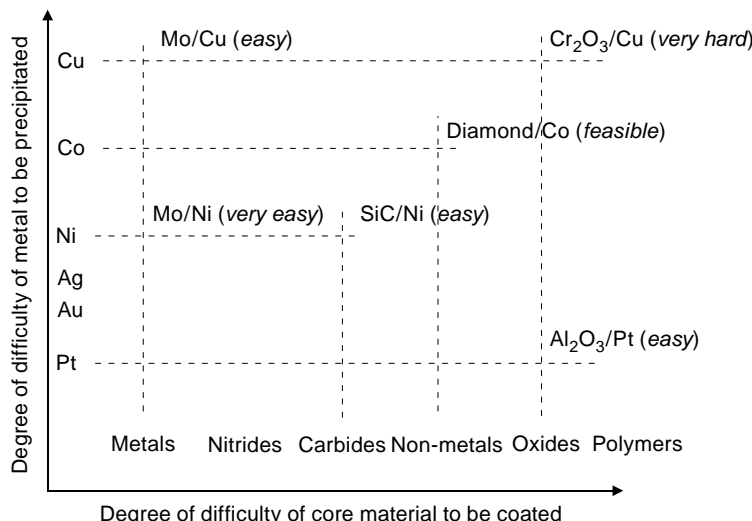


**Figure 1.13** Possibilities of metal coating formation by using the HYPREPOC process on cores from different materials (after Herbst and Lugscheider, 1996). Reproduced by permission of E. Lugscheider, Terolab Surface Group, Lausanne, Switzerland

When required, cores can be submitted to an activation using pretreatment with surface active reagents or catalytic metals (Pt, Pd). This increases the ‘reducibility’ on powder surfaces. The size of the core varies from a few tenths of a micrometre to more than one hundred micrometres.

The reduction can be carried out by using the following metal salts:

- sulfates (see Equation (1.5));
- nitrates;
- acetates;
- carbonates;
- chlorides;
- organometallic salts.

The clad layer has a typical thickness of a few micrometres. This can be increased by multiple reduction. Typical cladded Ni/Al and Ni/graphite powders are shown in Figure 1.14.

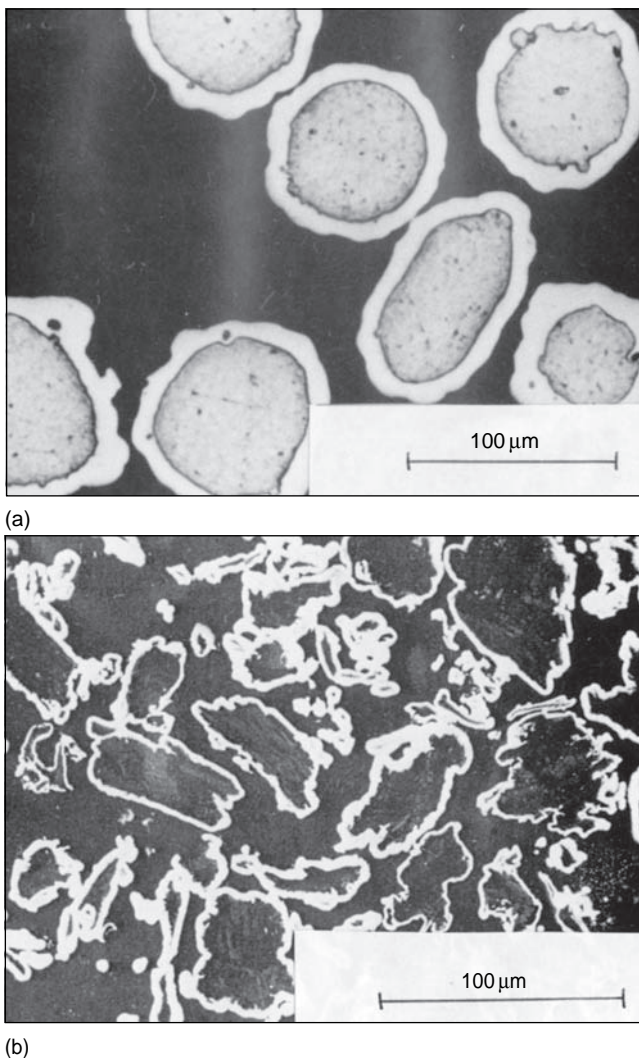


**Figure 1.14** Powders obtained by nickel precipitation on the cores of (a) aluminium and (b) graphite. Reproduced by permission of Sherritt Inc., formerly known as Sherritt Gordon Ltd, Fort Saskatchewan, Alberta, Canada

**Electrolytic Cladding** Under the influence of direct current (DC), many layers can be deposited on the cathode, provided that the coating material is connected as an anode and that it dissolves in a metal salt. The metal layers can reach a thickness of up to  $2000\text{ }\mu\text{m}$  (Lugscheider *et al.*, 1991) on flat surfaces. The layers on powders are spongy and

porous (see Figure 1.12). This results from the lack of homogeneity of the electric field around particles of irregular shapes.

**Painting (Porous Cladding)** The painting (porous-cladding) process consists of preparing a mixture of fine (typically less than 10 µm; Kushner *et al.*, 1988) particles with the binder, e.g. an epoxy or phenolic varnish. The mixture is then mechanically blended with the core particles and allowed to dry. Sometimes, the final blend is pressed into cakes (Houck, 1981) and then, after drying, subsequently crushed and screened to give the desired particle distribution. The varnish is ‘burnt out’ during thermal spraying. Al coating onto a Ni core is an example of porous cladding (Table 1.7).

**Table 1.7** Typical commercial powders produced by cladding

Powder type	Chemical composition (wt%)	Application	Production method	Grain size (µm)	Trade name
Alloy	Ni + 5Al	Bond coating	Precipitation of Ni, dense clad	-104 +45	Praxair NI-109
Cermet	WC + 20Co	Wear resistance	Porous clad of Ni Dense clad of Co	-90 +45 -45 +5	Amperit 282.2 Amperit 533.3

### Gas-Phase Cladding

Cladded layers can be deposited in the gaseous phase onto powders by two principal processes:

- chemical vapour deposition (CVD) or its modification, plasma-enhanced chemical vapour deposition (PECVD);
- physical vapour deposition (PVD).

**CVD and PECVD Cladding** CVD clads can be deposited by using the following processes (Pawlowski, 2003):

- thermal chemical vapour deposition;
- plasma-enhanced chemical vapour deposition;
- laser-assisted chemical vapour deposition (LCVD);
- metal–organic chemical vapour deposition (MOCVD).

The most popular approaches at present are the CVD and PECVD processes. *Thermal CVD* takes place at deposition temperatures varying from  $T_d = 800\text{K}$  up to  $1500\text{K}$  or more. At these temperatures, the coating material is a product of reactions such as:

- pyrolysis;
- thermal decomposition;
- reduction.

Core materials must be stable at such high temperatures. The deposition of layers with a homogenous thickness on the powder cores has to take place in fluidized beds.

The *PECVD* coating process is associated with a discharge (DC, RF or microwave) which produces a *low-temperature plasma* at pressures of about  $10^{-3}\text{ hPa}$ . The formation of a coating that results from the chemical reactions in the plasma environment takes place at considerably lower temperatures. For example, a  $\text{Si}_3\text{N}_4$  coating can be deposited at  $T_d = 1170\text{K}$  by thermal CVD and at  $T_d = 570\text{K}$  by PECVD. Most types of materials can be deposited. An essential problem is the stabilization of the fluidized bed which requires a large quantity of fluidizing gas and this becomes very difficult for particles of diameter ( $d_p$ ) lower than  $5\mu\text{m}$  (Lugscheider *et al.*, 1991).

**PVD Cladding** PVD clads can be deposited by the techniques of evaporation, sputtering, ion plating or laser ablation known as pulsed-laser deposition (PLD). The cores have to withstand a vacuum of about  $10^{-6}\text{ hPa}$  and temperatures up to  $1000\text{K}$ . With PVD cladding of powders, it is necessary to avoid the turbulence from rapid pumping or chamber ‘backfilling’; otherwise, the pumping system can be contaminated by powder. Homogenous coating onto the powder can be reached by, e.g. ‘tumbling’ of particles exposed to a gaseous flux of species. An example of such cladding is a  $0.5\text{--}1.0\mu\text{m}$ -thick Cu film onto a SiC powder with particles of a mean size of  $d_p = 142\mu\text{m}$  (Wang *et al.*, 1997). Typical, commercially available cladded powders are shown in Table 1.7.

### 1.1.5 MECHANICAL ALLOYING (MECHANOFUSION)

Mechanical alloying, also called mechanofusion (MF), is a relatively new experimental method of manufacturing small batches of the following powders:

- alloys;
- cermet and composite clads;
- cermet and composite agglomerates.

The morphology of cladded powders correspond to porous cladding while agglomerates are similar to spray-dried powders. There is also a possibility of obtaining agglomerates with a unique lamellar morphology (Figure 1.15).

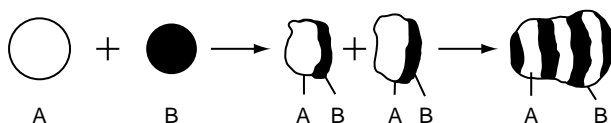


**Figure 1.15** Mechanofused powder of lamellar morphology (shown on the right-hand size) prepared from the initial powders A and B (Chen *et al.*, 1992). Reproduced by permission of ASM International from Chen *et al.*, 1992, in *Proceedings of the 13th ITSC*, C.C. Berndt (Ed.), ASM International, Materials Park, OH, USA, pp. 355–361

MF is an attritor process in which the energy of friction is transformed into heat that allows plastic deformation of the powder material (Figure 1.16). In practice, many types of milling machines are used. In the example shown in Figure 1.16 there is a cylindrical chamber

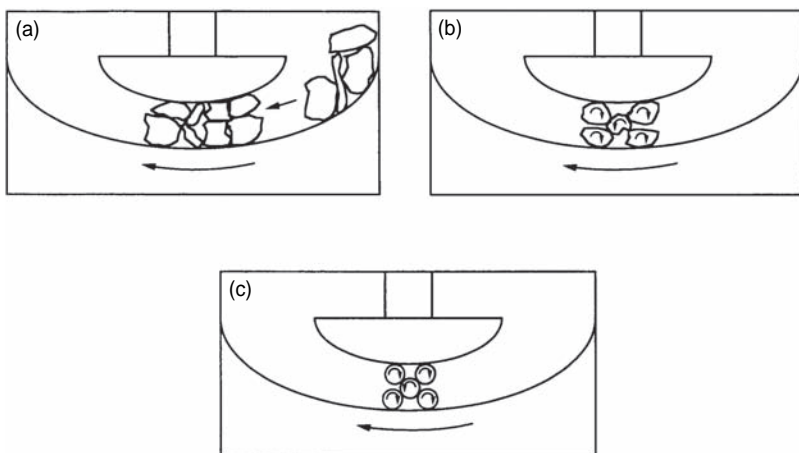


**Figure 1.16** Mechanofusion process showing (a) reduction in particle size and (b,c) progressing particle morphological changes (Herman *et al.*, 1992). Reproduced by permission of ASM International from Herman *et al.* (1992), *J. Therm. Spray Technol.*, 1, 129–135

containing powder and a semicylindrical arm that presses the powder against the chamber wall.

The morphology of a mechanofused powder depends on the properties of the used materials and on the following operational parameters:

- rotation speed of milling;
- milling time;
- sizes of initial powders;
- ratio of sizes of different powders.

The powders prepared by this method are mainly applied to obtain a batch of an experimental powder. Some examples of the powders are shown in Table 1.8.

**Table 1.8** Parameters used in mechanofusion of new powders

Chemical composition of powder	Al + 51 at% Ni	NiCrAl + (25–75) wt% (ZrO <sub>2</sub> + 7 wt% Y <sub>2</sub> O <sub>3</sub> )	MoSi <sub>2</sub> + 20 vol% SiC
Application	Oxidation resistance	Graded TBC	Oxidation and wear resistance
Sizes of initial powders ( $\mu\text{m}$ )	Ni: 7, Al: 30	NiCrAlY: -40 + 80, ZrO <sub>2</sub> : -70 + 35	Mo: 22, Si: 9.5, SiC: 11
Milling time (h)	15	0.5–4.0	8 followed by 0.25 <sup>a</sup>
Milling speed (rpm)	200–220	100–200	190 followed by 75
Powder morphology	Lamellar	Agglomerated	Porous clad
Final powder treatment	No	Arc plasma	Heat treatment at 1450 K for 1 h
Reference	Chen <i>et al.</i> , 1992	Khor and Gu, 1997	Wielage <i>et al.</i> , 2000

<sup>a</sup> Initial milling was carried out under an inert Ar atmosphere and the mixture was Si + 33 at% Mo, allowing formation of MoSi<sub>2</sub>.

### 1.1.6 SELF-PROPAGATING HIGH-TEMPERATURE SYNTHESIS (SHS)

Self-propagating high-temperature synthesis (SHS) is a kind of combustion process in which an exothermic and self-sustaining chemical reaction proceeds in the reaction volume, gradually transforming the

reactant powder mixture into the desired product (Bertuli *et al.*, 1995). The reactants are usually prepared as a rod which is ignited at one end and the combustion front progresses with a velocity  $v_c$ , leaving behind reacted material having a constant adiabatic temperature,  $T_{ad}$  (Figure 1.17).

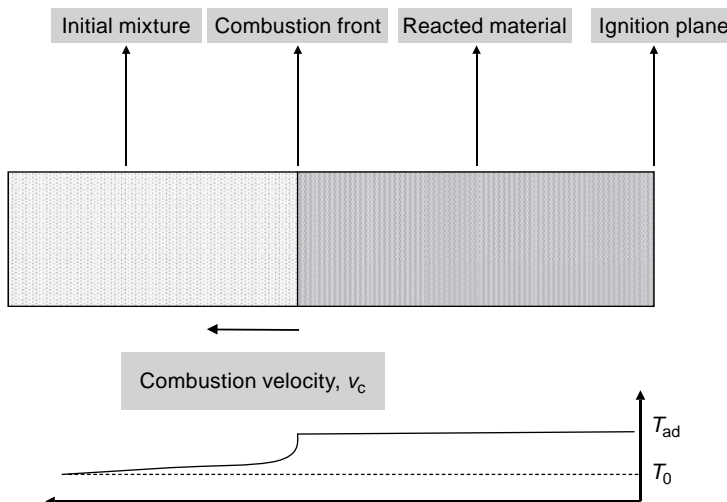


**Figure 1.17** Representation of an SHS reaction moving along a rod and an instantaneous temperature distribution (after Varma, 2000)

The adiabatic temperature can reach 4000 K and the combustion front moves with a velocity ranging from  $v_c = 0.1$  to 10 cm/s (Bertuli *et al.*, 1995; Varma, 2000). A successful design of an SHS process needs to fulfil the following conditions:

- The reaction involved in the SHS process must be exothermic – in other words, the standard enthalpy of formation,  $\Delta_f H^\circ$ , must be strongly negative. A threshold value of  $\Delta_f H^\circ = -70$  kJ/mol was reported (Blatchford *et al.*, 2001). Examples of compounds that are well-adapted to be synthesized by this process include TiC ( $\Delta_f H^\circ = -184$  kJ/mol) and TiB<sub>2</sub> ( $\Delta_f H^\circ = -324$  kJ/mol). Varma (2000) cites the following compounds that are suitable for the SHS process:
  - carbides (TiC, SiC);
  - borides (TiB<sub>2</sub>, LaB<sub>6</sub>);

- silicides ( $TiSi_2$ ,  $MoSi_2$ );
  - aluminides and titanites ( $AlNi$ ,  $TiNi$ );
  - nitrides ( $NbN$ ,  $Si_3N_4$ );
  - hydrides ( $MgH_2$ ,  $ZrNiH_3$ );
  - oxides ( $YBCO$ ,  $La_{0.8}Sr_{0.2}CrO_3$ ).
- At least one component of the initial mixture should form a liquid or vapour phase in order to increase the diffusion rate towards the combustion front. An example is the formation of  $MoSi_2$  in which Mo dissolves into a Si melt bath (Figure 1.18).

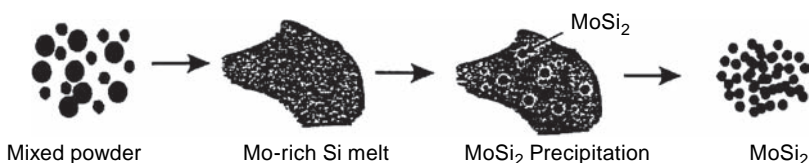


**Figure 1.18** Stages of formation of  $MoSi_2$  from a Mo (●) and Si (●) powder mixture during an SHS process (Hidouci and Pelletier, 1998). This article was published in *Mater. Sci. Eng., A*, 252, A. Hidouci and J.M. Pelletier, ‘Microstructure and mechanical properties of  $MoSi_2$  coatings produced by laser processing’, 17–26, Copyright Elsevier (1998)

Ignition of the reaction can be made by using an external source, such:

- a laser;
- an electric arc;
- a tungsten heating coil;
- an oxyacetylene torch.

Composite powders can be formed by adding a non-reactive powder to the initial mixture. For example, a NiCr powder was added to the reacting precursors of Ti and C in order to obtain a cermet of  $NiCr + TiC$  (Bertuli *et al.*, 1995). As the combustion synthesis is very rapid, only a few seconds are necessary to turn the mixture into a new solid that may have a uniform microscopic structure (Figure 1.19).

The composite powders produced with this method are, however, rather porous and need a high-temperature treatment, such as the *plasma spheroidization* method applied by Ovcharenko and Solonenko (1995). Another technological solution is post-treatment of sprayed SHS



**Figure 1.19** A batch of TiN obtained by the SHS method at the Advanced Research Centre for Powder Metallurgy and New Materials, International (ARCI), Hyderabad, India. Reproduced by permission of Dr G. Sundararajan, Director-ARCI

powders by using a high-power laser (Tondu *et al.*, 2000). Some examples of the experimental powders produced by using the SHS method are shown in Table 1.9.

**Table 1.9** Examples of experimental powders produced by the SHS method

Chemical composition	MoSi <sub>2</sub>	(Ni + 20 vol% Cr) + 40 vol% TiC	(Fe + 20 wt% Cr) + 70 wt% TiB <sub>2</sub>
Application	High-temperature corrosion resistance	Wear resistance	
Combustion reaction	Mo + 2Si → MoSi <sub>2</sub>	Ti + C → TiC	Ti + 2B → TiB <sub>2</sub>
Sizes of precursors (μm)	< 44	Ni, Ti, Cr: < 44; C: < 1	B: < 45; C: < 1; Cr < 180; Fe < 60
Adiabatic temperature (K)	1860	1720	—
Combustion velocity (cm/s)	0.38	0.18	—
Reference	Bertuli <i>et al.</i> , 1995		Blatchford <i>et al.</i> , 2001

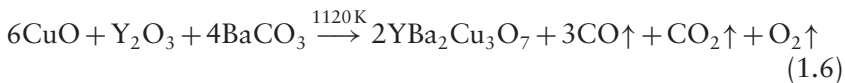
### 1.1.7 OTHER METHODS

There is a great number of powder production methods that are less frequently used than those described above. A few characteristic methods were selected and categorized following the phase in which the powder is formed, as follows:

- solid-phase method;
- liquid-phase method;
- gase-phase method.

#### Solid-Phase Method

Among the techniques of powder fabrication in the solid phase, *calcination* seems to be one that is used relatively frequently. *Calcination* means heating at high temperatures but below the melting point and may also correspond to a high-temperature chemical reaction in the solid state. This method can thus be applied to obtain powders of compounds. For example, a synthesis of  $\text{YBa}_2\text{Cu}_3\text{O}_7$  from copper oxide, yttria and barium carbonate follows a reaction at  $T = 1120\text{ K}$ .



The byproducts are gaseous oxygen and carbon oxides. In fact, the useful powder should be prepared with excess CuO which is known to evaporate more effectively than other oxides in spraying processes (Figure 1.20).

The product from calcination is crushed to form a powder. This powder is usually porous and, prior to spraying, should be subjected to a high-temperature heat treatment.

#### Liquid-Phase Method

The preparation of a *sol-gel* is a representative liquid-phase technique. This is a chemical method that allows powders of metal oxides or oxide systems to be produced. It utilizes metal-organic precursors to form metal salts. In aqueous or organic solvents, the precursors are hydrolysed and condensed to form inorganic polymers with metal oxides having M–O–M bonds (Brinker *et al.*, 1996). The most common precursors

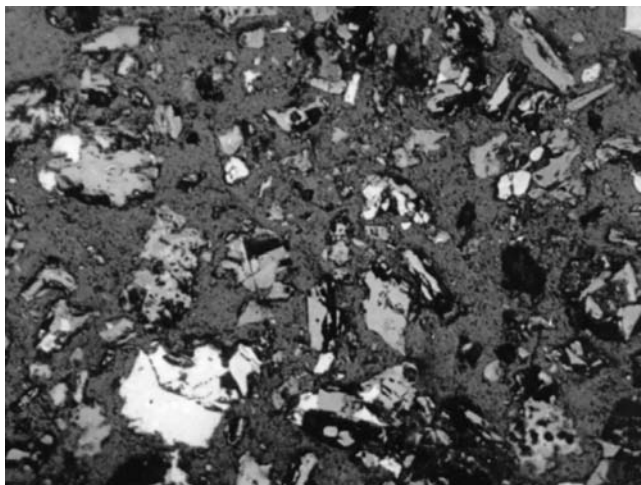
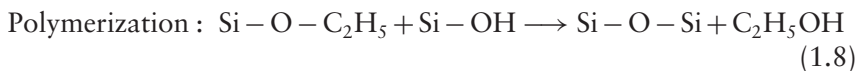
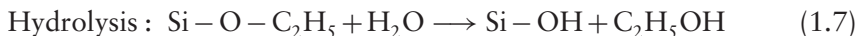


**Figure 1.20** Optical micrograph (in bright field) of a cross-section of a powder prepared by calcination and composed of  $\text{YBa}_2\text{Cu}_3\text{O}_7$  and  $\text{CuO}$ . The product from calcination was crushed and subjected to a number of heat treatments at 1220 K and finally, the fraction  $-56 + 28 \mu\text{m}$  was sieved out for plasma spraying. The volume-averaged atomic ratio of the elements in the shown powder is  $\text{Y} : \text{Ba} : \text{Cu} = 1.2 : 0.5 : 3.53$ , while the white inclusions probably correspond to  $\text{CuO}$  (Pawlowski, 1990)

for sol-gel powders are metal alkoxides  $\text{M}(\text{OR})_n$ . To take the example of  $\text{SiO}_2$  powder formation, the initial precursor is tetraethylorthosilicate,  $\text{Si}(\text{OC}_2\text{H}_5)_4$ , a colourless liquid that is available commercially. Two chemical reactions that allow a metal oxide to be obtained are *hydrolysis* and *polymerization* (Klein, 1991):



The conditions of polymerization (mechanical agitation, temperature, etc.) permit the shape and size of powder particles to be determined (Nelson *et al.*, 1974). The obtained particles are dried at temperatures about 400 K and then calcined at temperatures above 1170 K. The sol-gel method was reportedly used to obtain  $\text{ZrO}_2-\text{Cr}_2\text{O}_3$  powders with controlled contents of oxides and sizes in the range from 53 to 75  $\mu\text{m}$  (Scott and Woodhead, 1982). An important advantage of the powders prepared in this way is their spherical shape.

### Gas-Phase Method

The particles of powders prepared using this technique are often smaller than 100 nm and can be used to prepare *nano-powders*. Synthesis in the gas phase is a first step in powder preparation, which is followed by agglomeration, usually by spray drying (Kear, 1997). The synthesis is usually carried out in an electrode-less RF or microwave plasma in a glow discharge or in a zone of ‘post-discharge’. Gas-phase synthesis is especially useful for the production of less common powders such as

- $\beta$ -SiC powders with particle diameters in the range  $d_p = 10\text{--}50\text{ nm}$  from the gaseous precursors  $\text{SiH}_4$  and  $\text{CH}_4$  injected into an argon RF plasma (Kameyama *et al.*, 1990).
- $\text{CN}_x$  ( $x \approx 0.6$ ) powders of submicrometre particles (Figure 1.21) from vapours created by ablation using a pulsed  $\text{CO}_2$  laser with a graphite target. The graphite vapours react with a low-temperature nitrogen plasma in the *post-discharge zone*.

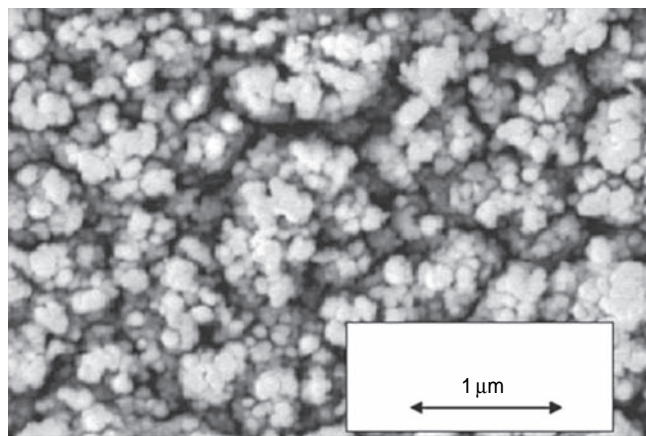


**Figure 1.21** Morphology of  $\text{CN}_x$  generated in the gaseous phase by ablation of a graphite target using a  $\text{CO}_2$  laser and reaction of graphite vapours with a nitrogen plasma in ‘post-discharge’ under a pressure,  $p$ , of 3 hPa (Alkhawwam *et al.*, 2000)

An important limitation of gas-phase methods is the small quantity of powder that can be produced in this way.

## 1.2 METHODS OF POWDERS CHARACTERIZATION

The powders are characterized by the manufacturers and certificates of characterization are provided with the products. However, errors can always occur and so it is recommended to check some of the powder parameters before spraying. The most important parameters are:

- grain size;
- chemical and phase composition;
- internal and external morphology, including shape and internal porosity;
- high-temperature behaviour, measured by DSC, DTA and TGA;
- apparent density and flowability.

### 1.2.1 GRAIN SIZE

As grain-size analysis is carried out by using only a few grams of powder and a typical batch of powder corresponds to a tenth of a kilogram, it is important to select a representative sample. The sampling can be carried out with the help of a special *sampler* described in the ASTM Standard, B 215–04.<sup>6</sup> Grain-size analysis could be done by using one of the following methods:

- Mechanical-sieve analysis (described, e.g. in ASTM Standard, B 214–07<sup>7</sup>). This method is useful for particle sizes with  $d_p > 10 \mu\text{m}$  and important powder densities (metals and alloys rather than ceramics). Small and light grains are more difficult to sieve. Sieving is, however, is practical when considering two-dimensional (2-D) sections of particles.
- X-ray absorption and laser light scattering devices (laser sizers) that are practical for volumes of particles.

<sup>6</sup> ‘Standard methods of sampling of metal powders’, 1 October 2004.

<sup>7</sup> ‘Standard test method for sieve analysis of granular metal powders’, 1 January 2007.

- Scanning electron microscopy (SEM) or optical microscopy (OM) images/micrographs. The number of powder particles in these micrographs should be large enough to allow statistical evaluation. This evaluation is made by using image analysis which allows direct measurement of 2-D sections of particles and indirect determination of their geometry in three dimensions. Figure 1.22 shows an example of a scanning electron micrograph used for evaluation of powder particle sizes.

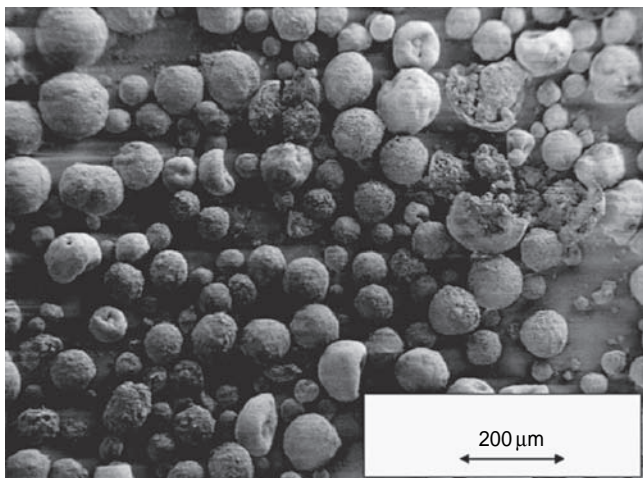


**Figure 1.22** Scanning electron micrograph (secondary electrons) of the hydroxyapatite (HA) powder described in Table 1.6

More information about particle-size measurement can be found in the book by Allen (1981). Each of the enumerated methods has some drawbacks. Small particle agglomeration can be a problem using sieving with X-ray and laser methods. Image analysis of particle micrographs is said to be the most accurate (Poech *et al.*, 1993) but the selected powder must be representative for the entire batch. A good idea is to determine the particle sizes by using two different methods and to analyse carefully the results obtained. For example, the distributions of hydroxyapatite (HA) powder particles sizes obtained by two different laser ‘sizers’ and an image analysis of the micrograph shown in Figure 1.22 indicate a possible agglomeration of powder particles in one of the laser measurements (Figure 1.23).

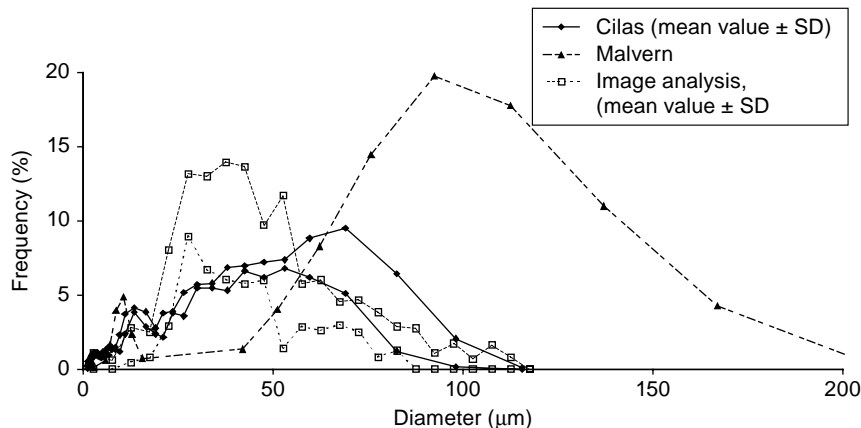


Figure 1.23 Distribution of hydroxyapatite (HA) powder particle sizes using the laser sizers ‘Cilas’ and ‘Malvern’ and image analysis of the micrograph shown in Figure 1.22

The grain-size distribution is often characterized by *mean diameters*. Some of these diameters are defined as follows (Masters, 1985):

- *Most frequent diameter*, which corresponds to the highest value on the frequency curve.
- *Arithmetic mean diameter*, which corresponds to the sum of the diameters of individual particles divided by their number.
- *Median diameter*,  $d_{50}$ , which corresponds to the diameters below which 50 % of the particles lie.
- *Volume–surface (Sauter) mean diameter*,  $d_{VS}$ , which can be found from the following expression:

$$d_{VS} = \frac{\sum_{i=1}^n N_i d_i^3}{\sum_{i=1}^n N_i d_i^2} \quad (1.9)$$

in which  $N$  is the total number of particles and  $N_i$  is the number of particles having a diameter,  $d_i$ . Some authors use diameters related to the cumulative plot, such as  $d_{90}$  (the diameter below which 90 % of the powder particles lie), as well as  $d_{75}$  or  $d_{10}$  (Pei *et al.*, 1996). Some manufacturers describe grain sizes following the German industrial standard DIN 32529 while others use the ASTM mesh designation standard. Table 1.10 shows the equivalence.

**Table 1.10** Conversion of equivalent diameters

Mesh number <sup>a</sup>	Grain size ( $\mu\text{m}$ )	DIN number <sup>b</sup>	Grain size (sieve opening) ( $\mu\text{m}$ )
100	150	0	-22.4 + 5.6
120	125	1	-45 + 22.4
140	106	2	-90 + 45
200	74	3	-45 + 5.6
230	63	4	-63 + 16
325	44	5	-106 + 32
400	37	6	-125 + 45

<sup>a</sup> ASTM Standard B 214-07.<sup>b</sup> DIN 32529.

## 1.2.2 CHEMICAL AND PHASE COMPOSITION

Powder users are principally interested in the following information:

- chemical composition averaged over many particles;
- elements distribution within the powder particles;
- crystal phases present in the powder.

### Chemical Analysis

The chemical composition of a powder can be found by using any of a number of analytical techniques. Inductively coupled plasma emission spectroscopy (ICPES) (Trassy and Mermet, 1984), X-ray fluorescence (XRF) spectroscopy (Jenkins *et al.*, 1981) and X-ray photoelectron spectroscopy (XPS) are typical methods. For example, the following methods allowed the determination of the chemical composition and were useful in ‘mastering’ the powder technology of the previously discussed powders:

- ICPES helped to find the atomic ratio of the  $\text{Ba}_2\text{Cu}_3\text{O}_x$  (YBCO) calcined powder shown in Figure 1.20 (Y:Ba:Cu = 1:2.05:3.53), thus confirming that the copper oxide content was, as desired, in excess.
- XPS was useful in determining the atomic concentration of the  $\text{Cr}_2\text{O}_3 + 5 \text{ wt\% SiO}_2$  spray-dried powder shown in Figures 1.8 and 1.9 (in at %): O + 37.3C + 8.6Cr + 6.2Na + 2.9Si. In this example, the

important carbon content is related to the surface contamination which is frequently visualized by XPS and sodium must have been present in the glass used to prepare the slurry.

### Element Distribution

Agglomerated or cladded powder particles contain different elements and it is sometimes important to know whether they are distributed homogeneously inside or outside of the powder particles. This information can be obtained from the metallographical cross-section of the powder particles (see Figures 1.9 or 1.20). The preparation technique of such a section is described in Chapter 7. The 2-D distribution (mapping) of the elements can be obtained using electron microprobe analysis (EMPA), usually equipped with a wavelength-dispersion spectrometer (WDS) facility (Loretto, 1984).

### Phase Analysis

Phase analysis can be carried with the well-known X-ray diffraction (XRD) technique (Cullity, 1977). More details about this technique can be found in Chapter 7. XRD is especially useful if the powder is submitted to a thermal treatment to improve or test its properties. For example, the cermet powder, NiCr + 75 wt% Cr<sub>3</sub>C<sub>2</sub>, described in Table 1.6, was submitted to thermogravimetric analysis (TGA). The results are shown in Figure 1.24. The following phases were found by XRD before and after the test (Saou and Simonin, 2003):

- before the test: Cr<sub>3</sub>C<sub>2</sub>, Cr<sub>3</sub>Ni<sub>2</sub>;
- after the test: NiCrO<sub>3</sub>, NiCr<sub>2</sub>O<sub>4</sub>, Cr<sub>3</sub>C<sub>2</sub>, Cr.

### 1.2.3 INTERNAL AND EXTERNAL MORPHOLOGY

Careful observation of the shape of the grains allows the manufacturing technique to be identified. External morphology can be determined directly by using SEM or OM (Figure 1.10). Internal morphology (porosity) can be determined by using a metallographical preparation of powder cross-sections, including embedding the powder in the resin and successive grinding and polishing (Figure 1.11). The specimens are

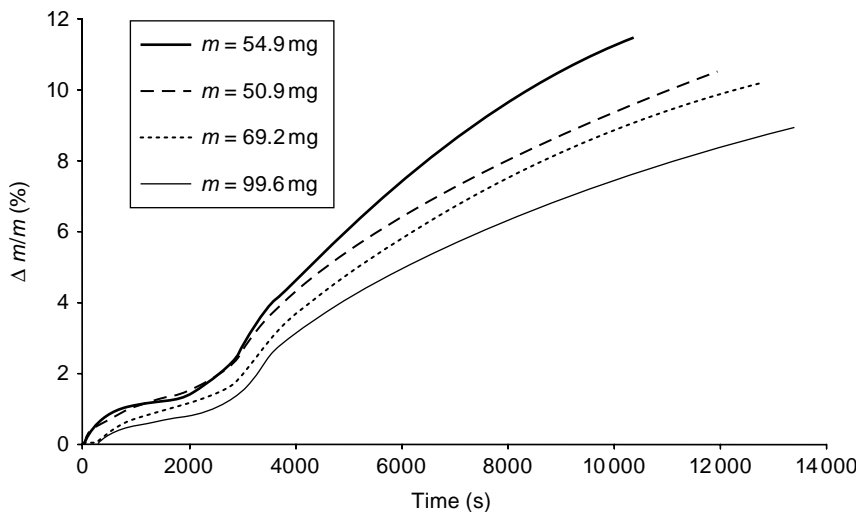


**Figure 1.24** Variation of weight versus time resulting from thermogravimetric measurements of four samples of NiCr + 75 wt% Cr<sub>2</sub>C<sub>3</sub> powder at 1273 K in air (Saou and Simonin, 2003)

observed by OM while porosity can be determined by using image analysis. A classification of powder shapes was proposed by Eschnauer and Kilp (1977), covering 15 fundamental shapes. Table 1.11 shows typical external and internal morphologies corresponding to the powder manufacturing techniques discussed in this present chapter.

**Table 1.11** External and internal morphologies of powders corresponding to their manufacturing techniques<sup>a</sup>

Morphology			
External		Internal	
Powder particle	Powder manufacturing technique	Powder particle	Powder manufacturing technique
Spheres with smooth surfaces	Gas atomization, spray drying followed by high-temperature treatment, sol-gel	Spheres without pores	Gas atomization, sol-gel, spray drying followed by high-temperature treatment
Spheres with rough surfaces	Spray drying	Porous spheres	Spray drying, MF

Irregular, rounded with smooth surfaces	Water atomization, MF, SHS followed by high-temperature treatment	Hollow spheres	Spray drying, spray drying followed by high-temperature treatment
Irregular, rounded with rough surfaces	MF, SHS	Angular, blocky, dense	Fusion and crushing
		Irregular, rounded, dense	Water atomization, SHS followed by high-temperature treatment SHS
Angular blocky	Fusing and crushing, sintering and crushing, calcination and crushing	Irregular, rounded, porous Angular, blocky, porous	Sintering and crushing
		Coated with dense layer Coated with porous layer Lamellar	Dense cladding Porous cladding, MF MF

<sup>a</sup> MF, mechanofusion; SHS, self-propagating high-temperature synthesis.

The determination of morphology may not be sufficient to identify the manufacturing technology, because some manufacturing methods result in powders being similar. Additional information, such as a chemical analysis, phase analyses or, last but not least, the powder price, may be necessary.

#### 1.2.4 HIGH-TEMPERATURE BEHAVIOUR

The high-temperature behaviour of powders is usually checked at their development stages. The most important measurements include the following:

- Differential scanning calorimetry (DSC) is discussed in detail in Chapter 7. DSC allows quantitative measurements of enthalpy changes in a heated powder sample with regard to an inert reference. This is useful in the detection of exo- and endothermic events, such as chemical reactions (which can be exo- or endothermic), crystallization (exothermic) or melting (endothermic). This method can also be used to determine the specific heat of a powder material. DSC is a complementary method to XRD phase analysis, especially for detection of phases in small quantities.

- Differential temperature analysis (DTA) is similar to DSC. Instead of measuring enthalpy changes, the temperature changes are registered in a powder sample with regard to an inert material. DTA is also used to determine the exo- and endothermic events in heated powder materials and is useful, in conjunction with XRD, in phase analysis.
- Thermogravimetric analysis (TGA) is based on the detection of the weight changes of a powder as a function of temperature and atmosphere. These changes typically result from powder decomposition or its oxidation. An example of such analysis, for the cermet NiCr + 75 wt% Cr<sub>2</sub>C<sub>3</sub>, is shown in Figure 1.24. The variation in powder weight results from its oxidation and decomposition.

### 1.2.5 APPARENT DENSITY AND FLOWABILITY

The measurements of apparent density and flowability are normalized, e.g. by ASTM standards B 212–99 and B 213–03, respectively.

The density measurement consists of weighing the sample of powder which fills the calibrated volume cup (25 cm<sup>3</sup>) and that of flowability on measuring the time necessary to ‘flow out’ a 50 g sample of powder from the calibrated orifice funnel ( $d = 2.54\text{ mm}$ ).

For example, the experimental powder of Cr<sub>2</sub>O<sub>3</sub> + 5 wt% SiO<sub>2</sub>, produced by spray drying, has an apparent density with a  $\rho_{\text{app}}$  as low as 1.22 g/cm<sup>3</sup>. This results from the internal porosity of the powder, as shown in Figure 1.9. A more dense Cr<sub>2</sub>O<sub>3</sub> powder produced by fusing and crushing has a nearly twofold higher density of  $\rho_{\text{app}} = 2.42\text{ g/cm}^3$  (Pawlowski *et al.*, 1993).

## 1.3 FEEDING, TRANSPORT AND INJECTION OF POWDERS

Feedstocks used in thermal spraying include wires, liquid suspensions, or most frequently, powders. Wires are wound on a roller and their feeding is controlled precisely by their rotation speeds. Liquid suspension feed rates are controlled by a peristaltic pump or a similar device. A powder is fed from a powder feeder. Its feed rate depends, to a degree, on the flowability of a powder. This can be improved by heating the powder prior to spraying at a temperature higher than 373 K. At this temperature, water evaporates, disintegrateing large agglomerates. For thermal spraying, powder is:

- fed from a powder feeder;
- transported by a pipeline up to the torch;
- injected to a flame or a jet.

### 1.3.1 POWDER FEEDERS

Any powder feeder contains a hopper (sometimes vibrating) which delivers powder, through orifice, onto rotating devices such as a star-shaped wheel or a disc with a orifice. The powder feed rate is controlled by the rotation speed. A modern powder feeder that allows simultaneous delivery of two powders is shown in Figure 1.25.

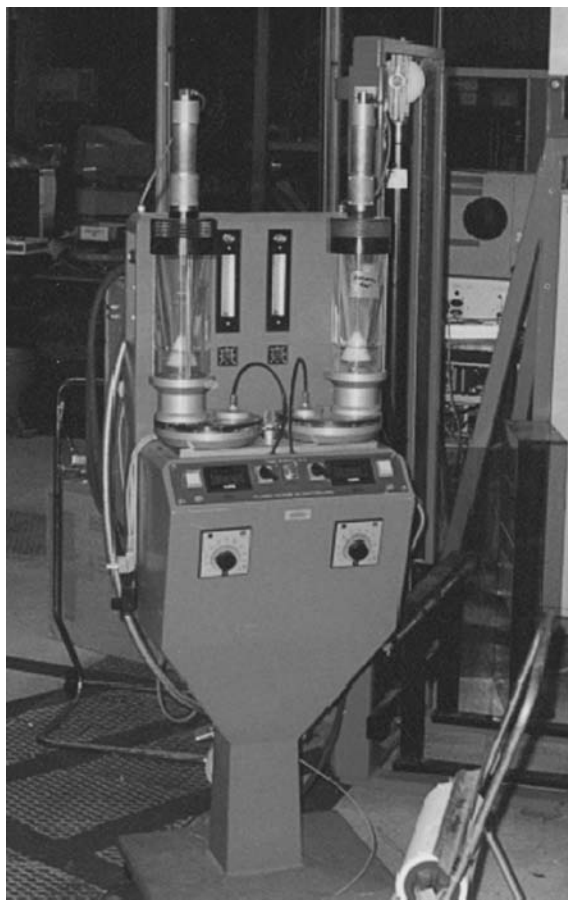


Figure 1.25 A modern powder feeder. Reproduced by permission of Sulzer-Metco, Wohlen, Switzerland

Typical values of powder feed rates,  $q_p$ , vary between 10 to 150 g/min. The average feed rate can be controlled by measuring the weight of powder collected during a short period of time (e.g. 1 min). Instantaneous feed rates, important at small values of  $q_p$ , can be controlled with optical sensors. Feed rate variations should not be greater than 5 % of the average value.

### 1.3.2 TRANSPORT OF POWDERS

Powder is transported through a pipeline as a suspension in a carrier gas. The gas should have a flow rate adapted to stable transport of the suspension. This flow rate depends on (Eck, 1961):

- diameter of the pipeline,  $d_{pi}$ ;
- density,  $\rho_p$ , and diameter,  $d_p$  of the powder particles;
- density,  $\rho_g$ , dynamic viscosity,  $\eta_g$ , and velocity,  $v_g$ , of the transport gas.

A very low powder feed rate results in oscillations and the minimum stable powder feed rate is given by:

$$(q_p)_{\min} = 0.25 \pi \rho_g Fro \sqrt{d_{pi}^5 g} \quad (1.10)$$

where  $Fro$  is the *Froud number*, given by:

$$Fro = \frac{v_g}{\sqrt{gd_{pi}}} \quad (1.11)$$

and  $g$  is the gravitation constant ( $9.81 \text{ m/s}^2$ ).

One can increase the powder feed rate to a maximum value, above which the powder transporting pipeline becomes blocked. The maximum powder feed rate is given by the following:

$$(q_p)_{\max} = 3 \times 10^{-5} Fro^4 (q_p)_{\min} \quad (1.12)$$

### 1.3.3 INJECTION OF POWDERS

The powder feeder is joined to a torch by a pipeline and an injector (Figure 1.26). A most important parameter relative to powder injection

is the particle velocity at the end of the injector,  $v_0$ , which is also the injection velocity of the particles into the plasma or flame. This velocity can be calculated by using a simplified *ballistic model* that assumes no interaction between the particles. Another supposition is that there is one force acting on a particle, namely the *drag force*.

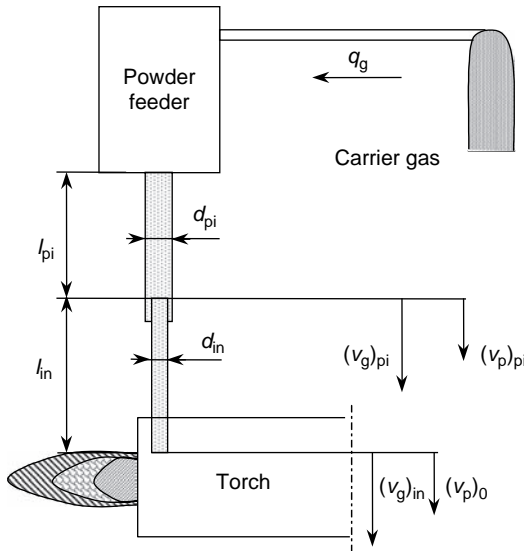


Figure 1.26 Schematic of transport of a powder to a torch

The velocity of carrier gas in the pipeline is given by:

$$(v_g)_{pi} = \frac{4q_g}{\pi d_{pi}^2} \quad (1.13)$$

The particle velocity at the end of the pipeline can be calculated from the force acting on a particle of a diameter  $d_p$  and is given by (Pawlowski, 1980):

$$(v_p)_{pi} = (v_g)_{pi} [1 - \exp(-kt_1)] \quad (1.14)$$

where  $k$  is a constant given by:

$$k = \frac{18\eta_g}{\rho_p d_p^2} \quad (1.15)$$

and  $t_1$  is the particle dwell time in the pipeline:

$$t_1 = \sqrt{\frac{2l_{pi}}{k(v_g)_{pi}}} \quad (1.16)$$

The dwell time of the particle in the injector,  $t_2$ , is given by:

$$t_2 = \frac{\sqrt{(v_p)_{pi}^2 + 2[(v_g)_{in} - (v_p)_{pi}]l_{in}k} - (v_p)_{pi}}{k[(v_g)_{in} - (v_p)_{pi}]} \quad (1.17)$$

where  $(v_g)_{in}$  is the velocity of the carrier gas in the injector, given by:

$$(v_g)_{in} = \frac{4q_g}{\pi d_{in}^2} \quad (1.18)$$

At the end of the injector, the particle has a velocity,  $v_0$ , given by:

$$v_0 = (v_g)_{in} - [(v_g)_{in} - (v_p)_{pi}] \exp(-kt_2) \quad (1.19)$$

Equation (1.19) shows the injection velocity of a particle of given diameter into a flame or jet. For example, these velocities for hydroxyapatite

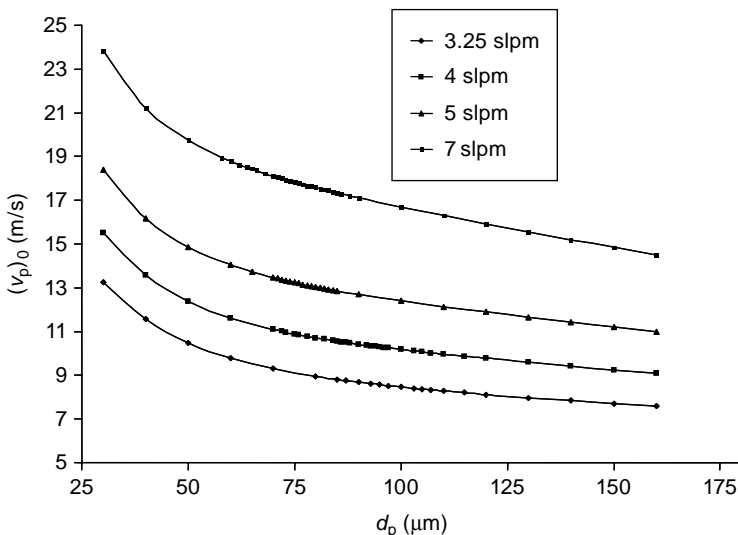


Figure 1.27 Injection velocities of HA particles versus particle diameter for different argon carrier gas flow rates (Dyshlovenko *et al.*, 2003)

(HA) powders, the properties of which are described in Table 1.6 and in Figure 1.23, were calculated by using the above equations and the results, for different carrier gas flow rates, are shown in Figure 1.27.

The absolute value of the injection velocity is an important parameter but the growth of a thermally sprayed coating is also affected by:

- the direction of injection velocity with regard to the flame or jet;
- the number of injectors and their spatial configuration (Boulos *et al.*, 1993).

## REFERENCES

- Alkhawwam, A., Jama, C., Ji, V., Boyaval, C., Pawlowski, L., Goudmand, P. and Dessaux, O. (2000). Synthèse d'un dépôt CN<sub>x</sub> polycristallin par l'ablation laser dans l'atmosphère d'azote en post-décharge, *Galv. Org. Traite. Surf.*, 701, 199–202.
- Allen, T. (1981). *Particle Size Measurements*, 3rd Edition, Chapman & Hall, London, UK.
- Bartnik, Z., Bialucki, P., Kozerski, S., Bork, P., Schrader, B., Clinton, G., Davies, K., Guglielmi, F. and Pawlowski, L. (1992). Improvements in manufacturing technology of wear resistant plasma sprayed Cr<sub>2</sub>O<sub>3</sub> coatings, in *Thermal Spray: International Advances in Coatings Technology*, C.C. Berndt (Ed.), ASM International, Materials Park, OH, USA, pp. 983–995.
- Beczkowiak, J. and Mundinger, K. (1989). Quality assurance during the production of fused chromium oxide, characterization of the powders and properties of the plasma sprayed coatings, in *Proceedings of the 12th International Thermal Spraying Conference*, The Welding Institute, Cambridge, UK, Paper 94.
- Bertuli, C., Smith, R.W. and Shtessel E. (1995). Self-propagating high-temperature synthesis (SHS) of ceramic and composite powders for thermal spray applications, in *Advances in Inorganic Films Coatings*, P. Vincenzini (Ed.), Techna, Faenze, Italy, pp. 131–140.
- Blatchford, M.T., Jones, M., Horlock, A.J., McCartney, D.G., Shipway, P.H. and Wood, J.V. (2001). Improvement in HVOF sprayed cermet coatings produced from SHS powders, in *Thermal Spray 2001: New Surfaces for a New Millennium*, C.C. Berndt, K.A. Khor and E.F. Lugscheider (Eds), ASM International, Materials Park, OH, USA, pp. 221–229.
- Boulos, M.I., Fauchais, P., Vardelle, A. and Pfender, E. (1993). Fundamentals of plasma particle momentum and heat transfer, in *Plasma Spraying: Theory and Applications*, R. Suryanarayanan (Ed.), World Scientific, Singapore, pp. 3–61.
- Brinker, C.J., Askley, C.S., Cairncross, R.A., Chen, K.S., Hurd, A.J., Reed, S.T., Samuel, J., Schunk, P.R., Schwartz, R.W. and Scotty, C.S. (1996). Sol-gel derived ceramic films—fundamentals and applications, in *Metallurgical and Ceramic Protective Coatings*, K.H. Stern (Ed.), Chapman & Hall, London, UK, pp. 113–151.
- Bork, P. (2001). Spray drying plants for manufacturing of dustless powders, *J. Therm. Spray Technol.*, 10, 578–583.

- Callister, W.D., Jr (1994). *Materials Science and Engineering, An Introduction*, 3rd Edition, John Wiley & Sons, Inc., New York, NY, USA.
- Chen, Z.J., Herman, H., Tiwari, R., Huang, C.C. and Cohen, R. (1992). Vacuum plasma sprayed mechanofused NiAl composite powders and their intermetallics, in *Proceedings of the 13th International Thermal Spraying Conference*, C.C. Berndt (Ed.), ASM International, Materials Park, OH, USA, pp. 355–361.
- Cheney, R.F., Port, D.J. and Spencer, J.R. (1975). Free flowing, sintered, refractory agglomerates, *US Patent*, 3 881 911, 6 May.
- Clegg, M.A., Silins, V. and Evans, D.J.I. (1973). Composite powders in thermal spray applications, in *Proceedings of the 7th International Metal Spraying Conference*, The Welding Institute, Cambridge, UK, pp. 62–72.
- Colin, E., Leaute, M. and Roger, T. (2001). Undergraduate students report, ENSCL, Villeneuve d'Ascq, France.
- Cullity, B.D. (1977). *Elements of X-ray Diffraction*, 2nd Edition, Addison-Wesley, Reading, MA, USA.
- Dittrich, F.J. (1965). New flame spray technique for forming nickel aluminide–ceramic systems, *Ceram. Bull.*, 44, 492–496.
- Drzeniek, H. and Steffens, H.-D. (1987). Cored tube wires for arc and flame spraying, in *Thermal Spray: Advances in Coatings Technology*, D.L. Houck (Ed.), ASM International, Materials Park, OH, USA, pp. 33–40.
- Dyshlovenko, S., Pateyron, B., Pawłowski, L. and Murano, D. (2003). Numerical simulations of hydroxyapatite powder behaviour in plasma jet, *Surf. Coat. Technol.*, 179(1), 110–117 and Corrigendum published in 187, (2–3), 408–9
- Eck, B. (1961). *Technische Strömungslehre*, 6th Edition, Springer-Verlag, Berlin, Germany.
- Eschnauer, H. and Kilp, F. (1977). Über das Herstellen pulverförmiger Zusätze zum thermischen Spritzen, *Schw. Schn.*, 29, 283–286.
- Gartner, F.W. and Walker, J. (1980). Rod deposition of ceramics, in *Proceedings of the 9th International Thermal Spraying Conference*, Nederlands Instituut voor Lastechniek, The Hague, Netherlands, Paper 102.
- Gorham Advanced Materials Institute (1990). *Thermal Spray Coatings*, Gorham, ME, USA.
- Herbst, C. and Lugscheider, E. (1996). Personal Communication.
- Herman, H., Chen, Z.J., Huang, C.C. and Cohen, R. (1992). Mechanofused powders for thermal spray, *J. Therm. Spray Technol.*, 1, 129–135.
- Hidouci, A. and Pelletier, J.M. (1998). Microstructure and mechanical properties of MoSi<sub>2</sub> coatings produced by laser processing, *Mater Sci. Eng.*, A, 252, 17–26.
- Holleck, H. and Schier, V. (1995). Multilayer PVD coatings for wear protection, *Surf. Coat. Technol.*, 76–77, 328–336.
- Houck, D.L. (1981). Techniques for production of flame and plasma spray powders, *Modern Dev. Powder Metall.*, 14, 485–504.
- Hurevich, V., Smurov, I. and Pawłowski, L. (2002). Theoretical study of the powder behavior of porous particles in a flame during plasma spraying, *Surf. Coat. Technol.*, 151–152, 370–376.
- Jenkins, R., Gould, R.W. and Gedcke, D. (1981). *Quantitative X-ray Spectrometry*, Marcel Dekker, New York, NY, USA.
- Johnson, D.W. (1987). Innovations in ceramic powder preparation in *Ceramic Powder Science* Vol. 21, Westerville, OH, Am. Ceram. Soc. (1987). G.L. Messing, K.S. Mazduyasni, J.W. McCauley, R.A. Haber (Eds.) 3–20.

- Kameyama, T., Sakanaka, K., Motoe, A., Tsunoda, T., Nakanaga, T., Wakayama, N.I., Takeo, H. and Fukuda, K. (1990). Highly efficient and stable r.f. thermal plasma system for the production of ultrafine and ultrapure  $\beta$ -SiC powder, *J. Mater. Sci.*, 25, 1058–1065.
- Kear, B.H. (1997). Thermal sprayed nanostructures: a new generation of high performance coatings, in *Proceedings of the United Thermal Spray Conference*, Indianapolis, IN, ana, USA, 15–18 september, invited paper.
- Keller, N., Bertrand, G., Comas, B. and Coddet, C. (2001). On the tailoring of spray dried thermal spray powders, in *Thermal Spray 2001: New Surfaces for a New Millennium*, C.C. Berndt, K.A. Khor and E. Lugscheider (Eds), ASM International, Materials Park, OH, USA, pp. 285–290.
- Khor, K.A.. and Gu, Y.W. (1997). Plasma spraying of functionally graded NiCrAlY/Yttria stabilized zirconia coatings using pre-alloyed powders, in *Thermal Spray:A United Forum for Scientific and Technological Advances*, C.C. Berndt (Ed.), ASM International, Materials Park, OH, USA, pp. 259–266.
- Kim, B.K., Lee, D.W. and Ha, G.H. (2001). Plasma spray coating of spray-dried  $\text{Cr}_2\text{O}_3 + 3$  wt%  $\text{TiO}_2$  powder, *J. Therm. Spray Technol.*, 10, 133–137.
- Klein, L.C. (1991). Sol-gel coatings, in *Thin Films Processes II*, J.L. Vossen and W. Kern (Eds), Academic Press, Boston, MA, USA, pp. 501–522.
- Klima, R. and Kotalik, P. (1997). On cavities in thermally spheroidized powder particles, *J. Therm. Spray Technol.*, 6, 305–308.
- Kushner, B.A., Rangaswamy, S. and Rotolico, A.J. (1988). Powder manufacturing processes and quality control procedures as related to thermal spray coatings, in *Proceedings of the International Symposium on Advanced Thermal Spray Technology and Allied Coatings*, High Temperature Society of Japan, Osaka, Japan, pp. 169–175.
- Loretto, M.H. (1984). *Electron Beam Analysis of Materials*, Chapman & Hall, London, UK.
- Lugscheider, E., Loch, M. and Eschnauer, H. (1991). Coated powders – the status today, in *Proceedings of the 2nd Plasma-Technik-Symposium*, Vol. 2, S. Blum-Sandmeier, H. Eschanuer, P. Huber and A.R. Nicoll (Eds), Plasma-Technik AG, Wohlen, Switzerland, pp. 339–351.
- Lugscheider, E., Loch, M. and Rass, I. (1992). Herstellung von Hartstoffverbundpulvern mittels Mikropelletisierung und Teilchenumhullung sowie anschließender Plasmaverdichtung, in *Hartstoffe in Werkzeugen*, Vol. 11, Forschungszentrum Jülich, Jülich, Germany, pp. 57–70.
- Lukasiewicz, S.J. (1989). Spray-drying ceramic powders, *J. Am. Ceram. Soc.*, 72, 617–624.
- Masters, K. (1985). *Spray Drying Handbook*, 4th Edition, George Godwin, London, UK.
- Meinhardt, H. Meyer, B. and Müller, J. (1990). Verdüste Pulver zur Herstellung von Oberflächenschichten durch thermisches Spritzen, in *TS90, DVS-Berichte*, Vol. 130, DVS, Düsseldorf, Germany, pp. 172–177.
- Nelson, R.L., Woodhead, J.L., Scott, K.T., Wassell, L.L. and Cross, A.G. (1974). The preparation and properties of powders for flame and plasma spraying, In *Proceedings of the 7th International Metal Spraying Conference*, The Welding Institute, Cambridge, UK, pp. 96–101.
- Ovcharenko, V.E. and Solonenko, O.P. (1995). Physical peculiarities of plasma spheroidization of composite powders having a microdisperse inner structure, in *Thermal Spraying: Current Status and Future Trends*, A. Ohmori (Ed.), High Temperature Society of Japan, Osaka, Japan, pp. 1151–1156.

- Pawlowski, L. (1980). Optimization of arc plasma spraying parameters, *Surf. J.*, **11**, 8–16.
- Pawlowski, L. (1990). *Thermal Spraying of YBa<sub>2</sub>Cu<sub>3</sub>O<sub>x</sub> – Materials Aspects*, Unpublished Research Report, Monash University, Melbourne, Australia.
- Pawlowski, L. (2003). *Dépôts Physiques*, PPUR, Lausanne, Switzerland.
- Pawlowski, L., Zaccino, R., Dal Maschio, R., Sgavio, V.M., Andresen, J. and Driller, Fr.J. (1993). Structure–properties relationship in plasma sprayed chromium oxide coating, in *TS93, DVS-Berichte*, Vol. 152, DVS, Düsseldorf, Germany, pp. 132–138.
- Pei, P., Kelly, J., Malghan, S. and Dapkunas, S. (1996). Analysis of zirconia powder for thermal spray: reference material for particle size distribution, in *Thermal Spray: Practical Solutions for Engineering Problems*, C.C. Berndt (Ed.), ASM International Materials Park, OH, USA, pp. 263–273.
- Poech, M.H., Isfahani, S. and Opielka, H. (1993). Size distribution analysis of powders used for thermal spraying, *Powder Metall. Int.*, **5**, 233–237.
- Saou, F. and Simonin, R. (2003). Undergraduate students report, ENSCL, Villeneuve d'Ascq, France.
- Schwier, G. (1985). Pulver zum thermischen Spritzen in der Luft- und Raumfahrt und ihre Charakterisierung, in *Schweißen und verwandte Verfahren im Luft und Raumfahrzeugbau*, DVS-Berichte, Vol. 98, DVS, Düsseldorf, Germany, pp. 87–90.
- Scott, K.T. and Woodhead, J.L. (1982). Gel-processed powders for plasma spraying, *Thin Solid Films*, **95**, 219–225.
- Sikorski, A.K., Bialucki, P. and Kozerski, S. (1996). Properties of ferrochromium thermal sprayed layers with different carbon contents, in *Thermische Spritzkonferenz*, E. Lugscheider (Ed.), Vol. 175, DVS, Düsseldorf, Germany, pp. 65–67.
- Simm, W. and Steine, H. Th. (1985). Einfluss der Herstellverfahren von Metallpulvern auf die Qualität von Spritzschichten, in *Schweißen und verwandte Verfahren im Luft und Raumfahrzeugbau*, DVS-Berichte, Vol. 98, DVS, Düsseldorf, Germany, pp. 91–94.
- Thiel, S., Heimann, R.B., Hermann, M., Berger, L.-M., Nebelung, M., Zschunke M. and Wielage, B. (1996). Thermal spraying of silicon nitride-based powders, in *Thermal Spray: Practical Solutions for Engineering Problems*, C.C. Berndt (Ed.), ASM International, Materials Park, OH, USA, pp. 325–331.
- Tondu, S., Schnick, T., Pawlowski, L., Wielage, B., Steinhäuser, S. and Sabatier, L. (2000). Laser glazing of FeCr-TiC composite coatings *Surf. Coat. Technol.*, **123**, 247–251.
- Trassy, C. and Mermet, J.M. (1984). *Les Applications Analytiques des Plasma HF*, Lavoisier, Paris, France.
- Tului, M., Arezzo, F. and Pawlowski, L. (2003). Optical properties of plasma sprayed ZnO + Al<sub>2</sub>O<sub>3</sub> coatings, *Surf. Coat. Technol.*, **179**(1), 47–55.
- Varma, A. (2000). Form from fire, *Sci. Am.*, **283**, 44–47.
- Veprek, S. (1999). The search for novel superhard materials, *J. Vac. Sci. Technol. A*, **17**, 2401–20.
- Vouristo, P., Stenberg, T., Mäntylä, T., Berger, L.-M. and Nebelung, M. (1996). Properties of TiC–Ni and (Ti, Mo)C–NiCo coatings sprayed from agglomerated and sintered powders, in *Thermische Spritzkonferenz*, Vol. 175, E. Lugscheider (Ed.), DVS, Düsseldorf, Germany, pp. 58–61.

- Wang, B., Ji, Z., Zimone, F.T., Janowski, G.M. and Rigsbee, J.M. (1997). A technique for sputter coating of ceramic reinforcement particles, *Surf. Coat. Technol.*, **91**, 64–68.
- Wielage, B., Steinhäuser, Reisel, G., Morgenthal, I. and Scholl, R. (2000). Vacuum plasma spraying of prereacted MoSi<sub>2</sub> and SiC-reinforced MoSi<sub>2</sub> produced by a new kind of powder processing, in *Thermal Spray: Surface Engineering via Applied Research*, C.C. Berndt (Ed.), ASM International, Materials Park, OH, USA, pp. 865–869.

# 2

## Pre-Spray Treatment

### 2.1 INTRODUCTION

The pieces arriving in a spraying shop are new or already coated. The new ones are usually covered with grease<sup>1</sup> that protects the surface against corrosion. The used pieces have old coatings that still adhere to some of their parts. The grease and the coating must be removed in a *cleaning* process. Cleaned pieces are often shaped in order to obtain desired dimensions or/and to avoid sharp angles that are difficult to be coated. The shaping process can be followed directly by a surface-activation process. Sometimes, however, the pieces should be stored before spraying. A coating is to be applied on a chosen area. The remaining area should be covered with ‘masks’ at surface activation and at spraying. Finally, immediately prior to the deposition process, the surface has to be activated. Without activation the coating would not adhere to the substrate surface. *Activation* by abrasive grit blasting, i.e. *roughening*, remains presently the most frequently applied process. Recently, a couple of new technologies, such as water-jet treatment or laser ablation, have appeared to offer valuable alternatives.

---

<sup>1</sup> Supposing the most frequent case of a piece made of a metal or an alloy.

## 2.2 SURFACE CLEANING

Degreasing of new metal substrates can be realized by using organic solvents, such as methyl alcohol or acetone. Hot water (under high pressure) or water vapour degreasing is another possibility that is used especially for the cleaning of large pieces (rollers). The process should be carried out in a clean room and the remaining liquid should be carefully recycled. The hands and the respiratory system of the operator should be protected.

Used pieces that arrive in the spray shop for refurbishment have old coatings which need to be stripped out. The ceramic coatings on large rollers, such as *corona rolls* coated with sprayed  $\text{Al}_2\text{O}_3$  or *anilox rolls* coated with sprayed  $\text{Cr}_2\text{O}_3$ , can be removed by using abrasive grit blasting or a water jet. Ceramic coatings can be stripped from the rollers by machining. Diamond or boron nitride wheels are applicable. Small pieces, such as turbine blades coated with *thermal-barrier coatings* (TBCs), including external  $\text{ZrO}_2 + 7 \text{ wt\% Y}_2\text{O}_3$  sprayed by plasma in air or deposited by electron-beam physical vapour deposition (EBPVD), and intermediate  $\text{Al}_2\text{O}_3$  *thermally grown oxide* (TGO) on bond coatings of  $\text{NiCrAlY}$  sprayed by plasma under vacuum can be refurbished by:

- chemical treatment;
- electric arc treatment.

An example of *chemical treatment* is shown by e.g., Warnes and Schilbe (2001). They reported the successful stripping of ceramic top coatings by immersion in molten potassium hydroxide. The possible reaction driving the removal of the ceramic is given by the following equation:



The hydroxide penetrates through the zirconia top coating and attacks the thermally grown alumina layer as shown in the above equation. The zirconia coating becomes detached from the bond coating and the remaining alumina TGO is removed by rinsing the component in cold water. This treatment has the advantage to be very short as the duration of immersion in molten hydroxide is not longer than 9 min.

Takeda and Takeuchi (1997) reported *vacuum electric arc* removal of chromium oxide from stainless steel substrates of the type SUS430. The removal rate depends on the arc current and reaches a value of  $6 \text{ cm}^2/\text{s}$  for a  $5 \mu\text{m}$  thick oxide when the arc current ( $I$ ) reaches 200 A. The reason why the electric arc ‘attaches’ to the oxide is reportedly related

to the *work function* of an electron. This function is generally lower for oxides than for metals. This is why the ‘cathode spot’ of the arc stays preferentially on the oxide ‘islands’, heats and vaporizes them. This treatment can be applied to remove oxides on turbine blades. Further studies are, however, necessary to prove whether this method of oxide stripping is also possible for thick coatings of zirconia.

## 2.3 SUBSTRATE SHAPING

Substrates need to be shaped in order to meet their dimensional specifications. Some material has to be removed in the places where the coating is to be deposited. Shaping is also necessary to avoid sharp angles or sharp ends where it is difficult to spray a coating or, on the other hand, where adherence to the substrate is poor. The adherence becomes lower because of the high concentration of thermal stresses inside the coatings sprayed in such places. Examples of acceptable and unacceptable substrates geometries are shown in Figure 2.1.

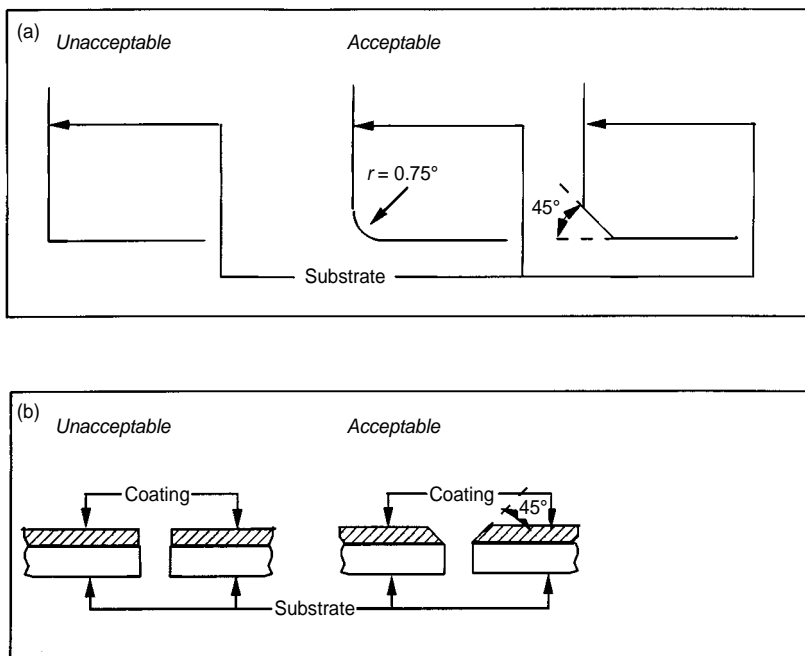


Figure 2.1 Examples of some acceptable and unacceptable substrate geometries applicable to thermal spraying (after Malik, 1973)

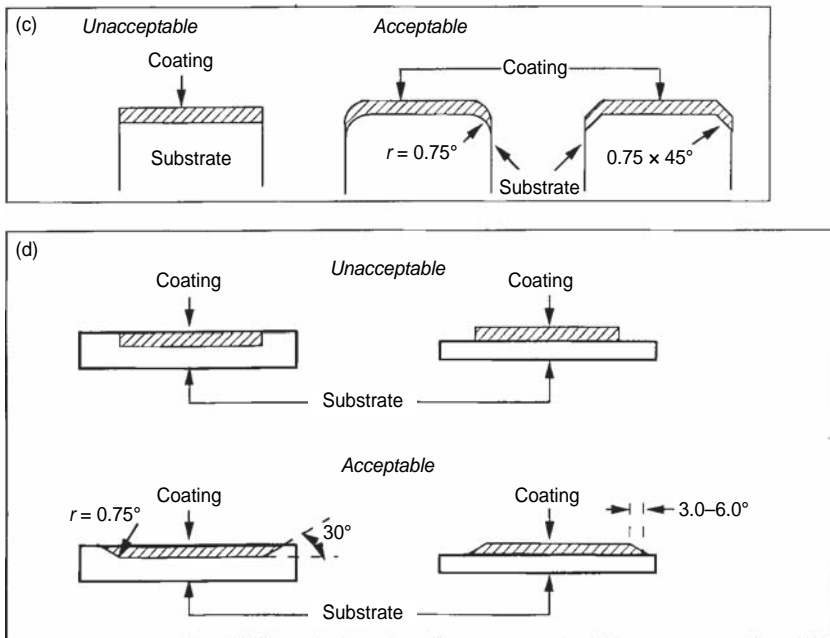


Figure 2.1 (Continued)

## 2.4 SURFACE ACTIVATION

The following methods of surface activation are in current use:

- abrasive grit blasting;
- water-jet treatment;
- laser ablation (the PROTAL™ process);
- chemical attack.

Abrasive grit blasting, shown schematically in Figure 2.2, is used to activate metallic substrates. Grit is sucked into a nozzle, accelerated in a compressed air stream and sprayed onto the substrate surface.

The principal parameters of grit blasting are collected in Table 2.1.

A typical laboratory installation for abrasive grit blasting is shown in Figure 2.3. The abrasive grit is recovered and re-used until it becomes 'worn' and unable to roughen the substrate.

The most rapidly worn part of the grit blasting installation is the nozzle. This is why it is recommended to use nozzles of hard structural

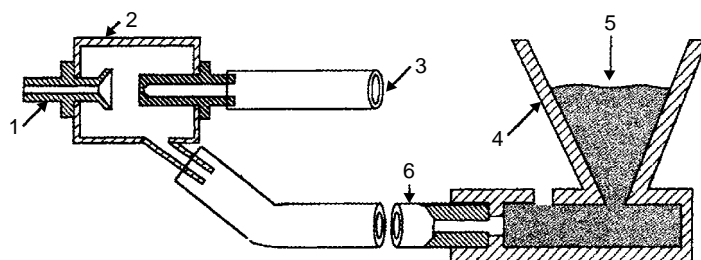


**Figure 2.2** Representation of abrasive grit blasting: (1) nozzle; (2) suction chamber; (3) compressed-air inlet; (4) grit feeder; (5) abrasive grit; (6) hose. Reproduced by permission of Battelle Columbus Laboratories

**Table 2.1** The principal parameters of grit blasting

Process element	Parameter
Grit	Material, grit size, elastic modulus, hardness
Blasted surface	Elastic modulus, hardness, thickness
Grit-feed principle	Suction, gravitational effect
Blasting atmosphere	Cabinet blasting, open-air blasting
Blasting technique	Duration, compressed air pressure, angle of grit impact, distance between nozzle and substrate

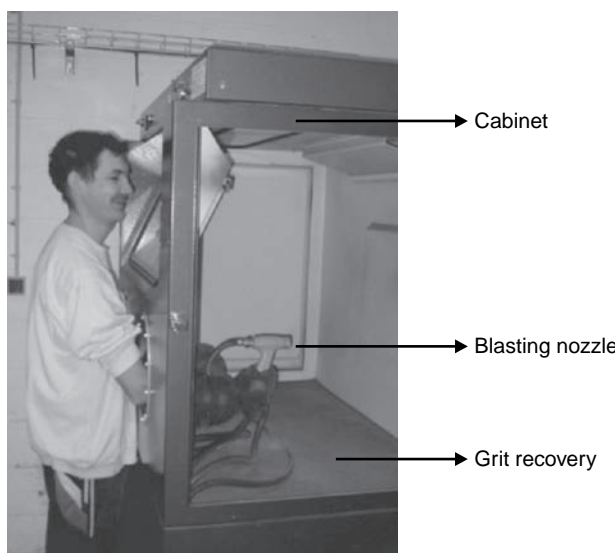


**Figure 2.3** A typical laboratory abrasive grit blasting cabinet with a manually guided nozzle

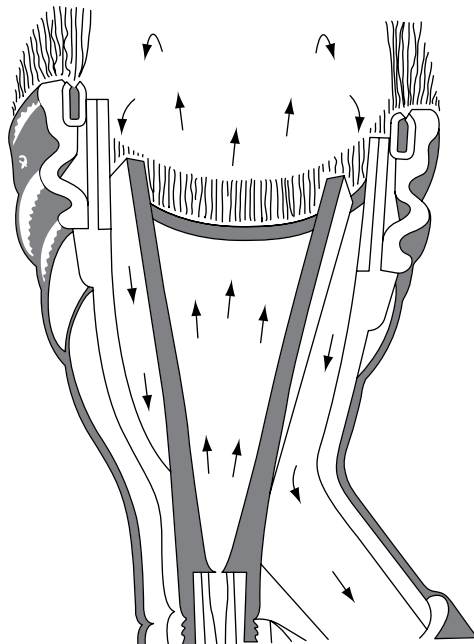


Figure 2.4 Illustration of the *Vacu-blast* nozzle used in open-air blasting. Reproduced by permission of Wheelabrator Group, Inc.

ceramics, such as  $B_4C$  or ceramic composites such as  $Al_2O_3 + (W,Ti)C$  (Jianxin *et al.*, 2003).

Small pieces should be grit-blasted inside a cabinet. This is because of the intensive dust formation that can be dangerous for the operator's health. Large pieces, such as *corona* or *anilox* rolls, are blasted in the open air by the use of a double-walled nozzle (*Vacu-blast* nozzle), which allows recovery of the grit (Figure 2.4).

Presently, grit blasting installations are often automatized, especially if they are used to process extensive series of products. One of the results of grit-blasting is an increase in surface roughness. *Roughness* can be characterized by many parameters, such as  $R_a$  (equivalent to average roughness (AA) or central-line average (CLA)) or  $R_{max}$ .  $R_a$  describes the overall quality of polishing while  $R_{max}$  is useful in describing the polished surface on which no valleys or holes are allowed. An example is the surface of an *anilox roll* which, at the production stage of polishing, should not have any surface imperfections. Such imperfections may eventually lower the quality of printing processes when using this type of roll.

An important parameter of blasting is *grit*. The most-used grits are (Roseberry and Boulger, 1977):

- metal grits of steel or cast iron of irregular shape;
- metal grits of spherical shape;
- ceramic grits of irregular shape (mainly silica, alumina and silica carbide).

The choice of the size of the grit results from the following desired characteristics:

- thickness of the sprayed piece (a finer grit is required if the piece is thin);
- roughness of the ‘as-sprayed’ coating (a finer grit results in a finer surface after spraying).

It is worth mentioning that silica sand is usually used as a fine grit while alumina sand is used as a coarse grit. Another important point is the ‘wearing’ of the grit which results in a decrease in its size. In fact, the grit must be changed after every 10 to 20 h of processing, depending on the pressure and hardness of the activated substrate. Other recommendations concerning the grit size are presented in Table 2.2.

**Table 2.2** Recommendations concerning the grit sizes used in substrate roughening (after Roseberry and Boulger, 1977)

Grit	Grit size ( $\mu\text{m}$ )	Application
Coarse	-2000 + 600	For coatings thicker than 250 $\mu\text{m}$ and best adherence
Medium	-1400 + 425	For coatings thinner than 250 $\mu\text{m}$ , fair adherence and smooth surfaces
Fine	-600 + 180	For coatings thinner than 250 $\mu\text{m}$ , used in ‘as-sprayed’ conditions (no finishing)

Surface roughness is the parameter which is closely related to grit-blasting and, on the other hand, strongly influences the adhesion of the coating to the substrate. An increase in the roughness results in an increase in the adhesion (Figure 2.5). The influence of the blasting parameters, such as blasting duration, blasting pressure and blasting angle, on the coating bond strength or surface roughness have been tested by, respectively, Apps (1974), Wigren (1987) and, more recently,

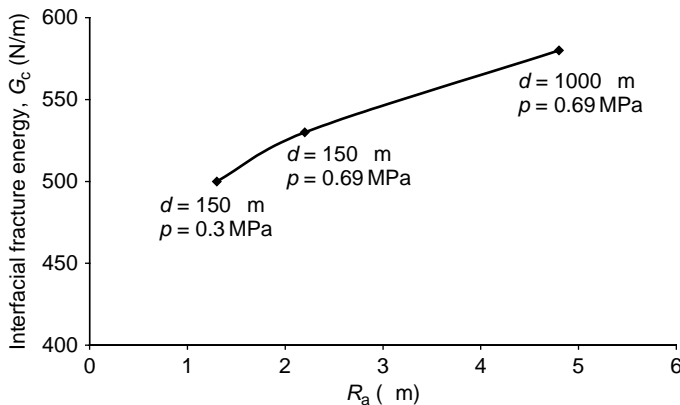


**Figure 2.5** Adhesion of an NiCrAlY bond coating to SAE 1010 mild steel (expressed by the interfacial fracture energy and measured by using a 4-point bending test) versus surface roughness. Different roughnesses were achieved by changing the grit size (diameter),  $d$ , and blasting pressure,  $p$ , with a constant blasting distance ( $l$ ) of 75 mm (after Hofinger *et al.*, 2002). Reproduced from *J. Therm. Spray Technol.*, 11(3), 2002, 387–392, ‘Effect of substrate surface roughness on the adherence of NiCrAlY thermal spray coatings’, I. Hofinger, K. Raab, J. Möller and M. Bobeth, Figure 11, Copyright (2002). With kind permission of Springer Science and Business Media

by Mellali *et al.* (1997). Some of the results obtained by Wigren (blasting of Inconel 718 with the *Vacu-blast* system and alumina grit) are showed in Figure 2.6. The parameter  $R_a$  reaches its maximum after relatively short blasting times and longer processing does not influence the surface roughness (Figure 2.6(a)).

Similarly, blasting at an angle of  $\alpha = 90^\circ$  allows us to reach a higher surface roughness in a shorter time. Finally, the  $R_a$  parameter grows linearly with increasing blasting pressure (Figure 2.6(b)). The results of Apps (1974) are somewhat contradictory. He reports that the bond strength of aluminium coatings sprayed onto mild steel reaches a maximum of nearly 25 MPa after grit-blasting using new alumina grit, at an angle of  $\alpha = 25^\circ$ . However, direct comparison of these results is not possible because of the fact that these authors used different substrates of different elastic moduli, different parameters to investigate the influence of blasting angle (Wigren – on roughness, Apps – on bond strength) and different alumina grits. The study of Mellali *et al.* (1997), however, confirms the findings of Wigren by showing that blasting at an angle  $\alpha$  between 60 and  $90^\circ$  results in similar roughnesses of the blasted surfaces (Figure 2.7).

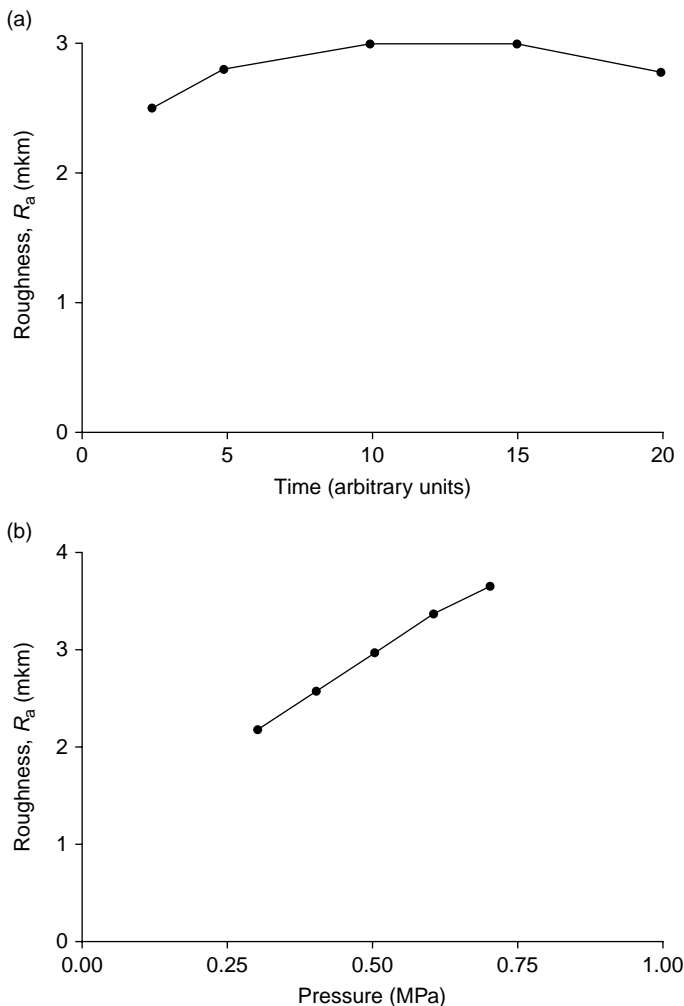


**Figure 2.6** Roughness of Inconel 718 (blasted using alumina grit, with a feed rate of  $q = 2 \text{ kg/min}$ , a blasting distance of  $l = 150 \text{ mm}$  and an angle of  $\alpha = 90^\circ$ ) versus (a) blasting duration and (b) blasting pressure (after Wigren, 1987). Reproduced by permission of ASM International from J. Wigren (1987), ‘Grit blasting as surface preparation before plasma spraying’, in *Thermal Spray: Advances in Coatings Technology*, D.L. Houck (Ed.), ASM International, Materials Park, OH, USA, pp. 99–104

At certain blasting angles, it is possible to create a special surface profile which results from the *undercutting* of asperities by rebounding particles (Figure 2.8).

The distance between the blasting nozzle and the workpiece does not strongly influence the surface roughness. If the distance becomes

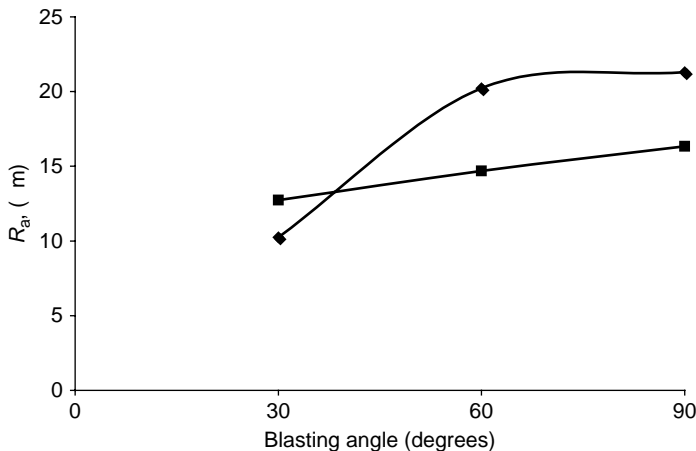


**Figure 2.7** Roughness of aluminium AU4G (◆) and carbon steel 100C6 (■) (blasted using alumina grit of size ( $d$ ) of  $1400\text{ }\mu\text{m}$  at a distance ( $l$ ) of  $100\text{ mm}$ ) versus blasting angle (after Mellali *et al.*, 1997). Reproduced from *J. Therm. Spray Technol.*, 6(2), 1997, 217–227, ‘Alumina grit blasting parameters for surface preparation in the plasma spraying operation’, M. Mellali, A. Grimaud, A.C. Leger, P. Fauchais and J. Lu, Figure 6, Copyright (1997). With kind permission of Springer Science and Business Media

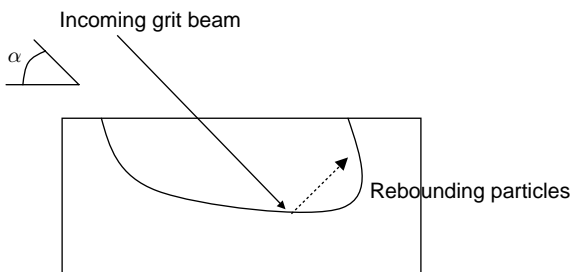


**Figure 2.8** Profile of a blasted surface with ‘undercutting’ of asperities (Bellot *et al.*, 2001). This article was published in *Sensors Actuators, A*, 92, E. Bellot, A. Sayah and M.A.M. Gijs, ‘Oblique powder blasting for 3-D micromachining of brittle materials’, 358–363, Copyright Elsevier (2001)

too great, the roughness, as expected, decreases. Wigren estimated a threshold value at  $l = 250\text{ mm}$ . Finally, it is important to carry out the roughening and spraying processes over small intervals of time (not more than a few hours). Too long an interval allows surface oxidation and may decrease the bond strength of the sprayed coating.

Another problem related to blasting is contamination of the activated surface by the grit. Some of the grit particles can remain implanted in this

surface. Some applications, such as biomedical ones, require coatings without any contamination. This can be achieved by:

- blasting by using coarse particles of coating material (if it is hard enough);
- ‘cryo-blasting’ with, e.g. solid CO<sub>2</sub> particles which evaporate after processing (Brewis *et al.*, 1999).

Water-jet treatment is another way of keeping the activated surface clean. This technique was applied to activate superalloys of Inconel 718, Rene 80 and Mar-M 509 before shrouded plasma spraying (SPS) of MCrAlY coatings of type LCO-22<sup>2</sup> (Taylor, 1995; Knapp and Taylor, 1996). Typical parameters for such treatments are shown in Table 2.3.

**Table 2.3** Typical operational parameters for water-jet treatment

Parameter	Value
Water pressure (MPa)	207–345
Water flow rate (l/min)	3.5–4.5
Nozzle diameter (mm)	0.4
Distance between nozzle and substrate (cm)	7.6
Scan velocity (cm/min)	30–130
Scan width (mm)	1.5
Scans overlapping (%)	50

The results of Knapp and Taylor indicate that the surface begins to get roughened starting from a water pressure of  $p = 200$  MPa. The morphology of a water-jet treated surface is much finer than that of a sand-blasted one. Finally, the bond strength of MCrAlY coatings to substrates, tested following the Standard ASTM C633-79, was in the range of 70 of 80 MPa for water-jet treated surfaces and 46–78 MPa for alumina grit-blasted ones. However, one important question remains to be answered, namely whether water-jet treatment does not corrode the substrates of some metals.

Another possible surface activation technique that does not contaminate the substrate is laser ablation. This technique uses a laser, typically Nd:YAG, of short pulses (tenths up to hundreds of nanoseconds) which rapidly vaporizes a superficial layer on the substrate surface. Moreover, the plasma created by these pulses expands and acts on the substrate in

<sup>2</sup> The coating description for *Praxair ST*.

the form of ‘mechanical shocks’. A laser installation that can be used for such a treatment is shown in Figure 2.9.



Figure 2.9 A *Laserblast*<sup>TM</sup> installation for laser cleaning and activation of substrates. Reproduced by permission of Quantel, Les Ulis, France

Surface activation with a pulsed laser is already commercialized under the name of *PROTAL*<sup>TM</sup> and was applied to activate the titanium alloy AISI 2017 before plasma spraying of  $\text{Al}_2\text{O}_3 + 13 \text{ wt\% TiO}_2$  (Coddet *et al.*, 1998). However, the prices of lasers considerably hamper the application of this method in the coatings industry.

Chemical etching is also a possible surface activation method but at present it is not often used any more. Diluted acids, such as sulfuric, nitric or hydrochloric, as well as their mixtures, can be used to activate most metals and alloys. Incompatibility with other manufacturing procedures in spray workshops and environmental standards reduce the attractiveness of activation by chemical attack.

## 2.5 MASKING

Coatings are sprayed in desired places on substrates. Some of their applications, especially those in the electronics field, require very

precise and multiple masking to obtain resistors, capacitors and other functional fields. Masking should also be applied at the surface-activation stage. Masks that adequately protect substrates against abrasive grit erosion are made of Teflon™, plastics or rubber (Hibler and Gerber, 1990). Masking prior to spraying can be carried out with metallic or glass fibre tapes, which can be cut to desired dimensions. There are also commercially available liquids, such as, Metco Anti-Bond™, which prevent the adhesion of hot particles during spraying and can be dissolved with water after processing. The ‘holes’ and ‘slots’ in the sprayed piece can be protected with Teflon™ or metal inserts.

A mechanical mask which is useful in the spraying of fine patterns can be made with the help of *photolithography* (Figure 2.10).

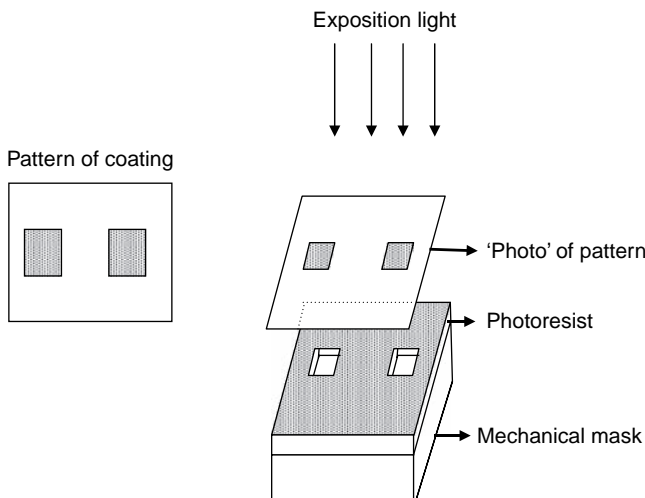


Figure 2.10 Principles of photolithography

Initially, a ‘photo’ with a pattern to be sprayed is prepared. Then, a thin film of a uv-sensitive polymer (*photoresist*) is applied onto the surface of a metallic sheet. The photoresist is then exposed to uv light through the ‘photo’. The exposed part of the film hardens and the other part can be easily removed with water. Finally, chemical etching removes the metal which is unprotected by the polymer, leaving a metal sheet with the desired pattern that can be used as a mechanical mask. More details about photolithography can be found in work of Lucas *et al.* (1999).

## REFERENCES

- Apps, R.L. (1974). The influence of surface preparation on the bond strength of flame sprayed aluminium coatings into mild steel, *J. Vac. Sci. Technol.*, **11**, 741–746.
- Belloy, E., Sayah, A. and Gijs, M.A.M. (2001). Oblique powder blasting for 3-D micro-machining of brittle materials, *Sensors Actuators, A*, **92**, 358–363.
- Brewis, D.M., Critchlow, G.W. and Curtis, C.A. (1999). Cryoblasting as a pretreatment to enhance adhesion to aluminium alloys: an initial study, *Int. J. Adhesion Adhesives*, **19**, 253–256.
- Coddet, C., Montavon, G., Marchione, T. and Freneaux, O. (1998). Surface preparation and thermal spray in a single step: the Protal™ process, in *Thermal Spray, Meeting the Challenges of the 21st Century*, C. Coddet (Ed.), ASM International, Materials Park, OH, USA, pp. 1321–1325.
- Hibler, A. and Gerber, K. (1990). Fortschrittliche Maskierungsmethoden beim thermischen Spritzen, in *Thermische Spritzkonferenz TS90*, Vol. 130, DVS, Düsseldorf, Germany, pp. 32–34.
- Hofinger, I., Raab, K., Möller, J. and Bobeth, M. (2002). Effect of substrate surface roughness on the adherence of NiCrAlY thermal spray coatings, *J. Therm. Spray Technol.*, **11**, 387–392.
- Jianxin, D., Yihua, F., Zeliang, D. and Peiwei, S. (2003). Wear behavior of ceramic nozzles in sand blasting treatments, *J. Eur. Ceram. Soc.*, **23**, 323–329.
- Knapp, J.K. and Taylor, T.A. (1996). Water roughened surface analysis and bond strength, *Surf. Coat. Technol.*, **86–87**, 22–27.
- Lucas, K.D., Henderson, C.L. and Strojwas, A.J. (1999). Photolithography, in *Wiley Encyclopedia of Electrical and Electronic Engineering*, Vol. 16, J.G. Webster (Ed.), John Wiley and Sons, Inc., New York, NY, USA, pp. 300–320.
- Malik, M.P. (1973). Plasma sprayed coatings in aircraft and engine components, in *Proceedings of the 7th International Metal Spray Conference*, The Welding Institute, Cambridge, UK, pp. 257–267.
- Mellali, M., Grimaud, A., Leger, A.C., Fauchais, P. and Lu, J. (1997). Alumina grit blasting parameters for surface preparation in the plasma spraying operation, *J. Therm. Spray Technol.*, **6**, 217–227.
- Roseberry, T.J. and Boulger F.W. (1977). *A Plasma Flame Handbook*, Report No. MT-043, US Department of Commerce, National Technical Information Service, Springfield, VA, USA.
- Takeda, K. and Takeuchi, S. (1997). Removal of oxide layer on metal surface by vacuum arc, *Mater. Trans. JIM*, **38**, 636–642.
- Taylor, T.A. (1995). Surface roughening of metallic substrates by high pressure pure waterjet, *Surf. Coat. Technol.*, **76–77**, 95–100.
- Warnes, B.M. and Schilbe, J.E. (2001). Molten metal hydroxide removal of thermal barrier coatings, *Surf. Coat. Technol.*, **146–147**, 147–151.
- Wigren, J. (1987). Grit blasting as surface preparation before plasma spraying, in *Thermal Spray: Advances in Coatings Technology*, D.L. Houck (Ed.), ASM International, Materials Park, OH, USA, pp. 99–104.

# 3

# Thermal Spraying Techniques

## 3.1 INTRODUCTION

Following its definition, thermal spraying is a process in which molten, semi-molten or solid particles are deposited on a substrate. Consequently, the spraying technique is a way of generating a ‘stream’ of such particles. Coatings can be generated if the particles can plastically deform at impact with the substrate, which may only happen if they are molten or solid and sufficiently rapid. Their heating and/or acceleration are practical if they occur in a stream of gas.<sup>1</sup> Thus, an academic classification of spray techniques is based on the way of generation of such streams. Table 3.1 shows some of the methods of generation of streams of gases. Some other sources of energy input into the gas, other than those listed in the table, are also possible. Photonic heating by focusing of a halogen lamp or a laser beam may generate a small-volume plasma that can be ‘theoretically’ used for spraying. Spray techniques can also be classified following technical and economical demands related to the sprayed coatings. These demands generate the ‘axes’ around which new techniques are being developed. These axes are related to the techniques characterized by the following:

---

<sup>1</sup> Spray techniques without a gas stream are easily imaginable; for example, a thin wire charged with a high-intensity electric current which ‘explodes’, forming a stream of radially moving liquid particles (like an ‘electric-fuse’).

**Table 3.1** Methods of generation of jets and flames used in thermal spraying

Energy input to gas	Variation	Spray technique
Electric discharge	DC arc	AS, APS, VPS
	Pulsing arc	Torches described by Vollrath <i>et al.</i> (1992) or by Whitterspoon <i>et al.</i> (2004)
	HF (RF) glow discharge <sup>a</sup>	RF plasma spraying (Mailhot <i>et al.</i> , 1998; Bouyer <i>et al.</i> , 2003) <sup>b</sup>
Combustion	Continuous	HVOF, FS
	Explosive	D-gun™
Decompression of gas	—	CGSM

<sup>a</sup> RF discharge is also used to initiate a discharge in a DC arc.

<sup>b</sup> See the catalogue of Tekna, Sherbrooke, Canada.

- *High kinetic energy of sprayed particles*, being in contact with jets or flames of high velocity but having a relatively low temperature. The ‘time of flight’ is short and they impact on the substrate without being molten. Examples of this family of techniques are high-velocity oxygen fuel (HVOF) spraying, high-velocity air fuel (HVAF<sup>2</sup>) spraying, D-gun™, Super D-gun™, Sonarc™ (Steffens and Nassenstein, 1996) or the cold-gas spraying method (CGSM). These techniques are adapted to spray materials of relatively low melting point, which:
  - modify their chemical composition at spraying, such as, carbides which decarburize;
  - melt incongruently, forming the phases less interesting from the point of view of future application, such as, ‘multi-oxides’, e.g. HA or YBCO.
- *Controlled atmosphere* surrounding a jet or flame. The atmosphere modifies the chemical composition of the jet or its physical properties, such as, level of turbulence or the mean free path of the species. Examples of such techniques are, e.g. vacuum plasma spraying (VPS) (called sometimes LPPS), controlled-atmosphere plasma spraying (CAPS), inert plasma spraying (IPS), shrouded plasma spraying (SPS), shrouded HVOF spraying (Fukushima and Kuroda, 2001) and underwater

<sup>2</sup> JetStar™ HVAF spray system – see the catalogue of Praxair ST, Appleton, WI, USA, revised September, 1997.

plasma spraying (UPS), described by Minami *et al.* (1998). These techniques are adapted to spray materials that oxidize easily, such as:

- metallic elements of very high chemical affinity to oxygen, such as, Ti or Ta;
- alloys that oxidize when spraying in an air atmosphere and which should form a coating without oxides, e.g. NiAl or NiCrAlY.
- *High productivity* with high throughput of the sprayed material. The jets or flames in these techniques are usually more voluminous with regard to other ones. This family of techniques can be subdivided into that which produce coatings of:
  - low quality, which include techniques, such as, FS or AS and which are used mainly to spray metals (Mo, Ni) or alloys (NiCr, NiAl) onto large surfaces;
  - high quality, which includes techniques such as, high-power plasma spraying (HPPS), water-stabilized plasma (WSP) spraying or three-cathode-plasma spraying with axial powder injection, represented by torches, such as, Triplex<sup>TM</sup> or Axial III<sup>TM</sup> and which are used mainly to spray oxides ( $\text{Cr}_2\text{O}_3$ ,  $\text{Al}_2\text{O}_3$ ,  $\text{ZrO}_2$ ) onto large surfaces.
- *Nanostructured coating spraying* which enables small crystal grains ( $d < 100 \text{ nm}$ ) to be obtained inside the coatings. This family of techniques has produced modifications of existing techniques which keep the size of the grains (and eventually the thickness of coatings) small. These techniques use very fine powders (agglomerated or not) or precursors as liquid suspensions or solutions which transform at spraying into the desired coating material. Modifications to the existing techniques are related mainly to the design of spray material feeders and of injectors, so enabling fine particles or liquids to be injected into a jet or flame.

## 3.2 FLAME SPRAYING (FS)

### 3.2.1 HISTORY

Flame spraying (FS) is chronologically the first spraying technique. It was developed by the Swiss engineer Schoop at the beginning of the last century (Schoop and Guenther, 1917). This process was used initially

for low-melting metals, such as tin or lead, and was later extended to more refractory metals and even ceramics.

### 3.2.2 PRINCIPLES

#### Powder Flame Spraying (FS-Powder)

In a flame spraying<sup>3</sup> torch, the chemical energy of combustion of the fuel gas in oxygen is used to generate a hot flame (Figure 3.1). The gas inlet is axial (1) and powder (2) can be introduced axially or perpendicularly to the torch (3). Rods and wires can be used instead of powder (Smith, 1974a). The particles become molten in the flame (6) and accelerated in the direction of the workpiece (4). The modern powder flame spraying torch, is shown in Figure 3.2.

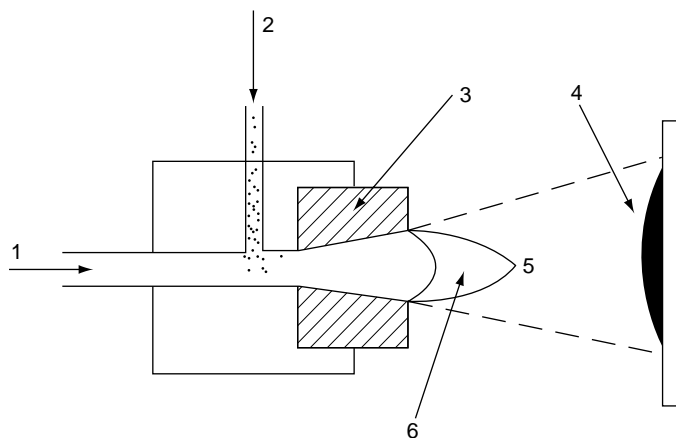


**Figure 3.1** Schematic of flame spraying of a powder: (1) working gases (fuel and oxygen); (2) injection of powder; (3) torch body; (4) sprayed coating; (5) stream of particles; (6) combustion flame

#### Wire Flame Spraying (FS-Wire)

In the torch used to spray wires or rods (see Figure 3.3), a flame is also generated by combustion of fuel gas (2) in oxygen (1). The flame melts

---

<sup>3</sup> Flame spraying is sometimes called combustion flame spraying.

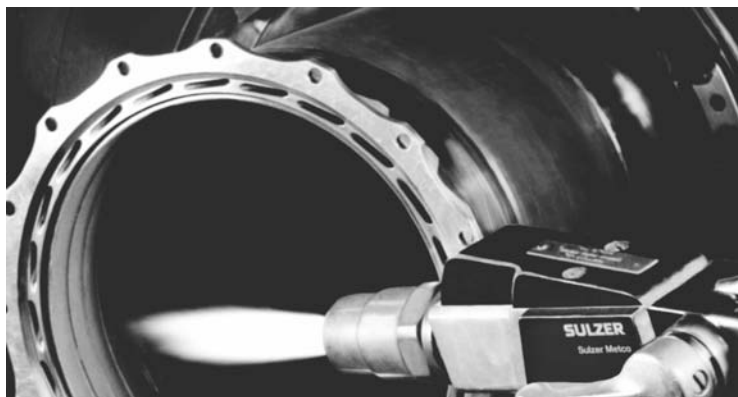


Figure 3.2 Modern flame spraying equipment. Reproduced by permission of Sulzer-Metco AG, Wohlen, Switzerland

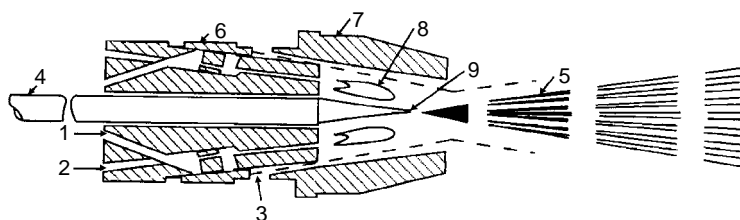


Figure 3.3 Schematic of flame spraying of wires/rods: (1) oxygen inlet; (2) fuel gas inlet; (3) compressed air inlet; (4) wire/rod; (5) stream of molten droplets; (6) nozzle for working gases; (7) compressed-air cap; (8) flame; (9) molten end of wire/rod

the end of the wire/rod (4) which becomes atomized by compressed air (3) to form droplets. These form a stream (5) and are propelled towards the substrate.

A modern torch used for spraying wires or rods is shown in Figure 3.4.

### 3.2.3 PROCESS PARAMETERS

#### Flame

- *Working gas composition:* oxygen-to-fuel ratio might vary from 1:1 to 1.1:1, which results in a carburizing or oxidizing atmosphere, respectively.
- *Flame temperatures* are in the range from 3000 to 3350 K.



Figure 3.4 A modern wire flame spraying torch. Reproduced by permission of Saint Gobain Coating Solutions, SNMI, Avignon, France

- *Flame velocities* are in the range from 80 to 100 m/s.
- *Working gases' flow rates and pressures* depend on the type of torch.

## Powder

- *Chemical properties:* chemical composition, element distribution, crystal phases and their distribution. Although metals, alloys and ceramics are used in most applications, polymers can also be sprayed by using specially designed torches proposed by some manufacturers (e.g. Saint Gobain SNMI, Avignon, France).
- *Physical properties:* density, melting point, latent heat of fusion and pressure of vapours.
- *Particles morphology:* a spherical shape is desired in order to facilitate powder handling and to decrease the spraying ‘spot’.
- *Particles size distribution:* a narrow distribution is desirable in order to improve spraying efficiency.
- *Particles sizes:* usually in the range 5–100 µm.
- *Feed rate:* varies from 50 to 100 g/min.

## Rods or Wires

- *Chemical composition:*
  - Rods<sup>4</sup> are ceramics, such as,  $\text{Al}_2\text{O}_3$ ,  $\text{Al}_2\text{O}_3 + \text{TiO}_2$ ,  $\text{TiO}_2$ ,  $\text{Cr}_2\text{O}_3$ , etc.
  - Wires are metals, such as, Mo, Zn and Al or alloys, such as, brass and stainless steel, plus *self-fluxing alloys*, etc.
- *Diameter:* ranges from 3 to 6 mm (frequently, 2.3, 3.17 and 4.75 mm).
- *Feed rate:* varies from 40 to 650 g/min, with the resulting deposition efficiency of a 100  $\mu\text{m}$  coating varying from 1 to 23  $\text{m}^2/\text{h}$ .<sup>5</sup>

## Powder Injection

- *Injection direction:*
  - Radial: in older types of torches.
  - Axial: in modern types of torches.
- *Powder feeders:*
  - Gravitational feeding in older types of torches.
  - Rotating plate feeding in modern types of torches.
- *Carrier gas flow rate:* 3 to 5 slpm.

## Principal Processing Parameters

- *Spray distance* is in the range 120–250 mm.
- *Spray atmosphere* is air.
- *Substrate surface temperature:*
  - Should be kept in the range 373–473 K when spraying ceramics onto metals in order to avoid the residual stresses.
  - When melting the self-fluxing coating, the temperature may rise up to 1000 K.

---

<sup>4</sup> Short ceramic rods cans be inserted into a long polymeric cover which can be handled as wires.

<sup>5</sup> See the catalogue of Saint Gobain SNMI, Avignon, France.

- *Post-spraying treatment* in order to improve the density and bond strength:
  - Fusion of *self-fluxing alloy* coatings.
  - Furnace annealing.

### 3.2.4 COATING PROPERTIES

The bond strength determined using tensile adhesion test (see Chapter 8) can reach 60 MPa for flame-sprayed NiAl alloys or even 70 MPa for self-fluxing ones. Typical values are in the range of 15 MPa for ceramics coatings to 30 MPa for metals and alloys. Porosities are in the range of 10 to 20 % (self-fluxing coatings are, after heat treatment, virtually ‘pore-free’) and typical thicknesses are in the range of 100 to 2500 µm.

## 3.3 ATMOSPHERIC PLASMA SPRAYING (APS)

### 3.3.1 HISTORY

The torch for plasma spraying is based on the *Gerdien-type plasma generator* (Gerdien and Lotz, 1922). The process of spraying with the use of a plasma has been patented by Gage *et al.* (1962), as well as by Giannini and Ducati (1960).

### 3.3.2 PRINCIPLES

The plasma generator, depicted in Figure 3.5, consists of a circular anode (1), usually of copper, and a cathode of thoriated tungsten (2). The cathode is made of graphite in a water-stabilized torch. The electric arc discharge, supported by a generator through the connectors (3, 4) heats up the working gases (5), which expand in the atmosphere, forming a jet. The powder (6), suspended in a carrier gas, is injected into the jet. The particles of the powder after being melted and accelerated in the jet impact the substrate and form the coating.

A commercial plasma torch installed onto a robot arm is shown in Figure 3.6.

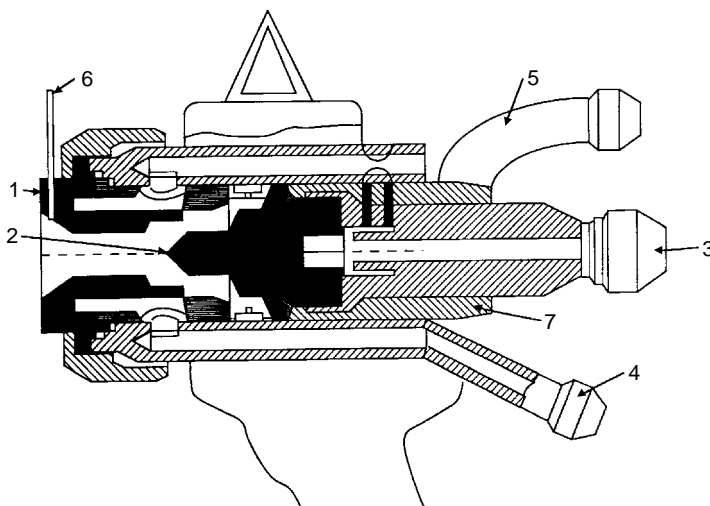


**Figure 3.5** Schematic of a section of a plasma torch: (1) anode; (2) cathode; (3) water outlet and cathode connector; (4) water inlet and anode connector; (5) inlet for working gases; (6) powder injector; (7) electrical insulator

### 3.3.3 PROCESS PARAMETERS

#### Arc Plasma

- *Working gases composition:* typically Ar or mixtures of Ar + H<sub>2</sub>, Ar + He and Ar + N<sub>2</sub>, sometimes N<sub>2</sub> and a mixture of N<sub>2</sub> + H<sub>2</sub>, with a typical flow rate being about 40 to 50 slpm but in some installations it may reach 80 slpm. High-energy torches use flow rates as high as 500 slpm (Jungklaus *et al.*, 1996). Some manufacturers propose a composition of three gases, such as Ar + He + H<sub>2</sub> or Ar + He + N<sub>2</sub>. Each gas has its own role in the formation of a plasma jet (Janisson *et al.*, 1999):
  - Ar stabilizes the arc inside a nozzle;
  - He, N<sub>2</sub> or H<sub>2</sub> enhance the heat transfer to the particles, due to their high heat conductivity.

Ternary gas mixtures are available commercially (e.g. *Spral 22<sup>TM</sup>*, Air Liquide). Water vapour forms a plasma gas in a water-stabilized torch (water consumption is about 5 l/h (WSP 500, 1997). Reactive plasma-forming gases, including hydrocarbons or carbon dioxide, can also be used. The torch generating such a reactive plasma must be, however, equipped with a graphite cathode (Fridlyand, 1995). An arc

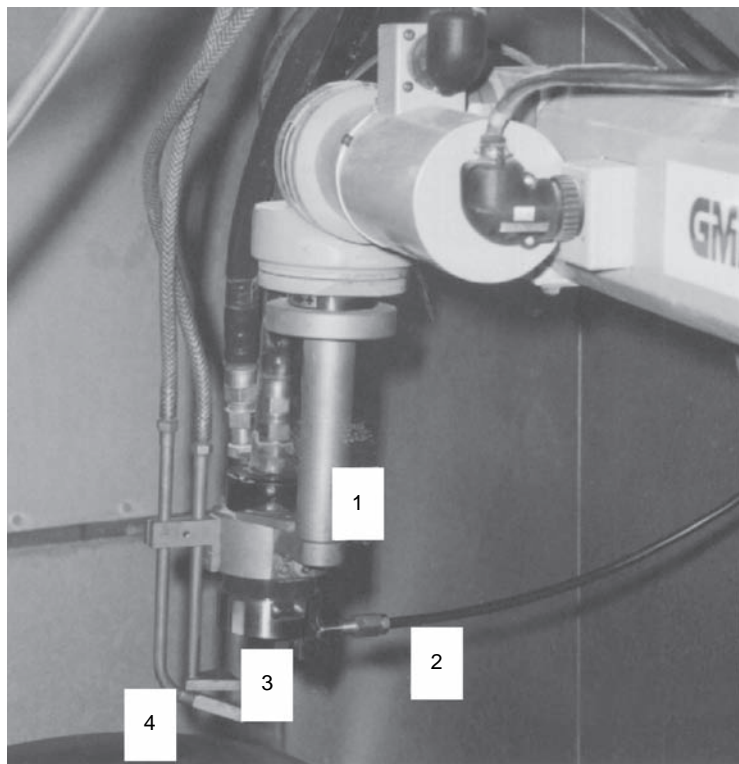


Figure 3.6 A modern plasma torch installed on a robot: (1) torch; (2) compressed-air barrier; (3) compressed-air cooling; (4) powder injector (Pawlowski *et al.*, 1991). Plasma torch installed in The Monash University, Melbourne, Australia

is characterized by an electric current of a few hundreds of amps and a voltage which depends on two principal parameters:

- the distance between cathode and anode (a greater distance increases the voltage);
- the choice of secondary gas (diatomic gases, such as hydrogen, increase the arc voltage).

Typical arc voltages in plasma torches, such as *F4* of Sulzer Metco or *SG100* of *Praxair ST*, range between 30 and 70 V. The temperature of a plasma in a typical plasma torch is about 14 000 K and its velocity at the nozzle exit can reach 800 m/s. The temperature is reported to be 28 000 K in a water-stabilized torch. The velocity reaches 2900 m/s in a high-power plasma spray installation (Plazjet, 1995). The working gases mostly influence the degree of melting of the sprayed particles.

The latter is easier with molecular gases, such as water vapour (in a water-stabilized torch) or hydrogen (in a typical plasma torch) due to the greater thermal conductivity when compared to atomic gases. On the other hand, monatomic gas jets may reach a high velocity. This is why mixtures of a monatomic gas with a molecular gas have been often used to achieve the melting of particles, as well as their high velocities during spraying. Monatomic He is used as a secondary gas because of its high thermal conductivity and its ability to form a narrow spray jet (Ingham and Fabel, 1975).

- *Electric power* is up to 80 kW in typical plasma torches, but can reach 200 kW in a water-stabilized torch (WSP 500, 1997) or even 250 kW in high-power ones (Plazjet, 1995).
- *Geometry of electrodes*: the cathode tip should have different shapes for different working gases. The geometry (profile, diameter) of an anode influences the plasma flow pattern, temperature and velocity. For example, application of a convergent–divergent anode–nozzle was reported to reduce arc voltage fluctuations (Schwenk *et al.*, 2003). The electric arc ‘contacts’ the anode and cathode in one or more places (‘roots’) resulting in deterioration and wear (Fisher, 1972). In some applications, e.g. *corona rolls*, it is necessary to monitor<sup>6</sup> this deterioration in order to reduce the content of metal transferred from the anode or cathode into the coating. Wear of the electrodes occurs due to the high density of heat flux reached in an arc spot,  $10^8 \text{ W/m}^2$  (Fridlyand, 1995)
- *Plasma stabilization*: usually achieved by using a sheath or vortex of working gas. Water-stabilized torches are available commercially (WSP 500, 1997).

## Powder

- See the section dealing with powders for flame spraying.
- *Particles sizes* are usually in the range 20–90 µm.<sup>7</sup>
- *Powder type*: the most used powders are oxide ceramics.

<sup>6</sup> The simplest but the most time-consuming method is weighing the electrodes. Oscilloscopic observation of arc current and voltage may also help in electrode-deterioration diagnostics (Dorier *et al.*, 2000).

<sup>7</sup> In some important applications, e.g. plasma spraying of hydroxyapatite for surgical implants, it is important not to entirely melt the sprayed particles. In this case, the particles sizes are up to 150 µm (see, e.g. Deram *et al.*, 2002).

## Powder Injection

- *Injection direction:*
  - radial: in a typical torch for plasma spraying; can be outside of the anode–nozzle (see Figures 3.5 and 3.6 and torch F4 (Sulzer-Metco)) or inside<sup>8</sup> it (e.g. torch SG100 of Praxair ST);
  - axial: as discussed later, three-cathodes torch as Axial III™.
- *Injection angle:* usually 90°, although sometimes 60° backwards or downwards of the plasma jet;
- *Injection ports:* most often one, although sometimes two or three; multiple injectors enable the spraying of composite coatings;
- *Powder feeders:* usually the rotating plate type;
- *Powder feed rate* is typically in the range of 50 to 100 g/min, but can reach 200 g/min in HPPS or axial injection torches. Values as high as  $q_p = 1650$  g/min have been reported in a water-stabilized torch (WSP 500, 1997);
- *Carrier gas flow rate* is in the range 3 to 10 slpm.

## Principal Processing Parameters

- *Spray distance* is in the range 60 to 130 mm.
- *Spray atmosphere* is air.
- *Linear velocity of the torch with regard to the substrate* is in the range 50 to 2000 mm/s.
- *Substrate temperature* is an important parameter when spraying ceramics onto metals due to the generation of residual stresses (see compressed-air cooling in Figure 3.6). In such cases, the temperature should be kept in the range 373 to 473 K.
- *Post-spraying treatment* is used to improve coating density and other properties. The methods of treatment, discussed in the next chapter, include, among others:
  - Furnace annealing;
  - Laser treatment;

---

<sup>8</sup> Injection inside the anode–nozzle results in a longer trajectory of the particles in a plasma jet and therefore enables using a lower power input to spray the given powder although internal injectors need to be cleaned more often.

- Sealing with organic and inorganic sealants;
- Spark-plasma treatment

### 3.3.4 COATING PROPERTIES

The bond strength of plasma-sprayed ceramics on metallic substrates is in the range 15 to 25 MPa.<sup>9</sup> Plasma-sprayed bonding alloys (NiAl or NiCrAl) or metals (Mo) may reach a strength of 70 MPa or even higher. The porosity of APS coatings is usually in the range 1–7%, but might be intentionally greater. The thicknesses of these coatings are typically in the range 300 to 1500 µm.

## 3.4 ARC SPRAYING (AS)

### 3.4.1 PRINCIPLES

A schematic of an AS installation is shown in Figure 3.7.

Two wires<sup>10</sup> (5), being consumable arc electrodes, are drawn from spools and form a liquid droplet due to arc heating (4). The droplet is blown by the atomizing gas (1). The gas atomizes the molten droplet

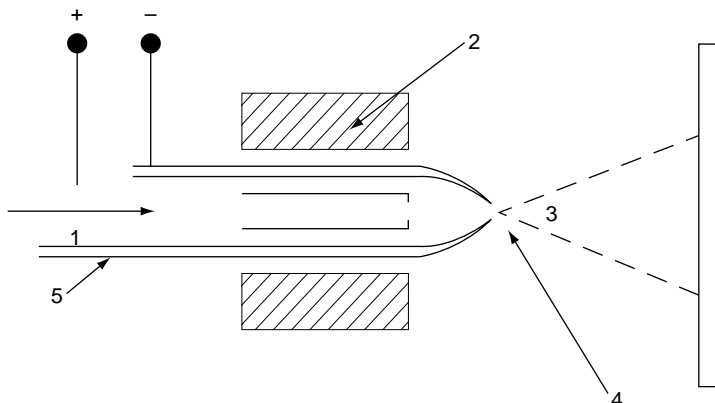


**Figure 3.7** Schematic of an arc-spraying installation: (1) atomizing gas flow; (2) torch outer shield; (3) stream of molten particles; (4) electric arc; (5) consumable arc electrodes

<sup>9</sup> Measured following the standard ASTM 633-01 or one of its previous versions.

<sup>10</sup> One-wire arc spraying was also studied and reportedly results in a narrow stream of droplets (Carlson and Heberlein, 2001).



Figure 3.8 A modern torch used for arc spraying. Reproduced by permission of Sulzer-Metco AG, Wohlen, Switzerland

and propels fine particles (3) towards a substrate. If the wires are made of different metals, a ‘pseudo-alloy’ coating can be produced. A modern torch used for arc spraying is presented in Figure 3.8.

### 3.4.2 PROCESS PARAMETERS

#### Electric Arc

- *Electric power:* is typically in the range 5–10 kW;
- *Arc temperature:* may reach 6100 K with an arc current of 280 A (Marantz, 1974);
- *Arc voltage:* typically in the range 20–40 V – an increasing voltage corresponds to increases in the sizes of the sprayed droplets.

## Wires

- *Materials:* all electrically conductive materials are applicable. These are traditionally metals, such as Zn, Al or Mo and alloys like NiCr, NiAl or NiCrAl, but cored wires are also in extensive use. The cored wires are composed of two phases, i.e. sheath and filler, such as a WC–W<sub>2</sub>C filler inside a Co sheath (Drzeniek and Steffens, 1987) and typically the sheath corresponds to approximately 50 % of the total composition (Sampson, 1993). Composite materials can also be deposited by a combination of an electric arc and HVOF spraying (Sonarc™). The powder is sprayed by HVOF and the wire by an arc. An example of such a composite is a coating sprayed by using NiCr wire and SiC powder (Steffens and Nassenstein, 1996).
- *Diameter:* typically 1.6–5.0 mm.
- *Particle velocity:* molten particles formed of wires can reach velocities up to 150 m/s (Rudzki, 1983). These velocities are similar to those observed when using the HVOF process in the Sonarc™ technique.

## Principal Processing Parameters

- *Deposition rate* is in the range 50 to 1000 g/min. Some manufacturers<sup>11</sup> ‘advertise’ deposition rates as high as 3300 g/min;
- *Spray distance:* 50–170 mm;
- *Spray atmosphere* is air but an arc-spraying torch can be installed in a vacuum, or reactive or inert atmospheres;
- *Atomizing gas* is usually air but can be nitrogen or a mixture of oxygen with fuel gas (in Sonarc™ technique);
- *Atomizing gas pressure* is in the range 0.2 to 0.7 MPa;
- *Atomizing gas flow rate* is in the ‘broad’ range 20 to 1300 slpm.
- *Post-spraying treatment* by furnace annealing can be applied in order to improve the densities and bond strengths of the coatings.

### 3.4.3 COATING PROPERTIES

The tensile bond strength is in the range 10 to 30 MPa for Zn and Al coatings (Schmidt and Matthäus, 1980) but can reach a value of

---

<sup>11</sup> OSU, Duisburg, Germany for spraying of Zn.

70 MPa for NiAl coatings or for NiCr + SiC composites sprayed by using Sonarc<sup>TM</sup>. The porosity is in the range 10 to 20 %. The thicknesses of the coatings are in the range 100 to 2000  $\mu\text{m}$ .

### 3.5 DETONATION-GUN SPRAYING (D-GUN)

#### 3.5.1 HISTORY

The D-gun<sup>TM</sup> process was developed by Union Carbide<sup>12</sup> (Poorman *et al.*, 1955) in the early 1950s and D-gun<sup>TM</sup> sprayed coatings are available through the coating service of this organization. The detonation-gun process was also developed in the 1960s at the Paton Institute in Kiev (Ukraine) (Borisov *et al.*, 1990; Kadyrov, 1988) and this technology seems to be at present commercially available (e.g. by Demeton Technologies, West Babylon, NY, USA).

#### 3.5.2 PRINCIPLES

The D-gun<sup>TM</sup>, shown schematically in Figure 3.9, includes a long, water-cooled barrel with an ID of about 25 mm (Schwarz, 1980).

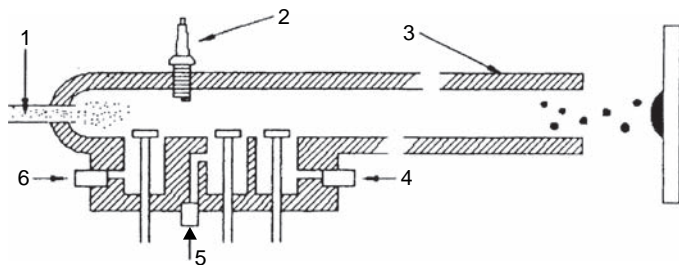


**Figure 3.9** Schematic of the D-gun<sup>TM</sup> process: (1) powder injection; (2) spark plug; (3) gun barrel; (4) oxygen input; (5) nitrogen input. Reproduced by permission of Praxair Technology, Inc., Indianapolis, IN, USA

A mixture of oxygen (4) and acetylene (5) is fed into the barrel, together with a charge of powder (1). The gas is ignited, explodes and its detonation wave accelerates the powder. In order to avoid 'backfiring',

---

<sup>12</sup> Today's name: Praxair.

i.e. explosion of the fuel gas supply, an inert gas, such as nitrogen, is used between the portions of exploding mixture. Nitrogen also purges the barrel. The detonation process therefore has the following cycles (Kadyrov and Kadyrov, 1995):

- Injection of oxygen and fuel into the combustion chamber;
- Injection of powder and nitrogen to prevent ‘backfiring’;
- Ignition of mixture and acceleration of powder;
- Purging of barrel by nitrogen.

There are 1–15 detonations per second with purges of nitrogen between them. Figure 3.10 shows a detonation gun installed at the Advanced Research Centre for Powder Metallurgy and New Materials International (ARCI) in Hyderabad India.

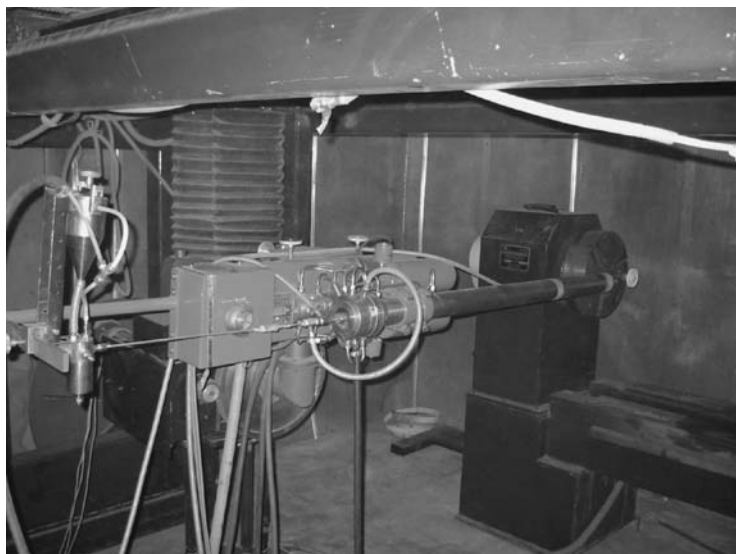


**Figure 3.10** Detonation gun in operation at the ARCI, Hyderabad, India. Reproduced by permission of Dr G. Sundararajan, Director – ARCI

### 3.5.3 PROCESS PARAMETERS

#### Detonation Wave

- *Working gases composition:* mixture of a fuel gas, usually H<sub>2</sub> or hydrocarbons, such as acetylene (C<sub>2</sub>H<sub>2</sub>), propane (C<sub>3</sub>H<sub>8</sub>) and butane

( $C_4H_{10}$ ), with oxygen ( $O_2$ ). The composition giving the maximum temperature of 4500 K corresponds to oxygen with 45 vol% of acetylene (Tucker, 1982). The detonation wave may attain a velocity of 2930 m/s (Smith, 1974b) while the velocity of the particles reportedly reached 750 m/s in the D-gun<sup>TM</sup> and 1000 m/s in the ‘Super D-gun’<sup>TM</sup>, (Irving *et al.*, 1993). Kadyrov and Kadyrov (1995) report velocities varying between 1000 and 3000 m/s.

- *Geometry of the barrel:* the length is in the range 450–1350 mm and the diameter 21–25 mm (Borisov *et al.*, 1990).
- *Firing rate* is in the range 1–15 Hz.

## Powder

- See previous sections dealing with powders.
- *Particle sizes* are usually in the range 5–60  $\mu\text{m}$ .
- *Powder type:* the most used powders are composites with carbide reinforcements.

## Powder Injection

- *Powder feed rate* is in the range 16–40 g/min (Borisov *et al.*, 1990).
- *Composition of carrier gas:* nitrogen or air (Vuoristo *et al.*, 1992).

## Principal Processing Parameters

- *Spray distance* is reported to be about 100 mm (Schwarz, 1980).
- *Spray atmosphere* is air.

### 3.5.4 COATING PROPERTIES

The porosities of D-gun<sup>TM</sup> coatings are very small: the reported values are 0.5 % for WC–Co coatings and about 2 % for  $Al_2O_3$  ones (Tucker, 1982). The tensile bond strengths were 83 and 70 MPa, respectively. The thicknesses of the detonation gun-sprayed coatings do not exceed 300  $\mu\text{m}$ .

### 3.6 HIGH-VELOCITY OXY-FUEL (HVOF) SPRAYING

#### 3.6.1 HISTORY

The HVOF torch was developed at the end of the 1970s and at the beginning of the 1980s. The principles of this technique are similar to that of the D-gun,<sup>TM</sup> with the difference in the way of burning the fuel medium in oxygen. The burning is continuous for HVOF and repetitive for D-gun.<sup>TM</sup> Many authors, Bick and Jürgens (1983) and Kreye *et al.* (1986), among others, agree that the initial work was carried out at the Thayer School of Engineering (Hanover, NH, USA) and by Browning Engineering (West Lebanon, NH, USA). The rapid development of this technique and the wide dissemination of HVOF installations have resulted from the efforts of many coating shops to obtain the high quality of D-gun<sup>TM</sup> coatings. Presently, this technique has become a standard one in the spraying of carbides and many applications in the aeronautical industry that have been previously realized using electrolytic chromium are now being replaced by carbides and alloys sprayed by the HVOF process (Grasset, 2003).

#### 3.6.2 PRINCIPLES

In the HVOF process (Figure 3.11), the fuel gas or liquid is introduced into the combustion chamber together with oxygen. An ignition initiates

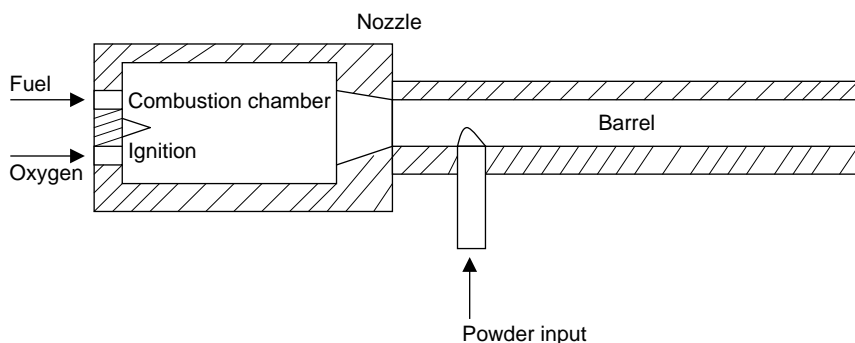


Figure 3.11 Schematic of an HVOF torch

the combustion and the exhaust gas, formed by a nozzle, passes through a barrel and emerges into the open atmosphere. The powder is introduced radially or axially into the jet. The combustion chamber, nozzle and barrel are intensively cooled by water.

Figure 3.12 shows a modern HVOF torch.



Figure 3.12 A modern HVOF torch.

### 3.6.3 PROCESS PARAMETERS

#### Flame

- The *working medium* is oxygen ( $O_2$ ) in the gaseous form and fuel, such as:
  - Hydrocarbon gases, e.g. among others, ethylene ( $C_2H_2$ ), propylene ( $C_3H_6$ ), propane ( $C_3H_8$ ) and natural gas, being a mixture of many hydrocarbons with some ‘non-hydrogen components’ (Yang *et al.*, 1995).
  - Hydrocarbon liquids, such as kerosene, which is a product of distillation of petroleum at temperatures of 320 to 550 K. Kerosene is used as a fuel in jet engines and is used in the HVOF torch JP-5000 (Praxair ST). The liquid is atomized prior to combustion.

Three main parameters determine the properties of the emerging jet, as follows:

- Pressure in the combustion chamber, which varies from about 0.3–1 MPa in a typical HVOF torch up to 4 MPa (Dvorak and Torday, 1996). The high combustion pressure results in an increase in the velocity of the sprayed particles. This increase may be most probably attributed to the greater viscosity of the flame. Moreover, the high chamber pressure (> 4 MPa) seems to be well-adapted for spraying wires (Browning *et al.*, 1995).
- Profile of the nozzle–barrel (see Figure 3.11). The following profiles are used (Sakaki and Shimizu, 2001): (i) convergent barrel; (ii) a convergent–divergent nozzle ('de Laval'); (iii) a convergent–divergent barrel. These profiles influence the pattern of the flame flow and its velocity.
- Stoichiometry of the fuel with an oxygen mixture with regard to the combustion reaction. An example of a stoichiometric reaction, for propylene as a fuel gas, is shown in following equation:



Under stoichiometric conditions, oxygen is completely burnt. Otherwise, it remains as one of the combustion products. The equivalence ratio,  $\Phi$ , is defined as follows (Swank *et al.*, 1994):

$$\Phi = \frac{F/O}{F/O_{st}} \quad (3.2)$$

The ratio  $\Phi$  is equal to 1 under stoichiometric conditions. Values of this ratio varying between 0.6 and 1.2 are practicable. At  $\Phi = 1$ , the temperatures of the flame and that of the sprayed particles were found to reach their maximum values (Swank *et al.*, 1994).

- *Flame properties:* a characteristic structure of an HVOF flame results from the 'supersonic' character of the expanding gas flow. The speed of sound is reached at the exit of the torch and expansion of the flow results in a pattern of expansion and compression waves and 'shock diamonds' which are characteristic of a supersonic flow (Oberkampf and Talpallikar, 1996a). The calculations of these authors, carried out for the 'Diamond Jet' torch, working with propylene and oxygen and

a  $\Phi$  ratio slightly lower than 1 (Oberkampf and Talpallikar, 1996b), enabled them to find a maximum flame temperature of about 2500 K and a velocity of about 1600 m/s.

A slightly greater temperature of about 3000 K and a velocity of 2000 m/s were calculated by Chang and Moore (1995) for a JP-5000 torch supplied with a liquid fuel of formula  $C_{10}H_{20}$  and oxygen under stoichiometric conditions. A similar velocity of 2000 m/s was found for the flame in a 'Jet-Kote' torch by Kreye (1991).

### Powder<sup>13</sup>

- See previous sections dealing with powders.
- *Particle sizes* are usually in the range 5–45  $\mu\text{m}$ .
- *Powder type*: the most used powders are composites with carbide reinforcements and metal or alloy matrices.

### Powder Injection

- The *injection direction* is:
  - radial inside the barrel (e.g. torch JP-5000 of Praxair ST);
  - axial into the combustion chamber (e.g. torch HV2000 of Praxair ST).
- *Powder feed rate* is in the range 20 to 120 g/min.
- *Carrier gas* is nitrogen or argon.
- *Powder feeders* are usually of the rotating-plate type.

### Principal Processing Parameters

- *Spray distance* is in the range 150 to 300 mm. This distance is a bit larger than those found during plasma spraying because of the high convective heating of the substrate.
- For other parameters, see Section dealing with processing parameters at flame spraying.

---

<sup>13</sup>The HVOF technique can also be used to spray wires. For example, Schiefer *et al.* (2002) sprayed Ni-based alloy and stainless steel using different HVOF torches and obtained low-porosity coatings.

### 3.6.4 COATING PROPERTIES

The tensile bond strengths of HVOF-sprayed carbide composites might be as high as 90 MPa (Kreye, 1991) – this value exceeds the maximum strength of most of the resins. The porosity of HVOF-sprayed coatings is lower than 1 %. Typical thicknesses are in the range 100–300 µm.

## 3.7 VACUUM PLASMA SPRAYING (VPS)

### 3.7.1 HISTORY

Credit for the development of vacuum plasma spraying (sometimes called Low-Pressure Plasma Spraying,<sup>14</sup> LPPS) is usually given to Muehlberger (1973) who was then with Plasmadyne (Santa Ana, CA, USA). A few years later, various research groups initiated the application of the VPS technique to deposit hot corrosion-resistant coatings (Wilms, 1980) and to produce pure coatings of copper (Braguier and Tueta, 1980) or tantalum (Pawlowski, 1980) for electronics applications. Today, VPS installations are available commercially and are used mainly to spray hot corrosion-resistant coatings onto gas turbines blades. On the other hand, low-pressure plasma sprayed coatings with thicknesses lower than 50 µm have become an interesting economical and technical alternative to gas-phase deposition methods, such as PVD and CVD (Loch *et al.*, 2002).

### 3.7.2 PRINCIPLES

A vacuum plasma spraying installation (Figure 3.13) is composed of a plasma torch with a nozzle (2) supplied by the working gases (1) and an electric arc generator (6). Powder is introduced by a port (5) to a plasma jet working in a vacuum (3).

An additional transferred arc (4) is used to clean up and heat the surface prior to spraying. A commercial VPS unit is shown in Figure 3.14.

---

<sup>14</sup> Some authors, e.g. Keller *et al.* (1995), make a distinction between the VPS process adapted to spray small quantities of samples and LPPS which is a continuous process.

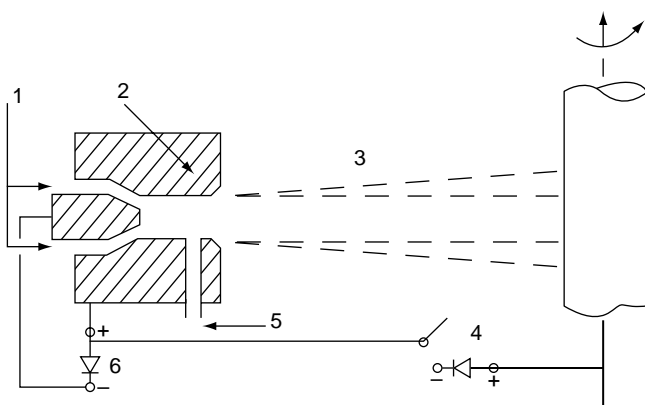


**Figure 3.13** Schematic of the vacuum plasma spraying process: (1) working gases inlet; (2) anode; (3) vacuum environment; (4) transferred arc generator (if the substrate is negatively polarized, the arc cleans up the surface, while if the substrate is positively polarized, the arc heats the surface); (5) powder injection port; (6) plasma generator



**Figure 3.14** A commercial vacuum spraying installation: (a) external view; (b) plasma torch for spraying. Reproduced by permission of Sulzer Metco AG, Wohlen, Switzerland



Figure 3.14 (Continued)

### 3.7.3 PROCESS PARAMETERS

#### Arc Plasma

- *Working gases composition:* typically Ar mixed with H<sub>2</sub>, He or N<sub>2</sub>, with a flow rate ranging from 90 to 200 slpm. The temperature of the plasma cannot be expressed by one value because the temperature of the heavy species (ions or molecules) may vary considerably from that of the electrons. Thornton (1982) estimated that the temperature of the electrons is ten times greater than that of the ions at a pressure of 130 Pa. Values for the temperature of the electrons range from 10 000 to 15 000 K, while the velocity of the plasma flow ranges from 1500 to 3500 m/s. The plasma jet is much longer than that issuing from a plasma torch into an open atmosphere and can reach 250 mm.
- *Electric power input* is substantially greater than in APS and usually more than 80 kW.
- *Geometry of anode–nozzle:*
  - A converging–diverging nozzle of the ‘de Laval’ type is often used (Henne *et al.*, 1986).
  - A *dripping anode* is an effect of agglomeration of small particles into a large molten droplet which, on spraying, may fall on to the

substrate and lower the quality of the coating. Use of a coarser powder, modification of the plasma working gas (Ar + He seems to be better than Ar + H<sub>2</sub>) and a special geometry for the anode may help in avoiding this effect (Loch *et al.*, 2002).

### Powder

- See previous sections dealing with powder.
- *Particles sizes* are usually in the range 5 to 20 µm.

### Powder Injection

- The *position of the injector* in the nozzle must be optimized. In some positions, the pressure in the nozzle would be higher than the pressure in the powder feeder and powder cannot penetrate the plasma (Vinayo *et al.*, 1985).

### Principal Processing Parameters

- *Spray distance* is in the range 300 to 400 mm.
- *Spray atmosphere* is low vacuum: the pressure prior to spraying is about 1.3 Pa, while the dynamic pressure at spraying is 655 Pa–13.3 kPa.
- *Substrate cleaning and preheating* by the transferred arc is possible in two modes of operation:
  - Positive mode (as depicted in Figure 3.13) with a positive polarity on the substrate. The effect of this polarity is an arc diffused onto all of the surface of the substrate without any particular melting spots.
  - Negative mode (substrate becomes the cathode). This mode results in melting of the substrate, especially in particular spots, which are characterized by a small electron work function. This is the case for metal oxides and thus oxides are removed from the metallic substrate in this polarization mode (Takeda *et al.*, 1990).

### 3.7.4 COATING PROPERTIES

The tensile bond strength of alloys coatings, which are most frequently deposited by using the VPS technique, is greater than 80 MPa which

renders impossible the application of a conventional epoxy resin test. The porosities of the coatings are usually lower than 1 or 2 % and a careful choice of the operational spray parameters enables the deposition of coatings without any pores. VPS deposits have typical thickness ranging from 150 to 500  $\mu\text{m}$ .

### 3.8 CONTROLLED-ATMOSPHERE PLASMA SPRAYING (CAPS)

Any spray technique having a processing atmosphere which is neither the surrounding air or at low pressure belongs to the ‘CAPS family’.

#### 3.8.1 HISTORY

Mash *et al.* (1961) and Stetson and Hauck (1961) seem to be the first who reported on plasma spraying into a chamber filled with an inert gas. Their technique can be called Inert Plasma Spraying (IPS). Another way to protect the powder-charged plasma jet against contact with the surrounding atmosphere, known as Shrouded Plasma Spraying (SPS), was developed by Okada and Maruo (1968) and Jackson (1969). They used a shielding nozzle attached to the anode of the plasma torch, in close contact with the substrate, which enables the plasma forming gases to be evacuated. More recently, this technique was used to deposit bond alloys for thermal barriers in the workshops of Union Carbide (now Praxair ST) (Taylor *et al.*, 1985). On the other hand, many of the modern VPS installations offer the possibility to work not only under vacuum but also at pressures higher than atmospheric. A commercial CAPS installation enables spraying in a ‘soft vacuum’, inert or reactive atmospheres at pressures up to 2000 hPa (Jäger *et al.*, 1992). Finally, an interesting technique, offering the possibility for simultaneous control of the spray atmosphere and substrate temperature was proposed by Ducos (1989). This technique is known as Atmosphere Temperature-Controlled Spraying (ATCS).

#### 3.8.2 PRINCIPLES

A commercial CAPS installation is shown in Figure 3.15. The plasma torch is similar to that used for atmospheric plasma spraying. The spraying process takes place inside a chamber having walls that can

withstand pressures up to 0.4 MPa. Manipulations inside the chamber are made with the help of a robot for the plasma torch and a turntable for the sprayed parts (Keller *et al.*, 1995).



**Figure 3.15** A commercial CAPS installation. Reproduced by permission of Centro Sviluppo Materiali (CSM) S.p.A, Rome, Italy and the University of Rome 1, Rome, Italy

An ATCS installation also includes nozzles for cooling of the sprayed parts (Figure 3.16).

### 3.8.3 PROCESS PARAMETERS

#### Arc Plasma

- See previous sections dealing with powders.
- The typical geometry of the shielding nozzle attached to the plasma torch in the SPS technique is an angle of 10°–18° with regard to the axis and a length of 90 to 110 mm (Okada and Maruo, 1968).

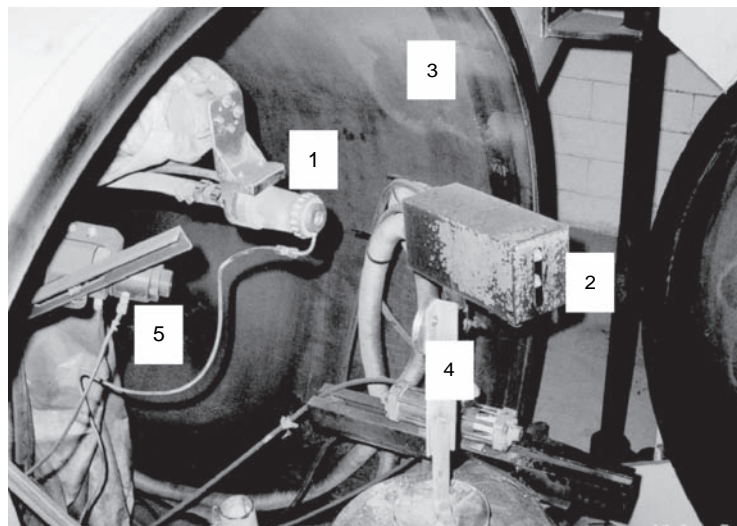


**Figure 3.16** A commercial ATCS installation: (1) plasma torch; (2) cryogenic gas cooling nozzles; (3) shielding chamber; (4) substrate; (5) pyrometer. Reproduced by permission of Centro Sviluppo Materiali (CSM) S.p.A, Rome, Italy

## Powder

- Powders sprayed by IPS or SPS are generally easy to oxidize (e.g. Ti, W – Keller *et al.*, 1995 or Ta – Pawlowski, 1975) or toxic (e.g. Be – Stetson and Hauck, 1961).
- The ATCS technique was tested for spraying  $ZrO_2 + Y_2O_3$  powders because of the generation of coating microstructures, thus enhancing the thermal shock resistance (Cosack *et al.*, 1992).

## Principal Processing Parameters

- *Spraying distance*: 100–130 mm in the SPS technique (Okada and Maruo, 1968) and 100–250 mm when using the IPS or ATCS techniques (depending on the pressure in the chamber).
- *Shielding gases* in the SPS technique: He or  $N_2$ .
- *Shielding gases flow rates* in the SPS technique: 50–150 slpm.
- *Spraying atmosphere* in the IPS and ATCS techniques: Ar, He or  $N_2$ , to which is added the working gas.

- *Cryogenic liquid flow rate* in the ATCS technique is in the range 1.8–2.5 l/min and the liquid is atomized with a gas of the same chemical composition, having a typical flow rate of 300 slpm (Cosack *et al.*, 1992).

### 3.8.4 COATING PROPERTIES

The tensile bond strengths of SPS-deposited coatings are in the range 20–45 MPa (WC–Co and NiCrSiB coatings – Okada and Maruo, 1968). The coating thicknesses and porosities are similar to those found in the APS techniques; however, the metallic coatings deposited with all of these techniques under an inert atmosphere contain less oxygen. The ATCS-deposited oxides can be sprayed to achieve greater thicknesses (1000–2000 µm) without any structural defects.

## 3.9 COLD-GAS SPRAYING METHOD (CGSM)

### 3.9.1 HISTORY

The cold-gas spraying method was developed in Novosibirsk, Russia at the end of the 1980s by Alkhimov *et al.* (1990). This research team worked on the design of high-speed ‘re-entry vehicles’ and during the experiments, using a supersonic wind tunnel with metal tracer particles, it was observed that sometimes the particles build up a coating on the target instead of eroding it (Steenkiste and Smith, 2003). The process was patented in Europe<sup>15</sup> and in the United States<sup>16</sup> and, starting from 1994, one of the inventors, Professor Papyrin, joined a consortium under the auspices of the National Center for Manufacturing Sciences, Ann Arbor, MI, USA. This consortium included several major American companies, e.g. Ford, General Electric and General Motors and studied the possibilities of technological development of the CGSM process (McCune *et al.*, 1995). At present, there are two companies that have commercialized CGSM installations:

<sup>15</sup> Allkimov, A.P., Papyrin, A.N., Kosarev, V.F., Nesterovich, N.I. and Shushpanov, M.M. (1995). Method and device for coating, *European Patent 0 484 533 B1*, January 25.

<sup>16</sup> Allkimov, A.P., Papyrin, A.N., Kosarev, V.F., Nesterovich, N.I. and Shushpanov, M.M. (1994). Gas-dynamic spray method for applying a coating, *US Patent 5 302 414*, April 12.

- CGT, Ampfing, Germany.
- K-Tech, Albuquerque, NM, USA.

### 3.9.2 PRINCIPLES

A typical cold-spraying system is shown schematically in Figure 3.17. The gas, typically N<sub>2</sub> or He, is compressed to 3.5 MPa and heated to 873 K by a heating coil. After introduction to a convergent-divergent nozzle, the working gas expands to reach ‘supersonic velocities’. The powder is injected into a nozzle ‘throat’ and its particles are accelerated to high velocities and heated to temperatures well below the melting point. Figure 3.18 shows a commercial CGSM installation.

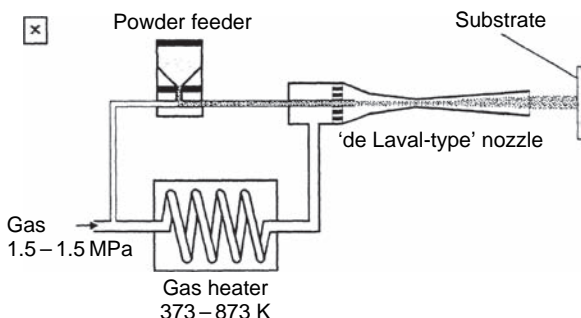


Figure 3.17 Principles of the cold-gas spraying method (after Stoltenhoff *et al.*, 2002)

### 3.9.3 PROCESS PARAMETERS

#### Working Gases

- *Chemical composition:* air, N<sub>2</sub>, He and their mixtures. More types of powders can be sprayed if He is used as a working gas. This gas is, however, expensive and helium recovery equipment seems to be necessary in industrial applications (Lauricelle and Jaynes, 2003). Such a system enables more than 95 % of general recovery but spraying should be made in a closed tank.<sup>17</sup>

<sup>17</sup> Heinrich, P. and Krömmmer, W. (2002). Cold spraying and ways to recycle helium, Catalogue of Linde AG, Unterschleissheim, Germany.



Figure 3.18 External view of a commercial vacuum spray installation. Reproduced by permission of Cold Gas Technology (CGT) GmSH, Ampfing, Germany

- *Working gas flow rate:* values of 18–20 g/s for air are reported (Steenkiste and Smith, 2004). A gas heater in the CGT set-up enables gas volumes of 90 m<sup>3</sup> to be heated to an operating temperature in less than 1 min (Richter *et al.*, 2002).
- *Pressure and temperature:* values ranging from 1.4 To 2.5 MPa of inlet gas pressure and outlet gas temperatures up to 1000 K are reported (Stoltenhoff *et al.*, 2002).

## Nozzle

The nozzle has a converging–diverging profile ('de Laval'). The hot gas has sonic velocities in the convergent region and supersonic velocities in the divergent region. The nozzle exits are usually cylindrical but rectangular ones have also been reported (size 2 × 10 mm or 5 × 12.5 mm) by Steenkiste and Gorkiewicz (2004).

## Powder

- *Selection criteria:* only the powders of materials than can deform plastically can be sprayed by using present CGSM installations. As ceramics do not deform in this way and polymers

do not represent any interest for processing by cold spraying, the remaining class of materials corresponds to metals and alloys. Metals of one crystal structure have similar deformation behaviour. The following groups of metals can be distinguished (Vlcek *et al.*, 2003):

- f.c.c.-structure metals, such as Al, Cu, Ag, Au, Pt, Ni and  $\gamma$ -Fe;
- b.c.c.-structure metals, such as W, Ta, Mo, Nb, V, Cr,  $\alpha$ -Fe and  $\beta$ -Ti;
- h.c.p.-structure metals, such as Cd, Zn, Co, Mg and Ti.

The f.c.c. metals have a large number of sliding planes which explains their good deformability. The h.c.p. metals have lesser deformability, while the b.c.c. metals have the lowest deformability. Another indicator of sprayability is the melting point. The low value of  $T_m$  is beneficial for the ability to spray. On the other hand, materials that harden under mechanical stress, such as the stainless steel 317L or the alloy TiAl8V4, are difficult to spray. In practice, the most popular material sprayed by CGSM is Cu. Important technological metals and alloys, such as Ta, NiCr, NiCrAlY or CuAl, have been successfully processed by this technique. Helium was used to spray most of these. Coatings of metal-ceramic composites, such as NiCr + Cr<sub>3</sub>C<sub>2</sub>, have also been obtained in this way (McCune *et al.*, 1995).

- *Particle sizes:* these are generally similar to those used in the VPS technique, i.e. in the range of 5–20  $\mu\text{m}$ . Small-size particles are better adapted to be processed, but they are difficult to be fed in a constant way. Greater-size particles (up to 200  $\mu\text{m}$ ) were reportedly successfully processed (Steenkiste and Smith, 2004).
- *Particle temperatures and velocities:* values of  $T_p = 500\text{ K}$  and  $v_p = 600\text{ m/s}$  were calculated for Cu particles (15  $\mu\text{m}$ ) with an optimized initial working gas (nitrogen) pressure and temperature (Stoltenhof *et al.*, 2002).
- *Powder injection* is axial in most installations.

## Substrate

Coatings were successfully sprayed onto metallic and ceramic substrates. Substrate roughening is not necessary and a well-adhering coating can be sprayed onto polished surfaces.

## Principal Processing Parameters

The following processing parameters influence quality of the coatings in the most significant way (Freslon, 2003; Steenkiste and Smith, 2004):

- Working gas temperature;
- Working gas pressure;
- Working gas composition (He, N<sub>2</sub> or air);
- Size distribution of powder particles;
- Spray distance;
- Nozzle type.

### 3.9.4 COATING PROPERTIES

The tensile bond strengths of CGSM coatings were reported to be 26–44 MPa for Cu and 33–35 MPa for Al, and the porosities of these deposits were 4.5 and 3.7 %, respectively (Steenkiste and Smith, 2004). Values in the range 26 to 62 MPa were reported for Ta by Steenkiste and Gorkiewicz (2004). The thicknesses of the deposits vary from 250 µm (NiCr) to 650 µm (Al), according to Stoltenhoff *et al.* (2002). These authors found that the oxygen content increased only slightly from 0.10 % in the initial NiCr powder to 0.12 % in the sprayed coating.

## 3.10 NEW DEVELOPMENTS IN THERMAL SPRAY TECHNIQUES

Developments in spray techniques follow, in general, the lines shown in Section 3.1 and the needs of a particular application, such as:

- Coatings onto small areas deposited by a microplasma;
- Coatings inside cylinder bores obtained by the ‘RotaPlasma™’ technique.

Non-conventional plasma torches have been discussed recently by Fauchais *et al.* (2001). The techniques of thermal spraying that seem to have the most promising future are as follows:

- A torch with the axial injection of a powder has been under development over a long period of time at The University of Limoges in the group of Professor Fauchais. Studies made in this laboratory used a hollow cathode in a DC plasma torch (Vardelle *et al.*, 1994). Powder feeding was, however, often stopped at the high-temperature cathode tip which necessitated replacement of the entire cathode. The resulting electrode lifetime was too short for industrial applications. The breakthrough came from the Northwest University in Vancouver, BC, Canada. This consisted of using a powder injector placed between three cathodes. Axial III™ has been commercialized by Northwest Mettech in Richmond, BC, Canada. The Axial III™ process uses plasma-forming gases, i.e. a mixture of Ar + N<sub>2</sub> + H<sub>2</sub> with a total flow rate of 240 slpm and an arc current of about  $I = 150\text{ A}$  (Burgess, 2002). The torch enables spraying of up to 150 g/min alumina using the Axial III™ technique, following the Mettech catalogue.
- A torch with three cathodes in which the total arc is divided in to three separated arcs (Figure 3.19).

The Triplex™ torch has been commercialized by Sulzer Metco AG, Wohlen, Switzerland and was developed by Professor Landes (Landes, 1992). At present, this torch is ‘rented’ to company customers (Barbezat, 2003). As far as the Triplex™ torch is concerned, it operates with a total arc current varying from  $I = 200$  to  $600\text{ A}$  and a voltage varying from  $U = 45$  to  $100\text{ V}$ , respectively. The plasma-forming gases are Ar + He and the maximum flow rate is about 60 slpm for Ar and 40 slpm for He (Zierhut *et al.*, 1998). The fluctuations of the arc are smaller, which reduces the ‘noise’ of the system to 90 dB. This torch enables a very high powder throughput, reported to be, for Al<sub>2</sub>O<sub>3</sub>,  $q_p = 120\text{ g/min}$  for the Triplex™ torch (Barbezat *et al.*, 1999).

- Suspension or liquid spraying is a technical solution for obtaining coatings having fine microstructures. Spraying of fine powders is not an appropriate way to obtain such coatings. This is due to the pneumatic transport of small powder particles which are not stable for particle sizes of 5–10 μm and finer. Smaller powder particles, especially those of ceramic materials, cannot be used in conventional feeders. An illustration of liquid plasma spraying is shown in Figure 3.20, while a view of a suspension atomizer attached to a plasma torch is given in Figure 3.21.

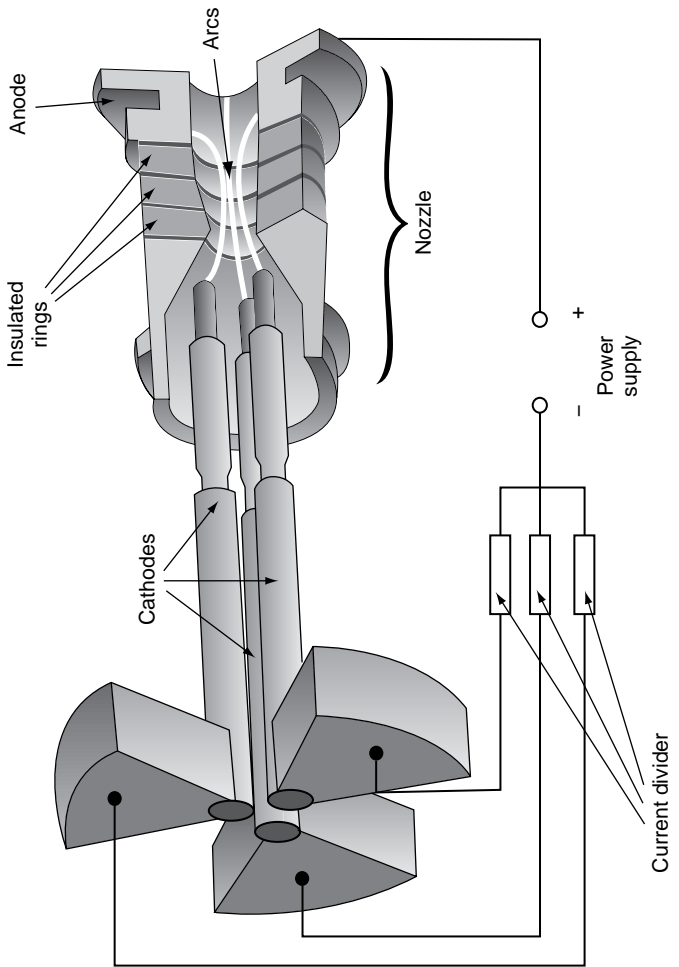


Figure 3.19 Construction of a three-cathode torch (Zierhut *et al.*, 1998). Reproduced by permission of ASM International from J. Zierhut *et al.* (1998), 'Triplex – an innovative three-cathode plasma torch', in *Thermal Spray: Meeting the Challenges of the 21st Century*, C. Coddet (Ed.), ASM International, Materials Park, OH, USA, pp. 1419–1424

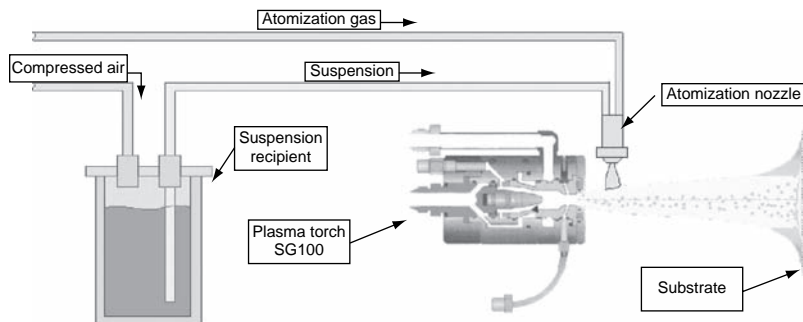


Figure 3.20 Principle of suspension/solution plasma spraying

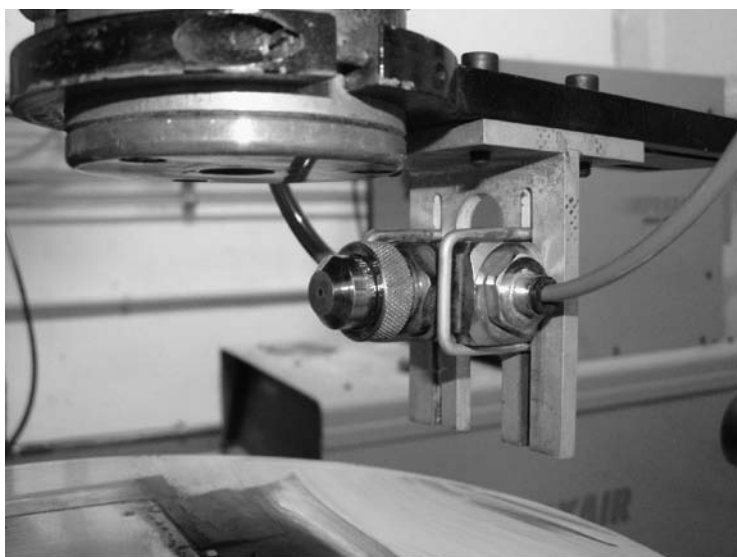


Figure 3.21 A suspension atomizer attached to a commercial plasma torch (Tomaszek and Pawlowski, 2004). The arrangement installed in Ecole Nationale Supérieure de Chimie de Lille, Villeneuve d'Ascq, France

Materials that can be sprayed in the form of a suspension are shown in Table 3.2. Two possibilities can be considered:

- Preparation of solution of liquid precursors, typically metal-organics, such as aluminium nitrate (see (2) in Table 3.2), which react in the flame or jet, resulting in the formation of small solid particles.
- Preparation of a suspension of fine solid particles having the ‘final’ composition of the coating. This possibility enables the transfer of

**Table 3.2** Preparation of solutions of liquid precursors for thermal spraying

Number	Area of application	Composition of solution	Spraying technique	Post-spraying treatment	Final coating	Reference
1	Electric insulation	aluminium isopropoxide with distilled water and nitric acid	APS	Annealing at 873–1273 K in air	AlOOH, $\gamma\text{-Al}_2\text{O}_3$ , $\delta\text{-Al}_2\text{O}_3$	Karthikeyan <i>et al.</i> , 1998
2	Electric insulation	$\text{Al}(\text{NO}_3)_3 \cdot 9\text{H}_2\text{O}$	FS	No	$\alpha\text{-Al}_2\text{O}_3$	Tikkannen <i>et al.</i> , 1997
3	Heat insulation, TBC	Aqueous solution of zirconium and yttrium salts	APS	No	Tetragonal $\text{ZrO}_2$	Padture <i>et al.</i> , 2001; Bhateria <i>et al.</i> , 2002; Xie <i>et al.</i> , 2003

knowledge gained in the area of preparation of powders by spray drying of slurry (Masters, 1985).

Coatings sprayed using liquids or suspensions have much finer surfaces than those sprayed using powders. They are also thinner and need more combustion or electrical energy to be sprayed. This results from the fact that a considerable part of the energy is used to evaporate the liquid. The most important area of application of solution or suspension thermal spraying are nano-structured coatings which have improved mechanical or electrical properties. An important advantage is a possible cost-saving. In fact, the smooth surfaces of suspension-sprayed coatings may render it unnecessary to use post-spray mechanical finishing. Finally, suspension spraying may be the last step in powder spraying as the spray torch with the sprayed material remains the same. The resulting coatings would have a gradient of crystal grain size (Tomaszek and Pawłowski, 2004).

- Rotating torches to spray inside cylinders. These torches have been commercialized by Sulzer Metco, Wohlen, Switzerland as RotaPlasma™ and their major application is to coat the cylinder bores of car motors (Barbezat, 2004).
- Microplasma spray torches having jet diameters between 2 and 4 mm and lengths between 30 and 50 mm which can be used to coat small surfaces with less-refractory materials (Fauchais *et al.*, 2001; Li and Sun 2004).

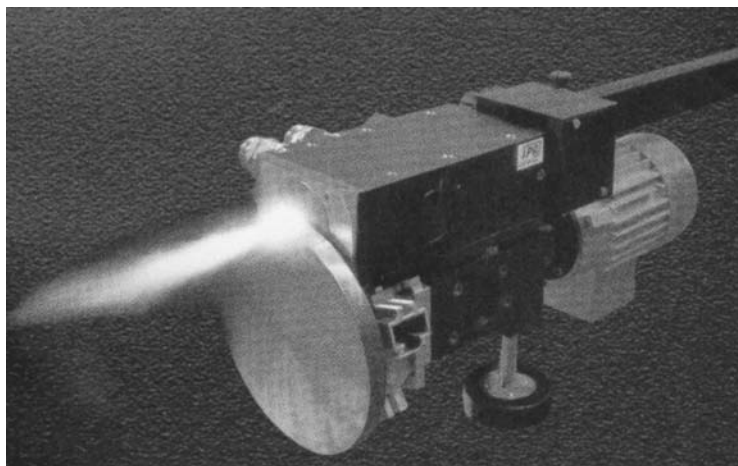


Figure 3.22 A water-stabilized plasma spray torch type WSP 500. Reproduced by permission of HAI Advanced Material Specialists, Inc., Santa Fe Springs, CA, USA

- Torches with a laminar flow of argon having a long plasma column, resulting in arc voltages in the range 60–80 V and arc currents in the range 500–600A (Fauchais *et al.*, 2001; Ma *et al.* 2005).
- Water-stabilized torches (Figure 3.22) which use water vapour as the plasma working gas. Although the principle of this torch has been known for many years (Zverina and Vesely, 1976), missing ‘legal consensus’ with regard to commercialization among the inventors has hampered implementation of this technology (Chraska, 2003). Such problems now seem to have been solved and the torch is currently being commercialized in the USA. Its major application could be spraying of oxide ceramics with high powder throughput that may reach 1000 g/min (WSP 500, 1997). This torch is very well-adapted to spray coating onto large rollers in the printing and paper industries.
- RF plasma spraying which is characterized by a large internal nozzle diameter that can reach 50 mm (6–8 mm being the ID of a typical dc torch). As the electrode of an RF torch is a coil external to the nozzle, the sprayed coatings are not contaminated by the products from electrode wear (Nutsch and Dzur, 1996). The plasma jet in a typical installation is much slower (15 to 25 times) than in a DC one. Contact with the surrounding atmosphere can be easily avoided, what may render RF-sprayed coatings virtually oxygen-free. On the other hand, the RF process uses large particles (up to 150 µm) and can be

considered for the manufacturing of 'bulk' pieces of metal. The next step in this technology, considered by Professor Boulos and his group from Sherbrooke University and his company Techna (Sherbrooke, Qu, Canada), is RF spraying in vacuum (Mailhot *et al.*, 1998). The nozzle has a 'de Laval' profile with a critical 'throat' diameter of 10 mm and the dynamic pressure at spraying is about 470 hPa. The installation was successfully tested for the spraying of dense YSZ coatings, aiming at applications in SOFC.

- High-energy torches for spraying were initially reported by Morishita and Whitfield (1988), Morishita (1991) and Bunya *et al.* (1992). The latter study describes a twin-anode torch. High-energy<sup>18</sup> plasma spraying is a technology that uses torches designed in such a way to increase the distance between the cathode and anode. This is usually achieved by 'anode segmentation'. An arc is initiated between the cathode and the 'closest segment' of the anode and is then transferred to the second anode. Consequently, the voltage between the anode and cathode increases (up to 400–500 V with an arc current of about 500 A in, e.g. the Plazjet™ torch) and the electric energy input to 'plasma working' is greater. The flow rate of the plasma working gases reaches 500 slpm, which increases the volume of the plasma and makes it possible to reach a high powder throughput of 150 g/min by a spray distance ranging between 18 and 28 cm (Jungklaus *et al.*, 1996). The technology is well-adapted to coat large rollers with ceramic coatings, in competition with water-stabilized plasmas in this market segment. The sprayed coatings exhibit excellent properties and values close to the absolute record of hardness of thermal spray coatings of HV 3 = 1775 and HV 3 = 2100 were reported for Cr<sub>2</sub>O<sub>3</sub> by Jungklaus *et al.* (1996) and Plazjet (1995), respectively.
- Underwater plasma spraying (UPS) was initiated at The Heriot-Watt University, Edinburgh, UK (Waldie and Harris, 1983) and at The Technical University of Aachen, Germany (Lugscheider and Bugsel, 1988). Typical arc plasma torches are used with slightly higher working gas flow rates and much lower spraying distances (around 20 mm). This technique makes possible off-shore and underwater coating deposition. The underwater spraying methods can be roughly categorized as follows: (Minami *et al.*, 1998):
  - *Dry methods*, in which a chamber protects the processing 'space'. A drawback of this method is its high cost.

---

<sup>18</sup> Sometimes, this technique is known as high-enthalpy plasma spraying.

- *Wet methods*, in which a cavity of smaller or greater size protects the processing ‘space’. Protection can be assured by compressed air or a water ‘curtain’ realized with the aid of a double-walled tube attached to the torch nozzle, at a distance of a few millimetres from the sprayed substrate.

The processing ‘space’ is filled with the plasma-forming gas, which makes it possible to spray oxidizing materials, such as Ti, with reasonably quality.

- Pulsed plasma spraying was developed by Vollrath *et al.* (1992). In this torch, an electronic switch transferred the arc with a frequency of up to 2 kHz from the closest anode to the furthest one. The torch and associated rights was bought by one of the major company producing spray equipment and, subsequently, then ‘hidden away’ in order to avoid competition with their torches. Another technique, based on the principle of a pulsed plasma has been reported recently by Whitterspoon *et al.* (2002). This technique uses a high-energy electric arc discharge in a small insulating capillary which heats the working gas to temperatures above 11600 K and increases the local pressure to more than 100 MPa. The created plasma expands in a barrel, in a way similar to that in the detonation gun technique. The sprayed powder is placed in the barrel just at the exit of the capillary. The discharges use energies from  $E = 1\text{ J}$  to  $1\text{ MJ}$ , which gives instantaneous powers ranging from  $P = 100\text{ kW}$  to  $1\text{ GW}$ . The technique was tested experimentally for a pulse rate of 1 Hz and the powder particles reached velocities above  $v_p = 2000\text{ m/s}$ . If further developed, this technique would be competing with the D-gun<sup>TM</sup> and HVOF techniques in the market segment of wear-resistant carbide spraying.

## REFERENCES

- Alkhimov, A.P., Kosarev, V.F. and Papyrin, A.N. (1990). Method of cold gas-dynamic deposition *Sov. Phys. Dokl.*, 35(12), 1047–1049 Transl. American Inst. of Phys., 1991
- Barbezat, G. (2003). Personal Communication.
- Barbezat, G. (2004). Application des dépôts projetés dans l’industrie automobile, in *Projection Thermique: Procédés, Revêtements, Applications*, Post-graduate formation MS12 of CNAM CACEMI, Paris, 21–22 October.
- Barbezat, G., Zierhut, J. and Landes, K.D. (1999). Triplex – a high performance plasma torch, in *United Thermal Spray Conference*, E. Lugscheider and P.A. Kammer (Eds), DVS, Düsseldorf, Germany, pp. 271–274.

- Bhatia, T., Özturk, A., Xie, L., Jordan, E.H., Gell, M., Ma, X. and Padture, N.P. (2002). Mechanism of ceramic coating deposition in solution–precursor plasma spray, *J. Mater. Res.*, **17**, 2363–2372.
- Bick, H. and Jürgens, W. (1983). Advanced high velocity thermal spraying of metallic and ceramic powders, in *Proceedings of the 10th International Thermal Spray Conference*, DVS, Düsseldorf, Germany, pp. 92–94.
- Borisov, Yu.S., Stachov, E.A. and Klimenko, V.S. (1990). Detonation spraying: equipment, materials and applications, in *Thermische Spritzkonferenz TS90*, Vol. 90, DVS, Düsseldorf, Germany, pp. 26–32.
- Bouyer, E., Henne, R., Müller-Steinhagen, H., Schäfer, D. and Asano, H. (2003). Improved heat transfer by RF plasma produced structured surfaces, in *Thermal Spray: Advancing the Science and Applying the Technology*, C. Moreau and Marple B. (Eds), ASM International, Materials Park, OH, USA, pp. 559–566.
- Braguier, M. and Tueta, R. (1980). Supersonic and vacuum arc plasma spraying apparatus characteristics and application to metallic coatings, in *Proceedings of the 9th International Thermal Spray Conference*, Nederlands Instituut voor Lastechniek, The Hague, Netherlands, pp. 167–72.
- Browning, J.A., Matus, R.J. and Richter, H.J. (1995). A new HVOF thermal spray concept, in *Thermal Spraying Current Status and Future Trends*, A. Ohmori (Ed.), High Tempere. Soc. Japan, Osaka, Japan, pp. 7–10.
- Bunya, A., Tateno, H., Kitoh, M., Fukami, S., Itoh, T. and Nagasaka, H. (1992). A plasma spraying system with two cathodes, in *Thermal Spray: International Advances in Coatings Technology*, C.C. Berndt (Ed.), ASM International, Materials Park, OH, USA, pp. 99–110.
- Burgess, A.W. (2002). Hastelloy C-276 parameter study using the axial III plasma spray system, in *Proceedings of the International Thermal Spray Conference 2002 Essen*, E. Lugscheider and C.C. (Eds), Berndt DVS Verlag, Düsseldorf, Germany, pp. 516–518.
- Carlson, R. and Heberlein, J. (2001). Effects of operating parameters on high definition single wire arc spraying, in *Thermal Spray 2001: New Surfaces for a New Millennium*, C.C. Berndt, K.A. Khor and E. Lugscheider (Eds), ASM International, Materials Park, OH, USA, pp. 447–453.
- Chang, C.H. and Moore, R.L. (1995). Numerical simulation of gas and particle flow in a HVOF torch, *J. Therm. Spray Technol.*, **4**, 358–366.
- Chraska, P. (2003). Personal Communication.
- Cosack, T., Pawłowski, L., Schneiderbanger, S. and Sturlese, S. (1992). TBC on turbine blades by plasma spraying with improved cooling, in *Proceedings of 37th ASME Int. Gas Turbine & Aeroengine Congress and Exposition*, Köln, Germany, June 1–4, ASME, New York, NY, USA, paper 92-GT-319.
- Deram, V., Minichiello, C., Vannier, R.N., Le Maguer, A., Pawłowski, L. and Murano, D. (2002). Microstructural characterizations of plasma sprayed hydroxyapatite coatings, *Surf. Coat. Technol.*, **166**, 153–159.
- Dorier, J.-L., Hollenstein, C., Salito, A., Loch, M. and Barbezat, G. (2000). Influence of external parameters on arc fluctuations in a F4 dc plasma torch used for plasma spraying, in *Thermal Spray: Surface Engineering via Applied Research*, C.C. Berndt, (Ed.), ASM International, Materials Park, OH, USA, pp. 37–43.
- Drzeniek, H. and Steffens, H.-D. (1987). Cored tube wires for arc and flame spraying, in *Thermal Spray: Advances in Coatings Technology*, D.L. Houck (Ed.), ASM International, Materials Park, OH, USA, pp. 33–40.

- Ducos, M. (1989). Atmosphere and temperature controlled plasma spraying thick coatings and coating on composite resin fibre, in *12th International Thermal Spray Conference*, The Welding Institute, Abington Hall, Abington Cambridge CB1 GAL, UK, Paper 66.
- Dvorak, M. and Torday, R. (1996). HVOF coatings produced at increased combustion chamber pressures, in *Thermische Spritzkonferenz TS96*, Vol. 175, DVS, Düsseldorf, Germany, pp. 6–9.
- Fauchais, P., Vardelle, A. and Dussoubs, B. (2001). Quo vadis plasma spraying?, in *Thermal Spray 2001: New Surfaces for a New Millennium*, C.C. Berndt, K.A. Khor, and E. Lugscheider (Eds), ASM International, Materials Park, OH, USA, pp. 4–5.
- Fisher, I.A. (1972). Variables influencing the characteristics of plasma sprayed coatings, *Int. Metal. Rev.*, 17, 117–129.
- Freslon, A. (2003). Dépôts résistants à la corrosion par la projection à froid, in *1st International Meeting on Thermal Spraying*, L. Pawłowski (Ed.), ENSCL, Lille, France, 3–4 December, pp. 185–185 unpublished conference proceedings.
- Fridlyand, M.G. (1995). Effect of reactive plasma-forming gases on plasma spray operating conditions: a technical note, *J. Therm. Spray Technol.*, 4, 137–142.
- Fukushima, T. and Kuroda, S. (2001). Oxidation of HVOF sprayed alloy coatings and its control by a gas shroud, in *Thermal Spray 2001: New Surfaces for a New Millennium*, C.C. Berndt, K.A. Khor and E. Lugscheider (Eds), ASM International, Materials Park, OH, USA, pp. 527–532.
- Gage, R.M., Nestor, D.M. and Yenni, Y.M. (1962). Collimated electric arc powder deposition process, *US Patent*, 3 016 447.
- Gerdien, H. and Lotz, A. (1922). *Wissen. Veröffen. Siemens Werken*, 2, 489–496.
- Giannini, G. and Ducati, A. (1960). Plasma stream apparatus and method, *US Patent* 2 922 869.
- Grasset, G. (2003). Projection thermique et codéposition électrolytique, deux alternatives, in *1st International Meeting on Thermal Spraying*, L. Pawłowski (Ed.) ENSCL, Lille, 3–4 December, pp. 197–202 unpublished conference proceedings.
- Henne, R., von Bradke, M., Schnurnberger, W. and Weber, W. (1986). Development and manufacture of electrolyzer components applying plasma under reduced pressure, in *Advances in Thermal Spraying*, Pergamon Press, New York, NY, USA, pp. 61–71.
- Ingham, H.S., Jr and Fabel, A.J. (1975). Comparison of plasma spray gases, *Weld. J.*, 54, 101–105.
- Irving, R., Knight, R. and Smith, R.W. (1993). The HVOF process – the hottest topic in the thermal spray industry, *Weld. J.*, July, 25–30.
- Jackson, J.E. (1969). Method of shielding gas effluent, *US Patent* 347 347.
- Jäger, D., Stover, D. and Schlump, W. (1992). High pressure plasma spraying in controlled atmosphere up to two bars, in *Proceedings of the 13th International Thermal Spray Conference*, C.C. Berndt (Ed.), ASM International, Materials Park, OH, USA, pp. 69–74.
- Janisson, S., Vardelle, A., Coudert, J.F., Meillot, E., Pateyron, B. and Fauchais, P. (1999). Plasma spraying using Ar–He–H<sub>2</sub> gas mixtures, *J. Therm. Spray Technol.*, 8, 545–552.
- Jugklaus, H., Lugscheider, E., Schwier, G., Heinrich, P. and Mathesius, H. (1996). Ceramic coatings by high power plasma spraying (HPPS), in *Thermische Spritzkonferenz TS96*, Vol. 175, DVS, Düsseldorf, Germany, pp. 44–48.
- Kadyrov, V. (1988). Detonation gas powder technique, in *Proceedings of the International Symposium on Advances in Thermal Spraying Technologies and Allied Coatings*, High Temperature Society of Japan, Osaka, Japan, pp. 43–48.

- Kadyrov, E. and Kadyrov, V. (1995). Gas dynamical parameters of detonation powder spraying, *J. Therm. Spray Technol.*, **4**, 280–286.
- Karthikeyan, J., Berndt, C.C., Reddy, S., Wang J.-Y., King, A.H. and Herman, H. (1998). Nanomaterial deposits formed by DC plasma spraying of liquid feedstock, *J. Am. Ceram. Soc.*, **81**, 121–128.
- Keller, S., Tommer, P., Clarke, R. and Nicoll, A.R. (1995). Key factors in the development of plasma spray systems and the spray process, in *Thermal Spraying – Current Status and Future Trends*, A. Ohmori (Ed.), High Temperature Society of Japan, Osaka, Japan, pp. 275–281.
- Kreye, H. (1991). High velocity flame spraying – process and coating characteristics, in *2nd Plasma-Technik-Symposium*, Blum-Sandmaier, S., Eschnauer, H., and Nicoll, A.R. (Eds), Vol. 1, Plasma Technik, Wohlen, Switzerland, pp. 39–47.
- Kreye, H., Fandrich, D., Müller, H.-H. and Reiners, G. (1986). Microstructure and bond strength of WC-Co coatings deposited by hypersonic flame spraying, in *Advances in Thermal Spraying*, Pergamon Press, New York, NY, USA, pp. 121–128.
- Landes, K. (1992). Plasmaspritzgerät zum Versprühen von festen, pulverförmigem oder gasförmigen Material *German Patent*. DE 41 05 407 A1 of 21 February.
- Lauricelle, F. and Jaynes, S. (2003). Helium recovery: design consideration for cold spray systems, in *Thermal Spray 2003: Advancing the Science, Applying the Technology*, C. Moreau and B. Marple (Eds), ASM International, Materials Park, OH, USA, pp. 113–116.
- Li, C.-J. and Sun, B. (2004). Microstructure and property of Al<sub>2</sub>O<sub>3</sub> coating microplasma sprayed using a novel hollow cathode torch, *Mater. Lett.*, **6**, 179–183.
- Loch, M., Barbezat, G. and Meyer, P. (2002). Progress in the area of low pressure plasma spraying, in *ITSC 2002 Essen, Proceedings of the International Thermal Spray Conference* E. Lugscheider and C.C. Berndt, (Eds), DVS Verlag, Düsseldorf, Germany, pp. 347–350.
- Lugscheider, E. and Bugsel, B. (1988). Underwater plasma spraying, in *1st Plasma-Technik-Symposium*, Vol. 3, Eschnauer H., Huber P., Nicoll A.R., Sandmaier S., (Eds.) Plasma Technik, Wohlen, Switzerland, pp. 55–62.
- Ma, W., Pan, W.X. and Wu, C.K. (2005). Preliminary investigations on low pressure plasma spray processing, *Surf. Coat. Technol.*, **191**, 166–174.
- Mailhot, K., Gitzhofer, F. and Boulos, M.I. (1998). Supersonic induction plasma spraying of yttria stabilised zirconia films, in *Thermal Spray, Meeting the Challenges of the 21st Century*, C. Coddet (Ed.), ASM International, Materials Park, OH, USA, pp. 1419–1424.
- Marantz, D.R. (1974). The basic principles of electric-arc spraying, in *The Science and Technology of Surface Coatings*, B.N. Chapman and J.C. Anderson, (Eds), Academic Press, London, UK, pp. 308–321.
- Mash, D.R., Weare, N.E. and Walker, D.L. (1961). Process variables in plasma jet spraying, *J. Met.*, **4**, 473–478.
- Masters, K. (1985). *Spray Drying Handbook*, George Godwin, London, UK.
- McCune, R.C., Hall, J.N., Papirin, A.N., Riggs II, W.L. and Zajchowski, P.H. (1995). An exploration of the cold gas-dynamic spray method for several materials systmes, in *Advances in Thermal Spray Science and Technology*, C.C. Berndt and S. Sampath (Eds), ASM International, Materials Park, OH, USA, pp. 1–5.

- Minami, N., Hongawa, T., Nojiri, Y., Nishida, Arata, T. and Katsumura M. (1998). Study on underwater thermal spraying, in *Thermal Spray, Meeting the Challenges of the 21st Century*, C. Coddet (Ed.), ASM International, Materials Park, OH, USA, pp. 1381–1386.
- Morishita, T. (1991). Coatings by 250 kW plasma jet spray system, in *2nd Plasma-Technik-Symposium*, Vol. 1, Plasma Technik, Wohlen, Switzerland, pp. 137–142.
- Morishita, T. and Whitfield, R.W. (1988). Study on extended-arc plasma jet spray system at 175 kW, in *Proceedings of the International Symposium on Advances in Thermal Spraying Technologies and Allied Coatings*, High Temperature Society of Japan, Osaka, Japan, pp. 95–98.
- Muehlberger, E. (1973). A high energy plasma coating process, in *Proceedings of the 7th International Metal Spraying Conference*, The Welding Institute, Cambridge, UK, pp. 245–256.
- Nutsch, G. and Dzur, G. (1996). Plasma spraying with inductively coupled plasma as a process variation of the atmospheric plasma spraying, in *Thermische Spritzkonferenz TS96*, Vol. 175, DVS, Lugscheider E. (Ed.) Düsseldorf, Germany, pp. 48–52.
- Oberkampf, W.L. and Talpallikar, M. (1996a). Analysis of a HVOF thermal spray torch. Part 2: computational results, *J. Therm. Spray Technol.*, **5**, 62–68.
- Oberkampf, W.L. and Talpallikar, M. (1996b). Analysis of a HVOF thermal spray torch. Part 1: numerical formulation, *J. Therm. Spray Technol.*, **5**, 53–61.
- Okada, M. and Maruo, H. (1968). New plasma spraying and its application, *Br. Weld. J.* **15**, 371–386.
- Padture, N.P., Schlichting, K.W., Bhatia, T., Özturk, A., Cegeten, B., Jordan, E.H., Gell, M., Jiang, S., Xiao, T.D., Strutt, P.R., Garcia, E., Miranzo, P. and Osendi, M.I. (2001). Toward durable TBC with novel microstructures deposited by precursor plasma spray, *Acta Mater.*, **49**, 2251–2257.
- Pawlowski, L. (1975). Some properties of arc plasma sprayed tantalum coatings, in *International Round Table on Study and Applications of Transport Phenomena in Thermal Plasma*, Odeillo, France, 12–16 September, Paper IV.4 unpublished conference proceedings.
- Pawlowski, L. (1980). The vacuum plasma sprayed copper and tantalum coatings, in: *Proceedings of the 9th International Thermal Spray Conference*, Nederlands Instituut voor Lastechniek, The Hague, The Netherlands, pp. 299–305.
- Pawlowski, L., Gross, A. and McPherson, R. (1991). Microstructure of plasma sprayed  $\text{YBa}_2\text{Cu}_3\text{O}_x$  high-temperature superconductor, *J. Mater. Sci.*, **26**, 3803–3808.
- Plazjet (1995). Catalogue of TAFA, Concord, CA, USA.
- Poorman, R.M., Sargent, H.B. and Lamprey, H. (1955). Method and apparatus utilizing detonation wave for spraying and other purposes. *US Patent* 2 714 553.
- Richter, P., Krömmer, D.W. and Heinrich, P. (2002). Equipment engineering and process control for cold spraying, in *Proceedings of International Thermal Spray Conference 2002 Essen*, E. Lugscheider and C.C. Berndt (Eds), DVS Verlag, Düsseldorf, Germany, pp. 375–379.
- Rudzki, G.J. (1983). *Surface Finishing Systems*, Finishing Publications Ltd, Teddington, UK.
- Sakaki, K. and Smimizu, Y. (2001). Effect of the increase in the entrance convergent section length of the gun nozzle of HVOF and GGC processes, *J. Therm. Spray Technol.*, **10**, 487–496.

- Sampson, E. (1993). Advances in thermal spray coatings broaden their applications, *Weld. J.*, July, 39–41.
- Schiefer, M.F.O., Voyer, J., Gärtner, F. and Qi, X. (2002). Corrosion behaviour of high velocity combustion wire sprayed coatings, in *Proceedings of International Thermal Spray Conference 2002 Essen*, E. Lugscheider and C.C. Berndt, (Eds), DVS Verlag, Düsseldorf, Germany, pp. 553–558.
- Schmidt, H. and Matthäus, D. (1980). Stage of development of the arc metal arc spraying systems: experiences and data, in *Proceedings of the 9th International Thermal Spray Conference*, Nederlands Instituut voor Lastechniek, The Hague, Netherlands, pp. 225–231.
- Schoop, M.U. and Guenther, H. (1917). *Das Schoopsche Metallspritverfahren*, Franck Verlag, Stuttgart, Germany.
- Schwarz, E. (1980). Detonation for nuclear and related industries, in *Proceedings of the 9th International Thermal Spray Conference*, Nederlands Instituut voor Lastechniek, The Hague, Netherlands, pp. 91–101.
- Schwenk, A., Nutsch, G. and Gruner, H. (2003). Modified nozzle for the atmospheric plasma spraying, in *Advancing the Science and Applying the Technology*, C. Moreau and B. Marple (Eds), ASM International, Materials Park, OH, USA, pp. 573–579.
- Smith, C.W. (1974a). The basic principles of flame spraying, in *Science and Technology of Surface Coatings*, B.N. Chapman and J.C. Anderson (Eds), Academic Press, London, UK, pp. 271–279.
- Smith, R.G. (1974b). The basic principles of detonation spraying, in *Science and Technology of Surface Coatings*, B.N. Chapman, and J.C. Anderson (Eds), Academic Press, London, UK, pp. 262–270.
- Steenkiste, van T., and Gorkiewicz (2004). Analysis of tantalum coatings produced by the kinetic spray process, *J. Therm. Spray Technol.*, 13, 265–273.
- Steenkiste, van T. and Smith, J.R. (2004). Evaluation of coatings produced via kinetic and cold spraying processes, *J. Therm. Spray Technol.*, 13, 274–282.
- Steffens, H.-D. and Nassenstein, K. (1996). The ‘Sonarc’ process: combination of arc and HVOF spraying, in *Thermische Spritzkonferenz TS96*, Vol. 175, DVS, Lugscheider E. (Ed) Düsseldorf, Germany, pp. 53–57.
- Stetson, A.R. and Hauck, C.A. (1961). Plasma spraying technique for toxic and oxidizable materials, *J. Met.*, 13, 479–482.
- Stoltenhoff, T., Voyer, J. and Kreye, H. (2002). Cold spraying – state of the art and applicability, in *Proceedings of the International Thermal Spray Conference 2002 Essen*, E. Lugscheider and C.C. Berndt (Eds), DVS Verlag, Düsseldorf, Germany, pp. 366–374.
- Swank, W.D., Fincke, J.R., Haggard, D.C., Irons, G. and Bullock, R. (1994). HVOF particle flow field characteristics, in *Thermal Spray Industrial Applications*, ASM International, Materials Park, Ohio, USA, pp. 319–324.
- Takeda, K., Ito, M. and Takeuchi, S. (1990). Properties of coatings and applications of low temperature plasma spray, *Pure Appl. Chem.*, 62, 1773–1782.
- Taylor, T.A., Overs, M.P., Gill, B.J. and Tucker, R.C., Jr (1985). Experience with MCrAl and TBC produced via inert gas shouded plasma deposition, *J. Vac. Sci. Technol.*, A, 3, 2526–2531.
- Thornton, J.A. (1982). Plasma in deposition processes, in *Deposition Technologies for Films and Coatings*, R.F. Bunshah (Ed.), Noyes Publishers, Park Ridge, NJ, USA, pp. 19–62.

- Tikkanen, J., Gross, K.A., Berndt, C.C., Pitkänen, V., Keskinen, J., Raghu, S., Rajala, M. and Karthikeyan, J. (1997). Characteristics of the liquid flame spray process, *Surf. Coat. Technol.*, **90**, 210–216.
- Tomaszek, R. and Pawlowski, L. (2004). Unpublished data.
- Tucker, R.C., Jr (1982). Plasma and detonation gun deposition techniques and coating properties, in *Deposition Technologies for Films and Coatings*, R.F. Bunshah (Ed.), Noyes Publishers, Park Ridge, NJ, USA, pp. 454–489.
- Vardelle, M., Vardelle, A., Fauchais, P. and Saray, I. (1994). Comparison of classical and axial injection torches for spraying alumina coatings, *Mater. Manufact. Proc.*, **9**, 735–755.
- Vinayo, M.E., Gaide, L., Kassabji, F. and Fauchais, P. (1985). Optimization of some spraying parameters under low pressure and controlled atmosphere, in *Proceedings of the 7th International Symp. Plasma Chemistry* C.J. Timmermans (Ed.), IUPAC, Eindhoven, The Netherlands, pp. 1161–1166.
- Vlcek, J., Gimeno, L., Huber, H. and Lugscheider, E. (2003). A systematical approach to material eligibility for the cold spray process, in *Thermal Spray 2003: Advancing the Science Applying the Technology*, C. Moreau and B. Marple, (Eds), ASM International, Materials Park, OH, USA, pp. 37–44.
- Vollrath, J.D., Doolette, A. and Ramakrishnan, S. (1992). The electronic plasma gun, in *Proceedings of the 13th International Thermal Spray Conference*, C.C. Berndt (Ed.), ASM International, Materials Park, OH, USA, pp. 117–120.
- Vuoristo, P.M.J., Niemi, K.J. and Mäntylä, T.A. (1992). On the properties of detonation gun and plasma sprayed ceramic coatings, in *Proceedings of the 13th International Thermal Spray Conference*, C.C. Berndt (Ed.), ASM International, Materials Park, OH, USA, pp. 171–175.
- Waldie, B. and Harris, W.K. (1983). Plasma spraying underwater, in *Proceedings of the 6th International Symposium on Plasma Chemistry*, Montreal, QU, Canada, 24–28 July, Boulos M.I. and Munz R.J. (Eds.), Paper B-3–4.
- Whiterspoon, F.D., Massey, D.W., Kincaid, R.W., Whichard, G.C. and Mohzi, T.A. (2002). High velocity pulsed plasma thermalspray. *J. Therm. Spray Technol.*, **11**, 119–128.
- Wilms, V. (1980). LPPS deposited coatings for the protection against hot gas corrosion – a first evaluation, in *Proceedings of the 9th International Thermal Spray Conference*, Nederlands Instituut voor Lastechniek, The Hague, The Netherlands, pp. 317–324.
- WSP 500 (1997). Catalogue of Hardface Alloys, Santa Fe Springs, CA, USA.
- Xie, L., Ma, X., Jordan, E.H., Padture, N.P., Xiao, D.T. and Gell M. (2003). Identification of coating deposition mechanisms in the solution–precursor spray process using model spray experiments, *Mat. Sci. Eng. A*, **362**, 204–212.
- Yang, Y.M., Liao, H. and Coddet, C. (1995). New performance for HVOF thermal spraying systems with use of natural gas, in *Thermal Spraying – Current Status and Future Trends*, A. Ohmori, (Ed.), High Temperature Society of Japan, Osaka, Japan, pp. 307–312.
- Zierhut, J., Halsbeck, P., Landes, K.D., Barbezat, G., Muller, M. and Schutz, M. (1998). Triplex – an innovative three-cathode plasma torch, in *Thermal Spray, Meeting the Challenges of the 21st Century*, C. Coddet, (Ed.), ASM International, Materials Park, OH, USA, pp. 1419–1424.
- Zverina, K. and Vesely, V. (1976). Materials used for technologies of plasmatic spraying on the base of water stabilized plasma burners, in *Proceedings of the 8th International Thermal Spray Conference*, American Welding Society, Miami, FL, USA, pp. 252–258.

# 4

## Post-Spray Treatment

Post-spray treatment has been widely recognized in the last decade as the key to the quality of coatings (Pawlowski, 1998). Consequently, many new post-spray techniques have been developed and applied to treat sprayed deposits. Besides brand new techniques, such as spark plasma sintering (Prawara *et al.*, 2003) or laser shock processing (Schnick *et al.*, 1999), classical ones, such as laser ‘glazing’ or chemical impregnation, have found a lot of new applications. Finally, such post-spraying treatments as grinding, polishing and lapping retain their important roles in the production of wear-resistant coatings.

### 4.1 HEAT TREATMENT

Heat treatment of sprayed coatings is realized in the following ways:

- electromagnetic heating, which involves the following energy sources (as a function of increasing frequency):
  - spark plasma sintering;
  - microwave;
  - laser;
  - electron beam (e-beam);
- furnace treatment;
- combustion flame treatment.

Considerable research efforts have recently put into spark plasma sintering and laser treatment. Many industrially sprayed coatings are submitted to furnace and combustion flame treatment. The latter is part of flame spray processing of *self-fluxing alloys*.

#### 4.1.1 ELECTROMAGNETIC TREATMENT

##### Spark Plasma Sintering

Spark sintering (Figure 4.1) is a process of rapid sintering of porous materials which is similar to hot pressing. In this process, a sample is inserted into a graphite die. Pulses of DC electric current are applied through electrodes attached to the die. The pulses results in *Joule-effect*

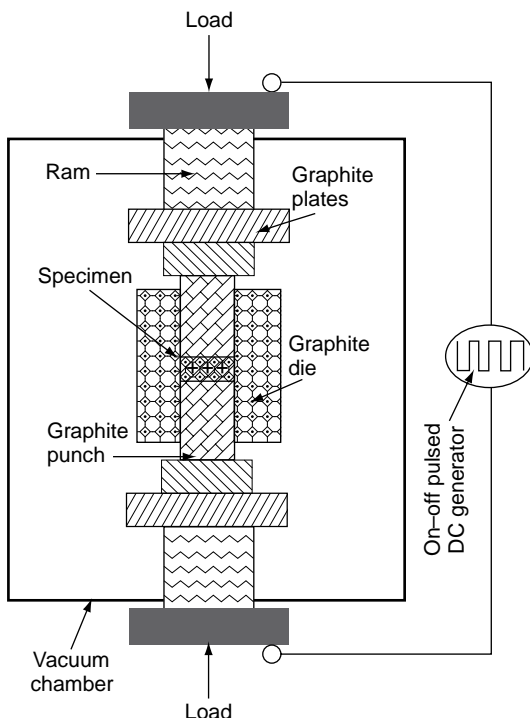


Figure 4.1 Schematic of a spark-plasma spraying set-up (after Prawara *et al.*, 2003). This article was published in *Surf. Coat. Technol.*, 162, B. Prawara, H. Yara, Y. Miyagi and T. Fukushima, 'Spark plasma sintering as a post-spray treatment for thermally sprayed coatings', 234–241, Copyright Elsevier (2003)

heating in densified samples. Heating occurs by electronic conduction in metals and alloys or by ionic conduction in oxides. In the latter, the electric field generates discharges (spark plasma) in voids and pores which promote effective heating while ionic conduction heats the bulk material at higher temperatures (Khor *et al.*, 2003). The electric current of the spark discharge reaches 500–2500 A (Khor *et al.*, 2002). Additionally, the external pressure (up to 10 MPa) promotes good contact between the electrodes and the sintered sample.

The major parameters of the treatment include:

- the heating rate, which is typically a few hundreds of K/min;
- the treatment temperature, which ranges from 700 to 1800 K;
- the time of holding at the temperature of treatment, which is typically a few minutes;
- the compression pressure, which varies from 4 to 50 MPa.

Spark plasma treatment has been applied for different types of coatings and the effects of this treatment are summarized in Table 4.1. An important advantage is the short processing time. The drawback is the necessity of keeping small the size of the treated samples.

**Table 4.1** Examples of spark plasma treatment of different coatings

Application	Coating material	Spray technique	Temperature of treatment (K)	Microstructure modifications	Reference
Biomaterials	Hydroxyapatite	APS	773–1073	Increase in coating crystallinity and formation of texture	Khor <i>et al.</i> , 2002
Solid-oxide fuel cells	Yttria-stabilized zirconia	APS	1473–1773	Reduction of porosity from 11 to 3 %; increase in thermal conductivity; decrease in electric resistivity	Khor <i>et al.</i> , 2003
Hot-gas corrosion resistance	Composite B-doped $M_5Si_3 + 5\text{ wt\% SiO}_2$	VPS	1373–1773	High oxidation resistance at 1473–1673 K	Murakami <i>et al.</i> , 2004
Wear resistance	WC–Co	APS	1073	Restoration of WC in some treatment conditions	Li <i>et al.</i> , 2005

### Microwave Sintering

Microwave radiation covers a spectrum of wavelengths ranging from 300 MHz to 300 GHz. A frequency of 2.45 GHz seems to be the most universal in scientific and technical applications (Agrawal, 1998). In this type of processing, the heat is generated in the internal part of the sintered sample. Thus, the temperature profile is inverted with regard to the furnace heating. The coupling of energy can be very high and almost 100 % of electromagnetic energy can be transferred into heat. The mechanism of microwave absorption in dielectrics includes dipole reorientation and space and ionic charge conduction. Metals, in general, do not absorb but reflect microwave energy. Some of the energy is adsorbed by the thin external layer around the metallic sample. This heating is realized by eddy-current losses and may be enhanced by keeping the sample inside a dielectric cavity (Roy *et al.*, 1999). Microwave sintering has been used mainly in the field of ceramics for the following materials:

- WC-Co composite sintering, enabling 99.8 % of the theoretical density to be achieved at a sintering temperature of 1573 K during a total processing time of 90 min. The mechanical properties of microwave-sintered samples, used mainly for cutting and drilling tools, were better than those sintered in a conventional way (Agrawal, 1998).
- Fe alloys with Ni or Cu were sintered into a microwave chamber at temperatures of 1373–1573 K for 5 to 60 min in an atmosphere of flowing H<sub>2</sub> or its mixture with N<sub>2</sub>. The Rockwell hardness and modulus of rupture were greater for microwave-sintered samples than for those sintered conventionally (Roy *et al.*, 1999).
- Al<sub>2</sub>O<sub>3</sub> sintering of a 10 kg batch of powder prepared by a sol-gel method and having particle sizes in the range 800 to 1000 µm. The sintering was carried out in a continuously working set-up, as shown in Figure 4.2 at temperatures ranging from 1673 to 1773 K over 15 to 45 min (Cheng *et al.*, 2000).

The literature does not contain any examples of thermally sprayed coatings densified by microwave sintering. However, this technique seems to be interesting and to have potential to become a useful post-spray method.

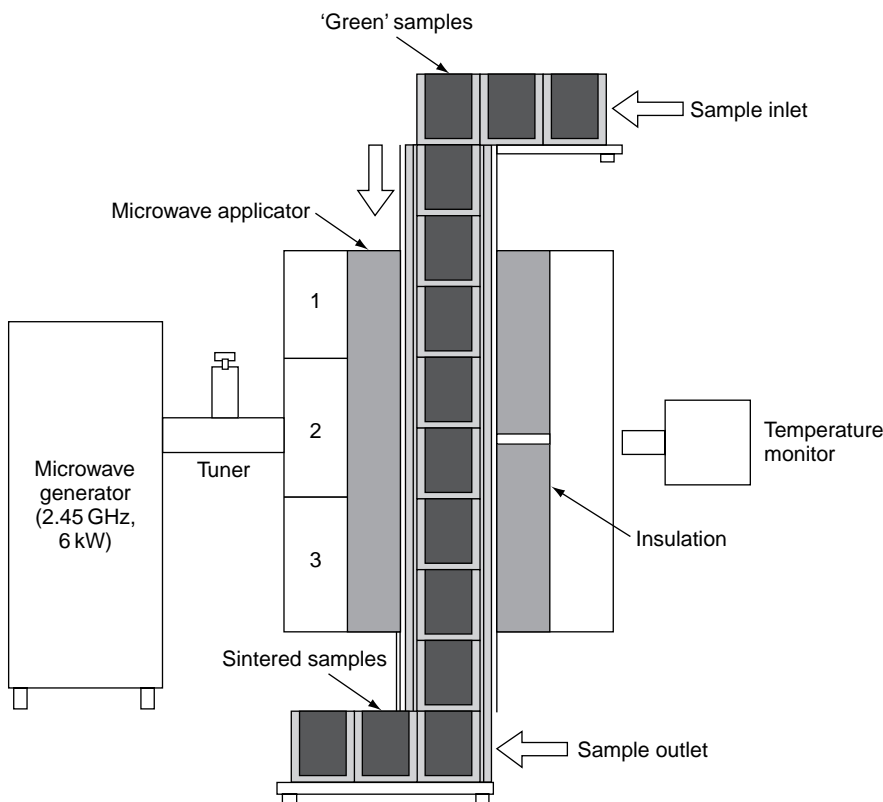


**Figure 4.2** Schematic of continuous microwave sintering of alumina grit: (1) pre-heating zone; (2) sintering zone; (3) cooling zone (after Chen *et al.*, 2000). This article was published in *J. Mater. Proc. Technol.*, 108, J. Cheng, D. Agrawal, R. Roy and P.S. Jayan, 'Continuous microwave sintering of alumina grits', 26–29, Copyright Elsevier (2000)

### Laser Treatment

Lasers have found many applications in the deposition and treatment of coatings. This is why the technology of laser treatment will be described in further detail. The coatings are deposited by the one-step laser deposition technique (1SLD), which consists of injecting powder into a melt caused by a focused laser beam. The powder melts and builds up a coating. This process is similar to deposition techniques using 'weld surfacing', such as PTA (Hocking *et al.*, 1989). The most recent

industrial applications of 1SLD is *rapid prototyping*<sup>1</sup> which enables the realization of solid pieces having complicated 3D shapes in one process. More information about 1SLD can be found, e.g. in the review by Pawłowski (1999) or in the book by Pawłowski (2003). Two-step laser deposition (2SLD) consists of laser treatment of the pre-deposited coating. The latter is frequently made by thermal spraying, especially with the techniques of APS, VPS or HVOF. The 1SLD and 2SLD processes can be implemented in three different ways (Figure 4.3):

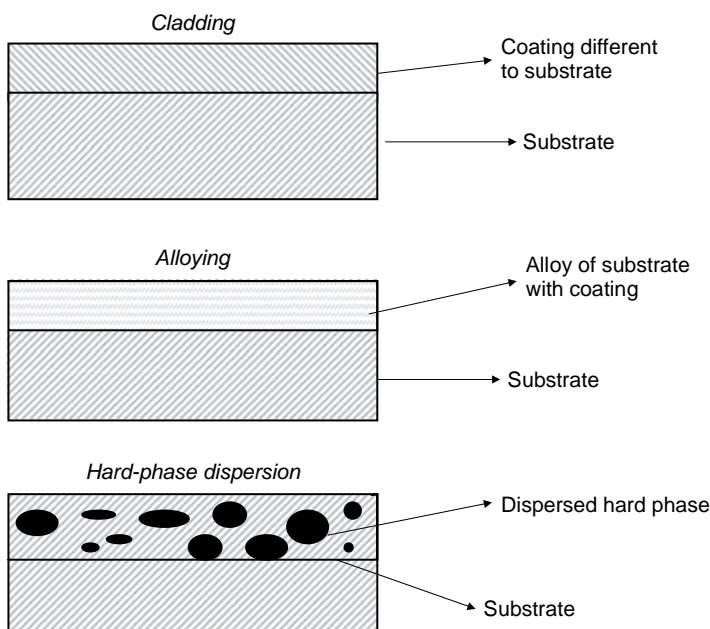


Figure 4.3 Variations in laser deposition and laser treatment techniques

- *Cladding*, in which the coating is chemically different to the substrate;
- *Alloying*, in which the coating and substrate form an alloy;
- *Hard-phase dispersion*, in which hard particles form a composite with the substrate.

**Fundamentals of Laser Technology** The principles of laser design and its characteristics are far beyond the scope of this book. The

<sup>1</sup> Rapid prototyping is a method of realizing pieces having complicated shapes with the help of laser or thermal spraying – more details can be found in, e.g. Pawłowski (1999).

interested reader can find further information in the monograph of Siegman (1986). This present section gives only those topics related to the treatment of coatings. Laser radiation is generated in an optical resonator (cavity) which contains an optically active (lasing) medium, such as a gas (e.g.  $\text{CO}_2 + \text{N}_2 + \text{He}$  in a  $\text{CO}_2$  laser) or a solid (Nd-doped YAG). The medium is initially excited with a gas discharge ( $\text{CO}_2$  laser) or a flash of light in a Nd-doped YAG laser. The electromagnetic wave starts to oscillate in the cavity. The geometry of the cavity determines the wave mode, which, in turn, determines the distribution of energy. The energy is radiated as a plane wave from one of its (partly transparent) mirrors (Figure 4.4).

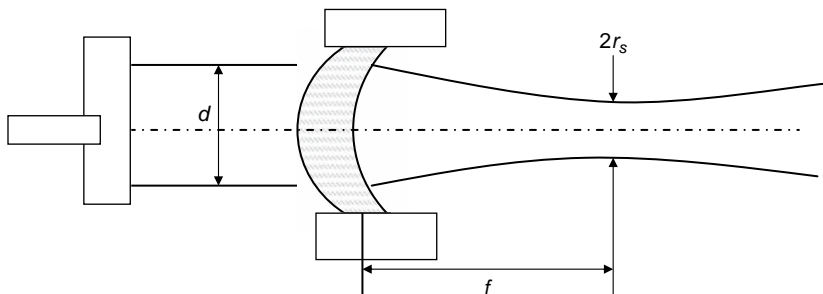


**Figure 4.4** Schematic of a beam issuing from a laser cavity:  $d$ , beam diameter;  $f$ , focal distance of the lens;  $r_s$ , radius of the spot area

In most cases, the distribution of energy corresponding to a fundamental mode,  $\text{TEM}_{00}$ .<sup>2</sup> The quality of the laser beam can be described by a factor  $K$ . This factor is equal to 1 for this mode and is smaller for higher modes. The light emitted by lasers is monochromatic (one wavelength) and spatially coherent. The lasers mainly used today have a wavelength of  $10.6\text{ }\mu\text{m}$  ( $\text{CO}_2$  laser) and  $1.06\text{ }\mu\text{m}$  (Nd-doped YAG and Nd-doped glass lasers). The laser beams diverge slightly (typically by a degree of a few milliradians). Probably, the most important property of laser treatment is the *power density*. This density is defined for a CW laser as:

$$q = \frac{P}{S} \quad (4.1)$$

<sup>2</sup> Mode  $\text{TEM}_{00}$ , resulting in a Gaussian distribution of laser energy, will be considered in the following discussion.

and for pulsed lasers as:

$$q = \frac{E}{S\tau} \quad (4.2)$$

The power density determines the kind of laser treatment (Table 4.2). For high-power density applications, such as engraving or laser shock processing, the beam is focused onto the substrate (Figure 4.4) and the spot area is a circle. The spot radius depends on the wavelength beam quality factor and on the properties of the focusing lens, i.e. focal distance and diameter, in the following fashion (Herziger and Loesen, 1993):

$$r_s \cong \left( \frac{2\lambda}{\pi} \right) \left( \frac{f}{d} \right) \left( \frac{1}{K} \right) \quad (4.3)$$

It is clear that short wavelengths, high beam quality and a large-diameter lens with a short focal distance are necessary to obtain a small spot area. For low-power density applications (heating, 1SLD, 2SLD), the beams can be shaped with the use of integrators, e.g. the *kaleidoscope* described by Chwa *et al.* (2001) to obtain practical rectangular spots. The laser beam is focused onto the surface of the treated material. The fraction of absorbed density by the treated material,  $a$ , for low laser power

**Table 4.2** Laser power densities used for different types of treatment (Pawlowski, 1999)

Number	CW/Pulsed	$q(\text{kW/cm}^2)$	Phase of treated coating	Example of treatment
1	Both	Less than 1	Solid	Phase transformation, heating
2	Both	1 to $10^3$	Liquid	Alloying, cladding, hard-phase dispersion, rapid prototyping
3	Pulsed, $\tau =$ microseconds to milliseconds	Above $10^3$	Vapour	Engraving
4	Pulsed, $\tau =$ nanoseconds	Above $10^6$	Solid	Laser shock processing

densities, at a depth  $x$  below the irradiated surface ( $x = 0$  at the surface) is given by:

$$a = (1 - R)\exp\left(-\frac{x}{L}\right) \quad (4.4)$$

**Table 4.3** Optical data for selected metals and oxides at wavelengths of about 1 and 10  $\mu\text{m}$  (Pawlowski, 1999)

Material	$\lambda$ ( $\mu\text{m}$ )	$R$	$L$ ( $\mu\text{m}$ )
Al	9.54	0.99	0.21
	0.83	0.87	0.022
Ni	9.54	0.98	0.14
	1.03	0.72	0.046
W	10	0.98	0.16
	1	0.58	0.068
$\text{SiO}_2$	10.6	0.2	40
	1.06	0.04	$> 10^6$

Values of reflectivity and optical absorption depth for some materials are collected in Table 4.3. Metals reflect a major part of the laser energy ( $R \approx 1$  in the far infrared at  $\lambda = 10 \mu\text{m}$  – see Table 4.3). The radiation at  $\lambda = 1 \mu\text{m}$  is less reflected. Consequently, the Nd-doped YAG laser is a better tool to treat metals and alloys than the  $\text{CO}_2$  one. The laser light has a frequency of more than  $10^{13} \text{ Hz}$  and is absorbed by the energy coupling with free electrons in metals and alloys (Allmen, 1980). Thus, the optical absorption depth,  $L$ , is typically smaller than  $1 \mu\text{m}$  for these materials. Ceramics have a completely filled valence band and no free electrons are available. The radiation is consequently absorbed by the high-frequency phonons. The energy coupling is weak and the laser radiation is absorbed much deeper ( $L$  = centimetres or metres) and quite often ceramics are totally transparent (Table 4.3). Far-infrared radiation is better absorbed by ceramics and the  $\text{CO}_2$  laser is a more useful tool for treating this class of materials.<sup>3</sup> A simple technological solution to improve the absorption of laser radiation is application of a film of absorbing materials (graphite, black paint) on the surface of the treated sample. The light is transformed in heat and increases the temperature at the surface of the material.

<sup>3</sup>  $\text{CO}_2$  laser radiation cannot be conducted by  $\text{SiO}_2$  optical fibres. On the other hand, Nd-doped YAG laser radiation can be conducted by these fibres. Therefore, the Nd-doped YAG laser, coupled to fibres, is used for many operations in industry.

The temperature as a function of time,  $T(x, t)$ , decreases exponentially with the distance,  $x$ , from the surface of the material following the equation:

$$T(x, t) = \left[ \frac{(1-R)q\tau}{\rho c_p \sqrt{\pi}} \right] \left\{ \frac{\exp [-x^2/(4at)]}{\sqrt{4at}} \right\} \quad (4.5)$$

Equation (4.5) corresponds to the approximation of the semi-infinite body (Bass, 1983; Carslaw and Jaeger, 1959). The temperature at heating can reach melting and boiling points. The distribution of temperature in two dimensions, calculated numerically for a graphite substrate irradiated by pulses from different types of lasers is shown in Figure 4.5.

The evaporation of material generates vapours which can absorb a major part of the incoming power. The gas becomes ionized and the plasma can reach high temperatures. The absorption of incoming radiation by the plasma results in a decrease in energy coupling at laser treatments associated with the evaporation of materials, such as engraving or drilling. On the other hand, the formation of such a plasma has enabled a new process, called ‘Laser Shock Processing’ (LSP) or, as proposed by Dane *et al.* (1998), ‘Shot Peening with Laser’, to be developed. The technique uses the shock waves created by an expansion of the plasma. The plasma results from an interaction of a laser pulse having a power density  $q = 1$  to  $10 \text{ GW/cm}^2$  and a duration<sup>4</sup>  $\tau = 1$  to  $30 \text{ ns}$  (Peyre *et al.*, 1996) with the material. Two methods of LSP are possible:

- *direct ablation*, in which the plasma is in direct contact with the coating;
- *confined treatment*, in which the plasma contacts a system with double layers.

One layer is water or glass and second is a black paint or aluminium foil. In such a way, the plasma, which does not enter directly into contact with the treated material, increases (3 to 5 times) the pressure of

---

<sup>4</sup> To achieve such short pulses, the laser should be equipped with a Q-switch (Siegman, 1986).

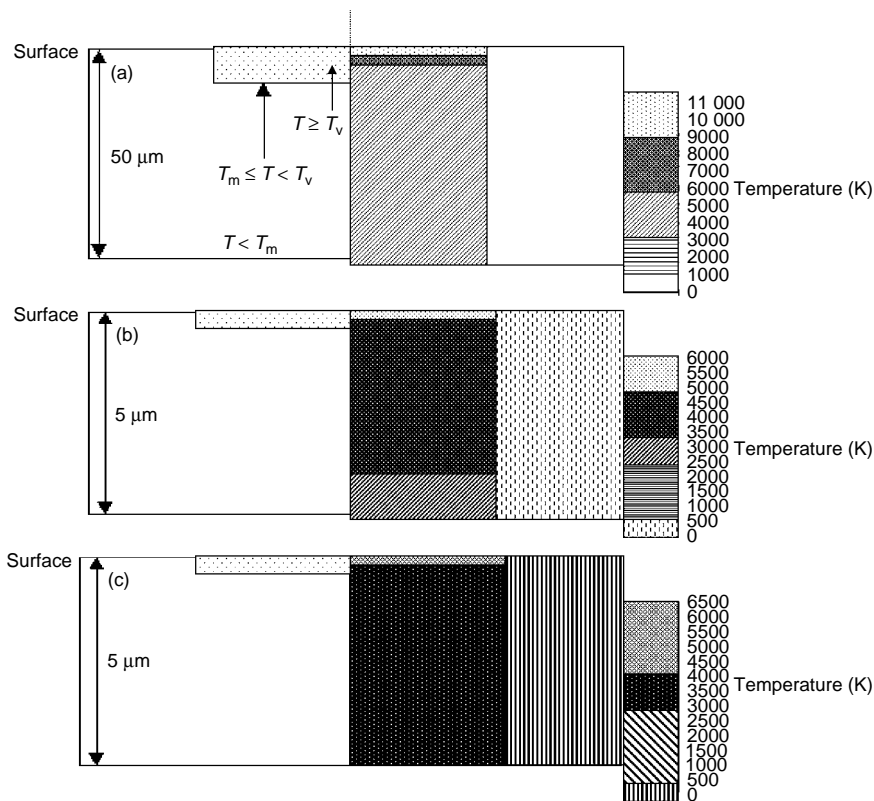


**Figure 4.5** Thermal fields in graphite at the end of a pulse duration of constant laser power density ( $q = 1.27 \times 10^{11} \text{ W/m}^2$ ) for different lasers: left-hand side, evaporated matter; right-hand side, temperature fields. (a) CO<sub>2</sub> laser:  $\tau = 4 \mu\text{s}$ ;  $\lambda = 10.6 \mu\text{m}$ ;  $t = 4.00 \times 10^{-6} \text{ s}$ ;  $R = 0.005 \text{ m}$ ;  $Z = 5 \times 10^{-5} \text{ m}$ . (b) Nd-doped YAG laser:  $\tau = 20 \text{ ns}$ ;  $\lambda = 1.06 \mu\text{m}$ ;  $t = 2.00 \times 10^{-8} \text{ s}$ ;  $R = 0.02 \text{ m}$ ;  $Z = 5 \times 10^{-6} \text{ m}$ . (c) KrF excimer laser:  $\tau = 20 \text{ ns}$ ;  $\lambda = 0.248 \mu\text{m}$ ;  $t = 2.00 \times 10^{-8} \text{ s}$ ;  $R = 0.02 \text{ m}$ ;  $Z = 5 \times 10^{-6} \text{ m}$  (after Skrzypczak *et al.*, 2001). This article was published in *Surf. Coat. Technol.*, 138, M. Skrzypczak, P. Bertrand, J. Zdanowski and L. Pawłowski, 'Modeling of temperature fields in the graphite target at pulsed laser deposition of CN<sub>x</sub> films', 39–47, Copyright Elsevier (2001)

the shock wave (Devaux *et al.*, 1991). Upon treatment, the laser beam crosses the transparent water overlay and is absorbed by a metallic target (aluminium foil). The foil is partly vaporized and creates the expanding plasma. An incoming water flow confines this expansion in a direction opposite to the coating (Masse and Barreau, 1995). The pressures of the laser shocks, measured in the treated substrates with piezoelectric

gauges, are in a range of 3 to 10 GPa (Peyre *et al.*, 1996; Devaux *et al.*, 1991). The pressure (GPa) acting on a treated sample surface depends on the laser power density ( $\text{W}/\text{cm}^2$ ) in the following way:

$$p = 3.22 \times 10^{-9} \sqrt{q} \quad (4.6)$$

An increase in the laser power density above the threshold of  $q = 10 \text{ GW}/\text{cm}^2$  results in a dielectric breakdown in water rather than in a further increase in the shock pressure.

**Table 4.4** Selected characteristics of industrial lasers applied in post-spray coating treatment (Herziger and Loosen, 1993; Pawlowski, 1999)

Parameter	Laser type		
	$\text{CO}_2$	Nd-doped YAG	Diode laser <sup>a</sup>
Wavelength ( $\mu\text{m}$ )	10.6	1.06	0.82–0.98
Excitation technique	Gas discharge	Flash or arc lamp	—
Pulsed/CW	Both	Both	CW
Maximum average power (kW)	25	2	5
Beam quality	Very high	Low	Low
Efficiency (%)	5–10	2–5	—
Price	125 k€ for a laser of average power of 1 kW	200 k€ for a laser of average power 1 kW	48 k€ for a laser of average power 0.5 kW <sup>b</sup>

<sup>a</sup> Information gathered from Dr E. Fogerassy, CNRS, Strasbourg, France and Professor I. Smurov, ENISE, Saint Etienne, France (February 2005).

<sup>b</sup> Quote from *Laserline*, Mülheim, Germany (December 2002).

The industrial lasers used to deposit and treat coatings today are mainly  $\text{CO}_2$  and Nd-doped glass or Nd-doped YAG lasers. Their properties are collected in Table 4.4. Another important industrial laser is the *excimer* one, which is used at present for polymer surface treatment. A great advantage of a diode laser is its small size what renders it practicable in many *in situ* applications. The head of the laser can be installed directly onto a robot arm (Figure 4.6). This is not possible for voluminous and precise resonators of  $\text{CO}_2$  and Nd-doped YAG lasers.



Figure 4.6 A diode laser of 1 kW installed on the arm of a robot in the laboratory of IREPA LASER, Illkirch, France. Reproduced by permission of IREPA LASER, Strasbourg, France

### **Laser Treatment Process Parameters**

- Laser and optical system
  - wavelength;
  - continuous wave or pulsed (pulse duration and pulse frequency);
  - beam shape and quality (modes);
  - Focusing lens (diameter, focus).
- Treated coating
  - chemical composition and thermophysical properties;
  - dimensions and surface preparation (roughness, oxidation, black paint, etc.).
- Processing
  - treatment atmosphere (inert, reactive gas, vacuum);
  - scan velocity;
  - beam tracks overlapping.

**Laser Treatment of Coatings (Two-Step Laser Deposition)** A schematic of the Two-Step Laser Deposition (2SLD) process, representing laser treatment of a pre-deposited coating, is shown in Figure 4.7.

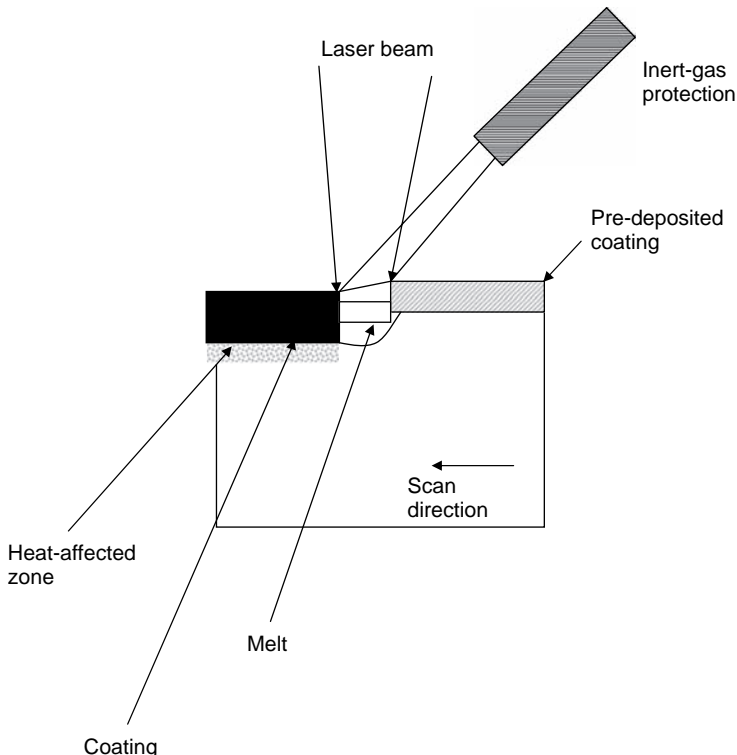


Figure 4.7 Schematic of laser treatment of coatings, known as two-step laser deposition (2SLD)

The laser treatment, being the second step of a final coating preparation needs expertise in mastering two different processes. Pawlowski (1999) describes some examples of technologies other than thermal spraying, e.g. painting, screen-printing, paste deposition and thin films by PVD, that were used for pre-deposition of coatings to be treated later by a laser. The microstructure of laser-treated coatings in the liquid phase is typical for rapidly solidified materials and such coatings have been mainly developed to resist wear.

**Laser Treatment of Thermal Spray Coatings** Application of a laser can improve the properties of thermally sprayed coatings. These improvements having been recently studied for the following applications:

- biomedical coatings;
- thermal-barrier coatings;
- wear-resistant composite coatings;
- wet and hot corrosion-resistant alloys;
- A particular application, such as wear-resistant coatings engraved with a laser – known as *anilox rolls*.

Most laser treatments correspond to the process of *cladding* and only a few reports concern *alloying* or *hard-phase dispersion*. Therefore, this discussion will be presented in a way which takes into account the phase of the sprayed coating during laser treatment, as follows:

- solid phase;
- liquid phase;
- gas phase.

#### *Treatment in the solid phase*

Treatment in the solid phase has been realized for hydroxyapatite (HA) coatings. The coatings were sprayed by mainly using the APS method (Pawlowski *et al.*, 1997; Ranz *et al.*, 1998), and a few times by VPS or HVOF. The major problem of spraying is related to the fact that HA decomposes at a temperature of 1723 K (water pressure of 500 mmHg) as shows it Eq. (4.7) into  $\alpha$ -Ca<sub>3</sub>(PO<sub>4</sub>)<sub>2</sub> ( $\alpha$ -TCP) and Ca<sub>4</sub>P<sub>2</sub>O<sub>9</sub> (TTCP):



On solidification of the molten calcium phosphate, formation of many phases is possible including, in addition to  $\alpha$ -TCP and TTCP, calcium oxide (CaO). All of these phases have a different Ca/P ratio which can be determined inside the sprayed coating by using electron microprobe analysis (EMPA). The profile obtained enables us to understand that each particle of HA may transform during thermal spraying into a lamella in the coating, as shown in Figure 4.8.

The idea behind laser treatment in the solid phase is to transform the amorphous phase in the outer region of a lamella back into the

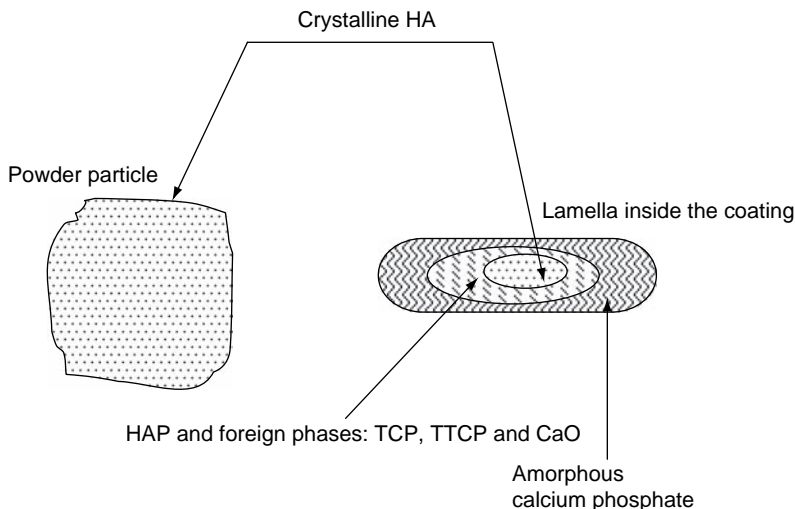


**Figure 4.8** Possible phase distribution inside a lamella obtained by plasma spraying of an HA powder particle (Deram *et al.*, 2003)

crystalline hydroxyapatite. This is a valuable technological solution which would enable a dense and well-adhering coating to be pre-deposited with any of the spray techniques and, later on, restoring the crystalline hydroxyapatite phase by using a laser. The latter must be the major phase in biomedical applications of coatings.<sup>5</sup> The parameters of some laser treatments realized in the solid phase are collected in Table 4.5. The laser treatment optimized by Pawłowski *et al.* (1997) enabled the content of crystalline HA to be restored from 23 to 90% in as-sprayed coatings (Figure 4.9). The following study by the same research group (Ranz *et al.*, 1998) enabled the phase content to be regulated by the temperature of the coating surface, i.e. by the laser processing conditions. The optimum temperature of the treatment was in the range 1073–1373 K, well below the decomposition temperature. Under these conditions, the amorphous calcium phosphate was indeed transformed into crystalline HA (Figure 4.10).

Another example of laser treatment in the solid phase concerns composites reinforced with carbides. Carbides are known to decompose at high temperatures. Therefore, laser treatment using laser shock

<sup>5</sup> Not less than 95 % following ASTM Standard F 1185-03: Standard specification for composition of hydroxyapatite for surgical implants.

**Table 4.5** Principal parameters of laser treatment in the solid phase of HA coatings pre-deposited by atmospheric plasma spraying

Substrate	Laser processing		Final coating		Reference
	Laser $q$ (kW/cm <sup>2</sup> )	Scan speed (cm/s)	Thickness (μm)	Phase composition	
'Medium' carbon steel	Nd-doped YAG, pulsed, $\tau = 2.7$ ms	Laser power up to 400 W	—	—	Khor and Cheang (1994)
Ti <sub>6</sub> Al <sub>4</sub> V	CO <sub>2</sub> , CW	Laser power up to 70 W	0.025–2.5	150	90 % of HA + $\alpha$ -TCP + TTCP + CaO (see Figure 4.10) Pawlowski <i>et al.</i> (1997)
Ti <sub>6</sub> Al <sub>4</sub> V	CO <sub>2</sub> , CW, kaleidoscope	0.52–0.68	2–5	150	HA + amorphous calcium phosphate (see Figure 4.11) Ranz <i>et al.</i> (1998)

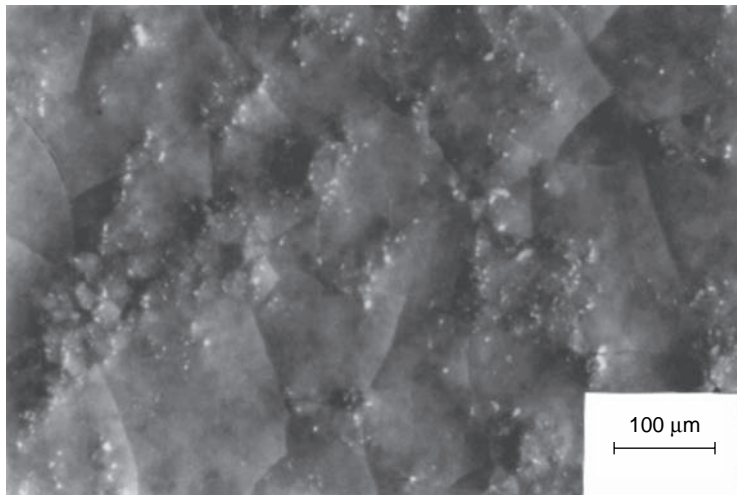


**Figure 4.9** Optical micrograph of the surface of an HA coating pre-deposited using plasma spraying in air and then laser treated in the solid phase (Pawlowski *et al.*, 1997)

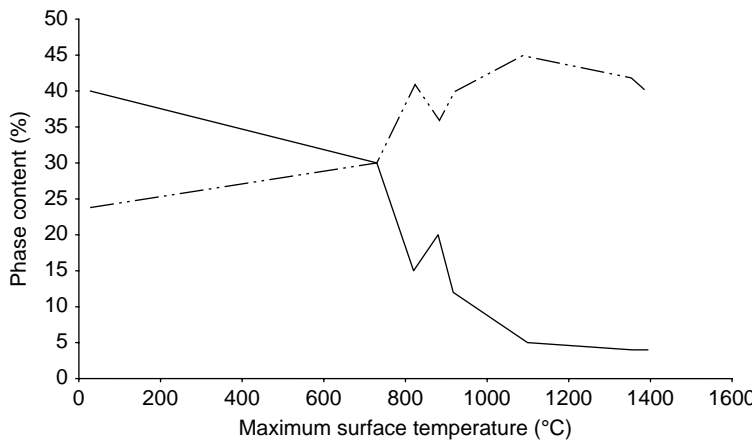


Figure 4.10 Phase composition in atmospheric-plasma-sprayed HA coatings subjected to laser treatment with different processing parameters, resulting in different treatment temperatures: (—) amorphous calcium phosphate; (..—..) crystalline HA (Ranz *et al.*, 1998). Reproduced by permission of ASM International from Ranz *et al.*, 1998, in *Thermal Spray: Meeting the Challenges of the 21st Century*, C. Codet (Ed.), ASM International, Materials Park, OH, USA, pp. 1343–1349

processing (LSP) carried out at room temperature can be a promising way to improve their properties. Al + SiC coatings pre-deposited by using HVOF were treated with LSP by Schnick *et al.* (1999). The composites were processed using the parameters collected in Table 4.6. A modification of the initial coating microstructure is shown in Figure 4.11.

Table 4.6 Parameters of the laser shock treatment of an Al + SiC composite pre-deposited using HVOF on an aluminum alloy substrate (Schnick *et al.*, 1999)

Pre-deposition		Laser shock processing				Final coating	
Technique	Powder composition (wt%)	Laser and pulse data	$q$ (GW/cm <sup>2</sup> )	Overlapping (%)	Pressure of one shock (GPa)	Thickness (μm)	Microstructure
HVOF	Al + (15–50) SiC	Nd-doped YAG, $\tau = 5\text{--}20\text{ ns}$ , $E = 80\text{ J}$	5–10	50	4–5.5	100–400	See Figure 4.11

The treatment modified the microstructure and morphology of the coatings in the following ways:

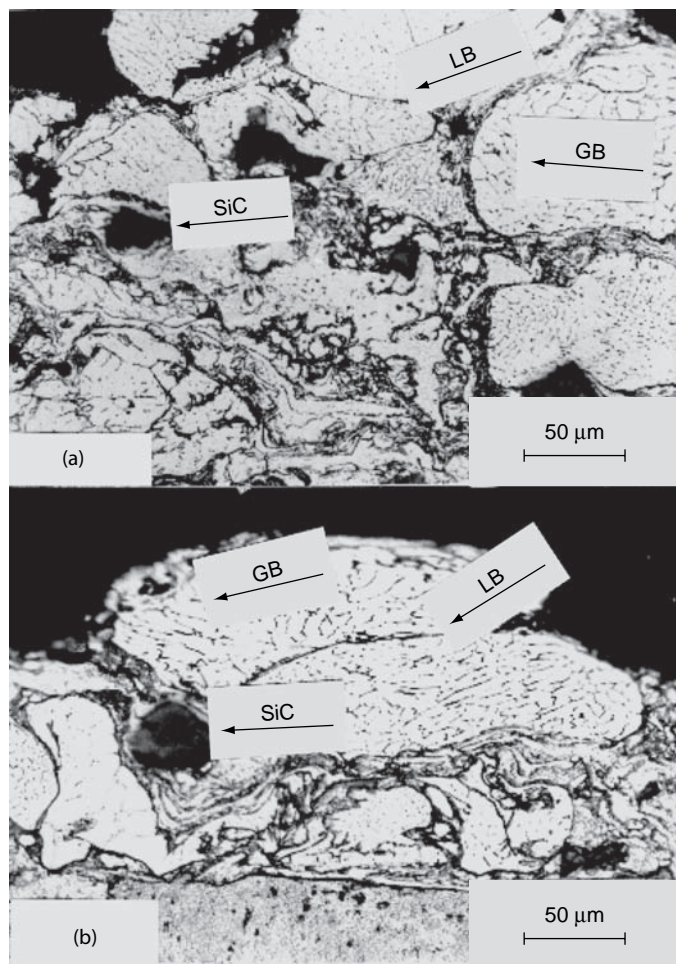


Figure 4.11 Scanning electron micrographs (secondary electrons) of the cross-section of an Al + 15 wt% SiC particulate composite: (a) sprayed coating; (b) coating after laser shock processing: SiC, silicon carbide reinforcement; LB, lamella boundary; GB, grain boundary

- Contact between the Al matrix and the SiC reinforcement (compare the boundaries between the lamellae in Figures 4.11(a) and 4.11(b)).
- Lamellae of the Al matrix became plastically deformed, which was associated by the formation of many crystal grains inside the Al lamellae in Figure 4.11(b).
- The laser-treated coating surface became smoother.

However, in spite of the improved microstructure, the *oscillating wear* resistance of the treated composites was worse than that of the as-sprayed deposits. This effect was explained by the formation of structural defects at the coating surface during the laser processing.

#### *Treatment in the liquid phase*

Laser treatment in the liquid phase is sometimes called *re-melting* or *glazing*. This concept to improve the properties of sprayed coatings is only a few years older than the laser itself (Ingham, 1967). At present, it is the most popular variation of laser treatment of thermally sprayed coatings. Some examples of the laser treatment of sprayed metals, alloys, oxide ceramics and carbide-reinforced composites are shown in Table 4.7.

#### *Metals*

Metals, such as Ti (Pangborn and Beaman, 1980; Ohmori *et al.*, 1993) or Ni (Dallaire and Cielo, 1982; Das, 1994), were 'laser-re-melted'. Ohmori and his colleagues used an interesting hybrid method similar to the PROTAL™ technique described previously for substrate preparation, namely simultaneous laser treatment and reactive plasma spraying. The method was tested to obtain wear-resistant TiN coatings by spraying Ti powder in an atmosphere of N<sub>2</sub>, associated with heating by a CO<sub>2</sub> laser (see Table 4.7). Ayers and Schaefer (1979) indicated that the laser beam quality influences the depth of the treatment. The melting of the coating is associated with evacuation of expanding gases entrapped in the closed pores which might leave holes on the coating surface. Finally, processing parameters, such as substrate speed and laser power density, should be carefully optimized to avoid residual stresses that may relax to form cracks. Laser re-melting seals the metal coatings and eliminates the post-spray porosity. Thus, to obtain a dense metal coating without holes on its surface, pre-deposition with VPS and laser treatment in a vacuum is a recommended technological solution. The roughness resulting from the laser treatment (with the parameters shown in Table 4.7) and the methods to control this were analysed by Das (1994).

#### *Alloys*

Modelling of a vacuum-plasma-sprayed NARloy-Z alloy (Co + 3 wt% Ag + 0.5 wt% Zr) was analysed theoretically by Singh *et al.* (1996). The formation of amorphous and nanostructured crystals of phases of different intermetallic compounds, such as AlNi<sub>3</sub>, was observed in laser-glazed coatings, plasma-sprayed by using the NiCrBSi self-fluxing alloy by Liang and Wong (1997). The treatment was carried

**Table 4.7** Examples of laser treatment in the liquid phase for different types of sprayed materials

Technique	Pre-deposition Powder composition (wt%)	Substrate composition (wt%)	Laser treatment				Final coating			Application Reference
			Type of treatment	Laser	$q$ (kW/cm <sup>2</sup> )	Scan speed (cm/s)	Atmosphere	Overlapping (%)	Thickness (μm)	
VPS	Ti	Mild steel, SS41	Alloying	CO <sub>2</sub> , CW (presumably)	Laser power, 200–600 W	30 $p = 13\text{ kPa}$	N <sub>2</sub> , under —	—	100–150 μm	Formation of 16 to 70 vol% of TiN
APS	Ni	Al	Alloying	Nd-doped YAG, $\tau = 4\text{ ms}$ , $f = 10\text{ Hz}$	Laser average power, 120 W	0.21	Air (presumably)	> 50	150–1100 μm	Concentration of Ni in coating, 5.7–21.5 wt%
APS	Self-fluxing alloy: Ni+11Cr+11Fe+1.5Si+1B 12Al+0.3Y	Al+8Si+1Cu+0.5Mg	Cladding	CO <sub>2</sub> , CW	36	1 <i>Allloys</i>	Ar	—	400	Al, Al <sub>3</sub> Ni, AlNi <sub>3</sub> , Al <sub>3</sub> N <sub>2</sub>
VPS		Mild steel, St38b	Cladding	CO <sub>2</sub> , CW	13	12–22	Air	66	100–150	See Figure 4.13
										Wear resistance and Wielage <i>et al.</i> , 1998

Table 4.7 (Continued)

Technique	Pre-deposition Powder composition (wt%)	Substrate composition (wt%)				Laser treatment				Final coating		Application Reference
		Type of treat- ment		Laser	$q$ (kW/cm <sup>2</sup> )	Scan speed (cm/s)	Atmosphere	Overlap- ing (%)	Thickness (µm)	Microstructure		
APS	Duplex: $ZrO_2 +$ 8wt% $Y_2O_3$ on $MoCrAlY$ $(Ca_3(PO_4)_3$ $(OH)$	Ni alloy	Cladding	CO <sub>2</sub> , CW	3–7	Oxide ceramics 20	Air	—	380 (ceramics)	See Figure 4.15	TBCs	Troczynski <i>et al.</i> , 1998
APS	Stainless steel	Stainless steel	Cladding	CO <sub>2</sub> , pulsed, $\tau =$ 0.74ms, $f =$ 47Hz	59–64	0.64–0.96	Air	32–50	—	See Figure 4.16	Bio- medical	Dyshlovenko, 2005
APS	(Fe + 13Cr) + 5.5TiC, by SHS	Steel, St38	Cladding	CO <sub>2</sub> , CW, kaleido- scope	8	Composites 0.25–1	Air	—	200–400	See Figure	Wear resistance	Tondu <i>et al.</i> , 1998
—	WC + 17Co	Steel, AlSi 1043	Cladding	CO <sub>2</sub> , CW, integrator	Energy density (300–2300 J/cm <sup>2</sup> )	0.83	Ar	2.5	—	Dendritic crystals	Wear resistance	Mateos <i>et al.</i> 1997

out with a CO<sub>2</sub> laser (see Table 4.7). Another example of an alloy tested for adhesive wear resistance was NiCrAlY, obtained in two-step laser deposition with the parameters shown in Table 4.7. Figure 4.12 shows densification of this coating after laser treatment and a small zone of dilution, as well as the formation of a heat-affected zone in the substrate.

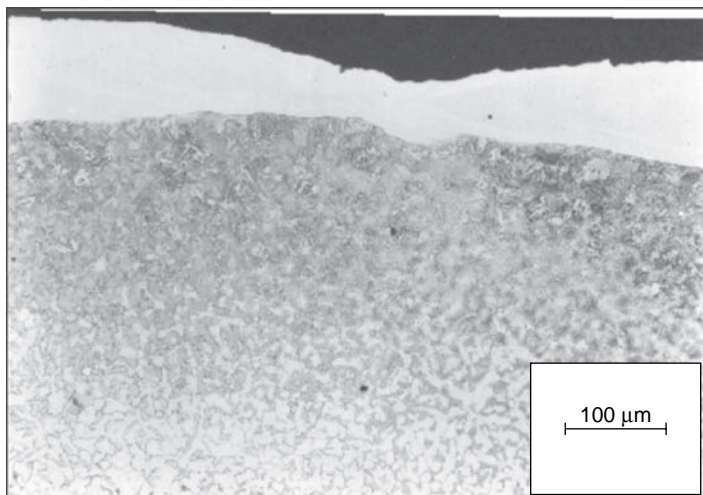


Figure 4.12 Optical micrograph of a polished cross-section of a CoCrAlY coating obtained by two-step laser deposition (2SLD) with the parameters shown in Table 4.7

Many studies have been devoted to the application of 2SLD to obtain corrosion-resistant and wear-resistant coatings. The following materials were tested:

- Hastelloy C, Hastelloy 6 and NiCr coatings against wet corrosion were studied by Dallaire and Cielo (1983), Capp and Rigsbee (1984) and Bhat *et al.* (1983), respectively.
- NiCoCrAlYTa, CoCrAlY and NiCrBSi coatings against hot corrosion were tested by Streiff *et al.* (1987), Wielage *et al.* (1998) and Liang and Wong (1997), respectively.
- A phosphor bronze against wear, prepared by simultaneous vacuum plasma spraying and CO<sub>2</sub> laser treatment was proposed recently by Alam *et al.* (1997).

**Oxide ceramics** As opposed to metals and alloys, laser-re-melted ceramic coatings are cracked on their surfaces (Figure 4.13). The molten surface solidifies by forming a small ‘column’ and are useful in some applications, such as thermal barriers. It is also possible to observe the holes resulting from evacuation of the gas entrapped inside the pores heated at laser treatment and expanding through liquid coating’s material to the atmosphere. The  $\text{Al}_2\text{O}_3$  coatings deposited by APS onto a low-thermal-expansion Kovar alloy were tested by Gorecka-Drzazaga *et al.* (1984). These authors observed transformation of a metastable  $\gamma$ -phase of alumina present in the sprayed coatings back into the stable  $\alpha\text{-}\text{Al}_2\text{O}_3$  in laser-re-melted samples.

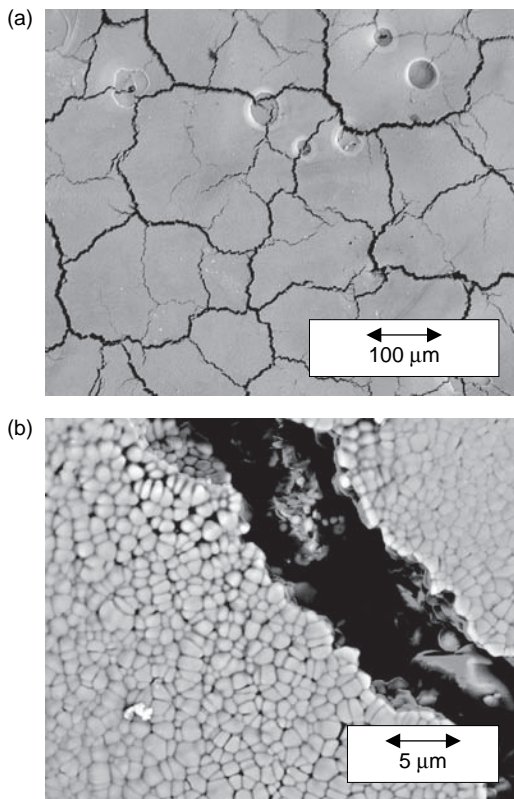


Figure 4.13 Scanning electron micrograph (backscattered electrons) of the surface (under two different magnifications) of a thermal-barrier coating composed of an  $\text{MoCrAlY}$  bond coating and a  $\text{ZrO}_2 + 8 \text{ wt\% Y}_2\text{O}_3$  top coating after laser treatment with the parameters shown in Table 4.7

Similarly, alumina alloyed with titania ( $\text{Al}_2\text{O}_3 + 13 \text{ wt\% TiO}_2$ ) transformed from the  $(\gamma + \alpha)\text{-Al}_2\text{O}_3$  phases and the rutile form of  $\text{TiO}_2$  present in the sprayed deposit into  $\alpha\text{-Al}_2\text{O}_3$  and spinel ( $\text{Al}_2\text{TiO}_5$ ) in a laser-re-melted deposit (Aihua *et al.*, 1992). The crystal structure transformation was reportedly associated with:

- coating densification;
- formation of a columnar structure in a zone re-melted with the laser;
- increase in microhardness from  $HV_{0.2}$  of 950 to 2000 in this zone;
- improvement of wear and corrosion resistance.

Another study, coming from this group of authors (Aihua *et al.*, 1993) tested ceramics of the same composition when plasma-sprayed onto the top of a multicoating composed of a NiAl bond layer and a cermet of  $\text{NiAl} + 50 \text{ wt\% } (\text{Al}_2\text{O}_3 + 13 \text{ wt\% TiO}_2)$  used as the intermediate layer. The multicoating was applied onto an AlSi alloy and re-melted with a  $\text{CO}_2$  CW laser. The samples were subsequently subjected to thermal shocks (773 K for 5 min, followed by water quenching to 283 K). The laser-treated specimen was more resistant to thermal shocks than the as-sprayed coatings. These authors pointed out that the stresses generated by thermal shock testing were more easily relieved by the formation of network cracks in the laser-treated samples.

Another important thermally sprayed oxide ceramic,  $\text{ZrO}_2$ , was also the subject of many studies on laser glazing, including, e.g. that of Zaplatynski (1982), Galasso and Veltri (1983), Jasim *et al.* (1989, 1991, 1992), Tsai and Tsai (1995), Chen *et al.* (1996), Fu *et al.* (1997) and Troczynski *et al.* (1998). In most of these studies, zirconia was a part of a *duplex* coating system which includes  $\text{ZrO}_2$  as the top coating and MCrAlY alloy as the bonding one. The reason for the interest in laser treatment results from the formation of a *columnar microstructure* in the sprayed deposits (Figure 4.14).

This type of microstructure with small vertical columns (see Figure 4.13) is similar to that of zirconia obtained by EBPVD (Maricochi *et al.*, 1997) and might also be observed in the coatings obtained by cryogenic gas cooling during the spraying process (Cosack *et al.*, 1992). Since thermal barriers are subjected to intensive thermal shocks during service, the distance between the columns could increase (at heating) and decrease (at cooling) without damaging the entire TBC. Thus, the strain tolerance of the TBC with a columnar microstructure is improved. However, the surface of the coating is divided into *segments*, visible

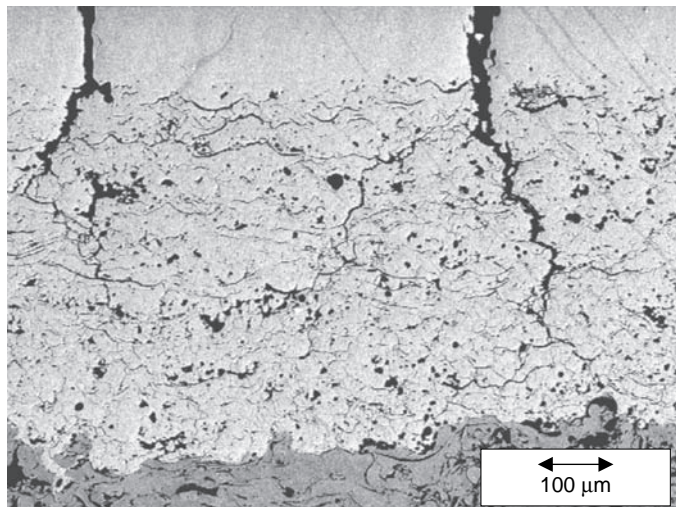


**Figure 4.14** Scanning electron micrograph (backscattered electrons) of the polished cross-section of a thermal-barrier coating composed of an MoCrAlY bond coating and a  $\text{ZrO}_2 + 8 \text{ wt\% Y}_2\text{O}_3$  top coating after laser treatment with the parameters shown in Table 4.7

on the cross-section shown in Figure 4.14. The segments weaken the mechanical resistance of the coating and enable easy penetration of hot gas into it, which promotes corrosion-related failure. Laser glazing results, moreover, in decrease in the coating roughness, which improves the aerodynamics of TBCs onto turbine blades.

The density of segments was reported to be smaller when a pulsed (instead of CW)  $\text{CO}_2$  laser was applied (Jasim *et al.*, 1992). The phase content of the laser-re-melted zirconia depended upon the percentage of yttria stabilizer in the powder used to spray in the following way:

- for 8 wt%, the structure was mainly tetragonal non-transformable ( $t'$ ) and cubic (c) (Jasim *et al.*, 1989);
- for 12 and 20 wt%, it was cubic (c) – Tsai and Tsai (1995) and Galasso and Veltri (1982), respectively.

The shape of the crystals in laser-treated zirconia was reported (Jasim *et al.*, 1992) to be cellular at a laser specific energy less than  $1 \text{ J/mm}^2$  and dendritic at the higher energies. The number of shocks withstood, without failure, during thermal shock testing of laser-re-melted TBCs, with regard to that of as-sprayed coatings, varies in different studies:

- the same number was found in the initial study of Zaplatynski (1982);
- a four times greater number was reported in a more recent study of Tsai and Tsai (1995).

The corrosion resistance of a glazed specimen was improved by sealing the coatings in the following ways (adopted by different authors):

- Chen *et al.* (1997) initially re-melted the coating to a depth of about 100 µm and applied a zirconia suspension to the coating surface, followed by treatment with a lower laser power density to a depth of 50 µm.
- Troczynski *et al.* (1998) employed sol-gel sealing with laser treatment.

Laser treatment of atmospheric-plasma-sprayed hydroxyapatite at a power density that enables formation of a liquid phase (see Table 4.7) results in the decomposition of HA into TTCP and  $\alpha$ -TCP phases, following Equation (4.7). XRD diagrams of laser-treated HA coatings are shown in Figure 4.15.

As the phases of HA decomposition are less biocompatible than HA itself, laser glazing is less interesting for the technology of prostheses deposition than treatment in the solid phase.

Laser treatment of MMCs (mainly with carbide reinforcements) should improve the contacts between the reinforcement and the matrix and reduce/eliminate the porosity of the metal matrix. Consequently, the wear resistance of the composites is supposed to increase. The main problem on treatment is related to the melting of the carbide reinforcement, associated with its possible decomposition and the decrease in hardness or the ‘rounding’ of the ‘blocky’ carbide particulates which do not favour wear resistance. The first solution using laser shock treatment was presented above. Another possibility is laser re-melting of MMCs in a way that keeps the carbide reinforcement solid and melts the metal matrix. This is, in principle, possible because the melting points of metals are usually much lower than those of carbides. It demands, however, careful control of the laser-treatment temperature. This approach was adopted by Tondu *et al.* (1998) who applied a very porous powder of composition (Fe + 13 wt% Cr) + 55 wt% TiC, prepared with an SHS method with an APS technique onto steel substrates. The sprayed coating was very porous (Figure 4.16) and was submitted to a laser glazing.

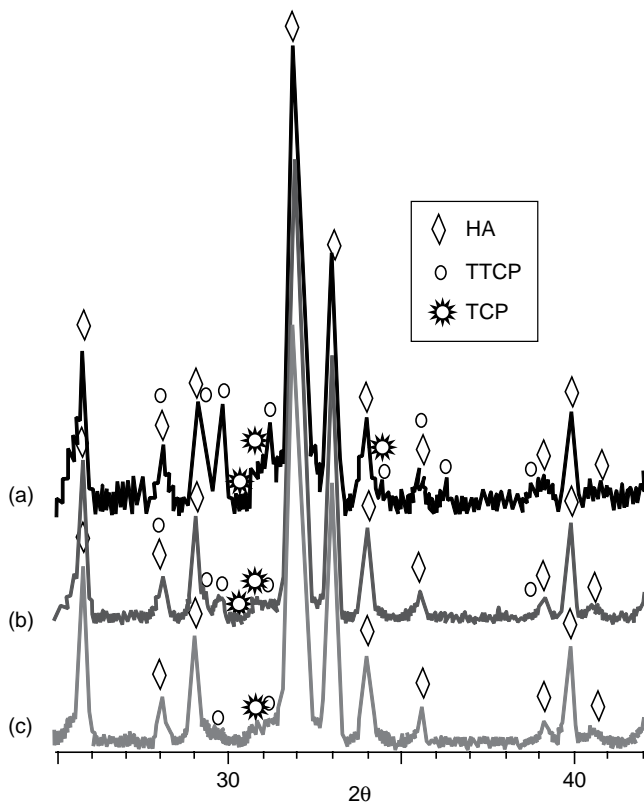


**Figure 4.15** XRD diagrams of hydroxyapatite coatings, (a) as-sprayed and with different power densities: (b)  $q = 5.8 \times 10^4 \text{ W/cm}^2$ ; (c)  $6.4 \times 10^4 \text{ W/cm}^2$ . Sample preparation details are shown in Table 4.7

The alloy matrix melts at 1811 K while, on the other hand, at 3049 K, the following eutectic reaction of the titanium carbide reinforcement with the graphite can take place:



On solidification from the melt, the formation of solid solutions of  $\alpha$ -Ti,  $\beta$ -Ti and/or  $\text{Ti}_2\text{C}$  are possible. Consequently, to melt the matrix and keep the reinforcement solid, the temperature of the coating surface on laser glazing was maintained at about 2273 K. Post-processing under these conditions enabled densification of the coating at the surface (Figure 4.16(b)) without decomposition of titanium carbide

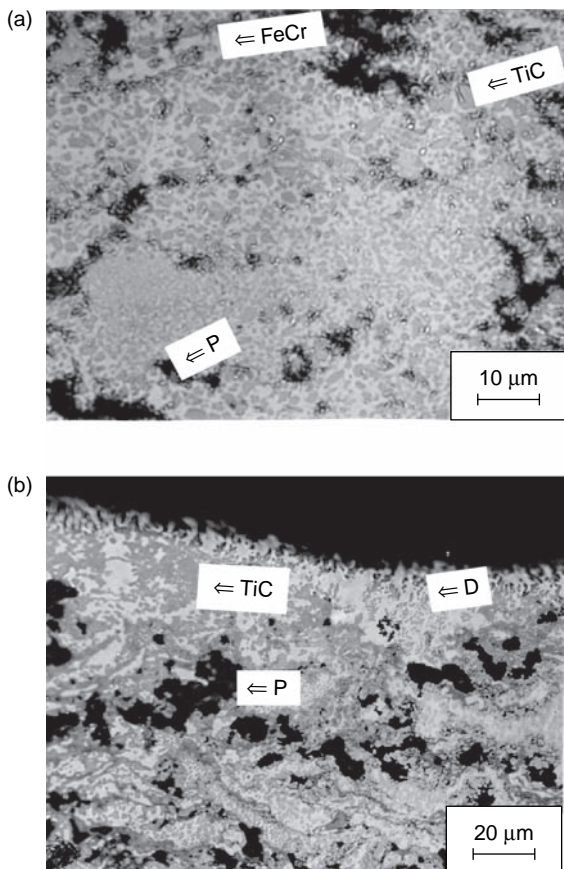


**Figure 4.16** Optical micrographs of a polished cross-section of an FeCr–TiC coating: (a) as-sprayed; (b) after laser treatment with the parameters shown in Table 4.7 (D, dendrite; P, pore)

(Figure 4.17). The adhesive-wear-resistance of laser-glazed coatings was considerably better than that of as-sprayed coatings.

#### *Treatment in the gas phase*

Treatment in the gas phase mainly concerns laser engraving which is part of the manufacturing of *anilox rolls* reviewed by Pawłowski (1996). The rolls are used to transport a precise quantity of ink in *flexographic* printing machines. The actual technology of the rolls includes the spraying of a  $\text{Cr}_2\text{O}_3$  coating with APS and subsequent laser engraving of the cells. The surface of a laser-engraved chromia coating is shown in Figure 4.18.

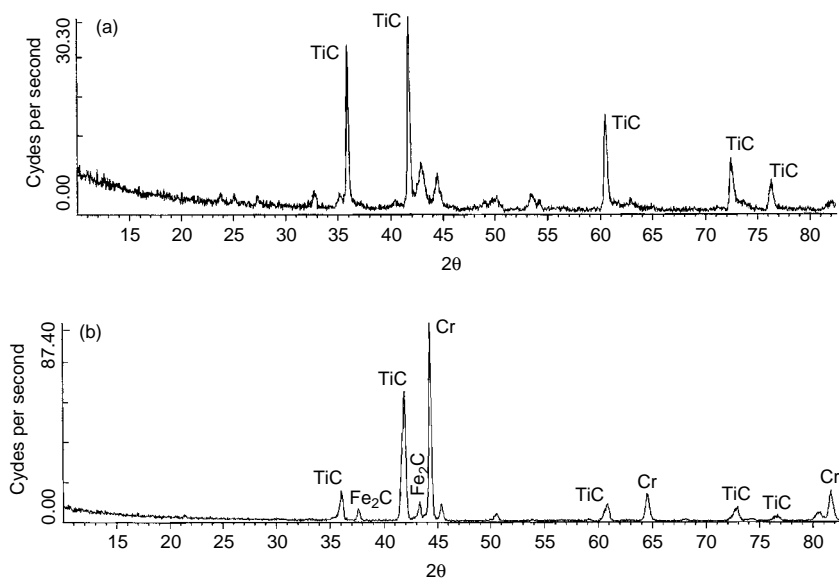


Figure 4.17 XRD diagrams of an FeCr–TiC composite: (a) as-sprayed; (b) laser-glazed. Sample preparation details are shown in Table 4.7

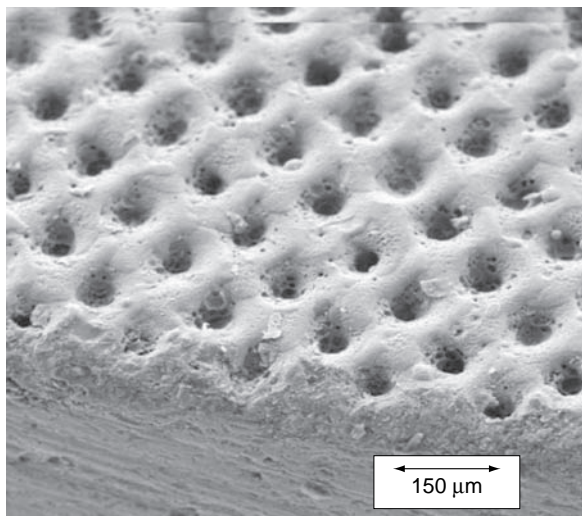


Figure 4.18 Scanning electron micrograph (secondary electrons), at an angle of  $40^\circ$ , of a pattern engraved on a  $\text{Cr}_2\text{O}_3$  coating: line density (LD),  $140 \text{ cm}^{-1}$ ; cell depth(s),  $\approx 34 \mu\text{m}$ ; angle of engraving, ( $\alpha$ ),  $60^\circ$  (Znamirowski *et al.*, 2003)

The principal parameters for laser engraving are as follows:

- Composition of the laser working gases in CO<sub>2</sub> lasers, including CO<sub>2</sub>, He and N<sub>2</sub> (nitrogen must be avoided for finer engraving).
- Density of lines (LD) in cm<sup>-1</sup>.
- Scan speed.
- Pulse length.
- Distance between the last lens and the roller surface.
- Pulse amplitude, which is expressed in % of the maximum value.
- Angle of engraving (see Figure 4.19), with  $\alpha$  in degrees.
- *Drop (%)* and *pitch* ( $\mu\text{m}$ ), which describe the shift of the neighbouring engraved lines. These parameters are interdependent, as shown in the following expression:

$$\text{Drop} = \frac{\tan \alpha \times \text{LD} \times \text{Pitch}}{100} \quad (4.9)$$

Laser engraving is made by mostly using a pulsed CO<sub>2</sub> laser. The frequency of pulsing varies typically from  $f = 5$  to 15 kHz. The typical cell line density is a few hundred per centimetre and an installation for laser engraving is shown in Figure 4.20.

On the other hand, manufacturers of the installations to engrave coatings have introduced sophisticated optical systems, such as the *New*

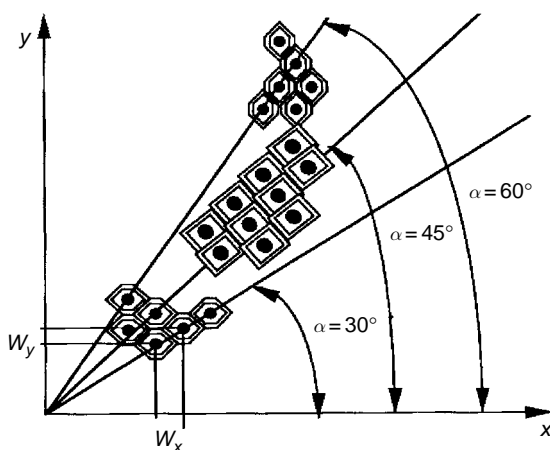


Figure 4.19 Shapes of cells upon engraving at different angles

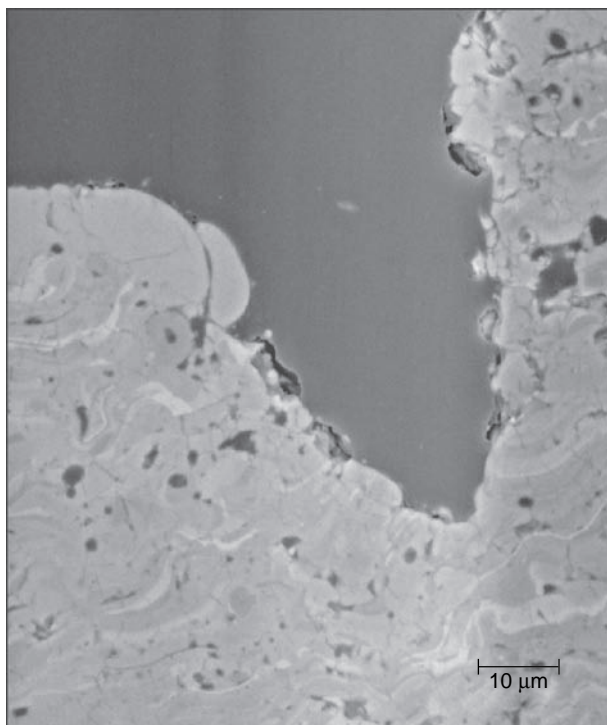


Figure 4.20 An installation for CO<sub>2</sub> laser engraving. Reproduced by permission of BS Lasergraphics, Itzehoe, Germany

*Anilox Technology* of ZED Instruments<sup>6</sup>, which enables, e.g. deflection of the laser beam across the surface of the engraved roll to achieve a better quality of engraving with high densities of cells or ‘double-engraving’ of the same cell to reach higher depths. The visible industrial tendency goes towards an increase of the density of the cells (*fine-pattern anilox rolls*). As the engraved cell diameter is physically limited by the laser emission wavelength of CO<sub>2</sub> (see Equation (4.3)), it is impossible to obtain a cell of a diameter less than 10 µm with a currently used CO<sub>2</sub> laser. This is why solid-state lasers, e.g. Nd-doped YAG, having shorter wavelengths, are increasingly tested in *anilox roll* production (Meiners, 1996; Birch, 1997). Recent developments in this field have concerned research on alternative coatings to Cr<sub>2</sub>O<sub>3</sub> ceramics and research to improve the production quality of laser engraving. Beczkowiak *et al.* (1996) initiated studies on the laser engraving of Al<sub>2</sub>O<sub>3</sub>, TiO<sub>2</sub>, Al<sub>2</sub>TiO<sub>5</sub> and Al<sub>2</sub>O<sub>3</sub>, alloyed with different contents of TiO<sub>2</sub> coatings applied by the APS technique. These authors found that the industrial laser engraving of Al<sub>2</sub>TiO<sub>5</sub> and Al<sub>2</sub>O<sub>3</sub>+60 wt% TiO<sub>2</sub> coatings produces cells which are quite similar to those engraved in Cr<sub>2</sub>O<sub>3</sub> coatings. These studies were followed up by the group at ENSCL (Lille, France) and their

<sup>6</sup> Catalogue of Zed Instruments, Hersham, UK (1993).

results were recently published (Znamirowski *et al.*, 2004; Tomaszek *et al.*, 2004). The publications show a careful analysis of the sprayed and engraved  $\text{TiO}_2$ ,  $\text{Al}_2\text{O}_3 + 13 \text{ wt\% TiO}_2$  and  $\text{Al}_2\text{O}_3 + 40 \text{ wt\% TiO}_2$  coatings' microstructures. Such studies enabled the workers to conclude that the specifications of anilox roll coatings, in terms of microhardness, small size of pores, homogeneity and  $\text{CO}_2$  laser light absorption, were fulfilled by the  $\text{Al}_2\text{O}_3 + 40 \text{ wt\% TiO}_2$  coating with a microstructure as shown in Figure 4.21.



**Figure 4.21** Scanning electron micrograph (backscattered electrons) of the inner part of a laser-engraved cell in an  $\text{Al}_2\text{O}_3 + 40 \text{ wt\% TiO}_2$  plasma-sprayed coating (line density (LD),  $100 \text{ cm}^{-1}$ )

The laser-engraving process was also simulated with a mathematical model by Groc *et al.* (1996, 1997). This model enabled prediction of the thickness of the liquid phase upon engraving. Liquid ceramics can be 'blown out' of the cell (*overflow effect*) and deteriorate the engraving quality. However, many further studies are necessary in order to convince manufacturers of the rolls and their customers to replace chromia by these ceramics.

## Electron Beam Treatment

Electron beam (e-beam) treatment is very useful post-spray technique if a small and precisely defined area can be worked out. The electrons can be confined to a very small spot. The spot is even smaller than that of laser light which is the result of the shorter wavelength of the electromagnetic wave associated with an electron beam (regulated by the electric-field intensity) and very well-developed electron optics. A major drawback is the necessity to carry out the treatment under vacuum. The latter restricts, to a degree, the dimensions of the treated piece or renders the treatment more expensive (cost of the vacuum chamber and an efficient pumping system). The vacuum at treatment should be a high level, with a dynamic pressure of  $p < 10^{-4}$  Pa. Moreover, the treated samples should be electrically conductive. Otherwise, their surfaces would charge negatively and repulse the oncoming electrons.

### *Principal parameters of e-beam treatment*

- Electric power which is a product of:
  - voltage (typically a tenth of a kV);
  - current (typically a tenth of a mA);
- Oscillation (deflection) which describes a zig-zag line of the e-beam over the substrate. The deflection has the following parameters:
  - width (a few mm to a few cm);
  - frequency (tenths of a Hz to a few kHz);
  - wave shape, which can be a sinusoidal triangle;
  - direction.
- Scan speed (a few mm to a few cm);
- Working distance, which is the distance between the last lens and the substrate.

The e-beam technique was applied to treat metals and alloy coatings by the following authors:

- Burman *et al.* (1987) subjected FeCrAlY coatings pre-deposited using atmospheric plasma spraying to electron beam re-melting. The oxides present in the as-sprayed coatings were reportedly eliminated by this treatment.

- Wielage and Fleischer (1998) treated, with electrons, the coatings of Cu and NiAl obtained on Mg alloy substrates by vacuum plasma spraying. This treatment was associated with the fusion of the substrate (*alloying*) and the *intermetallic alloys*, such as Mg<sub>2</sub>Ni and Mg<sub>2</sub>Cu, were formed. The formation of these alloys improved the hardness and wear of the initial coatings.
- Brandl *et al.* (2004) and Utu *et al.* (2005) used e-beam treatment to re-melt CoNiCrAlY alloys pre-deposited by HVOF. The electron treatment resulted in the formation of new phases, such as intermetallic AlCo and the oxides Al<sub>2</sub>O<sub>3</sub> and AlYO<sub>3</sub>. These authors interpreted the oxide formation as crystallization of the amorphous phases which were already present in pre-deposited coatings. The electron-re-melted coatings were tested against hot-gas corrosion. They exhibited a better resistance, which resulted from the formation of well-adhering oxide ‘scales’, which were responsible for a parabolic oxidation rate.

The superficial properties of metals and alloys at depths of a few micrometres can be modified by low-energy and high-current electron beams (Rotshtain *et al.*, 2004)

#### 4.1.2 FURNACE TREATMENT

This section deals with the heat treatments realized in different gas atmospheres. Diffusion treatment is described, together with the impregnation methods. Treatment in a furnace heats, in a more or less homogenous way, the coating and the substrate it was sprayed onto. If the substrate and coating materials have different thermal expansion coefficients (TCEs), thermal stresses are introduced during the heating cycle. These stresses must not be greater than the fracture stress in ceramics and/or the ultimate stress in metals and alloys. Consequently, the maximum temperature for furnace treatment of coated pieces is limited.

##### Treatment of Oxide Coatings

Most oxide ceramics has high-temperature phase transformations. Care has to be paid to control transformation-related stresses. For example,

a thermally sprayed  $\text{Al}_2\text{O}_3$  coating is usually composed of an  $\gamma$ -phase which transforms to the  $\alpha$ -phase above 1270 K. As this transformation is associated with density change (the  $\gamma$ -phase has a density of about  $3.60 \text{ g/cm}^3$ , while the  $\alpha$ -phase has a density of  $3.98 \text{ g/cm}^3$ ), the coating resulting from high-temperature furnace treatment has cracks and is more porous than the as-sprayed one (Thompson and Whittemore, 1968). Furnace treatment is a part of the manufacturing procedure of *free standing bodies*. The treatment aims at densifying by sintering the coatings which are initially detached from the substrate. This treatment increases usually their elastic moduli. It can also restore the superconducting effect in  $\text{YBa}_2\text{Cu}_3\text{O}_x$  (see Table 4.8). The latter was realized in two steps. In the first, an annealing was carried out in air in order to transform the simple cubic phase obtained in as-sprayed deposits into orthorhombic  $\text{YBa}_2\text{Cu}_3\text{O}_x$ . The second treatment was made in oxygen in order to increase the oxygen content in the material to reach a value of  $x \approx 7$ . Finally, cyclic thermal heating of thermal barrier coatings having the *duplex* configuration oxidize the interfaces between  $\text{ZrO}_2$  and an alumina-forming *superalloy*, such as e.g.,  $\text{NiCoCrAlY}$ . Thermally grown oxide (TGO) hampers the further oxidation of the bond coating (Table 4.8).

### Treatment of Metal and Alloy Coatings

A copper coating has been treated under hydrogen, in order to reduce the oxide content and improve the electric resistivity, by Braguier *et al.* (1973). At present, the cold-spray method offers an opportunity to obtain similar copper coatings without any post-spray treatment. Treatment in nitrogen gas and a plasma, in a carburizing atmosphere, enabled the hardening of a steel substrate under a ceramic coating (Nestler *et al.*, 1996, 1999). On the other hand, vacuum treatment is used at production of TBCs. This treatment enhances the adhesion of the bond coatings deposited onto turbine blades. Table 4.8 shows the details of the described furnace treatments.

#### 4.1.3 HOT ISOSTATIC PRESSING (HIP)

HIP consists, on simultaneous applications, of the treated components, high-pressure (up to 300 MPa) and high temperatures (up to 2300 K).

Table 4.8 Examples of furnace treatment of thermal sprayed coatings

Sprayed material	Spray technique	Temperature of treatment (K)	Time of treatment (h)	Atmosphere	Improved property	Reference
<i>Oxide ceramics</i>						
$\text{Al}_2\text{O}_3$	APS	1422–1866	0.5–4	Air	Densification from $\rho = 3.38$ to $3.60 \text{ g/cm}^3$	Thompson and Wittemore, 1968
$\text{ZrO}_2$	APS	1370–1870	1–36	Air	Young modulus, $\times 4$	Eaton and Novak, 1987
$\text{YBa}_2\text{Cu}_3\text{O}_x$	APS	1223, followed by 673–773	1–100, followed by 24–36	Air, followed by $\text{O}_2$	Superconducting effect restored	Pawlowski <i>et al.</i> , 1991
<i>Metals and alloys</i>						
Thermal barrier coating of $\text{ZrO}_2$ and $\text{NiCoCrAlY}$ Cu	NiCoCrAlY by VPS and $\text{ZrO}_2$ by APS VPS	Cycling, with a maximum temperature of 1394 1070	Heating for 10 min, held for 40 min and then cooling for 10 min	Air	Formation of thermally grown oxide (TGO) on the top layer of the bond coating	Tang and Schoenung, 2005
$\text{Al}_2\text{O}_3$ onto $16\text{MnCr}5$ steel	APS	773–863	4–50	$\text{H}_2$	Improved resistivity from 14 to $7 \mu\Omega\text{cm} \mu\Omega\text{cm}$	Bragnier <i>et al.</i> , 1973
$\text{NiCoCrAlY}$	VPS	1323	4	$\text{N}_2$	Hardening of substrate	Nestler <i>et al.</i> , 1996
				Vacuum	Enhanced adhesion of bond coating	Cosack <i>et al.</i> , 1992

The sample is sealed in the vessel and the operating pressure (using argon as the working gas) is then applied with the help of compressors. The final pressure is obtained due to the expansion of the hot gas. The HIP treatment can be applied only to rather small sprayed specimens.

### Treatment of Ceramic and Cermet Coatings

The main transformations resulting from the hot isostatic pressing of ceramic coatings are as follows:

- densification, reduction of porosity and reduction of cracking;
- recrystallization of some phases, e.g. a non-transformable tetragonal phase in  $\text{ZrO}_2 + 8 \text{ wt\% Y}_2\text{O}_3$  coatings (Chen *et al.*, 1997);
- improvement of mechanical properties, e.g. strength, microhardness, etc;
- improvement of coating adhesion to the substrates.

Some examples of the hot isostatic treatment of sprayed ceramics and cermets are shown in Table 4.9.

### Treatment of Alloy Coatings

Hot isostatic treatment is applied for alloys coatings in order to improve their mechanical properties and their resistance against hot corrosion. Some examples of treatments are shown in Table 4.9.

#### 4.1.4 COMBUSTION FLAME RE-MELTING

The traditional deposition technique of flame spraying is often applied to obtain *self-fluxing* alloys, such as NiCrBSi containing Si and/or B, i.e. elements that lower the melting point of the alloy. The sprayed coatings can be easily rendered molten by using a combustion flame. The treatment is carried out at temperatures of about 1323 K and can also be realized by using induction melting and furnace heating (Matthes *et al.*, 1996)

**Table 4.9** Examples of hot isostatic treatment of thermally sprayed cermets, cermets and alloys

Sprayed material composition (wt%)	Spray technique	Temperature of treatment (K)	Pressure of treatment (MPa)	Time of treatment (h)	Improved property	Reference
<i>Ceramics and cermets</i>						
Al <sub>2</sub> O <sub>3</sub>	APS	1370–1570	100–130	1–2	Microhardness increases from 700 to 1200; tensile strength increases from a few MPa to 60 MPa	Kuribayashi <i>et al.</i> , 1986
ZrO <sub>2</sub> +8Y <sub>2</sub> O <sub>3</sub> onto NiAl bond coating	APS	1523	200 (Ar)	2	Densification; reduction of cracking; recrystallization of t' phase,	Chen <i>et al.</i> , 1997
Ti6Al4V+(20–80)HA	APS	1173–1273	180	1	Reduction of porosity; increase of pore size; increase in adhesion	Khor <i>et al.</i> , 1997
<i>Alloys</i>						
Fe+20Cr+9Al+1.5Y	APS	—	—	—	Improvement of hot-corrosion resistance	Burman <i>et al.</i> , 1987
Ni+21.5Co+16.3Cr+0.1Al	VPS	1173–1453	180–350	3	Homogenization of microhardness; increase in yield strength	Steffens <i>et al.</i> , 1988

## 4.2 IMPREGNATION

Impregnation is mainly used to ‘seal’ the ‘open porosity’ in sprayed coatings. Liquid sealants penetrate by capillary action into the pores and then solidify. Impregnation is sometimes accompanied by heat treatment which encourages diffusion of the sealant and homogenization of the microstructure. These impregnation methods can be categorized, according to the impregnation pressure, as follows (Knuutila *et al.*, 1999):

- atmospheric-pressure impregnation;
- low-pressure impregnation;
- over-pressure impregnation;
- combination of the above methods.

The choice of the method depends on the following:

- size of the treated component;
- required penetration depth;
- properties of the sealant.

Low-pressure and over-pressure impregnations are suitable for small components. Atmospheric-pressure impregnation is the only method for larger pieces. In this case, the sealant can be applied by brushing, dipping or spraying. The impregnation theory was developed in the review by Knuutila *et al.* (1999). In this section, the impregnation methods will be discussed in relation to:

- inorganic impregnation, including molten metals and CVD methods;
- organic impregnation.

### 4.2.1 INORGANIC SEALANTS

The following impregnation methods will be discussed in the following:

- sol-gel;
- aluminium phosphate;
- molten metals;
- other methods.

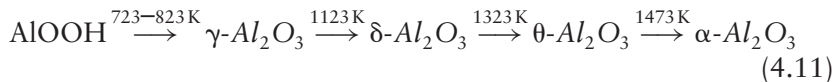
### Sol–Gel Method

This method involves the application of a liquid metal–organic precursor (sol) onto the surface of a coating. The precursor penetrates the latter, due to the action of capillary forces, as follows:

$$d^2 = \frac{\gamma \cos \Theta}{2\eta} rt \quad (4.10)$$

where the depth,  $d$ , can be obtained by assuming that the coating is an assemblage of capillaries having a radius,  $r$  (Troczyński *et al.*, 1999; Knuutila *et al.*, 1999).

‘Deep infiltration’ is consequently favoured by the time of impregnation, low viscosity of the sealant and its low wetting angle. The starting precursor is, e.g. aluminium isopropoxide ( $\text{Al}(\text{OC}_3\text{H}_7)_3$ ) dissolved in isopropyl alcohol. This sol was used by Troczyński *et al.* (1999) and Moriya *et al.* (1994) and is known to transform under gelation (see also Section 1.1.7) and then by *calcination* and heat treatment into alumina, according to the following chain of transformations (Perrin and Scharff, 1999):



The alumina obtained by the sol–gel method was used to seal:

- Alumina coatings obtained by APS using a *calcination* temperature of 673 K (Moriya *et al.*, 1994). This treatment helped to reduce the ‘interconnected porosity’ and improved the wet-corrosion resistance.
- Yttria-stabilized zirconia coatings by APS (as thermal barrier coatings) using calcination and a heat-treatment temperature of up to 1673 K (Troczyński *et al.*, 1999). In a similar study by Kartikeyan *et al.* (1996), aluminium hydroxide was used as the sol and calcination was carried out at 873 K for 1 h and was followed by heat treatment at 1273 K for 1 h. This treatment was intended to increase the hot-corrosion resistance of the TBCs.

### Aluminium Phosphate

An aqueous solution of aluminium hydroxide ( $\text{Al}(\text{OH})_3$ ) with orthophosphoric acid ( $\text{H}_3\text{PO}_4$ ) can be applied onto porous coating

surfaces. Continuous heat treatment at 373, 473 and 673 K (each step for 2 h) is needed to complete dehydratation of the aluminium phosphate solution. Such a treatment was applied to seal:

- Chromia coatings obtained by APS (Vippola *et al.*, 2002), as well as chromia and alumina (Leivo *et al.*, 1997). These coatings revealed an improved resistance against abrasive and erosive wear.
- Yttria-stabilized zirconia coatings obtained by APS. The sealing procedure represents part of the development of *thick thermal-barrier coatings* (TTBCs) with the top coatings having thickness up to 1000 µm (Ahmaniemi *et al.*, 2002).

### Molten Metals

This type of impregnation uses ‘foils’ of low-melting-point metals placed on the surfaces of the coatings and heat-treated in an vacuum oven above the melting point. This kind of impregnation was applied by the following authors:

- Ito *et al.* (1988) sealed titanium–molybdenum coatings obtained by APS with copper. The foils were heated at 1370 K ( $T_m = 1358$  K for copper) in a vacuum of 0.1 Pa for times ranging from 10 to 30 min. These authors found that the sealed coatings have better adhesion to mild steel substrates and better corrosion resistance.
- Ohmori *et al.* (1994) sealed alumina- and yttria-stabilized zirconia coatings with manganese. The plates were heated at 1573 K ( $T_m = 1519$  K for manganese) in a vacuum of  $10^{-3}$  Pa. This treatment was found to improve the mechanical properties of the coatings (micro-hardness and fracture toughness).

### Other Methods

**Chromium Diffusion** Chromium diffusion consists of the application to the surfaces of coatings of a penetrating agent, including pulverized chromium with other agents, e.g. alumina, ammonia chloride or/and water, to facilitate penetration. These coating can be embedded in a mixture (Takeuchi *et al.*, 1998) or sprayed onto it (Carr and Jones, 1984) and the coated pieces are consequently subjected to heat treatment

at 1203 K for 8 h or at 810 K ( $\times 14$ ), respectively. This treatment was applied to densify:

- zirconia coatings sprayed by plasma in air for use in adiabatic engines (Carr and Jones, 1984);
- chromium carbide–nickel chromium cermet coatings obtained by the same method for wear-resistant coatings with an improved resistance against thermal shocks (Takeuchi *et al.*, 1998).

**Chemical Treatment** Ceramic coatings can be sealed with glass-forming components, such as  $\text{SiO}_2$  or other oxides. This sealing can be accompanied by heat treatment at the glass-softening temperature. An example is sealing with a mixture of zirconium and yttrium nitrate aqueous solutions for atmospheric-plasma-sprayed yttria-stabilized zirconia (YSZ) coatings (Li *et al.*, 2005). After sealing, the samples were heated (twice) at 773 K for 30 min until complete decomposition of the nitrates and their transformation into YSZ. This treatment was applied to densify a solid electrolyte of a solid oxide fuel cell with a tubular shape. The similar atmospheric-plasma-sprayed YSZ coatings were densified by means of a 10  $\mu\text{m}$ -thick zirconia film obtained by CVD. Finally, the porous Ti coatings obtained by vacuum plasma spraying were treated by an NaOH solution at 313 K for 24 h. This treatment modified the morphology of the surfaces of the coatings and produced Ti–OH groups favourable for the bioactivity of deposits (Shi *et al.*, 2001).

#### 4.2.2 ORGANIC SEALANTS

Organic sealants can be one- or two-components resins. One-component systems are cured by the action of heat or uv light. The two component resins polymerize in the presence of hardeners. The organic sealants used are mainly (Knuutila *et al.*, 1999):

- epoxy resins;
- phenolic resins;
- silicone resins;
- polyurethanes;
- polyvinylesters;
- polymethacrylates;
- waxes.

An example of organic sealing is the application of silicone resins by rubbing onto the surface of an air plasma sprayed alumina coating in order to protect the coating against absorption of water. As-sprayed alumina is crystallized in the highly hygroscopic  $\gamma$ -phase. On the other hand, water has a high dielectric constant ( $\epsilon_r \approx 88$  at 1 kHz) which might increase the dielectric constant and the electrical losses of the sprayed alumina, which has a dielectric constant of about 10 at this frequency. In some applications of sprayed coatings, the dielectric constant of the sprayed alumina should not be too high, in order to keep this within the specified limits. This is the case for *corona rolls* used in the ‘corona treatment’ of polymeric foils. Impregnation with silicone resin ( $\epsilon_r \approx 2.5$ ) allows keeping of this specification. Another application is sealing by using different resins (silicone, epoxy, fluororesin) of wire-flame-sprayed Al + 2 wt% Zn coatings. This sealing improves the resistance of the coatings against salt-water corrosion (Tanaka and Takatani, 2001).

## 4.3 FINISHING

Thermally sprayed coatings must be ‘finished’ for many industrial applications. The requirements include the ‘tolerated dimension’, as well as roughness of the surfaces of the coatings. Grinding is used to achieve the desired dimension and polishing or lapping to obtain the required roughness.

### 4.3.1 GRINDING

For grinding ceramic coatings, diamond and cubic boron nitride (CBN) wheels are used. Metallic or metal matrices with carbide reinforcement composites can be ground with silicium carbide wheels (Ibrahim and Sampath, 1996). The most important grinding parameters include the following (Massad, 1985):

- type of abrasive (CBN, diamond);
- grit size;
- concentration of abrasive;
- type of bond (metal or resin);
- rotation speed of wheel;
- rotation (or linear) speed of ground piece;
- depth of grinding.

### 4.3.2 POLISHING AND LAPPING

Polishing is carried out by using the same machines as used for grinding but with finer abrasive. Careful control of the polishing parameters permits obtaining surfaces with  $R_a$  values less than  $0.2\text{ }\mu\text{m}$  (e.g. for chromium oxide coatings). Further improvement in the roughness could be achieved by lapping. Lapping is a process in which abrasives (such as diamond or alumina) are used in oil or grease mixtures (Boyd, 1985). It is recommended to use lapping if the vibrations of the grinding or polishing machines leave traces on the finished surfaces.

## REFERENCES

- Agrawal, D.K. (1998). Microwave processing of ceramics, *Curr. Opin. Solid State Mater. Sci.*, 3, 480–485.
- Ahmaniemi, S., Tuominen, J., Vuoristo, P. and Mäntylä, T. (2002). Sealing procedures for thick thermal barrier coatings, *J. Therm. Spray Technol.*, 11, 320–332.
- Aihua, W., Zengyi, T., Beidi, Z., Jiangmin, F., Xianyao, M., Shijun, D. and Xudong, C. (1992). Laser modification of plasma sprayed  $\text{Al}_2\text{O}_3 + 13\text{ wt\% TiO}_2$  coatings on a low carbon steel, *Surf. Coat. Technol.*, 52, 141–144.
- Aihua, W., Beidi, Z., Zengyi, T., Xianyao, M., Shijun, D. and Xudong, C. (1993). Thermal-shock behaviour of plasma sprayed  $\text{Al}_2\text{O}_3 + 13\text{ wt\% TiO}_2$  coatings on Al-Si alloy influenced by laser remelting, *Surf. Coat. Technol.*, 37, 169–172.
- Alam, S., Sasaki, S., Shimura, H., Kawakami, Y. and Hassan, M.A. (1997). Tribological and microstructural investigations of bronze coating by laser and plasma hybrid spraying technique, in *Surface Modification Technologies X*, T.S. Sudarshan, K.A. Khor and M. Jeandin (Eds), The Institute of Materials, London, UK, pp. 918–926.
- Allmen, von M. (1980). Coupling of beam energy to solids, in *Laser and Electron Beam Processing of Materials*, P.S. Peary (Ed.), Academic Press, New York, pp. 6–19.
- Ayers, J.D. and Schaefer, R.J. (1979). Consolidation of plasma sprayed coatings by laser remelting, *Proc. SPIE*, 198, 57–64.
- Bass, M. (1983). Laser heating of solids, in *Physical Processes in Laser–Materials Interactions*, M. Bertolotti (Ed.), Plenum Press, New York, NY, USA, pp. 77–115.
- Beczkowiak, J., Keller, H. and Schwier, G. (1996).  $\text{Al}_2\text{O}_3\text{--TiO}_2$  Schichten-eine Alternative zu  $\text{Cr}_2\text{O}_3$ , in *Thermische Spritzkonferenz TS'96*, Vol. 175, E Lugscheider (Ed.), E., DVS-Berichte, DVS-Verlag, Düsseldorf, Germany, pp. 68–71.
- Bhat, H., Herman, H. and Coyle, R.J. (1983). Laser processing of plasma sprayed NiCr coatings, in *Lasers in Materials Processing*, TMS-AIME, Warrendale, PA, USA, pp. 176–83.
- Birch, E. (1997). Applied Laser Engineering, West Molesey, UK, Personal Communication.
- Boyd, L.L. (1985). Method for finishing thermal sprayed coatings, in *Thermal Spray Coatings: New Materials, Processes and Applications*, F.N. Longo (Ed.), ASM International, Materials Park, OH, USA, pp. 135–138.

- Braguier, M., Bejat, J., Tueta, R., Verna, M., Aubin, G. and Naturel, C. (1973). Improvements of plasma spraying process for hybrid microelectronics, in *Conference on Hybrid Electronics and Microelectronics*, Canterbury, UK, 25–27 September, pp. 15–37.
- Brandl, W., Marginean, G., Maghet, D. and Utu, D. (2004). Effects of specimen treatment and surface preparation on the isothermal oxidation behaviour of the HVOF-sprayed MCrAlY coatings, *Surf. Coat. Technol.*, **188–189**, 20–26.
- Burman, C., Ericsson, T., Kvernes, I. and Lindblom, Y. (1987). Coatings with lenticular oxides preventing interdiffusion, *Surf. Coat. Technol.*, **32**, 127–140.
- Capp, M.L. and Rigsbee, J.M. (1984). Laser processing of plasma-sprayed coatings, *Mater. Sci. Eng.*, **62**, 49–56.
- Carr, J. and Jones, J. (1984). Post densified Cr<sub>2</sub>O<sub>3</sub> for adiabatic engine, *SAE Technical Paper*, No. 840 432, Warrendale, PA, USA.
- Carslaw, H.S and Jaeger, J.C. (1959). *Conduction of Heat in Solids*, 2nd Edition, Oxford University Press, London, UK.
- Chen, C., Wei, W.-C. and Chang, K.-J. (1996). Laser remelting process for plasma-sprayed zirconia coatings, *US Patent*, 5 576 069.
- Chen, H.C., Pfender, E. and Heberlein, J. (1997). Structural changes in plasma-sprayed ZrO<sub>2</sub> after hot isostatic pressing, *Thin Solid Films*, **293**, 227–235.
- Cheng, J., Agrawal, D., Roy, R. and Jayan, P.S. (2000). Continuous microwave sintering of alumina abrasive grits, *J. Mater. Proc. Technol.*, **108**, 26–29.
- Chwa, S.O., Ohmori, A., Yang, H. and Zhou, Z. (2001). Surface modification of plasma sprayed coating by using YAG laser equipped with a kaleidoscope, in *Thermal Spray 2001: New Surfaces for a New Millennium*, C.C. Berndt, K.A. Khor and E. Lugscheider, ASM International, Materials Park, OH, USA, pp. 575–582.
- Cosack, T., Pawłowski, L., Schneiderbanger, S. and Sturlese, S. (1992). Thermal barrier on turbine blades by plasma spraying with improved cooling, in *Proceedings of 37th ASME Int. Gas Turbine & Aeroengine Congress and Exposition*, Köln, Germany, June 1–4, ASME, New York, NY, USA, Paper 92-GT-319.
- Dallaire, S. and P. Cielo, P. (1982). Pulsed laser treatment of plasma sprayed coatings, *Metall. Trans.*, **B**, **13**, 479–483.
- Dallaire, S. and Cielo, P. (1983). Pulsed laser glazing, *Thin Solid Films*, **108**, 19–27.
- Dane, C.B., Hackel, L.A., Daly, J. and Harrison, J. (1998). Shot peening with lasers, *Adv. Mater. Proc.*, **153**, 37–38.
- Das, D.K. (1994). Surface roughness created by laser surface alloying of aluminium with nickel, *Surf. Coat. Technol.*, **64**, 11–15.
- Deram, V., Minichiello, C., Vannier, R.-N., Le Maguer, A., Pawłowski, L. and Murano, D. (2003). Microstructural characterizations of plasma sprayed hydroxyapatite coatings, *Surf. Coat. Technol.*, **166**, 153–159.
- Devaux, D., Fabbro, R. and Virmont, J., (1991). Generation of shock waves by laser-matter interaction in confined geometries, *J. Phys. IV, Coll. C7*, **1**, 179–182.
- Dyshlovenko, S. (2005). Modélisation des procédés de la projection plasma et du traitement laser de hydroxyapatite, *Ph.D. Thesis*, ENSCL, Lille, France.
- Eaton, H.E. and Novak, R.C. (1987). Sintering studies of plasma sprayed zirconia, *Surf. Coat. Technol.*, **32**, 227–236.
- Fu, Y., Batchelor, A.W., Xing, H. and Gu, Y. (1997). Wear behaviour of laser-treated plasma-sprayed ZrO<sub>2</sub> coatings, *Wear*, **210**, 157–164.
- Galasso, F.S. and Veltri, R. (1983). Observation of laser interaction with ceramics, *Am. Ceram. Soc. Bull.*, **62**, 253–254.

- Gorecka-Drzazga, A., Golonka, L., Pawłowski, L. and Fauchais, P. (1984). Application of the plasma spraying process to the production of metal-ceramics substrates for hybrid electronics, *Rev. Int. Hautes Temp. Refract.*, **21**, 153–165.
- Groc, M., Pawłowski, L., Smurov, I., Clinton, G. and Pitt, R. (1996). Modeling of the laser engraving at plasma sprayed  $\text{Cr}_2\text{O}_3$  coatings on anilox rolls, in *Thermal Spray: Practical Solutions for Engineering Problems*, C.C. Berndt (Ed.), ASM International, Materials Park, OH, USA, pp. 603–613.
- Groc, M., Pawłowski, L. and Smurov, I. (1997). Modeling of the laser engraving at plasma sprayed  $\text{Al}_2\text{O}_3$ ,  $\text{TiO}_2$  and  $\text{Al}_2\text{TiO}_5$  coatings for anilox rolls, in *Thermal Spray: A United Forum for Scientific and Technological Advances*, C.C. Berndt (Ed.), ASM International, Materials Park, OH, USA, pp. 41–49.
- Herziger, G. and Loosen, P. (1993). *Werkstoffbearbeitung mit Laserstrahlung*, Carl Hanser Verlag, München, Germany.
- Hocking, M.G., Vasantasree, V. and Sidky, P.S. (1989). *Metallic and Ceramic Coatings*, Longman, Burnt Mill, UK.
- Ibrahim, A. and Sampath, S. (1996). Effect of grinding mechanisms on surface finish and hardness of thermally sprayed WC-Co, in *Thermal Spray: Practical Solutions for Engineering Problems*, C.C. Berndt (Ed.), ASM International, Materials Park, OH, USA, pp. 493–499.
- Ingham, H.S. (1967). Flame spraying employing laser heating, *US Patent*, 3 310 423.
- Ito, H., Nakamura, R. and Shiroyama, M. (1988). Infiltration of copper into titanium molybdenum spray coatings, *Surf. Eng.*, **4**, 35–38.
- Jasim, K.M., West, D.R.F., Steen, W.M. and Rawlings, R.D. (1989). Laser surface sealing of plasma sprayed yttria stabilized zirconia ceramics, in *Laser Materials Processing, ICALÉO'88*, G. Buck (Ed.), Springer-Verlag, Berlin, Germany, pp. 17–30.
- Jasim, K.M., Rawlings, R.D. and West, D.R.F. (1991). Pulsed laser processing of thermal barrier coatings, *J. Mater. Sci.*, **26**, 909–916.
- Jasim, K.M., Rawlings, R.D. and West, D.R.F. (1992). Characterization of plasma-sprayed layers of fully yttria-stabilized zirconia by laser sealing, *Surf. Coat. Technol.*, **53**, 75–86.
- Kartikeyan, J., Berndt, C.C., Ristorucci, A. and Herman, H. (1996). Ceramic impregnation of plasma sprayed thermal barrier coatings, in *Thermal Spray: Practical Solutions for Engineering Problems*, C.C. Berndt (Ed.), ASM International, Materials Park, OH, USA, pp. 477–482.
- Khor, K.A. and Cheang, P. (1994). Laser post-treatment of thermally sprayed hydroxyapatite coatings. In: *Thermal Spray Industrial Applications*, eds. C.C. Berndt and S. Sampath, ASM Int., Materials Park, OH, USA, 153–7.
- Khor, K.A., Yip, C.S. and Cheang, P. (1997). Post-spray hot isostatic pressing of plasma sprayed Ti-6Al-4V/hydroxyapatite composite coatings, *J. Mater. Proc. Technol.*, **71**, 280–287.
- Khor, K.A., Yu, L.-G., Chan, S.H. and Cheang, P. (2002). Spark plasma sintering of plasma sprayed HA coatings, in *Proceedings of the International Thermal Spray Conference 2002 Essen*, E. Lugscheider and C.C. Berndt (Eds), DVS Verlag, Düsseldorf, Germany, pp. 1024–1028.
- Khor, K.A., Yu, L.-G., Chan, S.H. and Chen, X.J. (2003). Densification of plasma sprayed YSZ electrolytes by spark plasma sintering (SPS), *J. Eur. Ceram. Soc.*, **23**, 1855–1863.

- Knuutila, J., Sorsa, P. and Mäntylä (1999). Sealing of thermal spray coatings by impregnation, *J. Ther. Spray Technol.*, **8**, 249–257.
- Kuribayashi, H., Suganuma, K., Miyamoto, Y. and Koizumi, M. (1986). Effects of HIP treatment on plasma sprayed ceramic coating onto stainless steel, *Ceram. Bull.*, **51**, 1031–1035.
- Leivo, E.M., Vippola, M.S., Sorsa, P.P.A., Vuoristo, P.M.J. and Mäntylä, T.A. (1997). Wear and corrosion properties of plasma sprayed  $\text{Al}_2\text{O}_3$  and  $\text{Cr}_2\text{O}_3$  coatings sealed by aluminum phosphates, *J. Therm. Spray Technol.*, **6**, 205–210.
- Li, C.-J., Ning, X.-J., and Li, C.X. (2005a). Effect of densification processes on the properties of plasma-sprayed YSZ electrolyte coatings for solid oxide fuel cells, *Surf. Coat. Technol.*, **190**, 60–64.
- Li, H., Khor, K.A., Yu, L.G. and Cheang, P. (2005b). Microstructure modifications and phase transformation in plasma-sprayed WC-Co coatings following post-spray spark plasma sintering, *Surf. Coat. Technol.*, **194**, 96–102.
- Liang, G.Y. and Wong, T.T. (1997). Microstructure and character of laser remelting of plasma sprayed coating (Ni-Cr-B-Si) on Al-Si alloy, *Surf. Coat. Technol.*, **89**, 121–126.
- Maricocchi, A., Bartz, A. and Wortman, D. (1997). PVD TBC experience on GE aircraft engines, *J. Therm. Spray Technol.*, **9**, 193–199.
- Masse, J.E. and Barreau, G. (1995). Laser generation of stress waves in metal, *Surf. Coat. Technol.*, **70**, 231–234.
- Mateos, J., Cuetos, J.M., Fernandez, E. and Cadena, M. (1997). Effect of laser treatment on tungsten carbide coatings, in *Surface Treatment'97*, M.H. Aliabadi and C.A. Berbbia (Eds), Computational Mechanical Publishers, Southampton, UK, pp. 239–246.
- Matthes, K.J., Weichbrodt, K.-H., Lanzendorfer, G., Lugscheider, E., Nyland, A. and Sicking, R. (1996). Flammespritzen mit nachfolgendem Einschmelzen einer NiCrBSi-Legierung auf vergüteten Stählen, *Schw. Schn.*, **48**, 116–125.
- Massad, R.B. (1985). Diamond wheel grinding of thermal spray materials, in *Thermal Spray Coatings: New Materials, Processes and Applications*, F.N. Longo (Ed.), ASM International, Materials Park, OH, USA, pp. 139–146.
- Meiners, E. (1996). Mikrostrukturierung von Makrooberflächen – Laseranwendungen in der Druckformenherstellung, in *Proceedings of the 6th European Conference on Laser Treatment of Materials, ECLAT'96* F. Dausinger, H.W. Bergmann and J. Sigel (Eds), AWT, Stuttgart, Germany, pp. 663–674.
- Moriya, K., Tomino, H., Kandaka, Y., Hara, T. and Ohmori, A. (1994). Sealing of plasma-sprayed ceramic coatings by sol-gel process, in *Thermal Spray Industrial Applications*, C.C. Berndt and S. Sampath (Eds), ASM International, Materials Park, OH, USA, pp. 549–553.
- Murakami, T., Sasaki, S., Ito, K., Inui, H. and Yamaguchi, M. (2004). Microstructure of Nb substrates coated with  $\text{Mo}(\text{Si}, \text{Al})_2-\text{Al}_2\text{O}_3$  composite and B-doped  $\text{Mo}_5\text{Si}_3$  layers by spark plasma sintering, *Intermetallics*, **12**, 749–754.
- Nestler, M.C., Spies, H.-J., Herrmann, K., Klement, K. and Wewel, M. (1996). Thermo-chemische Nachbehandlung von Spritzschichten, in *Thermische Spritzkonferenz TS'96*, Vol. 175, E. Lugscheider (Ed.), DVS-Berichte, DVS-Verlag, Düsseldorf, Germany, pp. 190–193.
- Nestler, M.C., Spies, H.-J. and Herrmann, K. (1999). Improvement of coating characteristics and end-use performance of thermal sprayed coatings through post-treatments

- like hardening, nitriding or carburizing, in *Proceedings of the United Thermal Spray Conference, 1999, Düsseldorf*, E. Lugscheider and P. Kammer (Eds), DVS-Verlag, Düsseldorf, Germany, pp. 213–218.
- Ohmori, A., Hirano, S. and Kamada, K. (1993). Spraying TiN by a combined laser and low-pressure plasma spray system, *J. Therm. Spray Technol.*, **2**, 137–144.
- Ohmori, A., Zhou, Z. and Inoue, K. (1994). Improvement of plasma-sprayed ceramic coating properties by heat-treatment with liquid Mn, in *Thermal Spray Industrial Applications*, C.C. Berndt and S. Sampath (Eds), ASM International, Materials Park, OH, USA, pp. 543–548.
- Pangborn, R.J. and Beaman D.R (1980). Laser glazing of sprayed metal coatings, *J. Appl. Phys.*, **51**, 5992–5993.
- Pawlowski, L. (1996). Technology of thermally sprayed anilox rolls: state of art, problems and perspectives, *J. Therm. Spray Technol.*, **5**, 317–335.
- Pawlowski, L. (1998). Quality improvement of coating by a prespray and postspray process, *J. Therm. Spray Technol.*, **7**, 3–6.
- Pawlowski, L. (1999). Thick laser coatings: a review, *J. Therm. Spray Technol.*, **8**, 279–295.
- Pawlowski, L. (2003). *Dépôts Physiques. Techniques, microstructures et propriétés*, Presse Polytechnique et Universitaire Romande, Lausanne, Switzerland.
- Pawlowski, L., Gross, A. and McPherson, R. (1991). Microstructure of plasma sprayed  $\text{YBa}_2\text{Cu}_3\text{O}_x$  high-temperature superconductor, *J. Mater. Sci.*, **26**, 3803–3808.
- Pawlowski, L., Rapinel, H., Tourenne, F. and Jeandin, M. (1997). Traitement laser des dépôts plasma d'hydroxyapatite, *Galv. Org. Traite. Surf.*, **676**, 433–437.
- Perrin, R. and Scharff, J.-P. (1999). *Chimie Industrielle*, Dunod, Paris, pp. 400–406.
- Peyre, P., Fabbro, R., Berthe, L. and Dubouchet, C. (1996). Laser shock processing of materials, physical processes involved and examples of applications, *J. Laser Appl.*, **8**, 135–141.
- Pravara, B., Yara, H., Miyagi, Y. and Fukushima, T. (2003). Spark plasma sintering as a post-spray treatment for thermally-sprayed coatings, *Surf. Coat. Technol.*, **162**, 234–241.
- Ranz, X., Pawlowski, L., Sabatier, L., Fabbro, R. and Aslanian, T. (1998). Phases transformation in laser treated hydroxyapatite coatings, in *Thermal Spray: Meeting the Challenges of the 21st Century*, C. Coddet (Ed.), ASM International, Materials Park, OH, USA, 1343–1349.
- Rotshtein, V.P., Proskurovsky, D.I., Ozur, G.E., Ivanov, Yu.F. and Markov, A.B. (2004). Surface modification and alloying of metallic materials with low-energy high-current electron beams, *Surf. Coat. Technol.*, **180–181**, 377–381.
- Roy, R., Agrawal, D., Cheng, J. and Gedevanishvili, S. (1999). Full sintering of powdered-metal bodies in a microwave field, *Nature*, **399**, 668–670.
- Schnick, T., Tondu, S., Peyre, P., Pawlowski, L., Steinhäuser, Wielage, B., Hofmann, U. and Bartnicki, E. (1999). Laser shock processing of Al-SiC composite coatings, *J. Therm. Spray Technol.*, **8**, 296–300.
- Shi, J.M., Ding, C.X. and X.Q. Wu (2001). Preparation of bioactive and porous titanium coating by vacuum plasma spraying and chemical treatment, in *Thermal Spray 2001: New Surfaces for a New Millennium*, C.C. Berndt, K.A. Khor and E.F. Lugscheider (Eds), ASM International, Materials Park, OH, USA, pp. 593–597.
- Siegman, A.E. (1986). *Lasers*, University Science Books, Sausalito, CA, USA.

- Singh, J., Bhat, B.N., Poorman, R., Kar, A. and Mazumder, J. (1996). Laser glazing of vacuum plasma coated NARloy – Z, *Surf. Coat. Technol.*, **79**, 35–49.
- Skrzypczak, M., Bertrand, P., Zdanowski, J. and Pawlowski, L. (2001). Modeling of temperature fields in the graphite target at pulsed laser deposition of CN<sub>x</sub> films, *Surf. Coat. Technol.*, **138**, 39–47.
- Steffens, H.-D., Dammer, R. and Fischer, U. (1988). Post treatment of metal composites by hot isostatic pressing, *Surf. Eng.*, **4**, 38–42.
- Streiff, R., Pons, M. and Mazars, P. (1987). Laser induced microstructural modifications in a vacuum plasma sprayed NiCoCrAlYTa coating. *Surf. Coat. Technol.*, **32**, 85–95.
- Takeuchi, J., Murata, Y., Harada, Y., Tomita, T., Nakahama, S. and Go, T. (1998). An improvement of Cr<sub>3</sub>C<sub>2</sub>–NiCr sprayed coatings followed by chromium diffusion treatment, in *Thermal Spray: Meeting the Challenges of the 21st Century*, C. Coddet (Ed.), ASM International, Materials Park, OH, USA, pp. 1425–1430.
- Tanaka, M. and Takatani, Y. (2001). Evaluation of sealants on Al–Zn alloy sprayed coating by galvanostatic technique, in *Thermal Spray 2001: New Surfaces for a New Millennium*, C.C. Berndt, E.F. Khor and E.F. Lugscheider (Eds), ASM International, Materials Parks, OH, USA, pp. 621–625.
- Tang, F. and Schoenung, J.M. (2005). Local accumulation of thermally grown oxide in plasma-sprayed thermal barrier coatings with rough top-coat/bond-coat interfaces, *Scrip. Mater.*, **52**, 905–909.
- Thompson, V.S. and Whittemore, Jr, O.J. (1968). Structural changes on reheating plasma-sprayed alumina, *Ceram. Bull.*, **47**, 637–641.
- Tomaszek, R., Pawlowski, L., Zdanowski, J., Grimblot, J. and Laureyns, J. (2004). Microstructural transformation of TiO<sub>2</sub>, Al<sub>2</sub>O<sub>3</sub> + 13TiO<sub>2</sub> and Al<sub>2</sub>O<sub>3</sub> + 40TiO<sub>2</sub> at plasma spraying and laser engraving, *Surf. Coat. Technol.*, **185**, 137–149.
- Tondu, S., Schnick, T., Pawlowski, L., Wielage, B., Steinhäuser, S. and Sabatier, L. (1998). Laser glazing of FeCr – TiC composite coatings, *Surf. Coat. Technol.*, **123**, 247–251.
- Troczyński, T., Pawłowski, L., Third, N., Covelli, L. and Smurov, I. (1998). Physico-chemical treatment of zirconia coatings for thermal barriers, in *Thermal Spray: Meeting the Challenges of the 21st century*, C. Coddet (Ed.), ASM International, Materials Park, OH, USA, pp. 1337–1342.
- Troczyński, T., Yang, Q. and John, G. (1999). Post-deposition treatment of zirconia thermal barrier coatings using sol–gel alumina, *J. Therm. Spray Technol.*, **8**, 229–234.
- Tsai, H.L. and Tsai, P.C. (1995). Performance of laser-glazed plasma-sprayed (ZrO<sub>2</sub>–12 wt% Y<sub>2</sub>O<sub>3</sub>)/(Ni–22 wt% Cr–10 wt% Al–1 wt% Y) thermal barrier coatings in cyclic oxidation tests, *Surf. Coat. Technol.*, **71**, 53–59.
- Utu, D., Brandl, W., Marginean, G., Cartis, I. and Serban, V.A. (2005). Morphology and phase modification of HVOF-sprayed MCrAlY-coatings remelted by electron beam irradiation, *Vacuum*, **77**, 451–455.
- Vippola, M., Ahmanniemi, S., Vuoristo, P., Lepistö, Mäntylä, T. and Olsson, E. (2002). Microstructural study of aluminum phosphate-sealed, plasma-sprayed chromium oxide coatings, *J. Therm. Spray Technol.*, **11**, 253–260.
- Wielage, B. and Fleischer, K. (1998). Electron beam post-treatment of coatings plasma sprayed onto magnesium alloy, in *Thermal Spray: Meeting the Challenges of the 21st century*, C. Coddet (Ed.), ASM International, Materials Park, OH, USA, pp. 1448–1453.

- Wielage, B., Steinhäuser, S., Pawłowski, L., Smurov, I. and Covelli, L. (1998). Laser treatment of vacuum plasma sprayed CoCrAlY alloy, in *Surface Modification Technologies XI*, T.S. Sudarshan, M. Jeandin and K.A. Khor (Eds), The Institute of Materials, London, UK, pp. 687–698.
- Zaplatynski, I. (1982). Performance of laser-glazed zirconia thermal barrier coatings in cyclic oxidation and corrosion burner rig test, *Thin Solid Films*, **95**, 275–284.
- Znamirowski, Z., Czarczynski, W., Le Maguer, A. and Pawłowski, L. (2003). Plasma sprayed and laser engraved field electron emitters, *Surf. Coat. Technol.*, **165**, 211–215.
- Znamirowski, Z., Pawłowski, L., Cichy, T. and Czarczynski, W. (2004). Low microscopic field electron emission from surface of plasma sprayed and laser engraved  $TiO_2$ ,  $Al_2O_3 + 13TiO_2$  and  $Al_2O_3 + 40TiO_2$  coatings, *Surf. Coat. Technol.*, **187**, 37–46.

# 5

## Physics and Chemistry of Thermal Spraying

Particles of powders injected into flames and jets or formed from wires (rods) are subjected to rapid acceleration and intense heating prior to becoming in contact with the substrate. The liquid particles can evaporate and reduce their sizes. Oxidation of the metallic 'feedstock' can also happen. The microstructure of the sprayed coatings and their properties depend strongly on all of the phenomena occurring during particle flight. Knowledge of the properties of flames and jets and their interactions with sprayed particles covers the area of fluid mechanics and chemical engineering which are not well-mastered by materials or mechanical engineers and technicians, who are frequently involved in thermal spraying. Such knowledge, although relatively 'hermetic', is, however, necessary and parameters such as particle temperatures and velocities are at present possible to be measured with fair precision. Many workshops are already equipped or will be equipped soon with the commercially available instruments, hence enabling such measurements. On the other hand, numerical codes enabling the modelling of the phenomenon of interactions between jets and flames with particles are becoming increasingly popular. The state of knowledge approaches the point in which a spraying process is simultaneously monitored by different sensors (pyrometers, CCD cameras, thermocouples, etc.) and simulated numerically by a computer. The results of simulation are validated and corrected by input experimental data gathered by the sensors. In some cases, a point is reached where a full automatization of the spraying process becomes possible.

## 5.1 JETS AND FLAMES

The characterization of jets and flames<sup>1</sup> mainly concerns the experimental determination or numerical prediction of the spatial distribution of velocity and temperature. These parameters determine, in turn, the density, thermal conductivity and viscosity of gas streams, which influence the momentum and heat transfer between gas and particles. These data are essential for understanding and modelling the movement and heating of particles in flames. The resulting spatial distributions are, generally, independent of time. This is a major simplification because the jets and flames are not stable over time. The instabilities are intrinsic to any spray process and have different origins in different spray torches. The movement of an arc from one spot to another inside a plasma torch is an example of such instability, which has a frequency of a few kHz. The periodic arc root fluctuations generate variations in the plasma jet properties. These, in turn, result in variation in the particle velocities and temperatures. Their amplitudes were estimated, upon plasma spraying of zirconia and alumina, as  $\Delta v_p = 200$  m/s and  $\Delta T_p = 600$ K, respectively (Bisson *et al.*, 2003). Figure 5.1 shows a comparison of the time scales of all instabilities occurring during plasma spraying.

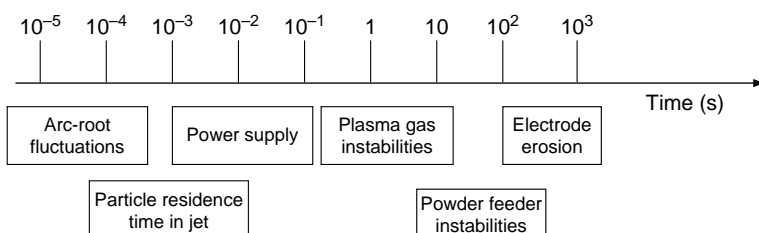


Figure 5.1 Time scale for various types of instabilities occurring during plasma spraying in comparison to the particle residence time in the jet (after Dussoubs *et al.*, 1997). Reproduced by permission of ASM International from Dussoubs *et al.*, 1997, *Thermal Spray: A United Forum for Scientific and Technological Advances*, C.C. Berndt (Ed.), ASM International, Materials Park, OH, USA, pp. 557–565

Another example of periodic variation are the detonations during D-gun™ spraying which have frequencies of about 10 Hz. The

<sup>1</sup> Jets are gas streams without combustion, occurring in, e.g. plasma spraying; flames are gas streams generated by combustion as occurs in flame spraying or high-velocity oxy-fuel spraying.

phenomena occurring inside of the torches generating the jets and flames are of primary importance for the instabilities but are only seldom studied theoretically (Baudry *et al.*, 2004). Furthermore, the mixing of a hot gas issuing from a torch with the ambient atmosphere is turbulent and the turbulences are unsteady. Consequently, the published spatial distributions of temperature or velocity of jet and flames are frequently averaged over time.

### 5.1.1 PROPERTIES OF JETS AND FLAMES

#### Differential Equations of Gas Flow

The equations governing homogenous gas flow express the following physical laws (Boulos *et al.*, 1994; Cheng *et al.*, 2003; Patankar, 1980):

- **Conservation of mass** for a gas without generation of chemical species:

$$\frac{\partial \rho_g}{\partial t} + \operatorname{div}(\rho_g \vec{v}_g) = 0 \quad (5.1)$$

- **Conservation of momentum** expresses the equilibrium of the forces acting on an elementary volume of a viscous liquid. The following forces are considered (Ouizaux and Perrier, 1978):

- force of gravity;
- force of liquid pressure;
- force of contact, valid for a viscous liquid;
- external forces (electric, magnetic, etc.).

The equation, which expresses the conservation of momentum, also called the *Navier-Stokes equation* or the basic equation of hydrodynamics, has the following form (Patankar, 1980; Eichert, 1996), which neglects the external forces:

$$\frac{\partial}{\partial t}(\rho_g \vec{v}_g) + \operatorname{div}(\rho_g \vec{v}_g \vec{x} \vec{v}_g) = \operatorname{div}(\eta_g \overrightarrow{\operatorname{grad}}(\vec{v}_g)) - \overrightarrow{\operatorname{grad}}(p_g) + \vec{V} \quad (5.2)$$

in which:

$$\vec{V} = \overrightarrow{\operatorname{grad}}\left(\frac{1}{3} \eta_g \operatorname{div}(\vec{v}_g)\right) \quad (5.3)$$

- Conservation of energy expresses the first law of thermodynamics. It has the following form (Patankar, 1980; Eichert, 1996):

$$\frac{\partial}{\partial t}(\rho_g H_g) + \operatorname{div}(\rho_g \vec{v}_g H_g) = \operatorname{div}(\lambda_g \overrightarrow{\operatorname{grad}} T_g) + S \quad (5.4)$$

For high-velocity flows, the total enthalpy of the gas has two components (Cheng *et al.*, 2003):

- kinetic enthalpy (second term on the right-hand side of Equation (5.5));
- static enthalpy, related to the internal energy (Equation (5.6));

$$H_g = h_g + \frac{v_g^2}{2} \quad (5.5)$$

$$h_g = \int_{T_0}^{T_g} c_p dT \quad (5.6)$$

- Turbulences should be considered for many jet and flames. The time-dependent equations of conservation are applicable for both laminar and turbulent flows. The jets and flames are turbulent in most spray techniques. The flows are inherently unsteady down to very short time scales. This is why time-averaged equations are used for turbulent flows. The most popular model used to describe turbulent flows is called ‘ $k-\varepsilon$ ’ or the ‘two-equation model’ and was developed by Launder and Spalding (1972, 1974). The values of  $k$  and of  $\varepsilon$  can be found from two separate differential equations presented by, e.g. Patankar (1980), Eichert (1996) or Cheng *et al.* (2003). Many authors (Dussoubs *et al.*, 1997; Eichert *et al.*, 1998) use, after Patankar (1980), one equation, called the *generalized conservation principle*. The equations of conservation enable us to find the profiles of temperature, velocity and density of jets or flames. They must be accompanied, however, by:

- boundary and initial conditions in all kind of jets/flames;
- thermodynamic data related to reaction between the species in combustion spraying, such as flame spraying and high-velocity oxy-fuel spraying, as well as data related to dissociation and ionization plus recombination in plasma spraying;
- transport properties of the gases used in thermal spraying;

- corrections necessary for sonic flows, characterized by a high Mach number,  $M > 1$ , to be considered in the detonation gun for high-velocity oxy-fuel modelling (Cheng *et al.*, 2003).
- **Boundary conditions** assume, in general, a cylindrical geometry. The cylinder has one part inside the barrel or the nozzle of a modelled torch and another part outside of it (Williamson *et al.*, 2002; Dyshlovenko *et al.*, 2006). Some authors model jets/flames which are totally outside of the torch (Bolot *et al.*, 1997; Dyshlovenko *et al.*, 2004). The cylinder, calleds *computational domain*, has two faces with radius  $R$ , i.e. an inflow and outflow boundary, an outer surface of length  $L$ , i.e. an open boundary (outside of the torch) – and also the torch wall (Figure 5.2).

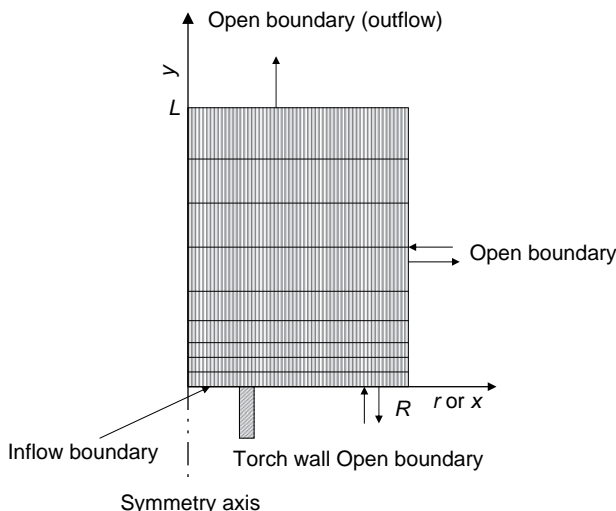


**Figure 5.2** Schematic of a computational domain outside of a torch used in simulations of jets/flames

The profiles of temperature and velocity of the ‘inflow’ into the computational domain are supposed to obey the *power law*. The following equation shows the power-law formula for the velocity distribution:

$$v = v_0 \left[ 1 - \left( \frac{r}{R} \right)^n \right] \quad (5.7)$$

The value of  $n$  is set based on the experimental data (e.g.  $n = 3$  in the study of Bolot *et al.*, 2004) and the centre-line value can be found, e.g. by fitting (Williamson *et al.*, 2002). The inflow conditions are necessary to be set for profiles of turbulent kinetic energy,  $k$ , and its dissipation rate,  $\varepsilon$ . Examples of such profiles are given by Williamson *et al.* (2002). For the open boundaries of the *computational domain* only the condition of ambient pressure is assumed and the flow can be calculated and can be either inwards or outwards of the domain (see, e.g. Dussoubs *et al.*, 1997). For the outflow face, the zero-gradient conditions for temperature and velocity are usually set. Finally, the solid boundary is either the torch wall or face (Figure 5.2). For this boundary, some authors use the condition of heat flux depending on the temperature (Baudry *et al.*, 2004) while others prescribe a constant temperature on this boundary (Williamson *et al.*, 2002).

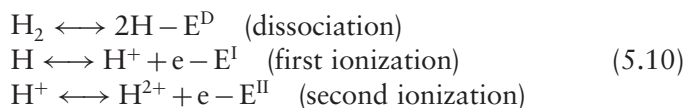
- **Thermodynamic data** concern the concentrations of the species in a jet or flame. To obtain these, first of all one has to compare the timescales of the turbulences with those of the chemical reactions. Most authors assume that the timescales of the chemical reactions are much faster than those of the turbulences (e.g. Eichert *et al.*, 1998). The gas is supposed to be in *local thermodynamical equilibrium* (LTE) and the possible reactions are completed immediately upon entering the computational domain (Cheng *et al.*, 2003). For combustion flames, a typical combustion reaction is shown in Chapter 3 (Equation (3.1)). The rate of creation or destruction of the species results from the reaction constant. This can be calculated from the *Arrhenius equation*:

$$k = AT^\beta \exp\left(\frac{E_a}{RT}\right) \quad (5.8)$$

The number of reaction and species that have to be taken into consideration can be important. For example, Bandyopadhyay and Nylén (2003) considered that the combustion of acetylene with oxygen upon flame spraying is associated with 44 possible reactions that may produce 15 species. The concentration of the latter was calculated from Arrhenius equation, which for a typical reaction during flame spraying, such as:



has the following coefficients:  $A = 3.31 \times 10^{10}$ ;  $E_a = 2.29 \times 10^8$  J/kmol;  $\beta = 0$ . The combustion reaction temperatures does not exceed 4000 K. Arc heating of a gas enables much higher temperatures to be reached. The reactions of dissociation, and the first and second ionizations have to be considered, as shown in the following equations for the hydrogen molecule:



In a gas heated by an arc, a dynamic equilibrium exists between dissociation, ionization and recombination and the thermodynamic properties (static enthalpy, specific heat, density, etc.) depend on the plasma composition. Methods for calculation of these properties have been presented by, e.g. Boulos *et al.* (1994). Thermodynamic data for the gases used in plasma spraying can be found in the studies of Capitelli *et al.* (1972), Pateyron *et al.* (1986), and Boulos *et al.* (1994). As an example, density data for pure Ar and Ar + 10 vol% H<sub>2</sub> plasmas are shown in Figure 5.3.

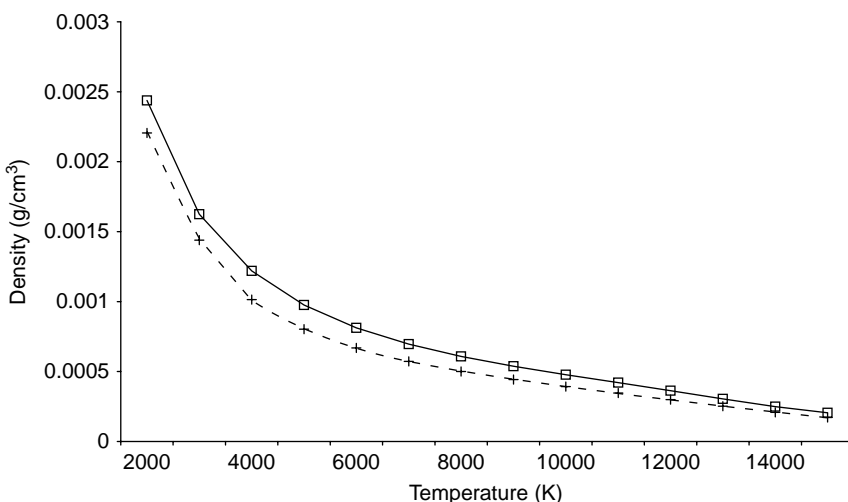


Figure 5.3 Variation of density with temperature in plasmas: (□) Ar; (+), Ar + 10 vol% H<sub>2</sub> (Capitelli *et al.*, 1972)

Thermodynamic data for the gases used in combustion flame spraying can be found, e.g. in the *JANAF tables* (Chase *et al.*, 1986).

- **Transport properties** of gases concern, in general, the coefficients which govern the flux of species under the action of the forces resulting from gradients of:
  - concentration – diffusion coefficient;
  - electric potential – electrical conductivity;
  - temperature – thermal conductivity;
  - velocity in a neighbouring layer of liquid – dynamic viscosity.

For a description of the velocities of jets and flames it is necessary to know the viscosity and thermal conductivity.<sup>2</sup> The velocity of a gas moving above a solid surface under *viscous conditions*<sup>3</sup> decreases when approaching the surface and is equal to zero on the surface. The decrease in the velocity can be described by a gradient. The latter has a finite value and results in the formation of an internal friction force,  $F$ , in the gas. *Dynamic viscosity* is a coefficient of proportionality, as shown in the following equation (the geometry of the gas flow is shown in Figure 5.2):

$$F = \eta_g \left( \frac{\partial v_{g,y}}{\partial x} \right) \quad (5.11)$$

Heat flux results in gases from a gradient in temperature while *thermal conductivity* can be defined from the following equation (geometry of gas flow as shown in Figure 5.2):

$$q_x = \lambda_g \left( \frac{\partial T_g}{\partial x} \right) \quad (5.12)$$

The transport properties of gases which are practicable in plasma spraying are available in the database of Pateyron *et al.* (1986) and in the book by Boulos *et al.* (1994). Even small percentages of hydrogen in argon at high temperatures increase the thermal conductivity of

---

<sup>2</sup> If the description takes into account the formation of an arc and the electromagnetic forces acting on a flow are considered in the equations of momentum conservation and energy conservation, knowledge of the electrical conductivity of the gas is also required (Baudry *et al.*, 2004).

<sup>3</sup> The size of the solid surface is much greater than the mean free path of the gas molecules.

the mixture (Figure 5.4). This is the main reason for improvement in the capacity of melting powder particles when plasma spraying using argon–hydrogen mixtures, with regard to pure argon processing.

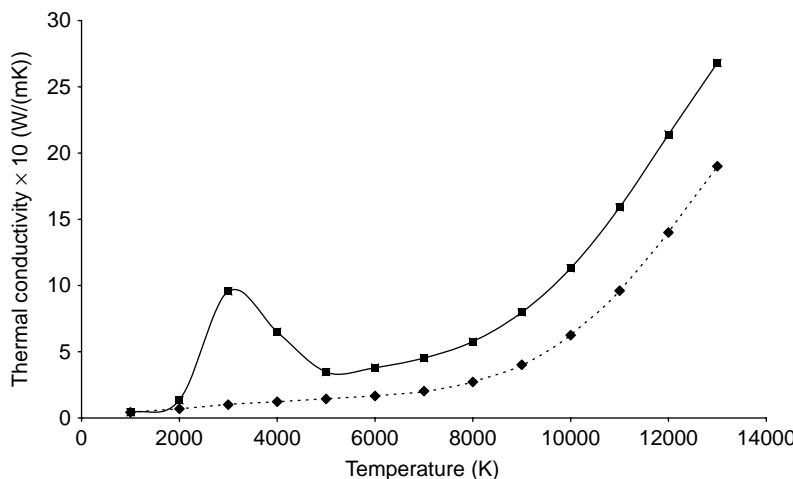


Figure 5.4 Variation of thermal conductivity with temperature in plasmas: ( $\blacklozenge$ ) Ar (Devoto, 1967); ( $\blacksquare$ ) Ar + 10 vol%  $\text{H}_2$  (Capitelli *et al.*, 1976)

- Sonic and supersonic flows reduce the rate of kinetic energy dissipation,  $\varepsilon$ , which should be included in differential equations of turbulent flow, in particular, in the  $k - \varepsilon$  model. The appropriate literature is given in Oberkampf and Talamali (1996).

### Modelling Methods

It is not possible to solve the equations of conservation and turbulent flow by using analytical methods in two and three dimensions. Only numerical methods are applicable. An excellent textbook on discretization of flow and heat-conduction problems, written by Patankar (1980), can be recommended to all who wish to find numerical solutions from the beginning. The discretization starts with the preparation of grids having 2-D or 3-D cells which are usually denser near to the torch (see Figure 5.2). Most researchers use commercial software employing methods known as computational fluid dynamics (CFDs). The following codes are frequently cited:

- PHOENICS,<sup>4</sup> used by, e.g. Eichert *et al.* (1998);
- ESTET,<sup>5</sup> used by, e.g. Dussoubs *et al.* (1997);
- FLUENT<sup>6</sup>, used by, e.g. Bolot *et al.* (2004);
- ‘Jets and Poudres’<sup>7</sup>, used by, e.g. Dyshlovenko *et al.* (2004, 2006).

Some examples of modelling methods are collected in Table 5.1. Typical profiles of temperatures and velocities of an Ar + H<sub>2</sub> plasma used in atmospheric plasma spraying are shown in Figure 5.5.

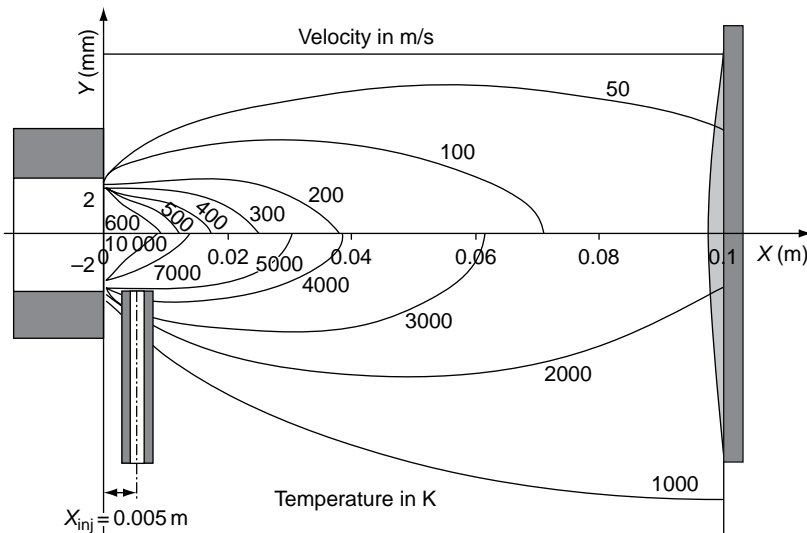


Figure 5.5 Calculated profiles of the temperatures and velocities of a plasma jet generated by an F-4 torch (details of the calculations are shown in Table 5.1)

### Experimental Determination of the Properties of jets and flames

The following properties of jets/flames, used in thermal spraying, are experimentally tested:

<sup>4</sup> The Phoenics Reference Manual, CHAM/TR200, CHAM, London, UK.

<sup>5</sup> Mattei, J.D. and Ouraou, M., EDF Report HE 44/93.20, EDF-LNH, 6 Quai Watier, 78400 Chatou, France.

<sup>6</sup> FLUENT Inc., Lebanon, NH, USA.

<sup>7</sup> Jets and Poudres can be downloaded from: [<http://jets.poudres.free.fr>].

**Table 5.1** Examples of modelling of jets and flames for different spray techniques

Spray technique/torch	Used gases/flow rate (slpm)	Solution method	Modelling details	Dimension of modelled flow	Remarks	Reference
FSIMetco 6P <sup>a</sup>	$C_2H_2 + O_2/(22.9 + 32)$ , also cooling air and Ar carrier gas	$k-\varepsilon$ model of turbulences	FLUENT	3-D	Modelling of real spray process	Bandyopadhyay and Nylen, 2003
APS/F-4	$Ar + H_2/(45 + 15)$	$k-\varepsilon$ model of turbulences	PHOENICS and FLUENT	2-D	Comparison of codes	Bolot <i>et al.</i> , 2004
APS/F-4MB	$Ar + H_2/(45 + 15)$	Equations of conservation, including electromagnetic forces	ESTET	3-D	Including modelling of arc behaviour	Baudry <i>et al.</i> , 2004
APS/F-4	Ar + 37.5 vol% N <sub>2</sub>	$k-\varepsilon$ model of turbulences	Jets et Poudres	2-D	Modelling of real spray process	Dyshlovenko <i>et al.</i> , 2004
Detonation gun	C <sub>3</sub> H <sub>8</sub> + O <sub>2</sub>	Solution of equations of conservation	Developed by authors	1-D	Modelling of real spray process (Figure 5.5)	Kadyrov, 1996
HVOF/Metco Diamond jet	C <sub>3</sub> H <sub>6</sub> + O <sub>2</sub> , also cooling air and Ar carrier gas	$k-\varepsilon$ model of turbulences	CFD-ACE	2-D	Modelling of real spray process	Oberkampf and Talpalikar, 1996
VPS/F4-VB	Ar(40)	$k-\varepsilon$ model of turbulences	—	2-D	Validated by flow experiments	Blais <i>et al.</i> , 2004
CCSM	Air	Isotropic flow of perfect gas	Analytical solution	1-D	Modelling of real spray process	Dykhuizen and Smith, 1998

<sup>a</sup>F-4, F-4MB, F-4VB, Metco 6P and Metco Diamond jet are torches commercialized by Sulzer-Metco, Wohlen, Switzerland.

- temperature distribution;
- velocity distribution;
- chemical composition (especially oxygen contents in jets/flames).

The experimental data are sometimes used to validate the modelling results. However, the modelling finally concerns the temperatures and velocities of the sprayed particles which are more closely correlated to the properties of the obtained deposits. Consequently, the validation is rather made for the properties of the stream of particles than that of jets/flames.

- Temperature can be estimated by the calorimetric method described in the Standard ASTM E 341-96<sup>8</sup>. This method, used by this present author many years ago (Pawlowski, 1978), is very simple and inexpensive, but only gives one, averaged value of the temperature. Its distribution can be obtained by emission spectroscopy in the hot emitting zone, often known as the *core zones*, and by thermocouples in the lower-temperature zones, also called *plumes* (Fauchais *et al.*, 1984). The temperature in the core zone is determined by employing emission spectroscopy (Kleimann *et al.*, 1970) using monochromators. Each emitting line has its own intensity which depends on the jet/flame temperature. Knowing the ratio of intensities of two lines, as well as their excitation energies and probabilities of spectral transitions, it is possible to determine the temperature in a precisely determined volume of the jet/flame. A *local thermodynamic equilibrium* (LTE) condition must be fulfilled in order to find one temperature value. As a jet/flame has a cylindrical symmetry, it is reasonable to suppose that the isotherms also have a cylindrical form. To obtain a radial temperature distribution from 2-D optical observation of the *core zone* from its side, an *Abel inversion* is often used (Czernichowski, 1985). Examples of the temperature distributions for such measurements made for a typical plasma torch are shown in Figure 5.6.

The determination of temperature in a plume is a standard method for temperatures above 6000 K. Under this condition, the strong atomic lines are emitting. At lower temperatures (occurring for all combustion flame spraying techniques), one has to analyse the emitting molecules, which is a much harder task. Another method that can be used at lower

---

<sup>8</sup> Standard method of measuring plasma arc gas enthalpy by energy balance, American Society for Testing Materials, Philadelphia, PA, USA (10 October 1996).

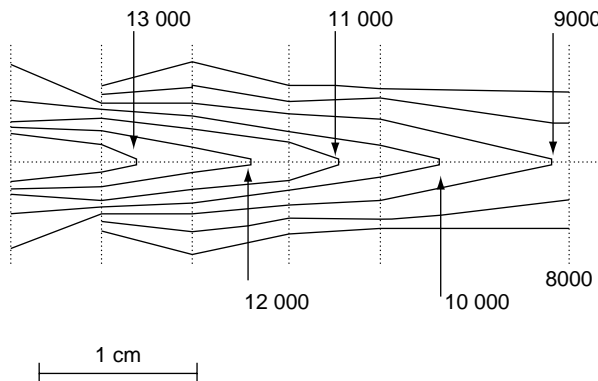


**Figure 5.6** Isotherms found for an F-4 torch working with an  $\text{Ar} + \text{H}_2$  plasma (35 + 11 slpm) at an electric power ( $P$ ) of 35.7 kW. The distribution starts with the powder-input point on the left-hand side, while the hottest isotherm is 13 000 K, at steps of 1000 K (Czernichowski, 1985)

temperatures is *laser induced fluorescence*, described by, e.g. Fauchais *et al.* (1984). Another difficulty arises if an LTE model is not applicable and there is more than one temperature. This corresponds to, e.g. a jet generated during vacuum plasma spraying. Different temperatures (electronic, excitational, vibrational, rotational, translational, etc.) should be measured by using different methods. A method that enables the determination of a local ‘stagnation’ enthalpy in a VPS jet is by using a small, intensively cooled *Pitot tube*. The ‘local’ enthalpy of the plasma can be found from calorimetric measurements of the water cooling the probe (Blais *et al.*, 2004). The temperatures in the plumes can also be determined with the help of high-temperature thermocouples (Fiszdon and Lesinski, 1975).

- Velocity measurements of flames and jets are frequently made by using the same methods employed for the determination of particles velocities (discussed later in more detail). These methods include, for example:
  - *Laser Velocimetry* (LV) measurements, which include *Laser Doppler Velocimetry* (LDV) and *Laser Two Focus* (L2F), are made using fine (size of about 1  $\mu\text{m}$ ) and light (alumina, kaolin, etc.) particles which are supposed to have velocities equal to those of jets/flames.
  - *The Photographic Streak Technique*, using a ‘rapid’ camera, enabling the disturbances in the flame to be followed from frame

to frame. This technique was used by, e.g. Frind *et al.* (1983), to determine the flame velocity in the VPS process.

- *Spectral methods*, based on the Doppler shifts of the lines emitted by the jet/flame (Cambray, 1977).

At present, most authors use commercial sensors, which enable the simultaneous measurements of velocity, temperature and size of particles. These sensors will be described more thoroughly in the section describing particle velocity measurements.

- The chemical composition of a jet/flame is determined by using probes that enable samples of gas to be taken at different axial distances from the torch. The chemical composition of the gas sample could be tested with any method of chemical analysis, such as, *mass spectrometry* (Fiszdon *et al.*, 1976). Examples of gas compositions during atmospheric plasma spraying are shown in Figure 5.7.

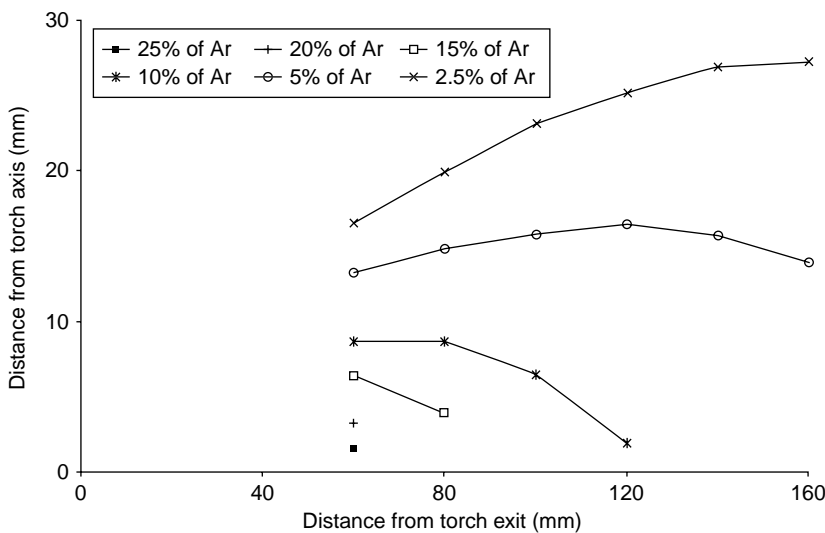


Figure 5.7 Isopleths of equal content of Ar during atmospheric plasma spraying using Ar + 30 vol% H<sub>2</sub> at an electric power (*P*) of 49 kW (Fiszdon *et al.*, 1976)

## 5.2 MOMENTUM TRANSFER BETWEEN JETS OR FLAMES AND SPRAYED PARTICLES

Jets and flames have very high velocities which are transferred to accelerate the sprayed particles. The particles arrive on the substrate

and form a coating. In most cases, the higher velocity at impact with the substrate results in better quality of the deposits. This is the main reason for development of new spray techniques, such as the family of high-velocity combustion spraying methods, including, among others, HVOF, HVAF, Sonarc<sup>TM</sup> or the cold gas-spray method.

### 5.2.1 THEORETICAL DESCRIPTION

Supposing that the movement of any particle at spraying is not perturbed<sup>9</sup> by others, known as the *ballistic model* or *Lagrangian approach* (Cheng *et al.*, 2003), the acceleration of a solid particle injected into the moving gas results from the action of the following forces (Lewis and Gauvin, 1973):

- drag force;
- force due to the pressure gradients;
- force due to the added mass (*Archimedean force*);
- *Basset history* term;
- external forces (gravitational, electrical, etc.).

In most practical cases met in thermal spraying, only the drag force counts and the equation of the particle motion has the following form:

$$\frac{1}{6} \rho_p \pi d_p^3 \frac{dv_p}{dt} = \frac{1}{8} C_D \pi d_p^2 \rho_g (v_g - v_p)^2 \quad (5.13)$$

The drag coefficient depends on the particle's velocity relative to the flame velocity (described by the *Re* number) in the following way:

$$C_D = \frac{24}{Re}, \quad Re < 0.2 \quad (5.14)$$

$$C_D = \frac{24}{Re} \left(1 + \frac{3}{16} Re\right), \quad 0.2 \leq Re < 2 \quad (5.15)$$

---

<sup>9</sup> There is much evidences that the ballistic model is not always true. For example, small particles coalesce in the plasma and become agglomerated and one can observe 'twinned' particles after spraying powders into water (Dyshlovenko *et al.*, 2006). The ballistic model is, however, a useful one for understanding most of the phenomena occurring between a hot gas and particles.

$$C_D = \frac{24}{Re} (1 + 0.11 Re^{0.81}), \quad 2 \leq Re < 21 \quad (5.16)$$

$$C_D = (1 + 0.189 Re^{0.632}), \quad 21 \leq Re < 200 \quad (5.17)$$

Equation (5.14) describes the movement in the *Stokes regime*, and Equation (5.15) in the *Oseen's regime*. Equations (5.16) and (5.17) were suggested by Beard and Pruppacher (1969). The Reynolds number used in the above equations corresponds to the relative movement of particle and jets/flames:

$$Re = \frac{\rho_g d_p (v_g - v_p)}{\eta_g} \quad (5.18)$$

The result obtained for velocity calculations of hydroxyapatite particles, plasma-sprayed by using an F-4 torch, are shown in Figure 5.8.

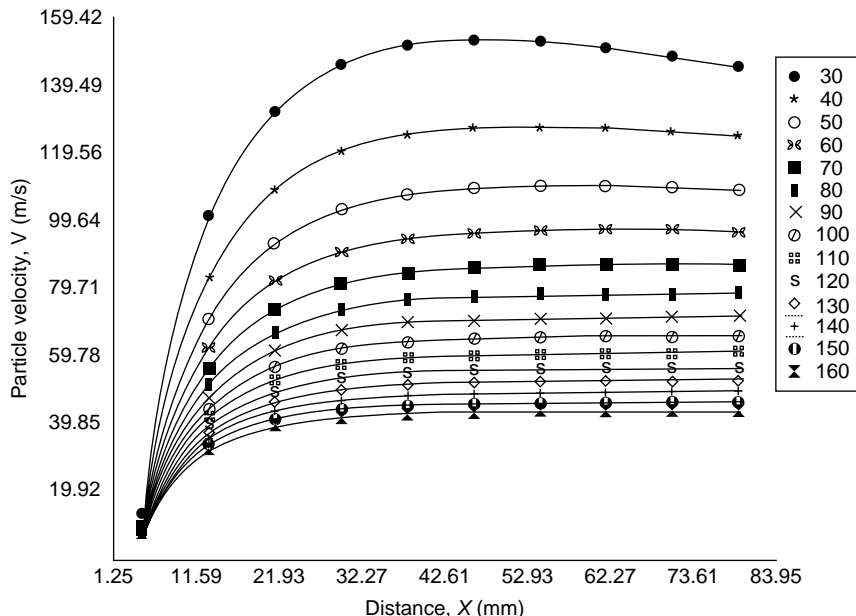


**Figure 5.8** Calculated velocities of hydroxyapatite particles as a function of the distance from the injection point. The profiles of the velocities and temperatures of the plasma jet are shown in Figure 5.5 (after Dyshlovenko *et al.*, 2004)

Two typical phenomena are visible in the figure and should be stressed:

- for large particles, after reaching their maximum velocities, the latter remain constant, independent of the velocities of jets/flames;
- the velocities of small particles are better correlated with the velocities of jets/flames.

The temperature of a particle's surface is much lower than that of the surrounding gas. Consequently, a boundary layer around the particle has a steep temperature gradient which influences the properties of the gas. The gradients should be somehow taken into account. One approach is to assume that the transport properties of the gas in the layer are averaged between the temperature of the gas and the temperature of the particle's surface. The averaged thermal conductivity (and viscosity) can be found from the following expression (Joshi and Sivakumar, 1991; Sobolev *et al.*, 1994):

$$\langle \lambda_g \rangle = \frac{1}{T_g - T_p} \int_{T_p}^{T_g} \lambda_g(T) dT \quad (5.19)$$

Another approach, proposed by, e.g. Chyou and Pfender (1989), consists of the application of correction factors to the drag coefficient. These factors consider the influence of:

- the steep temperature gradient in the boundary layer on the viscosity and density of the gas;
- the *noncontinuum effect* occurring when the sizes of the particles become comparable to the mean free path of the molecules of gas.

The noncontinuum effect, also called the *Knudsen effect*, depends on the *Knudsen number*, defined as follows:

$$Kn = \frac{l_{mf}}{d_p} \quad (5.20)$$

The mean free path becomes comparable to the particle sizes in rarefied gases. For example, its value for Ar at  $p = 5$  kPa and  $T_g = 5000$  K, is equal to  $l_{mf} = 23\mu\text{m}$  (Frind *et al.*, 1983). If  $Kn < 0.001$ , the Knudsen effect can be neglected. On the other hand, if  $Kn > 10$ , the gas cannot be treated as a continuous medium and its interaction with a solid body has

a molecular character. In the intermediate regime of  $0.001 < Kn < 10$ , it is necessary to introduce corrections for momentum and heat transfer (Joshi *et al.*, 1986). Another effect, worth discussing with regard to momentum transfer between the gas and the sprayed particles, is the *charge effect*, also known as the *load effect*. This effect can be described as the loss of momentum of a gas, which is equal to the gain in momentum by all particles injected into it. The fundamental equations describing this effect are given by Polak and Surov (1969). Fincke *et al.* (1990) and Vardelle *et al.* (1992) confirmed, experimentally, the reduction in the velocities of particles with an increase in the powder feed rate (Figure 5.9).

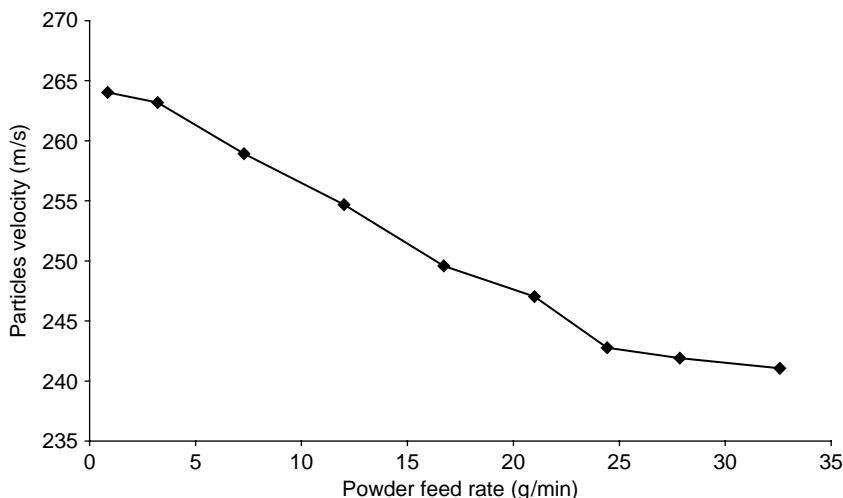


**Figure 5.9** Modification of the velocity of alumina particles, having particle sizes in the range  $-45 + 22.5\mu\text{m}$ , as a function of the increasing feed rate. The measurements were made, using laser velocimetry, for a point at a distance of 12 cm from the F-4 plasma torch, supplied with Ar + H<sub>2</sub> (32 + 12 slpm) and an electrical power of  $P = 34.8$  kW (after Vardelle *et al.*, 1992). Reproduced by permission of ASM International from Vardelle *et al.*, 1992, *Proceedings of the 13th International Thermal Spray Conference*, C.C. Berndt (Ed.), ASM International, Materials Park, OH, USA, pp. 543–547

The injection angle of the particles to the flames influences the trajectory of the particles in jets/flames. Some spray techniques enable axial injection, which results in a better concentration of sprayed particles near to the torch axis, where the temperature and velocity are the greatest. Many plasma spray torches have perpendicular (or close to perpendicular)

injection. The injection angle can be used to modify the trajectory of the sprayed particles. An exhaustive discussion of the effects of different injection techniques on the trajectories of particles in a plasma jet has been made by Vardelle *et al.* (2001).

In the family of spray techniques, which have a jet or flame with low temperature and high velocity, such as the D-gun<sup>TM</sup>, HVOF and especially CGSM, one has to consider the transformation of kinetic energy of the particles into heat upon impact with the substrate. Assuming adiabatic conditions, the transformation can be described by the following equation:

$$\frac{1}{2}m_p v_p^2 = m_p c_p \Delta T \quad (5.21)$$

Calculations of the temperature increase for different velocities of WC-Co, Al<sub>2</sub>O<sub>3</sub> and TiO<sub>2</sub> particles, shown in Figure 5.10, indicate that the effect of velocity on the temperature becomes important, beginning from 400 m/s. Such velocities, as shown, can be reached for all of the mentioned spray techniques. At a velocity about 900 m/s, which can be reached with the D-gun<sup>TM</sup> technique, the estimated temperature increase can be as high as 900 up to 1600 K.

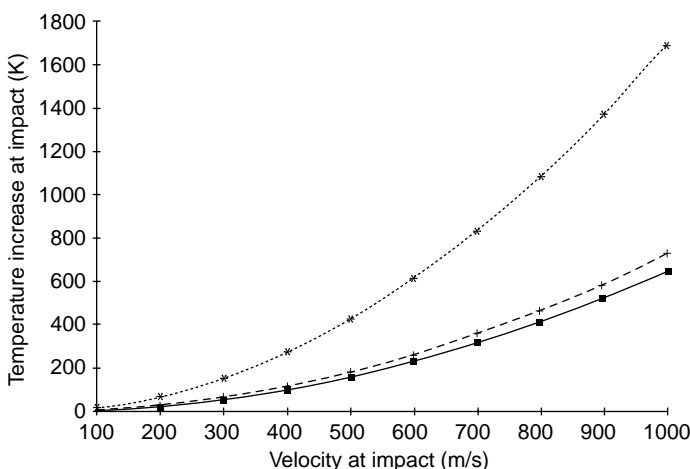


Figure 5.10 Theoretical temperature at impact of Al<sub>2</sub>O<sub>3</sub> (■), TiO<sub>2</sub> (+) and WC-Co (\*) particles; the specific heats ( $c_p$ ) were 775.4, 689.1 and 295.4 J/(kg K), respectively. The data for the oxides were taken from Samsonov (1978) while those of WC-Co were taken from Joshi (1992)

### 5.2.2 EXPERIMENTAL DETERMINATION OF SPRAYED PARTICLES' VELOCITIES

The methods used for experimental determination can be roughly categorized as follows:

- **mechanical methods**, with a rotating mirror or rotating substrate;
- **laser methods**, based on the frequency shift by the Doppler effect and the two-focus' laser;
- **optical methods**, based on the treatment of the optical signal gathered by a photomultiplier and/or a CCD camera, which are commercialized and used frequently in 'spray-shops'.

**Mechanical methods.** These, the oldest and simplest methods of measuring, consist of photographing the particle stream with a *rotating mirror*. The slope of the trace of the radiating particles registered on the film (of sufficiently high sensitivity) results from the superposition of their linear velocities in the flame and of the mirror surface (Lemoine and Le Goff, 1969; Lesinski, 1975). Thus, the particles' velocities can be easily found by measuring the slope, knowing the velocity of the mirror. This method is practicable if the luminosity of the 'flying' particles is intensive enough to leave a trace on the film. A similar principle is used in the *photographic streak technique* (Figure 5.11).

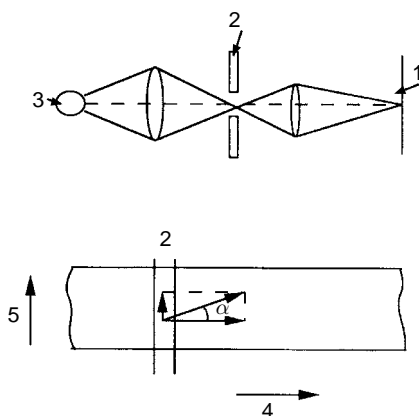


**Figure 5.11** Principles of the photographic streak technique for particle velocity measurements: (1) film; (2) slot; (3) particle; (4) film-motion direction; (5) particle-motion direction (Frind *et al.*, 1983)

The luminous particles are photographed by using a camera with a rapidly moving film (of a linear velocity,  $v_{fi}$ , of 175 m/s (Frind *et al.*, 1983)). The velocity of the particles can be determined from the formula:

$$v_p = \frac{v_{fi} \tan \alpha}{\text{Mag}} \quad (5.22)$$

A drawback of this method is the necessity of using high-sensitivity films. Otherwise, the particles of small emission (small or less heated) would not leave a trace on the film. A variation of the rotating mirror, method without this drawback, is the rotating substrate method, recently presented by Lebedev and Akedo (2003). A schematic of this method is shown in Figure 5.12.

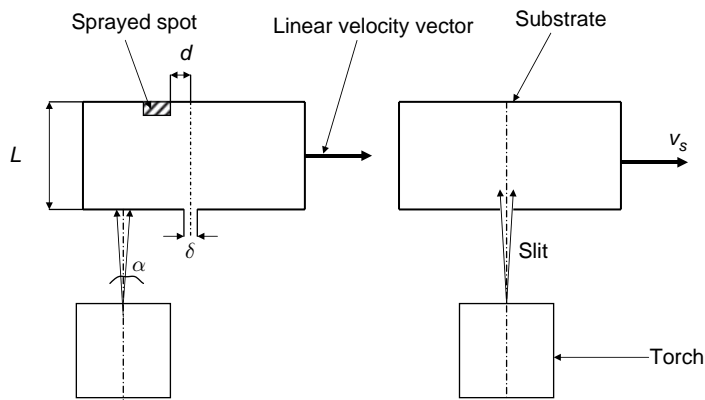


**Figure 5.12** Schematic of the rotating substrate method; the symbols used are given in Equation (5.23) (after Lebedev and Akedo, 2003). Reproduced by permission of ASM International from Lebedev and Akedo, 2003, *Thermal Spray 2003: Advancing the Science and Applying the Technology*, C. Moreau and B. Marple (Eds), ASM International, Materials Park, OH, USA, pp. 1117–1120

A disc consisting of two plates is revolving near to the spraying torch. One plate has a slit which allows the sprayed particles to enter and then impact onto the second disc, the substrate. Their maximum velocity can be found from the geometry of installation (see Figure 5.12) by using the equation:

$$v_p = \frac{v_s L}{d + \frac{\delta}{2} + L \sin \alpha} \quad (5.23)$$

A rotating substrate enables fine particles' velocities of up to 650 m/s to be measured by using a disc rotating at a speed of 6000 rpm. This method can be recommended for 'nanodimensional' particles' diagnostics.

Many measurements of particle velocities are made by using laser velocimeters. Two of the most popular systems are described in the following.

**Laser methods.** These include the Laser Doppler Velocimeter (LDV), which operates following the principles shown in Figure 5.13.

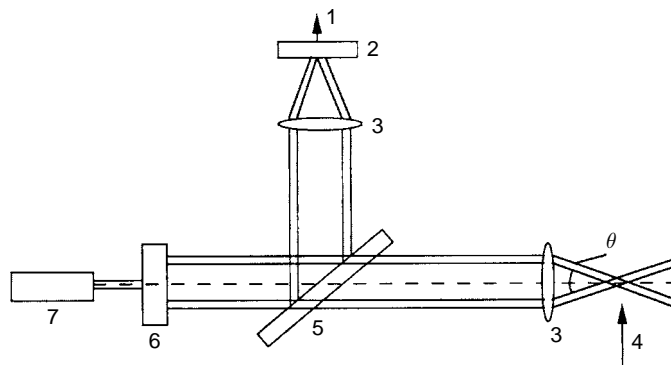


**Figure 5.13** Schematic of the dual-beam LDV system: (1) signal to processing electronics; (2) photodetector; (3) lens; (4) particle's motion direction; (5) semitransparent mirror; (6) beam splitter; (7) laser; the symbol  $\theta$  is used in Equation (5.24) (Wagner *et al.*, 1984). This article was published in *Surf. Technol.*, 22, N. Wagner, K. Gnädig, H. Kreye and H. Kronewetter, 'Particle velocity in hypersonic flame spraying of WC-Co', 61–71, Copyright Elsevier (1984)

A laser beam of wavelength  $\lambda$  is split into two beams, focused in the measurement volume. At this volume, a fringe pattern is created. The fringe spacing,  $d_{\text{fr}}$ , can be defined by the following equations:

$$d_{\text{fr}} = \frac{\lambda}{2 \sin(\frac{\theta}{2})} \quad (5.24)$$

$$\Delta f_D = \frac{v_p}{d_{\text{fr}}} \quad (5.25)$$

Laser light is scattered by the particles. Their movement, with a velocity  $v_p$ , results in a light frequency shift due to the *Doppler effect*. This shift is proportional to the particles' velocity.

If the laser light has enough intensity, the light can be received in the backscattered direction, as shown in Figure 5.13. The electronic system following the photodetector should enable the *Doppler frequency* to be measured. A typical laser used in the LDV has a wavelength of 514 nm and power of a few watts (Wagner *et al.*, 1984; Fincke *et al.*, 1990). Another method is the Laser Two Focus (L2F) one in which a laser beam is separated into two beams (Smith and Dykhuisen, 1987). These beams are focused to give two small test volumes. When the particles traverse the ‘start volume’, an electronic clock counts the time until these particles traverse the ‘stop volume’. The particles’ velocity is a product of the division of the known distance between the volumes by the measured time interval.

**Optical methods.** These include a method that is based on the treatment of the optical signal gathered by two photomultipliers. A schematic of this technique, which is quite similar to the L2F one, is shown in Figure 5.14.

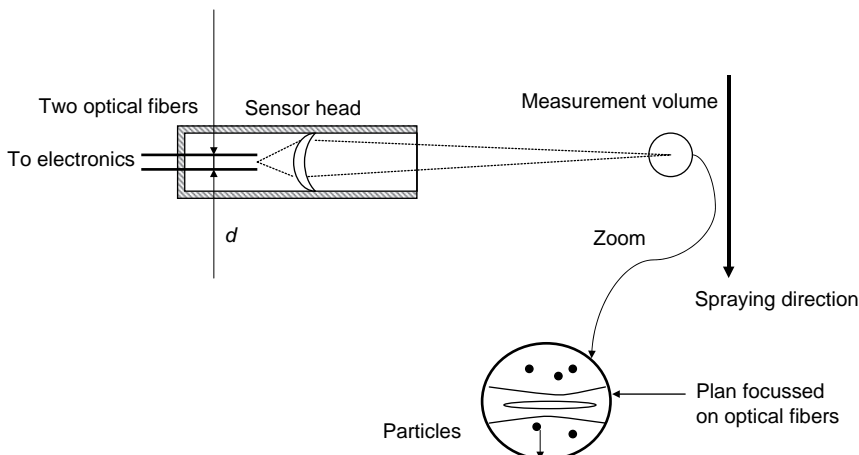


**Figure 5.14** Schematic of a sensor developed to measure the velocity of particles; the symbol  $d$  is used in Equation (5.26) (Bourque *et al.*, 2000). Reproduced by permission of ASM International from Bourque *et al.*, 2000, *Thermal Spray: Surface Engineering via Applied Research*, C.C. Berndt (Ed.), ASM International, Materials Park, OH, USA, pp. 45–50

Two areas in the stream of sprayed particles are focused on two optical fibres, which are connected to two photomultipliers. An averaged signal, corresponding to the intensity of the emitting particles, obtained by the

photomultiplier connected to the ‘downstream’ fibre is delayed with regard to the signal coming from the ‘upstream’ fibre. The mathematical treatment of the signals obtained from the photomultipliers enables us to find the lapse of time,  $\tau$ , that can be used to determine the velocity of the particles (Bourque *et al.*, 2000). Consequently, its average value can be found from the following equation:

$$\langle v_p \rangle = \frac{d\text{Mag}}{\tau} \quad (5.26)$$

The described sensor is coupled with a two-colour pyrometer in a system called DPV-2000<sup>TM</sup>, which is available commercially.

Another optical method uses a CCD camera which is focused on the particles’ charged plume. The plume is imaged for a short exposure time, ranging from 5 to 10 ms (Vuoristo *et al.* 2001). Over this time, the particles, depending on their velocity, travel a distance of 0.5 to 1.5 mm, which corresponds to 20–60 pixels on the CCD detector. A computer code enables us to measure their length and calculate their velocities. This system is incorporated into a commercialized SprayWatch<sup>TM</sup> installation, which enables velocities ranging from 10 to 1000 m/s to be determined.

### 5.2.3 EXAMPLES OF EXPERIMENTAL DETERMINATION OF PARTICLES VELOCITIES

The literature offers nowadays many results for particles’ velocity measurements. Commercial diagnostic tools, such as DPV-2000<sup>TM</sup> or SprayWatch<sup>TM</sup>, are used in many laboratories and ‘spray-shops’. A wealth of data can be found in scientific journals and proceedings of thermal spray conferences. In this section, some typical data are demonstrated for plasma spraying, in the open atmosphere and under reduced pressure, and for high-velocity combustion spraying.

#### Atmospheric Plasma Spraying

Some velocity-determination results using laser Doppler velocimetry of ceramic powders sprayed with a plasma in the open atmosphere are shown in Figure 5.15.

All measured velocities are in the range 120–350 m/s. Thus, sprayed particles reach the substrate at a spray distance of 100 mm after a

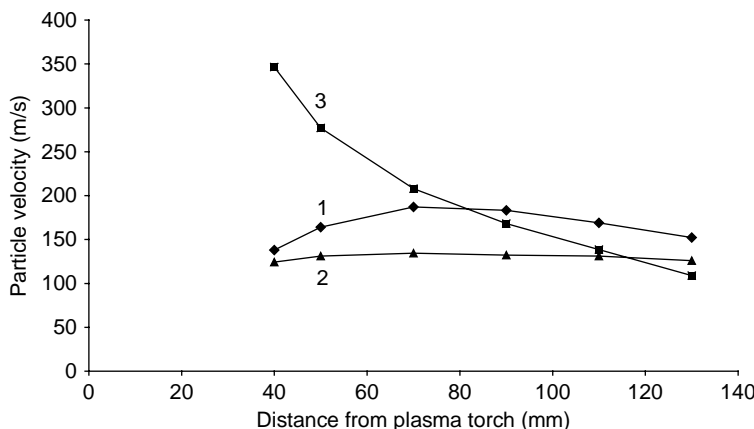


**Figure 5.15** Centreline velocities of some typical ceramic powders sprayed by a plasma in the open atmosphere: (1) zirconia ( $\text{ZrO}_2$ ) powder of size in the range from 10 to 40  $\mu\text{m}$ , sprayed using 75 slpm of Ar and 15 slpm of  $\text{H}_2$  with an electric power input of 29 kW (Vardelle *et al.*, 1986); (2) coarse alumina ( $\text{Al}_2\text{O}_3$ ) powder of size of about 46  $\mu\text{m}$ , sprayed using 50 slpm of  $\text{N}_2$  and 10 slpm of  $\text{H}_2$  with an electric power input of 24 kW (Vardelle *et al.*, 1980); (3) fine alumina ( $\text{Al}_2\text{O}_3$ ) powder of size of about 3  $\mu\text{m}$ , sprayed with an electric power input of 29 kW (McKelliger *et al.*, 1982)

flight in the plasma of a few hundreds of microseconds (fraction of a millisecond). On the initial part of their trajectories, the fine particles are very rapid, but at a spray distance of 80 mm, the velocities of the fine and coarse particles become almost equal. At a distance greater than 120 mm, the fine particles are slower than the coarse ones. The measured particles are of rather large sizes and keep their velocities relatively high, even at larger sprayings.

### Vacuum Plasma Spraying

The velocities, determined by using the laser-two-focus (L2F) method (Steffens *et al.*, 1985), of tungsten, kaolin and alumina particles, plasma-sprayed under vacuum, are showed in Figure 5.16.

The measurements show that very heavy tungsten grains of 23  $\mu\text{m}$ , do not even reach a velocity of 200 m/s. This could be due to the fact that the operational spray parameters selected by the authors could have been better optimized. The main reason for the low velocity of these particles results from the decreasing gas viscosity at low-pressure conditions. The velocities of the light and very fine kaolin

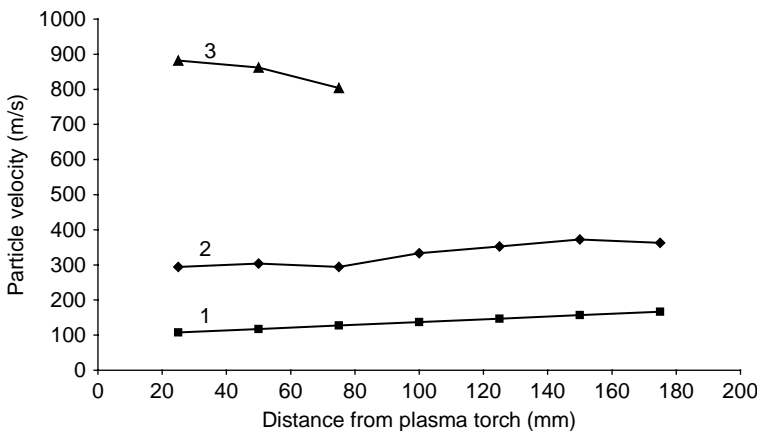


**Figure 5.16** Centreline velocities, determined by the L2F method, for some powders sprayed by a plasma under a dynamic pressure ( $p$ ) of 5 kPa, using 137 splm Ar and 41 splm He with an electric power input of 73 kW: (1) tungsten (W) powder of size of about 23  $\mu\text{m}$ ; (2) coarse alumina ( $\text{Al}_2\text{O}_3$ ) powder of size of about 23  $\mu\text{m}$ ; (3) very fine kaolin powder of size of about 0.55  $\mu\text{m}$

particles were probably similar to that of the low-pressure plasma jet, i.e. close to 1000 m/s. Finally, the velocities of alumina particles of similar size is about two times greater when spraying under lower pressures than those sprayed under an open atmosphere (see Figure 5.15).

### High-Velocity Oxy-Fuel Spraying

Particles' velocity data for HVOF spraying of fine alumina powders and very typical WC-Co powders (Barbezat, 1989) are shown in Figure 5.17. Fine alumina particles reach velocities of up to 1400 m/s, following closely the velocity of the flame. Tungsten carbides particles, which are very frequently sprayed using the HVOF technique, reach velocities of up to 400 m/s. This value is considerably higher than that which could be reached by atmospheric plasma spraying.

## 5.3 HEAT TRANSFER BETWEEN JETS OR FLAMES AND SPRAYED PARTICLES

Optimization of the processing parameters at spraying aims at melting most of the sprayed particles when impacting the substrate. In such conditions, dense coatings can be obtained. This is easier to achieve if

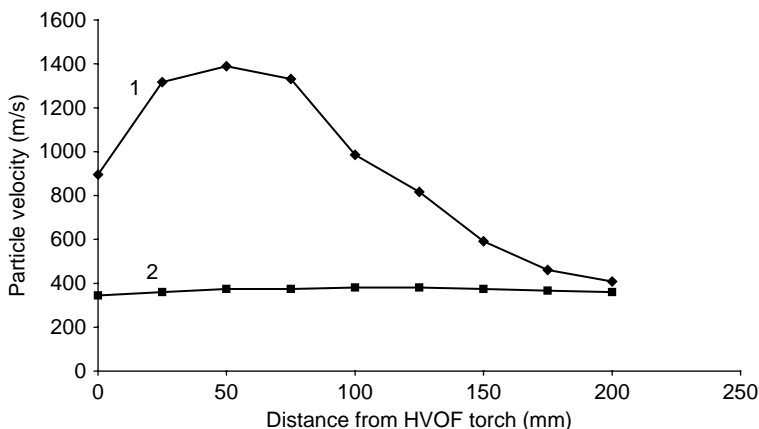


**Figure 5.17** Centreline velocities, determined by the L2F method, for some powders sprayed using a high-velocity combustion torch supplied with 430 slpm O<sub>2</sub> and 60 slpm fuel gas: (1) fine alumina (Al<sub>2</sub>O<sub>3</sub>) powder of size smaller than 2 µm; (3) coarse tungsten carbide (WC) + 12 wt % Co powder of size in the range 22 to 44 µm

the particles are small or if they conduct heat well than otherwise. The melting of large particles produced from poor heat conductors might need such a selection of spray parameters which lead to intensive evaporation. Vaporization is not a desired effect because it lowers the spray efficiency and may decrease the adhesion and cohesion of the coatings. Moreover, the generated vapours cool down the gas around the sprayed particles and reduce heat transfer. Finally, the vapours of some materials can be dangerous for the health of the operator. Another complication, resulting from the thermal gradients inside the particles is the formation of partly molten particles. Such particles contribute considerably to the formation of porosity in sprayed deposits.

### 5.3.1 THEORETICAL DESCRIPTION

The mechanism of heat transfer from a jet or a flame to a particle varies depending on its size and on its relative velocity. The latter changes during the particle's flight:

- **Convection** has a major contribution to the heat transfer shortly after injection of a particle when the hot gas has a much greater velocity. This might also be important at the end of its flight if the gas become cooler and slower than the particle.

- **Conduction** is important if the relative velocity decreases, which happens in the middle of a particle's flight.
- **Radiation** from a jet or flame to the particles and radiation losses from the particles is important for large particles.

The major property of a jet or flame which influences heat transfer is *thermal conductivity*. The *total* thermal conductivity can be decomposed into the contributions of the energy transporting species (Sayce, 1976):

$$\lambda_{\text{total}} = \lambda_{\text{atoms}} + \lambda_{\text{electrons}} + \lambda_{\text{ambipolar}} \quad (5.27)$$

where  $\lambda_{\text{ambipolar}}$  is a contribution to the heat transport of the atoms (such as H or N) that recombine back into molecules. The conduction and convection mechanisms are usually described by the Nusselt number ( $Nu$ ) that for the spherical shape of a particle is as follows:

$$Nu = \frac{hd_p}{\langle \lambda_{\text{total}} \rangle} = 2 + 0.66Re^{0.5}Pr^{0.33} \quad (5.28)$$

in which  $\langle \lambda \rangle$  is found from Equation (5.19). The first term (i.e. 2) on the right-hand side of Equation (5.28) describes the conduction mechanism. This mechanism is dominant if the  $Re$  number is small, i.e. when the particle has a velocity nearly equal to the velocity of the gas and the  $Re$  number is small. Such a case occurs when a particle is in the middle of its flight. Otherwise, the second term must be considered. In this,  $Re$  is defined by Equation (5.18) while the Prandtl number ( $Pr$ ) is defined as:

$$Pr = \frac{\eta_g(c_p)_g}{\lambda_g} \quad (5.29)$$

The *Knudsen effect* should be considered for small particles and/or for spraying under low pressures. This effect reduces the heat transfer. Chyou and Pfender (1989) carried out a calculation of the reduction in function of the particle size (Figure 5.18).

The *load effect* also leads to a reduction in the heat transfer from the hot gas. This effect consists of cooling down the flame due to the large quantity of particles (see Figure 5.19).

During the flight of molten particles, any collision with other one may lead to *agglomeration* or *twinning*. Agglomeration was observed for very fine alumina plasma sprayed into water (Pawlowski, 1980) and, more recently, for coarse hydroxyapatite powders (Figure 5.20).

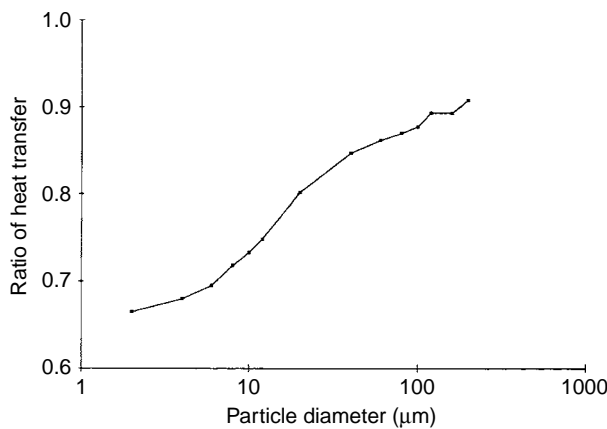


**Figure 5.18** Ratio of heat transfer with/without considering the *noncontinuum* effect. Calculations were made by Chyou and Pfnder (1989) for an argon plasma of  $T_g = 15\,000$  K under atmospheric pressure and a particle temperature ( $T_p$ ) of 2500 K

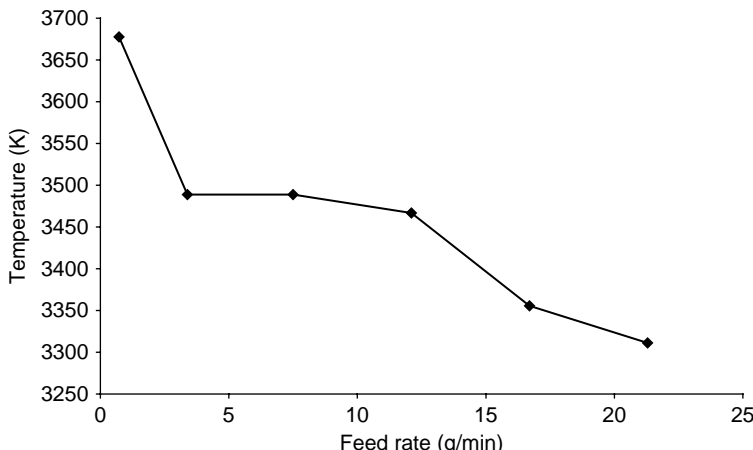


**Figure 5.19** Modification of the average centreline temperatures of alumina ( $\text{Al}_2\text{O}_3$ ) particles having particle sizes in the range  $-45$  to  $+22.5\mu\text{m}$ , measured by using two-colour pyrometry as a function of increasing powder feed rate. These measurements were made for a point at a distance of 12 cm from the F-4 plasma torch, supplied with  $\text{Ar} + \text{H}_2$  (32 + 12 slpm), with an electrical power ( $P$ ) of 34.8 kW (after Vardelle *et al.*, 1992). Reproduced by permission of Vardelle *et al.*, 1992, *Thermal Spray: International Advances in Coatings Technology*, C.C. Berndt (Ed.), ASM International, Materials Park, OH, USA, pp. 543–547

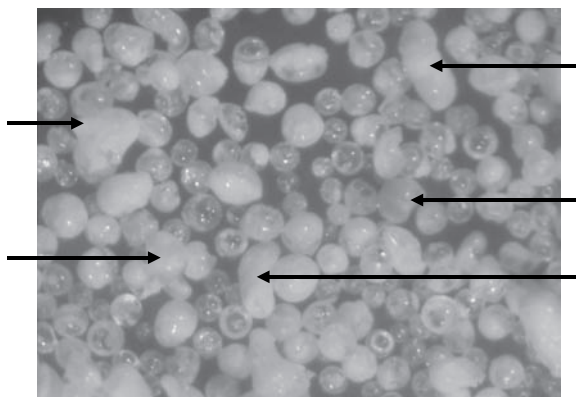


**Figure 5.20** Optical micrograph of a coarse hydroxyapatite powder sprayed into water; arrows indicate ‘twinned’ particles (Dyshlovenko *et al.*, 2006)

The agglomeration of small particles in a plasma has been discussed theoretically by Dundas (1975).

Heat transfer in arc spraying is slightly different than that in other spray techniques. The liquid particles are formed from ‘wires’ and during their flight towards the substrate they are cooled down by convection and conduction of the atomization gas and by radiation from their surfaces (Busse and Sobbe, 1989).

The description of the phenomena of particles heating in flames/jets can be categorized, as a function of the temperature distribution inside the particles. Two distinctive cases should be discussed:

- the particle has one temperature;
- the particle has a temperature gradient.

Dresvin (1972) suggested that this distinction depends on the Biot number ( $Bi$ ):

$$Bi = \frac{hd_p}{2\lambda_p} \quad (5.30)$$

He suggested that for  $Bi < 0.01$  the particles do not have a temperature gradient ‘inside’, while for  $Bi \geq 0.01$  they do have one. Consequently, particles which heat without any thermal gradient occurs when spraying a good heat conductor (large value of  $\lambda_p$ ), such as metals, alloys, carbides or small particles (low values of  $d_p$ ).

**Particles with one temperature,**  $T_p$ , are heated in a jet or flame in a way described by the equation<sup>10</sup> proposed by Borgianni *et al.* (1969):

$$\pi d_p^2 b(T_g - T_p) + h_r(T_g) = \frac{1}{6} \pi \rho_p c_p d_p^3 \frac{dT_p}{dt} + \pi d_p^2 \varepsilon_p \sigma T_p^4 \quad (5.31)$$

The left-hand side of Equation (5.31) describes the energy transferred from the plasma by convection, conduction (first term) and radiation (second term). The right-hand side describes the energy absorbed by the particle which results in an increase in the particle's enthalpy (first term) and radiation losses (second term). Let us assume the following simplifications:

- the energy-transfer mechanism is purely conductive, i.e.  $Nu = 2$ ;
- the mean thermal conductivity of the plasma/flame is given by Equation (5.19) and the lower limit of the integral is equal to 300 K, instead of the actual  $T_p$ ;
- the mean viscosity,  $\eta_g$ , of the plasma/flame is given by a similar equation to Equation (5.19);
- the length of the trajectory of all particles is constant and equal to  $L$ ;
- the plasma/flame has constant velocity,  $v_p$ ;
- the relative movement of the particle in a plasma/flame corresponds to *Stokes regime*.

Integration of Equation (5.31) leads to the following expression:<sup>11</sup>

$$AHF = \frac{L \left( \int_{300}^{T_g} \lambda_g dT \right)^2}{\langle \eta_g \rangle v_p} = \frac{H_m^2 d_p^2 \langle \rho_p \rangle}{16} = DMF \quad (5.32)$$

In the above equation the parameters related to the plasma/flame are on the left-hand side, while those related to the particle are on the right-hand side. The left-hand side is known as the Ability of Heating Factor (AHF) and the right-hand one, the Difficulty of Melting Factor (DMF). Equation (5.32) describes a situation in which a particle at the end of its trajectory in a plasma/flame is molten. It is clear that a particle of given diameter will be melted in a plasma/flame if:

---

<sup>10</sup> The given form of this equation supposes that no chemical reaction in the particle takes place.

<sup>11</sup> A similar equation was presented by Engelke (1962).

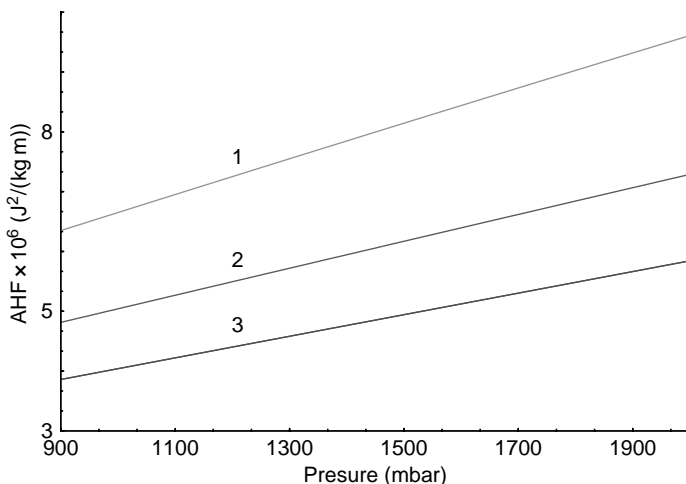
$$\text{AHF} \geq \text{DMF} \quad (5.33)$$

Table 5.2 shows the ‘difficulty of melting factors’ for some metals, and for comparison a factor for the ceramic ZrB<sub>2</sub>. The latter was analysed by Tului (2003). It is clear that this factor is greater for more refractory materials.

**Table 5.2** Difficulty of melting factors for particles of diameter  $d_p = 25\mu\text{m}$  of some metals and a ceramic

Material	$\text{DMF} \times 10^5 (\text{J}^2/(\text{kg m}))$
Cu	1.52
Ta	3.33
W	4.53
ZrB <sub>2</sub>	10.8

The ability of heating factors was analysed by using a calorimetric method for atmospheric plasma spraying by Pawłowski (1980) and, more recently, for inert gas plasma spraying under different pressures by Tului *et al.* (2002). The results of the latter are shown in Figure 5.21.



**Figure 5.21** Ability of heating factor versus chamber pressure of argon, at different compositions and flow rates of the plasma working gases, with an electric power input of 54 kW: (1) Ar + H<sub>2</sub>, 34 + 18 slpm; (2) Ar + H<sub>2</sub>, 40 + 12 slpm; (3) Ar + H<sub>2</sub>, 46 + 6 slpm (Tului *et al.*, 2002)

The optimization of the processing parameters becomes as easy as a comparison of the DMFs for powders to be sprayed with the AHFs of a torch in the used spray technique in order that the conditions for which the inequality (Equation (5.33)) is fulfilled. When calculating the factors for particles, care has to be paid to take the greatest particle sizes into consideration. This would assure the melting of all powder particles. The smaller particles would be, however, overheated and undesirable evaporation associated with reduction in their sizes is likely to occur.

**Particles with a temperature gradient** behaviour in a flame/plasma can be described by a heat-conduction equation. The *Fourier equation* has a very well-known form, as follows:

$$c_p(T)\rho(T)\frac{\partial T}{\partial t} = \text{grad}(\lambda(T)\text{grad}T) + q \quad (5.34)$$

As the particles are spherical or rounded in the initial state and, moreover, they become spherical after becoming molten in a flame/plasma, Equation (5.34) can be rewritten for spherical symmetry as follows:

$$c_p(T)\rho(T)\frac{\partial T}{\partial t} = \left(\frac{1}{r^2}r^2\frac{\partial}{\partial r}\right)\left(\lambda(T)r^2\frac{\partial T}{\partial r}\right) \quad (5.35)$$

The initial condition is:

$$T(r, 0) = 300 \text{ K} \quad (5.36)$$

The condition of symmetry gives another equation:

$$\frac{\partial T(0, t)}{\partial r} = 0 \quad (5.37)$$

The boundary conditions can be formulated by using the following assumptions:

- the material of the particle does not sublime and has melting and boiling points;
- the evaporation of the particle material has to be considered only if the temperature at its surface exceeds the boiling point;
- different situations that might occur during particle flight are depicted in Figure 5.22, while a diagram of the associated physical phenomena is shown in Figure 5.23.

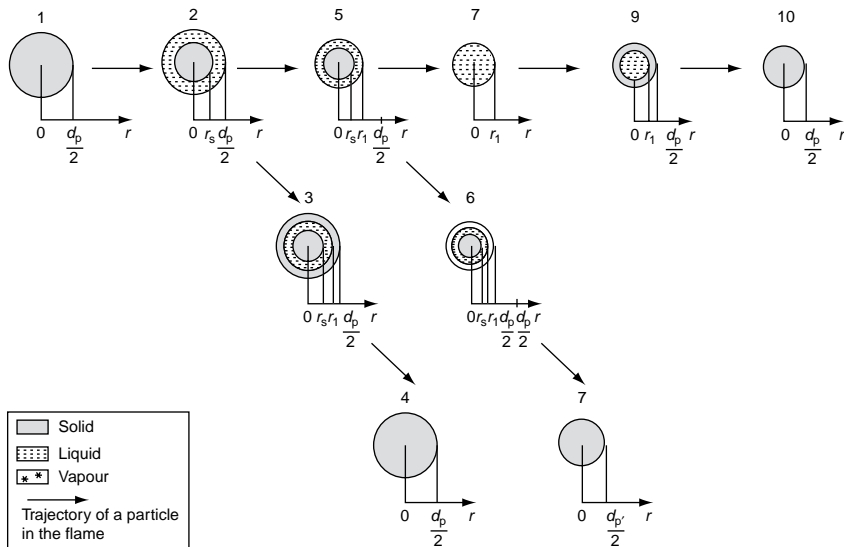


Figure 5.22 Possible phase compositions of a particle at flight in a plasma or flame

The boundary condition for stages 1 and 4 ( $r = d_p/2$ ), as well as for stages 7 and 9 ( $r = d'_p/2$ , where  $d'_p$  is the particle diameter after evaporation), is as follows:

$$\lambda(T) \frac{\partial T}{\partial r} = h(T_g - T_p) \quad (5.38)$$

At stage 1, the particle is heated until its temperature reaches the melting point. A liquid shell develops around the particle in stage 2. At stage 3, the particle starts to cool down and the liquid shell becomes solidified. Then, the particle solidifies entirely at stage 4. In the thermal history of the particle described by stages 1–4, the particle size is not changed. On the other hand, stage 5 initiates particle evaporation. The model of Knight (1979) for rapid surface vaporization with a back pressure can be used to investigate the particle evaporation. This model is based on the conservation of mass, momentum and energy across a thin layer. Knight showed that in the layer the following equation describes the temperatures and pressures of the vapours:

$$\begin{cases} \frac{p}{p_s} = \sqrt{\frac{T}{T_s}} \left[ (\beta^2 + 0.5) \exp(\beta^2) \operatorname{erfc}(\beta) - \frac{\beta}{\sqrt{\pi}} \right] \\ \quad + \frac{1}{2} (1 - \sqrt{\pi} \beta \exp(\beta^2) \operatorname{erfc}(\beta)) \\ \frac{T}{T_s} = \left\{ \sqrt{1 + \pi \left[ \left( \frac{\chi-1}{\chi+1} \right) \left( \frac{\beta}{2} \right) \right]^2} - \sqrt{\pi} \left[ \left( \frac{\chi-1}{\chi+1} \right) \left( \frac{\beta}{2} \right) \right] \right\}^2 \end{cases} \quad (5.39)$$

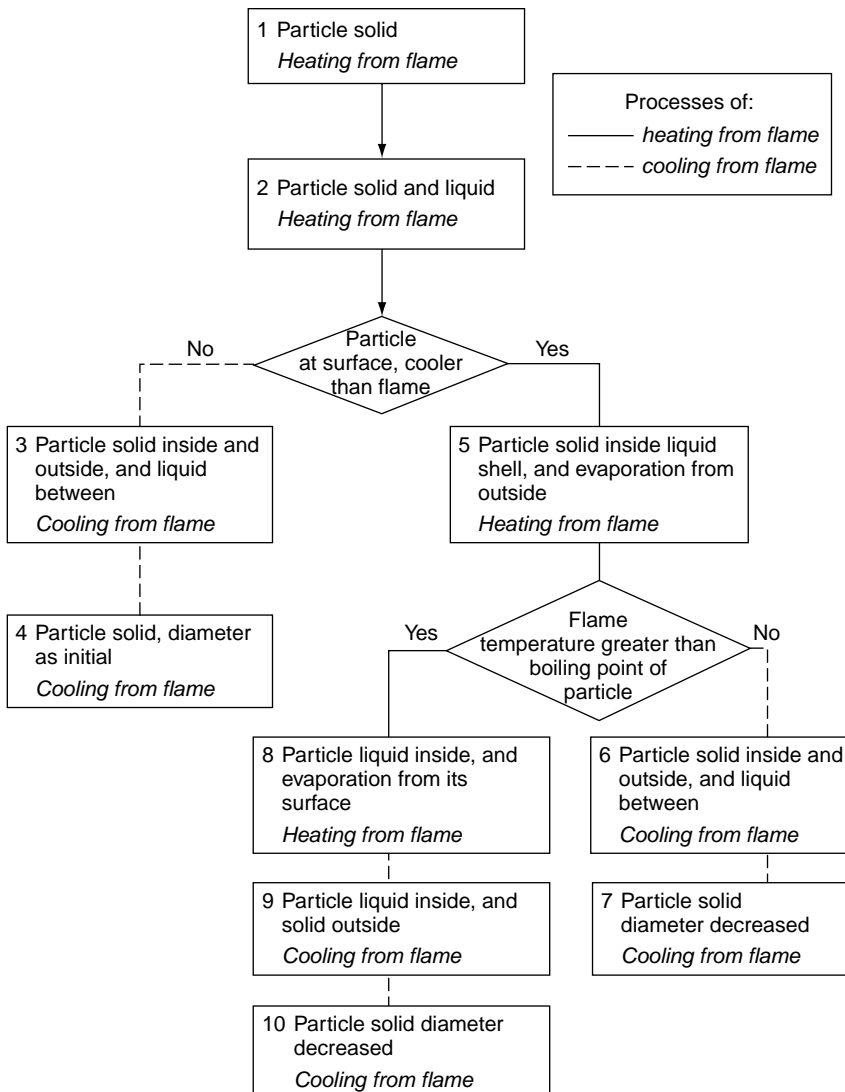


Figure 5.23 Diagram of possible physical phenomena occurring at flight in a plasma or flame

The saturated vapour pressure,  $p_s$ , can be determined experimentally or calculated by the Clausius–Clapeyron equation (Gusarov and Smurov, 2001). The value of the  $\beta$ -coefficient can be found from the following equation:

$$M = v_g / \sqrt{\chi RT} = \beta \sqrt{2/\chi} \quad (5.40)$$

Equation (5.39) is valid only if the flow outside the Knudsen layer is ‘subsonic’ (i.e.  $M \leq 1$ ). For a spherical particle, the radius decreases because of evaporation and hence:

$$\begin{cases} \frac{dr_p}{dt} = \sqrt{\frac{2R}{T_s}} \left( \frac{\beta p_s \mu}{\rho_p k} \right), & M < 1 \\ \frac{dr_p}{dt} = \sqrt{\frac{R \chi}{T_s}} \left( \frac{p_s \mu}{\rho_p k} \right), & M = 1 \end{cases} \quad (5.41)$$

The values of  $T_s$  and  $\beta$  are obtained by solving Equation (5.39). At the stages 7 and 10, the particle has cooled down after evaporation from its surface and thus the outer diameter is  $d'_p < d_p$ . The boundary condition for stage 2 at the surface  $r = d_p/2$  is given by Equation (5.38) and at the interface  $r = r_s$ , has the following form:

$$\left( \lambda_l(T) \frac{\partial T}{\partial r} \right)_{r=r_s(-)} = \left( \lambda_l(T) \frac{\partial T}{\partial r} \right)_{r=r_s(+)} + H_m \rho_l \frac{dr_s}{dt} \quad (5.42)$$

At the boundary, the temperatures  $T(r_{s(-)}, t)$  and  $T(r_{s(+)}, t)$  are equal to  $T_m$ . For the stages 3 and 6, the boundary conditions are as follows:

- at the surface,  $r = d_p/2$  (stage 3) or  $r = d'_p/2$  (stage 6), the boundary condition is given by Equation (5.38);
- at the interfaces,  $r = r_l$  and  $r = r_s$ , the boundary condition is described by Equation (5.42).

For stage 5, the boundary condition at the interface  $r = r_s$  is given by Equation (5.42) and at the surface  $r = r_1$  has the following form:

$$\lambda_l(T) \frac{\partial T}{\partial r} = h(T_g - T_e) + H_{ev} \rho_l \frac{dr_1}{dT} \quad (5.43)$$

The condition at boundary  $r = r_1$  at stage 8 is described by Equation (5.43). Finally, for stage 9, the condition at the surface  $d'_p/2$  is described by Equation (5.38) and at the interface  $r = r_l$  Equation (5.42) is valid. The boundary conditions are more complicated for materials which have phase transformations before melting. All of these transformations should be included in the temperature distribution. An example is shown in Figure 5.24.

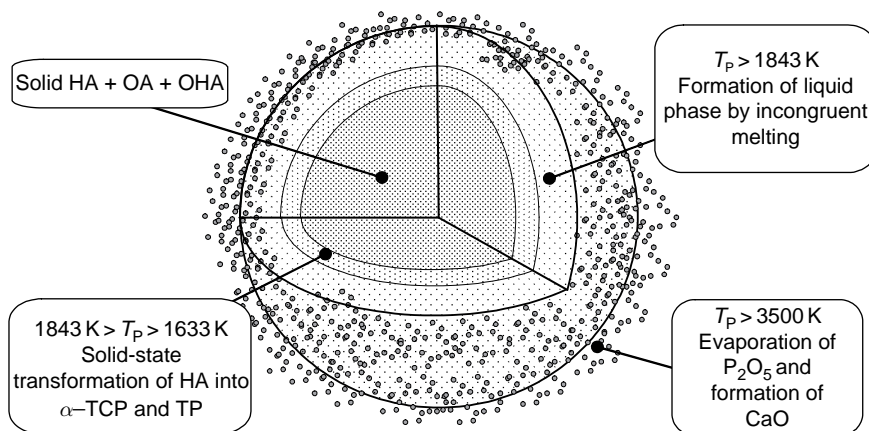


**Figure 5.24** Temperature field inside an HA particle at flight in plasma jet and possible crystal phase transformations on particle heating (Dyshlovenko *et al.*, 2006). The crystal phases considered are:  $\text{Ca}_{10}(\text{PO}_4)_6(\text{OH})_2$  (HA), which loses water gradually at high temperatures to become  $\text{Ca}_{10}(\text{PO}_4)_6(\text{OH})_{2-2x}\text{O}_x\text{v}_x$  (where 'v' stands for vacancy) (OHAP), which itself becomes  $\text{Ca}_{10}(\text{PO}_4)_6\text{O}$  (OAP) above 1373K;  $\alpha\text{-Ca}_3(\text{PO}_4)_2$  ( $\alpha$ -TCP);  $\text{Ca}_4\text{P}_2\text{O}_9$  (TP)

The boundary conditions at the interfaces of materials with phase transformations are similar to that given by Equation (5.42), by taking the temperature and enthalpy of the transformation, instead of those of melting.

To solve the Fourier equation, it is necessary to know the thermophysical properties of powder particle material. Corrections for the internal porosities of the particles should be made, if necessary, following the equations:

$$\rho_{\text{porous}} = \rho_{\text{dense}}(1 - P) \quad (5.44)$$

$$\lambda_{\text{porous}} = \frac{\lambda_{\text{dense}}(1 - P)}{1 + 0.5P} \quad (5.45)$$

Equation (5.45), known as the *Maxwell equation*, is one possibility. The other ones are shown by, e.g. Hurevich *et al.* (2002). The data for porous material can be considerably different, as shown in the examples for porous hydroxyapatite powder having a porosity  $P$  of 12 % in Figure 5.25.

The heating of porous particles starts with sintering of the precursors (as for spray-dried powders, described in Chapter 1, Section 1.1.3). The sintering of solid precursors takes a relatively long time (hundreds

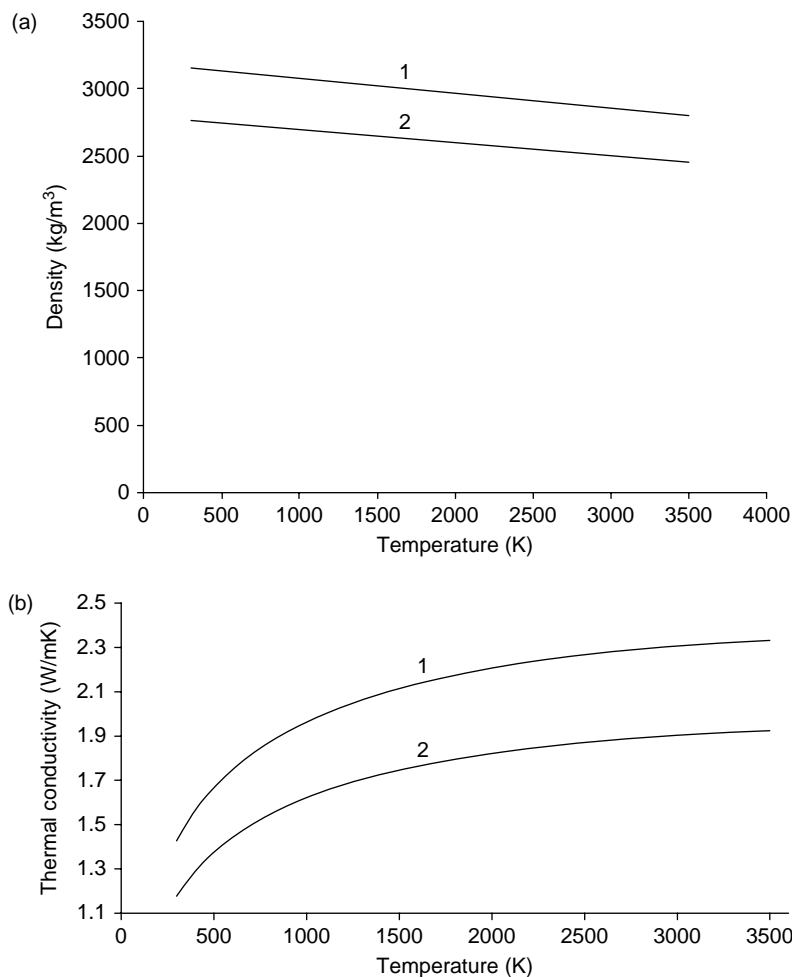


Figure 5.25 Density (a) and thermal conductivity (b) of dense (1) and porous ( $P = 12\%$ ) (2) hydroxyapatite as a function of temperature (Dyshlovenko *et al.*, 2006)

of seconds and more) but the sintering of liquid materials is nearly instantaneous (Hurevich *et al.*, 2002). Knowing that the typical ‘dwell time’ in a jet/flame is less than a few milliseconds, it can be reasonably concluded that no sintering in the solid state takes place ‘at flight of the particle’. Melting occurs from the particle surface and the pores agglomerate and evacuate out of the liquid material (Figure 5.26).

A comparison of the profiles of the flight of a porous particle inside the plasma jet is shown in Figure 5.27. It is clear that the temperature gradients are much steeper for more porous materials.

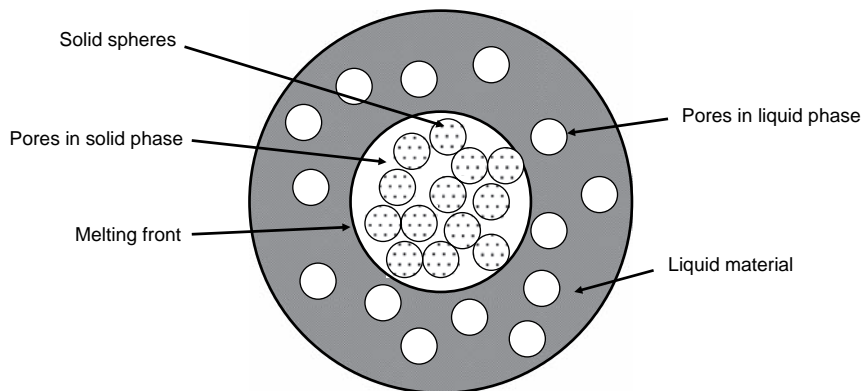


Figure 5.26 Representation of the melting of a porous powder particle

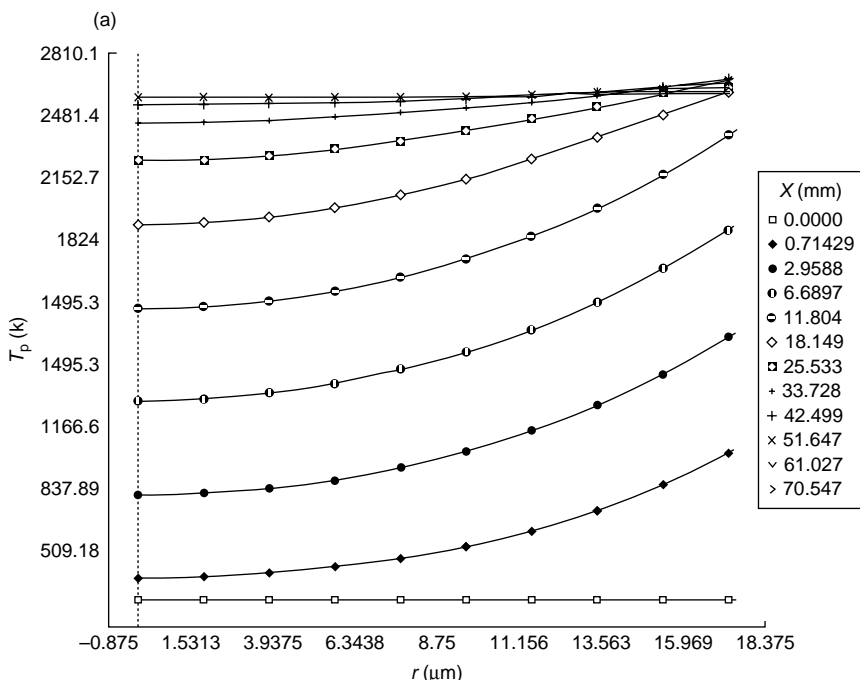


Figure 5.27 Modelled temperature profiles inside a  $\text{Cr}_2\text{O}_3$  particle with a diameter ( $d_p$ ) of 35  $\mu\text{m}$ , plasma-sprayed at an electric power of 29 kW, using  $\text{Ar} + \text{H}_2$  (75 + 15 slpm), at different distances ( $X$ ) from the injection port: (a) porosity,  $P = 0\%$ ; (b) porosity,  $P = 20\%$  (Hurevich *et al.*, 2002)

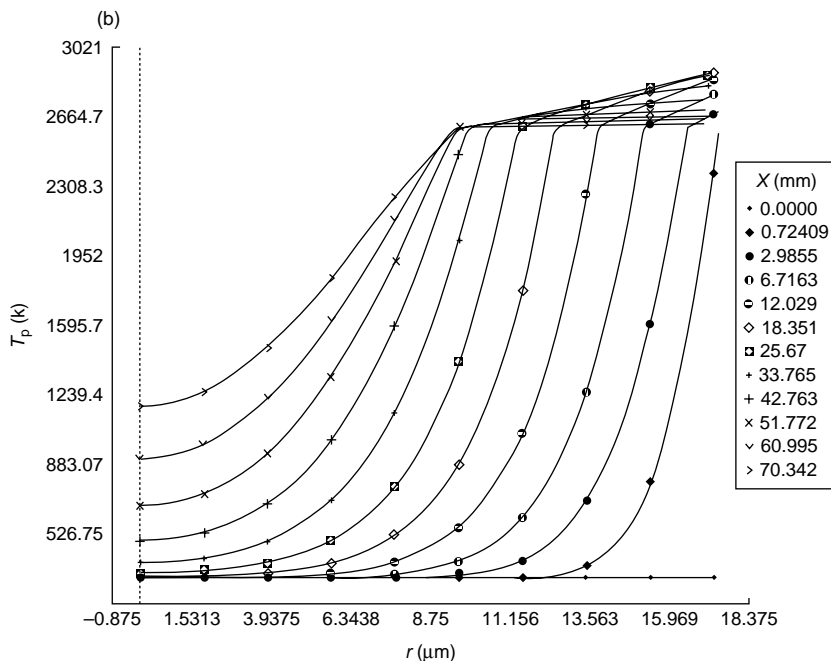


Figure 5.27 (Continued)

In ‘real’ processing situations, the powder is not ‘mono-sized’ and the particles impacting the substrate can be in any of the states shown in Figure 5.22. Usually, optimization of the spraying parameters is carried out with regard to the largest particles in the sprayed powder. Consequently, smaller particles become overheated and evaporate intensively.

Modelling of the particles’ temperatures in a flame/plasma is usually carried out together with modelling of their trajectories. Quite frequently, ‘maps’ of the temperatures and velocities of gases are also generated by numerical models (see Table 5.1). Table 5.3 shows some representative studies.

Most of the recent studies model all elements of the spray process, starting with modelling of the jet or flame, followed by modelling the dynamic and thermal interactions between the particles and the gas. The Knudsen effect is frequently considered, although the load effect is not. Finally, many studies have validated the models by using the particles’ temperature and/or velocity sensors. A few of these, namely those of Dyshlovenko *et al.* (2006) for APS and of Zagorski and Stadelmaier (2001) models (as discussed in Fincke *et al.*, 2001) consider the entire

Table 5.3 Examples of modelling of particles' temperatures and velocities when spraying using different spray techniques

Process	Powder particle material	Modelling of jet/flame	Considered effects			Experimental validation	Remarks	Reference
			Knudsen	Load	Evaporation			
APS	$\text{Ca}_{10}(\text{PO}_4)_6(\text{OH})_2$	Yes	No	No	Yes	Yes	Validation by microstructural investigations of coatings	Dyshlovenko, <i>et al.</i> , 2006
APS	ZrO <sub>2</sub>	Yes	No	No	No	Yes	Validation by DPV-2000 measurement	Remesh <i>et al.</i> , 2003
Detonation gun	WC-Co	Yes	No	No	No	No	1-D analytical model	Kadyrov, 1996
Detonation gun	Al <sub>2</sub> O <sub>3</sub>	Yes	No	No	No	No	—	Ramadan and Butler, 2004
HVOF	Al <sub>2</sub> O <sub>3</sub> , Ni, WC-12 wt%	Yes	Yes	No	No	No	—	Sobolev <i>et al.</i> , 1994
HVOF	Inconel, WC Co	Yes	No	No	No	Partly from data of manufacturer	1-D model	Tawfik and Zimmerman, 1997
VPS	NiCrAlY	Yes	Yes	No	—	Yes	Validation by microstructural investigations of coatings	Zagorski and Stadelmeier, 2001

spray process, including the coatings' growth and validate the modelling by using microstructural investigations.

### 5.3.2 METHODS OF PARTICLES' TEMPERATURE MEASUREMENTS

Optical methods *must* be used to determine the temperature of the particles 'in flight'. Two methods can be used:

- *one-colour pyrometry*, described and used by, e.g. Kruszewska and Lesinski (1977);
- *two-colour pyrometry*, described and used by, e.g. Hantsche (1973).

**One-colour pyrometry.** The installation has a calibrated photomultiplier which can be used to observe a stream of sprayed particles. The calibration involves the application of a tungsten ribbon lamp, pin hole and chopper. The changing intensity of the tungsten lamp radiation corresponds to the known temperature. The chopper and pin hole simulate the particle of a known diameter moving with a known velocity. This technique enabled the authors to find the distribution of the temperature as a function of the particle injection velocity.

**Two-colour pyrometry.** The installation, shown schematically in Figure 5.28, treats the optical signal from a small volume of the flame (e.g.  $1.5 \times 20.2 \times 0.12\text{mm}^3$  in the study of Vardelle *et al.*, 1989) which is focused on the entrance of two monochromators and then transformed by the photomultipliers into an electrical signal.

Finally, the signals are treated to obtain the temperature by the well-established principles of radiation thermometry. The radiometry is based on the *black-body* concept. The black-body radiates at a temperature,  $T$ , as a function of the power density, which for the wavelength  $\lambda$  is described by the Wien relationship:

$$I(\lambda, T) = 2\pi h c^2 \lambda^{-5} \exp\left(-\frac{hc}{\lambda kT}\right) \quad (5.46)$$

A *grey-body*, a body having an emission coefficient independent of the wavelength, radiates  $\varepsilon$  times less than a black-body ( $0 < \varepsilon \leq 1$ ). Typically, one can assume that emitting particles are grey-bodies between two wavelengths ( $\lambda_1$  and  $\lambda_2$ ) tested by the monochromators (Cetegen

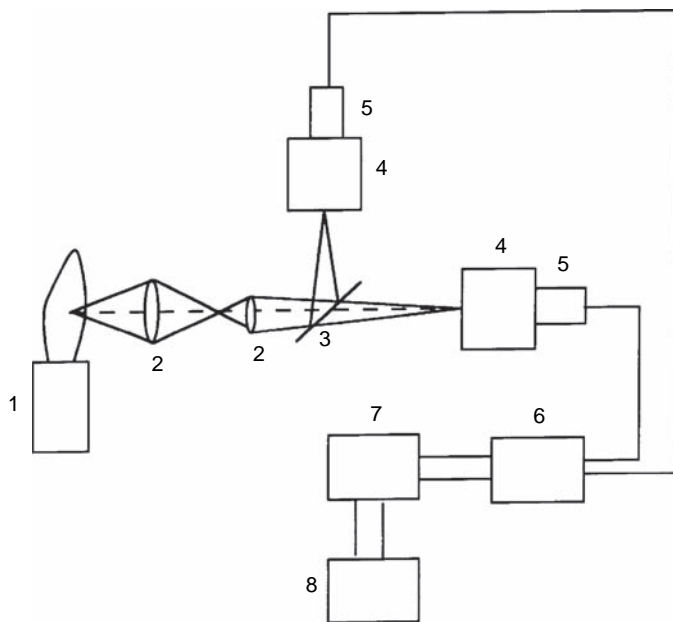


**Figure 5.28** Schematic of the two-colour pyrometry technique: (1) torch; (2) lens; (3) semitransparent mirror; (4) monochromator; (5) photomultiplier; (6) signal treatment; (7) A/D converter; (8) computer (after Vardelle *et al.*, 1989)

and Yu, 1999). Consequently, the temperature can be found from the following relationship:

$$T = \frac{A \left( \frac{1}{\lambda_2} - \frac{1}{\lambda_1} \right)}{\ln \left[ \left( \frac{\lambda_1}{\lambda_2} \right)^5 \frac{I(\lambda_1, T)}{I(\lambda_2, T)} \right]} \quad (5.47)$$

The constant  $A$  can be found from Equation (5.46). When measuring temperatures in chemically reacting gases, it is important to avoid the strong spectral emission regions that may interfere with the emitting particles. The set-up must be calibrated by using a tungsten ribbon lamp. The commercial set-ups, DPV-2000™ and SprayWatch™, use the principle of two-colour pyrometry. The precision of the temperature measurements using this principle was estimated to be in the range 5 to 20 % (Vardelle *et al.*, 1989; Fincke *et al.*, 1990).

At present there are a wealth of data concerning particles temperature measurements at processing with virtually all spray techniques. These data can be useful in process optimization. Examples of such

measurements of Ni particles, plasma-sprayed in the open air and in an argon atmosphere, using the same electric power of 29.4 kW and the same working gas composition and flow rate ( $\text{Ar} + \text{H}_2$ , 45+12 slpm) are shown in Figure 5.29.

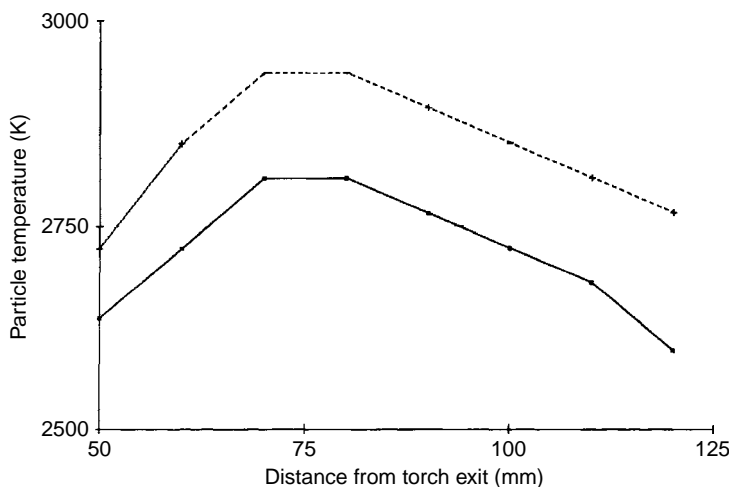


**Figure 5.29** Average centreline temperatures of Ni particles, plasma-sprayed in the open air (■) and in an Ar atmosphere (+)(after Vardelle *et al.*, 1989)

The results shown in Figure 5.29 indicate that at any distance from the torch the IPS-processed powder has a higher temperature than the APS one. The authors explain this by the effect of longer and larger isotherms when-plasma spraying in an argon atmosphere.

## 5.4 CHEMICAL MODIFICATION AT FLIGHT OF SPRAYED PARTICLES

Modification of the chemical composition can be mainly related to the following properties of jets and flames, used as working gases at spraying:

- high temperature;
- chemical activity.

A *high temperature* results in melting and evaporation of the particles injected or introduced into the gases. Evaporation can modify the initial chemical composition of the particles by *selective evaporation phenomena*. This effect was observed during atmospheric plasma spraying of  $\text{YBa}_2\text{Cu}_4\text{O}_x$ , which resulted into coatings having the composition  $\text{YBa}_2\text{Cu}_3\text{O}_{5.6}$  (Pawlowski *et al.*, 1990).  $\text{CuO}$  was evaporated more intensively than  $\text{BaO}$  and  $\text{Y}_2\text{O}_3$  at processing. Consequently, the authors used an excess of this oxide in order to obtain the desired chemical composition in sprayed coatings. The evaporation intensity of molecules ( $dN/(dt(S))$ ) for a clean surface can be expressed by the *Hertz-Knudsen equation*:

$$\frac{dN}{dtS} = (2\pi\mu kT)^{-0.5} (p^* - p) \quad (5.48)$$

The vapour pressure,  $p^*$ , being an element/compound property, depends strongly on the temperature at the origin of selective evaporation. Another two phenomena observed at spraying, may be at least partly related to the high enthalpy of the gas used for spraying:

- decarburization;
- reduction.<sup>12</sup>

Decarburization, reviewed extensively by Lovelock (1998), occurs when spraying such carbides as WC (being usually alloyed or agglomerated with Co). Many studies have revealed the formation of  $\text{W}_2\text{C}$  from WC and a loss of carbon (as high as 50–66 %) in plasma WC–Co coatings with regard to the initial powders. Reduction, observed for many ‘multi-oxides’, such as described above for YBCO, was also observed in oxides such as  $\text{ZrO}_2$  (Ingo *et al.*, 1990),  $\text{Cr}_2\text{O}_3$  (Pawlowski, 1996) or  $\text{TiO}_2$  (Figure 5.30).

The mechanisms of decarburization and reduction at spraying have not been yet studied. It can be tentatively explained by diffusion of carbon or oxygen atoms from the melt. The diffusion may be driven by the concentration of these atoms, which is locally higher inside the molten particles than on their surfaces.

The *chemical activities* of the jet or flames used in spray processes may result from the working gases. In fact,  $\text{N}_2$  or hydrocarbons are

---

<sup>12</sup> Reduction is also caused by the action of reducing gases, such as hydrogen.

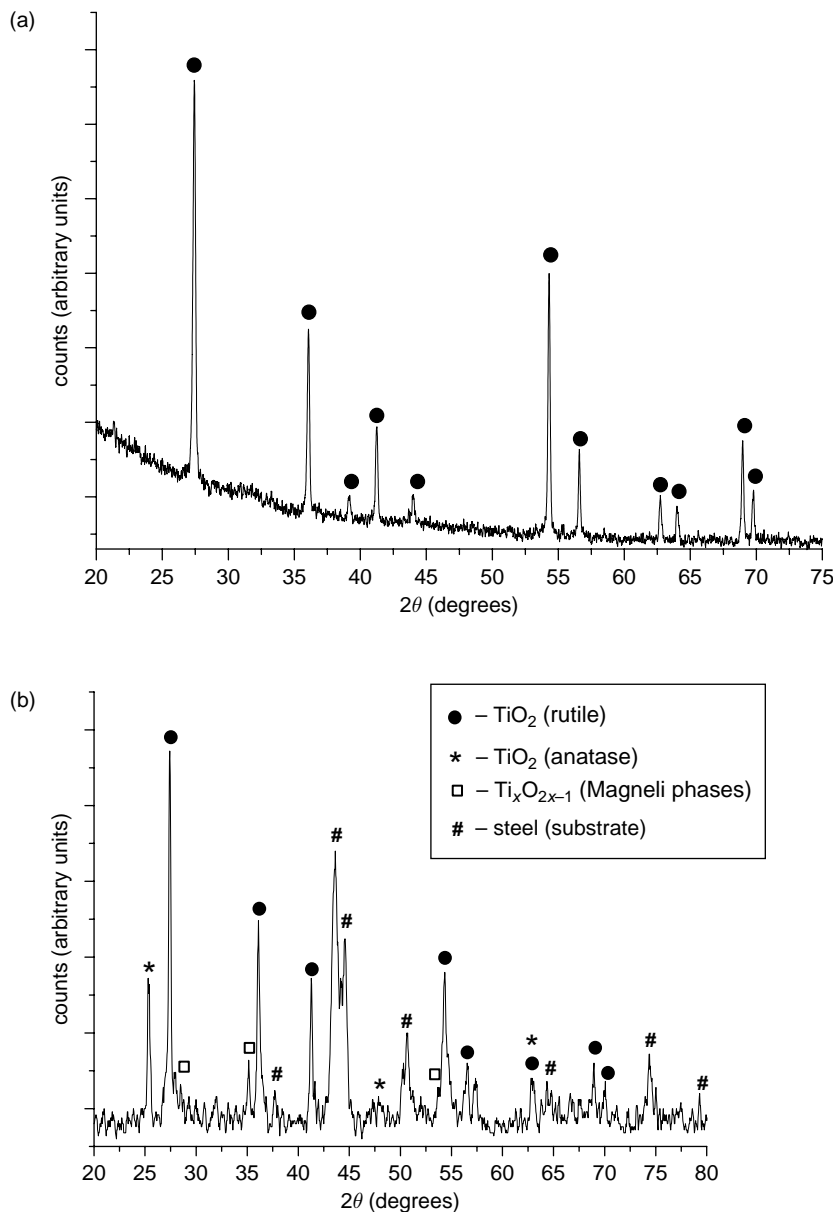


**Figure 5.30** X-ray diagrams of an initial fine powder of rutile ( $\text{TiO}_2$ ) (a) used to prepare a water suspension and of a  $10 \mu\text{m}$  thick film (b) suspension plasma sprayed in the open atmosphere. The diffraction of Fe, from the steel substrate, occurs because of penetration of the X-rays through the thin oxide film (Tomaszek *et al.*, 2006)

chemically active. In general, their affinities to the sprayed materials are considerably smaller than that of oxygen. Oxygen (in air) penetrates to a jet or flame by their turbulent mixing with the open atmosphere. The mixing is very efficient, as shown in the measurements made for atmospheric plasma spraying (see Figure 5.7). In fact, the Ar working gas content drops down to 50 vol % at a distance of 34 mm from the torch exit, following the measurement made by Fisdon *et al.* (1976). Oxidation which concerns metal and alloy particles is a time-dependent process. The kinetics of this process, expressed as the evolution of the initial mass,  $\Delta m$ , at the time of exposition,  $t$ , can be of two fundamental types (Perrin and Scharff, 1999):

- linear,  $\Delta m \sim t$ , characteristic for alkaline metals with a non-continuous oxide film;
- parabolic,  $\Delta m \sim t^{0.5}$ , characteristic for metals such as Fe, Ni or Cu with a continuous oxide film.

The time of exposition in flames or jets, estimated from the typical velocities of the particles and the spray distances, ranges from a fraction of a millisecond to slightly above 1 ms is very short. Moreover, the liquid material inside a molten particle can move under the action of shear forces resulting from the high-velocity gas flow around the particle (Figure 5.31).

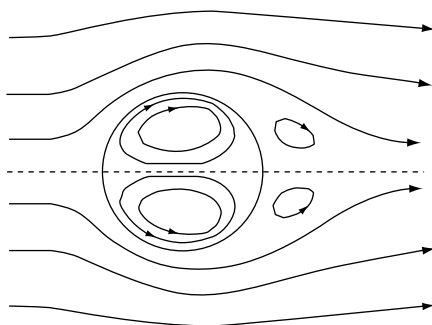


**Figure 5.31** Possible movement of liquid material inside a liquid particle resulting from the action of shear forces induced by the high-velocity gas around the particle (Neiser *et al.*, 1998). Reproduced from *J. Therm. Spray Technol.*, 7(4), 1998, 537–545, ‘Oxidation in wire HVOF-sprayed steel’, R.A. Neiser, M.F. Smith and R.C. Dykhuizen, Figure 11, Copyright (1998). With kind permission of Springer Science and Business Media

Such a convection move of the liquid can be explained by the relatively high rate of oxidation, because the liquid motion constantly ‘sweeps’ fresh liquid to the surface of the particle. This fresh liquid is then available for in-flight oxidation (Neiser *et al.*, 1998). Studies of oxidation carried out by different authors underline the fundamental difficulty of separating the oxidation, in-flight, of particles from the oxidation of splats on the substrate. The oxidation in-flight can be characterized by:

- formation of metastable oxides, which was observed at plasma-spraying of stainless steel by Syed *et al.* (2003);
- presence of sub-micron, spherical inclusion of oxides and metals in sprayed deposits (confirming formation of oxides in the liquid state), observed at high-velocity wire spraying of mild steel by Neiser *et al.* (1998).

## REFERENCES

- Bandyopadhyay, R. and Nylén, P. (2003). A computational fluid dynamic analysis of gas and particle flow in flame spraying, *J. Therm. Spray Technol.*, **12** 492–503.
- Barbezat, G. (1989). Hochgeschwindigkeit-Flammspritzen von Schutzschichten, *Metalloberfläche*, **43**, 459–466.
- Baudry, C., Vardelle, A., Mariaux, G., Delalondre, C. and Meillot, E. (2004). Three-dimensional and time-dependent model of the dynamic behavior of the arc in plasma spray torch, in *Proceedings of the International Thermal Spray Conference '04*, CD-Rom, ISBN 3-87155-792-7, DVS-Verlag, Düsseldorf, Germany.
- Beard, K.V. and Pruppacher, H.R. (1969). A determination of terminal velocity and drag of small water drops by means of a wind tunnel, *J. Atm. Sci.*, **26**, 1006–1072.
- Bisson, J.F., Gauthier, B. and Moreau, C. (2003). Effect of plasma fluctuations on in-flight particle parameters, *J. Therm. Spray Technol.*, **12**, 38–43.
- Blais, A., Jodoin, B., Dorier, J.-L., Gindrat, M., Hollenstein, Ch. and Barbezat, G. (2004). Supersonic plasma jet modelling at low pressure using recent advances of the enthalpy probe measurement technique, in *Proceedings of the International Thermal Spray Conference '04*, CD-Rom, ISBN 3-87155-792-7, DVS-Verlag, Düsseldorf, Germany.
- Bolot, R., Imbert, M. and Coddet, C. (1997). Mathematical modeling of free plasma jet discharging into air and comparison with probe measurements, in *Thermal Spray: A United Forum for Scientific and Technological Advances*, C.C. Berndt (Ed.), ASM International, Materials Park, OH, USA, pp. 549–555.
- Bolot, R., Li, J. and Coddet, C. (2004). Modelling of thermal plasma jets: a comparison between PHOENICS and FLUENT, in *Proceedings of the International Thermal Spray Conference '04*, CD-Rom, ISBN 3-87155-792-7, DVS-Verlag, Düsseldorf, Germany.
- Borgianni, C., Capitelle, M., Cramarosa, F., Triolo, L. and Molinari, E. (1969). The behavior of metal particles injected into an argon induction plasma, *Comb. Flame*, **13**, 181–194.

- Boulos, M., Fauchais, P. and Pfender, E. (1994). *Thermal Plasmas: Fundamental and Applications*, Plenum Press, New York, NY, USA.
- Bourque, G., Lamontagne, M. and Moreau, C. (2000). A new sensor for on-line monitoring the temperature and velocity of thermal spray particles, in *Thermal Spray: Surface Engineering via Applied Research*, C.C. Berndt (Ed.), ASM International, Materials Park, OH, USA, pp. 45–50.
- Busse, K.-H. and Stobbe, H. (1989). Spray particle behaviour during atmospheric arc spraying, in *Proceedings of the 12th International Thermal, Spray Conference*, The Welding Institute, Cambridge, UK, Paper 35.
- Cambray, P. (1977). Mesure de vitesse dans les jets de plasma, *Rev. Phys. Appl.*, **12**, 1039–1042.
- Capitelli, M., Fiocelli, E. and Molinari, E. (1972). Equilibrium compositions and thermodynamic properties of mixed plasma, Report, University of Bari, Italy (available upon request).
- Capitelli, M., Gorse, C. and Fauchais, P. (1976). Transport coefficients of Ar-H<sub>2</sub> high temperature mixtures, *J. Chim. Phys.*, **73**, 755–759.
- Cetegen, B.M. and Yu, W. (1999). *In situ* particle temperature, velocity and size measurement in dc arc plasma thermal sprays, *J. Therm. Spray Technol.*, **8**, 57–67.
- Chase, Jr., M.W., Davies, C.A., Downey, Jr., J.R., Frurip, D.J., McDonald, R.A. and Syverud, A.N. (1986). *JANAF Thermochemical Tables*, 3rd Edition, American Chemical Society, Washington, DC, USA.
- Cheng, D., Trapaga, G., McKelliget, J.W. and Lavernia, E.J. (2003). Mathematical modelling of high velocity oxy-fuel thermal spraying of nanocrystalline materials: an overview, *Model. Simul. Mater. Sci Eng.*, **11**, R1–R31.
- Chyou, Y.P. and Pfender, E. (1989). Behavior of particulates in thermal plasma flows, *Plasma Chem. Plasma Proc.*, **9**, 45–70.
- Czernichowski, A. (1985). Internal report, W. Haldenwanger, Berlin, Germany.
- Devoto, R.S. (1967). Transport coefficients of partially ionized argon, *Phys. Fluids*, **10**, 354–364.
- Dresvin, S.V. (1972). *Physics and Technology of Low Temperature Plasmas*, Atomizdat, Moscow, Russia (in Russian).
- Dundas, P.H. (1975). Agglomeration in large scale plasma spheroidization processes, in *International Round Table on Study and Application of Transport Phenomena in Thermal Plasmas*, C. Bonnet (Ed.), CNRS, Odeillo, France, Paper I.2.
- Dussoubs, B., Fauchais, P., Vardelle, A., Vardelle, M. and Themelis, N.J. (1997). Computational analysis of 3-D plasma spray jet, in *Thermal Spray: A United Forum for Scientific and Technological Advances*, C.C. Berndt (Ed.), ASM International, Materials Park, OH, USA, pp. 557–565.
- Dykhuizen, R.C. and Smith, M.F. (1998). Gas dynamic principles of cold spray, *J. Therm. Spray Technol.*, **7**, 205–212.
- Dyshlovenko, S., Pateyron, B., Pawlowski, L. and Murano, D. (2004). Numerical simulation of hydroxyapatite powder behaviour in plasma jet, *Surf. Coat. Technol.*, **179**, 110–117.
- Dyshlovenko, S., Pawlowski, L., Pateyron, B., Smurov, I. and Harding, J.H. (2006). Modelling of plasma particles interactions and coating growth for plasma spraying of hydroxyapatite, *Surf. Coat. Technol.*, **200**, 3757–3769.

- Eichert, P. (1996). Etude de l'écoulement gazeux, au sein et à l'extérieur d'une torch de projection à plasma d'arc soufflé à l'aide du code PHOENICS™, *PhD Thesis*, Institut Polytechnique de Sévenans, Belfort, France.
- Eichert, P., Imbert, M. and Coddet, C. (1998). Numerical study of an ArH<sub>2</sub> gas mixture flowing inside and outside a dc plasma torch, *J. Therm. Spray Technol.*, **7**, 505–512.
- Engelke, J.K. (1962). Heat transfer to particles in the plasma flame, in *Proceedings of the American Institute of Chemical Engineering Meeting*, Los Angeles, CA, USA, pp. 1–9.
- Fauchais, P., Coudert, J.F., Vardelle, A., Vardelle, M. and Lesinski, J. (1984). Diagnostics under thermal plasma conditions, *Mater. Res. Soc. Symp. Proc.*, **30**, 37–51.
- Fincke, J.R., Swank, W.D. and Jeffrey, C.L. (1990). Simultaneous measurement of particle size, velocity and temperature in thermal plasmas, *IEEE Trans. Plasma Sci.*, **18**, 948–957.
- Fincke, J.R., Swank, W.D., Bewley, R.L., Haggard, D.C., Gevelber, M. and Wroblewski, D. (2001). Diagnostics and control in the thermal spray process, *Surf. Coat. Technol.*, **146–147**, 537–543.
- Fiszdon, J. and Lesinski, J. (1975). Accélération et fusion des grains dans un jet du plasma d'argone-hydrogène, in *International Round Table on Study and Application of Transport Phenomena in Thermal Plasmas*, C. Bonnet (Ed.), CNRS, Odeillo, France, Paper IV.1.
- Fiszdon, J., Gauk, W. and Daniault, J. (1976). Mesures des paramètres du jet de plasma pour plasmatron de projection, *Rev. Int. Htes Tempér. Réfract.*, **13**, 11–15.
- Frind, G., Goody, C.P. and Prescott, L.E. (1983). Measurements of particle velocity in two low pressure plasma jets, in *Proceedings of the 6th International Thermal Spray Conference*, M.I. Boulos and R.J. Munz (Eds), McGill University, Montreal, Canada, pp. 120–126.
- Gusarov, A. and Smurov, I. (2001). Target–vapour interaction and atomic collisions in pulsed laser ablation, *J. Phys. D*, **34**, 1147–1156.
- Hantsche, H. (1973). Temperature measurements of powder particles in a plasma jet, in *Proceedings of the 7th International Metal Spray Conference*, The Welding Institute, Cambridge, UK, Paper 16.
- Hurevich, V., Smurov, I. and Pawlowski, L. (2002). Theoretical study of the powder behavior of porous particles in a jet during plasma spraying, *Surf. Coat. Technol.*, **151–152**, 370–376.
- Ingo, G. (1990). Origin of darkening in 8 wt% yttria–zirconia plasma sprayed thermal barrier coatings. *J. Am. Ceram. Soc.*, **74**, 381–388.
- Joshi, S.V. (1992). Comparison of particle heat-up and acceleration during plasma and HVOF spraying, *Powder Met. Int.*, **6**, 373–380.
- Joshi, S.V. and Sivakumar, R. (1991). Particle behaviour in high velocity oxy-fuel spraying, *Surf. Coat. Technol.*, **50**, 67–74.
- Joshi, S.V., Park, J.Y., Taylor, P.R. and Richardson, L.S. (1986). Knudsen effect on plasma–particle mass transfer. I – formulation and application to self-diffusion, *Plasma Chem. Plasma Proc.*, **6**, 281–298.
- Kadyrov, E. (1996). Gas–particle interaction in detonation spraying systems, *J. Therm. Spray Technol.*, **5**, 185–195.
- Kleimann, H., Reynaud, R. and Pelourson, A. (1970). Mesure expérimentale de la température d'excitation d'un dard de chalumeau à plasma, *High Temp. High Press.*, **2**, 617–630.

- Knight, C.J. (1979). Theoretical modeling of rapid surface vaporization with back pressure, *AIAA J.*, **17**, 519–523.
- Kruszewska, B. and Lesinski, J. (1977). Temperature distribution of solid particles in a plasma stream, *Rev. Phys. Appl.*, **12**, 1209–1211.
- Launder, B.E. and Spalding, D.B. (1972). *Mathematical Models of Turbulence*, Academic Press, New York, NY, USA.
- Launder, B.E. and Spalding, D.B. (1974). The numerical computation of turbulent flow, *Comp. Meth. Appl. Mech. Eng.*, **3**, 269–289.
- Lebedev, M. and Akeko, J. (2003). Simple self-selective method of velocity measurement for particles in spray coating, in *Thermal Spray 2003: Advancing the Science and Applying the Technology*, C. Moreau and B. Marple (Eds), ASM International, Materials Park, OH, USA, pp. 1117–1120.
- Lemoine, A. and Le Goff, P. (1969). Vitesse de grains d'un matériau refractaire injectés dans un chalumeau à plasma d'arc, *Chim. Ind. Gén. Chim.*, **102**, 1304–1311.
- Lesinski, J. (1975). Investigation on heat and momentum transfer between solid particles and argon-hydrogen plasma, *PhD Thesis*, Institute of Nuclear Research, Warsaw, Poland (in Polish).
- Lewis, J.A. and Gauvin, W.H. (1973). Motion of particles entrained in a plasma jet, *AIChE J.*, **19**, 982–990.
- Lovelock, K.H. de Villiers (1998). Powder/processing/structure relationship in WC–Co thermal spray coatings: a review of the published literature, *J. Therm. Spray Technol.*, **7**, 357–373.
- McKelliget, J., Szekeley, J., Vardelle, M. and Fauchais, P. (1982). Temperature and velocity fields in a gas stream exiting a plasma torch, *Plasma Chem. Plasma Proc.*, **2**, 317–332.
- Neiser, R.A., Smith, M.F. and Dykhuizen, R.C. (1998). Oxidation in wire HVOF-sprayed steel, *J. Therm. Spray Technol.*, **7**, 537–545.
- Oberkampf, M.L. and Talpalikar, M. (1996). Analysis of a high-velocity oxygen-fuel (HVOF) thermal spraying torch. Part 1: numerical formulation, *J. Therm. Spray Technol.*, **5**, 53–61.
- Ouziaux, R. and Perrier, J. (1978). *Mécanique des Fluides Appliquée*, Dunod, Paris, France.
- Patankar, S.V. (1980). *Numerical Heat Transfer and Fluid Flow*, McGraw Hill, New York, NY, USA.
- Pateyron, B., Elchinger, M.F., Delluc, G. and Aubreton, J. (1986). Banque de Données de l'Université et du CNRS, Université de Limoges, Limoges, France.
- Pawlowski, L. (1978). Analysis of the application possibility of the plasma spraying process in microelectronics based on research on the vacuum plasma spraying of copper and tantalum coatings, *PhD Thesis*, Wroclaw University of Technology, Wroclaw, Poland (in Polish).
- Pawlowski, L. (1980). Optimization of arc plasma spraying parameters, *Surf. J.*, **11**, 8–16.
- Pawlowski, L. (1996). Technology of thermally sprayed anilox rolls: state of art, problems and perspectives, *J. Therm. Spray Technol.*, **5**, 317–335.
- Pawlowski, L., Hill, A., McPherson, R., Garvie, D., Przelozny, Z. and Finlayson, T. (1990). Properties of plasma sprayed  $\text{YBa}_2\text{Cu}_3\text{O}_x$  high-temperature superconductors, in *Thermal Spray: Research and Applications*, T.F. Bernecki (Ed.), ASM International, Materials Park, OH, USA, 641–646.

- Perrin, R. and Scharff, J.-P. (1999). *Chimie Industrielle*, Dunod, Paris, France.
- Polak, L.S. and Surov, N.S. (1969). Research on interaction between the particles and plasma in nozzle, *Fiz. Chim. Obrab. Mater.*, (2), 19–29 (in Russian).
- Ramadan, K. and Butler, P.B. (2004). Analysis of particle dynamics and heat transfer in detonation thermal spraying systems, *J. Therm. Spray Technol.*, 13, 248–264.
- Remesh, K., Yu, S.C.M., Ng, H.W. and Berndt, C.C. (2003). Computational study and experimental comparison of the in-flight particle behavior for an external injection plasma spray process, *J. Therm. Spray Technol.*, 12, 508–522.
- Samsonov, G.V. (1978). *Physico-Chemical Properties of Oxides*, Metallurgija, Moscow, Russia (in Russian).
- Sayce, I.G. (1976). Heat and mass transfer in thermal plasmas, *Pure Appl. Chem.*, 48, 215–228.
- Smith, M.F. and Dykhuizen, R.C. (1987). The effect of chamber pressure on particle velocities in low-pressure plasma deposition, in *Thermal Spray: Advances in Coatings Technology*, D.L. Houck (Ed), ASM International, Materials Park, OH, USA, pp. 21–25.
- Sobolev, V.V., Guilemany, J.M., Garmier, J.C. and Calero, J.A. (1994). Modelling of particle movement and thermal behaviour during HVOF spraying, *Surf. Coat. Technol.*, 63, 181–187.
- Steffens, H.-D., Busse, K.-H. and Selbach, H. (1985) Measurements of particle and plasma velocity in a low pressure plasma jet, in *Proceedings of the 7th Symposium on Plasma Chemistry*, C.J. Timmermans (Ed.), Eindhoven University of Technology, Eindhoven, The Netherlands, Paper B-5-2.
- Syed, A.A., Denoirjean, A., Denoijen, P., Labbe, J.C. and Fauchais, P. (2003). In flight oxidation of metallic particles in plasma spraying, in *Thermal Spray2003: Advancing the Science and Applying the Technology*, C. Moreau and B. Marple (Eds), ASM International, Materials Park, OH, USA, pp. 985–992.
- Tawfik, H.H. and Zimmerman, F. (1997). Mathematical modeling of the gas and powder flow in HVOF systems, *J. Therm. Spray Technol.*, 6, 345–352.
- Tomaszek, R., Pawlowski, L., Gengembre, L., Laureyns, J., Znamirowski, Z. and Zdanowski, J. (2006). Microstructural characterization of plasma sprayed TiO<sub>2</sub> functional coating with gradient of crystal grain size, *Surf. Coat. Technol.*, 201, 45–56.
- Tului, M. (2003). Propriétés optiques d'oxydes et de borures obtenus par projection plasma sous différentes pressions, *PhD Thesis*, ENSCL, Lille, France.
- Tului, M., Ruffini, F., Arezzo, F., Lasisz, S., Znamirowski, Z. and Pawlowski, L. (2002). Properties of atmospheric air and inert gas high-pressure plasma sprayed ZrB<sub>2</sub> coatings, *Surf. Coat. Technol.*, 151–152, 483–489.
- Vardelle, A., Vardelle, M., McPherson, R. and Fauchais, P. (1980). Study on the influence of particle temperature and velocity distribution within a plasma jet coating formation, in *Proceedings of the 9th International Thermal Spray Conference*, Nederlands Instituut voor Lastechniek, The Hague, The Netherlands, Paper 30.
- Vardelle, A., Vardelle, M. and Fauchais, P. (1986). Les transferts de quantité de mouvement et de chaleur entre plasma et particules solides dans un plasma d'arc en extinction, *Rev. Int. Haut. Temp. Réfract.*, 23, 69–85.
- Vardelle, M., Vardelle, A. and Fauchais, P. (1989). Etude comparative du traitement thermique des poudres en projection plasma à l'air et en atmosphère contrôlée, *Rev. Int. Haut. Temp. Réfract.*, 25, 83–91.

- Vardelle, A., Vardelle, M., Fauchais, P., Proulx, P. and Boulos, M.I. (1992). Loading effect by oxide powders in dc plasma jet, in *Thermal Spray: International Advances in Coatings Technology*, C.C. Berndt (Ed.), ASM International, Materials Park, OH, USA, pp. 543–547.
- Vardelle, M., Vardelle, A., Fauchais, P., Li, K.-I., Dussoubs, B. and Themelis, N.J. (2001). Controlling particle injection in plasma spraying, *J. Therm. Spray Technol.*, **10**, 267–284.
- Vuoristo, P., Ahmaniemi, S., Nuutinen, S., Mäntylä, Hämäläinen, E., Arola, N. and Vattulainen, J. (2001). Optimisation and monitoring of spray parameters by a CCD camera based imaging thermal spray monitor, in *Thermal Spray2001: New Surfaces for a New Millennium*, C.C. Berndt, K.A. Khor and E.F. Lugscheider (Eds), ASM International, Materials Park, OH, USA, pp. 727–736.
- Wagner, N., Gnädig, K., Kreye, H. and Kronewetter, H. (1984). Particle velocity in hypersonic flame spraying of WC-Co, *Surf. Technol.*, **22**, 61–71.
- Williamson, R.L., Fincke, J.R. and Chang, C.H. (2002). Numerical study of the relative importance of turbulence, particle size and density, and injection parameters on particle behavior during thermal plasma spraying, *J. Therm. Spray Technol.*, **11**, 107–118.
- Zagorski, V.V. and Stadelmaier, F. (2001). Full-scale modelling of a thermal spray process, *Surf. Coat. Technol.*, **146–147**, 162–167.

# 6

## Coating Build-Up

Coatings are built up from the individual particles that strike the substrate. The particles can be fully or partly melted or solid at the moment of impact. The solid ones would rebound or remain weakly connected to the rest of the coating. Such particles are not desired because they worsen most of the coating's mechanical characteristics. This is why careful optimization of the spray parameters should lead to their elimination or, at least, their reduction in the coating. At the beginning of the coating build-up, particles impact directly onto the substrate. The phenomena occurring at this stage determine the adhesion of the coating to the substrate. The molten particles deform, become lamellae and solidify into columnar or fine-grained equiaxial crystals. The spraying torch moves over the substrate and the first layer<sup>1</sup> is usually composed of 5–15 lamellae, depending on the processing parameters, such as powder feed rate, spray distance, particles size and linear speed of the torch, is formed. The phenomena occurring inside the generated layer determine the crystal structure and size, porosity formation and formation of microcracks. The torch returns after a little time, depending on the work piece size, to the same spot. Meanwhile, the surface of

---

<sup>1</sup> In the following discussion, a layer will be defined as a coating deposited during one pass of the spraying torch.

the layer is subjected to the action of the environment, i.e. oxidation (for metals or alloys) and/or cooling. The cooling leads to generation of residual stresses, which may, eventually, cause the coating to crack. During spraying of one layer of coating, the torch also heats up the previously deposited material by convection. Additional heat fluxes result from solidification of the particles and their cooling down to the temperature of equilibrium. The final coating's thickness is reached in a few tenths to a few hundreds passes of the torch over the substrate. Thereafter, the coating is cooled down to room temperature. This last stage of build-up is often crucial, because of the generation of thermal stresses. The latter sometimes causes detachment of the entire coating from its substrate.

## 6.1 IMPACT OF PARTICLES

Molten particles on impact with a substrate (or a previously deposited coating) transform into lamellae. The transformation is associated with the processes of deformation and solidification, being in turn dependent on such factors as:

- particle velocity, size and phase content (totally liquid, partly liquid, etc.) on impact;
- particle material properties in the liquid state (viscosity, surface tension, etc.);
- ability of wetting the substrate by liquid particles;
- temperature of substrate;
- substrate roughness.

The solidification and deformation processes occur more or less simultaneously. The temperature at the particle's interface with the substrate at impact, called the *contact temperature*, influences adhesion of the lamellae and, consequently, adhesion of the coating to the substrate. The mechanisms of adhesion can be, most probably, mechanical anchorage and, less probably, metallurgical bonding. The temperature in the particles bodies that can be at present measured by using high-speed and high-sensitivity sensors strongly influences the microstructure of the coatings. First of all, its evolution with time, determines material solidification and cooling rates, which, in turn, influence formation of crystals phases and crystal size.

### 6.1.1 PARTICLE DEFORMATION

Particle deformation, associated with its solidification, is the most fundamental problem in thermal spraying. This problem is very important because of the following reasons:

- Deformation is independent of the way an impacting particle was accelerated and heated before impact, i.e. is independent of the spraying method. What counts is the velocity at impact and phase content of the particle (and to a degree, temperature distribution inside the phases) at the moment of impact.
- Lamellar microstructure, characteristic for as-sprayed coatings, result from the deformation of particles. The first, known to this author, exception to this rule comes from suspension and solution-sprayed coatings (Tomaszek *et al.*, 2006). These coatings have the microstructure which may include slightly deformed grains; hollow grains and other features being intensively studied at present.
- Finally, the development of numerical and experimental tools enables us, at present, to analyse in depth the problems related to deformation. Consequently, a wealth of theoretical and experimental data has been generated in the last decade.

### Theoretical Description

A useful analogy to particle ‘splashing’ can be found in the impact of raindrop. Everyone, who has experienced rain on the front window of a car, could have observed raindrops disintegrating when the car is accelerated. More fundamental studies, reviewed by Dykhuizen (1994), state two fundamental observations from studies of raindrops that can be transferred to thermal spraying:

- liquid that makes up the portions of raindrops that impact the first surface ends up at the periphery of the splat;
- raindrops impacting on smooth and dry surfaces do not ‘splash’, in contrast to those impacting rough and wet ones.

Starting from the moment of the first contact with the substrate, the particle begins to deform. Two approaches can be applied to analyse theoretically this stage (Dykhuizen, 1994):

- a incompressible model which assumes that the liquid does not compress and offers a simplified description of radial flow of the liquid droplet at impact;
- a compressible model which assumes that the liquid compresses at impact.

The models are unfortunately not very useful for thermal spraying because they do not consider solidification of particles at impact. They can be, however, useful to explain the phenomena at impact. Impact can be divided into two stages – a compressible one, starting with contact with the substrate and finishing with the formation of a truncated sphere, including compressed liquid near to the contact circle (Figure 6.1).

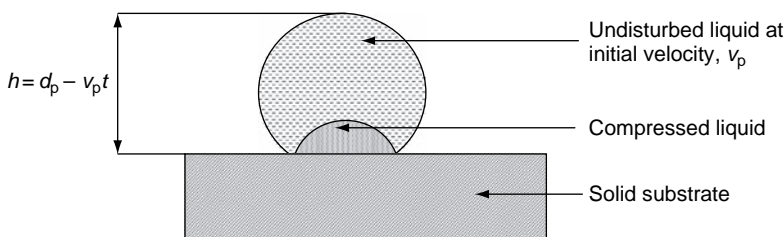


**Figure 6.1** Subcritical flow regime at the impact of a liquid particle onto a rigid substrate (after Dykhuizen, 1994)

This stage is called *subcritical flow regime*. Its duration was estimated by Kudinov (1977) and Houben (1988) at  $10^{-10}$ – $10^{-9}$  s. The time scale of the entire impact process can be estimated as the time necessary for spreading<sup>2</sup> of the particle using the following equation in which the *Re* number is defined in Equation (6.3) (Trapaga and Szekely, 1991):

$$t_i = \frac{2 d_p}{3 v_p} Re^{0.2} \quad (6.1)$$

The impact creates a shock wave inside the lamellae and in the substrate. At the end of the subcritical stage, the liquid starts to expand radially to reach its final shape. This stage is called the *postcritical flow regime*.

<sup>2</sup> 90 % of spreading, to be exact.

During this stage, the liquid expands radially taking one of the forms similar to those shown in Figure 6.2 – at the same time, solidification occurs.

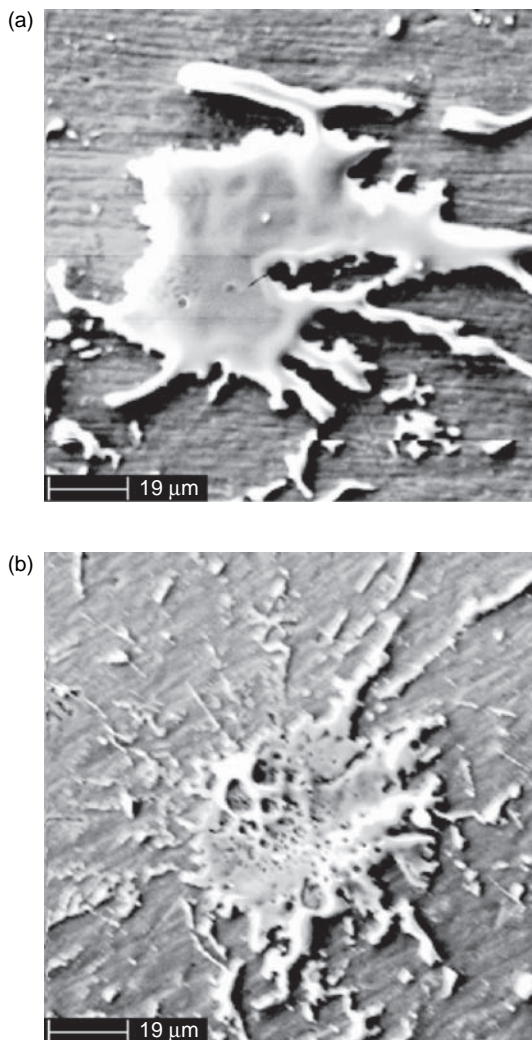


**Figure 6.2** Morphologies of splats of hydroxyapatite, plasma-sprayed in the open air onto stainless steel using a SG100 torch supplied with Ar + 2.5 vol% H<sub>2</sub> and electric powers of (a) 11 kW and (b) 24 kW (after Dyshlovenko *et al.*, 2006b)

The state of the art for the formation of splats has been reviewed by Dykhuizen (1994), Sobolev and Guilemany (1999a,b) and Fauchais

*et al.* (1999). The first person, who initiated the analysis of splats in a rigorously scientific way was Professor Jan Madejski<sup>3</sup> in his studies published in 1976 (Madejski, 1976 a,b,c). As typical for thermal spray process lamellae (shown in Figure 6.2), it is easier to estimate the surface area  $S$  rather than the diameter. This is why Madejski tried to find the parameter  $\xi$  defined as:

$$\xi = \frac{2}{d_p} \sqrt{\frac{S}{\pi}} \quad (6.2)$$

Madejski did not consider the compressibility of the liquid in the splat but included surface tension, viscosity and solidification. These elements allow the splat size to be determined as a function of the dimensionless parameters relative to splat formation, i.e.  $Re$ ,  $We$  and  $Pe$ :

$$Re = \frac{\rho_l d_p v_p}{\eta_l} \quad (6.3)$$

$$We = \frac{\rho_l d_p v_p^2}{\sigma} \quad (6.4)$$

$$Pe = \frac{v_p d_p}{a_s} \quad (6.5)$$

In general terms, he was solving the equations describing the radial movement of a liquid cylinder (*equation of energy balance*). The resulting analysis flattening parameter,  $\xi$ , depends on the  $Re$  and  $We$  numbers, which result from the supposition that the kinetic energy of the impacting particle is dissipated by a viscous flow. The solutions found by Madejski (1976 a,b) for different combinations of the dimensionless numbers, as well as solutions found by other authors, are shown in Table 6.1. In fact, the deforming particle solidifies. The thickness of the solidified lamella can be found from the time of impact (see also Figure 6.1):

$$b = d_p - v_p t \quad (6.6)$$

---

<sup>3</sup> Sadly, Professor Madejski died in 2000. Interested readers can read about his career on the Internet page made by his co-workers at the Gdansk University of Technology, Poland: [[http://www.imp.gda.pl/inst\\_zew/ppw/Madejski.htm](http://www.imp.gda.pl/inst_zew/ppw/Madejski.htm)].

**Table 6.1** The parameter  $\xi$  describing the spread of liquid particles impacting the substrate following the models developed by different authors under the general assumption that the predominant mechanism of ‘splashing’ is viscous dissipation of the kinetic energy of the particle

Number	Re	We	$\xi$	Reference
1	—	—	$1.06Re^{0.125}$	Jones, 1971
2	Optional	$\infty$	$1.2941(Re + 0.9517)^{0.2}$	Madejski, 1976 a,b
3	$> 100$	$\infty$	$1.2941Re^{0.2}$	
4	$> 100$	$> 100$	$\frac{3\xi^2}{We} + \frac{1}{Re} \left( \frac{\xi}{1.2941} \right)^5 = 1$	
5	$\infty$	$> 100$	$(We/3)^{0.5}$	
6	—	—	$Re^{0.2}$	Trapaga and Szekely, 1991
7	—	—	$0.83Re^{0.21}$	Yoshida <i>et al.</i> 1992

The second part of Madejski’s theory considered solidification of the layer formed by deformation. The thickness of the solidified layer depends on time in a way that can be found by assuming that conduction of heat towards the substrate is the dominant mechanism, as shown in the following equation:

$$h = U(a_s t)^{0.5} \quad (6.7)$$

Setting Equation (6.6) equal to Equation (6.7), one supposes that deformation of the particles stops if the thickness of the deformation is equal to the thickness of the solidified lamellae. This enables us to find the flattening parameter  $\xi$  under the assumption that solidification is the determining parameter. A simplified equation with regard to that of Madejski (1976 a,b) was given by Dykhuizen (1994):

$$\xi = 0.82 \left[ \frac{Pe}{U^2} \right]^{0.25} \quad (6.8)$$

The constant  $U$  can be found under the assumption that the substrate has a constant temperature  $T_0$  and infinite thermal conductivity by solving the following transcendental equation (Dykhuizen, 1994):

$$\frac{c_p(T_m - T_0)}{H_m \sqrt{\pi}} = \left( \frac{U}{2} \right) \operatorname{erf} \left( \frac{U}{2} \right) \exp \left( \frac{U}{2} \right)^2 \quad (6.9)$$

Finally, the processes of deformation and solidification of the particle are simultaneous. Deformation, however, stops when a particle becomes

solidified. In this sense, the solidification is the ‘controlling mechanism’ of lamellae formation (Madejski, 1976a; Dykhuizen, 1994). The model of Madejski is an excellent introduction to understanding particle deformation and it has been refined by different authors to take into account the following elements which better correspond to the real conditions of thermal spraying:

- wetting of substrate by particle material and thermal contact resistance;
- roughness of substrate;
- spraying at angles different from normal;
- oxidation of particle at ‘splashing’;
- particular features of the formation of splats from submicrometric (less than 1  $\mu\text{m}$ ) or nanometric (less than 100 nm) particles.

Short descriptions of recent work in these areas follow.

**Wetting** affects the contact area between the splat and the underlying substrate. It can be described by an angle  $\alpha$  that increases for improved wetting<sup>4</sup> (Figure 6.3).

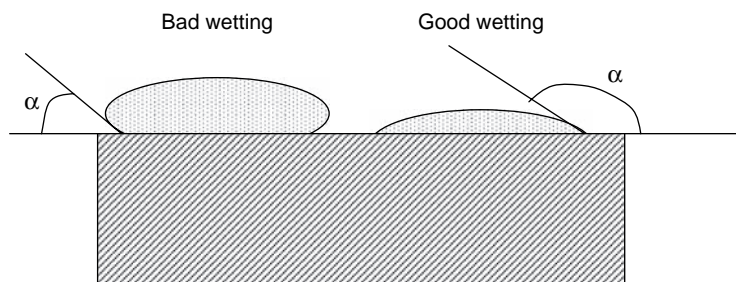


Figure 6.3 Wetting angles between a splat and the substrate (after Sobolev and Guilemany, 1999b)

Good wetting would result in a *pancake* shape for the lamellae rather than that of a *flower* shape (Moreau *et al.*, 1991). Obviously, when spraying particles of the same material as the substrate the wetting is better than spraying on any other type of material. Bad wetting may

<sup>4</sup> The small angle  $\alpha$  is considered by Sobolev and Guilemany (1999b) as a sign of good wettability which is in contradiction with the discussion in this section. Most probably, these authors wrote  $\alpha$  and meant  $180^\circ - \alpha$ .

be, consequently, the origin of formation of gas cavities at the interface between the lamellae and the substrate (Sobolev and Guilemany, 1999b). Small contact angles reduce the contact area and increase the thermal contact resistance. The *thermal contact resistance* between two materials in contact is proportional to the temperature gap caused by a thermal energy flux, as shown in the following equation:

$$R_{\text{th}} = \frac{\Delta T}{q} \quad (6.10)$$

The model of Madejski considers an ideal contact between the substrate and lamellae ( $R_{\text{th}} = 0$ ). The values of  $R_{\text{th}}$ , in the range  $10^{-7}$ – $10^{-8}$  m<sup>2</sup>K/W, considered as being very low, can increase during flattening of the lamellae (Espie *et al.*, 2001). High values of  $R_{\text{th}}$  increase the solidification time and, thus may increase flattening of the lamellae. Quantification of the wetting effect is difficult because of the low precision of data related to many materials at high temperatures and in the liquid state.

**Roughness** of the substrate is introduced by sand blasting and has to be considered in any practical cases. Filling the ‘irregularities’ of the substrate by expanding splat obviously reduces its final size, as shown in Table 6.2, which presents the results of numerical calculation made by Feng *et al.* (2002). The influence of roughness can be taken into account through the action of friction forces between the liquid and substrate. These forces hamper movement of the liquid onto the rough substrate (Sobolev and Guilemany, 1999(a); Feng *et al.*, 2002).

**Table 6.2** Sizes of splats and total flattening times obtained by numerical simulation of the impact of a 50 µm aluminum droplet with a velocity of 100 m/s on steel substrates having different surface morphologies (Feng *et al.*, 2002).<sup>a</sup> Reproduced from *J. Therm. Spray Technol.* 11(1), 2002, 62–68, ‘Finite element analysis of effect of substrate surface roughness on liquid droplet impact and flattening process’, Z.G. Feng, M. Domaszewski, G. Montavon and C. Coddet, Table 2, Copyright (2002). With kind permission from Springer Science and Business Media

Parameter	Smooth surface	Fine surface	Coarse surface
$\xi$	6.52	3.91	2.57
Flattening time (µs)	3.74	2.93	2.20
Splat diameter (µm)	317.0	178.6	125.5
Splat height (µm)	1.24	2.62	5.24

<sup>a</sup>These authors used roughness factors (being presumably equal to the ratios of the ‘irregularity height’ to the particle diameter) which are equal to 0.025 for a smooth (polished) surface, 0.25 for a fine (machined) surface and 4.0 for a coarse (sand-blasted) surface.

'Off-normal' spraying is a case of coating deposition into cavities (e.g. car cylinder bores). The first factor to be considered in spraying under an angle  $\alpha$  ( $\alpha = 0^\circ$  for spraying with the torch perpendicular to the substrate) is reduction in the particle velocities. The effective velocity at impact becomes equal to  $v_{\text{eff}} = v_p \cos \alpha$ . Moreover, the splats become more elongated, becoming elliptic rather than circular (Sobolev and Guilemany, 1999b). The pressure with which the droplet acts on the substrate decreases with a factor  $\cos \alpha$ . This may result in weaker mechanical (contact area) and thermal interactions ( $R_{\text{th}}$ ) and, consequently, in worse adherence.

**Oxidation** of lamellae can take place during the time of solidification (order of microseconds) before the next particles arrives. An oxide layer can be formed on the lamella's top. The calculation of Sobolev and Guilemany (1999a), made for NiCr (with  $\text{Cr}_3\text{C}_2$  being a part of the cermet) did show that the oxidation of chromium in the splat to give  $\text{Cr}_2\text{O}_3$  is less intensive than oxidation 'in-flight'. In fact, the relative mass of oxide formed 'in-flight' was reportedly about 7.2 wt% and this formed upon splat solidification – only 1.6 wt%.

**Splats** obtained by spraying fine submicrometric or nanometric particles in suspensions have different shapes to those sprayed with powders of the same material (Figure 6.4).

The shape of a suspension-sprayed splat is mainly a 'pancake', without 'splashing'. This could be due to the lower temperature of the particles at impact<sup>5</sup> but there could be a more fundamental explanation, namely, the superficial tension forces outside a small droplet are great enough to be able to avoid particle 'splashing'. Poirier *et al.* (2003) pointed out that pre-heating of the substrate can also have an influence on 'splashing' when suspension-spraying.

### Experimental Observations of Splats

Experimentally observed lamellae have two principal morphologies which can be called, following Houben (1988), *pancake* and *flower* (Figure 6.5).

Generally, a *pancake* lamella is formed at impact of:

<sup>5</sup> A considerable amount of the thermal energy of the flame or plasma is consumed in evaporating the suspension medium, such as water in this present case.

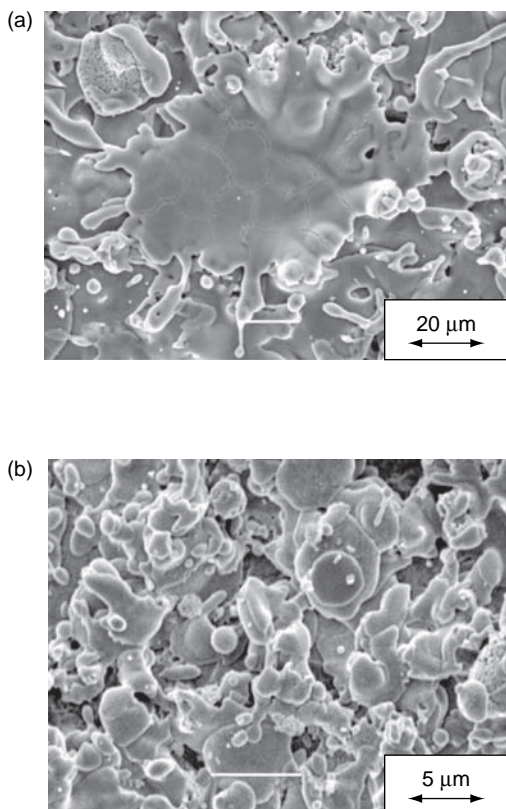


**Figure 6.4** Scanning electron micrographs (secondary electrons) of the surfaces of  $\text{TiO}_2$  coatings sprayed using (a) coarse particles of size  $d_{\text{vs}} = 23 \mu\text{m}$  and (b) fine particles of size  $d_{\text{vs}} = 0.33 \mu\text{m}$  as a suspension in water (after Tomaszek *et al.*, 2006)

- particles with relatively low thermal and/or kinetic energies;
- very fine particles (discussed previously).

Inversely, *flower* lamella, associated with the ‘splashing’ of a particle, are formed during high-energy impact. At a similar energy of impact, substrate temperature would be an important factor. At lower temperatures, the formation of the *flower* shape is more probable than that of the *pancake*. The morphologies of hydroxyapatite lamellae, plasma-sprayed in air using high and low electric power inputs (see Figure 6.2), as well as those obtained by Steffens and collaborators (1993) for different spray processes applied for molybdenum (Table 6.3), support reasonably well

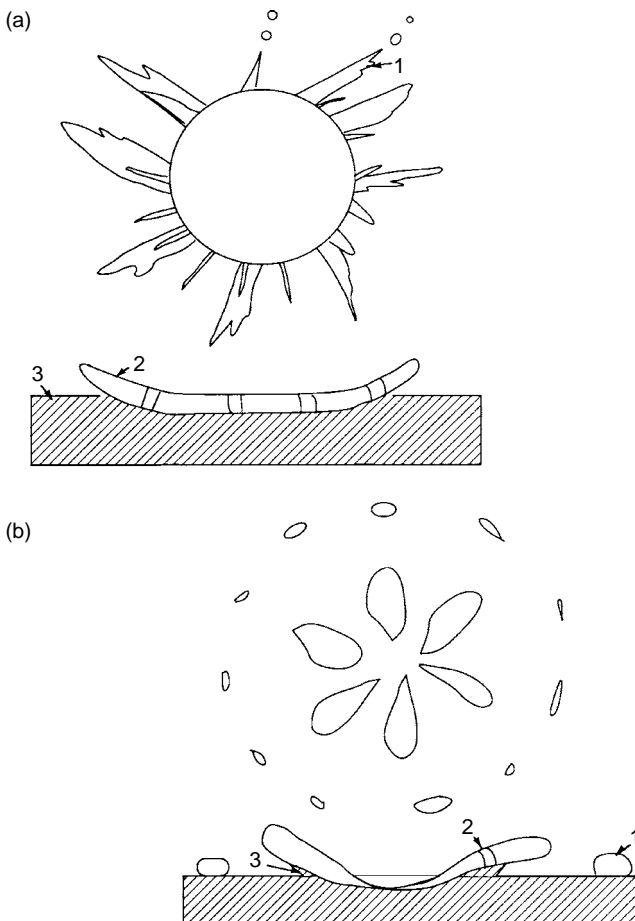


Figure 6.5 Principal morphologies of lamellae obtained from sprayed particles: (a) pancake; (b) flower: (1) corona; (2) crack; (3) deformed substrate

this categorization. The experimental studies related to impact are of two general types.

Free fall of large (millimetre size) particles made, e.g. by Fukumoto *et al.* (2002). This approach allows precise determination of the temperatures and velocities of the splats at impact and keep well under control the experimental conditions. There is, however, a problem with scaling up, as stressed by Dykhuizen (1994), namely, the solidification time of large particles is about one tenth of a millisecond. This is much longer than the time under 'real' thermal spray conditions, which is one tenth of a

**Table 6.3** Morphologies of molybdenum lamellae sprayed using different techniques (Steffens *et al.*, 1993).

Technique	Consumable		Spray process variables	Lamellae form	Remarks
	Powder size ( $\mu\text{m}$ )	Wire diameter (mm)			
FS	—	3.18	(1) Working gas pressure (0.5 and 0.7 MPa); (2) Spray distance (40–200 mm)	Pancake with corona	Corona wider spread if greater spray distance
FS	$-45 + 22.5$	—	Spray distance (120–280 mm)	Pancake with corona	Form does not depend on varying parameters
APS	$-45 + 22.5$	—	Spray distance (40–200 mm)	Pancakes, flowers and intermediate forms	More flowers by increasing spray distance
AS	—	1.6	(1) Atomization gas pressure (0.2–0.7 MPa); (2) Spray distance (40–200 mm)	Pancakes, flowers	More flowers by increasing atomization gas pressure

microsecond. Three orders of magnitude difference raises doubts about the possibility of transfer of such experiments to thermal spraying.

**Thermal spraying** of small particles made, e.g. by Vardelle *et al.* (1980) or Li *et al.* (2003). Such experiments need the determination of particle velocities and temperatures with one of the methods discussed in Chapter 5. These methods are not very precise and, most of all, they have a statistical character, i.e. they do not allow following the history of one particle from injection into the flame/jet up to impact with the substrate.

The study of Fukumoto *et al.* (2002) correlated the formation of ‘splashing’ (formation of a *flower* shape) with substrate temperature, namely, at low temperatures the bottom part of the lamella solidifies rapidly and the liquid part of the impacting particle, arriving at

high velocity, cannot be held by surface tension forces. Inversely, at higher substrate temperatures the bottom part of the lamella remains liquid and allows formation of the *pancake* shape for the splat. For each pair of impinging liquid particle and substrate material there is a substrate temperature of transition between these two morphologies. Below this temperature, 'splashing' occurs and a *flower* splat is formed. In contrast, above this temperature the *pancake* morphology of the splat is generated. For example, for a Ni splat onto AISI 304 stainless steel, the temperature of transition is about 550 K (Fukumoto *et al.*, 1998). Vardelle *et al.* (1980) carried out experiments on the atmospheric plasma spraying of alumina particle. Their investigations confirmed the model of Madejski (entry 3 of Table 6.1). On the other hand, Ohmori and Li (1993) suggested that the experimentally determined sizes of Al and Al<sub>2</sub>O<sub>3</sub> splats fit better to the model of Jones (entry 1 of Table 6.1). Similar conclusions were reached by Li *et al.* (2003) for copper particles sprayed by APS. Finally, the study of Fantassi *et al.* (1992), made for open-air plasma-sprayed zirconia particles, showed a good correlation with the predictions of Yoshida *et al.* (entry 7 of Table 6.1). Such a dispersion of experimental results could have resulted from neglecting the solidification mechanism of particle flattening at impact; the viscous flow mechanism being much simpler for experimental correlation. Similarly, the precision of the experiments (temperatures and velocities of the particles prior to impact) is not high and the high-temperature data of the materials must often be approximated.

In the practice of thermal spraying, it is important to know the thickness of a lamellae.<sup>6</sup> This can be found, knowing that the volume of the lamella is equal to that of the particle, from the following equation:

$$h = \frac{2 d_p}{3 \xi^2} \quad (6.11)$$

To take an example, let us evaluate the thicknesses of the lamellae of sprayed Al<sub>2</sub>O<sub>3</sub> obtained by plasma spraying in the open air and in vacuum using the data previously cited in this book (see Figures 5.15 and 5.16, respectively). The liquid alumina density and viscosity, as a function of material temperature, starting from 2300 to 2700 K, were

---

<sup>6</sup> We assume that a lamella can have any shape but only one thickness, *h*.

taken from the thesis of Balting (1990). The  $Re$  numbers are found to be greater than 250 while the  $We$  numbers can be estimated, starting from the coefficient of surface tension for liquid alumina,  $\sigma = 0.68 \text{ N/m}$  (McPherson, 1980), to be greater than 4000. Thus, the equation shown in entry 3 of Table 6.1 can be applied. Consequently, the flattening parameter  $\xi$  and, using Equation (6.11), the thickness of the lamella can be found. Figure 6.6 shows the results of these calculations as a function of the particle temperature at impact.

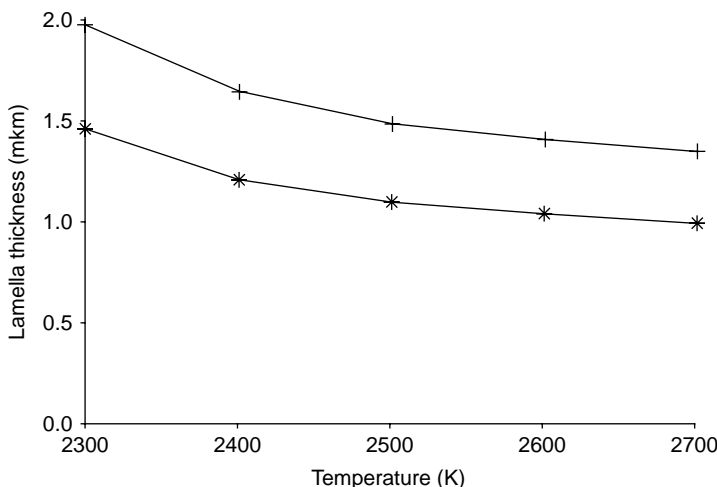


**Figure 6.6** Thicknesses of  $\text{Al}_2\text{O}_3$  lamellae sprayed by using a plasma in: (+) air after impact of  $46 \mu\text{m}$  particles (see Figure 5.15) having a velocity ( $v_p$ ) of  $131 \text{ m/s}$ ; (\*) vacuum after impact of  $54 \mu\text{m}$  particles (see Figure 5.16) having a velocity ( $v_p$ ) of  $358 \text{ m/s}$

The thicknesses of lamellae, plasma-sprayed in air, using alumina particles with a size of  $d_{50} = 50 \mu\text{m}$ , were determined experimentally by Zoltowski (1968) to be equal to  $h = 3 \mu\text{m}$ . His results converge reasonably well with the present predictions.

Experimental studies of splats are at present frequently realized in order to:

- optimize the spray process – see, e.g. Newberry and Grant (2000 ) or Mørks *et al.* (2003);
- contribute to the understanding of flattening and ‘splashing’ mechanisms – see, e.g. Fukumoto *et al.* (1998, 2001).

### 6.1.2 PARTICLE TEMPERATURE AT IMPACT

The temperatures in particles during solidification determine the adhesion of a coating to the substrate. On the other hand, the kinetics of solidification and the cooling determine the size of the crystals. The latter influences many mechanical and electrical properties of coatings. At present, rapid pyrometers enable the experimental determination of temperature evolution of lamellae solidifying and cooling down on a substrate.

#### Theoretical Description

The temperature fields in solidifying particles and in a substrate can be found by solution of the heat conduction equation (see Chapter 5, Equation (5.34)). The solution with solidification, known as the *Stefan* problem of this equation in one-dimension, is given in the classical textbook of Carslaw and Jaeger (1959). This solution was adapted for thermal spraying by the use of a thin slab onto a ‘semi-infinite’ body approximation, by, e.g. Kudinov (1977), Zaai (1983) or El-Kaddah *et al.* (1984). Different approximations of two ‘semi-infinite’ bodies were adopted by Dallaire (1982). The solution proposed by Kudinov (1977) is based on the following simplifications:

- the substrate is a ‘semi-infinite’ body, having before impact an initial temperature  $T_0$ ;
- the particle is liquid prior to the impact and has a temperature  $T_m$ ;
- the contact between the particle and substrate is ideal;
- the heat is propagated in one direction, perpendicular to the substrate surface.

The contact temperature,  $T_c$ , at the interface between the substrate and particle during the time of its solidification,  $t_s$ , is given by:

$$T_c = T_0 + \frac{K_e(T_m - T_0)}{K_e + \Phi(\alpha)} \quad (6.12)$$

in which:

$$K_e = \frac{\lambda_p a_s^{0.5}}{\lambda_s a_p^{0.5}} \quad (6.13)$$

In addition,  $\Phi(\alpha)$  is the probability integral, defined as:

$$\Phi(\alpha) = \frac{2}{\sqrt{\pi}} \int_0^{\alpha} \exp(-t^2) dt \quad (6.14)$$

and  $\alpha$  is the root of the following transcendental equation:

$$K_e + \Phi(\alpha) = \frac{K_L \exp(-\alpha^2)}{\alpha} \quad (6.15)$$

in which  $K_L$  is the left-hand side of Equation (6.9). Equation (6.15) can be solved numerically. The solidification time,  $t_s$ , is given by the following equation (similar to Equation (6.7)):

$$t_s = \left( \frac{b}{2\alpha} \right)^2 \frac{1}{a_s} \quad (6.16)$$

Calculations of the contact temperatures and solidification times (the latter based on experimental estimations of lamella thickness) are presented in Table 6.4. The results for the contact temperatures do not depend on the particular spray technique for the obvious reason that the particle is supposed to be molten and homogeneous at  $T_m$ . However, the solidification time *does* depend on the lamella thickness, in such a way that the thinner lamellae solidify quicker.

**Table 6.4** Contact temperatures and solidification times for nickel sprayed on a steel substrate using different spray techniques

Spray technique	Experimental			Calculations		Reference
	$T_m$ (K)	$T_0$ (K)	$b$ ( $\mu\text{m}$ )	$T_c$ (K)	$t_s$ ( $\mu\text{s}$ )	
APS	1728	373	18	1273	23	Kudinov, 1977
AS		300 (probably)	5	1230	1	Steffens <i>et al.</i> , 1991a
AS			40	1230	100	

### Experimental Determinations of Temperatures of Splats

In ‘real’ situations, the particles impacting the surface can have a temperature different to  $T_m$ , which makes the presented calculations useful but very simplified. Progress in this area has been realized

thanks to the application of fast pyrometers. In fact, starting from the beginning of 1990, the temperature evolution of splats has been studied in this way. A typical set-up used by Gougeon and Moreau (2001) is shown in Figure 6.7.

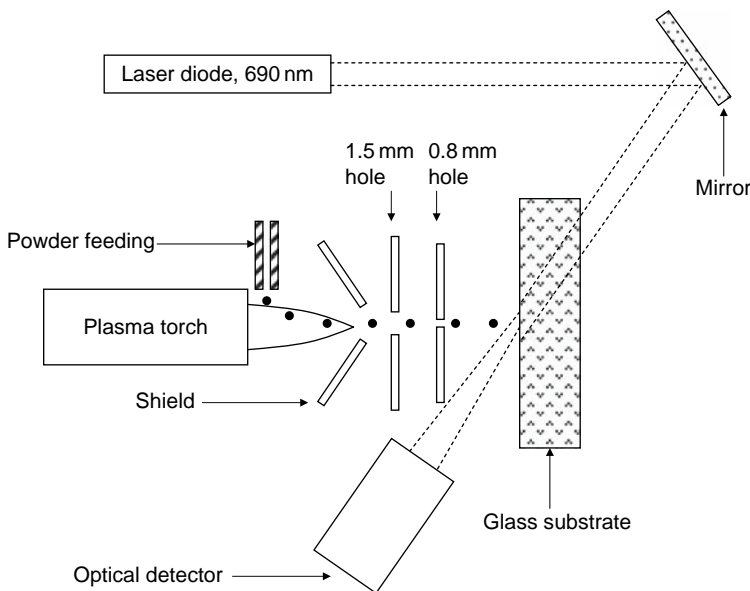


**Figure 6.7** Schematic of the experimental set-up used by Gougeon and Moreau (2001) to study the evolution of shape and temperature of molybdenum splats on a glass substrate. Reproduced from *J. Therm. Spray Technol.*, 10(1), 2001, 76–82, ‘Simultaneous independent measurements of splat diameter and cooling time during impact on a substrate of plasma-sprayed molybdenum particles’, P. Gougeon and C. Moreau, Figure 1a, Copyright (2001). With kind permission of Springer Science and Business Media

A sprayed particle, selected from the stream by the water-cooled shield and the following holes, impacts the substrate. Entry to the pyrometer is masked optically in a way which enables observation of the fields prior to and after the particle's impact. Observation of the thermal radiation prior to and after impact enables the particle temperature to be determined (by the principle of two-colour pyrometry described in Chapter 5, Section 5.3.2). An optical filter selecting the incoming radiation also enables observation of the signal coming from the 690-nm laser. The latter enables us to find the area of a splat on the substrate. This area is opaque and reduces the intensity of the 690-nm light coming from the field observed on the substrate. The electrical signal coming from the

detector made it possible to find that deformation of the molybdenum particle (sieved between 32 and 45  $\mu\text{m}$ ) on the glass substrate took about 2  $\mu\text{s}$  (which confirms fairly well the theoretical predictions shown in Table 6.2). The flattening parameter was found to be about  $\xi = 6.7$ . After having reached the maximum diameter, the splat decreased its diameter, which was interpreted as being due to its disintegration. In fact, microscopical observation of the splats revealed a *pancake* shape with a corona around them. Other set-ups described in the literature also enable the particle velocity at impact to be determined (Fantassi *et al.*, 1992). Moreau *et al.* (1991) observed the behaviour of niobium particles sprayed on to steel and glass substrates (Figure 6.8).

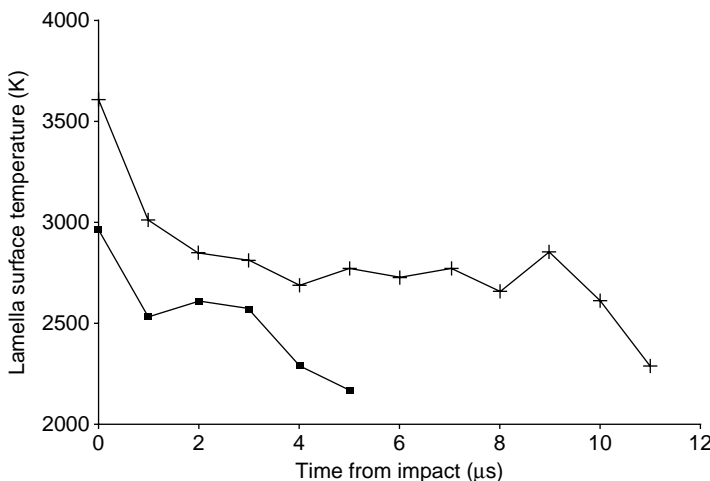


**Figure 6.8** Evolution of the temperature of a niobium splat, plasma-sprayed using a powder having a particle size in the range  $-45$  to  $+22.5 \mu\text{m}$ . The power input to the plasma torch ( $P$ ), supplied with working gases of  $\text{Ar} + \text{H}_2$  ( $50 + 2.7 \text{ slpm}$ ), was  $38.5 \text{ kW}$  and the glass (+) and steel (■) substrates were placed at a distance of  $115 \text{ mm}$  from the torch

The splat obtained on steel has the *pancake* morphology and after impact it cooled down rapidly to  $2500 \text{ K}$ . Then, its temperature started to rise for a few microseconds, which was explained as release of the latent heat of fusion (*recalescence effect*). The splat obtained on glass has a higher temperature than that on steel. This can be related to the lower thermal conductivity of glass in comparison to steel and the resulting thus higher contact temperature. Moreover, this splat has the *flower* morphology, with a *corona*. This could have resulted from the weak

wetting of glass by liquid niobium and from the important thermal contact resistance between the splat and substrate. The thermogram has a number of variations resulting from superposition of the thermal signal arising from many small components of the 'flower' and its corona. It must be, however, stressed that oxidation of niobium<sup>7</sup> could have

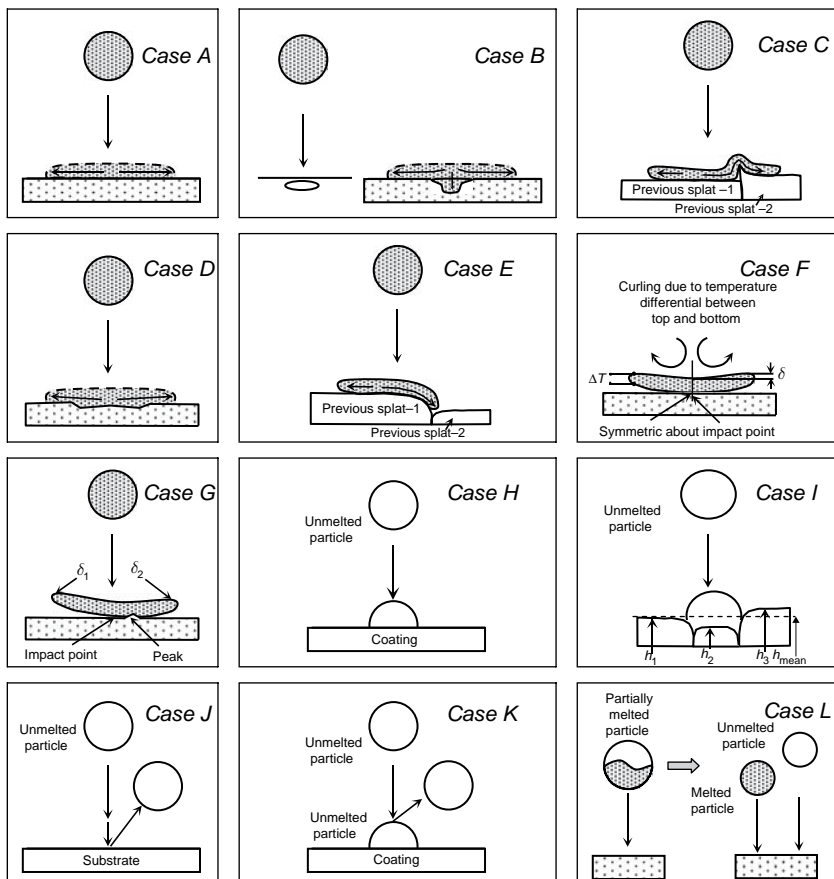


**Figure 6.9** Different situations occurring for a particle impacting a substrate (after Doltsinis *et al.*, 1998). These situations are described in Table 6.5. Reproduced by permission of CIMNE from I.S. Doltsinis, J. Harding and M. Marchese, 'Modelling the production and performance analysis of plasma-sprayed ceramic thermal barrier coatings', *Arch. Comput. Methods Eng.*, 5(2), 59–166 (1998)

<sup>7</sup> Niobium and tantalum have high affinities to oxygen and are usually sprayed under an inert atmosphere or in vacuum.

influenced the thermogram. The cooling rates of sprayed Nb particles were found to be about  $2 \times 10^8$  K/s on steel and  $5-6 \times 10^7$  K/s on glass. Similar values of the rates for tungsten particles plasma-sprayed onto steel of  $3-7 \times 10^7$  K/s were estimated by Fantassi *et al.* (1992). The temperature of the lamella upon impact also depends on the particle velocity before impact (see Chapter 5, Figure 5.10). This effect becomes important for velocities  $v_p > 400$  m/s. Another important factor is the thermal contact resistance between the bottom part of the lamella and the surface at contact. A study made by Moreau *et al.* (1992) for Mo particles plasma-sprayed on to a steel substrate indicated that the splat cooling time was shorter when the coating built-up. This can be explained by a decrease in the thermal contact resistance at the interface between the molybdenum splat and the molybdenum coating with regard to the resistance between the molybdenum splat and the steel substrate. An increase in substrate roughness of an ‘intermediate’ coating, between the substrate and the final coating, would also increase the thermal contact resistance.

The cases discussed in the previous sections were mainly related to the formation of one splat on an idealized substrate. The ‘real’ coating growth is associated with many different situations, related to the state of the incoming particle and to the position on the substrate being impacted by it. Dotschinis *et al.* (1998) have considered twelve such situations, which are shown in Figure 6.9 and described in Table 6.5.

### 6.1.3 NUCLEATION, SOLIDIFICATION AND CRYSTAL GROWTH

Solidification starts after contact of the liquid particle with the substrate (or previously deposited coating). The heat is released through the cool substrate in the direction of the bottom part of the lamella. As discussed previously sometimes the solidification finishes well after splat deformation (viscous flow mechanism) while sometimes the solidification is faster (solidification mechanism) or, in a very particular case, these two processes are simultaneous. The bottom contact surface of the lamella serves as a ‘heat-sink’ and nucleation of the crystals starts from this surface. For the first splats striking the cold and smooth substrate,

**Table 6.5** Descriptions of different situations which possibly occur at the impact of a particle on a substrate (see Figure 6.9). Reproduced by permission of CIMNE from I.S. Doltsinis, J. Harding and M. Marchese, ‘Modelling the production and performance analysis of plasma-sprayed ceramic thermal barrier coatings’, *Arch. Comput. Methods Eng.*, 5(2), 59–166 (1998)

Case	Rule
A	The splat is formed on the surface, following one of the equations given in Table 6.1. The shape of the underlying surface is maintained
B	The porosity under the splat below the uppermost layer, under the impact region, is ‘hammered down’ to the uppermost layer below it. The pore is destroyed and the splat follows the surface
C	The splat encounters a ‘dead-end’, fills the space available and then flows over the outer surface above (interlocking mechanism)
D	The splat ‘covers’ the roughness created by other splats
E	The splat comes to a ‘vertical drop’ and then falls straight down until the surface is ‘found’ again
F	The splat ‘curls-up’, provided that it is in the topmost layer
G	The underlying region contains a large peak, the splat is ‘pinned’ by the peak and curling occurs with respect to the peak
H	The unmelted particles form hemispheres on the coating
I	The hemisphere is assumed to lie on the ‘mean-line’ of the surface and the cavities below are filled
J	The unmelted particles do not adhere to the substrate surface. On impact, they bounce off
K	The unmelted particles do not adhere to other unmelted particles. If they “hit” one of them, they bounce off
L	A partially melted particle is divided in two parts: the molten part follows rules A to G while the unmelted part follows rules I, J and K

nucleation would be heterogeneous<sup>8</sup> and the grains grow as columns. Two elements have to be taken into account, as described below.

**Undercooling effect**, which renders the temperature of nucleation lower than the melting point. This effect is more pronounced for homogeneous nucleation. For instance, Dyslovenko *et al.* (2006a) found that the undercooling effect for hydroxyapatite particles solidifying in-flight is in the range  $\Delta T/T_m = 0.12\text{--}0.14$ . Wilden *et al.* (2001) observed that the dendritic structure of growing grains (while simulating numerically the solidification of nickel grains plasma-sprayed under vacuum onto a steel substrate) is finer for a smaller undercooling effect (i.e. the nucleation temperature is closer to the melting point).

<sup>8</sup> Heterogenous nucleation starts near to an inclusion different to that of the melt, e.g. a cold substrate. Homogenous nucleation occurs in the absence of such inclusions.

**Thermal contact resistance**, between the bottom part of the splat and the substrate, would hamper heat evacuation and slow down solidification of the lamella. The resistance is different in different locations below the lamella (curling effect – see Figure 6.9, case F).  $R_{th}$  is different on the interface splat/substrate (coating's interface) and the splat/splat (inside the coating). The solidification front can be planar, cellular or dendritic, depending on the cooling rate (Salimijazi *et al.*, 2005). At heterogeneous nucleation on the coating interface, the cooling rate is the greatest and a planar solidification front is the most probable. The front moves rapidly towards the top of the lamella with a velocity in the range of a few cm/s (McPherson, 1981) to a few m/s (Sampath and Herman, 1989). The residual liquid temperature increases due to the *recalescence effect* (see Figure 6.8 and related discussion) under such conditions, solidification results in a columnar structure (Figure 6.10(a)).

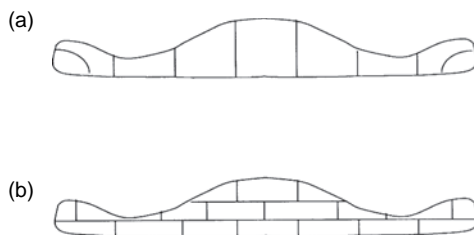


Figure 6.10 Possible microstructures of a lamella after solidification: (a) columnar; (b) equiaxial, also called a 'brick wall'

The columnar microstructure has been recently observed experimentally by many authors in coatings of different materials sprayed using different techniques (e.g. Salimijazi *et al.* (2005) in vacuum plasma-sprayed titanium alloy) and also several years ago (e.g. Wilms and Herman (1976) in alumina coatings plasma-sprayed in the open atmosphere). The superficial density of the columnar grains depends on the substrate temperature. This was calculated for plasma-sprayed alumina by Robert *et al.* (1998) to be in the range 20 to 80 grains/ $\mu\text{m}^2$ . Experimental observations using atomic force microscopy confirmed the calculated values.

However, many observations have revealed the fine-grained equiaxial microstructure shown in Figure 6.10(b) (Sampath and Herman (1989)). The formation of such a microstructure inside the lamella would be favoured by the low rate of heat removal at the interface with the substrate (or previously deposited coating) – thus by the increase in

thermal contact resistance (resulting from substrate oxidation and/or roughness) and/or increase in substrate temperature (Wilden and Frank, 2005). In this case, the nucleation becomes homogeneous (i.e. starts inside the lamella) and the *undercooling effect* is greater. The fine equiaxial grains were observed in atmospheric plasma-sprayed molybdenum coatings (Moreau *et al.*, 1992) and in  $\text{Al}_2\text{O}_3 +$  (3–5) wt%  $\text{Y}_2\text{O}_3$  sprayed in the same way by Wilms and Herman (1976). Safai and Herman (1981) reported fine equiaxial-grain microstructure in the central part of an aluminium lamella sprayed by a plasma in air. The ‘brick wall’ microstructure could also be formed as a result of the coating recrystallization. Such a microstructure was observed by, e.g. Sampath and Herman (1989) in nickel coatings plasma-sprayed under vacuum. This spraying technique is associated with the high temperature of the substrate which could have favoured recrystallization.

If, on cooling down of the melt in the lamella, no nuclei are formed but a glass or amorphous grain microstructure is produced. Formation of such a microstructure is favoured by:

- adding to the spray feedstock glass-forming additives, e.g.  $\text{Y}_2\text{O}_3$  or  $\text{SiO}_2$ ;
- a very high cooling rate.

In fact, an amorphous phase was observed by Wilms and Herman (1976) in yttria–alumina coatings close to the interface with the substrate, where the heat removal rate is the greatest.

With rapid solidification, some crystals, e.g. in metals having the cubic structure, grow in a preferential direction. Consequently, one may expect in the columnar grains perpendicular to the substrate a preferential crystallographical orientation which is called *texture*. The texture in the <200> direction was indeed observed in Ni and NiAl coatings deposited by APS and VPS (to a lesser degree) by Sampath and Herman (1989). The texture was more pronounced on the coating’s back-side, where solidification was more rapid. Preparation of the substrate by sand blasting results in the important roughness and reduces the texture effect. The dimensions of the crystals in the thermally sprayed coatings vary between a few nanometres and one micrometre (see Table 6.6). Thermal spraying onto a quenched or cooled with liquid  $\text{N}_2$  substrate having a temperature of about 100 K (entry 1 of Table 6.6) leads to the formation of very small crystals of bcc-iron with dimensions of 3–10 nm. As the temperature of the coating during vacuum-plasma spraying is high and recrystallization of the material is possible, the crystal grains

**Table 6.6** Examples of dimensions of crystals in coatings sprayed by using different techniques

Number	Testing technique	Spraying technique	Initial powder composition (wt%)	Substrate preparation	Crystal size (nm)	Reference
1	TEM grains observation	APS	Fe-bal., Cr-17, Ni-2, Si-1, C-0.2	Cu substrate cooled with liquid N <sub>2</sub>	3 of Fe (bcc)	Bhat and Herman, 1982
2	Peak broadening in X-ray diagrams	VPS	Cu	Al <sub>2</sub> O <sub>3</sub> substrate polished and cleaned prior to deposition	29–37 (40 for initial powder)	Pawlowski, 1980
3		APS	TiO <sub>2</sub>	Stainless steel, sand-blasted	29–43 of rutile (48–56 in initial powder)	Tomaszek <i>et al.</i> , 2006
4		Suspension plasma spraying			45 of rutile (58 in initial pigment)	
5	AFM observation of lamella surface	APS	Al <sub>2</sub> O <sub>3</sub>	Cu kept at 573 K	Radii of solidified columns ranging from 53 to 101	Robert <i>et al.</i> , 1998
6	TEM grains observation	VPS	Ti-bal., Al-(4.6–5.7), V-(4.0–4.3)	Cu mandrel kept at 973 K	100–1000	Salimijazi <i>et al.</i> , 2005

are relatively large (entries 2 and 6 of Table 6.6). The crystals in VPS Cu coatings have nearly the same dimensions as the crystals in the powder used for spraying. Similarly, rutile crystals in suspension plasma-sprayed TiO<sub>2</sub> coatings have a similar size to that in the pigment used to prepare the initial suspensions. The latter are, in turn, comparable to the external size of the powder particles. The rutile crystals in coarse TiO<sub>2</sub> powder becomes smaller after open-air plasma spraying (entries 4 and 3, respectively, in Table 6.6). Finally, atomic force microscopy enabled the diameters of the columnar grains in Al<sub>2</sub>O<sub>3</sub> to be found in the range from 53 to 101 nm (entry 5 in Table 6.6).

### 6.1.4 MECHANISMS OF ADHESION

The most obvious and most common mechanism of sprayed coatings' adhesion is mechanical anchorage of the splats to irregularities of the substrate (Figure 6.11). These irregularities result from sand blasting or other methods of substrate pre-spray preparation (Laszlo, 1961). The splat on solidification becomes attached to the substrate by the force resulting from liquid shrinkage.

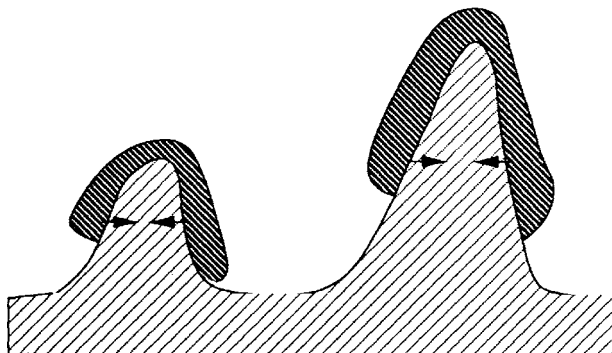


Figure 6.11 Illustration of mechanical anchorage of splats to irregularities of the substrate surface

It must be, however, noted that the splat does not contact the substrate over all of its bottom area. It is obviously true for *flower*-type lamellae and also for *pancake* splats with curling (see Figure 6.9, case F). The zones in contact are sometimes called *welding points* (Kudinov, 1977) or *active zones* (Steffens *et al.*, 1991a) and correspond to a small fraction of the splat area (20–30 % in the opinion of McPherson and Cheang (1989)). Clearly, adhesion of the coating improves, if the *active zone* area becomes greater. Formation of a *pancake* splat is a way to achieve this. Consequently, following the theory of Fukumoto *et al.* (2002), an increase in the substrate temperature would promote the formation of such a type of splat which, in turn, should improve adhesion. This was, in fact, proved by Pershin *et al.* (2003) for plasma-sprayed nickel coatings on steel substrates. These authors found that an increase of substrate temperature from 300 to 920 K results in an increase of adhesion strength from 10 to 74 MPa, measured with ASTM C633-79 test. The areas of the *active zones* is reduced by:

- oxides in metal and alloy coatings;
- air and/or working gas dissolved in liquid particles ‘in-flight’;
- air and/or working gas-filled pores entrapped by arriving particles on the substrate (see Figure 6.9, case E).

Addition of a deoxidizing element in the initial feedstock may, by reducing the oxide content, increase the areas of the active zones. Such an experiment was carried out and proved to be true for a pre-alloyed Ni + 5 wt% Al. Al becomes more easily oxidized than Ni, thus preventing the latter against oxidation. The powder was plasma-sprayed in air and the obtained coating indeed contained less oxygen with regard to that sprayed when using pure Ni. Moreover, the analysed splats were mainly *pancakes* in comparison to *flowers* in the Ni deposit (McPherson and Cheang, 1989). Another way to increase the *active zone* is deposition in an oxygen-reduced atmosphere (inert or low pressure). The low-pressure spraying also reduces the quantity of working gas absorbed by the liquid particle ‘in-flight’. In fact, the interfaces between metallic substrate and the vacuum sprayed metals and alloys coatings do not show any pores. On the other hand, oxides might result from substrate oxidation that could have occurred at roughening. Vacuum plasma spraying offers the possibility to clean the substrate by the action of the arc. Other spray techniques do not have this possibility and the substrate is always slightly oxidized during the time elapsed between surface roughening and the beginning of coating deposition. The oxidized spots may:

- act as the points of anchorage;
- be dissolved in liquid lamellae as the same oxide;
- react with another oxide to form a spinel.

As far as the formation of spinel is concerned, this was investigated experimentally (by, e.g. Steffens *et al.* (1991a)) but were not yet observed at the coating’s interface. Inside the *active zones*, adhesion can be realized by one of the following mechanisms:

- physical interaction;
- metallurgical interaction;
- other types of interactions, e.g. epitaxy.

Epitaxy is a particular mechanism that can occur if the sprayed material has the same or a similar crystal structure; the following discussion will be reduced to the first two mechanisms.

**Physical interaction** between the atoms of the lamella and of the substrate result from the action of *van der Waals forces* (Steffens and Müller, 1972) and can occur only if there is close and constant contact. The surfaces must approach each other to reach the field of attraction of the atoms, i.e. less than 1 nm. The prerequisite conditions for physical interaction between the contacting surfaces are as follows (Zaat, 1983):

- surfaces are clean,
- surfaces are activated by, e.g. plastic deformation;
- their contact is close.

**Metallurgical interaction** which can have two possible mechanisms:

- diffusion;
- chemical reaction between the lamella and substrate.

Diffusion occurs by the vacancies generated in high concentration in a rapidly solidified lamella. Diffusion can be activated by a high contact temperature. This was experimentally observed for the first time by Kitahara and Hasui (1974) on the interface between molybdenum and tungsten coatings sprayed onto aluminium. This could be explained by the high melting points of molybdenum ( $T_m = 2893\text{ K}$ ) and tungsten ( $T_m = 3668\text{ K}$ ) which could have induced a high contact temperature on solidification.  $T_c$  was also probably higher than the melting point of the aluminium substrate ( $T_m = 933\text{ K}$ ). The contact temperature may increase due to the exothermic reactions occurring on impact. Ingham (1975) discussed the exothermic reactions in two types of Ni-Al powders (Al covered with a dense Ni clad and a porous clad of Al around the Ni core) during the powders particle's flight. This reaction resulted in the formation of NiAl or  $\text{Ni}_3\text{Al}$ . Sampath *et al.* (1987) indicated that the components of Ni-Al powders would rather react (in-flight under open-atmosphere spray conditions) with oxygen (to form  $\text{NiO}$  or  $\text{Al}_2\text{O}_3$ ) than with each other. As far as the reaction on impact is concerned, its probability remains small because of the short solidification time.

Formation of a chemical compound between the materials of the sprayed particle and the substrate may also result in strong metallurgical bonding. The formation of many intermetallic phases was reported by Kitahara and Hasui (1974) while spraying different metals onto aluminium substrates. Intermetallic compounds, such as,  $\text{FeMo}$ ,  $\text{Fe}_2\text{Mo}$  and  $\text{Fe}_2\text{W}$ ,  $\text{Fe}_7\text{W}_6$ , were observed in Mo and W coatings air plasma-sprayed onto mild steel substrates. Similarly, Zhuang *et al.* (1988)

reported the formation of an intermetallic phase between the Mo coating sprayed onto a steel substrate.

## 6.2 COATING GROWTH

### 6.2.1 MECHANISM OF COATING GROWTH

A section of a thermally sprayed coating displays many lamellae piled up one upon another, as shown in Figure 6.12.

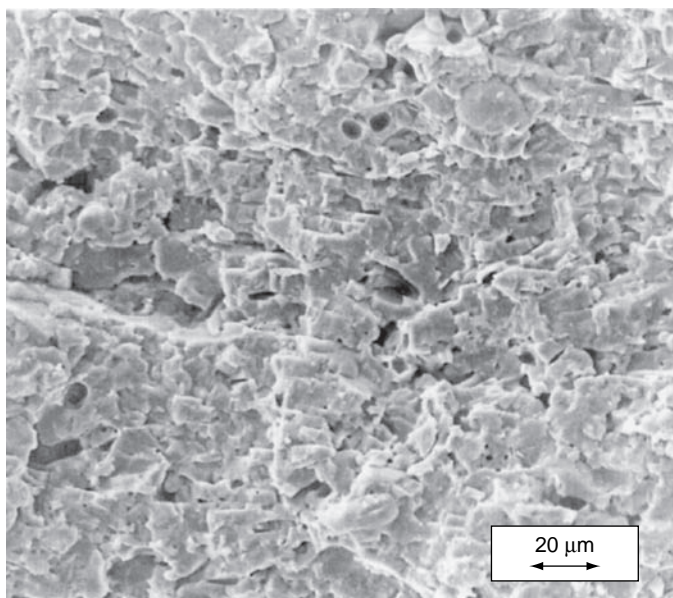


**Figure 6.12** Scanning electron micrograph (secondary electrons) of a fractured section of an  $\text{Al}_2\text{O}_3$  coating obtained from a powder having a size ( $d_{50}$ ) of  $34 \mu\text{m}$ , delivered at a feed rate of  $65 \text{ g/min}$  by plasma spraying in air using an F4 torch with an electric power of  $43 \text{ kW}$  and a 'stand-off' distance of  $90 \text{ mm}$

$\text{Al}_2\text{O}_3$  lamellae have a thickness of about  $h = 4 \mu\text{m}$  which enables us<sup>9</sup> to find the flattening parameter, which is equal to  $\xi = 2.4$ . The area covered by a lamella is about  $S = 4900 \mu\text{m}^2$ . On the other hand, knowing the

<sup>9</sup> In this simplified calculation, the powder particles of alumina are supposed to have one diameter, equal to  $d_p = 34 \mu\text{m}$ , and a density of  $\rho_p = 4.0 \text{ g/cm}^3$ .

powder feed rate and supposing that 50 % of the particles striking the substrate stick to it, one can find the number of particle being deposited on the substrate during 1 s. This number is equal to  $6.85 \times 10^6$  particles/s. The splats formed thereof, if placed near to each other, can cover an area of  $340\text{ cm}^2$ . As a typical spray spot has a diameter of 2.5 cm and an area of  $4.9\text{ cm}^2$ , it is clear that during one second as many as 69 splats (and  $4\mu\text{m}$  thick lamellae) would form on top of each other and the coating would grow to a thickness of  $274\mu\text{m}$ . However, the spraying torch moves with regard to the substrate and the coating grows more slowly. In fact, a typical torch moves over the substrate with a certain linear velocity which is equal to the velocity of the spraying spot. The number of lamellae in one layer, i.e. deposited during one torch pass, depends on the velocity. Taking as an example alumina deposited with the APS technique and the processing parameters described in Figure 6.12 and the data used in the above analysis, it is possible to find that for linear velocities of:

- 450 mm/s – the number of lamellae included in one layer is about 3.8, which corresponds to the thickness of a layer, in one pass, of  $15\mu\text{m}$ ;
- 900 mm/s – the number of lamellae included in one layer is about 1.9, which corresponds to the thickness of a layer, in one pass, of  $7.6\mu\text{m}$ ;
- 1800 mm/s – the number of lamellae included in one layer is about 0.9, which corresponds to the thickness of a layer, in one pass, of about  $3.6\mu\text{m}$ .

Linear velocity is an important parameter of spray technology. A high linear velocity leads to a lower thickness of a layer but, on the other hand, the torch returns rapidly to the same spot which reduces the contact with the environment. Moreover, the substrate temperature variations are smaller. Inversely, at a low linear velocity the coating grows rapidly. A large layer thickness leads to the difference in the temperature between its lower and upper part. Consequently, especially for materials having a high thermal dilatation coefficient, such as zirconia, residual stresses can be generated. Finally, the proper choice of linear velocity is a matter of compromise. For spraying of ceramic coatings onto metal substrates, high linear velocities should be used. When spraying cylindrical elements, the linear velocity can be ‘decomposed’ into the traverse speed (movement of the torch) and the rotation speed (movement of the cylinder). Example of such calculations for different diameters of a cylinder are shown in Table 6.7. The mass of powder deposited onto

**Table 6.7** Calculation of rotation and traverse speeds for cylinders of different diameters for a linear velocity of spraying of 1800 mm/s, assuming that the spraying torch moves 4 mm during one rotation of the cylinder

Cylinder diameter (mm)	Rotation speed (1/min)	Traverse speed (mm/s)
50	689	46
100	343	23
150	229	15
200	172	11
250	137	9
300	115	8

the substrate is spatially distributed and its distribution is closed to Gaussian. The distribution becomes more diffused with the increasing distance of spraying. Again, while choosing the spray parameters, it is important to take this distribution into account in such a way as to avoid periodical variation of the coating thickness. One way to avoid such a variation is shortening of the neighbouring passes of the spraying torch. The time for the splats flattening and their cooling decreases with the coating's growth. This is due to the smaller thermal contact resistance between the lamellae themselves than that between the lamellae and the substrate (Moreau *et al.*, 1992). The coating's growth can be simulated numerically. First, studies on 2-D simulations, enabling prediction of coating microstructure were made by using the *Monte Carlo* method by Knotek and Elsing (1987). The model developed by Cirolini *et al.* (1991) and Doltsinis *et al.* (1998) used the rules of growth presented in Table 6.5. Later, the program associated with the model was slightly modified and applied to simulate the growth of a plasma-sprayed hydroxyapatite coating (Figure 6.13).

Models for coating growth in three dimensions have also just started to be developed, e.g. for the plasma spraying of ZrO<sub>2</sub> (Wei *et al.*, 2004) and Ni (Xue *et al.*, 2004).

### 6.2.2 TEMPERATURE OF COATINGS AT SPRAYING

During thermal spraying, a substrate with a deposited coating is heated by the thermal fluxes coming from the torch and the sprayed particles. These are specified in Table 6.8. The thermal fluxes depend on the spraying technique. Some numerical data for plasma spraying in the

(a)



(b)



**Figure 6.13** Computer simulations of a cross-section of a hydroxyapatite coating, sprayed using an SG100 torch supplied with an Ar + 5 vol% H<sub>2</sub> plasma and 24 kW of electric power, from a powder having a mean diameter ( $d_{50\%}$ ) of 120 µm with a carrier flow rate of (a) 3 slpm and (b) 3.5 slpm (Dyshlovenko *et al.*, 2006a)

**Table 6.8** Thermal fluxes with heating directed towards the substrate during thermal spraying

Thermal flux	Flux description	Technique
Radiative	Radiation of plasma jets in all directions	Plasma spraying in the open air, at low pressure or in an inert atmosphere
Convective	Convective flux coming from the jets and flames, directed towards the substrate	Plasma spraying in the open air, in an inert atmosphere or, to a lesser degree, under vacuum; flame spraying, high-velocity flame spraying; detonation spraying
Splats solidification	Liberated latent heat of fusion, directed towards the cooler zones of coating and/or substrate	All spraying techniques
Lamellae cooling	Flux resulting from lamellae cooling down to the temperature of equilibrium, directed towards the cooler zones of coatings and/or substrates	All spraying techniques

open atmosphere and under vacuum are compiled in Table 6.9. The total thermal flux for open-air spraying is about  $2 \text{ MW/m}^2$  and, for a given example, seems to be smaller for vacuum plasma processing.<sup>10</sup> The convective flux  $q_c$  can be expressed as:

$$q_c = h_c(T_g - T_s) \quad (6.17)$$

in which  $T_g$  is the temperature of gas at the surface of the processed coating and  $T_s$  is the actual temperature of the coating surface. This flux, as well as the radiative one, depends strongly on the processing parameters. Table 6.10 shows these fluxes for different spray distances and ways of cooling for atmospheric plasma spraying using a torch installed with a compressed-air barrier and cooling (see Figure 3.6) onto a circular end of a cylinder. Application of an efficient thermal barrier is supposed to cut entirely the convective heat flux and the sprayed coating remains cooled with the stream of compressed air (entry 1 of Table 6.10). In most cases, the coatings sprayed by plasma and flame (low and high

<sup>10</sup> For comparison, on laser cladding the flux of energy ( $q$ ) is in the range  $10\text{--}10^4 \text{ MW/m}^2$  (Pawlowski, 2003)

**Table 6.9** Thermal fluxes for plasma spraying in the open air and under vacuum

Spray parameters and thermal fluxes	Open-air plasma spraying		Vacuum plasma spraying (Lee, 1983)
	Marynowski <i>et al.</i> , 1965	Mariaux <i>et al.</i> , 2003	
Electric power input (kW)	30	21.5	65
Working gases flow rate (slpm)	Ar + 5.6 H <sub>2</sub> (70)	Ar + 15 H <sub>2</sub> (45)	Ar + He
Powder/feed rate (g/min)	TiC	Al <sub>2</sub> O <sub>3</sub> (15)	Cu
Spray distance (cm)	7.5	Variable	45
Working pressure (hPa)	1000	1000	79.8
Radiative flux (MW/m <sup>2</sup> )	0.045	2 (on jet axis) and 1.5 at 2 cm 'off-axis'	—
Convective flux (MW/m <sup>2</sup> )	1.13	—	—
Flux of solidification of splat and cooling of lamellae (MW/m <sup>2</sup> )	1.42	About 2.5 % fluxes of plasma	—
Total flux (MW/m <sup>2</sup> )	2.6	—	0.617

**Table 6.10** Convective heat transfer coefficients and radiative heat fluxes for different atmospheric-plasma spray distances and different configuration of compressed-air cooling at a constant electric power input of 32 kW and flow rate of the working gases, Ar + H<sub>2</sub> (70 + 15 slpm) (after Pawlowski *et al.*, 1982)

Number	Processing parameter	Convective heat transfer coefficient (W/(m <sup>2</sup> K)) <sup>a</sup>	Radiative flux (W/m <sup>2</sup> )
1	Spray distance, 6 cm; cooling-air velocity, 110 m/s; barrier-air velocity, 140 m/s	416–0.017 × T <sub>s</sub>	3470
2	Spray distance, 10 cm; no cooling; no barrier	1150–0.083 × T <sub>s</sub>	1250
3	Spray distance, 15 cm; no cooling; no barrier	1040–0.113 × T <sub>s</sub>	555

<sup>a</sup> Temperatures in the regression equations are expressed in °C.

velocities) in air are cooled by compressed air or, sometimes, cryogenic liquids, at deposition. Air cooling and relative motion of the torch with regard to the substrate generate convective cooling, which is superposed with convective heating of the working gas. In fact, only plasma spraying under vacuum cannot be accompanied by convective cooling. This is why the temperatures at this kind of deposition remain relatively high (Sampath, 1993). Thermal fluxes are also the boundary conditions for the heat conduction equation (see Chapter 5, Equation (5.35)) enabling us to predict the temperature fields during spraying. The analytical solutions in one-dimension, for a ‘semi-infinite’ body-approximation, simulating the deposition of alumina by a static plasma torch in air, were presented by Madejski (1976b) and Pawłowski (1981). Bao *et al.* (2004) made similar calculations for flame-spray deposition of a polymer with a torch scanning a mild-steel substrate. The calculated temperature rises in a ‘parabolic-like’ way up to an asymptotic value, with small modulations resulting from the torch scans. A more realistic, 2-D analytical model of the coating temperatures during spraying was developed by Madejski (1976c). A numerical 2-D model, part of a large software program simulating coating growth, was reported by Cirolini *et al.* (1991). The 1-D numerical simulations during spraying of alumina were validated experimentally by Pawłowski *et al.* (1982). The measurements were carried out with the help of an ir camera (Figure 6.14), equipped with an InSb detector. The emission coefficients of alumina over the tested temperature range were found to be about  $\epsilon = 0.78\text{--}0.82$  at room temperature and  $\epsilon = 0.42\text{--}0.45$  at 1270 K.

The results of this determination for alumina coatings deposited onto copper and mild steel substrates by using the spray parameters presented in Table 6.10 (entry 3) are shown in Figure 6.15.

The temperature of the surface after 15 s of spraying is equal to  $T = 670\text{ K}$  when depositing onto a copper substrate and  $720\text{ K}$  for the mild-steel substrate. The difference results from the better heat conduction of copper. A knowledge of the temperature fields in coatings and substrates is prerequisite to initiate a discussion of the thermal stresses generated at spraying.

### 6.2.3 GENERATION OF THERMAL STRESSES AT SPRAYING

Pre-spray treatment of a substrate introduces mechanical stress. For example, sand-blasting results in a strong compressive stress near to the treated surface of a substrate (which later becomes the interface with

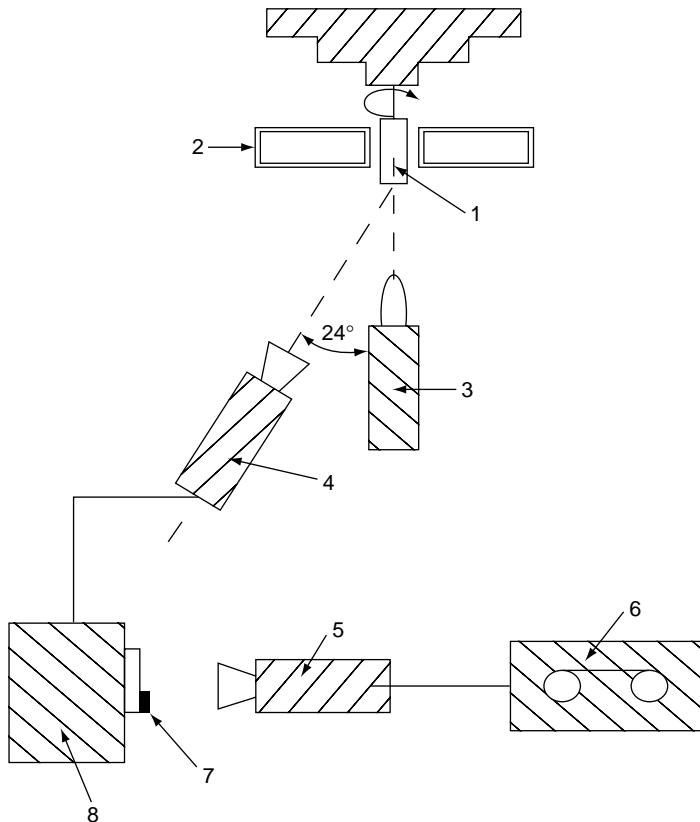


**Figure 6.14** Experimental set-up used by Pawlowski *et al.* (1983) to determine the surface temperature of an alumina coating at deposition: (1) substrate; (2) water-cooled contrast plate; (3) plasma torch; (4) ir camera; (5) video camera; (6) magnescope; (7) chronometer; (8) display unit

the coating). The reported stress values range between  $-150\text{ MPa}$  at a depth of  $100\mu_{\text{m}}$  below the surface in AlSi9 alloy (Gadow *et al.*, 2005) to  $-800\text{ MPa}$  at the same depth in a 35CrMo4 steel substrate (Laribi *et al.*, 2003). The stress is superimposed with the ones introduced by coating deposition giving the residual stress. To obtain the final pattern of stresses in a coating, one has to apply a specific mechanical stress to the residual one. The stress introduced at coating deposition, discussed by Clyne and Gill (1996), can be ‘decomposed’ as follows:

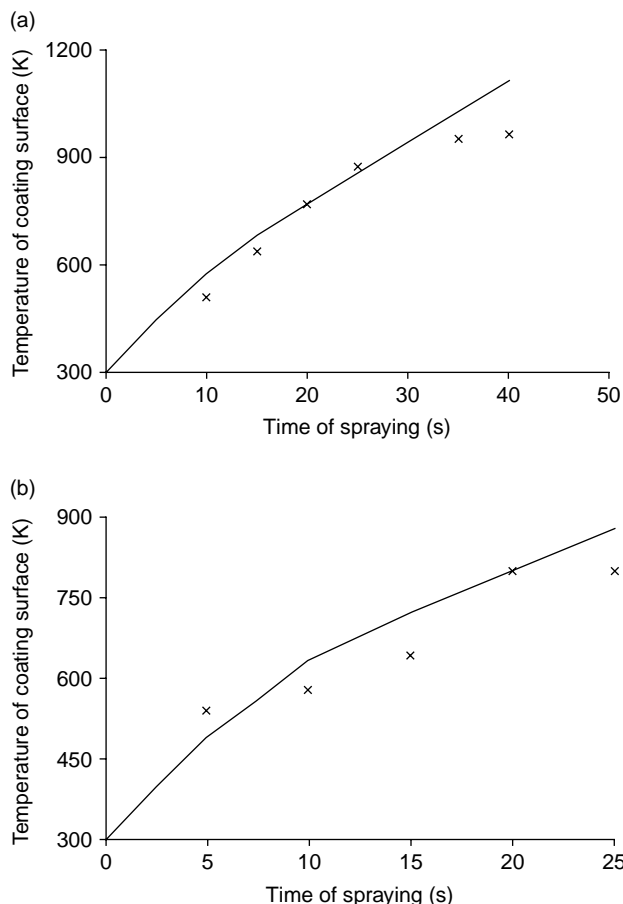


Figure 6.15 Calculated (solid line) and experimental points (+) corresponding to the  $\text{Al}_2\text{O}_3$  coating surface temperature during spraying by a plasma in air, using the parameters shown in Table 6.10 (entry 3), on (a) copper and (b) mild-steel substrates

- *quenching stress*, generated during solidification of the lamella;
- stresses generated in one pass of the torch;
- *cooling stress*, generated in the coating and substrate after processing;
- *phase-transformation stresses*, generated in the coating or substrate at crystal-phase transformation associated with the density change.

Quenching stress is generated when a sprayed particle impacts a substrate, which then deforms, solidifies and cools down rapidly (quenches) to the 'actual' temperature. The stress in a splat and,

consequently, in a lamella formed from the particle, is always tensile.<sup>11</sup> The value of the tensile stress,  $\sigma_q$ , can be estimated from the following equation:

$$\sigma_q = TEC_{co}(T_m - T_s)E_{co} \quad (6.18)$$

The quenching stress can be determined thanks to *in situ* measurements of the change of the curvature of the plate being coated. The elastic and Poisson moduli of the coating have to be known (Kuroda and Clyne, 1991; Kuroda *et al.*, 1992). The stress reached its highest value at NiCr deposition on mild steel, increased with surface temperature. The smallest stress occurred with  $Al_2O_3$  coatings. This difference can be explained by micro-cracking of the ceramic lamellae. Such cracking could have relaxed the stress. This explanation is confirmed by calculation of the quenching stress during Ni deposition of carbon steel, carried out by Fan *et al.* (2005). They observed tensile stresses of about 200 MPa in the lamellae changing into compressive stresses of –100 MPa in the substrate close to the interface. Such a sharp change in the sign of the stress enhances the probability of cracking. The quenching stress can relax by ‘creeping’ upon deposition of metals and alloys.

**Stresses generated in a one-torch pass** can be generated if the layer deposited in one pass is thick (linear velocity of the torch too slow and/or powder feed rate too large), especially at deposition of a thermal conductivity coating, e.g. zirconia. The temperature gradient between the surface and the interface of the layer then becomes large enough to generate stress. The stress relaxes with a characteristic pattern of cracks, as shown in Figure 6.16.

**Cooling stress** is generated when the coating and substrate cool down after deposition and is due to a ‘mismatch’ of their thermal expansion coefficients ( $TEC$ ). These kinds of stresses are not specific to thermal spraying and the theory and basic equations for stresses generated in units of different geometries have been presented in many textbooks, e.g. Abramov (1961). The simplified models for cooling stress, specific for thermal spraying, which also takes into account quenching stress, have been presented by Kuroda and Clyne (1991) and Takeuchi *et al.*

---

<sup>11</sup> All stresses discussed in this section have directions parallel to the coatings’ surfaces (in-plane stresses).

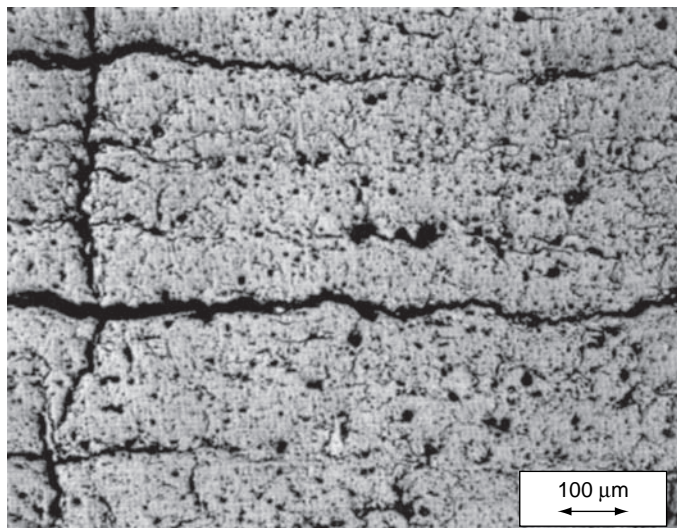


Figure 6.16 Optical micrograph of an air plasma-sprayed  $\text{ZrO}_2 + 7 \text{ wt\% } \text{Y}_2\text{O}_3$  coating with a pattern of cracks, most probably generated during one pass of the torch (Pawlowski *et al.*, 1983)

(1990). Their models assume just one temperature in the coating and the substrate after spraying, which is obviously not correct. A more sophisticated numerical model, which takes into account the temperature and properties gradients, was created by Ferrari *et al.* (1991). The cooling stress cannot be separated, neither from quenching, nor from the one-torch-pass or phase-transformation stresses. All of these are superimposed as residual stresses. Only in some particular cases is the separation of one of the stresses possible. For instance, the quenching stress in ceramic coatings on metals gives only a minor contribution because of the micro-cracking mechanism. The determination of residual stresses can be made by measuring the deformation of the ‘plate’, having removed successive layers of the coating sprayed onto it. A successive simple mathematical treatment enables the determination of the stress profile versus the corresponding coating thickness (Hobbs and Reiter, 1987). A modification of this method is the electrochemical ‘thinning’ of the coating instead of the substrate, applied by, e.g. Laribi *et al.* (2003). Another method, consisting of the drilling of a ‘relieving stress hole’ in a coating and then measuring the strains in various radial directions in its vicinity, was described by Bialucki *et al.* (1986) and used by Gadow *et al.* (2005). The residual stress at the coating

surface<sup>12</sup> can also be determined by the use of X-ray diffraction. This method is based on the assumption that the stress deforms the crystal lattice in the following way:

- compressive stress decreases the elementary cells' dimensions;
- tensile stress acts inversely.

This method was applied by, e.g. Weglowski and Pawlowski (1981) and discussed in detail by Matejicek *et al.* (1998). The experiments consist of measuring strains and, in order to calculate the residual stress, one needs the values of the elastic and Poisson moduli, as well as the thermal expansion coefficients. Sprayed coatings have different elastic moduli to bulk materials. The Poisson moduli and thermal expansions are less different. This is why measurements of stress should be accompanied by determinations of elastic moduli (Kuroda and Clyne, 1991; Kuroda *et al.*, 1992). The residual stresses measured in thermally sprayed coatings are presented in Table 6.11. The prediction of the stress directions in sprayed coatings seems, in general, to follow the model of Takeuchi *et al.* (1990) and is dependent on the relationship between the thermal expansion coefficients of the substrate ( $TEC_s$ ) and the coating ( $TEC_{co}$ ), in the following way:

- $TEC_{co} < TEC_s$  – the stresses in the coating are tensile or compressive;
- $TEC_{co} \approx TEC_s$  – the stresses in the coating are tensile;
- $TEC_{co} > TEC_s$  – the stresses in the coating are tensile.

The result from entry 5 of Table 6.11 shows, in contrast to expectations, compressive stresses instead of tensile ones. This was explained by Matejicek and co-workers by the higher temperature of deposition when vacuum plasma spraying than that under open-air processing. The temperature has reportedly amplified the effect of the slight 'mismatch' in thermal expansion coefficients ( $TEC \approx 13 \times 10^{-6}$  1/K for Ni;  $TEC \approx 14 \times 10^{-6}$  1/K for used steel). Consequently, this case rather corresponds to the situation  $TEC_{co} < TEC_s$  for which compressive stress can be expected. The small stress in YSZ coatings (entry 6 of Table 6.11) results from its relaxation by a micro-cracking mechanism. An increasing thickness can have two effects on the residual stress: its increase (entry 1 of Table 6.11) and a steep decrease to a constant value (entry 7 of Table 6.11). The difference

---

<sup>12</sup> Penetration depths of X-rays of  $\sim 16\text{ }\mu\text{m}$  for Ni and  $\sim 8\text{ }\mu\text{m}$  for  $\text{ZrO}_2$  were reported by Matejicek *et al.*, 1998.

Table 6.11 In-plane residual stresses in thermally sprayed coatings (after Takeuchi *et al.*, 1990)

Number	Reference	Spray technique	Stress determination method	Substrate	Coating	Deposition variable	Stress direction	Residual stress in coating, $\sigma$ (MPa) <sup>a</sup>
$TEC_{co} > TEC_s$								
1	Bialucki <i>et al.</i> , 1986	APS	Hole drilling	Mild steel	NiCr (80/20)	Coating thickness, $d$	Tensile	150 to 280, $d$ increases— $\sigma$ increases About 240 at surface
2	Szieslo, 1983	AS	Hole drilling	Mild steel	Stainless steel 304	—	Tensile	
$TEC_{co} \approx TEC_s$								
3	Matejicek <i>et al.</i> , 1998	APS	X-ray	Steel	Ni+16.5Cr+5.5Al+0.5Y	Coating 200 $\mu\text{m}$ thick	Tensile	99 + / - 15 for five specimens 62/241
4	—	APS	X-ray/hole drilling	—	Ni	Coating 100 $\mu\text{m}$ thick	Tensile	
5	—	VPS	—	—	—	Coating 600 $\mu\text{m}$ thick	Compressive	-116 / - 55
$TEC_{co} < TEC_s$								
6	Matejicek <i>et al.</i> , 1998	APS	X-ray	Steel	ZrO <sub>2</sub> + 8 wt% Y <sub>2</sub> O <sub>3</sub> Mo	Coating 200 $\mu\text{m}$ thick	Tensile	15 + / - 10 for five specimens
7	—	—	—	Steel/ aluminum	Coating thickness, $d$ , from 50 to 900 $\mu\text{m}$ and coating temperature, $T_{co}$ from 50 to 350 °C	and compressive	-50 to +100/ -200 to -200 $T_{co}$ $d$ increases $\sigma$ increases $d$ decreases $\sigma$ decreases	

<sup>a</sup> The sign “-” corresponds to compressive stress, while the sign “+” corresponds to tensile stress.

can be explained by using different test methods. Bialucki *et al.* (1996) reported stress evolution with thickness in one coating, while Matejicek *et al.* (1998) investigated the stresses reached at the surface of a sprayed coating with different thicknesses. This method gives very different values for the stresses (entry 4 of Table 6.11). Moreover, the coating temperatures at deposition reported by these two research group could have been different. An increase of this temperature results in an increase of the stress value and a change in its sign. In fact, at low temperatures quenching stresses can be predominant. At higher deposition temperatures, a thermal ‘mis-match’ effect takes over and compressive stress is more likely to occur. This is enhanced by a large difference in the *TEC*, as shown by entry 7 in Table 6.11 for an Mo coating ( $TEC \approx 6 \times 10^{-6} \text{ 1/K}$ ) onto steel ( $TEC \approx 14 \times 10^{-6} \text{ 1/K}$ ) and aluminum ( $TEC \approx 23 \times 10^{-6} \text{ 1/K}$ ) substrates. Reduction in the deposition temperature by intensive cooling, e.g. cryogenic, also reduces one-torch-pass stresses. This enables deposition of thicker layers in one pass and an increase in the deposition efficiency. The temperature can also be reduced by an increase in the torch’s linear velocity. Another two elements of technology influence the stress pattern:

- intermediate coatings;
- post-spray treatment.

An intermediate coating can reduce the variation of the residual stress in alloy coatings (Figure 6.17) and reduce the stress in ceramic coatings (Weglowski and Pawlowski, 1981). Further reduction in stresses can be achieved by the application, between the bond and the top ceramic coating, of a cermet coating which has a chemical composition and a *TEC* intermediary between these two materials. This has great practical importance when depositing a crack-free alumina coating onto an aluminum substrate for such application as, e.g. *corona rolls* (Pawlowski, 1991). Post-spray treatment can induce cracking due to the *phase transformation stress*, but, on the other hand, can sometimes reduce the residual stress (Figure 6.17).

**Phase transformation stress** is generated if the temperature during post-spraying heat treatment is greater than the phase transition temperature. This stress can be calculated from the following equation (Kingery *et al.*, 1976):

$$\sigma = \frac{E_{co} \left( 1 - \frac{\rho'}{\rho''} \right)}{3(2\nu_{co} - 1)} \quad (6.19)$$

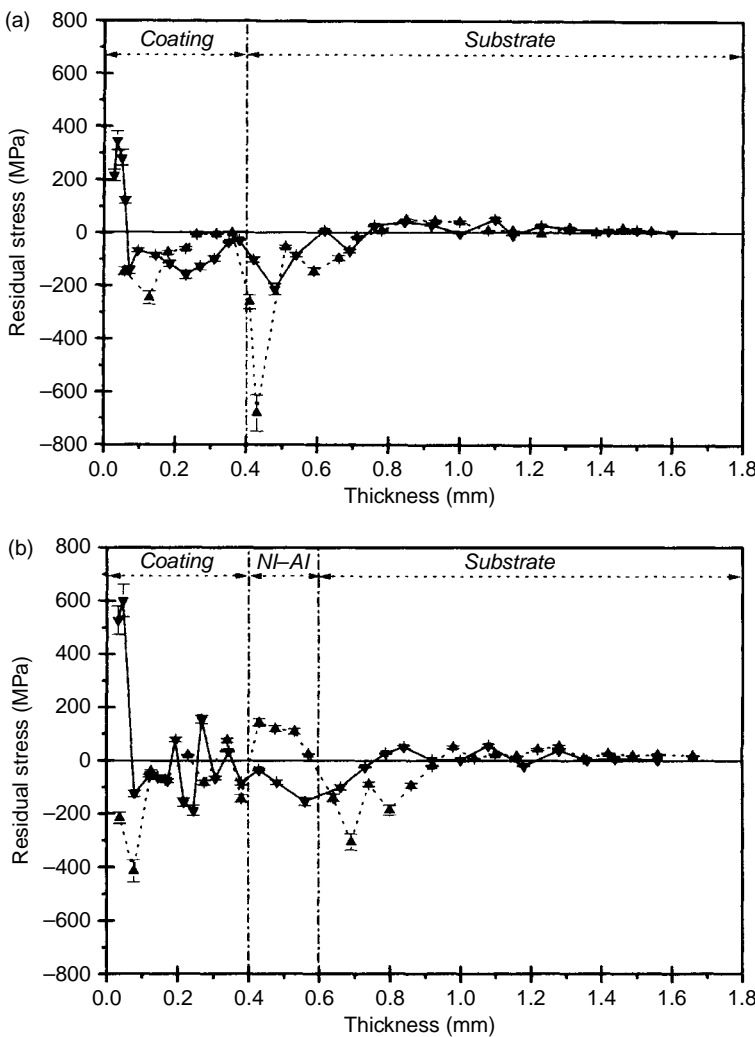


**Figure 6.17** Profiles of residual stresses determined by the plate-deformation method in an arc-sprayed coating of Cr–Ni and Cr–Mn steels, as-sprayed ( $\blacktriangle$ ) or subjected to post-spray annealing, in air at 1120 K for 1 h ( $\blacktriangledown$ ), deposited directly onto (a) a 35CrMo4 steel substrate and (b) an NiAl bond coating (after Laribi *et al.*, 2003). Reproduced from *J. Therm. Spray Technol.*, 12(2), 2003, 234–239, ‘Metallurgical characterization and determination of residual stresses of coatings by thermal spraying’, M. Laribi, A.B. Vannes, N. Mesrati and D. Treheux, Figure 7, Copyright (2003). With kind permission of Springer Science and Business Media

in which  $\rho'$  and  $\rho''$  concern the densities of the coating material, prior and after phase transformation, respectively. This stress would be generated, for example, in an as-sprayed, free-standing alumina sample heated to a temperatures above 1373 K. At this temperature, phase

$\gamma$  having a density  $\rho' = 3.67 \text{ g/cm}^3$  transforms to phase  $\alpha$  of density  $\rho'' = 3.98 \text{ g/cm}^3$ .

### 6.2.4 COATINGS SURFACES

The surface of a thermally sprayed coating is composed of lamellae formed of molten, partially molten and unmelted particles, as shown in Figure 6.18.

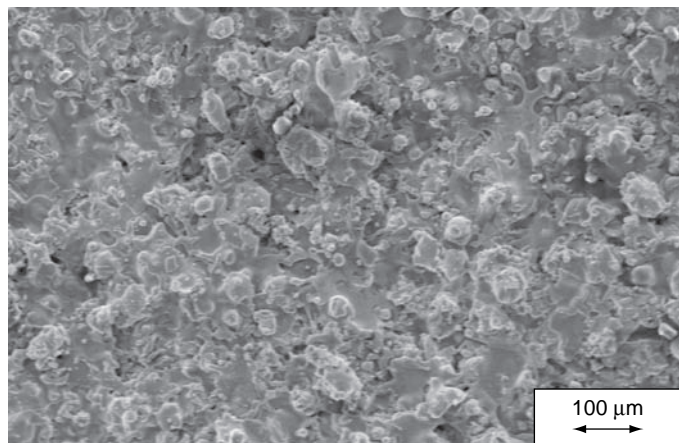


**Figure 6.18** Scanning electron micrograph (secondary electrons) of the surface of a  $\text{Cr}_2\text{C}_3 + 25 \text{ wt\% NiCrAlY}$  coating, plasma-sprayed in air (Nykiel and Pawłowski, 2004)

The coating can be characterized by roughness, which increases with the powder particle size (or wire diameter) and decreases with the particle velocity and temperature at impact. In addition, the substrate roughness influences, to a degree, the coating roughness. The authors' own experience is that a smoother substrate results in a smoother coating although some authors have other opinions (Smyth and Anderson, 1975).

## 6.3 MICROSTRUCTURE OF THE COATINGS

### 6.3.1 CRYSTAL PHASE COMPOSITION

Phase diagrams, so useful in materials engineering, have a limited usefulness in thermal spraying. The prediction of phase composition of a coating by knowing the composition of the initial powder is more

complicated than analysis of a diagram. The main difficulties result from:

- rapidity of solidification and cooling of splats, which often results in the formation of an amorphous phase at solidification or of a metastable phase at cooling;
- position in the diagram (in other words, the chemical composition) that can be modified at processing by the selective evaporation of a component of a ‘multicomponent’ powder;
- analysis of another diagram may prove necessary because of chemical reactions (oxidation, reduction, ‘decarburation’).

The phase composition of a coating depends on the following factors of the ‘entire’ technology:

- The chemical and phase composition of the initial powder, as well as the morphology of its particles. The latter results from the powder manufacturing method (discussed in Chapter 1).
- The deposition process and, in particular, the spraying atmosphere, as well as all of the processing parameters which influence the solidification and cooling rapidity. These two processes are integral parts of the thermal history of a particle which transforms into a lamella in sprayed coatings. The initial particle melts and is evaporated in a few milliseconds. Then, after impact, the substrate deforms, solidifies and cools down to the ‘actual temperature’ of the coating. Finally, the lamella cools down to room temperature (see Figure 6.19).
- Post-spraying treatment can be accompanied by coating recrystallization. High-energy treatment, such as the use of a laser, may lead to coating-fusion, hence resulting in the formation of new phases.

## Composition and Morphology of Powders

To discuss the influence of the composition and morphology of a powder, an example for an NiAl powder is taken. This powder is in ‘standard use’ as a bond-intermediate coating and also as a high-temperature corrosion-resistant coating. It can be manufactured by the following methods:<sup>13</sup>

---

<sup>13</sup> Further details about powder manufacturing methods can be found in Chapter 1.

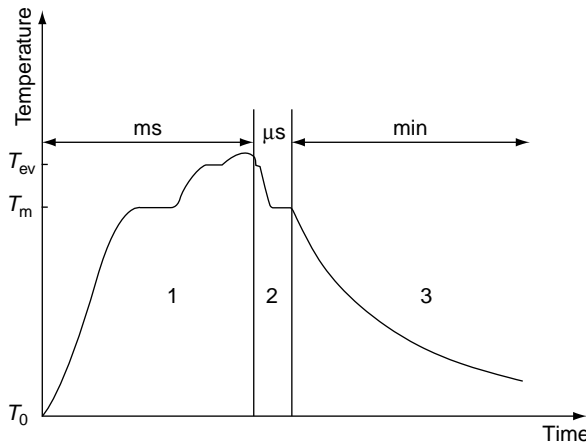


**Figure 6.19** Thermal history, corresponding to the following transformations of a particle injected into a jet/flame (region I), becoming a splat which solidifies (region II) and ending up as a lamella inside the coating which then cools to room temperature (region III)

- porous cladding, resulting in small grains of Al, ‘glued’ onto an Ni core, to obtain irregular rounded particles with a macroscopic chemical composition of Ni + 5 wt% Al;
- dense cladding, resulting in a continuous Ni layer around an Al core, to obtain spherical particles with a macroscopic composition of Ni+20 wt% Al;
- water atomization, resulting in irregular rounded particles having microscopic and macroscopic compositions of Ni+5 wt% Al;
- gas atomization, resulting in spherical particles of microscopic and macroscopic compositions of Ni+5 wt% Al.

The powders prepared in these ways were plasma-sprayed in air and under vacuum and the microstructures of the obtained deposits were studied by Sampath *et al.* (1987) with the details shown in Table 6.12. The coatings sprayed under vacuum have a composition which results from the reaction between Ni and Al – if these elements are present for reaction (i.e. not yet being a part of the intermetallic compound) or have the same composition as the initial powder. The coatings sprayed in air also contain nickel and aluminium oxides resulting from the reaction between these elements and oxygen from air (in cladded-powder sprayed coatings) or contain  $\text{Al}_2\text{O}_3$ , together with a solid solution of  $\alpha$ -Ni (in atomized powder sprayed coatings). The major influence on the phase

**Table 6.12** Phase composition determined by X-ray diffraction and electron micro-probe analysis, in coatings plasma-sprayed in air and under vacuum when using NiAl powders prepared differently and having different chemical compositions (after Sampath *et al.*, 1987). Reproduced by permission of ASM International from Sampath *et al.*, 1987, *Thermal Spray: Advances in Coating Technology*, D.L. Houck (Ed.), ASM International, Materials Park, OH, USA, pp. 47–53

Powder chemical composition (wt%)	Powder production method	Spray technique	Crystal phases in powder	Crystal phases in coating <sup>a</sup>
Ni + 5Al	Porous cladding	APS	α-Ni (solid solution), Al	α-Ni, NiO plus traces of Al and $\text{Al}_2\text{O}_3$
		VPS		α-Ni, traces of $\text{Ni}_3\text{Al}$ , NiAl and $\text{Ni}_2\text{Al}_3$
Ni + 20Al	Dense cladding	APS		α-Ni, NiO, Al and $\text{Al}_2\text{O}_3$
		VPS		α-Ni, $\text{Ni}_3\text{Al}$ , NiAl and $\text{Ni}_2\text{Al}_3$
Ni + 5Al	Gas-atomized	APS	α-Ni	α-Ni and $\text{Al}_2\text{O}_3$
	Water-atomized	VPS		α-Ni
		APS		α-Ni and $\text{Al}_2\text{O}_3$
		VPS		α-Ni

<sup>a</sup> Starting from the most intense phase.

composition of the coatings is the spraying atmosphere. Oxidation could have a place on the powder particle flights or on the substrates (in splats or lamellae). It can be concluded that Ni and Al form intermetallic compounds in the absence of oxygen or oxides in its presence.

## Deposition Process

The following factors of the deposition process influence the phase composition of sprayed coatings:

- High temperatures of particles in jets/flames which exceed the melting point and therefore the resulting possible selective evaporation of a component of a multicomponent compounds, such as CuO which evaporates selectively from  $\text{YBa}_2\text{Cu}_3\text{O}_x$ .
- Gases of jets/flames that can react with an element of the particle surface in-flight and/or the splat and lamella formed thereof. Typical phenomena are reduction and decarburation.

- Nucleation and solidification of the splat that may result in formation of metastable phases, depending on the nucleation energy. The latter depends on the temperature and the size of the splat.
- Rapid cooling of the lamella.

Discussions concerning the above will be presented below for three refractory oxides,  $\text{Al}_2\text{O}_3$ ,  $\text{TiO}_2$  and  $\text{ZrO}_2$ , two low-temperature multi-oxides,  $\text{Ca}_{10}(\text{PO}_4)_6(\text{OH})_2$  (hydroxyapatite) and  $\text{YBa}_2\text{Cu}_3\text{O}_x$  and the important carbide, WC, which when prepared as a cermet with Co or CrNi is frequently used to obtain wear-resistant coatings.

**$\text{Al}_2\text{O}_3$**  Alumina is highly refractory and a very stable ceramic (melting point,  $T_m = 2327\text{ K}$ ; standard enthalpy of formation,  $\Delta_f H^\circ = -1675.7\text{ kJ/mol}$ ). Consequently, the oxide does not modify its composition upon spraying. At solidification, some authors have reported the formation of an amorphous phase in the lamellae, close to the interface of the substrate (Wilms and Herman, 1976). The modification of alumina with regard to the initial material occurs at solidification of the splat. The process results in formation of the  $\gamma\text{-Al}_2\text{O}_3$  phase instead of the stable  $\alpha\text{-Al}_2\text{O}_3$  phase. McPherson (1973) explained this formation by a lower energy for nucleation from the liquid for the  $\gamma$ -phase than for the  $\alpha$ -phase. The  $\alpha$ -alumina presented in the as-sprayed coatings results from inclusion of the unmelted grains (Figure 6.20)

It is possible to obtain the  $\alpha$ -phase for the melt by alloying alumina with other oxides, such as chromia. Such alloying modifies the height of the nucleation energy barrier.

**$\text{TiO}_2$**   $\text{TiO}_2$ , being a relatively less-refractory oxide with a melting point of  $T_m = 2143\text{ K}$  and a standard enthalpy of formation of  $\Delta_f H^\circ = -944.0\text{ kJ/mol}$ , is used frequently as a coating in chemical catalysis and a dielectric in capacitors, and is being studied for such new applications as electron emitters (Tomaszek *et al.*, 2007) or in photocatalysis (Toma *et al.*, 2005). The oxide is often alloyed with others ( $\text{Al}_2\text{O}_3$ ,  $\text{Cr}_2\text{O}_3$ ) in such compositions as, e.g.  $\text{Al}_2\text{O}_3 + 13\text{ wt\% TiO}_2$ , which has a liquidus at a lower temperature than the melting points of more refractory component. Commercial  $\text{TiO}_2$  powders are often prepared by fusing and crushing and contain mainly rutile and sub-oxides, being the Magnéli phases of a general formula,  $\text{Ti}_x\text{O}_{2x-1}$  ( $5 < x < 9$ ) (Berger, 2004). On plasma-spraying of coarse particles (mean size,  $d_{\text{VS}} = 23\text{ }\mu\text{m}$  in Figure 6.21(a); rutile crystal size,  $d_{\text{cr}} = 48\text{--}56\text{ nm}$ ) coatings are produced, having a composition similar to the initial particles, namely

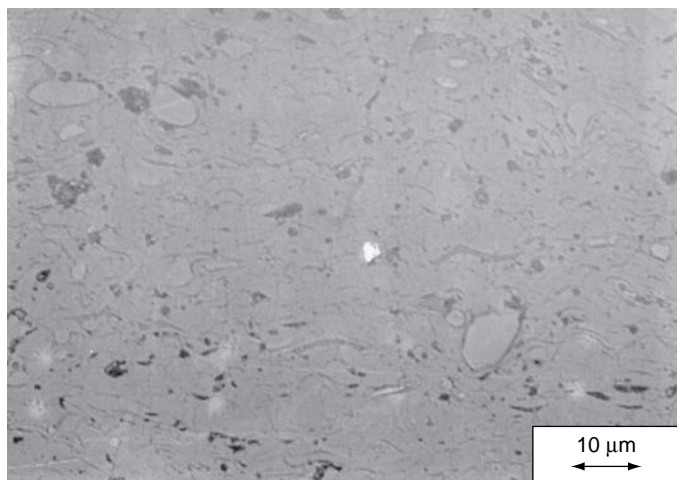


**Figure 6.20** Optical micrograph of an alumina coating used for corona rolls production, obtained by plasma-spraying using 43 kW of electric power and an F-4 torch at a spraying distance of 90 mm. The image analysis fraction of unmelted grains is about 4.4 % and the porosity is about 9.8 %. The initial powder was produced by fusing and crushing and has sizes  $-45 + 22.5 \mu\text{m}$

rutile (crystal size,  $d_{\text{cr}} = 29\text{--}43 \text{ nm}$ , being clearly smaller than that of the powder) and sub-oxides.

When plasma-spraying fine particles of the same powder (ball-milled for 8 h to a mean size of  $d_{\text{VS}} = 0.45 \mu\text{m}$ , crystal size of rutile,  $d_{\text{cr}} = 58 \text{ nm}$  and prepared as a water suspension – Figure 6.21(b)), the coating crystallizes in a mixture<sup>14</sup> of rutile (crystal size,  $d_{\text{cr}} = 45 \text{ nm}$ ), anatase and sub-oxides. The presence of anatase was confirmed by Raman spectroscopy (Tomaszek *et al.*, 2006). Further confirmation comes from the literature (Toma *et al.*, 2005) for a similar pigment sprayed in the same way. On the other hand, anatase is not expected to be formed on solidification of a stoichiometric  $\text{TiO}_2$  melt under equilibrium conditions. Its formation may be rather interpreted as a result of rapid solidification of liquid particles on impact. Li and Ishigaki (2002) explained this from calculations of the ratio of critical energies for nucleation of anatase and rutile from the melt as a function of temperature. These calculations did show that at temperatures lower than 2075 K, nucleation of anatase occurs

<sup>14</sup> Professor Heimann, during a recent meeting at the University of Bochum, Germany, in October 2005, identified the presence of brookite in plasma-sprayed coatings. Brookite is, as rutile and anatase, a possible phase of  $\text{TiO}_2$  crystallization, but its presence in sprayed coatings is mentioned very seldom in the literature.

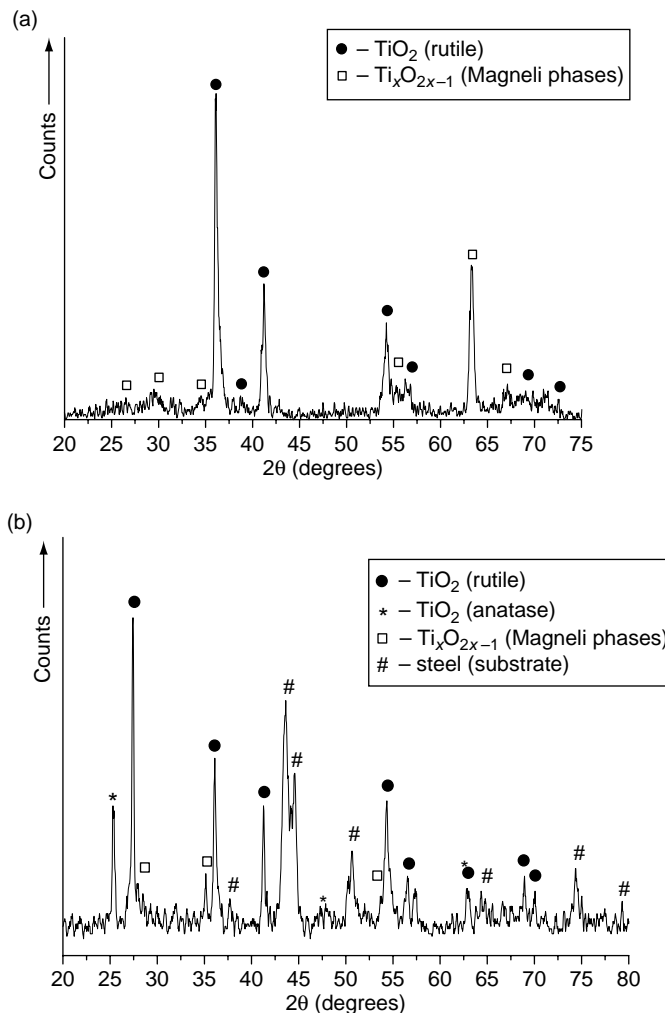


Figure 6.21 X-ray diffraction diagrams of (a) a coarse  $\text{TiO}_2$  powder plasma-sprayed coating and (b) a fine  $\text{TiO}_2$  pigment plasma-sprayed as a water suspension (Tomaszek *et al.*, 2006)

and above this temperature, rutile nucleates. On the other hand, the effect of overcooling is an intrinsic phenomenon in solidification under spraying condition. Consequently, the temperature of solidification is expected to be lower than that under equilibrium conditions. Calculations of this lowering, made recently for hydroxyapatite coatings, did show a relative lowering of  $\Delta T/T_m = 0.12\text{--}0.14$  (see Section 6.1.3). As the melting point of rutile under equilibrium conditions is equal to

$T_m = 2143\text{ K}$  (Samsonov, 1978), the relative lowering would be about  $\Delta T = 260\text{ K}$  and the temperature of solidification would be equal or less than about  $1880\text{ K}$  under spraying conditions. Consequently, one may expect the formation of anatase during solidification of the splats. However, anatase can transform back to rutile on cooling of the coating. This transformation would be more pronounced for larger particles due to the greater quantity of heat of fusion liberated and the slower cooling rate. Consequently, fine particles in suspension-sprayed coatings would more probably contain anatase and coarse particles – rutile. The presence of rutile in suspension-sprayed coatings can be explained by unmolten, large particles which are visible on the coating surface. As the formation of anatase would not depend on the phase composition of the initial powder, this explanation is valid for the results from the study made by Toma *et al.* (2005). It is important to stress that anatase is more useful than rutile in applications of coatings in catalysis.

Titanium dioxide looses oxygen during fusion of powders. Consequently, on spraying powders crystallized in the rutile phase, one can expect the presence of sub-oxides, such as Magnéli phases, in the obtained coating. This was, in fact, observed, during suspension plasma-spraying of rutile pigments. The sub-oxides were accompanied by rutile (coming presumably from unmolten particles) and anatase, formed by the above explained effect.

**ZrO<sub>2</sub>** ZrO<sub>2</sub>, which is a refractory material with a melting point,  $T_m = 2983\text{ K}$  and a standard enthalpy of formation,  $\Delta_f H^\circ = -1100.6\text{ kJ/mol}$ , is used mainly with stabilizers such as CaO or Y<sub>2</sub>O<sub>3</sub> in order to avoid phase transformations (Figure 6.22). These transformations lead to generation, on heating or cooling, of stresses that may be detrimental for coatings (see Section 6.2.3).

The most frequently plasma-sprayed coatings use powders composed of ZrO<sub>2</sub> alloyed with 6–12 wt% of Y<sub>2</sub>O<sub>3</sub>. The coatings crystallize into the non-transformable, tetragonal t'-phase. The mechanism of this phase formation is as follows:

- liquid zirconia lamellae containing, e.g. 8 wt% of Y<sub>2</sub>O<sub>3</sub>, solidify at about  $2970\text{ K}$  and crystallize in the cubic phase down to about  $2700\text{ K}$ ;
- at this temperature, the formation of the tetragonal transformable t-phase takes place (with some content of the cubic phase);
- finally, at about  $800\text{ K}$  a martensitic transformation into the monoclinic phase (with some content of cubic phase) *should* occur. Instead, a transformation into the non-transformable t'-phase is *observed*.

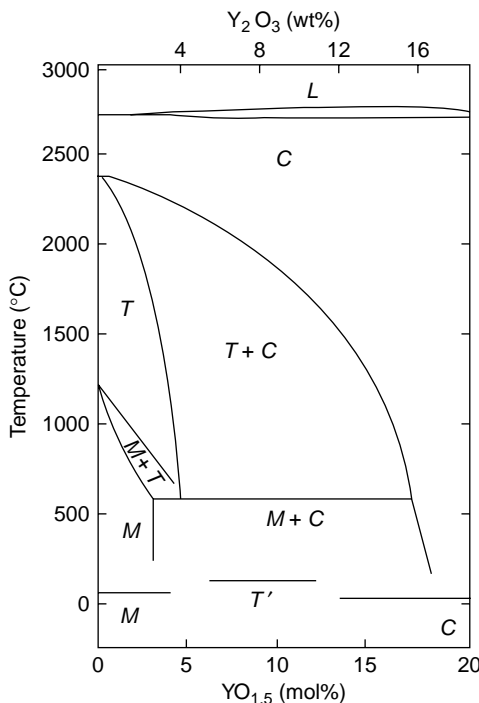


**Figure 6.22** Phase diagram of yttria-stabilized zirconia: L, liquid; M, monoclinic; C, cubic; T, tetragonal; T', non-transformable tetragonal (after Alperine and Lelait, 1992). Reproduced by permission of ASME International from 'Microstructural investigation of plasma sprayed yttria partially stabilised zirconia', by S. Alperine and L. Lelait, *International Gas Turbine Aeroengine Congress Exposition*, Cologne, Germany, 1–4 June, 1992, Paper 92-GT-317

McPherson (1989) explained the formation of this phase by a reduction in the martensitic transformation temperature to below room temperature, due to the small crystal sizes in the lamellae.

$\text{Ca}_{10}(\text{PO}_4)_6(\text{OH})_2$  Atmospheric plasma spraying is the most widely accepted method to obtain HA coatings on titanium-alloy prostheses. The 'multi-oxide' has many transformations at relatively low temperatures. Heat treatment in a plasma jet provokes dehydration and can result in high-temperature decomposition of HA. The dehydration produces (with increasing temperature):

- oxyapatite (OA),  $\text{Ca}_{10}(\text{PO}_4)_6\text{O}$ ;
- oxyhydroxyapatite (OHA),  $\text{Ca}_{10}(\text{PO}_4)_6(\text{OH})_{2-x}\text{O}_x\text{V}_x$ , in which 'V' stands for vacancy.

The decomposition, in turn, results in generation of different calcium phosphate crystalline phases, such as calcium oxide ( $\text{CaO}$ ),  $\alpha$ -tricalcium phosphate ( $\alpha\text{-TCP}$ ),  $\alpha\text{-Ca}_3(\text{PO}_4)_2$ ,  $\beta$ -tricalcium phosphate ( $\beta\text{-TCP}$ ),  $\beta\text{-Ca}_3(\text{PO}_4)_2$ , tetracalcium phosphate (TTCP) ( $\text{Ca}_4\text{P}_2\text{O}_9$ ) and/or the amorphous calcium phosphate (ACP). The decomposition is predictable with the use of the phase diagram shown in Figure 6.23, by taking into account possible evaporation of the less-refractory oxide,  $\text{P}_2\text{O}_5$ .

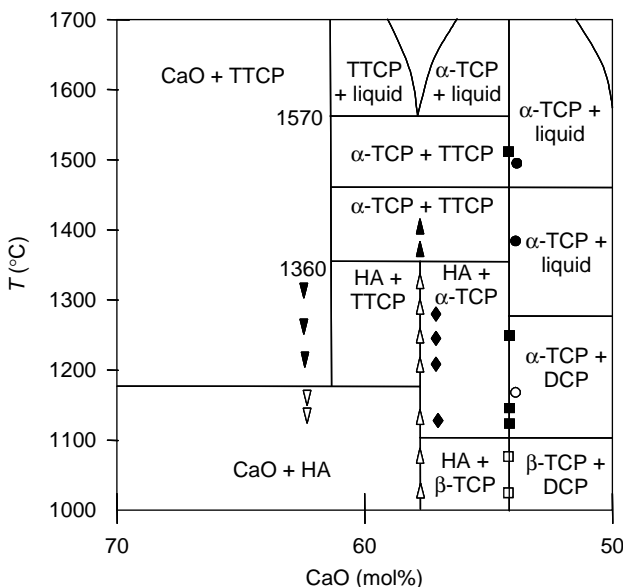


**Figure 6.23** Part of the phase diagram of  $\text{CaO}-\text{P}_2\text{O}_5$  under a water pressure of 500 mmHg (see text for identification of the various phases) (after Ribaud, 1973). Reproduced by permission of Lavoisier SAS from P.V. Ribaud, 'Composition et stabilité de phases à structure d'apatite dans le système  $\text{CaO}-\text{P}_2\text{O}_5$ -oxyde de fer- $\text{H}_2\text{O}$  à haute température', *Ann. Chim.*, 8, 1807–1813 (1973)

Fast cooling of the crystal phases inside the particles at impact with the cold surface results in conservation of the high-temperature phases in the coatings. The liquid parts of the particles are most probably transformed at impact into amorphous phases inside the coating (Dyshlovenko *et al.*, 2006a). The fractions of the phases HA, OA-OHA, TTCP,  $\alpha$ -TCP and ACP in sprayed coatings is the most important factor which determines

their biological behaviour, such dissolution of the coatings in physiological liquids (Weng *et al.*, 1997). The composition changes inside the coatings because of the thermal history of each lamella (Figure 6.24).

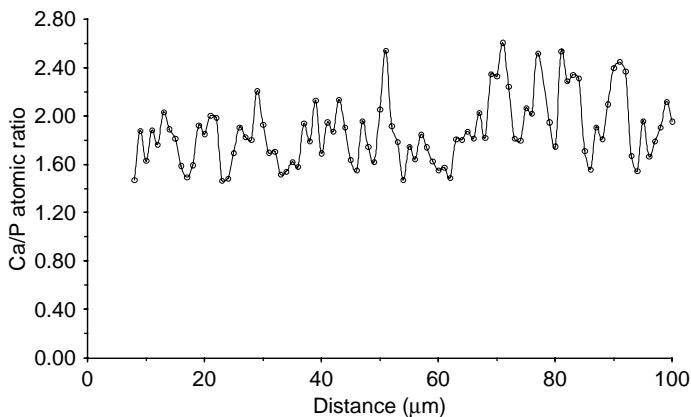


Figure 6.24 Profile of the Ca/P atomic ratio along the line of analysis inside an HA coating plasma-sprayed in air (Deram *et al.*, 2003)

The possible phase composition of a typical lamella in the coating is shown in Figure 6.25.

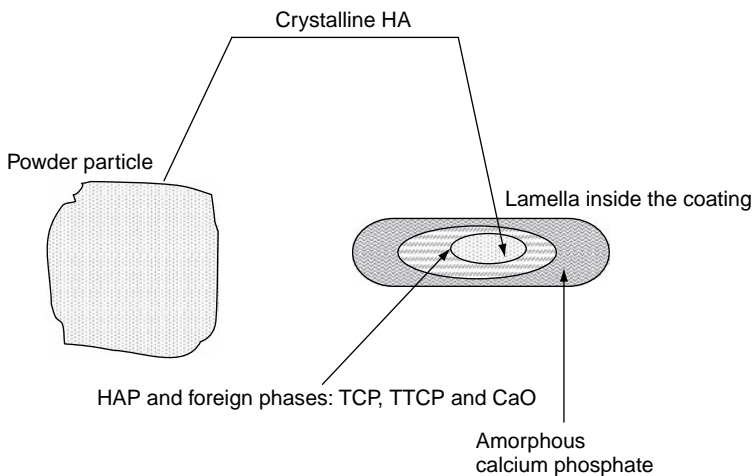
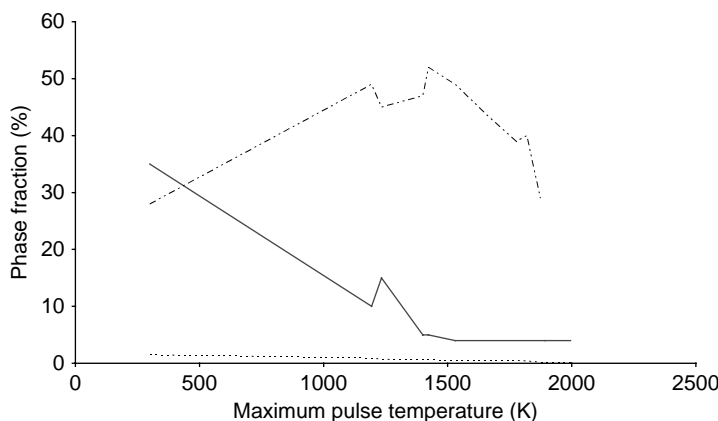


Figure 6.25 Possible phase distribution inside a lamella obtained by plasma spraying of an HA powder particle

The amorphous phase can be transformed back into crystalline hydroxyapatite after heat treatment. Treatment using a CO<sub>2</sub> CW laser made it possible to restore crystallinity in the coatings and to decrease the fraction of the amorphous phase (Figure 6.26)



**Figure 6.26** Fractions of different phases in a plasma-sprayed HAP coating after CO<sub>2</sub> laser treatment, characterized by temperature increasing with the pulse duration (the initial crystallinity of the coating was about 30 %): (—), amorphous HAP; (- - - -); crystalline HAP; (---) CaO/HAP ratio (Ranz *et al.*, 1998). Reproduced by permission of ASM International from Ranz *et al.*, 1998, *Thermal Spray: Meeting the Challenges of the 21st Century*, C. Codet (Ed.), ASM International, Materials Park, OH, USA, pp. 1343–1351

**YBa<sub>2</sub>Cu<sub>3</sub>O<sub>7-x</sub>** A high-temperature superconductor, YBa<sub>2</sub>Cu<sub>3</sub>O<sub>7-x</sub> (YBCO) has a temperature of transition of about  $T = 90\text{ K}$ , i.e. above the liquid nitrogen temperature of 77 K. YBCO powder is usually prepared by calcination and its grains crystallize in the orthorhombic phase of a superconducting composition, i.e. YBa<sub>2</sub>Cu<sub>3</sub>O<sub>x</sub> (see Chapter 1, Figure 1.20). The DTA scan of the powder shown in Figure 1.20 shows a large melting ‘event’ at a temperature of about 1270 K (Pawlowski, 1990). The finding is confirmed by the data published by Roth *et al.* (1987) who indicated a temperature of 1283 K as the highest temperature of the orthorhombic phase. On plasma spraying in air, the powder crystallizes in a metastable primitive cubic phase of very fine crystals (Figure 6.27(a)).

The cubic phase when left in air transforms to the Y<sub>2</sub>BaCuO<sub>5</sub> phase (see the phase diagram in Figure 6.28).

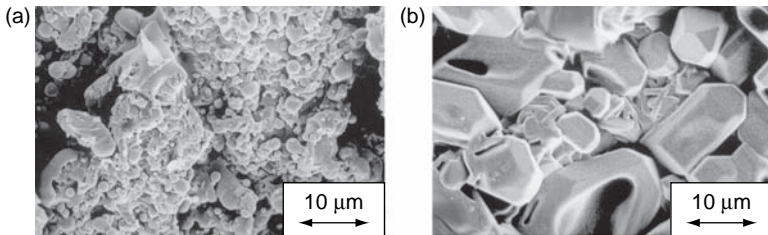


**Figure 6.27** Scanning electron micrographs (secondary electrons) of YBCO (a) as-sprayed and (b) after heat treatment at 1220 K for 3 h. The powder was prepared by calcination and has the macroscopical composition,  $\text{YBa}_2\text{Cu}_4\text{O}_{7-x}$  ( $x < 0.5$ ) and particle sizes in the range  $-56 + 28 \mu\text{m}$ . The coatings were plasma-sprayed with an SG-100 torch using 42 kW of electric power at a spray distance of 100 mm. The as-sprayed coatings had the macroscopical composition,  $\text{YBa}_2\text{Cu}_4\text{O}_{5.6}$ .

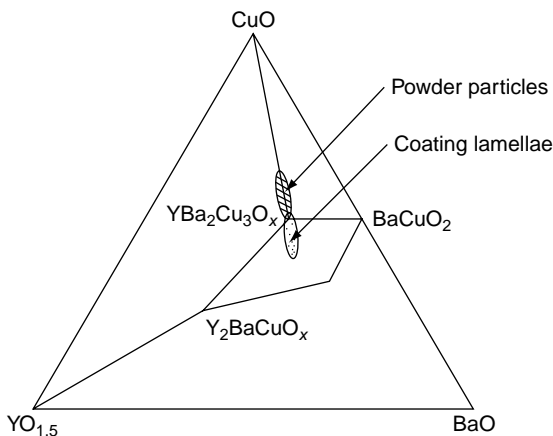


**Figure 6.28** Equilibrium phase diagram at about 1223 K showing some of the tie lines (all of these are identified in the study of Roth *et al.*, 1987) and the possible variations of chemical composition in the initial powder (due to the solid-state reaction) and in the sprayed coating (due to selective evaporation of CuO) (after Pawlowski *et al.*, 1991)

Heat treatment at temperatures higher than 1120 K enables the fine primitive cubic-phase grains to transform into orthorhombic grains after only 3 h of treatment (Figure 6.27(b)).

**WC** Tungsten carbide, WC, frequently applied for wear-resistant coatings, contains about 6 wt% C and its microhardness (HV) is equal to 2400.  $\text{W}_2\text{C}$  contains about 3.16 wt% C and has a greater microhardness (HV = 3000) but is more brittle (De Villiers Lovelock, 1998). Pure WC

does not melt under atmospheric conditions, but instead decomposes into a liquid phase and graphite above 3050 K (Figure 6.29).

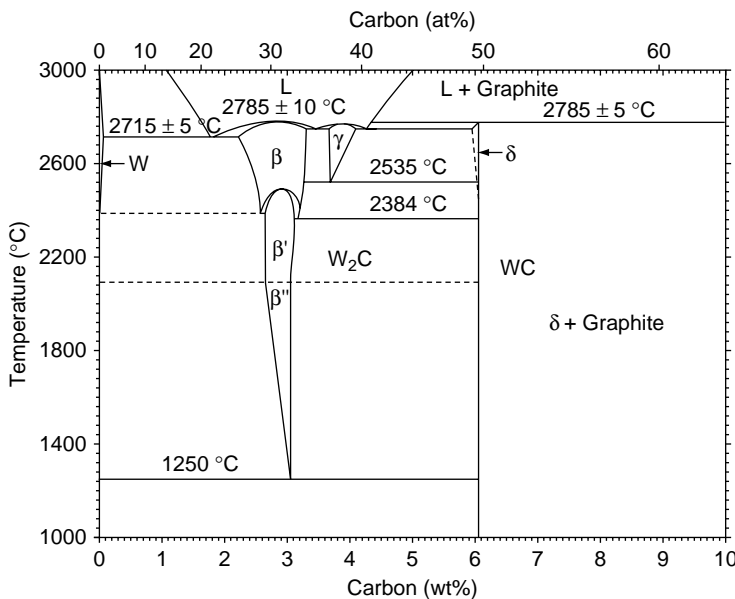


**Figure 6.29** Equilibrium phase diagram for the binary system, W–C (from De Villiers Lovelock, 1998). Reproduced from *J. Therm. Spray Technol.*, 7(3), 1998, 357–373, ‘Powder/processing/structure relationship in WC–Co thermal spray coatings: a review of the published literature’, H.L. De Villiers Lovelock, Figure 1b, Copyright (1998). With kind permission from Springer Science and Business Media

WC is mainly sprayed as a cermet with Co (less often with Ni, NiAl or NiCr) and its crystals in the particles have sizes in the range 1 to 10 µm. Upon spraying by a plasma or high-velocity flame, the following phenomena were reported (De Villiers Lovelock, 1998):

- loss of carbon and formation of  $\text{W}_2\text{C}$  or even W;
- reaction of WC with Co to give such compounds as  $\text{Co}_3\text{W}_3\text{C}$ ;
- oxidation of decarburized W to form  $\text{WO}_3$ ;
- selective evaporation of cobalt, observed especially during air-plasma spraying.

The phenomena depend mainly on the powder production method (casting and crushing, sintering and crushing, spray-drying and densification) and the spray technique (APS and HVOF).

### 6.3.2 COATINGS' INHOMOGENEITY

The coatings are not homogeneous because they are sprayed by using powders having different sizes. Furthermore, the powder particles have neither identical morphologies nor chemical and phase compositions. For example,  $\text{Cr}_2\text{O}_3$  powders containing particles which are slightly reduced to the lower oxide would result in a coating having inclusions of metallic chromium (Figure 6.30)

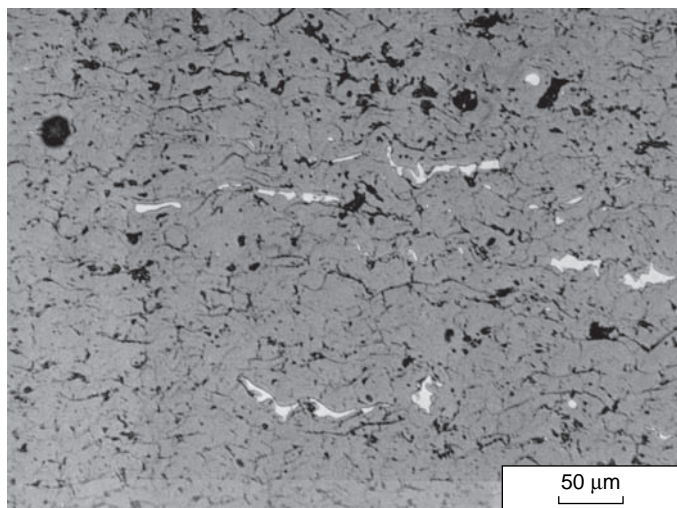


**Figure 6.30** Optical micrograph (in bright field) of a polished cross-section of a chromium oxide coating plasma-sprayed in air. The powder (shown earlier in Chapter 1, Figure 1.4) was sprayed by using an F4 torch using 50 kW of electric power with  $\text{Ar} + \text{H}_2$  working gases at a flow rate of 60 + 12 slpm

Powders feeders do not deliver a powder in a constant fashion to a torch. Similarly, in the spray techniques using wires (AS- and FS-wire), the particles formed on the wire tip can have sizes varying as much as 5 to 200  $\mu\text{m}$  (Höhle *et al.*, 1983). The electric arc used in the APS and VPS spraying techniques moves inside the nozzle, which results in flame temperature and velocity instabilities over time (see Chapter 5, Figure 5.1). The radial injection of powder to the flames associated with the particle size distribution originates from the variations in particle velocity and temperature in jets and flames.

Because of all of these factors, the particles arriving at the substrate have different velocities and can be:

- molten;
- partly molten;
- solid.

The **molten particles** form *pancake* or *flower* lamellae and contact the substrate (or previously deposited coating) only on a part of their bottom surfaces. The gaps between such lamellae have sizes of 0.01 to 0.1  $\mu\text{m}$  (McPherson and Shafer, 1982).

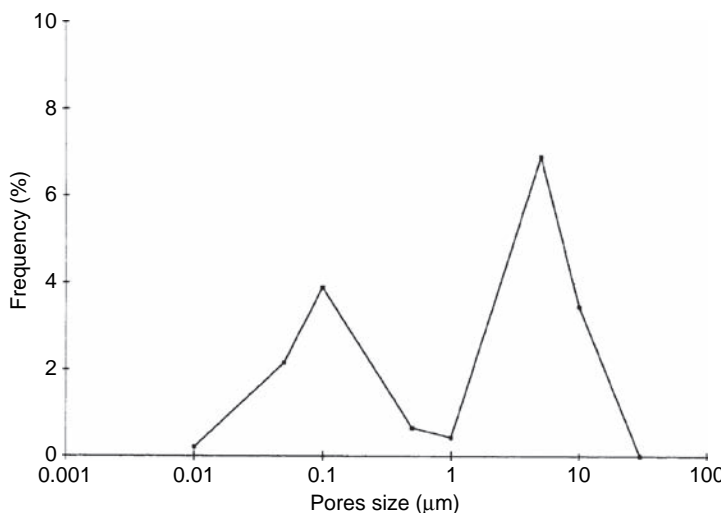


Figure 6.31 Distribution of the pore sizes in an alumina coating sprayed using a detonation gun (Bartenev, 1997)

The **partly molten** or **solid** particles cannot adapt well to the previously deposited coating. In fact, at the contacts of such lamellae, pores are generated having sizes of a few micrometres. The distribution of the pore sizes is thus bimodal<sup>15</sup> (Figure 6.31) and becomes monomodal and centred around 0.01–0.1  $\mu\text{m}$ , if the spray parameters are optimized in such a way to melt most of the impacting particles.

As Bartenev (1977) observed, regarding the bimodal distribution of the pores sizes in alumina coatings sprayed by a detonation gun one

---

<sup>15</sup> Some researchers have doubts about the bimodal distribution of pores, e.g. Dr Seiji Kuroda from the National Research Institute for Metals, Osaka, Japan.

can suppose that such a distribution is characteristic for all thermally sprayed coatings.

### 6.3.3 FINAL MICROSTRUCTURE OF SPRAYED COATINGS

Many of the defects in thermally sprayed coatings result from badly optimized processing parameters. Some of these, however, are ‘technology-specific’. A coating having all possible microstructural defects is shown in Figure 6.32.

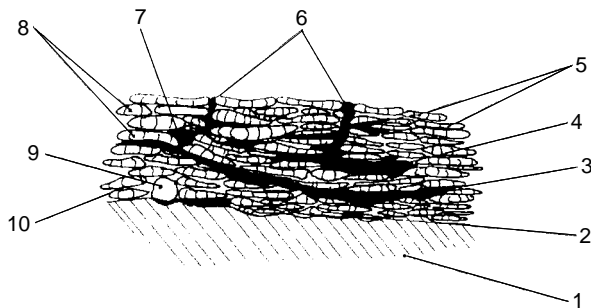


**Figure 6.32** Cross-section of a thermally sprayed coating with all microstructural defects: (1) substrate; (2) weak contact to the substrate; (3) crack resulting from one-torch-pass stresses; (4) crack resulting from relaxation of vertical stresses; (5) lamellae solidified with columnar crystals; (6) crack resulting from relaxation of in-plane stresses; (7) large pore (a few micrometres in size); (8) well-deformed lamellae; (9) powder particle that remained solid upon spraying; (10) small pore (submicrometre size)

Parameter optimization results, in general, in decreasing porosity. Some coatings are sprayed in a way which generates a large amount of porosity. A well-known example is biocompatible hydroxylapatite which is intentionally sprayed in such a way that keeps part of the particles solid in order to avoid undesirable phase transformations (Figure 6.33). The resulting coating is very porous.

Generally, the microstructure of a coating determines its properties. Consequently, an important part of technology design is specification of the desired property and a knowledge of how this property is related to the coating’s microstructure.

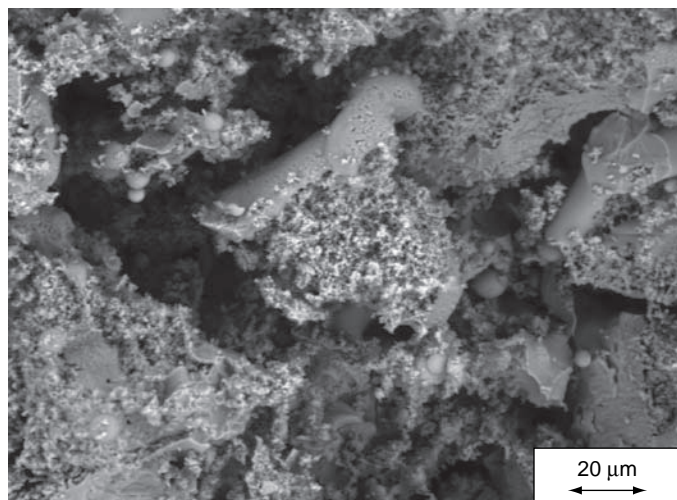


**Figure 6.33** Scanning electron micrograph (secondary electrons) of an HAP coating sprayed ‘industrially’ which shows unmelted particles disagglomerated after impact with the substrate (Deram *et al.*, 2003)

## 6.4 THERMALLY SPRAYED COMPOSITES

Composites are generally described as being a kind of mixture of two materials from the following different classes:

- metals and alloys;
- ceramics;
- polymers.

A coating on a substrate can be seen as a composite if the substrate and coating belong to different classes of materials. In thermal spraying, composites are rather understood as being a kind of a mixture of different materials in a coating. The composite coatings can be classified as a function of the mixing technology as follows (Pawlowski, 2003):

- a multi-coating in which the final coating contains many layers of different materials;
- A granular composite containing a matrix and a second phase, called the ‘reinforcement’.

As multi-coatings do not have a different deposition technology to that of individual coatings, only granular composites will be discussed in detail in the following.

#### 6.4.1 CLASSIFICATION OF SPRAYED COMPOSITES

A composite contains a matrix of metals and alloys (often Ni alloys) or ceramics ( $\text{Al}_2\text{O}_3$ ,  $\text{ZrO}_2$  stabilized with  $\text{Y}_2\text{O}_3$ ). The second phase serves mainly to mechanically reinforce the matrix or to modify another property, e.g. thermal expansion. Reinforcements have morphologies of:

- whiskers, such as  $\text{SiC}$  or  $\text{Si}_3\text{N}_4$ ;
- fibres, such as stainless steel,  $\text{W}$ ,  $\text{B}$ ;
- particles, such as  $\text{TiC}$  or  $\text{SiC}$ .

#### 6.4.2 COMPOSITE COATING MANUFACTURING

The possible morphologies of sprayed composites are shown in Figure 6.34.

Composite coatings should be manufactured in the following ways which enable a homogeneous distribution of reinforcements in the matrix:

- *Whiskers* are small monocrystals that have a cylindrical shape and a typical diameter of  $0.05\text{--}8 \mu\text{m}$  and length of  $3\text{--}80 \mu\text{m}$ . They can be blended with matrix powders to give the desired properties. The blend is sprayed onto a substrate (Iwamoto *et al.*, 1987; Berndt and Yi, 1987). The resulting coating is rather inhomogeneous because of imperfect mixing and of the similar trajectory in the plasma/flame of the reinforcement and the matrix. They have different shapes and are different materials. Consequently, their trajectories should be such that the whiskers remain solid and the matrix particles become molten. This was the way of processing used by Tsunekawa *et al.* (1987). The most recommended method of homogenous implantation of whiskers into coatings leads by an appropriate preparation of the powder. Namely, a spray-drying technique makes it possible to prepare powders with particles including

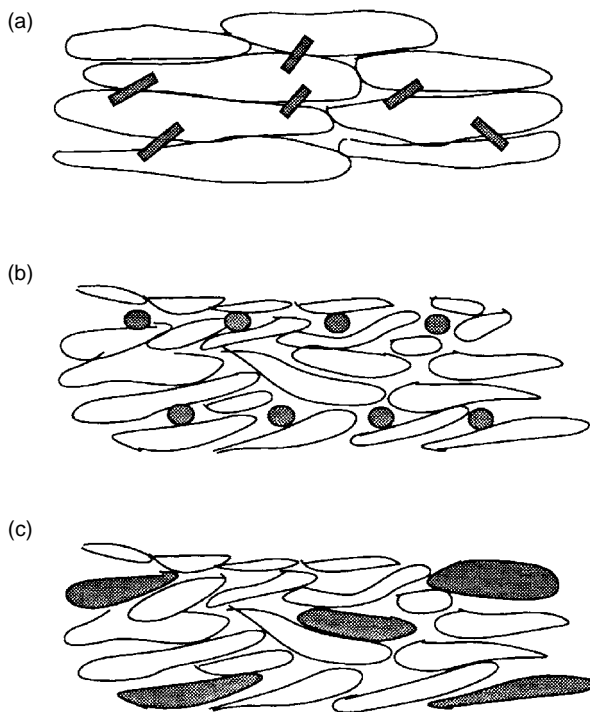


Figure 6.34 Thermally sprayed composites reinforced with (a) whiskers, (b) fibres and (c) particles

a homogenously distributed matrix and reinforcement precursors (see Chapter 1, Section 1.1.3).

- **Fibres** are wrapped around cylindrical substrates. The matrix is sprayed in a way so as to fill the space between them (Figure 6.34(b)). Then, another fibre can be wrapped around the substrate and the matrix sprayed. This procedure can be repeated until the desired thickness of coating is reached (Steffens *et al.*, 1991b). The fraction of fibres in the composite usually varies from 5 to 40 vol%.
- **Particulate** reinforcements can be prepared by blending with the matrix powder. Another possibility is the simultaneous injection of two different powders by two injection ports (Pawlowski, 1991). Finally, composite powders can be prepared by spray-drying. The precursors of the reinforcement and matrix are formulated, in desired proportions, with other components of the slurry.

## REFERENCES

- Abramov, V.V. (1961). *Residual Stresses and Deformation in Metals*, Mashgiz, Moscow USSR (in Russian).
- Alperine, S. and Lelait, L. (1992). Microstructural investigations of plasma sprayed yttria partially stabilized zirconia TBC, in *International Gas Turbine Aeroengine Congress Exposition*, Cologne, Germany, 1–4 June, Paper 92-GT-317.
- Bao, Y., Zhang, T. and Grawne, D.T. (2004). Computational model for the prediction of the temperatures in the coating during thermal spray, in *Proceedings of the International Thermal Spray Conference'04*, CD-Rom, ISBN 3-87155-792-7, DVS-Verlag, Düsseldorf, Germany.
- Balting, U. (1990). Research of plasma sprayed  $\text{Al}_2\text{O}_3$  coating/substrate composite using simulation, *PhD Thesis*, University of Aachen, Germany (in German).
- Bartenev, S.S. (1977). Distribution of the pores size and the gas permeability of oxide coatings, *Proshk. Metall.* **11**, 98–101 (in Russian).
- Bhat, H. and Herman, H. (1982). Plasma spray-quenched martensitic stainless steel coatings, *Thin Solid Films*, **95**, 227–235.
- Berger, L.-M. (2004). Titanium oxide—new opportunities for an established coating material, in *Proceedings of the International Thermal Spray Conference'04*, CD-Rom, ISBN 3-87155-792-7, DVS-Verlag, Düsseldorf, Germany.
- Berndt, C.C. and Yi, P. (1987). Strength enhancement of plasma sprayed coatings, in *Thermal Spray: Advances in Coatings Technology*, D.L. Houck (Ed.), ASM International, Materials Park, OH, USA, pp. 297–309.
- Bialucki, P., Kaczmar, W. and Gladysz, P. (1986). Residual stresses measurements of plasma sprayed coatings, in *Advances in Thermal Spraying*, Pergamon Press, New York, NY, USA, pp. 837–845.
- Carslaw, H.S. and Jaeger, J.C. (1959). *Conduction of Heat in Solids*, Oxford University Press, Oxford, UK.
- Cirolini, S., Harding, J.H. and Jacucci, G. (1991). Computer simulation of plasma sprayed coatings, I—Coating deposition model, *Surf. Coat. Technol.*, **48**, 137–145.
- Clyne, T.W. and Gill, S.C. (1996). Residual stresses in thermally sprayed coatings and their effects on interfacial adhesion, *J. Therm. Spray Technol.*, **5**, 404–418.
- Dallaire, S. (1982). Influence of temperature on the bonding mechanism of plasma sprayed coatings, *Thin Solid Films*, **53**, 41–54.
- Deram, V., Minichiello, C., Vannier, R.-N., Le Maguer, A. and Pawlowski, L. (2003). Microstructural characterizations of plasma sprayed hydroxyapatite coatings, *Surf. Coat. Technol.*, **166**, 153–159.
- De Villiers Lovelock, H.L. (1998). Powder/processing/structure relationship in WC-Co thermal spray coatings : a review of the published literature, *J. Therm. Spray Technol.*, **7**, 357–373.
- Doltsinis, I.S., Harding, J. and Marchese, M. (1998). Modelling the production and performance analysis of plasma-sprayed ceramic thermal barrier coatings, *Arch. Comput. Meth. Eng.*, **5**, 59–166.
- Dykhuizen, R.C. (1994). Review of impact and solidification of molten thermal spray droplets, *J. Therm. Spray. Technol.*, **3**, 351–361.
- Dyshlovenko, S., Pawlowski, L., Pateyron, B., Smurov, I. and Harding, J.H. (2006a). Modelling of plasma particles interactions and coating growth for plasma spraying of hydroxyapatite, *Surf. Coat. Technol.*, **200**, 3757–3769.

- Dyshlovenko, S., Pawlowski, L., Roussel, P., Murano, D. and Le Maguer, A. (2006b). Relationship between plasma spray operational parameters and microstructure of hydroxyapatite coatings and powder sprayed into water, *Surf. Coat. Technol.*, **201**, 2054–2061.
- El-Kaddah, N., McKelliget, J. and Szekely, J. (1984). Heat transfer and fluid flow in plasma spraying, *Metall. Trans. B*, **15**, 59–70.
- Espie, G., Fauchais, P., Labbe, J.C., Vardelle, A. and Hannoyer, B. (2001). Oxidation of iron particles during APS: Effect of the process on formed oxide. Wetting of droplets on ceramics substrates, in *Thermal Spray 2001: New Surfaces for a New Millennium*, C.C. Berndt, K.A. Khor and E.F. Lugscheider (Eds), ASM International, Materials Park, OH, USA, pp. 821–827.
- Fan, Q., Wang, L., Wang, F. and Wang Q. (2005). Modeling of temperature and residual stress fields resulting from impacting process of a molten Ni particle onto a flat substrate, in *Proceedings of the International Thermal Spray Conference'05*, CD-Rom, ISBN 3-87155-793-5, DVS-Verlag, Düsseldorf, Germany.
- Fantassi, S., Vardelle, M., Fauchais, P. and Moreau, C. (1992). Investigation of the splat formation versus different particulate temperatures and velocities prior to impact, in Proceedings of the 13th International Thermal Spray Conference, C.C. Berndt (Ed.), ASM International, Materials Park, OH, USA, pp. 755–760.
- Fauchais, P., Vardelle, A. and Dussoubs, B. (1999). Quo vadis thermal spraying ?, *J. Therm. Spray Technol.*, **10**, 44–66.
- Feng, Z.G., Domaszewski, M., Montavon, G. and Coddet, C. (2002). Finite element analysis of effect of substrate surface roughness on liquid droplet impact and flattening process, *J. Therm. Spray Technol.*, **11**, 62–68.
- Ferrari, M., Harding, J.H. and Marchese, M. (1991). Computer simulation of plasma sprayed coatings. II. Effective bulk properties and thermal stress calculations, *Surf. Coat. Technol.*, **48**, 147–154.
- Fukumoto, M., Huang, Y. and Ohwatari, M. (1998). Flattening in thermal sprayed particle impinging on flat substrate, in *Thermal Spray: Meeting the Challenges of the 21st Century*, C. Coddet (Ed.), ASM International, Materials Park, OH, USA, pp. 401–406.
- Fukumoto, M., Nishioka, E. and Nishiyama, T. (2001). Proposal of new criterion for splashing for splashing of thermal sprayed particle onto flat substrate surface, in *Thermal Spray 2001: New Surfaces for a New Millennium*, C.C. Berndt, K.A. Khor and E.F. Lugscheider (Eds), ASM International, Materials Park, OH, USA, pp. 841–848.
- Fukumoto, M., Nishioka, E. and Matsubara, T. (2002). Effect of interface wetting on flattening of freely fallen metal droplet onto flat substrate surface, *J. Therm. Spray Technol.*, **11**, 69–74.
- Gadow, R., Riegert-Escribano, M.J. and Buchmann (2005). Residual stress analysis in thermally sprayed layer composites, using hole milling and drilling method, *J. Therm. Spray Technol.*, **14**, 100–107.
- Gougeon, P. and Moreau, C. (2001). Simultaneous independent measurements of splat diameter and cooling time during impact on a substrate of plasma-sprayed molybdenum particles, *J. Therm. Spray Technol.*, **10**, 76–82.
- Höhle, H.-M., Steffens, H.-D. and Beczkowiak, J. (1983). Optimization of electric arc and flame spraying conditions by application of high-speed cinematography, in *Proceedings of the 10th International Thermal Spray Conference*, Vol. 80, DVS, Düsseldorf, Germany, pp. 146–148.

- Hobbs, M.K. and Reiter, H. (1987). Residual stresses in  $ZrO_2$ -8 %  $Y_2O_3$  plasma sprayed thermal barrier coatings, in *Thermal Spray: Advances in Coatings Technology*, D.L. Houck (Ed.), ASM International, Materials Park, OH, USA, pp. 285–290.
- Houben, J.M. (1988). Relation of the adhesion of plasma sprayed coatings to the process parameters, size, velocity and heat content of the spray particles, *PhD Thesis*, University of Eindhoven, Eindhoven, The Netherlands.
- Ingham, H.S., Jr (1975). Bonding of flame sprayed Ni-Al, *J. Vac. Sci. Technol.*, **12**, 773–776.
- Iwamoto, N., Umesaki, N., Endo, S. and Morimura, T. (1987). Characterization of plasma sprayed and whisker reinforced alumina coatings, *J. Mater. Sci.*, **22**, 1113–1119.
- Jones, H. (1971). Cooling, freezing and substrate impact of droplets formed by rotary atomization, *J. Phys. D: Appl. Phys.* **4**, 1657–1660.
- Kingery, W.D., Bowen, H.K. and Uhlmann, D.R. (1976). *Introduction to Ceramics*, John Wiley & Sons, Inc., New York, NY, USA.
- Kitahara, S. and Hasui, A. (1974). A study of bonding mechanism of sprayed coatings, *J. Vac. Sci. Technol.*, **11**, 747–753.
- Knott, O. and Elsing, R. (1987). Monte Carlo simulation of the lamellar structure of thermally sprayed coatings, *Surf. Coat. Technol.*, **32**, 261–271.
- Kudinov, V.V. (1977). *Plasma Coatings*, Izdatelstvo Nauka, Moscow, USSR (in Russian).
- Kuroda, S. and Clyne, T.W. (1991). The quenching stresses in thermally sprayed coatings, *Thin Solid Films*, **200**, 49–66.
- Kuroda, S., Fukushima, T. and Kitahara, S. (1992). Significance of the quenching stress in the cohesion and adhesion of thermally sprayed coatings, in *Proceedings of the 13th International Thermal Spray Conference*, C.C. Berndt (Ed.), ASM International, Materials Park, OH, USA, pp. 903–909.
- Laribi, M., Vannes, A.B., Mesrati, N. and Treheux, D. (2003). Metallurgical characterization and determination of residual stresses of coatings by thermal spraying, *J. Therm. Spray Technol.*, **12**, 234–239.
- Laszlo, T.S. (1961). Mechanical adherence of flame-sprayed coatings, *Ceram. Bull.*, **40**, 751–755.
- Lee, D. (1983). A finite elements modeling of low pressure plasma deposition process—I, Temperature analysis, *Int. J. Mech. Sci.*, **25**, 543–551.
- Li, Y. and Ishigaki, T. (2002). Thermodynamic analysis of nucleation of anatase and rutile from  $TiO_2$  melt, *J. Cryst. Growth*, **242**, 511–516.
- Li, C.-J., Liao, H.-L., Gougeon, P., Montavon, G. and Coddet, C. (2003). Experimental correlation between flattening degree and Reynolds number of spray particles, in *Thermal Spray'03: Advancing the Science and Applying the Technology*, C. Moreau and B. Marple (Eds), ASM International, Materials Park, OH, USA, pp. 863–869.
- Madejski, J. (1976a). Solidification of droplets on a cold surface, *Int. J. Heat Mass Transf.*, **19**, 1009–1013.
- Madejski, J. (1976b). Solidification de liquide projetée sur la surface d'un demi espace, *Bull. Acad. Pol. Sci., Série Sci. Technol.*, **24**, 67–70.
- Madejski, J. (1976c). Champs thermiques au cours de la projection des poudres au pistolet à plasma, *Bull. Acad. Pol. Sci., Série Sci. Technol.*, **24**, 59–66.
- Mariaux, G., Legros, E. and Vardelle, A. (2003). Modeling of coating formation and heat flux to substrate by particles and plasma jet, in *Thermal Spray'03: Advancing the Science and Applying the Technology*, C. Moreau and B. Marple (Eds), ASM International, Materials Park, OH, USA, pp. 895–903.

- Marynowski, C.W., Halden, F.A. and Farley, E.P. (1965). Variables in plasma spraying, *Electrochem. Technol.*, 3, 109–115.
- Matejicek, J., Sampath, S. and Dubsky, J. (1998). X-ray residual stresses measurement on metallic and ceramic plasma sprayed coatings, *J. Therm. Spray Technol.*, 7, 489–496.
- McPherson, R. (1973). Formation of metastable phases in flame and plasma prepared alumina, *J. Mater. Sci.*, 8, 851–858.
- McPherson, R. (1980). On the formation of thermally sprayed alumina coatings, *J. Mater. Sci.*, 15, 3141–3149.
- McPherson, R. (1981). The relationship between the mechanism of formation, microstructure and properties of plasma sprayed coatings, *Thin Solid Films*, 83, 297–310.
- McPherson, R. (1989). A review of microstructure and properties of plasma sprayed ceramic coatings, *Thin Solid Films*, 39/40, 173–181.
- McPherson, R. and Cheang, P. (1989). Microstructural analysis of Ni-Al plasma sprayed coatings, in *Proceedings of the 12th International Thermal Spray Conference*, The Welding Institute, Cambridge, UK, Paper 17.
- McPherson, R. and Shafer, B.V. (1982). Interlamellar contact within plasma sprayed coatings, *Thin Solid Films*, 97, 201–204.
- Moreau, C., Cielo, P., Lamontagne, M., Dallaire, S., Krapez, J.C. and Vardelle, M. (1991). Temperature evolution of plasma sprayed niobium particles impacting on a substrate, *Surf. Coat. Technol.*, 46, 173–187.
- Moreau, C., Cielo, P. and Lamontagne, M. (1992). Flattening and solidification of thermal sprayed particles, in *Proceedings of the 13th International Thermal Spray Conference*, C.C. Berndt (Ed.), ASM International, Materials Park, OH, USA, pp. 761–766.
- Marks, M.F., Tsunekawa, Y., Okumiya, M. and Shoeib, M.A. (2003). Splat microstructure of plasma sprayed cast iron with different chamber pressures, *J. Therm. Spray Technol.*, 12, 282–289.
- Newbery, A.P. and Grant, P.S. (2000). Droplet splashing during arc spraying of steel and the effect on deposit microstructure, *J. Therm. Spray Technol.*, 9, 250–258.
- Nykiel, Z. and Pawłowski, L. (2004). ENSCL, Lille, France, unpublished data.
- Ohmori, A. and Li, C.J. (1993). The structure of thermally sprayed ceramic coatings and its dominant effect on the coating properties, in *Plasma Spraying*, R. Suryanarayanan (Ed.), World Scientific, Singapore, pp. 179–203.
- Pawłowski, L. (1978). Analysis of applications possibility of plasma spraying process in microelectronics basing on research on vacuum plasma sprayed copper and tantalum coatings, *PhD Thesis*, Wroclaw University of Technology, Wroclaw, Poland (in Polish).
- Pawłowski, L. (1980). The vacuum plasma sprayed copper and tantalum coatings, in *Proceedings of the 9th International Thermal Spray Conference*, Nederlands Instituut voor Lastechniek, The Hague, The Netherlands, pp. 299–305.
- Pawłowski, L. (1981). Temperature distribution in plasma sprayed coatings, *Thin Solid Films*, 81, 79–88.
- Pawłowski, L. (1990). The Monash University, Melbourne, Australia, unpublished data.
- Pawłowski, L. (1991). The properties of plasma sprayed aluminum-aluminum oxide cermets, *Surf. Coat. Technol.*, 48, 219–224.
- Pawłowski, L. (2003). *Dépôts Physiques. Techniques, Microstructures et Propriétés*, Presses Polytechniques et Universitaires Romandes, Lausanne, Switzerland, p. 84 and p. 220.

- Pawlowski, L., Vardelle, M. and Fauchais, P. (1982). A model of the temperature distribution in an alumina coating during plasma spraying, *Thin Solid Films*, **94**, 307–319.
- Pawlowski, L., Lombard, D., Gitzhofer, F. and Fauchais, P. (1983). Propriétés de couches  $\text{ZrO}_2\text{--Y}_2\text{O}_3$  et Ni-Al projetées par plasma, The University of Limoges, Limoges, France, unpublished data.
- Pawlowski, L., Gross, A. and McPherson, R. (1991). Microstructure of plasma sprayed  $\text{YBa}_2\text{Cu}_3\text{O}_x$  high-temperature superconductor, *J. Mater. Sci.*, **26**, 3803–3808.
- Pershin, V., Lufitha, S. Chandra, S. and Mostaghimi, J. (2003). Effect of substrate temperature on adhesion strength of plasma-sprayed nickel coatings, *J. Therm. Spray Technol.*, **12**, 370–376.
- Poirier, T., Vardelle, A., Elchinger, M.F., Vardelle, M., Grimaud, A. and Vesteghen, H. (2003). Deposition of nanoparticles suspensions by aerosol flame spraying: model of the spray and impact processes, *J. Therm. Spray Technol.*, **12**, 393–402.
- Ranz, X., Pawlowski, L., Sabatier, L., Fabbro, R. and Aslanian, T. (1998). Phases transformations in laser treated hydroxyapatite coatings, in *Thermal Spray: Meeting the Challenges of the 21st Century*, C. Coddet (Ed.), ASM International, Materials Park, OH, USA, pp. 1343–1351.
- Ribaud, P.V. (1973). Composition et stabilité de phases à structure d'apatite dans le système  $\text{CaO}\text{--P}_2\text{O}_5$ –oxyde de fer– $\text{H}_2\text{O}$  à haute température, *Ann. Chim.*, **8**, 1807–1813.
- Robert, C., Denoirjean, A., Vardelle, A., Wang, G.-X. and Sampath, S. (1998). Nucleation and phase selection in plasma sprayed alumina: modeling and experiment, in *Thermal Spray: Meeting the Challenges of the 21st Century*, C. Coddet (Ed.), ASM International, Materials Park, OH, USA, pp. 407–412.
- Roth, R.S., Davis, K.L. and Dennis, J.R. (1987). Phase equilibria and crystal chemistry in the system Ba–Y–Cu–O, *Adv. Ceram. Mater.*, **2**(3B), 303–312.
- Safai, S. and Herman, H. (1981). Plasma sprayed materials, in *Treatise on Materials Science and Technology*, Vol. 20, Academic Press, New York, NY, USA, pp. 183–213.
- Salimijazi, H.R., Coyle, T.W., Mostaghimi, J. and Leblanc, L. (2005). Microstructure and failure mechanism in as-deposited, vacuum plasma-sprayed Ti-6Al-4V alloy, *J. Therm. Spray Technol.*, **14**, 215–223.
- Sampath, S. (1993). Microstructural characteristics of plasma spray consolidated amorphous powders, *Mater. Sci. Eng.*, **A**, 167, 1–10.
- Sampath, S. and Herman, H. (1989). Microstructural development of plasma sprayed coatings, in *Proceedings of the 12th International Thermal Spray Conference*, The Welding Institute, Cambridge, UK, Paper 53.
- Sampath, S., Herman, H. and Rangaswamy, S. (1987). Ni-Al re-evaluated, in *Thermal Spray: Advances in Coating Technology*, D.L. Houck (Ed.), ASM International, Materials Park, OH, USA, pp. 47–53.
- Samsonov G.V. (1978). *Physicochemical Properties of Oxides*, Metallurgija, Moscow, USSR (in Russian).
- Smyth, R.T and Anderson, J.C. (1975). Production of resistors by arc plasma spraying, *Electrocomp. Sci. Technol.*, **2**, 135–145.
- Sobolev, V.V. and Guilemany, J.M. (1999a). Flattening of droplets and formation of splats in thermal spraying: a review of recent work–Part 1, *J. Therm. Spray Technol.*, **8**, 87–101.
- Sobolev, V.V. and Guilemany J.M. (1999b). Flattening of droplets and formation of splats in thermal spraying: a review of recent work–Part 2, *J. Therm. Spray Technol.*, **8**, 301–314.

- Steffens, H.-D. and Müller, K.-N. (1972) Grundlagen der Haftung der thermisch gespritzten Schichten, *Adhäsion*, 2, 34–38.
- Steffens, H.-D., Wielage, B. and Drozak, J. (1991a). Interface phenomena and bonding mechanism of thermally sprayed metal and ceramic composites, *Surf. Coat. Technol.*, 45, 299–308.
- Steffens, H.-D., Kern, H., Fischer, G., Kaczmarek, R. and Janczak, J. (1991b). Mechanical behaviour of plasma sprayed fibre reinforced composites, in *Proceedings of the 2nd Plasma Technik Symposium*, S. Blum-Sandmaier, H. Eschnauer, P. Huber and A.R. Nicoll, Plasma Technik, AG, Wohlen, Switzerland, pp. 151–158.
- Steffens, H.-D., Drozak, J. and Haumann, D. (1993). Morphology of thermal sprayed particles in different spraying processes illustrated by the behaviour of molybdenum, in *Thermische Spritzkonferenz TS93*, Vol. 130, DVS, Düsseldorf, Germany, pp. 366–370.
- Szieslo, U. (1983). Residual stresses within thermal sprayed layers, in *10th International Thermal Spraying Conference*, Vol. 80, DVS, Düsseldorf, Germany, pp. 222–225.
- Takeuchi, S., Ito, M. and Takeda, K. (1990). Modelling of residual stresses in plasma sprayed coating: effects of substrate temperature, *Surf. Coat. Technol.*, 43/44, 426–435.
- Thompson, V.S. and Whittemore, O.J., Jr (1968). Structural changes on reheating plasma-sprayed alumina, *Ceram. Bul.*, 47, 637–641.
- Toma, F.-L., Bertrand, G., Klein, D., Coddet, C. and Meunier, C. (2005). Photocatalytic decomposition of nitrogen oxides over TiO<sub>2</sub> coatings elaborated by liquid feedstock plasma spraying, in *Proceedings of the International Thermal Spray Conference'05*, CD-Rom, ISBN 3-87155-793-5, DVS-Verlag, Düsseldorf, Germany.
- Tomaszek, R., Pawłowski, L., Gengembre, L., Laureyns, J., Znamirovski, Z. and Zdanowski, J. (2005). Microstructural characterization of plasma sprayed TiO<sub>2</sub> functional coating with gradient of crystal grain size, *Surf. Coat. Technol.*, 201, 45–56.
- Tomaszek, R., Znamirovski, Z., Pawłowski, L. and Zdanowski, J. (2007). Effect of conditioning on field electron emission of suspension plasma sprayed TiO<sub>2</sub> coating, *Vacuum*, 81(10), 1278–1282.
- Trapaga, G. and Szekely, J. (1991). Mathematical modeling of the isothermal impingement of liquid droplets in spraying processes, *Metal. Trans. B*, 22, 801–814.
- Tsunekawa, Y., Okumiya, M., Niimi, I. and Okumura, K. (1987). Flame spraying fabrication of silicon carbide whisker-reinforced aluminium, *J. Mater. Sci. Lett.*, 6, 191–193.
- Vardelle, A., Vardelle, M., McPherson, R. and Fauchais, P. (1980). Study on influence of particle temperature and velocity distribution within a plasma jet coating formation, in *Proceedings of the 9th International Thermal Spray Conference*, Nederlands Instituut voor Lastenchniek, The Hague, The Netherlands, Paper 30.
- Weglowski, S. and Pawłowski, L. (1981). A study of residual stresses in plasma sprayed alumina coating, in *Proceedings of the 5th International Symposium on Plasma Chemistry* Edimburgh, UK, 1–14 August, pp. 592–601.
- Wei, G., Xiong, H., Zheng, L. and Zhang, H. (2004). An advanced ceramic coating buildup model for thermal spray processes, in *Proceedings of the International Thermal Spray Conference'04*, CD-Rom, ISBN 3-87155-792-7, DVS-Verlag, Düsseldorf, Germany.
- Weng, J., Liu, Q., Wolke, J.G.C. and de Groot, K (1997). The role of amorphous phase in nucleating bone-like apatite on plasma-sprayed hydroxyapatite coatings in simulated body fluid, *J. Mater. Sci. Lett.*, 16, 335–337.

- Wilden, J. and Frank, H. (2005). Thermal spraying-simulation of coating structure, in *Proceedings of the International Thermal Spray Conference'05*, CD-Rom, ISBN 3-87155-793-5, DVS-Verlag, Düsseldorf, Germany.
- Wilden, J., Frank, H. and Müller, T. (2001). Microstructure simulation of thermally sprayed particles, in *Thermal Spray 2001: New Surfaces for a New Millennium*, C.C. Berndt, K.A. Khor and E.F. Lugscheider (Eds), ASM International, Materials Park, OH, USA, pp. 875–882.
- Wilms, V. and Herman, H. (1976). Plasma spraying of  $\text{Al}_2\text{O}_3$  and  $\text{Al}_2\text{O}_3\text{-Y}_2\text{O}_3$ , *Thin Solid Films*, **39**, 251–262.
- Xue, M., Mostaghimi, J. and Chandra, S. (2004). Prediction of coating microstructure, in *Proceedings of the International Thermal Spray Conference'04*, CD-Rom, ISBN 3-87155-792-7, DVS-Verlag, Düsseldorf, Germany.
- Yoshida, T., Okada, T., Hamatami, H. and Kumaoka, H. (1992). Integrated fabrication process for solid fuel cells using novel plasma spraying, *Plasma Sources Sci. Technol.*, **1**, 195–201.
- Zaat, J.H. (1983). A quarter of century of plasma spraying, *Annu. Rev. Mater. Sci.*, **13**, 9–42.
- Zhuang, H.Gu., Gu, Z., Wu, S. and Zhou, X. (1988). Bonding mechanism of Mo coating and its quality improvement, in *Advances in Thermal Spraying Technology and Allied Coatings Symposium*, Osaka, Japan, 13–15 May, pp. 319–325.
- Zoltowski, P. (1968). Les couches en alumine effectuées au pistolet à plasma, *Rev. Int. Htes Temp. Refract.*, **5**, 253–265.

# 7

## Methods of Coatings' Characterization

The characterization of coatings is important in:

- research and development (R&D) of a new product (see Figure 7.1);
- quality control in a production routine.

At the R&D stage, the coatings are characterized thoroughly by using many techniques. Inversely, the quality control is rapid and superficial. The techniques used in the latter have to be rapid and easy to carry out by less qualified personnel. The simplest way of controlling the coating's quality is careful observation of its surface. Such an observation enables such defects as adhesion failures, superficial cracks, etc., to be detected. More advanced microstructural investigations are often made by scanning electron microscopy (SEM), X-ray diffraction (XRD), transmission electron microscopy (TEM), mercury intrusion porosimetry (MIP) or other techniques. The properties of coatings determine their behaviour during service. The best possible test is the one made under conditions simulating 'real-service' conditions. However, such a test is expensive and sprayed coatings are most frequently characterized by testing their physical or chemical properties. Mechanical properties such as microhardness, tensile strength, fracture strength, elastic modulus, toughness or wear resistance are most often determined. The thermophysical properties of the coatings and particularly thermal conductivity, determined usually by measurements of the thermal dilatation and density at 300 K,

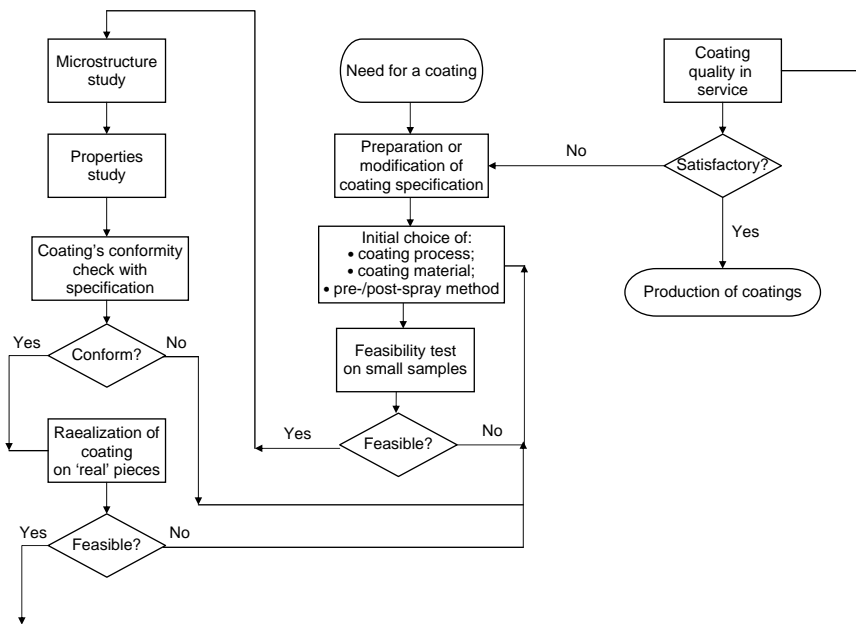


Figure 7.1 Development of a coating for a given application

specific heat and diffusivity, are also fairly frequently tested. These measurements are often accompanied by thermal shock resistance tests. The electrical and magnetic properties of the coatings are also frequently tested. Non-destructive tests with the use of thermal or acoustic waves have been introduced for the control of coatings' quality. Finally, many properties are 'cross-linked' and there is a possibility to estimate one property by measuring another. An example of such cross-linking, given by Margadant *et al.* (2001), is a correlation between the anisotropy of NiCr coatings (characterized by small-angle neutron scattering) and its electrical conductivity (determined by 4-point probe testing), as well as its elastic modulus (found by ultrasonic testing). Such cross-linking may help in reducing the number of characterization tests.

## 7.1 METHODS OF MICROSTRUCTURE CHARACTERIZATION

The microstructure of thermally sprayed coatings has a lot of particular features, as discussed in Chapter 6. This is why it is difficult to select one appropriate microstructure characterization method. On the other hand,

microstructural investigation of coatings is a useful and often necessary step in the selection of processing parameters and in achievement of specified properties (see Figure 7.1). The full coating microstructure description contains the following information (Jacobson, 1982):

- chemical composition on the macro- and micro-scale;
- grains' morphology and their orientation (texture);
- defects, such as voids or second phases, or more rarely microdefects, such as stack faults or dislocations, content and their distribution;
- distribution of the above features at different depths of coating.

The word *microstructure* does not correspond any longer to the size of the observed coatings' features. At present, the sizes vary from a few nanometres<sup>1</sup> to a few milimetres. The microstructure is tested by exciting a sample using a primary beam of species or electromagnetic waves. The sizes of the species and the wavelengths of the waves should be smaller than that of the observed features. The following species are used for excitation in different characterizations of thermally sprayed samples:

- electrons in scanning electron microscopy (SEM), electron microprobe analysis (EMPA), energy-dispersive spectroscopy (EDS), transmission electron microscopy (TEM), selected-area diffraction (SAD) and wavelength-dispersion spectroscopy (WDS);
- neutrons in neutron diffraction.

The following electromagnetic waves are practicable for excitation of samples in testing:

- infrared radiation in infrared spectroscopy (IRS);
- visible light in optical microscopy (OM) and Raman spectroscopy (RS);
- X-rays in X-ray diffraction (XRD) and X-ray photo-electron spectroscopy (XPS).

Such techniques as scanning tunnelling microscopy (STM) and atomic force microscopy (AFM) use electric field excitation. On the other hand, one can associate, using the *de Broglie* hypothesis, the species with kinetic energy  $E_k$  with a wave. The wavelength of the wave associated with an electron, is given by the following equation:

$$\lambda = \frac{h}{\sqrt{2m_e e E_k}} \quad (7.1)$$

---

<sup>1</sup> Consequently, the word nanostructure would match better to such small features.

Excitation of a sample by a primary beam results in emission of:

- species of a similar kind to the exciting one by:
  - rebounding;
  - backscattering;
  - emission from the internal shells of an atom;
- electromagnetic waves, such as infrared and visible light or X-rays.

The emitted species or waves carry information about the sample. This information should be extracted by using an appropriate spectrometer. There is a great number of different techniques used to characterize films and coatings and new techniques (or modifications of old ones) are still presented in scientific reviews. They can be roughly divided as techniques related to:

- chemical composition analyses;
- diffraction;
- microstructural analyses.

The techniques described in this chapter are collected in Table 7.1. Details about the described techniques are collected in Table 7.2.

**Table 7.1** Techniques used for the characterization of thermally sprayed coatings

Chemical composition	Diffraction	Microstructure
EDS	SAD	AFM (surface)
EMPA	DRX	OM (cross-section)
IR	Neutron diffraction <sup>a</sup>	STM (surface)
RS	—	TEM (small crystals)
XPS	—	—
XRF	—	—

<sup>a</sup> This technique is used relatively seldomly because of the expensive equipment required. The interested reader can find further information, e.g. in Keller *et al.* (2001).

**Table 7.2** Characteristics of the analytical methods used in the analysis of sprayed coatings (Pawlowski, 2003; Malingrey, 1984; Despujols, 2000)

Method	Excitation source	Energy of source (keV)	Detected signal	Depth of analysis (nm)	Resolution in depth (nm)	Lateral resolution (μm)	Sample preparation	Limit of analysis (ppm)	Tested coating features
AFM	Electric field	—	Electrons	< 1	0.001–1000	0.1–10 <sup>5</sup>	Easy	—	Surface morphology
EDS	Electrons	1–30	X-rays	10 <sup>3</sup> –10 <sup>4</sup>	1	1	Easy	10 <sup>3</sup>	Qualitative chemical composition mapped in one and two dimensions
EELS	Electrons	0.00002–2	Electrons	< 5	0.3	10 <sup>3</sup>	—	10 <sup>3</sup>	Chemical composition
EMPA	Electrons	1–50	X-rays	< 100	1	1	Easy	10 <sup>2</sup>	Chemical composition mapped in one and two dimensions
IRS OM	Infrared light Visible light	— —	Infrared light Visible light	— —	— 250	— 0.7	Easy Difficult	— —	Molecular structure Voids, unmelted particles
RS	Infrared/visible light	—	Infrared/visible light	—	—	—	Easy	—	Phase mapping in two dimensions
SAD	Electrons	20–120	Electrons	< 100	100	< 0.001	Difficult	—	Phase identification of small crystals

Table 7.2 (Continued)

Method	Excitation source	Energy of source (keV)	Detected signal	Depth of analysis (nm)	Resolution in depth (nm)	Lateral resolution ( $\mu\text{m}$ )	Sample preparation	Limit of analysis (ppm)	Tested coating features
SEM	Electrons	1–30	Electrons	< 10 (secondary electrons)	—	1	Easy	—	Surface morphology
STM	Electric field	—	Electrons	< 1	0.001–10 <sup>3</sup>	0.1–10 <sup>5</sup>	Easy	—	Surface morphology
TEM	Electrons	10 <sup>2</sup> –10 <sup>3</sup>	Electrons	< 100	100	< 0.001	Very difficult	—	Morphology of small grains
WDS	Electrons	1–30	X-rays	10 <sup>3</sup> –10 <sup>4</sup>	1	1	Easy	10 <sup>3</sup>	Quantitative chemical composition mapped in one and two dimensions
XPS	X-rays or uv light	0.2–2	Electrons	< 10	0.2–5	10–10 <sup>3</sup>	Easy	10 <sup>3</sup>	Quantitative chemical composition, valence state
XRD	X-rays	—	X-rays	> 10 <sup>3</sup>	—	—	Easy	—	Phase analysis, crystal grain size
XRF	X-rays	Power, 1–4 kW	X-rays	> 10 <sup>3</sup>	—	—	Easy	30	Quantitative and qualitative chemical composition

### 7.1.1 METHODS OF CHEMICAL ANALYSIS

#### Electron Microprobe Analysis (EMPA) and Related Techniques: Energy-Dispersive Spectroscopy (EDS) and Wavelength-Dispersive Spectroscopy (WDS)

An electron microprobe analyser is often part of a scanning or transmission electron microscope. The analyser is used to carry out chemical analysis in selected areas of the sprayed coatings. The electrons of a primary beam generate X-ray emission. The spectrum has a continuous component (called *Bremsstrahlung*) and characteristic peaks. The peaks are generated after changing one electronic level by an electron bound to an atom which has an inelastic shock with an electron from the primary beam. These peaks are 'element-specific' and, consequently, their detection makes possible the chemical analysis. There are two types of analysers which differ by the way of X-ray detection.

**Energy-Dispersive Spectroscopy (EDS)** Energy-dispersive spectrometers (EDSs) use liquid N<sub>2</sub>-cooled Si doped with Li as detectors. The X-ray photons generate electron-hole pairs. The number of pairs is proportional to the photon's energy. By putting the diode under an electric field, one can count the pairs which become transformed into an electric signal. Finally, an analog/digital converter enables numerical representation of the absorbed photons which is then classified by a multi-channel analyser as a function of their energies (Hantsche, 1988). The entire spectrum covers photon energies ranging from  $E = 1$  to 20 keV with a resolution of about 60 eV and can be recorded in some hundreds of seconds (Martin and George, 1998). This rapidity is a major advantage of the EDS technique with regard to that of WDS. Typical applications of EDS include:

- Mapping of the elements within an alloy, such as the 2-D distribution of Ni and Al in NiAl coatings plasma-sprayed with the use of dense cladded powders (Kozerski, 1986).
- Chemical qualitative analysis of the compounds grown during an NiCrAlY alloy vacuum plasma-sprayed coating exposition in hot air having a temperature exceeding 1200 K upon thermal cycling (Wu *et al.*, 1989).

**Wavelength-Dispersive Spectroscopy (WDS)** The X-rays emitted by a sample are guided towards a monochromator, which is a monocrystal with

a well-known structure (Hantsche, 1988). The radiation is diffracted, following *Bragg's law*, and the diffraction angle depends on its wavelength. The monochromators should cover the entire radiation spectrum. The following mono-crystals are frequently used (Loretto, 1984):

- LiF, for wavelengths  $\lambda = 0.1\text{--}0.3\text{ nm}$ ;
- SiO<sub>2</sub>, for wavelengths  $\lambda = 0.18\text{--}0.55\text{ nm}$ ;
- C<sub>8</sub>H<sub>5</sub>O<sub>4</sub>K, for wavelengths  $\lambda = 0.58\text{--}2.5\text{ nm}$ .

A detector measures the intensity of the radiation issuing from the monochromator. Typically, an inert-gas tube is used with the electrodes put under high voltage. The gas become ionized by the X-ray photons which produces small voltage variations. The latter are amplified and transformed electronically. A few minutes are necessary to obtain the entire spectrum when using a wavelength-dispersive spectrometer. This is a relatively long time in comparison to an EDS monochromator. High resolution and sensitivity to light elements ( $Z \leq 4$ ) are the principal advantages of this technique. Typical applications of WDS include 1-D or 2-D mapping of elements in a compound. An example of such an application is the determination of the profile of the atomic ratio of Ca/P along a line of analysis in an air plasma-sprayed hydroxyapatite coating (see Chapter 6, Figure 6.24). The ratio enables us to visualize the inhomogeneity of the phase composition in a sprayed coating. Another example is the profile of element concentration at a coating's interface, which makes it possible to determine the coating's adhesion mechanism (Kitahara and Hasui, 1974).

### Infrared Absorption Spectroscopy

The incoming light to a sample surface can be reflected, absorbed and transmitted. IR spectroscopy considers the absorbed part. The intensity of this light follows the *Beer-Lambert* law (see Chapter 4, Equation (4.4)). Some frequencies of the incoming light may excite the molecules by generating different kinds of vibrations (stretching, in-plane, wagging, etc.) producing *absorption bands*. The energies that correspond to the absorption bands correspond mainly to the mid-infrared spectrum, i.e.  $\lambda = 2.5\text{--}15\text{ }\mu\text{m}$  or wavenumbers<sup>2</sup> from about 600 to  $4000\text{ cm}^{-1}$ . A typical spectrometer has a heated resistance tube to generate radiation with a wide spectrum. The desired infrared radiation

---

<sup>2</sup> Wavenumber ( $\text{cm}^{-1}$ ) =  $10^4/\lambda$ , with  $\lambda$  in  $\mu\text{m}$ .

is selected by using optical devices acting in a similar way to a prism and focused on the sample. A solid sample can be studied by reflection (after having polished its surface) or by absorption. In this case, the solid has to be pulverized and the powder particles should be smaller than the wavelength. Then, the powder is mixed with a transparent powder such as KBr (Buzon and Roussel, 1981). The radiation, after having interacted with the sample, is detected by a receiver such as a *photoelectric cell* or a *bolometer*, which are able to detect radiation having a power in the range  $P = 10^{-9}\text{--}10^{-13}\text{ W}$  (Malingrey, 1984). IR spectroscopy can be applied to qualitatively analyse the content of water in the crystal lattice of plasma-sprayed HA coatings (see Figure 7.2).

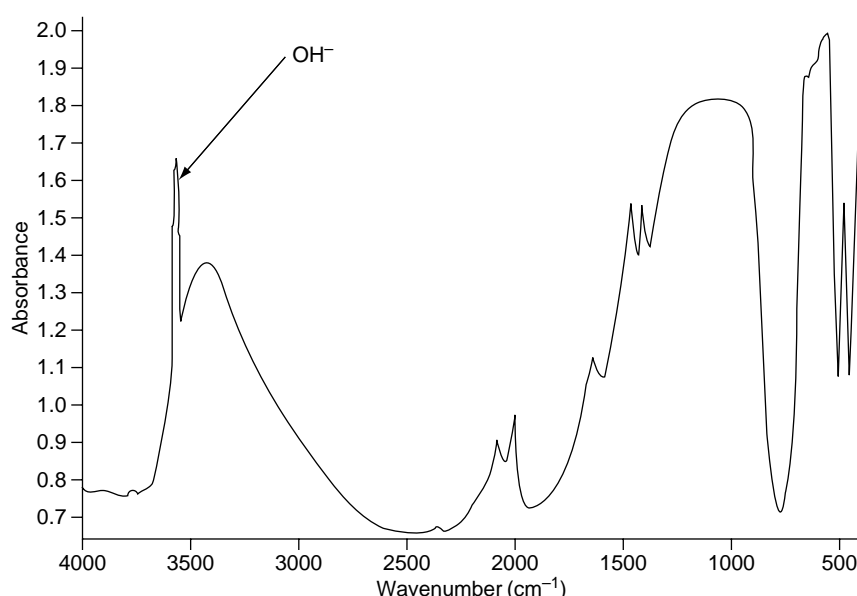


Figure 7.2 Spectrum of an HAP powder used for thermal spraying

The ‘structural water’ is lost upon spraying due to the high temperature of the plasma jet (see Chapter 6, Section 6.3.1)

### Raman Spectroscopy

The *Raman effect* results from the inelastic diffusion of monochromatic light having an initial frequency  $f_0$  by the vibrations and/or rotations of

molecules. The interaction between a photon and the molecule modifies the frequency of the incoming photons. The diffused light can have an energy lower than  $f_0$ . This case is called the *Stokes spectrum*. If the photons have a greater energy, the created *spectrum* is called *anti-Stokes*. The entire spectrum of a linear molecule vibrating with a frequency  $f_{\text{mol}}$ , diffusing monochromatic light, includes two types of signal (Turrel and Corset, 1996):

- a central signal having a frequency  $f_0$  smaller than the incident intensity;
- two signals having frequencies of  $f_0 + f_{\text{mol}}$  and  $f_0 - f_{\text{mol}}$ .

Again, in Raman spectroscopy wavenumber units are used rather than frequencies. A spectrometer is composed of a source of monochromatic light, such as a Nd:YAG laser, optical devices enabling the focusing of incident and diffused light, a spectrum analyser, such as a monochromator or a Fabry–Perot interferometer, and a light detector, such as a photodiode. Raman spectroscopy enables identification of microstructural features as oscillations and the rotations spectra are ‘molecule-specific’. An example of such identification of the phases present in a plasma-sprayed  $\text{TiO}_2$  coating is shown in Figure 7.3.

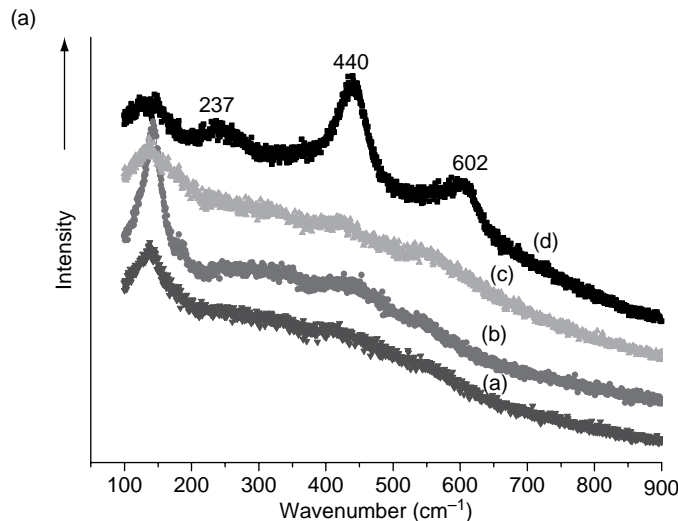


**Figure 7.3** (a) Raman spectrum of a plasma-sprayed  $\text{TiO}_2$  coating using a commercial powder and (b) a typical cross-section observed with an optical microscope showing the analysed spots (after Tomaszek *et al.*, 2006b)

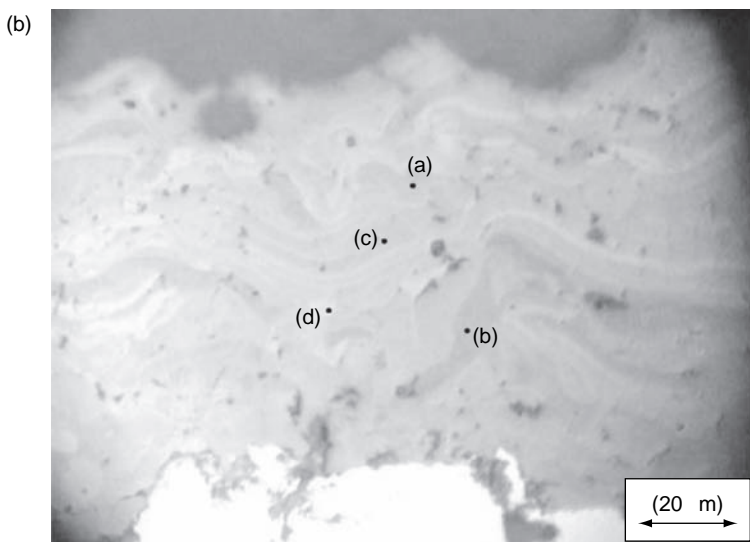


Figure 7.3 (Continued)

The spot 'd' shown in Figure 7.3(b) corresponds to rutile which has bands at  $237, 440$  and  $602\text{ cm}^{-1}$ . The spots 'a', 'b' and 'c' correspond to the Magnéli phases,  $\text{Ti}_x\text{O}_{2x-1}$ , having a low crystallinity and subjected to thermal stresses. These spots are characterized by broadened bands (at  $320\text{--}360\text{ cm}^{-1}$ ) and a frequency shifted by  $142\text{ cm}^{-1}$  with regard to that of rutile. This shifting could have resulted from oxygen vacancies. The presence of Magnéli phases in the tested samples was conformed by X-ray diffraction. Raman spectroscopy is useful in the determination of the crystal phases in plasma- and high velocity combustion-sprayed hydroxyapatite (Li *et al.*, 2004).

### X-Ray Photoelectrons Spectroscopy (XPS)

This method, also known as Electron Spectroscopy for Chemical Analysis (ESCA), consists of irradiation of a solid specimen with monochromatic photons under a very high vacuum. The radiation lies in the X-ray spectrum (typically,  $\text{MgK}\alpha$  or  $\text{AlK}\alpha$ ). The X-ray photons penetrate the solid and ionize the atoms which results in the emission of photoelectrons. The latter have a kinetic energies  $E_k$  which is the sum of the

ionization energies of different atomic orbitals and the incident photon energy, as shown in the following equation:

$$E_{\text{ion}} = hf - E_k \quad (7.2)$$

The kinetic energies are ‘atom-specific’. Consequently, one can identify atoms and their valence states (Wagner *et al.*, 1978). The samples do not need any special preparation. However, the method is very sensitive and the obtained results can correspond to some kinds of impurity, e.g. dirt, on its surface rather than to the sample bulk. The XPS method allowed confirmation of the change in valence states of cerium (from Ce (IV) to Ce (III)) in cerium oxide contained in powders of  $\text{ZrO}_2 + 2.5 \text{ wt\% } \text{Y}_2\text{O}_3 + 25.5 \text{ wt\% } \text{CeO}_2$  as the result of plasma-spraying in air (Ingo *et al.*, 1990). Another study of Ingo (1991) suggested that the coatings plasma sprayed in air and under vacuum of  $\text{ZrO}_2 + 8 \text{ wt\% } \text{Y}_2\text{O}_3$  darken and attribute this darkening to the partial reduction of  $\text{ZrO}_2$  to  $\text{Zr}_2\text{O}_3$ . The XPS technique enabled us to discover the presence of metallic chromium in commercial  $\text{Cr}_2\text{O}_3$  powders used in spraying (Figure 7.4).

The powders showing metallic chromium should be rather excluded from spraying coatings for such applications in which corrosion-resistance is specified (e.g. *anilox rolls*).

### X-Ray Fluorescence Spectroscopy (XRF)

X-ray radiation absorbed by a solid sample can produce electrons, analysed in the XPS technique, and photons. The emitted spectrum of the latter is polychromatic and is traditionally called *fluorescence*. The spectrum has a continuous envelope and some peaks, which are ‘element-specific’. The emission can be analysed, in a similar way to the EMPA technique, by an EDS or WDS detector. The X-ray tube used as the source of X-rays is typically of high power,  $P = 1\text{--}4 \text{ kW}$  (Despujols, 2000). The wavelength of the emitted X-rays can be modified by the voltage between the anode and cathode and, on the other hand, by the materials of the anode (sometimes called the *anticathode*). The sample has a surface of a few  $\text{mm}^2$  which is in contact with the incident X-ray beam and should be under vacuum to avoid contamination. The X-ray radiation reflected from the sample is analysed by an energy-dispersive or wavelength-dispersive spectrometer. The XRF technique enables both quantitative and qualitative chemical analysis and is frequently used to characterize thermally sprayed samples.

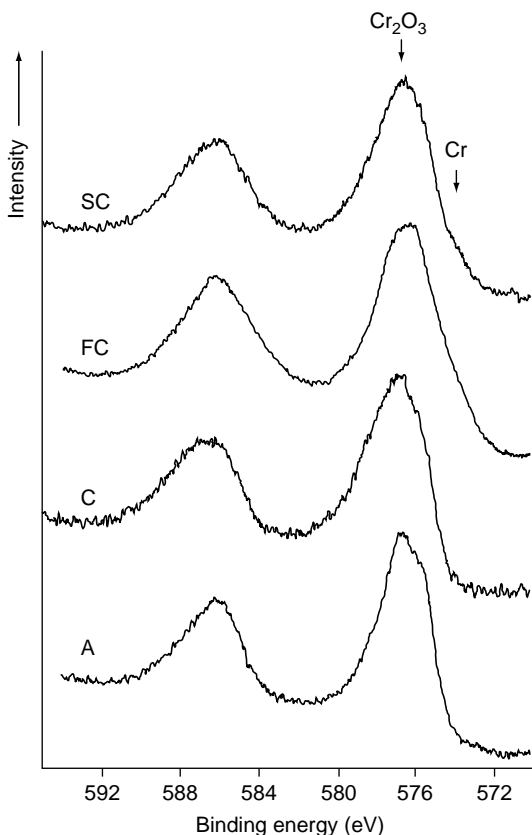


**Figure 7.4** X-ray photoelectron spectra, showing the Cr 2p photoelectron lines, of a number of Cr<sub>2</sub>O<sub>3</sub> powders prepared by: SC, sintering and crushing; FC, fusing and crushing; C, crystallization; A, spray-drying (after Pawlowski, 1996)

### 7.1.2 CRYSTALLOGRAPHIC ANALYSES

Crystallographic techniques are based on the principle of diffraction of X-rays (XRD) or the waves associated with the electrons (selected area diffraction (SAD)). The techniques can be useful in determination of:

- the phase present in a sample;
- crystal grains' texture;
- degree of crystallization of a grain visualized by transmission electron microscopy.

### Selected Area Diffraction (SAD)

The primary electron beam (e-beam) of a transmission electron microscope passes through a thin specimen. The wave associated with the beam is diffracted by the crystal plans of the specimen, following Bragg's law:

$$\lambda = 2d_{\text{hkl}} \sin \theta \approx 2d_{\text{hkl}} \theta \quad (7.3)$$

As the electromagnetic wave associated with an e-beam in TEM is short, e.g.  $\lambda = 0.0037$  nm, if the electrons are accelerated by a potential of  $U = 100$  kV (Loretto, 1984), the angle of diffraction is small and Bragg's law can be simplified, as shown in Equation (7.3).

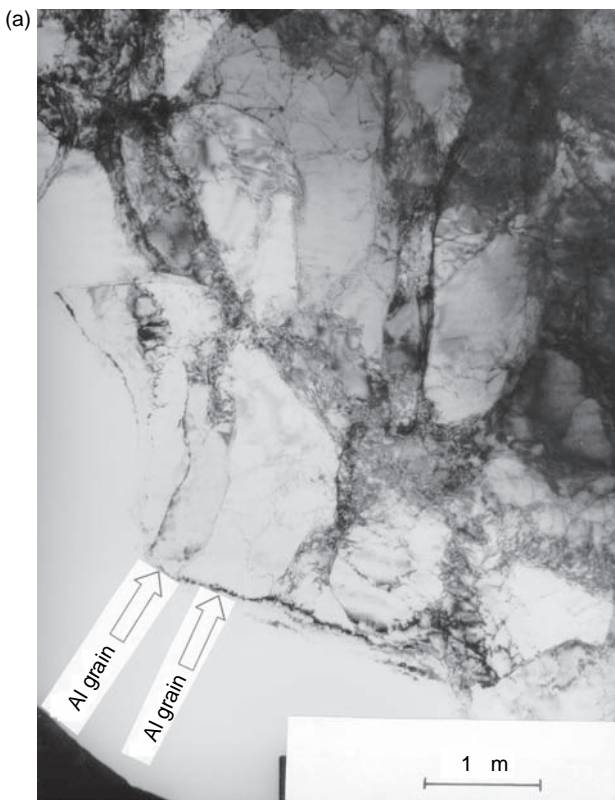


**Figure 7.5** (a) Transmission electron micrograph of the grains in an Al + SiC coating high velocity combustion sprayed and densified by 'laser shocks' (the scanning electron micrograph of this coating is shown earlier in Chapter 4, Figure 4.12) and (b) the diffraction image of the Al grains (after Podlesak *et al.*, 2000)

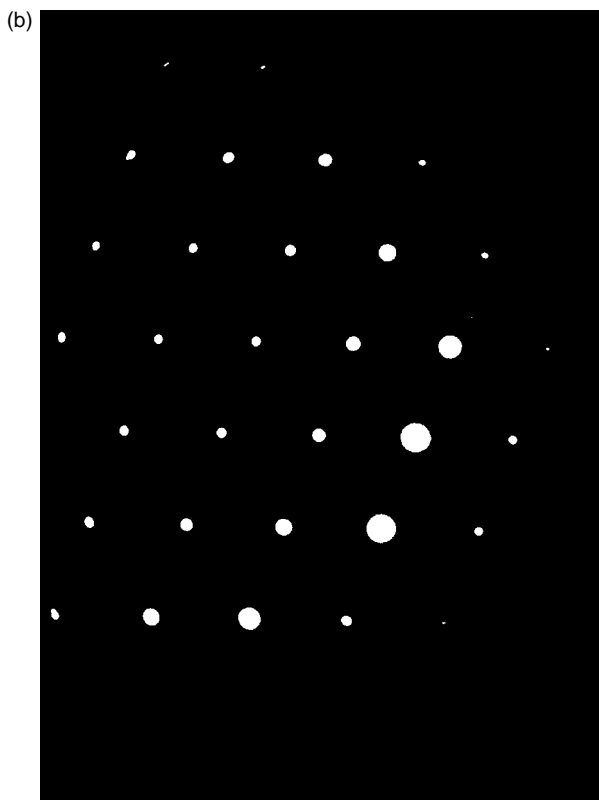


Figure 7.5 (Continued)

SAD can be well-adapted to show the degree of crystallization of a grain visualized by transmission electron microscopy. This can show, in particular, whether a grain is amorphous or crystallized. The Al grains, shown in Figure 7.5(a) are crystalline, confirmed by the individual spots corresponding to the diffracted beam shown in Figure 7.5(b).

The X-ray diagram of a poorly crystallized or amorphous sample is composed of diffused rings around a central spot (the primary beam).

### X-Ray Diffraction (XRD)

XRD is a routine technique used to carry out phase analysis of the powders used to spray and the coatings themselves. The most popular is

the Debye–Scherer method which employs monochromatic X-rays and finely powdered specimens. The principle of the method consists of the determination of the angle  $2\theta$ , which corresponds to the diffraction of a monochromatic X-ray beam of a wavelength  $\lambda$  on the crystallographic planes at a distant  $d_{hkl}$  from each other, following Bragg's law (see Equation (7.3)). The resulting  $d_{hkl}$  spacings' pattern can be attributed to a phase via the use of the 'actualized' yearly standard JCPDS<sup>3</sup> index cards. The X-rays are generated in a tube with an *anti-cathode* made of, e.g. Mo ( $\lambda = 0.071\text{ nm}$ ) or Cu ( $\lambda = 0.154\text{ nm}$ ). The source of radiation and its detector are usually placed on the circumference of a circle with the tested sample at its centre. Such a geometry is known as the Bragg–Brentano arrangement (Martin and George, 1998). This method is easy to conduct, especially with modern computerized diffractometers, and detailed descriptions of this technique can be found in many textbooks (e.g. Cullity, 1977). The coatings can be used with a substrate or can be detached off it prior to the test. The diagram obtained for the coating on a substrate may display two effects:

- stresses in the coatings, resulting in shifts of the peaks.
- peaks corresponding to the substrate if the coating is thin.

An example of these two effects is shown in the diagram in Chapter 6, Figure 6.21(b), obtained for a TiO<sub>2</sub> coating obtained by suspension plasma spraying onto a steel substrate. The peaks shown in this diagram are shifted by an angle  $2\theta$  of  $0.370^\circ$  in the direction of smaller angles with regard to the reference. This shifting could have resulted from tensile thermal stresses generated at cooling after processing. The XRD method enables identification of the phases of minimum content in the sample of about 5 wt%. The diffracted peaks become wider for small crystals. Knowing the full width of the peak at half maximum (FWHM) which together with a correction resulting from the experimental set-up gives a corrected-width  $\beta$ , the mean crystal size  $D$  can be calculated from the following equation (Cullity, 1977):

$$D = \frac{0.9\lambda}{\beta \cos \theta} \quad (7.4)$$

---

<sup>3</sup> Joint Committee on Powder Diffraction Standards, USA.

The values calculated from the above equation should be corrected for the strain resulting from microstresses. A *Williamson and Hall* diagram is useful in visualizing this effect (Deram *et al.*, 2003)

### 7.1.3 MICROSTRUCTURE ANALYSES

Observations of microstructure are made on the surface of a coating by scanning electron microscopy, scanning tunnelling microscopy and atomic force microscopy. The coatings' cross-section reveals their interior. Large features inside the coating, such as pores, cracks and lamellae, can be visualized by an optical microscope and a scanning electron microscope. Finally, a transmission electron microscope enables observation of the internal morphology of small crystals.

#### Optical Microscopy (OM)

Optical microscopy<sup>4</sup> is used at present in a routine way. It provides basic information about the coating and substrate microstructures. This approach enables analysis of the following (Fowler, 1991):

- voids;
- unmelted particles;
- deformation (mechanical or thermal) of the substrate under the tested coating;
- different phases in the tested coating, such as metallic and ceramic in a cermet coating;
- lamellae obtained from particles that have been modified chemically at spraying by reduction or oxidation;
- solid inclusions resulting from contamination by particles of copper or tungsten upon plasma spraying (in the coating's body) or from pre-spray processing (at the interface between the coating and substrate).

Prior to microscopic observation, the tested sample must be prepared metallographically. An observation can be made on the longitudinal or transverse section of the coating. The longitudinal section (perpendicular

---

<sup>4</sup> Thermally sprayed coatings are usually tested with an 'inverted microscope' (sometimes called a *metallographic microscope*).

to the coating's surface) provides an insight into the coating's body and into the interface between the substrate and coating and is more frequently applied.<sup>5</sup> This procedure has the following steps:

- First, as the area of microscopic observation is small, it is important to select a typical part of the sprayed piece (at the quality-control stage) or the part in which microstructural defects are to be expected, such as edges or sharp angles (at the R&D stage).
- The selected part should be impregnated with a low-viscosity resin. This serves to reinforce, in particular, porous and brittle coatings. Such an impregnation was used by, e.g. Rückert *et al.* (1989), to prepare sections of ZrO<sub>2</sub> coatings plasma-sprayed with spray-dried powders. These powders contain many fine voids (see Chapter 1, Figure 1.9) which were expected to render porous the sprayed deposit.
- The impregnated sample is 'sectioned'. Typically, diamond cutting wheels are used. Care should be paid to ensure that the wheel first engages into the coating and then into the substrate. Otherwise, coatings of low adhesion could detach from the substrate (Elssner *et al.*, 1990). Low-speed cutting is recommended. The specimen should be cooled when cutting with water or oil. The latter is applicable for water-sensitive materials, such as YBa<sub>2</sub>Cu<sub>3</sub>O<sub>7-x</sub>.
- The sectioned specimen is embedded in the resin. Typical mounts have diameters of 25–35 mm. A low-viscosity, 'cold-hardening resin', such as Epofix™, is recommended for embedding. A 'hot-hardening' resin is to be avoided for brittle coatings that might crack upon heating. Embedding under vacuum is also recommended for porous coatings (Pawlowski, 1998). Mounted samples are subjected to grinding which should produce a flat surface of the material that was not affected by the cutting, i.e. at least 0.2–2 mm should be removed. This step is usually made by the use of a coarse-grade SiC paper (grade from 220 to 1200) which is attached to the rotating disc in the grinding/polishing set-up, such as the one shown in Figure 7.6, in one or more steps.

The dense specimen can be ground by using a load of 300 N (see entry 1 in Table 7.3.) and the porous specimen with a much smaller load (entry 3 in Table 7.3). Application of a greater load for grinding of porous coatings would result in a *smearing effect*, i.e. artificial filling of the

---

<sup>5</sup> Longitudinal cross-sections are used in this present book.



Figure 7.6 A metallographical grinding and polishing machine. Reproduced by permission of Struers A/S, Rodovre, Denmark

voids in the coating. More details about mounting in a resin can be found in Puerta (2005).

- Grinding with coarse SiC papers might be followed by lapping with a diamond grain suspension ( $6\text{ }\mu\text{m}$  diamond grains) on a self-lubricating Petrodisc™ or other 'hard-surface' cloths. At this stage of metallographic preparation, it must be ensured that the specimen keeps its microstructural integrity and phenomena, such as 'smearing' the 'real' voids or pulling out the less-bound particles, do not occur. To stress the importance of keeping the coating integrity, Blann *et al.* (1989) and Diaz and Blann (1991) suggested calling this part of the metallographic preparation as the *sample-integrity stage*. At this stage, the load is generally lower than by grinding, namely  $F = 50\text{--}120\text{ N}$ . A lower load should be applied at a higher coating porosity.
- Polishing completes the metallographic preparation. The surface of the sample must be free of fine scratches and have a lustrous texture for microscopic examination. The final polishing is typically carried out by using diamond suspensions or pastes of gradually decreasing grains (from 3 down to  $0.25\text{ }\mu\text{m}$ ) on hard-surface clothes and could be finished by using  $\text{Al}_2\text{O}_3$  suspensions on soft cloths. In the last step, the interlammellar contacts within the coating should be revealed (see Chapter 6, Figure 6.20) and different phases should be recognized, such as metallic inclusions in  $\text{Cr}_2\text{O}_3$  coatings (see Chapter 6, Figure 6.29). The polishing should be conducted under a steadily reduced load.

Table 7.3 Typical metallographical procedures for different types of thermally sprayed coatings

Number	Reference	Particular aspect of microstructure	Coating	Spray technique	Stage <sup>a</sup>	Abrasive or cloth <sup>b</sup>	Lubricant <sup>c</sup>	Rotation speed (rpm)	Load (N)	Time (min)
1	Barbezat <i>et al.</i> , 1991	Dense metallic NiCrAl, NiCoCrAlY	VPS	G	S-220	W	300	300	300	1.5
2	Elsner <i>et al.</i> , 1990	Dense, oxide, Al <sub>2</sub> O <sub>3</sub> , Al <sub>2</sub> O <sub>3</sub> +TiO <sub>2</sub> ceramic	APS	G	S-220	W	300	90	Until flat	
3	Rückert, 1989	Porous, carbide ceramic	WC-12Co	APS	G	S-150	W	21	200μm removed 75μm removed	

<sup>a</sup> G, grinding; L, lapping; P, polishing.

<sup>b</sup> S, SiC; A, Al<sub>2</sub>O<sub>3</sub>; D, diamond; S, soft; M, medium; H, hard.

<sup>c</sup> A, alcohol-based; O, oil-based; W, water-based.

The interested reader can find useful procedures for the metallographic preparation of thermally sprayed coatings, e.g. in the journals *Structure*<sup>6</sup> and *Practical Metallography*. Procedures for typical coatings were recently reviewed by Eskling (1997). Observations are made most frequently by using the 'bright-field' facility of a microscope. In some situations, other facilities or methods can also be used, such as described in the following.

- Differential interference contrast (DIC) or Nomarski interference contrast (NIC) converts the differences in the polished depths into differences of brightness. These facilities enable distinction between the areas of polished cross-sections having a different hardness. For example, Gräf (1981) used this method to detect the nitrides in titanium coatings plasma sprayed under a nitrogen atmosphere. On the other hand, Shinde *et al.* (1987) used the DIC facility to identify the features generated in coatings upon degradation of a zirconia thermal-barrier coating (TBC) during heat treatment.
- The interference-layer technique, which consists of the application of thin films, such as ZnSe or ZnTe, by vacuum-evaporation (Pepperhoff, 1965) or Pb sputtered in oxygen (Gräf, 1981) onto the polished surface of the coating section. This method enabled Oberländer and Kvernes (1983) to visualize different phases in thermally cycled TBCs.
- Chemical etching is useful in revealing the microstructure of dense metallic coatings, such as those sprayed using a self-fluxing NiCrBSi alloy (Leistner, 1993) and also to observe the heat-affected zone in part of the substrate under the coating. The etchants depend on the coating material. H<sub>3</sub>PO<sub>4</sub> was used to etch a vacuum-sprayed Rene' 125 alloy by Ritter and Henry (1982). Other etchants have been described by Blann (1992).

Light microscopy is also useful in image analysis. This analysis can be made with a set-up which is frequently proposed by the microscopes' manufacturers. The procedure consists of setting the 'grey-level' on the microscope image to separate the microstructural features. The area of one feature is, by the use of a suitable mathematical treatment, related to the total area of the image (Fowler *et al.*, 1990; Pawłowski, 1987a). Image analysis enables quantitative analysis of the voids which are larger than 0.5 µm, being the resolution limit for light microscopy. The contribution to the total porosity, resulting from the

<sup>6</sup> *Structure* has been published on-line since 2004.

smaller voids, should be tested by using porosimeters. A fraction of the unmelted particles in the coatings cannot be determined by using an automatic analyser because of the missing ‘brightness difference’ concerning the matrix. This microstructural feature can be quantitatively determined by using a manual device. A manual device, developed by Pawlowski (1987a), enabled quantitative analysis of the coating shown in Chapter 6, Figure 6. 20. The coating was estimated to have:

- a total porosity of 9.6 % and a maximum void size of 15 µm;
- a fraction of unmelted grains equal to 4.4 % and a maximum size of 26 µm, which is well inside the limits given for manufacturers of the initial powder, i.e.  $-46 + 16 \mu\text{m}$ .

### Scanning Electron Microscopy (SEM)

E-beams of energies up to 50 keV and diameters down to 5 nm are used in SEM to scan the surfaces of samples. The scanned areas are

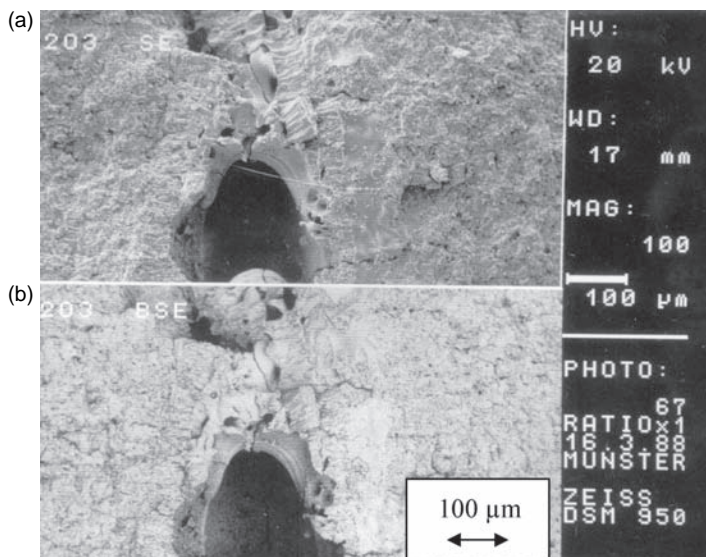


Figure 7.7 Scanning electron micrographs of  $\text{Al}_2\text{O}_3$  applied as a corona roll (a similar coating to that shown earlier in Chapter 6, Figure 6.20) after an ‘electric breakdown’, resulting in the formation of a channel. Observations of fractured section were made with (a) secondary electrons and (b) backscattered electrons

squares with sides of lengths between  $5\text{ }\mu\text{m}$  and 1 mm. The specimens to be observed can have much larger dimensions of up to  $100 \times 100\text{ mm}$ . The primary e-beam ionizes the atoms near to the surface which results in the emission of *secondary electrons* (SEs) of energies up to 50 eV. These electrons enable the surface morphology to be observed. The electrons of the primary beam are elastically scattered inside the sample and are called *backscattered electrons* (BSEs) and can be used to contrast the elements if the difference in their atomic numbers,  $\Delta Z$ , is greater than 3 (Postek *et al.*, 1980). The more energetic backscattered electrons are moving in a straight line, which attenuates the signal coming from the 'holes'. The surface relief is consequently less visible. This effect, known as the *shadow effect*, is shown in Figure 7.7.

Specimens for SEM investigations should have electrically conducting surfaces. Insulating materials are usually coated by a film of evaporated carbon or sputtered gold. Fracturing of the observed surfaces should be carried out shortly before investigation in order to avoid any contamination.

SEM with a secondary electron (SE) detector is used as a routine method to observe the following:

- individual lamella after a 'splash' (see Chapter 6, Figure 6.2);
- surfaces of as-sprayed coatings (see Chapter 6, Figures 6.4 and 6.18);
- the fractured cross-section of an as-sprayed coating, showing fine-grained microstructure (see Chapter 6, Figure 6.12), fine structure (see Chapter 6, Figure 6.26(a)) or recrystallized microstructure (see Chapter 6, Figure 6.26(b));
- the fractured surface of a coating degraded by thermal fatigue (Shinde *et al.*, 1987) or wear (Guyonnet and Fauchais, 1975);
- a metallographically polished cross-section, enabling distinction of 'real' voids from the *pull-outs*.

A scanning electron microscope, equipped with a back scattered electron (BSE) detector was used by Hermansson *et al.* (1985) to distinguish the  $\text{SiO}_2$  inclusions in  $\text{Cr}_2\text{O}_3$  coatings. These authors reported that such a detector enabled distinction of the reduced  $\text{CrO}$  within a  $\text{Cr}_2\text{O}_3$  matrix. Such a detector was also applied by Veilleux *et al.* (1987) to observe the phases in TiC coatings and by Diaz (1992) to visualize the spatial distribution of different elements in high-temperature alloy coatings. Finally, Shankar *et al.* (1983a) applied a BSE detector to visualize the different concentrations of Zr and Mg in a  $\text{ZrO}_2 + 20\text{ wt\%}$

MgO coating. Scanning electron microscopy also enables measurements of the absorbed electron current. This method was used to characterize the microstructure of plasma-sprayed alumina by Beauvais *et al.* (2004).

### Transmission Electron Microscopy (TEM)

Electrons of the primary e-beam in transmission electron microscopy have energies of  $E = 100\text{--}200\,\text{keV}$  and can even reach 1000 keV. The resolution in TEM imaging is as high as 0.2–0.3 nm. The specimens must be transparent for the electrons and should have thicknesses in the range 100–200 nm (for a 100 keV microscope), while the area of observation in a TEM foil is about  $S = 0.03\,\text{mm}^2$  (Jacobson, 1982). TEM also enables phase-analysis of the same area that the micrograph is taken, via the use of selected area diffraction (see Figure 7.5). Imaging in TEM is made by observation of the directly transmitted beam. Inserting an aperture which selects transmitted electrons from the diffracted ones, enables selected area diffraction (SAD). The minimum area suitable for SAD analysis is about 1000 nm. The e-beam traverses the specimen and loses energy in many ways, e.g. ionization. The ionization energy is ‘element-specific’ and it is possible to achieve chemical analysis by extracting this information from the transmitted e-beam. This technique is known as electron energy-loss spectrometry (EELS) and enables the analysis of elements from lithium upwards ( $Z > 3$ ). The specimens (usually called *foils*) suitable for TEM have typical diameters of 3 mm and must be ‘thinned’ from the centre down to 200–300 nm (thicker for high-voltage microscopes). A schematic of a typical preparation for a sample for TEM investigation is shown in Figure 7.8.

The specimens were initially cut with a diamond saw. Then, two segments, arranged with the coated sides face-to-face, were ‘glued’ with epoxy resin. Subsequently, the samples were cut to obtain flat specimens with a size of about 3 mm. Then, the thicknesses of the specimens were reduced, in a first step, to approximatively 100  $\mu\text{m}$  by using SiC grinding paper (graded 15, 10 and 5  $\mu\text{m}$ ) and, in a second step, by means of a one-sided ‘dimple-grinding’ to approximately 40  $\mu\text{m}$  in the central part. After ‘gluing’ onto a copper ring of 3 mm diameter, the specimen was thinned by ‘ion-milling’. To minimize artefacts, the energies of the ions were set to a few kV and the angles were as small as 3–5°. ‘Ion-beam thinning’

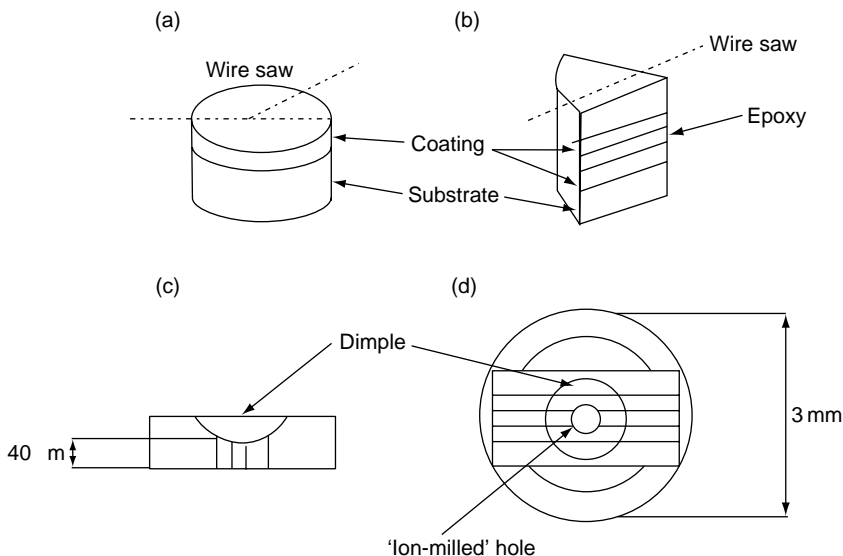


**Figure 7.8** Schematic of the preparation of an HVOF-sprayed and 'laser-shocked' treated Al+SiC composite sample for TEM investigation. The transmission electron micrograph and selective area diffraction (SAD) image of the sample are shown earlier in Figure 7.5 (after Podlesak *et al.*, 2000)

is a tedious process, with a thinning rate of a few inches per hour and it might take a few days to prepare the TEM foil. The microstructural features of the thermally sprayed coatings, evidenced by the use of TEM are collected in Table 7.4.

#### 7.1.4 OTHER APPLIED METHODS

The *Secondary-Ion Mass Spectrometry* (SIMS) technique was used by Dearnley *et al.* (1991) to detect the presence of hydrogen and oxygen ions which could have been dissolved in the particles during vacuum-plasma spraying of titanium. Another advanced method, *Extended X-ray Absorption Fine Structure* (EXAFS), was used by Sampath (1993) to analyse the fine structure of amorphous alloy powders processed by a plasma in air and under vacuum. Finally, *Mössbauer spectroscopy* was used by Leidheiser *et al.* (1984) to provide evidence that a flame-sprayed aluminium coating does not interact in any 'chemical way' with a cobalt substrate. These authors drew the conclusion that the coating

**Table 7.4** Features of the microstructure of thermally sprayed coatings, evidenced by using TEM and related methods

Number	Feature	Reference	Coating	Post-spray treatment <sup>a</sup>	TEM		
					Voltage (kV)	SAD <sup>a</sup>	EELS <sup>a</sup>
1	Columnar grains	Harmsworth and Stevens, 1992	ZrO <sub>2</sub> + 6–8 wt % Y <sub>2</sub> O <sub>3</sub>	N	—	N	N
2	Fine equiaxial grains (brick-wall)	Safai and Herman, 1977; Wang and Herman, 1989	Al Mg-Al <sub>2</sub> O <sub>4</sub>	N	— 120	Y Y	N
3	Amorphous grains	Wilms and Herman, 1976	Al <sub>2</sub> O <sub>3</sub>	N	—	Y	N
4	Twins	Finlayson <i>et al.</i> , 1990	YBa <sub>2</sub> Cu <sub>3</sub> O <sub>7-x</sub>	Annealing at 1123 K in O <sub>2</sub>	—	N	N
5	Unmelted particles	Fournier <i>et al.</i> , 1985	TiC	N	200–1000	N	Y
6	Interlamellar voids	McPherson and Shafer, 1982	Al <sub>2</sub> O <sub>3</sub>	N	—	N	N

<sup>a</sup> Y, yes; N, no.

adheres by a ‘mechanical-interlocking’ mechanism (see Chapter 6, Figure 6.11).

## 7.2 MECHANICAL PROPERTIES OF COATINGS

Thermally sprayed coatings are frequently applied for their wear-resistance. Wear is a very complicated process which depends on the following (Eyre, 1984):

- Input parameters, namely:
  - load;
  - temperature;
  - velocity;
  - time.
- Process parameters, namely:
  - materials in contact;
  - lubricant (if any);
  - environment;
  - geometry of contact;
  - surface preparation;
  - operational procedure.
- Output parameters, namely:
  - friction;
  - noise;
  - vibration;
  - worn mass or volume.

Consequently, wear is difficult to characterize. Inversely, hardness or microhardness is relatively easy to measure but these properties do not always help in predicting the mechanical aspects of coatings’ behaviour in service. This is why it is recommended to carry out a few complementary mechanical tests, or even to simulate the real conditions of coatings’ service. The tensile adhesion test (TAT) is universally used to characterize the adhesion of a coating to a substrate. Fracture mechanics-related adhesion tests are sometimes used to characterize adhesion.

Credit for initiating the work in this area must go to *Professor Reginald McPherson*.<sup>7</sup> Finally, classical 3- and 4-point bending tests are applied to characterize the strength of the coatings when detached from substrates (for materials that are used as ‘free-standing bodies’). Most of the mechanical properties are characterized by using just a few methods, as given in Table 7.5.

**Table 7.5** Tests for mechanical properties of coatings (Brotzen, 1994). Reproduced by permission of ASM International from Brotzen, 1994, *Int. Mater. Rev.*, 39, 24–45

Test	Mechanical property
Indentation	Hardness, microhardness, adhesion, toughness, modulus of elasticity, strength
Scratch test	Adhesion of thin films
Tensile test	Adhesion, modulus of elasticity, toughness
Bulge test	Estimations of modulus of elasticity and strength
Beam deformation test	Modulus of elasticity and strength

### 7.2.1 ADHESION DETERMINATION

The experimental measurement of adhesion can be achieved by defining the following (Rickerby, 1996):

- force of adhesion (often defined as the maximum force per unit area) exerted when two materials are separated;
- work of adhesion, namely the work in detaching two materials from one another.

The principle methods used to test thermally sprayed coatings are as follows:

- tensile adhesion test (TAT), also known as the ‘pull-off’ method;
- a family of tests, based on fracture mechanics, including the double-cantilever beam (DCB) method, bending tests and indentation test;
- other methods, such as the peel test, scratch test and ‘laser-shock’ test.

<sup>7</sup> Professor Reginald (Reg) McPherson had been for a long time associated with the Department of Materials Engineering at The Monash University in Melbourne, Australia. Sadly, died shortly after his retirement from active academic life. The Thermal Spray Society elected him in 1996 to their ‘Hall of Fame’.

### Tensile Adhesion Test

This involves a coating sprayed onto the face of a cylindrical specimen, 'glued' with a resin to the sand-blasted face of a similar uncoated specimen and applying a tensile load to such an assembly (Figure 7.9).

Tensile strength results from division of the maximum load applied at rupture by the cross-sectional area. The adhesion strength of the coating is given if the failure occurs only at the coating–substrate interface. The cohesive strength of the coating is given if rupture is entirely within the coating. If the failure occurs in a combination of these locations (most frequent test result), no interpretation can be provided. Users generally apply the ASTM 633-01<sup>8</sup> Standard but there are also other procedures and other national standards. The major recommendations of ASTM 633-01 concern:

- specimen diameter should be in the range 23 to 25 mm;
- specimen length should be 38.1 mm;
- coating thickness should be more than 380 µm;
- number of tested specimens should be at least five;
- tensile load should be applied, with a constant rate between 0.013 and 0.021 mm/s until rupture occurs.



**Figure 7.9** Views of (a) two specimens 'glued' together before testing, (b) installed in the loading fixture of a tension machine and (c) the two specimens after rupture

<sup>8</sup> Standard Test Method for Adhesion and Cohesion Strength of Thermal Sprayed Coatings (March 10, 2001).



Figure 7.9 (Continued)

A coating subjected to a TAT should be as thick as 380 µm for the reason of possible penetration of the resin into the voids of the sprayed porous coating. This is especially true for coatings which are obtained using 'less-energetic techniques' (e.g. flame spraying). The resin can penetrate into the interconnected pores, reinforce the coating and even become in contact with the substrate, hence increasing, artificially, their adhesion to the substrate. On the other hand, coatings sprayed using 'more-energetic' techniques, such as arc or plasma spraying, high-velocity oxy-fuel spraying or the detonation gun, are less porous and the resin does not deeply penetrate. *Auger Electron Spectroscopic* measurements of the depth of carbon penetration in air plasma-sprayed chromium oxide revealed that the resin does not penetrate more than 10–15 µm into the coatings (Pawlowski, 1987b). Consequently, the thickness of 380 µm required by the ASTM Standard is probably not necessary for coatings sprayed with these techniques. Very well-adhering vacuum-plasma sprayed alloy coatings are often impossible to test when using an epoxy resin. In fact, some authors, e.g. (1982) or Steffens and Beczkowiak (1983), 'brazed' their sprayed samples when using this method. The limitation of the ASTM test results from the penetration of the resin into the coating and its limited strength, which does not exceed  $p = 80\text{--}100 \text{ MPa}$ , which makes it impossible to test well-adhering coatings. Table 7.6 shows the results obtained for a TAT performed by

**Table 7.6** Results of a tensile adhesion test carried out for plasma-sprayed TiO<sub>2</sub> coatings of mean thickness 475 µm following the ASTM 633-01 Standard (Castejon *et al.*, 2005)

Test number	Tensile stress (MPa)	Type of rupture	Comment
1	70	Cohesive rupture in resin	Concluding test, samples 'glued' without coating
2	21.4	Cohesive rupture in coating	Concluding test
3	19.5	Cohesive rupture in coating	Concluding test
4	20.9	Cohesive rupture in coating	Concluding test
5	7.13	Adhesive rupture at NiCr/TiO <sub>2</sub> interface	Non-concluding test
<i>Mean value of tensile stress, 20.6 MPa</i>			

using the ASTM Standard for a  $\text{TiO}_2$ , 475- $\mu\text{m}$  thick coating sprayed onto an NiCr bond coat and specimens of stainless steel by Castejon *et al.* (2005). Most of the tested samples failed in a cohesive way. TATs were carried out for multi-coatings, such as thermal barriers, including air-plasma sprayed yttria-stabilized zirconia and the same materials by PVD, as well as  $\text{Cr}_2\text{O}_3$  layers obtained by high-temperature oxidation of Inconel 617 alloy. The adhesion/cohesion strength was as high as 70 MPa after deposition and is reduced to 30–40 MPa after thermal cycling (Andritschky *et al.*, 1995)

### Fracture Mechanics Tests

An adhesion test, developed on the base of fracture mechanics, was proposed by Berndt and McPherson (1980) using the double-cantilever beam (DCB) method. A DCB is used for determination of the critical strain energy release rate and is more thoroughly described in Section 7.2.4. A four-point bending test can also be applied for adhesion measurements in the way shown in Figure 7.10.

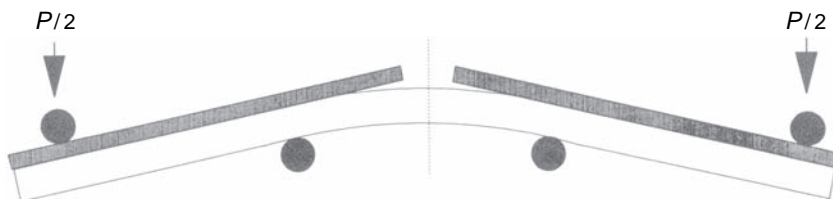


**Figure 7.10** Loading arrangement for the four-point bending test (Rickerby, 1996). Reproduced by permission of Chapman & Hall from D. Rickerby, 'Measurements of coating adhesion', in *Metallic and Ceramic Protective Coatings*, K.H. Stern (Ed.), Chapman & Hall, London, UK, 1996, pp. 306–334

The critical energy release rate is calculated by comparing the total strain energy before and after a propagation of events observed on a load-displacement trace. Then, the difference between the loads is divided by the area of contact. Finally, an indentation test, shown schematically in Figure 7.11, enables the determination of apparent interfacial toughness (Chicot *et al.*, 1996).

The indentation test is realized on a polished cross-section of a sprayed coating. A *Vickers indentation* is made at the interface of the coating with the substrate, using an appropriate alignment of the indenter.

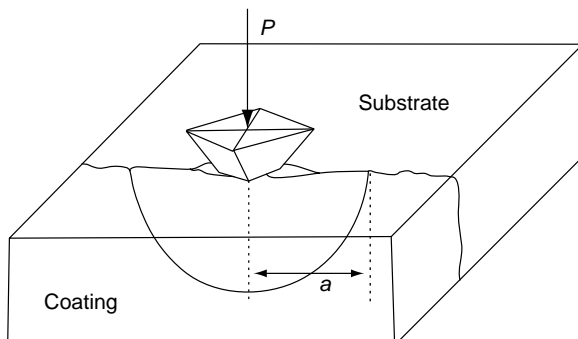


**Figure 7.11** Schematic of the interfacial indentation test (Chicot *et al.*, 1996). This article was published in *Thin Solid Films*, 283, D. Chicot, P. Démaréaux and J. Lesage, 'Interfacial indentation test for the determination of adhesive properties of thermal sprayed coatings', 151–157, Copyright Elsevier (1996)

The crack generated by the penetration is localized along the interface and has a semicircular shape (Figure 7.11). An appropriate mathematical treatment enables determination of the apparent interfacial toughness,  $K_c$ . Knowledge of the Young's moduli and hardnesses of the coating and substrate is necessary in the calculations. This method, with a slightly different geometry (indentation made on the surface of the deposit), was also applied to test the adhesion of thin films by Chiang *et al.* (1981). Another test, belonging to this family, uses a spherical indentor pushed down onto the coating's surface. This test was applied by Nygård *et al.* (1998) to verify the adhesion of a  $\text{Cr}_3\text{C}_2 + \text{NiCr}$  coating obtained by high velocity combustion spraying.

## Other Methods

The bond strength of an 'intentionally' porous coatings, e.g. titanium for medical applications, can be tested by using the ASTM F-1147 Standard.<sup>9</sup> Thin films, e.g. suspension-sprayed ones, can be tested by a *scratch test*. This test, described in many textbooks, e.g. that of Pawlowski (2003), consists of using an indenter which is moved linearly on the film surface under an increasing load. The load which corresponds

<sup>9</sup> Standard Test Method for Tension Testing of Calcium Phosphate and Metallic Coatings, American Society for Testing and Materials, *Annual Book of ASTM Standards*, Vol. 13-01, *Medical Devices*, ASTM F-1147 (1 April 2005).

to the detachment of the coatings is defined as critical one. Das *et al.* (1991) used this test to check the adhesion of plasma-sprayed yttria-stabilized zirconia coatings and Jaworski *et al.* (2007) to that of suspension plasma sprayed TiO<sub>2</sub> ones. A *peel adhesion test* has been proposed by Sexsmith and Troczynski (1994). This test allows determination of the peel strength, which is very closely related to the ‘real’ adhesion of a coating to a substrate. On the other hand, Grützner and Weiss (1991) pointed out that the TAT does not simulate very well the service conditions of sprayed coatings. These authors proposed rather a *shear test* in which the applied force acts parallel to the coating’s surface. Finally, a ‘laser-shock’ adhesion test was proposed by Berthe *et al.* (2002). Short laser pulses of duration of  $\tau = 10\text{ ns}$  and a power density  $q = 10^9 - 10^{13}\text{ W/cm}^2$  are used to generate a ‘laser shock’ which, in turn, serves to detach the coating from the substrate.

### 7.2.2 HARDNESS AND MICROHARDNESS

Tests of hardness are based on the principle of penetration of a hard diamond on the surface of a tested material. The diamond has the shape of a pyramid, with a base in the form of the following:

- square – in the *Vickers* test;
- rhombus – in the *Knoop* test;
- triangle – in the *Berkovitch* pyramid.

The specimens for the microhardness tests should be metallographically polished. Most of the measurements are made on longitudinal cross-sections, also used for OM observations. However, it is also possible to make measurements on transverse cross-sections and the values could diverge because of the lamellar microstructure of the coatings. In fact, the microhardness in a transverse cross-section is expected to be greater than that in a longitudinal one. Moreover, the coating’s thickness when testing a transverse section must be at least ten times thicker than the depth of the pyramid indentation (Burnett and Rickerby, 1987). Hardness is expressed as the ratio of the load to the area of indentation. For the *Vickers* test, the hardness is expressed by the following relationship:

$$HV = \frac{1.8544F}{d^2} \quad (7.5)$$

The Vickers number is denoted by  $HV$ , while the Knoop number is denoted by  $HK$ . The value of  $HV$  is expressed in  $\text{kgf}/\text{mm}^2$  if  $F$  is in  $\text{kgf}$ , with  $d$ , the length of the indentation diagonal, in  $\text{mm}$ . Sometimes, hardness is expressed in  $\text{GPa}$ .<sup>10</sup> Hardness depends, to a degree, on the applied load. The practicable loads are in the range of  $F = 0.1$  to  $50 \text{ N}$ . Usually, one uses the term ‘microhardness’ if the loads ( $F$ ) are lower than  $10 \text{ N}$  and ‘hardness’ if the loads are greater. Measurements under a low load ( $F < 0.5 \text{ N}$ ) describe the properties of individual lamellae and that under a greater load—the *whole* coating. Most authors give values under a  $1, 3$  or  $5 \text{ N}$  load. By convention, the load is an index of microhardness. Thus,  $HV_3$  corresponds to a value obtained under an  $F = 3 \text{ N}$  load. Commercially available testers follow the normalized procedures, e.g. the ASTM E-384-07 Standard.<sup>11</sup> Some authors recommend a minimum coating thickness for a given load. For example, Adam (1977) recommends the following values:

- $HV_3 = 1000$  – minimum thickness,  $40 \mu\text{m}$ ;
- $HV_3 = 500$  – minimum thickness,  $100 \mu\text{m}$ .

The *Rockwell* hardness test is used mainly for thick coatings of metals and alloys. The indenters can be different (steel balls of specific diameter or diamonds) and also the load depends on the type of tested material. The commercially available *Rockwell* testers are designed to follow normalized procedure, such as the ASTM E-18-07 Standard.<sup>12</sup>

### 7.2.3 ELASTIC MODULI, STRENGTH AND DUCTILITY

Elastic moduli and strengths are intrinsic properties of materials. The parameters are usually deduced from a stress–strain curve which is different for ductile and brittle materials. Ductile materials, such as metals and alloys, can be characterized by the ultimate strength and yield strength, and brittle materials by the fracture strength (Figure 7.12).

The elastic modulus ( $E$ -modulus) of coatings is influenced mainly by porosity and bad contact between the lamellae (McPherson, 1989). Post-spraying heat treatment, leading to sintering of the material, reduces

<sup>10</sup>  $1 \text{ GPa} = 100 \text{ kgf}/\text{mm}^2$ .

<sup>11</sup> Standard Test method for Microindentation Hardness of Materials, ASTM-384-07 (1 July 2007).

<sup>12</sup> Standard Test method for Rockwell Hardness and Rockwell Superficial Hardness of Metallic Materials, ASTM E-18-07 (1 April 2007).

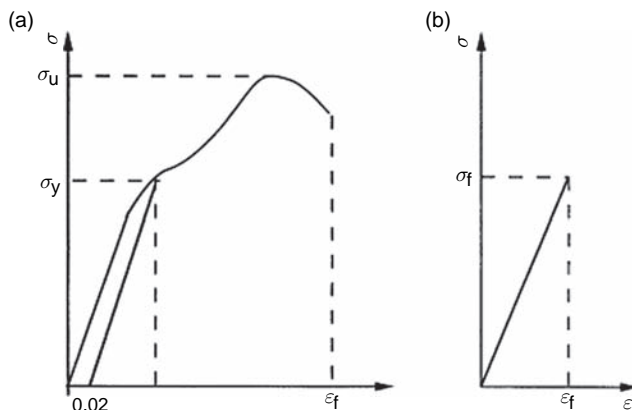


**Figure 7.12** Stress–strain curves for (a) ductile and (b) brittle materials:  $\sigma_y$ , yield stress corresponding to a sample permanent ‘off-set’ of 0.2 %;  $\sigma_u$ , ultimate stress;  $\sigma_f$ , fracture stress;  $\varepsilon_f$ , fracture strain

its porosity which increases the elastic modulus. Methods of elastic modulus testing can be categorized according to Buchmann *et al.* (2002) as follows:

- *destructive methods*, which include:
  - micro-indentation on a coating cross-section;
  - 3-point bending (see Figure 7.14);
  - 4-point bending (see Figure 7.10);
  - compression or tensile test;
  - cantilever beam method.
- *non-destructive methods*, which include:
  - laser acoustic method;
  - nano-indentation method on a coating surface;
  - ultrasonic tests.

The micro-indentation test is carried out on a metallographically polished coating cross-section using a method described by Oliver and Pharr (1992). The set-up should enable the recording of indentation-load/penetration-depth curves (Figure 7.13).

The load during micro-indentation measurements has values in the range  $F = 100\text{--}1000\text{ mN}$ . Analysis of the slope of the unloaded curve gives the ratio  $dF/dd$  (see Figure 7.13), knowing the elastic properties of

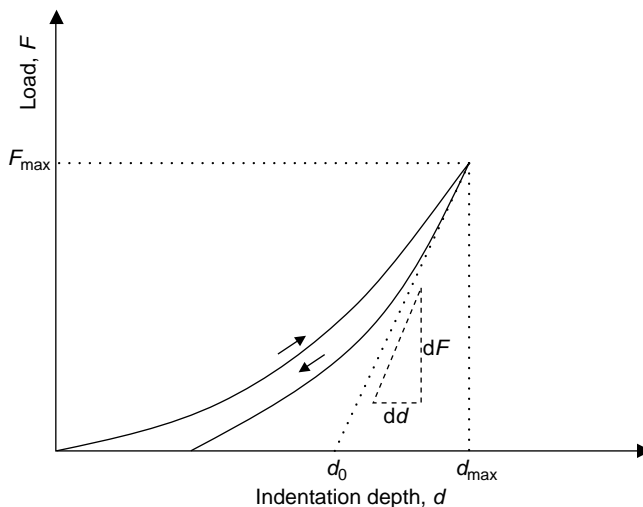


Figure 7.13 Loading–unloading curves obtained during an indentation test

the indenter.<sup>13</sup> The micro-indentation method was used, e.g. to determine the elasticity of plasma-sprayed  $\text{TiO}_2$  coatings (Buchmann *et al.*, 2002) or NiCrAlY bond coatings sprayed using different techniques (Gouldstone *et al.*, 2004). A similar calculation, but using a much lower load of about  $F = 1 \mu\text{N}$ , is used in the nano-indentation method. The indenter has the shape of the *Berkovitch* pyramid and indentation is made on the polished coating surface. This kind of measurement is typically made for thin films (Pawlowski, 2003). Micro- and nano-indenters are available commercially. A schematic of the 3-point bending method is shown in Figure 7.14. This method was applied by, e.g. Kuroda and Clyne (1991).

A schematic of the 4-point bending test, used, e.g. by Siemers and Mehan (1983), is shown above in Figure 7.10. Bending tests are based on the principle that application of a force acting in direction  $y$  (see Figure 7.14) induce an elastic displacement in direction  $x$ . The displacements are measured with a sensor and should be monitored acoustically to detect the formation of crack (Colin *et al.*, 1988). It is important to keep in mind the direction of mechanical testing because the  $E$ -moduli and strengths are different in the direction parallel to the coating surface and perpendicular to it. Analysis of acoustic activity under load allows recognition of the mode of failure, namely:

<sup>13</sup> For diamond,  $E_{\text{ind}} = 1050 \text{ GPa}$  and  $\nu_{\text{ind}} = 0.3$ .

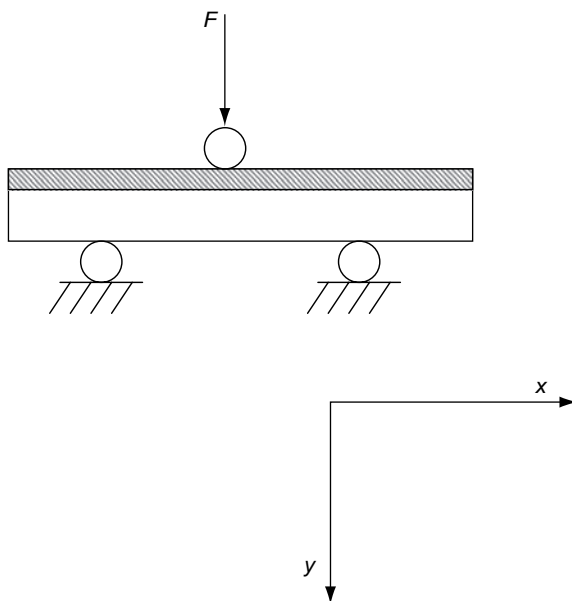


Figure 7.14 Schematic of the four-point bending method applied for coatings without substrates

- crack initiation accompanied by high acoustic activity;
- crack growth accompanied by low acoustic activity.

The  $E$ -modulus and strength can be found by knowing the applied load and the resulting deflection. Both variables are recalculated to give a stress-strain curve. ‘Strain-to-fracture’ can be calculated from the values of the  $E$ -modulus and the strength. The mechanical test can be conducted either for coatings on a substrate or without a substrate, i.e. *free-standing samples*. The latter can have the form of a cylinder or plate. Detailed descriptions of the 3- and 4-point-bending tests are given in the textbook by Timoshenko (1976). The static 3-point bending method was applied by Buchmann *et al.* (2002) to determine the  $E$ -modulus of free-standing FeCrB-based, HVOF-sprayed coatings. Beghini *et al.* (1997) used the static 4-point bending test to find the elastic moduli of  $\text{ZrO}_2\text{-Y}_2\text{O}_3$  by APS and NiCoCrAlY by HVOF. The measurements were made by using coated substrates and an appropriate mathematical treatment was necessary. A similar test for *free-standing samples* was made by Varis *et al.* (2001) for different alloy and ceramic coatings.

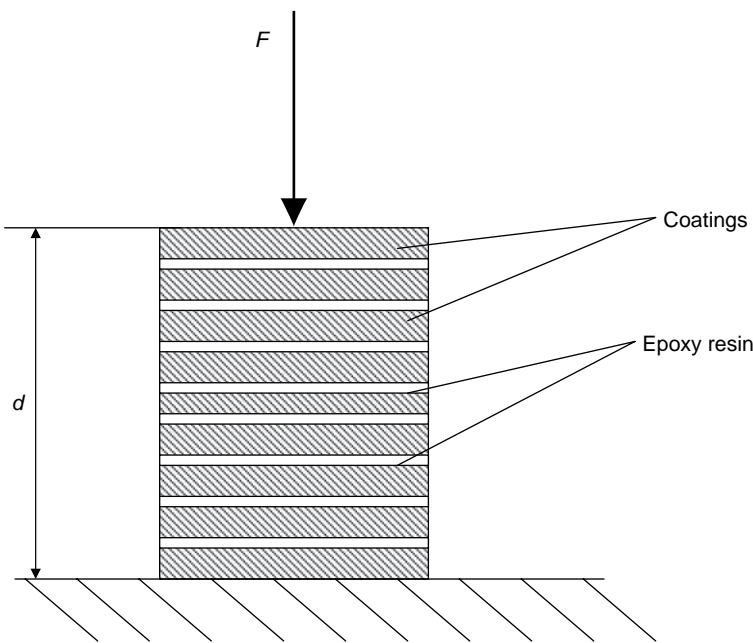
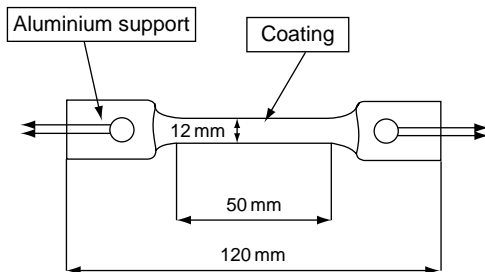


Figure 7.15 Schematic of the compression test, as used by Pawłowski (1987b)

Young's modulus in compression can be found by preparing a sample in the way presented in Figure 7.15.

A number of coatings detached from the substrates are 'glued' together with epoxy resin in order to obtain a sample of sufficient thickness. During the compression test, the applied load removes the epoxy and the coatings become closer. Then, a 'micro-fissuration' of ceramics takes place. The test is stopped when the sensor identifies macro-cracking of the coating. The  $E$ -modulus in compression was found by using this test for air plasma-sprayed  $\text{Cr}_2\text{O}_3$  coatings (Pawłowski, 1987b). The Young's modulus in tension can be found by using the sample presented in Figure 7.16.

The coating is sprayed onto an aluminium substrate which was, after processing, chemically etched. Parts of the substrate are not coated and serve as attachments to the testing machine. Varis *et al.* (2001) tested various ceramic and alloy coatings using such an arrangement. Mehan *et al.* (1987) proposed the use of short hollow cylinders (rings) for another tensile test. The procedure consists of inserting split D-shaped fixtures into a sprayed ring. The ring and aligned fixtures are placed in a tensile machine and then pulled apart. The load–elongation curve



**Figure 7.16** Illustration of the tensile test specimen used by Varis *et al.* (2001). Reproduced by permission of ASM International from Varis *et al.*, 2001, in *Thermal Spray 2001: New Surfaces for a Millennium*, C.C. Berndt, K.A. Khor and E.F. Lugscheider (Eds), ASM International, Materials Park, OH, USA, pp. 993–997

is used to compute the tensile properties. Tucker (1982) recommended this method to test thin coatings which have less residual stresses. The methods of detaching the coating from the substrate, used by different authors, consist of spraying:

- Onto a graphite mandrel which is later ‘burnt out’. This method was used by Holcombe (1978) to obtain an cylinder of plasma-sprayed  $\text{Y}_2\text{O}_3$ .
- A coating of low TEC, e.g.  $\text{Al}_2\text{O}_3$  or  $\text{Cr}_2\text{O}_3$ , onto a previous heated and slightly roughened metal mandrel of high TEC, such as aluminium, followed by cooling down and detaching the coating without any effort. This method can be used to manufacture plates and short hollow cylinders.
- A chemically resistant coating, such as Mo, onto an ‘easy-to-etch’ mandrel, e.g. Al, followed by its chemical removal. This method can be used to manufacture hollow cylinders.

Free-standing hollow cylinders can also be tested in compression by loading the sample, inserted between two parallel plates, until fracture occurs (Lutz, 1993). The *cantilever-beam* method, based on measurements of deformation of coated samples, fixed on one side and loaded on another, was recommended by Shadley *et al.* (2000) to determine the Young’s modulus and Poisson modulus of thermal-sprayed coatings. These authors propose the method as standard practice.

The Poisson modulus and Young’s modulus can also be determined by the use of laser-ultrasonics. The method consists of generation of

surface acoustic waves (SAWs) by a pulsed laser (nitrogen or Nd:YAG). The waves are detected by a wide-band piezoelectric transducer fixed on the surface. Oscilloscopic analysis of the spectrum enables the elastic moduli to be determined (Buchmann *et al.*, 2002; Lima *et al.*, 2003). The method is strongly influenced by the coating's inhomogeneity and gives rather an indication of Young's modulus than its precise value.

Ultrasonic methods are well adapted to test small free-standing samples (Glandus *et al.*, 1979) or bars such as the one shown in Figure 7.17.

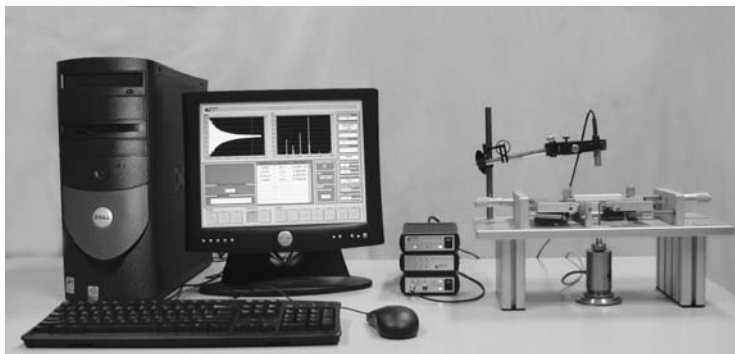


**Figure 7.17** A modern ultrasonic tester of the elastic properties of materials based on 'Impulse Excitation Technology'. Reproduced by permission of Integrated Material Control Engineering NV, Diepenbeek, Belgium

The method consists of generating vibrations in a specimen and determining their frequencies. The latter depend on the sample's shape, density and Young's and Poisson moduli which can be found by a suitable mathematical treatment, as presented by, e.g. Spinner and Tefft (1961) and Van Landuyt (1995).

The mechanical properties of sprayed materials are highly anisotropic due to their lamellar structure and care must be taken when interpreting the test results.

*Ductility* is a property of materials that deform plastically. It can be described as the permanent strain before fracture of a sample during tensile testing (Van Vlack, 1989). Ductility is typically described by the linear plastic strain accompanying fracture. It can be tested for free-standing samples by using tensile testers.

### 7.2.4 PROPERTIES RELATED TO MECHANICS OF COATING FRACTURE

The fracture mechanics approach that leads to evaluation of the mechanical properties of coatings is based on *linear elastic fracture mechanics*, as developed by Griffith. He observed that a material usually contain cracks and that rupture occurs by the spreading of the pre-existing cracks under the action of forces acting on the body. The spreading is accompanied by an increase in energy equal to an increase in the area of the created faces multiplied by the surface energy of the solid (Kelly and Macmillan, 1986). This hypothesis enabled a rigorous description of the cracking phenomena. In particular, an important technological property is the resistance against propagation of the crack. The resistance is a material-specific property and is equal to the critical energy per unit area ( $G_{lc}$ ) it is necessary to apply for propagating a crack (in the opening mode of fracture<sup>14</sup>). This energy is also called the *strain energy release rate*. The *fracture toughness*,  $K_{lc}$ , is also a material property, related to  $G_{lc}$  by the following equation (Kelly and Macmillan, 1986):

$$K_{lc} = \frac{G_{lc}E}{1-\nu^2} \quad (7.6)$$

The fracture strength,  $\sigma_f$ , for brittle materials depends on  $G_{lc}$ , following the well-known Griffith equation:

$$\sigma_f = \sqrt{\frac{EG_{lc}}{(1-\nu^2)\pi l}} \quad (7.7)$$

This equation describes the tensile stress that corresponds to initiating a crack of length  $l$ . The strength is related to the microstructure of the material because  $E$ -modulus depends on the coating porosity and contact between the lamellae. Consequently,  $G_{lc}$  would also depend on it because a crack can propagate easier between areas of weak contact.

---

<sup>14</sup> Mode I corresponds to the forces acting in the direction of opening the crack, mode II corresponds to the shear forces acting parallel to the crack surface and perpendicular to the crack front while mode III corresponds to the shear forces acting parallel to the crack surface and parallel to the crack front ('tearing') (Van Vlack, 1989).

McPherson (1989) gives the following equation for the *effective strain energy release rate* ( $G_{lc}$ )<sub>eff</sub>:

$$(G_{lc})_{\text{eff}} = 2mS_r G_{lc} \quad (7.8)$$

In Equation (7.8),  $S_r$  is the fraction of the lamellae surfaces in contact with other lamellae,  $m$  is a factor describing the ‘multiplication’ of the cracks and  $G_{lc}$  is a parameter for a non-porous material. McPherson suggests values of  $S_r = 0.25$  and of  $m = 4$  for an alumina coating sprayed by a plasma in air.

The toughness of sprayed coatings was tested by using the following methods:

- double-cantilever beam (DCB);
- double torsion (DT);
- indentation test.

Coatings, in the DCB and DT methods, are applied on one face of a substrate and ‘glued’ to the similar uncoated one. The uncoated surface is sand-blasted to promote adhesion of the ‘glue’ (Figure 7.18).

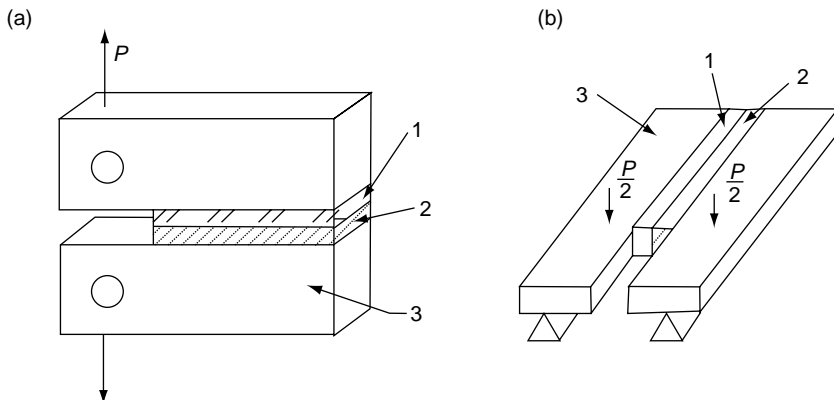


**Figure 7.18** Schematics of (a) the double-cantilever beam (DCB) and (b) the double-torsion (DT) tests for the determination of fracture toughness: 1, glue; 2, coating; 3, substrate;  $P$ , applied force

The coatings must be ‘pre-cracked’ initially. In the DCB method, a sample is loaded and unloaded many times as the crack propagation

progresses (Guo and Wang, 1992). To calculate the  $G_{lc}$  values, it is necessary to know the crack length  $l$ :

$$G_{lc} = \left( \frac{P_c^2}{2W} \right) \left( \frac{dC}{dl} \right) \quad (7.9)$$

In Equation (7.9),  $P_c$  is the critical load,  $W$  is the specimen width and  $C$  is the compliance, i.e. the crack opening divided by the load. On the other hand, results obtained from DT tests do not depend on the crack length. More details about the measurement techniques are given by Berndt and McPherson (1980), Colin *et al.* (1988), Guo and Wang (1992) and Troczynski and Camire (1994). Standard ASTM E 399-06<sup>15</sup> describes ‘pre-cracking’ shapes. A crack can propagate within a coating or at its interface with the substrate – the failure type (cohesive, adhesive or mixed) has to be indicated in the test report (similarly for the tensile adhesion test).

The indentation method is very simple and consists of analysis of the indentation made during the Vickers microhardness test (Ostojic and McPherson, 1987). The  $G_{lc}$  values found using indentation method were lower than those measured using the DCB test (Ostojic and McPherson, 1988). The indentation method was also applied by Lopez *et al.* (1991) to determine *fracture toughness*.

## 7.2.5 FRICTION AND WEAR

Friction and wear belong to the branch of science called *tribology* (Zambelli and Vincent, 1998). *Static friction* can be defined as the resistance against displacement of a solid body being initially at rest in contact with the surface of another body. Friction results in ageing of the surfaces, heat generation and leads to wear of the material. *Static friction* is much lower than *dynamic friction*. The latter concerns a body already in movement. Friction is usually described by a coefficient of friction  $\mu$ , defined as:

$$\mu = \frac{T}{N} \quad (7.10)$$

---

<sup>15</sup> Standard Test Method for Linear-Elastic Plane-Strain Fracture Toughness  $K_{lc}$  of Metallic Materials, ASTM E-399-06 (15 December 2006).

In Equation (7.10),  $T$  is the force of friction and  $N$  is the load. The coefficient of dynamic friction can be found by the use of a set-up shown in Figure 7.19.

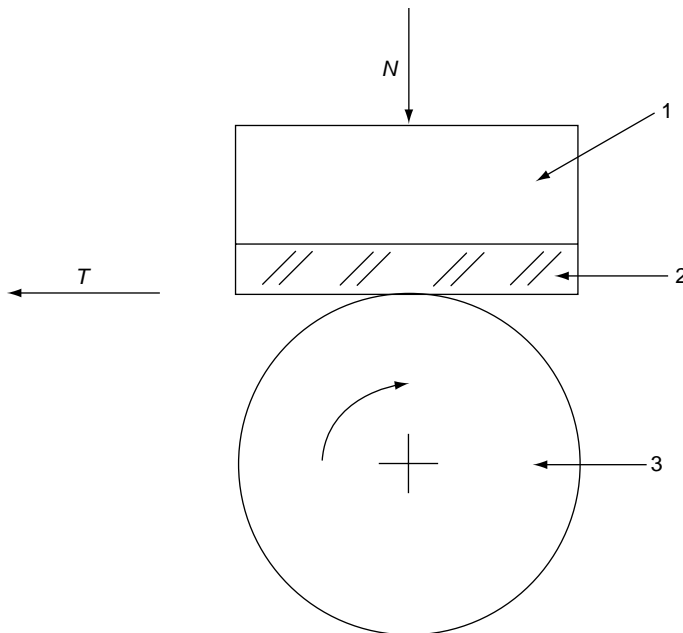


**Figure 7.19** Schematic of a bloc on a cylinder tribometer for the characterization of dynamic friction: 1, substrate; 2, coating; 3, rotating wheel;  $N$ , load;  $T$ , friction

The friction coefficient can be found with the help of different types of tribometers, such as (Zambelli and Vincent, 1998):

- pin on disc;
- bloc on cylinder (Figure 7.19);
- 4-spheres test.

The tribometers simulate friction by:

- sliding;
- rotation;
- rolling.

A tribological test gives a friction coefficient as a function of the distance 'run' of the sample and depends on the following coating parameters (Holmberg and Matthews, 1994):

- hardness with regard to that of the contacting surface;
- roughness;
- thickness;
- size and hardness of debris at testing.

The basic mechanisms of wear include (Föhl *et al.*, 1988):

- adhesion associated with transfer of material between the contacting surfaces;
- abrasion associated with cutting of the coatings;
- fatigue associated with micro-cracking of the coatings.

The resistance of thermally sprayed coatings has been mainly tested for the following types of wear:

**Adhesive wear** which appears when two surfaces slide past each other. This type of wear is proportional to the distances ‘run’ by the moving surfaces and to the load and inversely proportional to the coating’s hardness. Wear can be characterized by the use of commercial tribometers. The result of the test is *linear wear* which is defined as the depth of the worn trace of a contacting surface or *volumic wear* which is the volume of the worn coating multiplied by the ‘run’ distance and divided by the load. This kind of wear decreases if lubricant is applied between the surfaces in contact. *Adhesive wear* is also called *frictional wear* since it has the same mechanisms as friction, which is welding and subsequent shearing of surface asperities (Askwith, 1980). The following factors influence the adhesive wear:

- cleanliness of contacting surfaces, i.e. cleaner surfaces adhere better and get worn more;
- temperature, i.e. higher temperatures increase adhesive wear.

Many experiments have shown that there are two distinct classes of wear:

- *mild wear*;
- *severe wear*.

In *mild wear*, the debris is composed of fine particles and the wear rate increases proportionally to the load, relative velocity and distance travelled. The mechanism can also be called the *adhesion mechanism*. Starting from a certain point, the wear increases more than

proportionally. From this point, *severe wear* starts. The mechanism of this wear, also called the *fracture mechanism*, can be explained by lamellae, which are broken from the coatings which leads to an increase of friction coefficient. The lamellae act as an additional abrasive. Adhesive wear can be tested under dry and lubricated conditions. Generally, application of a lubricant results in much smaller wear and a much lower friction coefficient. Moreover, thermally sprayed coatings, due to their open porosity, retain lubricant (Yuansheng *et al.*, 1992). In dry conditions, coating roughness becomes an important factor and a smoother surface corresponds, most frequently, to a lower friction coefficient. Tucker (1982) discusses some examples of exceptions to this rule. Many coatings become smoother in service. The basic equations relating adhesive wear resistance  $w^{-1}$  and friction coefficient  $\mu$  to the wear conditions are as follows (Sandt and Krey, 1985):

$$w^{-1} = \frac{H}{kp} \quad (7.11)$$

$$\mu = \frac{d\gamma}{Hdx} \quad (7.12)$$

In Equations (7.11) and (7.12),  $k$  is the wear coefficient,  $p$  is the pressure in contact and  $dx$  is a sliding length. The coefficients  $k$  and  $d\gamma$  correspond to the micro-mechanism of wear. The  $k$ -coefficient could be divided into the following components:

$$k = k_{\text{def}} + k_f \quad (7.13)$$

Another form of *adhesive wear* is *scuffing wear* which is characterized by micro- or even macro fusion of two surfaces in contact. This kind of wear can occur in the pistons of diesel engines (Buran and Fischer, 1988). Scuffing wear resistance is, in practice, promoted by a high content of molybdenum or molybdenum carbide  $\text{Mo}_2\text{C}$  in coatings.

**Abrasive wear** occurs if the mating surface is harder than the coating (*two-body abrasion*). *Three-body abrasion* occurs if a sand or abrasive grit is introduced between two surfaces in contact. The *two-* and *three body abrasion* tests (the latter is normalized in the ASTM G 65–04<sup>16</sup> Standard as a rubber wheel abrasion test) are shown in Figure 7.20.

---

<sup>16</sup> Standard Test Method for Measuring Abrasion Using the Dry Sand/Rubber Wheel Apparatus, G 65–04 (1 November 2004).

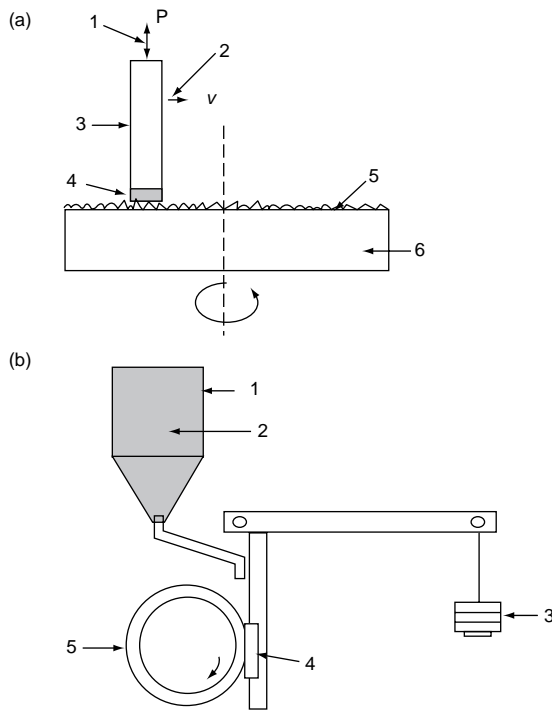


**Figure 7.20** (a) Schematic of the two-body abrasion test (also called the ‘pin-up disc’ abrasion test): 1, applied force; 2, linear movement; 3, substrate; 4, coating; 5, abrasive surface; 6, rotating disc. (b) Schematic of the three-body abrasion test (also called the ‘dry sand–rubber’ abrasion test): 1, sand container; 2, sand; 3, load; 4, coated sample; 5, rotating wheel

The results of the tests are usually given as volume or mass of the worn coating material divided by distance ‘run’ while testing.

**Erosive wear** is due to the action of impinging particles. The erosion rate  $E$  (in dimensionless units) in particulate erosion depends on the velocity,  $v$ , of impacting particles, impinging particles’ angle  $\alpha$  and their size,  $d$ , following the relationships (Taylor *et al.*, 1987):

$$E = kv^n f(\alpha) \quad (7.14)$$

$$E = kd^n \quad (7.15)$$

In the above equations,  $k$  and  $n$  are materials-related constants and  $f(\alpha)$  is a function depending on the impinging erodent angle. Taylor and co-workers found a value of  $n = 0.63$  for bulk stainless steel grade 304 and plasma-sprayed NiCrAl alloy. Eroding brittle materials develop

micro-cracking. This leads to the fracture and resulting wear (Alonso *et al.*, 1991). Ductile materials (metals or alloys) erode by micro-machining caused by impinging particles. At the brittle mode of erosion wear, the rate has a maximum at an impingement angle ( $\alpha$ ) of about  $90^\circ$ . In contrast, the ductile mode is characterized by the maximum erosion rate at low angles of  $\alpha = 15\text{--}30^\circ$ . *Cavitation erosion* is a kind of erosion associated with turbulent flow conditions, which results in localized pressure drops, causing the formation of vapour cavities and the repetitive collapse of these cavities, damaging the coating's surface through a combination of shock loadings and fatigue processes leading to material removal (Tiwari *et al.*, 1993). To test this kind of erosion, the ultrasonic wave's generator inside a water container vibrator is well adapted.

**Fatigue wear** occurs when the coating surface is in contact with a rotating body which has a rolling motion.

**Fretting wear** occurs when a coating surface is in contact with a body oscillating or vibrating with a small amplitude. This kind of wear be categorized as a function of oscillation (Blanpain *et al.*, 1995):

- linear under normal and constant load – mode I;
- radial under normal and variable load – mode II;
- rotational under normal and constant load – mode III.

**Corrosive wear** results from the action of an environment, such as moisture. The moisture can be contained in the atmosphere (moist air) or in industrial fumes and gases. The products of such corrosion are relatively easy to remove by rubbing. Corrosive wear requires the presence of both corrosion and sliding and hence the products of corrosion may protect the surface from further corrosion unless they are removed by sliding (Askwith, 1980).

**Impact wear** occurs if the coating is subjected to the repetitive action of an impacting second body (e.g. a ball).

Any kind of wear can be tested by the use of microscopic observations. The profile of the defects in the worn surface can be useful in recognition of the wear mechanism.

## 7.2.6 RESIDUAL STRESSES

There are a number of alternative methods for investigation of residual stresses. They can be roughly divided into destructive and non-destructive.

The most popular among the destructive ones is a *hole-drilling method* which involves surface-strain-gauge readings as material is removed by drilling. The surface strains are used to calculate the residual stresses as a function of coating depth (Pantucek *et al.*, 1991; Wenzelburger *et al.*, 2005). Among the non-destructive methods, the oldest one is the use of X-rays which is based on deformation of the crystal lattice due to residual stresses. This method, also called the ' $\sin^2 \psi$ ' method, is explained in many textbooks, such as that of Noyan and Cohen (1987), and is also practicable for another source of radiation – neutrons. This method was used, e.g. by Weglowski and Pawłowski (1983) and Noutomi *et al.* (1989), to test stresses in plasma-sprayed ceramic and metallic coatings. A limitation of the ' $\sin^2 \psi$ ' method is absorption of radiation which is a few  $\mu\text{m}$  for X-rays and a few cm for neutrons, and is difficult to determine for porous or graded coatings. Special mathematical efforts have to be undertaken in order to avoid the influence of diffraction from the regions which are not being considered (Kesler *et al.*, 1998). This renders difficult measurements of stress distribution versus coatings depth. Moreover, the testing is time-consuming and expensive. Finally, the simplest method of residual stress determination is a *curvature-monotoring method*, described for the first time by Hobson and Reiter (1988). The method consists of changing the curvature of a metallic substrate/deposit couple. The technique was developed by Gill and Clyne (1994) who made two important advances. First, a remote method of investigating curvature by video recording was applied for vacuum-plasma spraying. Secondly, a numerical procedure was developed which allows calculating stresses from the geometry of curvature and their origin, i.e. stresses resulting from a particle quenching mechanism and from thermal expansion coefficients ‘mis-match’. An important advantage of this method is its simplicity in comparison with the neutron and X-ray diffraction methods (Kesler *et al.*, 1998).

### 7.3 PHYSICAL PROPERTIES OF COATINGS

An important property of a coating is its thickness. This property is often specified at processing. The measurements can be a problem for suspension-sprayed coatings which are thinner than 20  $\mu\text{m}$  (Tomaszek *et al.*, 2006b). Porosity is also an important property, which influences considerably the mechanical and thermophysical characteristics of deposits. Thermophysical properties, which include thermal conductivity, thermal diffusivity, specific heat, emissivity and thermal-shock

resistance, are important, especially for thermal-barrier coatings. Finally, the methods of characterizing the resistance to aqueous and hot corrosion should be known in order to predict the coatings' behaviour under different conditions.

### 7.3.1 THICKNESS, POROSITY AND DENSITY

The thickness of sprayed coatings can be measured by using a micrometre screw with accuracy in the range 5–10 µm. The screws available commercially enable measurement of samples having different shapes and sizes. Thickness can also be measured, in a destructive way, by the metallographic preparation of coatings' cross-sections and their microscopic observation. This method is especially recommended for thin films obtained by suspension-plasma spraying (see Figure 7.21).

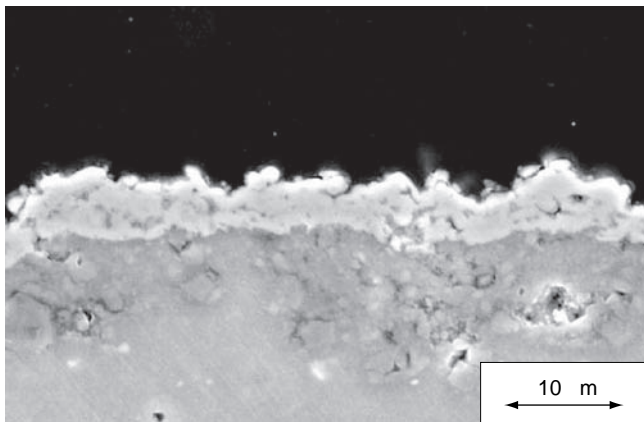


Figure 7.21 Scanning electron micrograph (secondary electrons) of a cross-section of a suspension-plasma sprayed  $\text{TiO}_2$  coating (Tomaszek *et al.*, 2006b)

Pores can be categorized, taking their size into account, by the following:

- *Regular pores* having sizes ranging from a few tenths of nanometres to a few tenths of micrometres. Regular pores are generated at coating deposition and during post-spray treatment. Their characterization methods are shown in Table 7.7.

- *Micropores* – vacancies in the crystal structure. Their size is in the range of nanometres. Micropores can be observed by transmission electron microscopy under high-resolution conditions.

Another classification takes into account the place of pores with regard to the coating's surface and interface. In such a way, one can distinguish:

- *open porosity*, which corresponds to all pores connected with the coating's surface;
- *closed porosity*, which describes all pores in the coating's interior;
- *transversal porosity*, which corresponds to all pores traversing the coating from surface to interface.

Different kinds of porosity and density can be measured by using the methods shown in Table 7.7.

### 7.3.2 THERMOPHYSICAL PROPERTIES

The thermophysical properties of coatings are important because of the application of thermal barriers in the aeronautical industry. Thermal transport properties, reviewed by Pawłowski and Fauchais (1992), include thermal conductivity and thermal expansion. The latter has a special importance in designing coatings systems with low-level residual stresses. This can be reached by, e.g. design of functionally graded coatings (Pawłowski, 1991; Tomaszek *et al.*, 2006b). There are three principal mechanisms of thermal conduction occurring in different materials:

- *Electronic thermal conduction*, which occurs in materials having free electrons (alloys and metals). Thermal conductivity is, at low temperatures, proportional to temperature and, at higher temperatures, is not temperature-dependent.
- *Lattice thermal conduction*, which occurs in materials without free electrons. Energy is transported by phonons, which at low temperatures are scattered by geometrical defects. Thermal conductivity then depends exponentially on temperature. Scattering by other phonons, called the *Umklapp process*, occurs at higher temperatures and thermal conductivity becomes inversely proportional to temperature.
- *Photon conduction* may also occur in dielectric materials. It may be described as emission, absorption and radiation. Thermal conductivity is then proportional to  $T^3$ .

Table 7.7 Methods of porosity and density determination

Parameter	Method of characterization	Principle	Remarks	Reference
Open porosity	Mercury intrusion porosimetry (MIP)	A sample is evacuated under low pressure, and then immersed in mercury at a low pressure. The mercury is then pressurized and a series of pressures and corresponding volumes of intruded mercury determined. From the pressure (ranging from 50 to 410 MPa), the surface tension of mercury and the assumed wetting angle, the pore diameter can be calculated	Useful for coatings thicker than a few tenths of micrometres	Whittmore, 1981
SAW/BET		The method consists of monitoring the frequency changes in a surface acoustic wave made to propagate through a coating. The coating must be deposited onto a piezoelectric substrate to which is also attached input and output transducers connected to a frequency analyser. The system is put inside a vacuum chamber. The chamber is then filled with nitrogen under different pressures. The variation of frequency is then related to the volume of gas absorbed	Useful for thick and thin films	Taylor <i>et al.</i> , 1998

Table 7.7 (Continued)

Parameter	Method of characterization	Principle	Remarks	Reference
Density, total porosity	Archimedean method	The tested sample should be crushed prior to the measurements and kept under a reduced pressure for some time in order to allow the immersion liquid (e.g. water) to penetrate all interconnected pores. This procedure allows determination of the density of the coating. This density is smaller than the ‘skeletal’ one (or bulk material density) because of closed pores, which remain in the sample. In some cases, e.g. samples containing one crystal phase, the ‘skeletal’ density can be determined from the geometry of the unit cell by X-ray crystallography The procedure is described in Section 7.1.3	Coating should be detached from the substrate	Standard Test Method for Density and Interconnected Porosity of Sintered Metal Structural Parts and Oil-Impregnated Bearings, ASTM B 328-96 (10 September 1996)
Image analysis			Coating cross-section is prepared metallographically	Pawlowski, 1987a
Transversal porosity	Electrochemical methods	The electrochemically inert coating (ceramic) is sprayed onto the metal substrate. The transversal porosity can be found by comparing the electrochemical current measured at the same potential for coated and uncoated samples	—	Celis <i>et al.</i> , 1993; Haure <i>et al.</i> , 2003

Thermal spray coatings are very heterogeneous and thermal energy transport occurs by many simultaneously acting mechanisms. Conduction in the coatings depends on the following elements of their microstructure:

- dimensions of crystal grains, which influence the mean free path of the energy carriers;
- impurities;
- porosity.

The porosity leads to a decrease in the thermal conductivity of the coating,  $\lambda_{\text{eff}}$ , with regard to that of the solid matrix,  $\lambda_m$ . The simplest formula is given by the model of Loeb (1954):

$$\frac{\lambda_{\text{eff}}}{\lambda_m} = 1 - P \quad (7.16)$$

McPherson (1984) created a model of the conductivity adapted for thermally sprayed coatings. This model takes into account small pores having sizes in the range of  $d = 0.01\text{--}0.1\mu\text{m}$ , filled with a gas. The conductivity of the coating depends on the conductivity of the gas and has the following form:

$$\frac{\lambda_{\text{eff}}}{\lambda_g} = \frac{1}{1 + \left[ \frac{(9\gamma-5)}{(\gamma+1)} \frac{(2-\alpha)}{\alpha} \frac{d}{x} \right]} \quad (7.17)$$

In the above equation,  $d$  is the mean free path in the gas contained in the pores,  $x$  is the coating thickness and  $\alpha$  is a semiempirical constant ( $0.5 < \alpha < 1$ ). The model does not take into account large pores and is consequently oversimplified. Thermal conductivity is linked with other thermophysical parameters by the following relationship:

$$\lambda = ac_p\rho \quad (7.18)$$

Thermal expansion depends mainly on the phase composition of the tested coating and on its geometry at testing. The thermal expansion coefficient (TEC) in the longitudinal direction is different from the coefficient in the transverse direction. This effect was explained by the lamellar microstructure of coatings (Berndt and Herman, 1983). Porosity was proved not to influence the TEC (Kuroda and Clyne, 1991).

The thermal conductivity of thermally sprayed coatings has often been tested by using 'home-made' devices. Generally, there are two methods used for thermal conductivity testing (Touloukian *et al.*, 1970):

- steady-state methods;
- time-dependent methods.

**Steady-state methods** are based on the determination of thermal conductivity from the following one-dimensional heat conduction equation:

$$\lambda = \frac{-q\Delta x}{S\Delta T} \quad (7.19)$$

A thermal flux generates a temperature gradient along a sample. The thermal conductivity can be found knowing this flux, geometry of the sample and the temperatures at the sample ends. One method using this principle, known as *hot wire*, was applied to determine the conductivities of refractory materials having a thermal conductivity up to 25 W/(mK) by de Boer *et al.* (1980).

**Time-dependent methods** do not require knowledge of heat flow and temperature fields variation with time. These methods enable thermal diffusivity<sup>17</sup> to be found. Then, knowing the density and specific heat, the thermal conductivity can be calculated. The thermal diffusivity of sprayed coatings has been tested using two methods:

- laser-flash (LF) method;
- modulated-beam (MB) method.

The laser-flash method has become very popular since it was first described by Parker *et al.* (1961). In this method (Figure 7.22), a thermally isolated sample, having two parallel faces, is subjected to a flash (laser, flash of a xenon lamp) on its front face.

An evolution of the temperature of the rear face is registered with a thermocouple or an ir detector. From this evolution, the thermal diffusivity can be found by using the relationship:

$$a = \frac{0.139d^2}{t_{0.5}} \quad (7.20)$$

---

<sup>17</sup> The German language defines, quite precisely, thermal diffusivity as *Temperaturleitfähigkeit*, i.e. the conduction of temperature.



Figure 7.22 Laser flash set-up installed at the University of Limoges, France

In this equation,  $d$  is the tested sample thickness and  $t_{0.5}$  is the time corresponding to half of the maximum temperature of the rear face (time starts with the beginning of the flash). An analysis of the boundary conditions in this method has been made by, e.g. Pawłowski (1985) and Pawłowski *et al.* (1985). The method has been also applied to determine the thermal contact resistance between sprayed multi-coatings (Gitzhofer *et al.*, 1985). The applicability of the method to the determination of the diffusivity of porous materials is discussed by Kerrisk (1971, 1972).

The modulated-beam method was first described by Cowan (1963). A small disc-shaped sample, used in this method, is heated uniformly by a sinusoidal or square wave. The temperature oscillations propagate through the sample. The phase shift between the temperature oscillations of the front and rear faces of the sample enable the thermal diffusivity to be determined. A detailed technical description of a set-up for thermal diffusivity determination can be found in the study of Brandt and Neuer (1979).

The specific heat is a material property which can be defined as:

$$c_p = \left( \frac{dq}{dT} \right)_p \quad (7.21)$$

In this equation,  $q$  is the quantity of heat on a mass unit. A comprehensive survey of the fundamentals of the physical background of

specific heat and the methods of its measurement is given by Touloukian and Buyco (1970). The specific heats of thermally sprayed coatings has been tested using *Bunsen ice calorimetry* (BIC) and *differential scanning calorimetry* (DSC), a method discussed in detail by Richardson (1984).

The density at temperature  $T$ ,  $\rho(T)$ , depends on the density at 300 K ( $\rho_{300}$ ) and on the thermal expansion coefficient (TEC), following the equation:

$$\rho(T) = \frac{\rho_{300}}{1 + 3(TEC)\Delta T} \quad (7.22)$$

In this equation,  $\Delta T = T - 300$  and TEC is defined as:

$$TEC = \frac{1}{L} \left( \frac{\partial L}{\partial T} \right) \quad (7.23)$$

In this equation,  $L$  is the length of the sample. The densities of sprayed samples have been mainly tested by using the *Archimedean method* and then adjusted to a given temperature by the use of TEC, in the way shown by Equation (7.22). The methods of thermal expansion measurements are reviewed by Touloukian *et al.* (1978).

*Spectral emissivity*,  $\varepsilon(\lambda, T)$ , is a function of wavelength and temperature and can be defined as follows (Gaussorgues, 1981):

$$\varepsilon(\lambda, T) = \frac{dq_r(\lambda, T)/d\lambda}{dq_{r,bb}(\lambda, T)/d\lambda} \quad (7.24)$$

*Total emissivity* is the spectral emissivity integrated over all wavelengths. *Normal emissivity* is the emissivity measured in the direction normal to the radiating surface. The emissivity of thermally sprayed coatings has been measured by the use of infrared thermography. The technique of the measurements is described by Martin and Fauchais (1981).

### 7.3.3 THERMAL SHOCK RESISTANCE

*Thermal Shock Resistance* (TSR), also called *thermal stress resistance*, describes the capacity of a brittle material to resist rapid temperature variations without failure. The TSR depends on the conditions of heating (steady-state flow, transient heating, heating by convection or radiation,

etc.) and may be expressed as the maximum allowable temperature difference in the body. Hasselman (1970) gives a summary of the used TSR parameters. Under steady heat-flow conditions, this parameter can be expressed as:

$$TSR = \frac{\sigma_f(1-\nu)}{ETEC} \quad (7.25)$$

In practice, *TSR* is tested for the system of a coating onto a substrate. Thus, residual stresses may influence it (Sheffler *et al.*, 1982). Most of the tests simulate the conditions of the service of the coatings. A typical thermal cycling (burner) rig used to test coated turbine blades is shown in Figure 7.23.

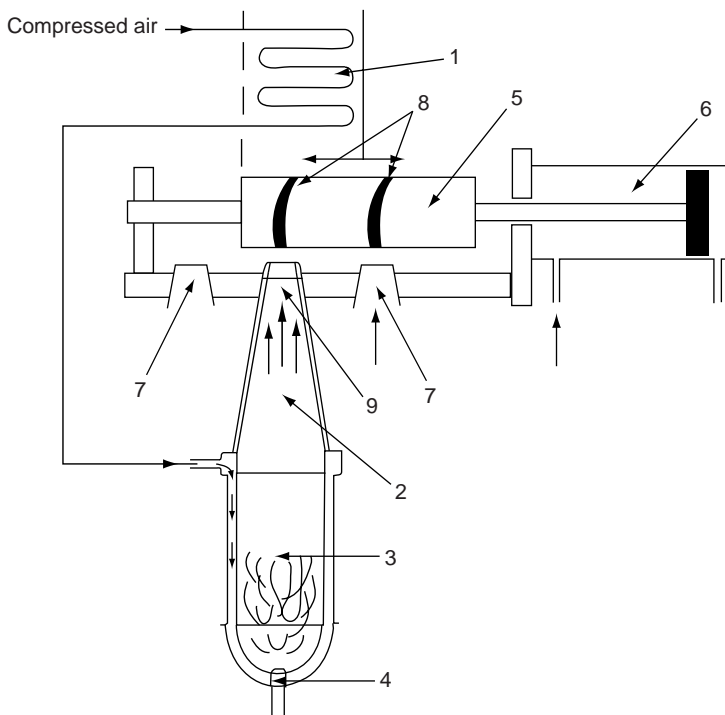


**Figure 7.23** Schematic of a typical thermal cycling (burner) rig used for testing turbine blades: 1, heat exchanger; 2, ceramic hot-gas nozzle; 3, combustor; 4, fuel nozzle; 5, specimen carrier; 6, pneumatic cylinder; 7, cooling-air nozzle; 8, test specimen; 9, Pt/PtRh thermocouple (Cosack *et al.*, 1992). Reproduced by permission of ASME International from 'Thermal barrier coatings on turbine blades by plasma spraying with improved cooling', by T. Cosack *et al.*, *International Gas Turbine Aeroengine Congress Exposition*, Cologne, Germany, 1–4 June, 1992, Paper 92-GT-319

The result for such a test is a number of thermal shocks that were resisted by the tested sample until failure. The test, using the rig shown in Figure 7.23, consists of subjecting the coated blades to a stream of hot fuel gas ( $T \approx 1760\text{ K}$ ) for 30 s, followed by a cooling cycle of the same duration in a compressed air stream. During the cooling cycle, the temperature of the coating steps down to  $T \approx 570\text{ K}$ .

## 7.4 ELECTRICAL PROPERTIES OF COATINGS

### 7.4.1 ELECTRICAL CONDUCTIVITY

Electron conductors, such as metals and alloys, are characterized by electric conductivity which is linked to thermal conductivity by the *Wiedemann–Franz–Lorenz law*:

$$\frac{\lambda}{\sigma T} = 2.45 \times 10^{-8} (\text{W}\Omega/\text{K}^2) \quad (7.26)$$

Electric conductivity decreases with temperature because electrons get scattered by the oscillations of the crystal lattices (phonons). The microstructure of sprayed coatings (contacts between lamellae, porosity, etc.) influences the resistivity of conductors and semiconductors by a reduction in the mean free path of the electricity carriers. The carriers are also scattered on the impurities on the crystal grain boundaries and on the pores. The resistivities of sprayed conductors can be regulated by adding a second non-conducting phase by forming, e.g. cermets, such as W with  $\text{Al}_2\text{O}_3$ , as studied by Pawłowski (1974). Electrons are organized in *Cooper pairs* in superconductors above the critical temperature,  $T_c$ , and electric charge is transported without any resistance. This effect disappears if:

- the electric current becomes greater than the critical one,  $I > I_c$ ;
- the magnetic field generated by the current<sup>18</sup> or by an external source becomes greater than the critical one,  $H > H_c$ .

Electrons are dispersed in dielectrics and semiconductors in two energetic bands:

---

<sup>18</sup> In superconductors of type II in which the magnetic field penetrates the material bulk (Rose-Innes and Rhoderick, 1978).

- the *valence band*, which has electrons being closely bound to the atoms;
- the *conduction band*, which has free electrons which are able to move in all directions.

The concentration of electrons in the *conduction band* increases if one delivers enough energy (thermal, electric) to the electrons in *valence band*. They are then able to jump over the *forbidden zone* which separates these bands. Consequently, electric conductivity increases with temperature. The electric current can be carried by ions in materials known as *ionic conductors*.

Variations of electric resistivity<sup>19</sup> with temperature are described by the thermal coefficient of resistance (TCR). The latter is rather positive for metals and alloys and rather negative for dielectrics and semiconductors. The DC resistivity of coatings can be determined by using a 4-point probe (Figure 7.24), utilizing the following equation (Maissel and Glang, 1970):

$$\rho = \frac{V2\pi s}{I} \quad (7.27)$$

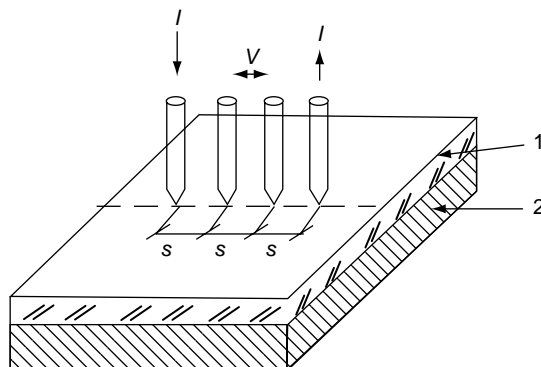


Figure 7.24 Schematic of a 4-point probe used to measure DC resistivity: 1, coating; 2, substrate;  $I$ , current;  $V$ , voltage;  $s$ , distance between the electrodes

In the above equation, the symbols used are the same as those shown in Figure 7.24. The resistance of planar samples can be found by knowing

<sup>19</sup> Electrical resistivity is inversely proportional to electric conductivity,  $\rho = 1/\sigma$ .

the resistivity and their geometry from Equation (7.28). The ratio  $R_s = \rho/d$  is known as the *sheet resistance* (in units of  $\Omega/\text{square}$ ) and it is practical to count the number of squares,  $n = l/w$ , for the sample whose geometry is shown in Figure 7.25(a).

$$R = \left(\frac{\rho}{d}\right) \left(\frac{l}{w}\right) = R_s n \quad (7.28)$$

Calculation of the ‘square numbers’ can be carried out for different geometries of thin-film rectangles by using the methods developed by Hall (1997). Finally, application of planar electrodes can be useful to test the resistivity of dielectric coatings (Nakamichi and Kawamura, 2001).

The most important parameters of superconductors are the critical temperature, critical current and critical magnetic field density (Chandler, 1989). These parameters can be determined by using a 4-point probe in a cryostat with controlled temperature and an external magnetic field or, indirectly, by using AC susceptibility measurements (Norris, 1988).

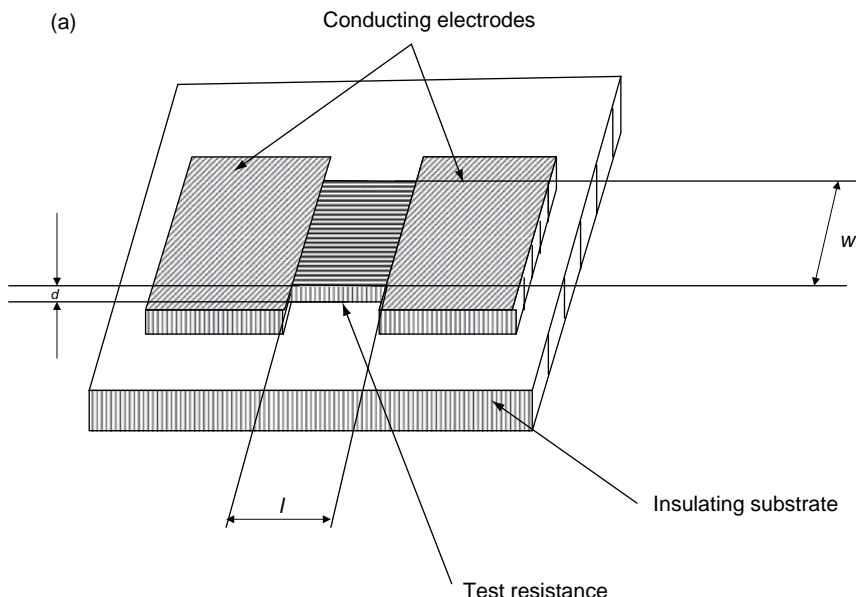


**Figure 7.25** (a) Geometry for measuring sheet resistance. (b) Set-up, involving a plasma-sprayed  $\text{Fe}_3\text{O}_4 + \text{NiO}$  resistor and Cu electrodes on a plasma-sprayed alumina substrate, used for determining thermal conductivity (Pawlowski, 1985)

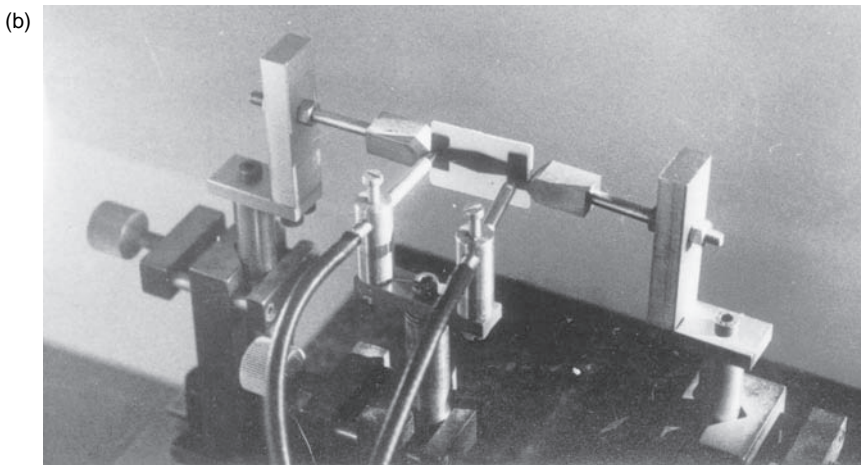


Figure 7.25 (Continued)

Finally, the *mobility of electric charges* (electrons, holes, ions) is defined as the velocity of a carrier in a unit electric field. This parameter was measured by Akani *et al.*, (1986).

#### 7.4.2 PROPERTIES OF DIELECTRICS

Dielectrics can be characterized by the presence of electrical dipoles that become ordered in an external electric field. The local field created by the dipoles is superposed onto the external field. The *dielectric constant*,  $\epsilon_r$ , indicates by how many times the final electric field in a dielectric is greater than that in vacuum. Its value depends on the frequency of the electric field, because the polarization mechanism of a dielectric varies with frequency. The following species react in an alternating electric field:

- polar molecules (e.g. H<sub>2</sub>O) at low frequencies;
- ions at intermediate frequencies;
- electrons at high frequencies.

Another important parameter of a dielectric is the *loss factor*. This factor, also called *tan δ*, describes the contribution of loss current in a capacitor. The latter results from electron or ion conduction. Materials with especially high dielectric constants are *ferroelectrics* (e.g. BaTiO<sub>3</sub>).

The constants for some thermally sprayed coatings, e.g. alumina, can be surprisingly high. In fact, formation of the highly hygroscopic  $\gamma\text{-Al}_2\text{O}_3$  leads to the dielectric constant in sprayed  $\text{Al}_2\text{O}_3$  coatings being in the range  $\varepsilon_r = 10\text{--}60$ . This constant is in superposition with the value for bulk alumina ( $\varepsilon_r = 6\text{--}9$ ) and for water ( $\varepsilon_r \approx 88$ , at 1 kHz). On the other hand, metal impurities and high porosity would lead to an undesired increase in  $\tan \delta$  in thermally sprayed dielectrics. Dielectric constants and loss factors are tested with commercially available capacitance bridges. Samples should be prepared as a capacitor with a dielectric coating sprayed onto the metal substrate – which is also the bottom electrode. The top electrode can be sprayed onto a coating of a ‘well-conducting’ metal or a ‘well-pressed’ conducting elastomer (see Figure 7.26). The dielectric constant can be found from the following relationship:

$$\varepsilon_r = \frac{Cd}{S\varepsilon_0} \quad (7.29)$$

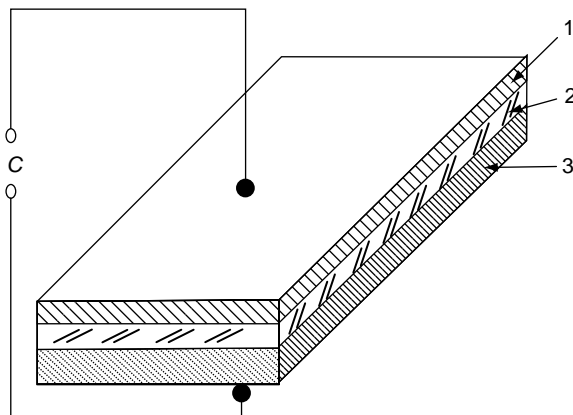


**Figure 7.26** Schematic of the set-up used to determine the dielectric constant: 1, top electrode; 2, dielectric coating; 3, metallic substrate;  $C$ , capacitance

Another important property of dielectrics is the *dielectric strength*, which is the maximum electric field intensity before electrical breakdown occurs. There are two principal mechanisms of breakdown:

- *Electronic breakdown*, which occurs when an ‘avalanche’ of electrons becomes accelerated in an electrical field. This type of breakdown can be recognized by a very narrow (nanodimensional) discharge channel.
- *Thermal breakdown*, which occurs when a dielectric becomes locally melted by *Joule heating*. This breakdown type can be recognized by a large (tenths of micrometre size – see Figure 7.27) discharge channel.

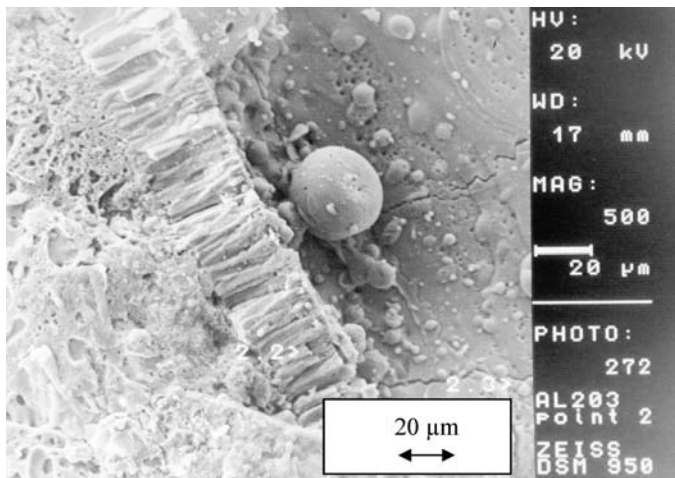


**Figure 7.27** Scanning electron micrograph (secondary electrons) of a breakdown channel in an  $\text{Al}_2\text{O}_3$  coating obtained by air-plasma spraying. The columnar form of the grains on the channel's boundary indicates the thermal character of the breakdown (Pawlowski, 1987b)

Thermal breakdown occurs more frequently in dielectrics (Yoshimura and Bowen, 1981). The porosity resulting from unmelted grains, resulting in pores having sizes in the range from a few micrometres to a few tenths of micrometres, is the coatings' microstructural feature which limits the dielectric strength of thermally sprayed coatings. The gas included in these pores (air or working gas) has a much lower strength, being about  $30 \text{ kV/cm}$  for air, than a ceramic matrix, which is about  $700 \text{ kV/cm}$  for polycrystalline alumina (Morse and Hill, 1970). The effect of the porosity on the dielectric strength might be estimated

by using the simplified statistical model of Gerson and Marshal (1959). This model does not take into account the bimodal distribution of the pores in sprayed deposits (Pawlowski, 1988). An interesting approach may offer a fractal model of the breakdown, developed by Wiesmann and Zeller (1986).

Dielectric coatings sprayed on to metallic substrates might be used to test dielectric strength. The testing involves application of a steadily growing voltage until the breakdown occurs. Care should be paid to avoid a corona discharge between the top electrode and the metallic substrate when testing. This effect can be reduced by the preparation of samples having a large surface area and milling the place of contact with the top electrode in order to promote the breakdown (Figure 7.28). Another possibility offers immersion of the sample in a transformer oil. The dielectric strength,  $E$ , can be calculated from the following equation (using the symbols shown in Figure 7.28):

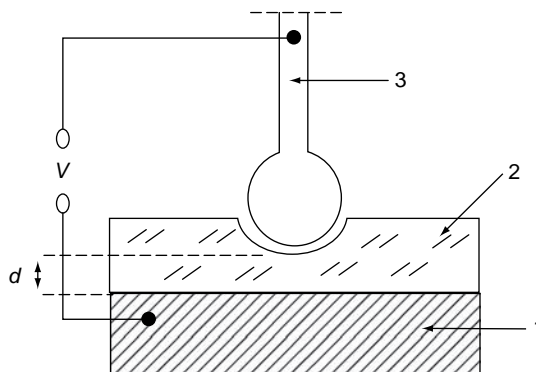
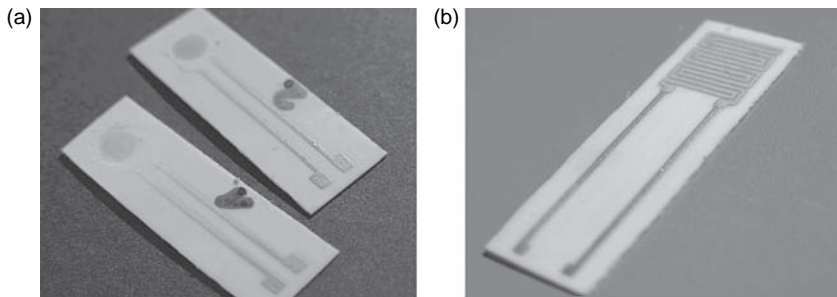


Figure 7.28 Schematic of the dielectric strength probe: 1, metallic substrate; 2, dielectric coating; 3, top electrode;  $V$ , test voltage;  $d$ , coating thickness

$$E = \frac{V}{d} \quad (7.30)$$

*Impedance spectroscopy* is a technique that consists of testing the impedance of a dielectric sample at different frequencies (from a few Hz to a few tenths of MHz) (Macdonald, 1987). The responses can be given as a function of temperature if the samples have an associated heater (see Figure 7.29) and may complete the microstructural investigation of the coatings. For example, Tomaszek *et al.* (2006a) confirmed

the presence of sodium impurities in suspension plasma-sprayed TiO<sub>2</sub> coatings.



**Figure 7.29** Views of (a) samples of a suspension plasma-sprayed coating on the top parts of the substrates and (b) the heater on the bottom part of the substrate(s)

### 7.4.3 ELECTRON EMISSION FROM SURFACES

Electrons can be emitted under the action of an electric field. The emission depends on the material work function (e.g. the work function for Ti,  $\Phi$ , is 4.35 eV) and may be enhanced by irregularities in its surface. This enhancement can be described by the  $\beta$ -factor, defined by the following equation (Znamirowski *et al.*, 2003a,b):

$$E = \frac{\beta V}{l} \quad (7.31)$$

In the above equation,  $V$  is the voltage between the electrodes and  $l$  is the distance between them. The factor  $\beta$  can be found from the characteristic emission current versus voltage curve or from the geometrical shape of the emitter (Znamirowski *et al.*, 2004). Electron emission can be tested with a ‘home-made’ set-up, such as the one shown in Figure 7.30.

## 7.5 MAGNETIC PROPERTIES OF COATINGS

Magnetic materials or *ferromagnetics* have magnetic domains. These domains can become ordered in an external magnetic field,  $H$ . The local magnetic field created by the domains amplifies the external field, giving

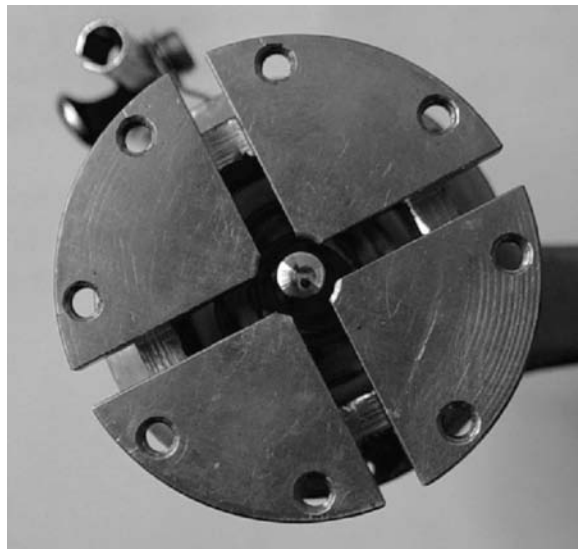


Figure 7.30 View of a sample holder with a hemispherical copper anode in the centre – a part of the set-up for the measurement of electron emission current (Znamirowski *et al.*, 2004)

an induction  $B$ . The parameters of magnetic materials can be found from the  $B$ - $H$  curve shown in Figure 7.31.

Magnets can be categorized as either ‘soft’ or ‘hard’. Soft materials need only a small external magnetic field to become magnetized and

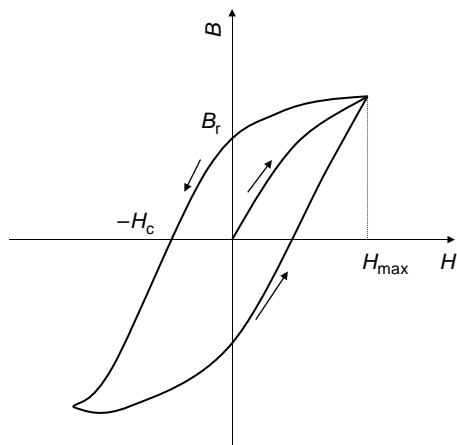


Figure 7.31 An example of a  $B$ - $H$  curve

upon removal of this field a certain residual induction,  $B_r$ , remains in the sample. To remove this magnetism, a small negative external magnetic field, called the coercive force,  $H_c$ , must be applied. Hard materials have  $B_r$  and  $H_c$  parameters much greater than soft ones. This means that it is difficult to both 'magnetize' and to 'demagnetize'. Hard magnets have  $H_c > 12$  Oe (Pawlowski, 2003). The maximum ratio  $B/H$  is known as the relative permeability,  $\mu_r$ . Hard magnets might also be characterized by the product,  $BH_{\max}$ . The magnetic properties of thermally sprayed materials are sensitive to residual stresses (Kumar and Das, 1980) and variations in the chemical composition under as-sprayed conditions (Preece and Andrews, 1973).

A  $B$ - $H$  curve at constant field may be obtained by the use of a vibrating sample magnetometer (Norris, 1988). In this method, the sample (free-standing or attached to a diamagnetic substrate) is suspended inside a small internal coil, which vibrates together with the sample. The external coil supplies a constant magnetic field. The voltage, which is proportional to the magnetization  $B$  of the sample, is generated and is measured together with the  $H$  field generated by the external coil. Cullity (1972) reviews other methods of  $B$ - $H$  curve determination.

## 7.6 CHEMICAL PROPERTIES OF COATINGS

Thermally sprayed coatings are frequently used to protect the surfaces of metals and alloys against aqueous corrosion. Such coatings mainly protect the structural 'pieces' in water, acids or bases. Another family of applications requires coatings to be resistant against hot gases. Such coatings are used in turbines motors.

### 7.6.1 AQUEOUS CORROSION

Metals and alloys immerseved in an aqueous solution, can dissolve by forming ions. For instance, iron can dissolve, following the reaction:



Loss of ions results in the formation of an electromotive force which slows down the dissolving process. In fact, in electrochemistry, one always considers two electrodes. The electrodes and electrolyte form

a cell, known as the *galvanic cell*. The one on which corrosion occurs, as oxidation, is the anode.<sup>20</sup> The processes of wet corrosion can be understood from different kinds of galvanic cells, namely (Bunshah, 1994):

- *Dissimilar electrode cells*, which correspond to two metals and an electrolyte. An example could be a copper pipe connected to iron pipe and transporting water.
- *Concentration cells*, which have identical electrodes, each in contact with a solution of differing composition. A most important case corresponds to the *different aeration cell*, in which one electrode is thoroughly aerated (becomes the cathode) and other less aerated (anode).
- *Differential temperature cells*, which are cells having the same electrodes at different temperature in an electrolyte of the same initial composition.

A first approach to know which metal dissolve another one is by comparison of the oxidation potentials – shown in Table 7.8. Metals which have a more positive potential are said to be more ‘noble’ and dissolve those which are less positive. For example, Zn is more reactive (‘sacrificial’) than Fe and Zn could be the anode in a galvanic cell with

**Table 7.8** Oxidation potentials of a number of metals with regard to the hydrogen electrode at 298 K (Lide, 1997)

Metal	Reaction	Oxidation potential V
Al	$\text{Al} = \text{Al}^{3+} + 3\text{e}^-$	-1.662
Ti	$\text{Ti} = \text{Ti}^{2+} + 2\text{e}^-$	-1.630
Zn	$\text{Zn} = \text{Zn}^{2+} + 2\text{e}^-$	-0.7618
Cr	$\text{Cr} = \text{Cr}^{3+} + 3\text{e}^-$	-0.407
Fe	$\text{Fe} = \text{Fe}^{2+} + 2\text{e}^-$	-0.447
Ni	$\text{Ni} = \text{Ni}^{2+} + 2\text{e}^-$	-0.257
Mo	$\text{Mo} = \text{Mo}^{3+} + 3\text{e}^-$	-0.200
Cu	$\text{Cu} = \text{Cu}^{2+} + 2\text{e}^-$	+0.3419
Au	$\text{Au} = \text{Au}^+ + \text{e}^-$	+1.692

<sup>20</sup> In electrochemistry, the cathode is the positive pole while the anode is the negative pole.

Fe. Aqueous corrosion-resistant coatings can be categorized as follows (Bunshah, 1994):

- *Anodic coating or sacrificial coating*, in which the coating is less 'noble' than the substrate, e.g. Zn or Al on Fe. If the electrolyte enters into contact with the coating and substrate, then the coating dissolves.
- *Cathodic coating*, in which the coating is 'nobler' than the substrate. This coating must be without pores or other defects which enable contact of the electrolyte with both electrodes. A typical example is a Ni coating on an Fe substrate.
- *Inert coating*, which protects the substrate in a 'physical way'. The coating does not have any electrochemical activity with regard to the substrate.
- *Inhibitive coating*, which is made of a material which slows down the rate of corrosion.

The corrosion rate can be measured by weighing a coated sample exposed to a corrosive environment as a function of exposure time. The rate is usually calculated as the loss of weight per unit area divided by the exposure time (Ailor, 1971). Corrosion can be tested in an electrochemical or polarization cell (Figure 7.32).

A reference electrode usually consists of calomel or hydrogen and the working electrode polarizes the tested sample. A standard procedure<sup>21</sup> consists of scanning the working electrode with a potential ranging from  $-30\text{ mV}$  to  $+30\text{ mV}$  and recording the current flowing between the two electrodes. A Typical curve of current versus applied potential is shown in Figure 7.33.

The tested sample is the anode. The polarization potential,  $U_{\text{corr}}$ , corresponds to the intrinsic potential of the anode. Above this potential, the current starts to flow and the anode is dissolved in the electrolyte. This zone is called the *active* zone, while the *passive* zone starts above the critical potential,  $U_c$ . In this zone, only a very small current flows. This zone corresponds to the formation of a thin 'passivated' film on the sample's surface, such as with  $\text{Cr}_2\text{O}_3$  on Cr. This zone ends with the *pitting potential*,  $U_{\text{pitt}}$ . Starting from this potential, important corrosion starts again in the same location on the sample's surface. Resistance to aqueous corrosion is better if the values of  $j_{\text{corr}}$  and  $j_{\text{pass}}$  are small and if the passive zone is extended.

<sup>21</sup> Standard Practice for Conventions Applicable to Electrochemical Testing, ASTM G 3-89, (24 February 1989).

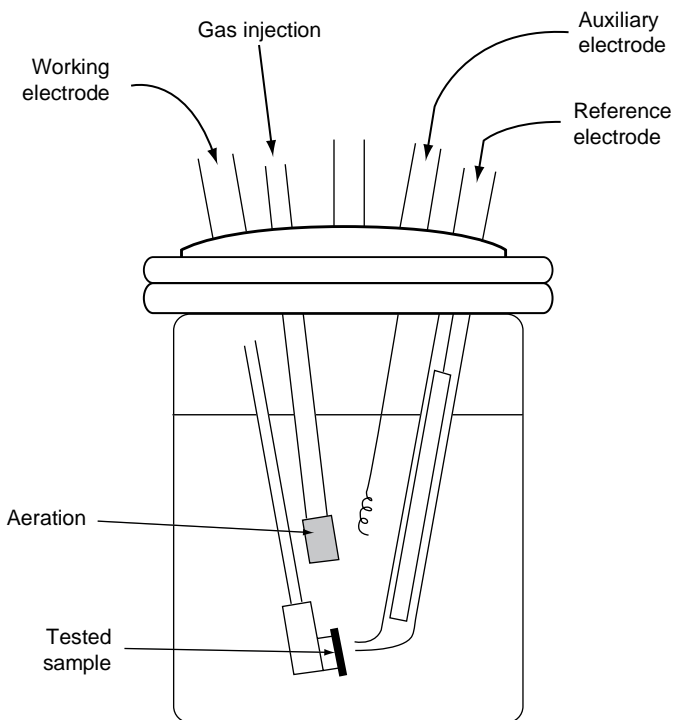


Figure 7.32 Schematic of a polarization cell

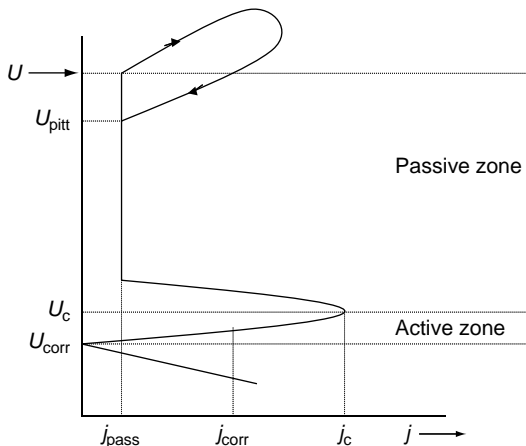


Figure 7.33 Typical curve of the current flowing in the electrolyte of a galvanic cell between the tested sample and the standard electrode as a function of polarization voltage

The following types of corrosion are recognized:

- *galvanic corrosion* of two metals having different oxidation potentials;
- *intergranular corrosion*, resulting in dissolution of the grain boundaries;
- *pitting corrosion*, which corresponds to the formation of points of corrosion in the passivated film;
- *crevice corrosion*, which occurs under the coating.

### 7.6.2 HOT-GAS CORROSION

Hot corrosion corresponds to the reaction of materials with gases (oxygen, carbon-containing gases, sulfur-containing gases) or liquids (metals, salts) at high temperature. The most frequent case is the oxidation of metals and alloys. The oxidation rate,  $k$ , can be found from the kinetics of oxide mass growth:

$$\frac{dw}{dt} = \frac{k}{w} \quad (7.33)$$

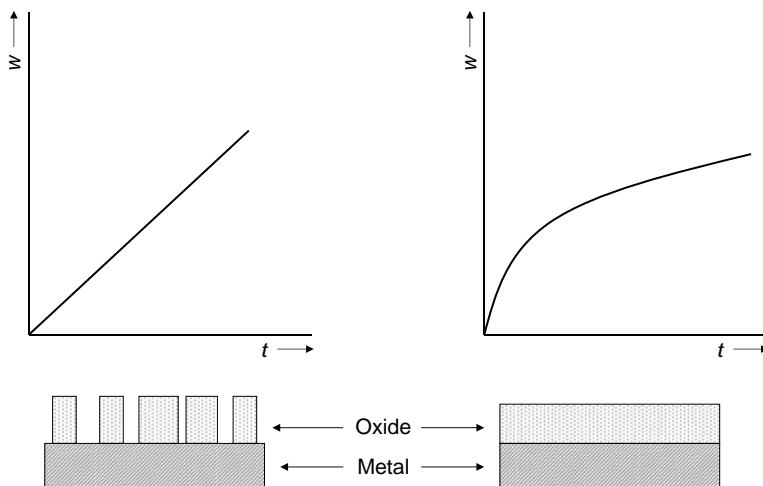


Figure 7.34 Linear (a) and parabolic (b) kinetics curves and the corresponding morphologies of the oxide scales

The  $w-t$  curve can be parabolic, which corresponds to a dense oxide scale, or linear. The latter corresponds to a scale which grows by forming isolated ‘islands’ of oxide (Figure 7.34).

Other kinetics corresponding to spallation, vaporization, etc. are discussed by Hocking *et al.* (1989). The kinetics of oxidation can be studied by the *thermogravimetric test*. A typical result shows a relative increase in the mass of sample at constant temperature as a function of time (see Chapter, Figure 1.24).

Hot-corrosion resistance can be studied under conditions close to that of the coatings’ service. For instance, burner rigs applied to study thermal shock resistance can also be used to this end by adding a corrosive medium to the hot gas. Hodge *et al.* (1980) doped the fuel in a burner rig with an aqueous solution of NaOH and  $\text{NH}_4\text{VO}_3$ . The corrosion tests are usually accompanied by microstructural analysis, hence enabling understanding of the corrosion mechanism.

## 7.7 CHARACTERIZATION OF COATINGS’ QUALITY

Characterization of the coatings’ quality is the last stage of their production. The properties that determine quality are usually characterized first at the coating R&D stage and later (see Figure 7.1), say, every few months. This approach is correct, assuming that in this period the consumables are of the same quality and the processing parameters are well-monitored and kept constant for a specified coating. Nowadays, many job-shops are managed by using the standards of the International Standard Association 9001–9005 which covers control of the quality of incoming feedstocks and processing procedures (Laboucheix, 1990). The daily control of coatings’ quality is made by a visual control of the coating and by microscopic observation of a cross-section of a sample sprayed simultaneously with the actually coated product. However, the product has a more complex shape than a small sample which may result in a different pre-spray surface quality and different residual stress patterns generated at processing. Consequently, the actual coating may contain defects which are detectable neither visually nor with microscopic observation. This is of special importance for those coatings applied with respect to the high safety standards required in the medical or aeronautical industries. Non-destructive techniques (NDTs) have been developed to meet this demand. Their status has been reviewed

by Bucklow (1980), Steffens *et al.* (1984) and Crostack *et al.* (1986). The following NDT methods have been studied for thermally sprayed coatings:

- thermal methods, such as the use of infrared cameras, thermal interferometry, liquid crystals and thermographic paints;
- acoustical methods, such as acoustic emission analysis (AEA) or ultrasonic methods;
- optical and photoacoustical methods, such as deformation holography, contour holography and holographic observation of acoustically vibrating samples (Meyer and Pohl, 1989);
- electromechanical methods, such as eddy-current testing and magnetic flux analysis;
- dye-penetration methods.

NDT methods should allow early detection of 'macro-defects', visualized in Chapter 6, Figure 6.32, which can result in subsequent coating delamination in service, namely:

- bad contact to the substrate, i.e. adhesion defects;
- vertical cracks;
- planar cracks;
- pore clusters.

The spatial resolution in these tests must be of tenths of micrometres. Moreover, in order to be accepted in industrial conditions the methods should:

- be easy to apply for large coating surfaces;
- enable rapid interpretation of the test results.

Nowadays, it is mainly acoustical and thermal methods which seem to fulfil some of these expectations.

The standardization of procedures for quality controls has progressed considerably and many standards are now being applied in 'job-shops'.

### 7.7.1 ACOUSTICAL METHODS

#### Ultrasonic Testing

An ultrasonic signal directed to a sample immersed in water would be reflected as:

- a *surface echo* from the coating surface;
- a *interface echo* from the interface or interfaces if intermediate coatings are applied (Lescreibaa and Vincent, 1996);
- *backwall echo* from the bottom part of a substrate (as shown in Figure 7.35).

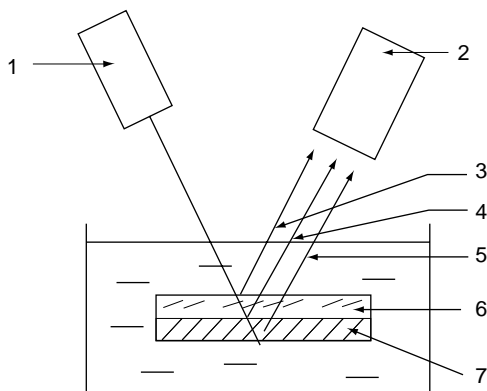


**Figure 7.35** Schematic of the basic configuration used for ultrasonic testing: 1, transmitter; 2, receiver; 3, *surface echo*; 4, *interface echo*; 5, *backwall echo*; 6, coating; 7, substrate; 8, water

Analysis of the interface echo is adapted to detection of defects inside the coating, while that of the backwall echo allows analysis of adhesion defects. Steffens *et al.* (1984) used ultrasonic waves (*backwall echo*) of a frequency of 3–5 MHz to detect adhesion defects in arc-sprayed carbon steel coatings on mild-steel substrates. Analysis of echo frequencies has enabled pore clusters to be distinguished. NiCr coatings on mild steel were tested by Suga *et al.* (1992) using X-Y scanning ultrasonic testing with a frequency of 2–7 MHz. The *backwall echo* was found to suit, at best, adhesion-defect analysis. A similar study was carried out by Namba *et al.* (1992) to study the APS and VPS of NiCrBSi alloys. The *backwall echo*, at a frequency of  $f = 10$  MHz, was reported to give satisfactory results and to give a fair correlation between adhesion tensile testing and ultrasonic testing. Smith *et al.* (1992) carried out a preliminary study of aluminium/polyester coatings deposited with APS and HVOF and the data received from ultrasonic 2-D scanning were correlated with microscopy observations. Finally, Lescreibaa and Vincent (1996) used the *interface echo* to test *duplex* coatings, with NiCrAlY as the bond coating and ZrO<sub>2</sub> as the top coating.

Ultrasonic testing has an important drawback which is the necessity to immerse the tested sample in a liquid. Consequently, larger parts and/or liquid-sensitive coatings cannot be tested in this way. Moreover, ultrasonics are *attenuated* in porous coatings and a loss of 500 dB per 1 cm of thickness has been reported by Patel and Almond (1985). Thus, thicker and more porous coatings would require a more powerful signal generator.

### Acoustic Emission Analysis (AEA)

Acoustic emission analysis is realized by clamping a piezoelectric transducer to the sample to be tested. The acoustic events occurring in the sample are amplified and the obtained signal classified by its amplitude. The events generated by cracking are successively counted. This cracking results from relaxation of residual, thermal or mechanical stresses. Consequently, acoustic emission analysis is particularly well adapted to monitor deposition processes or thermal cycling. For example, Steffens *et al.* (1984) found a correlation between the cumulative count of acoustic events and the following parameters for arc spraying of steel coatings:

- arc current;
- atomizing gas pressure.

Pacey and Stratford (1988) used acoustical analysis to distinguish the different arc currents applied in atmospheric-plasma spraying of  $\text{Al}_2\text{O}_3$  with 3 and 40 wt%  $\text{TiO}_2$ . Shankar *et al.* (1983a) monitored, using AEA, the thermal cycling of thermal-barrier coatings. Almond *et al.* (1983) and Shankar *et al.* (1983b) used AEA in 4-point bending and tensile adhesion/cohesion tests, respectively. Shankar and co-workers found that AEA enables a clear distinction between cohesive and adhesive failure modes. Ostojic and McPherson (1986) used AEA to test the long-term acoustic activity of flame- and plasma-sprayed coatings of  $\text{Al}_2\text{O}_3$ ,  $\text{Al}_2\text{O}_3 + 2.5$  wt%  $\text{TiO}_2$  and  $\text{Ni} + 5$  and 20 wt% Al immersed in water and benzene. It was found that the sealing reduces acoustic activity and that this activity decreases with time. Activity is more important for interaction with polar liquids (e.g. water). Another interesting application of acoustic emission analysis is the optimization of a number of coatings, their thicknesses and chemical compositions for an  $\text{Al}-\text{Al}_2\text{O}_3$  cermet applied between an Al substrate and an alumina top coat

(Pawlowski, 1987b). The top alumina coating specification was a dielectric strength as high as possible at  $T \approx 400\text{ K}$ . The samples, containing different coating compositions, were subjected to heating at 400 K and the configuration with the lowest cumulative count was selected. A designed coating configuration has been successfully applied to produce coatings on aluminium rolls for corona generators at W. Haldenwager, Berlin, Germany.

### 7.7.2 THERMAL METHODS

#### Infrared Thermography

An ir camera was used to detect the defects in thermally sprayed coatings by Green *et al.* (1983). A schematic of their system is shown in Figure 7.36.

Testing with an ir camera needs a source of heat (laser, stream of hot air, etc.). Diffusion of heat is influenced by defects in the coating which results in small differences in its surface temperature. These differences ( $\Delta T < 0.1\text{ K}$ ) can be distinguished by a camera detector. The tested surface must have no traces of oil, dirt or any other modification of emissivity. Otherwise, the camera will detect differences in coating emissivity

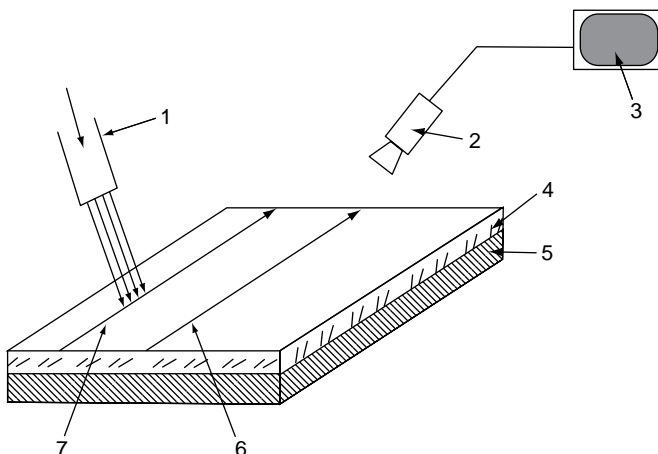


**Figure 7.36** Schematic of a set-up using an infrared camera to test thermally sprayed coatings: 1, stream of hot gas; 2, ir camera; 3, monitor; 4, coating; 5, substrate; 6, scanned line; 7, heat line (after Green *et al.*, 1983)

rather than defects (Gitzhofer *et al.*, 1987). Infrared thermography has been applied to:

- detect the defects in as-sprayed coatings;
- detect the formation of defects under thermal cycling;
- monitor the coating surface temperature during spraying.

Green *et al.* (1983) used ir thermography to visualize the defects of adhesion having sizes starting from 3.2 up to 12 mm in different types of coatings. Defect having sizes smaller than 6.4 mm could not be detected. A similar detection threshold of 5 mm was reported by Steffens *et al.* (1984). These authors recommended heating the sample up to  $T = 360\text{ K}$  and to make observations on cooling at temperatures ranging from 343 to 353 K.

Gitzhofer *et al.* (1987) have used ir thermography to observe yttria-stabilized zirconia coatings and NiCrAlY plasma-sprayed onto Al substrates during thermal cycling with a period of 20 s. The maximum surface temperature during the heating cycle reached 1573 K. The formation of vertical cracks was detected during testing. A similar test was made by Andrews and Taylor (2000) for a TBC subjected to furnace thermal shocks.

Pawlowski *et al.* (1983) applied ir thermography to determine the emissivity of some plasma-sprayed materials and to determine thermal conductivity (see Figure 7.26(b)), as well as to determine the temperature of the  $\text{Al}_2\text{O}_3$  coating surface during spraying.

### Thermal-Wave Interferometry

Static thermographic observations depend on the emissivity of the coating's surface. The differences in the observed temperature must be attributed by an operator to a defect within the coating or modification of emissivity. To avoid this drawback, thermal wave analysis was developed. The experimental set-up is shown in Figure 7.37.

The theory of thermal wave propagation in a coating was given by Jaarinens and Luukkala (1984). These authors recommended the application of thermal wave interferometry to determine the coating's thickness as well as to detect the defects of adhesion. The analysis of phases and amplitudes of thermal waves is possible, but phase analysis seems to be more sensitive for detecting the adhesion defects. Jaarinens and Luukkala (1984) used an Ar-ion laser chopped with a frequency  $f$  of 1–20 Hz

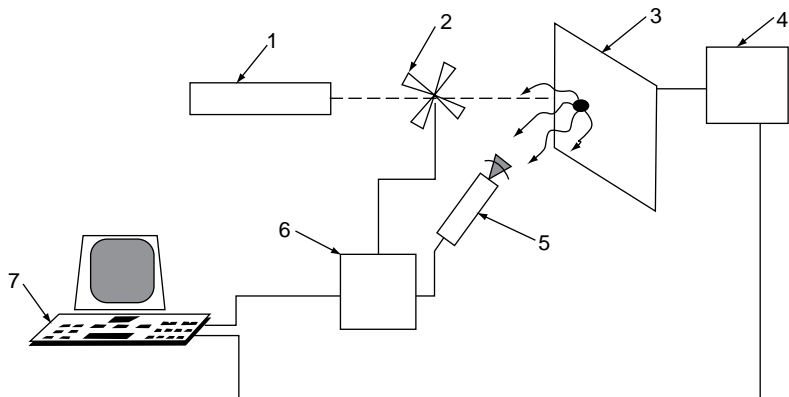


**Figure 7.37** Schematic of a system using thermal waves to identify the defects in thermally sprayed coatings: 1, heat source (laser); 2, modulator; 3, tested sample; 4, scanning unit; 5, ir detector; 6, electronic unit; 7, personal computer (after Patel and Almond, 1985)

and an ir detector to test WC and  $\text{Cr}_2\text{O}_3$  coatings on steel. Almond *et al.* (1985) also applied an Ar-ion laser chopped with a frequency  $f$  of 1–800 Hz. These authors used phase analysis to detect the difference in thicknesses (at frequencies of 10–25 Hz) and to determine the adhesion defects (at frequencies of 5–63 Hz) in  $\text{Cr}_2\text{C}_3 + \text{NiCr}$  coatings, plasma-sprayed onto stainless-steel substrates. Patel and Almond (1985) used the same system to test plasma-sprayed coatings of Mo, Al and NiAl on stainless-steel. They found that the adhesion defects in an Al coating were detectable at thermal wave frequencies up to  $f = 40$  Hz. The system developed at The University of Bath in the UK was adapted to ‘off-laboratory’ testing by the use of optical fibres (Morris *et al.*, 1989). A prototype of a thermal wave scanning system adapted for marine turbine shaft testing was developed by Green *et al.* (1984). The heat waves were generated by pulses of a heated air jet, which was switched on and off every 5 ms. The utility of the system for testing ‘non-bonding’ (sized down to 1.6 mm) and correlation with tensile adhesion/cohesion of NiCrAlMoFe coatings prepared by atmospheric-plasma spraying was successfully proven.

## REFERENCES

- Adam, P. (1977). Merkmale thermischer Spritzverfahren und ihr Einfluß auf die Eigenschaften der Schichten-Verfahrenstechnische Gesichtspunkten, *VDI Berichte*, 333, 97–103.

- Ailor, W.H. (1971). *Handbook of Corrosion Data and Evaluation*, John Wiley & Sons, Inc., New York, NY, USA.
- Akani, M., Suryanarayanan, R. and Brun, G. (1986). Influence of process parameters on the electrical properties of plasma sprayed silicon, *J. Appl. Phys.*, **60**, 457–459.
- Almond, D.P., Moghisi, M. and Reiter, H. (1983). The acoustic emission of plasma sprayed coatings, *Thin Solid Films*, **108**, 439–447.
- Almond, D.P., Patel, P.M., Pickup, I.M. and Reiter H. (1985). An evaluation of the suitability of thermal wave interferometry for the testing of plasma sprayed coatings, *NDT Int.*, **8**, 17–24.
- Alonso, F., Fagoaga, I. and Oregui, P. (1991). Erosion protection of carbon–epoxy composites by plasma sprayed coatings, *Surf. Coat. Technol.*, **49**, 482–488.
- Andrews, D.J. and Taylor, J.A.T. (2000). Quality control of thermal barrier coatings using acoustic emission, *J. Therm. Spray Technol.*, **9**, 181–190.
- Andritschky, M., Teixiera, V., Rebouta, L., Buchkremer, H.P. and Stöver, D. (1995). Adherence of combined physically vapour-deposited and plasma-sprayed ceramic coatings, *Surf. Coat. Technol.*, **76–77**, 101–105.
- Askwith, T.C. (1980). The basic mechanism of wear, *Surf. J.*, **11**, 2–9.
- Barbezat, G., Hochstrasser, J. and Nicoll, A.R. (1991). Caractérisation et contrôle des revêtements déposés par projection thermique, Plasma Technik AG, Wohlen, Switzerland, unpublished data.
- Beauvais, S., Guiport, V., Jeandin, M., Juve, D., Treheux, D., Robinson, A. and Saenger, R. (2004). Study of the influence of microstructure on electric properties of plasma sprayed alumina coatings using the scanning electron microscope mirror effect (SEMME) method, in *Proceedings of the International Thermal Spray Conference'04*, CD-Rom, ISBN 3-87155-792-7, DVS-Verlag, Düsseldorf, Germany.
- Beghini, M., Bertini, L., Frendo, F. and Giorni, E. (1997). Determination of thermal sprayed coatings elastic modulus using four point bedning point, in *Surface Treatment 97*, M.H. Aliabadi and C.A. Brebbia (Eds), Computational Mechanics Publications, Boston, MA, USA, pp. 60–70.
- Berndt, C.C. and Herman, H. (1983). Properties and phase studies of plasma sprayed Y-stabilized zirconia thermal barrier coatings, in *Proceedings of the 10th International Thermal Spray Conference*, Vol. 80, DVS, Düsseldorf, Germany, pp. 175–179.
- Berndt, C.C. and McPherson, R. (1980). A fracture mechanics approach to the adhesion of flame and plasma sprayed coatings, in *Proceedings of the 9th International Thermal Spray Conference*, Nederlands Instituut voor Lastechniek, The Hague, The Netherlands, pp. 310–316.
- Berthe, L., Bartnicki, E., Bolis, C., Boustie, M., Arrigini, M., Barradas, S., Jeandin, M., Barbezat, G., Dumont, B. and Desalos, Y. (2002). Developments in laser shock adhesion test (LASAT), in *Proceedings of the International Thermal Spray Conference 2002*, E. Lugscheider and C.C. Berndt (Eds), DVS-Verlag, Düsseldorf, Germany, pp. 587–591.
- Blann, G.A. (1992). The important role of microstructural evaluation in each phase of thermally sprayed coatings application, in *Thermal Spray: International Advances in Coatings Technology*, C.C. Berndt (Ed.), ASM International, Materials Park, OH, USA, pp. 959–966.
- Blann, G.A., Diaz, D.J. and Nelson, J.A. (1989). Raising the standards for coatings analysis, *Adv. Mater. Proc.*, **12**, 31–36.
- Blanpain, B., Mohrbacher, H., Liu, E., Celis, J.P. and Roos, J.R. (1995). Hard coatings under vibrational contact conditions, *Surf. Coat. Technol.*, **74–75**, 953–958.

- Brandt, R. and Neuer, G. (1979). Thermal diffusivity of solids – analysis of a modulated heating-beam technique, *High Temp. High Press.*, **11**, 59–68.
- Brotzen, F.R. (1994). Mechanical testing of thin films, *Int. Mater. Rev.*, **39**, 24–45.
- Buchmann, M., Escrivano, M., Gadow, R., Bürkle, G., Mahlich, M. and Fecht, H.J. (2002). On the elastic mechanical properties of thermally sprayed coatings, in *Proceedings of the International Thermal Spray Conference 2002*, E. Lugscheider and C.C. Berndt (Eds), DVS-Verlag, Düsseldorf, Germany, pp. 598–605.
- Bucklow, I.A. (1980). Possible methods for the NDT of sprayed coatings, *Surf. J.*, **11**, 3–12.
- Bunshah, R.F. (1994). Metallurgical application, in *Handbook of Deposition Technologies for Films and Coatings*, 2nd Edition, R.F. Bunshah (Ed.), Noyes, Park Ridge, NJ, USA, pp. 740–762.
- Buran, U. and Fischer, M. (1988). Properties of plasma spray coatings for piston ring running surfaces, in *1st Plasma Technik Symposium*, Vol. 2, S. Blum-Sandmeier, H. Eschnauer, P. Huber and A.R. Nicoll (Eds), Plasma Technik, Wohlen, Switzerland, pp. 25–36.
- Burnett, P.J. and Rickerby, D.S. (1987). Assessment of coating hardness, *Surf. Eng.*, **3**, 69–76.
- Buzon, J. and Roussel, J.C. (1981). Spectrometrie d'absorption dans l'infrarouge, *Tech. Ingén.*, P2 855, 1–10.
- Castejon, B., Ougoughi, L. and Pedoussaut, N. (2005). *Projection Plasma de Dioxyde de Titane*, Undergraduate student project under the direction of L. Pawłowski, ENSCL, Lille, France.
- Celis, J.P., Drees, D., Maesen, E. and Roos, J.R. (1993). Quantitative determination of through-coating porosity in thin ceramic PVD coatings, *Thin Solid Films*, **224**, 58–62.
- Chandler, P.E. (1989). High  $T_c$  – the role of plasma spraying, in *Proceedings of the 12th International Thermal Spray Conference*, The Welding Institute, Cambridge, UK, Paper 93.
- Chiang, S.S., Marshal, D.B. and Evans, A.G. (1981). A simple method for adhesion measurements, in *Surfaces and Interfaces in Ceramic and Ceramic–Metal Systems*, Materials Science Research, Vol. 14, E. Pash and A.G. Evans (Eds), Plenum Press, New York, NY, pp. 603–617.
- Chicot, D., Démarécaux, P. and Lesage, J. (1996). Interface indentation test for the determination of adhesive properties of thermal sprayed coatings, *Thin Solid Films*, **283**, 151–157.
- Colin, C., Boussuge, M., Valentin, D. and Desplanches, D. (1988). Mechanical testing of plasma sprayed coatings of ceramics, *J. Mater. Sci.*, **23**, 2121–2128.
- Cosack, T., Pawłowski, L., Schneiderbanger, S. and Sturlese, S. (1992). Thermal barrier coatings on turbine blades by plasma spraying with improved cooling, in *Proceedings of the 37th ASME International Gas Turbine and Aeroengineering Congress and Exposition*, Cologne, Germany, 1–4 June, Paper 92-GT-319.
- Cowan, R.D. (1963). Pulse method of measuring thermal diffusivity at high temperatures, *J. Appl. Phys.*, **34**, 926–927.
- Crostack, H.-A., Krüger, A. and Pohl, K.-J. (1986). Zerstörungsfreie Qualitätssicherung von Beschichtungen, *VDI Ber.*, **624**, 115–146.
- Cullity, B.D. (1972). *Introduction to Magnetic Materials*, Addison-Wesley, Reading, MA, USA.

- Cullity, B.D. (1977). *Elements of X-Ray Diffraction*, 2nd Edition, Addison-Wesley, Reading, MA, USA.
- Das, D.K., Srivastava, M.P., Joshi, S.V. and Sivakumar, R. (1991). Scratch adhesion testing of plasma-sprayed yttria-stabilized zirconia coatings, *Surf. Coat. Technol.*, **46**, 331–345.
- Dearnley, P.A., Hyland, M.M., Metson, J.B. and Roberts, K.A. (1991). Analysis of vacuum plasma sprayed  $\alpha$ -titanium, *J. Mater. Sci. Lett.*, **10**, 884–886.
- de Boer, J., Butter, J., Grosskopf, B. and Jeschke, P. (1980). Hot wire technique for determining high thermal conductivities, *Refract. J.*, September/October, 1–6.
- Deram, V., Minichiello, C., Vannier, R.-N., Le Maguer, A., Pawłowski, L. and Murano, D. (2003). Microstructural characterizations of plasma sprayed hydroxyapatite coatings, *Surf. Coat. Technol.*, **166**, 153–159.
- Despujols, J. (2000). Spectrométrie d'émission des rayons X, *Tech. Ingén.*, P2 695, 1–19.
- Diaz, D.J. (1992). The microstructural characterization of thermally sprayed coatings using digital X-ray mapping, in *Thermal Spray: International Advances in Coatings Technology*, C.C. Berndt (Ed.), ASM International, Materials Park, OH, USA, pp. 953–957.
- Diaz, D.J. and Blann, G.A. (1991). Thermally sprayed coatings, *ASTM Stand. News*, May, 48–53.
- Elssner, G., Kunkel, K., Dieser, K., Weber, S. and Kopp, W.-U. (1990). Preparation of ceramic sprayed coatings on metal substrates, *Pract. Metall.*, **27**, 211–230.
- Eskling, A. (1997). Sample preparation technique for metallography of surface coatings, in *Surface Modification Technology, X*, T.S. Sudarshan, K.A. Khor and M. Jeandin (Eds), The Institute of Materials, London, UK, pp. 641–654.
- Eyre, T.S. (1984). Wear: laboratory tests and field evaluation, *Surf. J.*, **15**, 7–13.
- Finlayson, T.R., Fayman, Y.C., Lowe, D.B., Przelozny, Z. and Smith, T.F. (1990). Flux pinning studies for plasma sprayed  $\text{YBa}_2\text{Cu}_3\text{O}_{7-x}$ , in *Proceedings of the 3rd International Symposium on Superconductors*, Senai, Japan, 6–9 November, pp. 1–4.
- Föhl, J., Weissenberg, T. and Wiedemeyer, J. (1988). General aspects for tribological applications of hard particle coatings, in *1st Plasma Technik Symposium*, Vol. 3, S. Blum-Sandmeier, H. Eschnauer, P. Huber and A.R. Nicoll (Eds), Plasma Technik, Wohlen, Switzerland, pp. 23–34.
- Fournier, D., Saint-Jacques, R.G., L'Esperance, G., Brunet, C. and Dallaire, S. (1985). Microstructure and composition of plasma sprayed TiC coatings, in *Proceedings of Electron Microscope and Analysis Group '85*, Newcastle upon Tyne, UK, 2–5 September, pp. 543–546.
- Fowler, D.B. (1991). Metallographic evaluation of thermally sprayed coatings, *ASTM Stand. News*, May, 54–57.
- Fowler, D.B., Riggs, W. and Russ, J.C. (1990). Inspecting thermally sprayed coatings, *Adv. Mater. Proc.*, **138**, 54–57.
- Gaussorgues, G. (1981). *La Thermographie Infrarouge*, Technique et Documentation, Paris, France.
- Gerson, R. and Marshall, T.C. (1959). Dielectric breakdown of porous ceramics, *J. Appl. Phys.*, **30**, 1650–1653.
- Gill, S.C. and Clyne, T.W. (1994). Investigation of residual stresses generation during thermal spraying by continuous curvature measurements, *Thin Solid Films*, **250**, 172–180.

- Gitzhofer, F., Pawlowski, L., Lombard, D., Martin, C., Kaczmarek, R. and Boulos, M. (1985). The apparent thermal diffusivity and thermal contact resistance in plasma sprayed multicoatings, *High Temp. High Press.*, **18**, 563–573.
- Gitzhofer, F., Martin, C. and Fauchais, P. (1987). Contrôle par thermographie infrarouge de l'apparition de fissures dans un matériau céramique projeté par plasma et soumis à un cyclage thermique, *Rev. Gén. Therm.*, **301**, 63–69.
- Glandus, J.C., Platon, F. and Boch, P. (1979). Measurements of the elastic moduli of ceramics, *Mater. Eng. Appl.*, **1**, 243–246.
- Gouldstone, A., Prchlík, L., Kulkarni, A. and Sampath, S. (2004). Elastoplastic characterization of thermal spray coatings using instrumented indentation, in *Proceedings of the International Thermal Spray Conference'04*, CD-Rom, ISBN 3-87155-792-7, DVS-Verlag, Düsseldorf, Germany.
- Gräf, I. (1981). Metallographic investigations of plasma sprayed titanium and titanium alloy coatings, *Zeiss Inform. Oberk.*, **25**, 13–19.
- Green, D.R., Schmeller, M.D. and Sulit, R.A. (1983). Thermal NDE method for thermal spray coatings, in *Proceedings of the 10th International Thermal Spray Conference Essen*, Vol. 80, DVS, Düsseldorf, Germany, pp. 24–27.
- Green, D.R., Wandling, C.R., Gatto, F.B. and Rogers, F.S. (1984). System for NDE of thermal spray coating bonds, in *2nd National Conference on Thermal Spray*, Long Beach, CA, USA, 31 October–2 November, pp. 125–133.
- Grützner, H. and Weiss, H. (1991). A novel shear test for plasma sprayed coatings, *Surf. Coat. Technol.*, **45**, 317–323.
- Guo, D.Z. and Wang, L.J. (1992). Measurements of the critical strain energy release rate of plasma-sprayed coatings, *Surf. Coat. Technol.*, **56**, 19–25.
- Guyonnet, J. and Fauchais, P. (1975). Projection au chalumeau à plasma de revêtements céramiques à coefficients de frottement variables, in *International Round Table Study of Applications of Transport Phenomena in Thermal Plasmas*, C. Bonnet (Ed.), CNRS, Odeillo, France, Paper IV.5.
- Hall, P.M. (1997). Resistance calculation for thin film rectangles, *Thin Solid Films*, **300**, 256–264.
- Hantsche, H. (1988). Röntgenmikroanalyse mit dem Raster-Elektronenmikroskop, in *Raster-Elektronenmikroskopie und Mikrobereichsanalyse*, G. Pfefferkorn (Ed.), Seminar No. 9658/01.028, Technische Akademie Esslingen, Esslingen, Germany.
- Harmsworth, P.D. and Stevens, R. (1992). Microstructure of zirconia–yttria plasma sprayed thermal barrier coatings, *J. Mater. Sci.*, **27**, 616–624.
- Hasselman, D.P.H. (1970). Thermal stress resistance parameters for brittle refractory ceramics: a compendium, *Ceram. Bull.*, **49**, 1033–1037.
- Haure, T., Denoirjean, A., Tristant, P., Desmaison, J., Fauchais, P. and Maître, A. (2003). Interconnected porosity of plasma sprayed alumina coatings: evaluation and modification, in *Thermal Spray 2003: Advancing the Science and Applying the Technology*, C. Moreau and B. Marple (Eds), ASM International, Materials Park, OH, USA, pp. 1317–1324.
- Hermannsson, L., Eklund, L., Askengren, L. and Carlsson, R. (1985). On the microstructure of plasma-sprayed chromium oxide, unpublished data.
- Hobson, M.K. and Reiter, H. (1988). Residual stresses in  $\text{ZrO}_2$ –8 %  $\text{Y}_2\text{O}_3$  plasma-sprayed thermal barrier coatings, *Surf. Coat. Technol.*, **34**, 33–42.

- Hocking, M.G., Vasantasree, V. and Sidky, P.S. (1989). *Metallic and Ceramic Coatings*, Longman, Burnt Hill, UK.
- Hodge, P.E., Stecura, S., Gedwill, M.A., Zaplatynsky, I. and Levine, S.L. (1980). Thermal barrier coatings: burner rig hot corrosion test results. *J. Mater. Energy Syst.*, 1, 47–58.
- Holcombe, C.E., Jr (1978). Fabrication of thin walled ceramic structures, *Am. Ceram. Soc. Bull.*, 57, 610.
- Holmberg, K. and Matthews, A. (1994). Coatings tribology: a concept, critical aspects and future directions, *Thin Solid Films*, 253, 173–178.
- Ingo, G.M. (1991). Origin of darkening in 8 wt% yttria–zirconia plasma sprayed thermal barrier coatings, *J. Am. Ceram. Soc.*, 74, 381–386.
- Ingo, G.M., Parapazzo, E., Bagnarelli, O. and Zucchetti, N. (1990). XPS studies on cerium, zirconium and yttrium valence states in plasma sprayed coatings, *Surf. Interface Anal.*, 16, 515–519.
- Jaarinen, J. and Luukkala, M. (1984). The use of thermal waves for non-destructive evaluation of plasma sprayed coatings, in *Proceedings of the 3rd European Conference on Nondestructive Testing*, Florence, Italy, 15–18 October, pp. 128–137.
- Jacobson, B.E. (1982). Microstructure of PVD-deposited films characterized by transmission electron microscopy, in *Deposition Technologies for Films and Coatings*, R.F. Bunshah (Ed.), Noyes Publications, Park Ridge, NJ, USA, pp. 288–234.
- Jaworski, R., Pawłowski, L., Roudet, F. and Petit, F. (2007). Characterization of mechanical properties of suspension plasma sprayed TiO<sub>2</sub> coatings using scratch test, *Surf. Coat. Technol.*, doi: 1016/j.surfcoat.2007.09.44.
- Keller, T., Wagner, W., Ilavsky, J., Margadant, N., Siegmann, S., Pisacka, J., Matejicek, J., Barbezat, G., Fiala, P. and Pirling, T. (2001). Microstructural studies of thermally sprayed deposits by neutron scattering, in *Thermal Spray 2001: New Surfaces for a New Millennium*, C.C. Berndt, K.A. Khor and E.F. Lugscheider (Eds), ASM International, Materials Park, OH, USA, pp. 653–660.
- Kelly, A. and Macmillan, N.H. (1986). *Strong Solids*, Clarendon Press, Oxford, UK.
- Kerrisk, J.F. (1971). Thermal diffusivity of heterogeneous materials, *J. Appl. Phys.*, 42, 267–271.
- Kerrisk, J.F. (1972). Thermal diffusivity of heterogeneous materials, II. Limits of steady state approximation, *J. Appl. Phys.*, 43, 112–117.
- Kesler, O., Matejicek, J., Sampath, S., Suresh, S., Gnaeupel-Herold, T., Brand, P.C. and Prask, H.J. (1998). Measurements of residual stresses in plasma-sprayed metallic, ceramic and composite coatings, *Mater. Sci. Eng.*, A, 257, 215–224.
- Kitahara, S. and Hasui, A. (1974). A study of bonding mechanism of sprayed coatings, *J. Vac. Sci. Technol.*, 11, 747–753.
- Kozerski, S. (1986). The oxide reduction in the plasma sprayed NiAl layers, in *Advances in Thermal Spraying*, Pergamon Press Canada, Willowdale, Canada, pp. 845–853.
- Kumar, K. and Das, D. (1980). Role of atmosphere in the crystallization of amorphous plasma sprayed SmCo deposits, *J. Appl. Phys.*, 51, 1031–1035.
- Kuroda, S. and Clyne, T.W. (1991). The quenching stresses in thermally sprayed coatings, *Thin Solid Films*, 200, 49–66.
- Laboucheix, V. (1990). *Traité de la Qualité Totale*, Dunod, Paris, France.
- Leidheiser, H., Jr., Music, S., Vertes, A., Herman, H. and Zatorski, R.A. (1984). Metal/flame-aluminium interface as studied by emission Mössbauer spectroscopy, *J. Electrochem. Soc.*, 131, 1348–1349.

- Leistner, E. (1993). Preparation and characterization of thermal sprayed coatings, in *Thermische Spritzkonferenz 93*, Vol. 152, DVS-Verlag, Düsseldorf, Germany, pp. 127–132.
- Lescriba, D. and Vincent, A. (1996). Ultrasonic characterization of plasma sprayed coatings, *Surf. Coat. Technol.*, **81**, 297–306.
- Li, H., Ng, B.S., Khor, K.A., Cheang, P. and Clyne, T.W. (2004). Raman spectroscopy determination of phases within thermal sprayed hydroxyapatite splats and subsequent *in vitro* dissolution examination, *Acta Mater.*, **52**, 445–453.
- Lide, D.L. (1997). *Handbook of Chemistry and Physics*, CRC Press, New York, NY, USA.
- Lima, R.S., Kruger, S.E., Lamouche, G. and Marple, B.R. (2003). Elastic modulus measurements via laser-ultrasonic and Knoop indentation techniques, in *Thermal Spray 2003: Advancing the Science and Applying the Technology*, C. Moreau and B. Marple (Eds), ASM International, Materials Park, OH, USA, pp. 1369–1378.
- Loeb, A.L. (1954). Thermal conductivity: VIII, a theory of thermal conductivity of porous materials, *J. Am. Ceram. Soc.*, **37**, 96–99.
- Lopez, E., Zambellei, G. and Nicoll, A.R. (1991). An indentation test for the measurement of cohesion of plasma sprayed composite coatings, in *2nd Plasma Technik Symposium*, S. Blum-Sandmeier, H. Eschnauer, P. Huber and A.R. Nicoll (Eds), Plasma Technik, Wohlen, Switzerland, pp. 285–291.
- Loretto, M.H. (1984). *Electron Beam Analysis of Materials*, Chapman & Hall, New York, NY, USA.
- Lutz, E.H. (1993). Plasma ceramics, *Powder Metall. Int.*, **25**, 131–137.
- Macdonald, J.R. (1987). *Impedance Spectroscopy*, John Wiley & Sons, Inc., New York, NY, USA.
- Maisel, L.I. and Glang, R. (1970). *Handbook of Thin Film Technology*, McGraw Hill, New York, NY, USA.
- Malingrey, B. (1984). Spéctrométrie d'absorption dans l'infrarouge, *Tech. Ingén.*, **P 2** 845, 1–14.
- Margadant, N., Siegmann, S., Patscheider, J., Keller, T., Wagner, W., Ilavsky, J., Pisacka, J., Barbezat, G. and Fiala, P. (2001). Microstructure–property relationship and cross-property correlations of thermal sprayed Ni-alloy coatings, in *Thermal Spray 2001: New Surfaces for a New Millennium*, C.C. Berndt, K.A. Khor and E.F. Lugscheider (Eds), ASM International, Materials Park, OH, USA, pp. 643–652.
- Martin, C. and Fauchais, P. (1981). Mesure par thermographie infrarouge de l'émissivité de matériaux céramiques, *Rev. Int. Hautes Temp. Refract.*, **18**, 95–108.
- Martin, J.L. and George, A. (1998). *Caractérisation Expérimentale des Matériaux II*, Presse Polytechnique et Universitaire Romande, Lausanne, Switzerland.
- McPherson, R. (1984). A model for thermal conductivity of plasma sprayed ceramic coatings, *Thin Solid Films*, **112**, 89–95.
- McPherson, R. (1989). A review of microstructure and properties of plasma sprayed ceramic coatings, *Surf. Coat. Technol.*, **39/40**, 173–181.
- McPherson, R. and Shafer, B.V. (1982). Interlamellar contact within plasma sprayed coatings, *Thin Solid Films*, **97**, 201–204.
- Mehan, R.L., Jackson, M.R., Raider, J.R. and Carter, W.T. (1987). The use of a ring test to evaluate plasma deposited metals, *J. Mater. Sci.*, **22**, 4476–4483.
- Meyer, E.H. and Pohl, K.-J. (1989). Further development of the holographic sound field imaging method for testing thermal sprayed coatings, in *Proceedings of the 12th International Thermal Spray Conference*, The Welding Institute, Cambridge, UK, Paper 33.

- Morris, J.D., Almond, D.P., Patel, P.M. and Reiter, H. (1989). Developments in thermal wave non-destructive testing systems for thermal spray coatings, in *Proceedings of the 12th International Thermal Spray Conference*, The Welding Institute, Cambridge, UK, Paper 99.
- Morse, C.T. and Hill, G.J. (1970). The electric strength of alumina: the effect of porosity, *Proc. Br. Ceram. Soc.*, 18, 23–35.
- Nakamichi, M. and Kawamura, H. (2001). Mechanical and electrical properties of  $\text{Al}_2\text{O}_3$ – $\text{TiO}_2$  coating as electrical insulator, in *Thermal Spray 2001: New Surfaces for a New Millennium*, C.C. Berndt, K.A. Khor and E. Lugscheider (Eds), ASM International, Materials Park, OH, USA, pp. 1039–1043.
- Namba, Y., Nakazato, H. and Honma, K. (1992). An ultrasonic method to study the adhesion of thermally sprayed coatings, in *Thermal Spray: International Advances in Coatings Technology*, C.C. Berndt (Ed.), ASM International, Materials Park, OH, USA, pp. 241–245.
- Norris, D.A. (1988). Synthesis and characterization of yttrium based superconductors, *BSc Thesis*, Department of Physics, Monash University, Australia.
- Noutomi, A., Kodama, M., Inoue, Y., Ono, T., Kawano, M. and Tani, N. (1989). Residual stresses measurement on plasma sprayed coatings, *Weld. Int.*, 11, 947–953.
- Noyan, I.C. and Cohen, J.B. (1987). *Residual Stress-Measurements by Diffraction and Interpretation*, Springer-Verlag, New York, NY, USA.
- Nygård, C.M., White, K.W. and Ravi-Chandar, K. (1998). Strength of HVOF coating–substrate interfaces, *Thin Solid Films*, 332, 185–188.
- Oberländer, B. and Kvernes, I. (1983). Metallographic studies on plasma sprayed duplex coating system, *Metallography*, 16, 117–135.
- Oliver, W.C. and Pharr, G.M. (1992). An improved technique for determining hardness and elastic modulus using load and displacement sensing indentation experiments, *J. Mater. Res.*, 7, 1564–1583.
- Ostojic, P. and McPherson, R. (1986). Acoustic emission study of environmental effects in thermally sprayed coatings, *Thin Solid Films*, 136, 215–227.
- Ostojic, P. and McPherson, R. (1987). Indentation toughness testing of plasma sprayed coatings, *Mater. Forum*, 10, 247–255.
- Ostojic, P. and McPherson, R. (1988). Indentation toughness: its characteristics in thermally sprayed coatings, *Mater. Sci. Forum*, 34–36, pp. 451–455.
- Pacey, R.A. and Stratford, V. (1988). *In-situ* acoustic emission monitoring of the plasma spraying process, in *1st Plasma Technik Symposium*, Vol. 2, S. Blum-Sandmeier, H. Eschnauer, P. Huber and A.R. Nicoll (Eds), Plasma Technik, Wohlen, Switzerland, pp. 135–144.
- Pantucek, P., Lugscheider, E. and Miller, U. (1991). Influence of surface temperature during plasma spraying on residual stresses in TBC's, in *2nd Plasma Technik Symposium*, Vol. 2, S. Blum-Sandmeier, H. Eschnauer, P. Huber and A.R. Nicoll (Eds), Plasma Technik, Wohlen, Switzerland, pp. 143–150.
- Parker, W.J., Jenkins, R.J., Butler, C.P. and Abbott, G.L. (1961). Flash method for determining thermal diffusivity, heat capacity and thermal conductivity, *J. Appl. Phys.*, 32, 1679–1684.
- Patel, P.M. and Almond, D.P. (1985). Thermal wave testing of plasma sprayed coatings and a comparison of the effects of coating microstructure on the propagation of thermal and ultrasonic waves, *J. Mater. Sci.*, 20, 955–966.

- Pawlowski, L. (1974). A study of electrical and structural properties of plasma sprayed  $\text{Al}_2\text{O}_3 + \text{W}$  coatings, in *Proceedings of the 2nd Polish Symposium on Plasma Chemistry*, Czestochowa, Poland, October, pp. 278–284.
- Pawlowski, L. (1985). Optimisation des Paramètres de Projection des Céramiques par Plasma d'Arc. Etude des Propriétés Physiques et Thermophysiques des Couches Projétées – Exemple d'Application: Substrats pour la Microélectronique Hybride, DSc Thesis, The University of Limoges, Limoges, France.
- Pawlowski, L. (1987a). Microstructural study of plasma sprayed alumina and nickel chromium coatings, *Surf. Coat. Technol.*, **31**, 103–116.
- Pawlowski, L. (1987b). W. Haldenwanger, Berlin, Germany, unpublished data.
- Pawlowski, L. (1988). The relationship between structure and dielectric properties in plasma sprayed alumina coatings, *Surf. Coat. Technol.*, **35**, 285–298.
- Pawlowski, L. (1991). The properties of plasma sprayed aluminium-aluminium oxide cermets, *Surf. Coat. Technol.*, **48**, 219–224.
- Pawlowski, L. (1996). Technology of thermally sprayed anilox rolls: state of art, problems and perspectives, *J. Therm. Spray Technol.*, **5**, 317–334.
- Pawlowski, L. (1998). Mikrogefügeuntersuchungen an thermisch gespritzten Schichten, *Structure*, **33**, 11–13.
- Pawlowski, L. (2003). *Dépôts Physiques. Techniques, Microstructures et Propriétés*, Presse Polytechnique et Universitaire Romande, Lausanne, Switzerland.
- Pawlowski, L. and Fauchais, P. (1986). The least square method in the determination of thermal diffusivity using flash method, *Rev. Phys. Appl.*, **21**, 83–86.
- Pawlowski, L. and Fauchais, P. (1992). Thermal transport properties of thermally sprayed coatings, *Int. Mater. Rev.*, **37**, 271–289.
- Pawlowski, L., Martin, C. and Fauchais, P. (1983). The application of infrared thermography in testing the coatings and optimizing the plasma spraying process, in *Proceedings of the 10th International Thermal Spray Conference Essen*, Vol. 80, DVS, Düsseldorf, Germany, pp. 31–36.
- Pawlowski, L., Fauchais, P. and Martin, C. (1985). Analysis of boundary conditions and transient signal treatment in diffusivity measurements by laser pulse method, *Rev. Phys. Appl.*, **20**, 1–11.
- Pepperhoff, W. (1965). Quantitative Auflichtmikroskopie mit Hilfe aufgedampfter Interferenzschichten, *Arch. Eisenhüt.*, **36**, 941–950.
- Podlesak, H., Schnick, T., Pawlowski, L., Steinhäuser, S. and Wielage, B. (2000). Microscopic study of Al-SiC particulate composites processed by laser shocks, *Surf. Coat. Technol.*, **124**, 32–38.
- Postek, M.T., Howard, K.S., Johnson, A.H. and McMichael, K.L. (1980). *Scanning Electron Microscopy. A Student's Handbook*, Postek and Ladd Research Industries, Inc., Williston, VT 05495, USA.
- Preece, I. and Andrews, C.W.D. (1973). Plasma spraying of ferrites, *J. Mater. Sci.*, **8**, 964–967.
- Puerta, D.G. (2005). The preparation and evaluation of thermal spray coatings: mounting, *J. Therm. Spray Technol.*, **14**, 450–452.
- Richardson, M.J. (1984). Application of differential scanning calorimetry to the measurements of specific heat, in *Compendium of Thermophysical Properties Measurements Methods*, K.D. Maglic, A. Cezairliyan and V.E. Peletsky (Eds), Plenum Press, New York, NY, USA.

- Rickerby, D. (1996). Measurements of coating adhesion, in *Metallic and Ceramic Protective Coatings*, K.H. Stern (Ed.), Chapman & Hall, London, UK, pp. 306–334.
- Ritter, A.M. and Henry, M.F. (1982). Microstructure of a plasma-sprayed superalloy coating/substrate, *J. Mater. Sci.*, 17, 2741–2752.
- Rose-Innes, A.C. and Rhoderick, E.H. (1978). *Introduction to Superconductivity*, Pergamon Press, Oxford, UK.
- Rückert, M. (1989). Plasma spray coating symposium, *Structure*, 20, 15–18.
- Rückert, M., Wigren, J. and Svantesson, J. (1989). Metallographic preparation of plasma sprayed ZrO<sub>2</sub> coatings sprayed under varying conditions, *Pract. Metall.*, 28, 227–237.
- Safai, S. and Herman, H (1977). Microstructural investigation of plasma sprayed aluminium oxide, *Thin Solid Films*, 45, 295–307.
- Sampath, S. (1993). Microstructural characteristics of plasma spray consolidated amorphous powders, *Mater. Sci. Eng.*, A, 167, 1–10.
- Sandt, A. and Krey, J. (1985). NiCrBSi-Schichten mit Hartstoff-Beimischungen, Teil II: Verhalten bei gleitender und abrasiver Verschleißbeanspruchung, *Metall*, 39, 15–19.
- Sexsmith, M. and Troczynski, T. (1994). Peel adhesion test for thermal spray coatings, *J. Therm. Spray Technol.*, 3, 404–411.
- Shadley, J.R., Rybicki, E.F., Xiong, Y., McGrann, R.T.R. and Savarimuthu, A.C. (2000). An ASM recommended practice for evaluation of Young's modulus and Poisson ratio of thermal spray coatings bonded to a substrate, in *Thermal Spray: Surface Engineering via Applied Research*, C.C. Berndt (Ed.), ASM International, Materials Park, OH, USA, pp. 1291–1295.
- Shankar, N.R., Berndt, C.C. and Herman, H. (1983a). Structural integrity of thermal barrier coatings by acoustic emission studies, in *Proceedings of the 10th International Thermal Spray Conference*, Vol. 80, DVS, Düsseldorf, Germany, pp. 41–45.
- Shankar, N.R., Berndt, C.C., Herman, H. and Rangawamy, S. (1983b). Acoustic emission from thermally cycled plasma sprayed oxides, *Ceram. Bull.*, 62, 614–619.
- Sheffler, K.D., Graziani, R.A. and Sinko, G.C. (1982). *JT9D Thermal Barrier Coated Vanes*, NASA Report CR-16964, NASA, Lewis Research Center, Cleveland, OH, USA.
- Shinde, S.L., Reimanis, I.E. and De Jonghe, L.C. (1987). Degradation in thermal barrier coatings, *Adv. Ceram. Mater.*, 2, 60–64.
- Siemers, P. and Mehan, R.L. (1983). Mechanical and physical properties of plasma sprayed stabilized zirconia, *Ceram. Eng. Sci. Proc.*, 3, 828–840.
- Smith, R.W., Jiao, D., Rose, J. and Roggs, W. (1992). An NDT method for measuring the quality of aluminium/polyester thermal sprayed coatings, in *Thermal Spray: International Advances in Coatings Technology*, C.C. Berndt (Ed.), ASM International, Materials Park, OH, USA, pp. 227–234.
- Spinner, S. and Tefft, W.E. (1961). A method for determining mechanical resonance frequencies and for calculating elastic moduli from these frequencies, *Proc. ASTM*, 61, 1221.
- Steffens, H.-D. and Beczkowiak, J. (1983) Adhesion by low pressure plasma spraying, in *Proceedings of the 10th International Thermal Spray Conference*, Vol. 80, DVS, Düsseldorf, Germany, pp. 218–221.
- Steffens, H.-D., Crostack, H.-A. and Beczkowiak, J. (1984). Testing and inspection of coatings, in *Coatings for High Temperature Application*, E. Lang (Ed.), Applied Science Publishers, London, UK, pp. 193–215.

- Suga, Y., Harjanto, Y. and Takahashi, J. (1992). Study on the ultrasonic test for evaluating the adhesion of sprayed coatings to a substrate, in *Thermal Spray: International Advances in Coatings Technology*, C.C. Berndt (Ed.), ASM International, Materials Park, OH, USA, pp. 247–252.
- Taylor, M.L., Murphy, J.G. and King, H.W. (1987). Brittle/ductile erosion of plasma sprayed ceramic and metallic coatings, in *Thermal Spray: Advances in Coatings Technology*, D.L. Houck (Ed.), ASM International, Materials Park, OH, USA, pp. 143–149.
- Taylor, D.J., Fleig, P.F. and Hietala, S.L. (1998). Technique for characterization of thin film porosity, *Thin Solid Films*, 332, 257–261.
- Timoshenko, S. (1976). *Strength of Materials*, Robert E. Kreiger Publishing Company, New York, NY, USA.
- Tiwari, R., Sampath, S., Herman, H. and Anekawa, Y. (1993). Cavitation-erosion of plasma sprayed nickel aluminides, in *Thermal Spray Coatings: Research, Design and Application*, C.C. Berndt and T.F. Bernecki (Eds), ASM International, Materials Park, OH, USA, pp. 423–428.
- Tomaszek, R., Nitsch, K., Pawlowski, L., Znamirovski, Z., Kondrat, A. and Brylak, M. (2006a). Impedance spectroscopy of suspension plasma sprayed titania coatings, *Surf. Coat. Technol.*, 201, 1930–1935.
- Tomaszek, R., Pawlowski, L., Gengembre, L., Laureyns, J., Znamirovski, Z. and Zdanowski, J. (2006b). Microstructural characterization of plasma sprayed TiO<sub>2</sub> functional coating with gradient of crystal grain size, *Surf. Coat. Technol.*, 201, 45–56.
- Touloukian, Y.S. and Buyco, E.H. (1970). *Thermophysical Properties of Matter*, Vol. 4, *Specific Heat, Metallic Elements and Alloys*, IFI Plenum, New York, NY, USA.
- Touloukian, Y.S., Powell, R.W., Ho, C.Y. and Klemens, P.G. (1970). *Thermophysical Properties of Matter*, Vol. 1, *Thermal Conductivity: Metallic Elements and Alloys*, IFI Plenum, New York, NY, USA.
- Touloukian, Y.S., Kirby, R.K., Taylor, R.E. and Lee, T.Y.R. (1978). *Thermophysical Properties of Matter*, Vol. 13, *Thermal Expansion, Nonmetallic Solids*, IFI Plenum, New York, NY, USA.
- Troczyński, T. and Camire, J. (1994). Resistance to fracture of thermal sprayed ceramic coatings, in *Thermal Spray: Industrial Applications*, C.C. Berndt and S. Sampath (Eds), ASM International, Materials Park, OH, USA, pp. 66–67.
- Tucker, R.C., Jr (1982). Plasma and detonation gun deposition techniques and coating properties, in *Deposition Technologies for Films and Coatings*, R.F. Bunshah (Ed.), Noyes Publications, Park Ridge, NJ, USA, pp. 454–489.
- Turell, G. and Corset, J. (Eds) (1996). *Raman Microscopy. Development and Applications*, Academic Press, London, UK.
- Van Landuyt, P. (1995). Revêtements vitreux sur titane pour application aux prothèses articulaires, PhD Thesis, Catholic University of Louvain, Louvain, Belgium.
- Van Vlack, L.H. (1989). *Elements of Materials Science and Engineering*, Addison-Wesley, Reading, MA, USA.
- Varis, T., Rajamäki, E. and Korpiola, K. (2001). Mechanical properties of thermal spray coatings, in *Thermal Spray 2001: New Surfaces for a Millennium*, C.C. Berndt, K.A. Khor and E.F. Lugscheider (Eds), ASM International, Materials Park, OH, USA, pp. 993–997.
- Veilleux, G., Saint-Jacques, R.G. and Dallaire, S. (1987). Cross-sectional transmission electron microscopy characterization of the interface between plasma sprayed TiC and inconel, *Thin Solid Films*, 154, 91–100.

- Wagner, C.D., Riggs, W.M., Davis, L.E., Moulder, J.F. and Muilenberg, G.E. (1978). *Handbook of X-ray Photoelectron Spectroscopy*, Perkin-Elmer Corporation, Eden Prairie, MN, USA..
- Wang, H.G. and Herman, H. (1989). Structure and properties of plasma sprayed spinel, *Ceram. Bull.*, **68**, 97–102.
- Weglowski, S. and Pawłowski, L. (1981). A study of residual stresses in plasma sprayed alumina coating, in Proceedings of the 5th International Symposium on Plasma Chemistry. Conference, B. Waldie, (Ed.), Edinburgh, UK, pp. 1–14 August, pp. 592–601.
- Wenzelburger, M., Lopez, D. and Gadow, R. (2005). Methods and application of residual stress analysis on thermally sprayed coatings and layer composites, *Surf. Coat. Technol.*, **201**, 1995–2001.
- Whittemore, O.J. (1981). Mercury porosimetry of ceramics, *Powder Technol.*, **29**, 167–175.
- Wiesmann, H.J. and Zeller, H.R. (1986). A fractal model of dielectric breakdown and prebreakdown in solid dielectrics, *J. App. Phys.*, **60**, 1770–1773.
- Wilms, V. and Herman, H. (1976). Plasma spraying of  $\text{Al}_2\text{O}_3$  and  $\text{Al}_2\text{O}_3\text{-Y}_2\text{O}_3$ , *Thin Solid Films*, **39**, 251–262.
- Wu, B.C., Chang, E., Chang, S.F. and Tu, D. (1989). Degradation mechanism of  $\text{ZrO}_2$ -8 wt%  $\text{Y}_2\text{O}_3$ /Ni-22Cr-10Al-1Y thermal barrier coatings, *J. Am. Ceram. Soc.*, **72**, 212–218.
- Yoshimura, M. and Bowen, H.K. (1981). Electrical breakdown strength of alumina at high temperatures, *J. Am. Ceram. Soc.*, **64**, 404–410.
- Yuansheng, J., Huadong, W., Nicoll, A.R. and Barbezat, G. (1992). The tribological behaviour of various plasma sprayed coatings against cast iron, *Surf. Coat. Technol.*, **52**, 169–178.
- Zambelli, G. and Vincent, L. (1998). *Matériaux et Contact*, Presse Polytechnique et Universitaire Romande, Lausanne, Switzerland.
- Znamirowski, Z., Czarczynski, W., Pawłowski, L. and Le Maguer, A. (2003a). Field emission from laser engraved surface, *Vacuum*, **70**, 397–402.
- Znamirowski, Z., Czarczynski, W., Le Maguer, A. and Pawłowski, L. (2003b). Plasma sprayed and laser engraved field electron emitters, *Surf. Coat. Technol.*, **165**, 211–215.
- Znamirowski, Z., Pawłowski, L., Cichy, T. and Czarczynski, W. (2004). Low microscopic field electron emission from surface of plasma sprayed and laser-engraved  $\text{TiO}_2$ ,  $\text{Al}_2\text{O}_3 + 13 \text{ TiO}_2$  and  $\text{Al}_2\text{O}_3 + 40 \text{ TiO}_2$  coatings, *Surf. Coat. Technol.*, **187**, 37–46.

# 8

## Properties of Coatings

The properties of coatings result from the initial material and processing technology. The latter includes deposition techniques and used parameters. The parameters are often specified by the manufacturer of a powder (or wire) for most popular spray torches. Sometimes, however, it is necessary to optimize them. A useful tool for such optimization is the *statistical design of experiments* (DOE), discussed shortly in this present chapter. The DOE enables a direct correlation between a given property and a set of process parameters that may influence it. These statistical tools are also able to find out the most significative parameters (called factors) influencing the property. The parameters are different for each property. This is why it was decided not to present them in a discussion of the coatings' properties.<sup>1</sup> These properties are discussed for the following groups of materials:

- ceramics (divided sometimes into carbides and oxides);
- metals and alloys;

---

<sup>1</sup> The interested reader can find the relevant data in the first edition of this book.

- polymers;
- composites.<sup>2</sup>

Obviously, it is not possible to collect all published properties of coatings. The collected data are selected to be representative for coating materials and spray techniques. This selection was necessary for the mechanical and thermophysical properties of coatings. These properties have been tested many times and there is a wealth of experimental data available. The electrical and magnetic properties are relatively harder to find and a less 'severe' selection has been made.

## 8.1 DESIGN OF EXPERIMENTS

The statistical methods used to optimize spray process parameters belong to the following groups.

Modelling by a generation of a polynomial equation of an optimized property versus significative spray parameters (factors) by applying full factorial design seems to be most frequently applied. It has been used by, for example:

- Troczynski and Plamondon (1992) to find the models of roughness, erosion, hardness, density and content of decomposition of the (W<sub>2</sub>C) phase at plasma spraying of WC + 12 wt% Co powder.
- Varacalle *et al.* (1995) to generate models of porosity, hardness and roughness of plasma-sprayed aluminum.
- Riley and Sturgeon (2005) to create models of deposition rate, deposition efficiency, roughness, adhesion, microhardness and α-Al<sub>2</sub>O<sub>3</sub> content in HVOF-sprayed alumina coatings.
- Dyshlovenko *et al.* (2006) to predict the fraction of crystalline hydroxyapatite, phases of its decomposition and of amorphous calcium phosphates in air-plasma-sprayed HA coatings.

The neural network method concept, which is based on the mechanism of biological nerve cells. The output pattern (coatings properties) is related to the input pattern (process parameters) by a number of neurons arranged in an array, called 'hidden layers' (Guessasma

---

<sup>2</sup> Although coatings of WC-Co or Cr<sub>3</sub>C<sub>2</sub>-NiCr are, in fact, composites, they are often classified as carbides. This is because carbides are always sprayed with a metal/alloy matrix.

*et al.*, 2002). The authors used the neural network method to predict hardness, Young's and Poisson moduli, adhesion and residual stress levels of  $\text{Al}_2\text{O}_3 + 13 \text{ wt\% TiO}_2$  coatings, plasma-sprayed onto different substrates.

The initial step in the factorial design of experiments is a choice of variables, the process parameters. In the simplest case, the parameters are put on low ( $-1$ ) and high ( $+1$ ) levels. The experimental space is defined inside these parameters values. A matrix for four variables corresponds to  $2^4 (=16)$  experiments, as shown in Table 8.1. In order to determine the possible nonlinear effects and to check the repeatability of the deposition process, it is recommended to realize a couple of experiments in the central point in which the variables have values equal to zero<sup>3</sup> (experiment nos 17 and 18 in Table 8.1). The choice of parameters needs some understanding of the process as there are about 50 process variables (Guessasma *et al.*, 2002). Typical variables for atmospheric-plasma spraying are as follows:

**Table 8.1** Experiments corresponding to full factorial design including four variables

Experiment no.	Variable 1	Variable 2	Variable 3	Variable 4
1	-1	-1	-1	-1
2	+1	-1	-1	-1
3	-1	+1	-1	-1
4	+1	+1	-1	-1
5	-1	-1	+1	-1
6	+1	-1	+1	-1
7	-1	+1	+1	-1
8	+1	+1	+1	-1
9	-1	-1	-1	+1
10	+1	-1	-1	+1
11	-1	+1	-1	+1
12	+1	+1	-1	+1
13	-1	-1	+1	+1
14	+1	-1	+1	+1
15	-1	+1	+1	+1
16	+1	+1	+1	+1
17	0	0	0	0
18	0	0	0	0

<sup>3</sup> If the variable is a spray distance and the 'high level' is 12 cm, the low level is 8 cm and then the central point is equal to 10 cm.

- composition of working gas, e.g. vol% of hydrogen in an argon-hydrogen mixture;
- spray distance;
- powder feed rate;
- electric power input;
- carrier gas flow rate.

For high-velocity oxy-fuel spraying, it is useful to also add another variable which is the ratio of fuel gas to oxygen (Rajamäki *et al.*, 2002). The properties of coatings sprayed in different experiments (responses) can be represented as a polynomial equation (regression equation) of the following form:

$$Y_u = b_0 + \sum b_j X_{uj} + \sum b_{ij} X_{ui} X_{uj} + \sum b_{ijk} X_{ui} X_{uj} X_{uk} + \dots \quad (8.1)$$

where  $i$ ,  $j$  and  $k$  vary from 1 to the number of variables, coefficient  $b_0$  is the mean of responses of all the experiments, coefficient  $b_i$  represents the effect of the variable  $X_i$  and  $b_{ij}$ ,  $b_{ijk}$  and  $b_{1234}$  are the coefficients of regression which represent the effects of interactions of the variables  $X_i X_j$ ,  $X_i X_j X_k$  and  $X_1 X_2 X_3 X_4$ , respectively. The coefficients in the equation can be easily found from the formula given in many textbooks, such as that of Perrin and Scharff (1999). The equation with all coefficients corresponds to the entire model inside the experimental space. However, not all of the calculated coefficients are useful and should be submitted to a *signification test*. One test, suggested by Lyonnet (1999) and applied by Dyshlovenko *et al.* (2006), is based on the assumption that the highest interaction coefficient is not significative ( $b_{1234}$  for a 4-variable experiment) and by calculations of the ratios:

$$\frac{b_1}{b_{1234}}, \frac{b_2}{b_{1234}}, \dots, \frac{b_{123}}{b_{1234}}, \frac{b_{234}}{b_{1234}} \quad (8.2)$$

The ratios are subsequently compared to the values generated by the Student's statistical test of degree of freedom equal to 1 and level of probability equal to 95 % ( $t_{1,95}$  %). All of the coefficients resulting in the ratios given by Equation (8.2) being smaller than the value of  $t_{1,95}$  % are supposed not to be significant. Some regression equations for different spray technologies are collected in Table 8.2. These enable obtaining the values of the response functions for the variables in the range between the low and high levels, knowing that they are normalized in the range  $-1 \leq X_i \leq +1$ . The response function for the additional experiments made in the

**Table 8.2** Statistical models of different coatings' properties valid inside the experimental space

Response function, Y	Coating material	Spray technique	Number of variables	Variables	Regression equation	Reference
Porosity (%)	Al	APS	3	$X_1 = \text{vol\% of He in Ar + He working gas};$ $X_2 = \text{vol\% of H}_2 \text{ in Ar + H}_2 \text{ working gas};$ $X_3 = \text{electric arc current};$ $X_4 = \text{electric arc power};$ $X_5 = \text{spray distance};$ $X_6 = \text{carrier gas flow rate}$	$Y = 7.7 + 0.9X_1 - 0.7X_3 - 1.85X_5$	Varacalle <i>et al.</i> (1995)
Fraction of amorphous phase (wt%)	$\text{Ca}_5(\text{PO}_4)_3(\text{OH})$	APS 4			$Y = 26.0 + 3.75X_2 + 12.75X_4 - 6.75X_5 - 3.5X_2X_4 - 3.5X_4X_6 - 2.75X_2X_4X_6$	Dyshlovenko <i>et al.</i> (2006)
Adhesion (MPa)	$\text{Al}_2\text{O}_3$	HVOF	3		$Y = 26.1 - 9.35X_5$	Riley and Sturgeon, (2005)

central points ( $X_i = 0$ ) should be equal to  $b_0$ . The regression equations can be expressed in the form of isopleths, also known as response surfaces (Troczynski and Plamondon, 1992). The isopleths for the response function – the fraction of the amorphous phase – are presented in Figure 8.1.

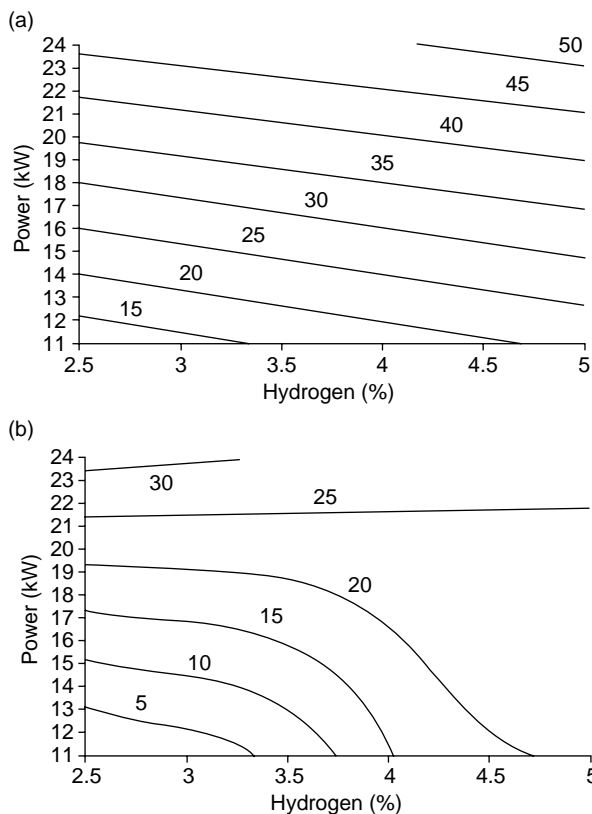


**Figure 8.1** Isopleths of the constant fraction of the amorphous phase in plasma-sprayed hydroxyapatite coatings as a function of the volume fraction of hydrogen and electric power for carrier gas flow rates of (a) 3 slpm and (b) 3.5 slpm (after Dyshlovenko *et al.*, 2006)

The isopleths in Figure 8.1 show the experimental conditions of obtaining the desired quantity of the amorphous phase in plasma-sprayed HA coatings. For instance, in order to achieve 25 wt% of the amorphous phase in the coatings sprayed using a carrier gas flow rate of 3.5 slpm, the electric power should be kept constant,  $P \approx 21.5$  kW, for any hydrogen volume fraction in an Ar + H<sub>2</sub> working gas between 2.5

and 5 %. More information about the response surface methodology can be found in textbooks such as that of Box and Draper (1987).

## 8.2 MECHANICAL PROPERTIES

### 8.2.1 HARDNESS AND MICROHARDNESS

Hardness and microhardness are the first approximations of the coatings' wear resistance and strength (Tucker, 1982). The test is easy to realize and can also serve to estimate the quality of spraying. This is because the processing faults frequently result in a higher porosity (fractures) and a growing number of un-melted grains which, in turn, lower the coatings' hardness.

#### Carbides

Carbides are, together with oxides, the hardest thermally sprayed coatings. The most frequently sprayed is tungsten carbide which is usually prepared as composite with cobalt or nickel. The Vickers microhardness,  $HV_3$ , of tungsten carbide is well above 1000 (Figure 8.2).

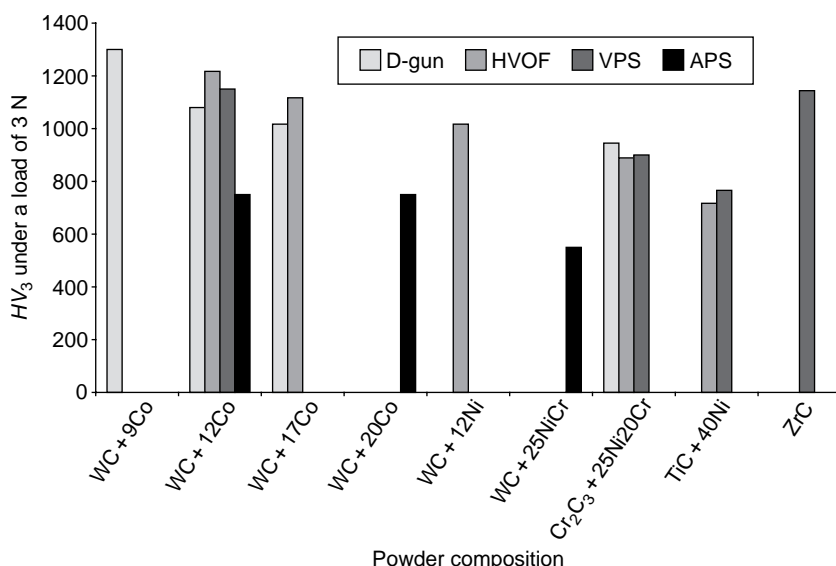


Figure 8.2 Vickers microhardness of carbide coatings obtained using different spray techniques (see also Table 8.3)

Tungsten carbide containing Co (9, 12, 17 and 20 wt%), as well as 12 wt% Ni and 25 wt% NiCr is the most frequently sprayed material. Some work has been carried out for TiC with Ni. These coatings are obtained with the D-gun<sup>TM</sup>, high-velocity combustion spraying and less frequently with air plasma spraying. Application of plasma spraying results in a lower, with regard to that of the detonation gun or high-velocity combustion spraying, hardness of coatings (Figure 8.2). Vacuum plasma spraying has been rather seldom used to deposit hard coatings. An example is the deposition of ZrC coatings. The detonation gun and high-velocity combustion spraying are suitable for spraying carbides, due to the carburizing atmosphere and high velocities of the flames. The atmosphere reduces carbide decomposition and oxidation. High velocity, in turn, reduces the time of interaction between the particles and the flame which results in preserving the carbide as a solid inside the molten metal or alloy matrix. The latter have relatively low melting points (usually lower than 1800 K), which is well below the temperature of the flames in the HVOF or D-gun<sup>TM</sup> techniques. When the matrix of the particles becomes molten and the carbide grains remain solid, the resulting coating is well-bonded and hard. Powder morphology and chemical composition seems to influence more significantly the coatings' hardness than the operational spray parameters (Vinayo *et al.*, 1985). The hardness of WC-Co coatings depends mainly on the following (Jarosinski *et al.*, 1993):

- amount, size and distribution of the WC phase;
- amount of the Co binder.

Generally, coatings having a greater amount of WC are harder but are simultaneously less strong than those coatings having less WC. Similarly, the wear resistance increases for small-sized WC distributed in a homogeneous way in the matrix. The high temperature of the jet during APS of tungsten carbide results in coatings with a lower hardness than D-gun<sup>TM</sup> or HVOF coatings. This is due to the decomposition of WC in the hot oxidizing flame into 'less-hard' W<sub>2</sub>C (see Chapter 6, Section 6.3.1). Tungsten carbide–cobalt powders can be prepared by casting and crushing, sintering and crushing, agglomeration and cladding with a dense clad. The comparative study of Jarosinski *et al.* (1993) indicated that high-velocity combustion-sprayed, agglomerated powders containing 17 wt% of Co and average carbide grain sizes of 5–7 µm result in coatings having the greatest microhardness (Figure 8.3).

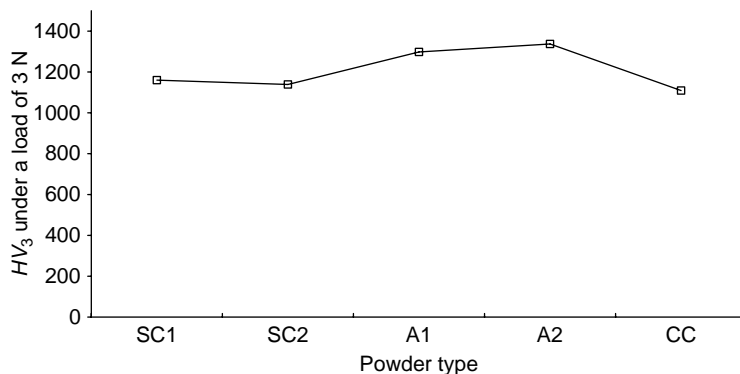


Figure 8.3 Vickers microhardness of WC-Co coatings (sprayed by Jarosinski *et al.*, 1993) with the high-velocity combustion-spraying technique using powders of different chemical composition (in wt%) and/or manufacturing techniques and sizes: SC1 – 85W, 4C, 10Co, sintered and crushed,  $d_{50\%} = 12.5 \mu\text{m}$ ; SC2 – 78W, 5C, 12Co, sintered and crushed,  $d_{50\%} = 14.5 \mu\text{m}$ ; A1 – 78W, 5C, 17Co, agglomerated,  $d_{50\%} = 4.5 \mu\text{m}$ ; A2 – 78W, 5C, 17Co, agglomerated,  $d_{50\%} = 8.7 \mu\text{m}$ ; CC – 85W, 4C, 10Co, casted and crushed,  $d_{50\%} = 9.4 \mu\text{m}$

Kreye *et al.* (1986) confirmed that the microhardness of coatings after high velocity combustion spraying of agglomerated powders of WC–12 Co is greater than that of coatings applied using cast-crushed and cladded powders. Tungsten carbide powders can be also sprayed with Ni (see Table 8.2) or with CrCo. Consequently, coatings sprayed with 14 wt% CrCo by high-velocity combustion-spraying gives, following Barbezat *et al.* (1993), a hardness of  $HV_3 = 1020$ . Nano-sized<sup>4</sup> WC–8Co and WC–12Co powders were also sprayed using this technique. The coatings have microhardnesses in the range of  $HV_1 = 1180$ –1550. These values were comparable to those obtained with conventional powders sprayed under similar conditions (Voyer and Marple, 2000)

Another, frequently deposited carbide is  $\text{Cr}_3\text{C}_2$ . This is used because of its better high temperature resistance than that of WC (see Chapter 1, Figure 1.24). This carbide is often blended with 25 wt% NiCr (80/20), as shown in Table 8.3. The hardness of coatings sprayed using chromium carbide is clearly lower than that of tungsten carbide, independently of the spray technique.  $\text{Cr}_3\text{C}_2$  decarburizes at spraying and the resulting coatings often contain  $\text{Cr}_7\text{C}_3$  (Barbezat *et al.*, 1993). Post-spray annealing (up to about 1000 K for 1 h) of the WC–17Co, WC–17Ni,

<sup>4</sup> Crystal grain size is smaller than 100 nm.

$\text{Cr}_3\text{C}_2$ –25NiCr and WC +  $(\text{WCr})_2\text{C}$  high-velocity combustion-sprayed coatings leads to the *supersaturation effect* of the matrix, observed by Kreye (1991). This effect leads to an increase in the coatings microhardness,  $HV_3$ , by 100 to 200 and consists of dissolution of carbon in the binder. This dissolution is confirmed by an increase in the binder's lattice constant. The annealing leads to a precipitation of the second phase, a return to the initial lattice constant and a resulting increase in hardness.

Titanium carbide composites with nickel, nickel–cobalt and nickel–cobalt–molybdenum alloys were applied by HVOF and the resulting coatings have hardnesses in the range of  $700 < HV_3 < 800$  (Figure 8.2 and Table 8.3). Titanium carbide–iron composite coatings were air-plasma sprayed using the powder prepared by spray drying from the following precursors (in wt%,) (after Cliche and Dallaire, 1991):

- 53.4 of FeTi;
- 35.5 of iron;
- 11.1 of graphite.

The resulting coatings had microhardnesses,  $HV_{0.5}$ , in the range of 1300–1700. Composite powders of  $\text{TiC} + (40\text{--}70)\text{ Ni20Cr}$  were prepared by the methods of blending, spray-drying and spray-drying with sintering by Lugscheider *et al.* (1991). The Vickers microhardness,  $HV_3$ , was  $\approx 600$  for coatings sprayed with an air plasma using spray-dried and sintered powders and  $\approx 800$  for those coatings sprayed with the high-velocity combustion technique using a spray-dried powder.

Zirconium carbide was plasma-sprayed in a vacuum onto a graphite substrate and the resulting microhardness was in the range  $867 < HV_3 < 1144$  (see also Figure 8.2 and Table 8.3). Heat treatment at  $T = 1998\text{ K}$  improved the microhardness which reached  $HV_3 = 1589$  at maximum.

## Oxides

The hardest sprayed oxide coating is that of  $\text{Cr}_2\text{O}_3$  (Figure 8.4).

The values shown in Figure 8.4 are typical although it is possible to find in the literature greater microhardnesses. To show only two examples, Niemi *et al.* (1991) measured the microhardness of chromia by plasma spraying and obtain a value as high as  $HV_2 = 1890$  on the transverse section of the coating. Similarly, Gansert *et al.* (1990) report

Table 8.3 Descriptions of used powders and selected properties of some carbides sprayed using different techniques (coatings microhardness data are shown in Figure 8.2)

Number	Reference	Powder characteristics		Coatings characteristics	
		Grain size ( $\mu\text{m}$ )	Chemical composition (wt%)	Crystalline phases	Density, ( $\text{kg}/\text{m}^3$ )
<i>D-gun™ or detonation gun</i>					
1	Tucker, 1982	—	WC + 9Co	—	14 200
2	Barbezat <i>et al.</i> , 1993	-45 + 11	WC + 12Co	WC, $\text{W}_2\text{C}$	0.5
3	Barbezat <i>et al.</i> , 1993	-63	WC + 17Co	WC, $(\text{WC}\text{O})_6\text{C}$	1.5
4	Barbezat <i>et al.</i> , 1993	—	Cr <sub>3</sub> C <sub>2</sub> + 25Ni20Cr	Cr <sub>3</sub> C <sub>2</sub> , Cr <sub>7</sub> C <sub>3</sub>	1.5
<i>High-velocity combustion spraying</i>					
5	Barbezat <i>et al.</i> , 1993	-45 + 11	WC + 12Co	WC, $\text{W}_2\text{C}$	0.3
6	Jarosinski <i>et al.</i> , 1993	$d_{50\%} = 8.7$	WC + 17Co	1.5 C loss	—
7	Barbezat <i>et al.</i> , 1993	—	WC + 12Ni	WC, $\text{W}_2\text{C}$ , (W, Co) <sub>6</sub> C	0.7
8	Barbezat <i>et al.</i> , 1993	-45 + 11	Cr <sub>3</sub> C <sub>2</sub> + 25Ni20Cr	Cr <sub>3</sub> C <sub>2</sub> , Cr <sub>7</sub> C <sub>3</sub>	0.8
9	Gärtner <i>et al.</i> , 2000	—	TiC + 40Ni	Loss of 33.9 wt% C, oxidation	—

Table 8.3 (Continued)

Number	Reference	Powder characteristics		Coatings characteristics		
		Grain size ( $\mu\text{m}$ )	Chemical composition (wt%)	Crystalline phases	Density, (kg/m $^3$ )	Porosity (%)
<i>Air-plasma spraying</i>						
10	Wolf and Longo, 1980	—	WC + 12Co	—	12 500	—
11	Tronche, 1986	—40 + 10	WC + 20Co	WC, W <sub>2</sub> C, W <sub>2</sub> (C,O)	12 770	8
12	Wolf and Longo, 1980	—	Cr <sub>3</sub> C <sub>2</sub> + 2.5Ni20Cr	—	6200	—
<i>Vacuum-plasma spraying</i>						
13	Wolf and Longo, 1980	—	WC + 12Co	—	12 500	—
14	Tronche, 1986	—40 + 10	WC + 20Co	(Co, W) <sub>6</sub> C	10 460	2
15	Wolf and Longo, 1980	—	(Bal.) Cr <sub>3</sub> C <sub>2</sub> , 25 Ni20Cr	—	6600	—
16	Varacalle <i>et al.</i> , 1994	—45 + 10	(Bal.) ZrC, 2HfC	—	—	1.0–2.4

$\text{Cr}_2\text{O}_3$  coatings sprayed using a high-energy plasma torch (working with powers up to 200 kW) having a microhardness  $HV_2$  of 1990.

Oxides are mainly deposited by plasma spraying. The reason is their high melting points which makes necessary the application of hot-plasma jets and reduces the usefulness of cool flames occurring in the combustion and detonation spray techniques. Moreover, the oxidizing atmosphere during atmospheric-plasma spraying hampers material deoxidation. On the other hand, the close interlamellar contacts and small porosity occurring in the high-velocity combustion spraying techniques, results in greater hardness. This is why efforts have been undertaken in order to adapt these techniques to spray oxides. The D-gun<sup>TM</sup> has been used to spray alumina and the resulting coating was significantly harder than the coating obtained by Tucker (1982) by a plasma in air (see Figure 8.4 and Table 8.4). The detonation gun was also applied by Niemi *et al.* (1991) to spray fine  $\text{Cr}_2\text{O}_3$  powder and obtained coatings which had a microhardness, measured on the transverse section, in the range of  $HV_2 = 1420\text{--}2100$ . Similarly, Kreye (1991) used high-velocity combustion guns to spray  $\text{Al}_2\text{O}_3$  and obtained  $HV_3 = 945$  and  $\text{Al}_2\text{O}_3 + 13\text{ wt\% TiO}_2$  to obtain  $HV_3 = 940$ . Another example of the hardness of  $\text{TiO}_2$  coating sprayed in this way is shown in Figure 8.4.

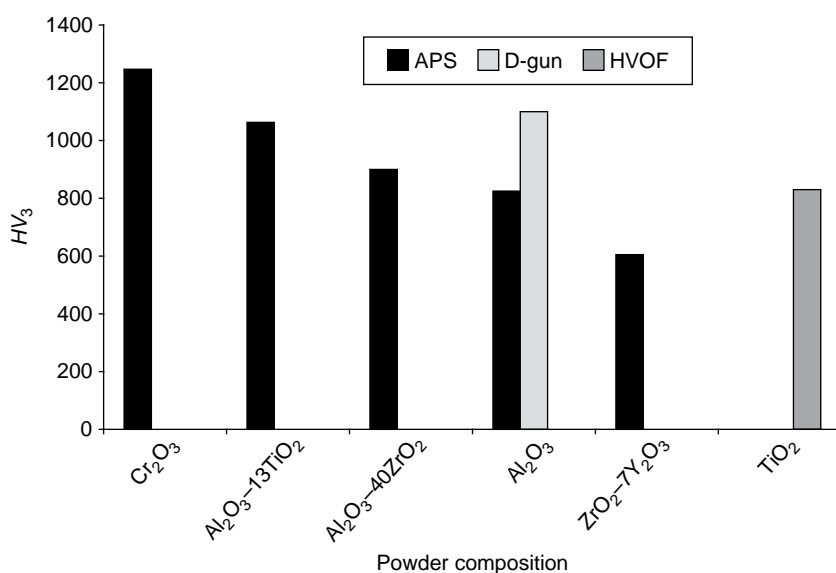
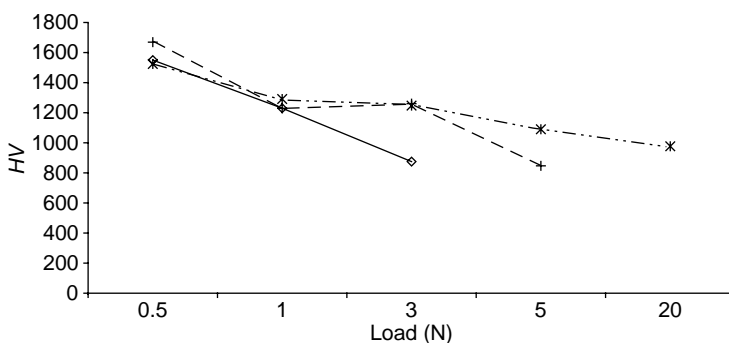


Figure 8.4 Vickers microhardness of sprayed oxides (see also Table 8.4)

**Table 8.4** Descriptions of used powders and selected properties of some oxides sprayed using different techniques (coatings microhardness data are shown in Figure 8.4)

Number	Reference	Powder characteristics			Coatings characteristics		
		Grain size ( $\mu\text{m}$ )	Chemical composition (wt%)	Crystalline phases	Density ( $\text{kg}/\text{m}^3$ )	Porosity (%)	
<i>Air-plasma spraying</i>							
1	Pawlowski <i>et al.</i> , 1993	$d_{50\%} = 7.4$	$\text{Cr}_2\text{O}_3$	Eskolaite	—	2	
2	Barbezat <i>et al.</i> , 1993	-30+5	$\text{Al}_2\text{O}_3$ , 13 $\text{TiO}_2$	—	—	—	
3	Barbezat <i>et al.</i> , 1993	-30+5	$\text{Al}_2\text{O}_3$ , 40 $\text{ZrO}_2$	—	—	—	
4	Tucker, 1982	—	$\text{Al}_2\text{O}_3$	—	3380	3	
5	Pawlowski, 1985	-106+10	$\text{ZrO}_2$ , 7 $\text{Y}_2\text{O}_3$	$\text{t}'$ , monoclinic	5550	9.5	
<i>D-gun™</i>							
6	Tucker, 1982	—	$\text{Al}_2\text{O}_3$	—	3400	2	
<i>High-velocity oxy-fuel spraying</i>							
7	Lima and Marple, 2003	-22+5	$\text{TiO}_2$	Mainly rutile	—	—	

The choice of load when testing microhardness can influence the measured values. A low-load microhardness indicates the degree of individual lamellae melting and can be influenced by small pores, while high-load measurements describe the overall coating in which the hardness depends on the interlamellar contacts' strength and porosity. Lima and Marple (2003) estimated that there is a *critical load* which separates load-dependent and load-independent hardnesses. Below this load, only information from a particular volume of the coating is obtained. A coating volume of about  $500 \mu\text{m}^3$  and an area of about  $250 \mu\text{m}^2$  correspond to a *critical load* equal to  $F = 3 \text{ N}$ . The lamellae are always harder than the coating as a whole (Figure 8.5) and the low-load microhardness might be as high as  $HV_3 = 1700$  for plasma-sprayed  $\text{Cr}_2\text{O}_3$ . The porosity and strength of the interlamellar contacts are characterized at high-load microhardness. An exceptionally high value of  $HV_{20} = 1000$  was achieved for a  $\text{Cr}_2\text{O}_3$  coating using a fine crystalline powder. This coating had only 2 % porosity and a very fine-grained microstructure (Pawlowski *et al.*, 1993).



**Figure 8.5** Vickers microhardness versus load for coatings sprayed using different oxides: (\*) chromia (see Figure 8.6 (A)); (+) chromia (see Figure 8.6 (A1)); (◇) alumina FC – fused and crushed  $\text{Al}_2\text{O}_3$  powder, which has a grain size of  $-45 + 22.5 \mu\text{m}$ , and was sprayed by a plasma in air with a torch supplied with 43 kW of arc power

The spray-dried powder particles (A1 in Figure 8.6) contain a lot of internal porosity (See Chapter 1, Figures 1.8 and 1.9) which most probably resulted in porous coatings and low hardness.

Vacuum-plasma spraying is not well adapted to deposit ceramic coatings. First, the energy input to the torch must be very high and, secondly, it is sometimes difficult to inject light ceramic powders into the plasma jet. An important advantage of sprayed coatings is their low porosity

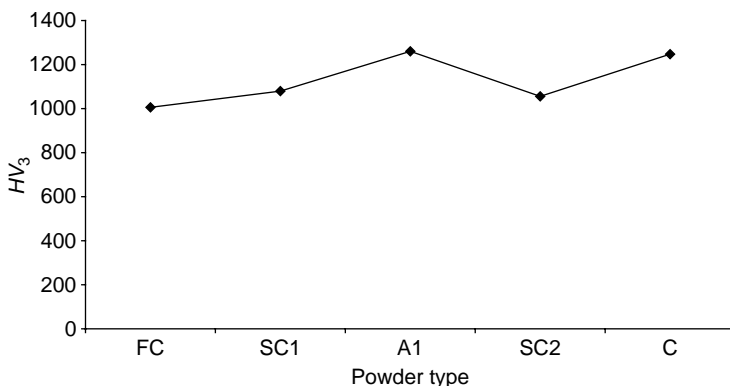


**Figure 8.6** Vickers microhardness of chromia coatings (sprayed in air by Pawlowski *et al.*, 1993) using different arc powers and  $\text{Cr}_2\text{O}_3$  powders having different chemical compositions (in wt%), grain sizes and/or manufacturing techniques: FC – 45.5 kW, 99.8 Cr<sub>2</sub>O<sub>3</sub>,  $d_{50\%}$  = 30.4 µm, fused and crushed; SC1 – 45.5 kW, bal. Cr<sub>2</sub>O<sub>3</sub> + 4SiO<sub>2</sub> + 3TiO<sub>2</sub>,  $d_{50\%}$  = 32.9 µm, sintered and crushed; A1 – 52.9 kW, Cr<sub>2</sub>O<sub>3</sub> + 5SiO<sub>2</sub>,  $d_{50\%}$  = 31.29 µm, agglomerated; SC2 – 44.1 kW, Cr<sub>2</sub>O<sub>3</sub> + 5SiO<sub>2</sub> + 3TiO<sub>2</sub>,  $d_{50\%}$  = 73.7 µm, sintered and crushed; C – 49 kW, ‘pure’ Cr<sub>2</sub>O<sub>3</sub>,  $d_{50\%}$  = 7.4 µm, crystalline

**Table 8.5** Microhardnesses,  $HV_3$ , of oxide coatings plasma-sprayed in air and in vacuum (Takeuchi *et al.*, 1991)<sup>a</sup>

Number	Oxide	Air-plasma sprayed	Vacuum-plasma sprayed
1	$\text{Al}_2\text{O}_3$	720	1310
2	$\text{Al}_2\text{O}_3$ + 40 wt% TiO <sub>2</sub>	690	810
3	Cr <sub>2</sub> O <sub>3</sub>	930	1500
4	TiO <sub>2</sub>	730	750

<sup>a</sup> All powders were fused and crushed. Powder sizes were, for air-plasma spraying, in the range –30 + 10 µm and, for vacuum-plasma spraying, in the range –20 + 10 µm.

(resulting from the high velocity of the particles’ impact) which results in a high microhardness (Table 8.5).

Titania is used in a pure form or as an alloy with other oxides ( $\text{Al}_2\text{O}_3$ , Cr<sub>2</sub>O<sub>3</sub>). The alloys have a lower ‘liquidus’ temperature than the melting point of the primary oxide. Titania is a relatively ‘low refractory material’ (see Chapter 6, Section 6.3.1) and can be sprayed by a plasma or by a high velocity combustion (see Figure 8.4). Spray-dried titania powder from a ‘nanostructured’ precursor was sprayed by Ibrahim *et al.* (2005) and the hardness values of the obtained coatings were

compared with fused and crushed feedstock. The following values of  $HV_3$  were obtained:

- 875, for fused and crushed powders by plasma spraying;
- 830, for fused and crushed powders by high-velocity combustion spraying;
- 800, for a spray-dried powder with ‘nano-structured’ precursors by high-velocity combustion spraying.

Coatings containing titania as an additive are typically less porous than primary oxides, but less hard. For example, Barbezat *et al.* (1993), found the following data for plasma-sprayed coatings:

- pure chromia coatings had an apparent porosity of 2.7 % and a microhardness of  $HV_3 = 1400$ ;
- chromia with 30 wt% of titania had a porosity of 0.8 % but a microhardness of  $HV_3 = 1100$ .

An additive of 40 wt% zirconia to alumina powder produces a coating which has a microhardness similar to that of pure alumina (see Figure 8.4) but its toughness is much greater due to the *transformation toughening effect* (Stevens, 1986). This effect consists of the absorption of ‘crack energy’ by a phase transformation of zirconia. Zirconia coatings used for thermal barriers are intentionally produced with some porosity. Such coatings are subjected to thermal cycling at high temperatures. Figure 8.7 presents the evolution of the microhardness of some typical yttria-stabilized zirconia coatings.

The microhardness of coatings increases with the temperature of annealing. This annealing leads to a decrease in porosity and to an improvement in the interlamellar contacts.

The microhardness,  $HV_1$ , of some ‘less-often sprayed’ oxides was determined by Kirner (1980) and Ctibor *et al.* (2000):

- barium titanate,  $BaO.TiO_2$ ,  $HV_1 = 420$ ;
- calcium titanate,  $CaO.TiO_2$ ,  $HV_1 = 965$ ;
- alumina magnesia spinel,  $Al_2O_3.MgO$ ,  $HV_1 = 600\text{--}900$ ;
- *zircon*,  $ZrO_2.SiO_2$ ,  $HV_1 = 450\text{--}600$ ;
- *mullite*,  $3Al_2O_3.2SiO_2$ ,  $HV_1 = 470$ .

The microhardness of hydroxyapatite, an important biomedical oxide, was tested by Lima *et al.* (2004a). The coatings were plasma-sprayed

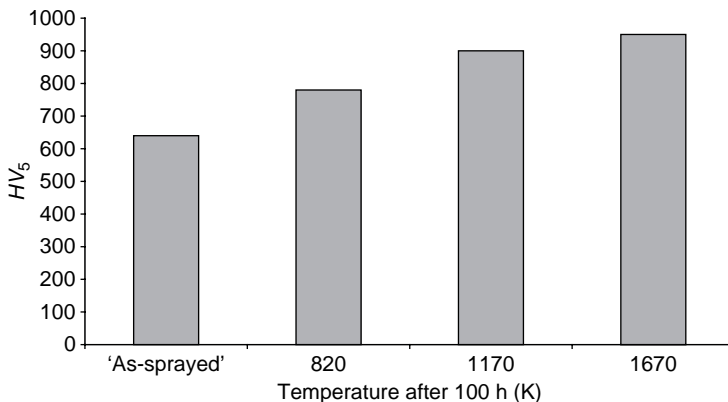


**Figure 8.7** Vickers microhardness of coatings of zirconia stabilized with 7 wt% yttria, sprayed by plasma in air and tested under the following conditions: 'as-sprayed' and after annealing in air at 820, 1170 and 1670 K for 100 h. The 'as-sprayed' coatings crystallized in the tetragonal 't-phase' and had a porosity of 9.6 %

using conventional and 'nano-structured' powders. The microhardness was equal to  $HV_3 = 230$  for conventional and  $HV_3 = 93$  for 'nano-structured' feedstocks.

## Metals

The hardest sprayed metal is molybdenum. The reported values of its hardness vary depending on the spray technique and spray atmosphere. Mo coatings obtained by wire flame spraying reached a microhardness of  $HV_1 = 1110$  and a Rockwell N hardness under a load of  $F = 150$  N equal to 85.4 (Houck and Whisenant, 1987). Overs *et al.* (1980) influenced the hardness of coatings by modifying the oxygen pressure during processing. The reported microhardnesses,  $HV_2$ , were in the range:

- 800–1300, for an oxygen pressure of  $p = 0.12$  MPa;
- 1500–1700, for an oxygen pressure of  $p = 0.28$  MPa.

Oxidation of molybdenum increases the hardness of coatings but has a detrimental influence on its cohesion (Tucker, 1982). Other reported values of the hardness for Mo were:

- $HV_3 = 520$ –600 for plasma-sprayed coatings (Adam, 1977);
- $HV_1 = 300$ –400 for arc-sprayed deposits (Milewski and Milewski, 1980).

The hardness of arc-sprayed titanium depends on the spray atmosphere. The controlled-atmosphere arc-spray installation shown by Müller (1973) made it possible to compare the microhardnesses of titanium sprayed under argon ( $HV_1 = 300$ ) to that sprayed under nitrogen ( $HV_1 = 1300$ ). The coatings sprayed under nitrogen were composed of nitrides such as TiN, and of titanium modifications, e.g.  $\alpha$ -Ti and  $\beta$ -Ti. Only the  $\alpha$ -Ti and  $\beta$ -Ti phases were present in coatings obtained under argon. Steffens *et al.* (1980) used vacuum-plasma spraying to obtain titanium coatings of such a low hardness as  $HV_1 = 151\text{--}185$ . A low hardness indicates a low content of oxygen in the coatings, which was estimated by the authors as 0.1–0.2 wt%.

Nickel was sprayed by using a plasma in air and under vacuum. Coatings having hardness varying from  $HV_3 = 120$  (Kretschmar, 1980) to  $HV_3 = 200$  (Tucker, 1982) were reported. Kretschmar found that the hardness of a vacuum-plasma coating is similar to that sprayed in air.

The hardnesses of aluminum and zinc coatings were tested using the *Brinell* method by Bardal *et al.* (1973). The reported values were 20–27 for arc-sprayed aluminium and 20 for flame-sprayed zinc.

## Alloys

Hard alloys are applied as top coatings, while less-hard and more ductile ones are used for bond coatings.

Top coatings are often sprayed by the use of *self-fluxing* alloys in the form of powders or wires. The alloys contain boron and silicon which have a ‘double role’ of lowering the melting point and absorption of oxygen (see Chapter 1, Figure 1.3). The coatings are traditionally flame-sprayed and then fused. Kretschmar (1980) tested the hardness of an NiCrBSiC alloy and reported a value of  $HV_3$  of 780 for an essentially non-porous coating (porosity less than 1%). As the coatings are ‘metallurgically bound’ to the substrates, many authors have used the *Rockwell* test to determine their hardnesses. For example, Weirich and Wilwerding (1983) flame-sprayed coatings using a *self-fluxing* alloy of a composition described in the German Standard DIN 32529. The coatings were subsequently post-spray fused and had hardnesses in the range  $HRC = 40\text{--}65$ . Milewski and Sartowski (1986) used the plasma and flame torches to spray an alloy of a composition (in wt%) of  $\text{Ni} + 13.7\text{Cr} + 5.4\text{Fe} + 4.2\text{Si} + 3.1\text{B}$ . Flame-sprayed coatings had a hardness of  $HV_1 = 645$ , while plasma-sprayed ones were slightly softer, i.e.  $HV_1 = 600$ .

Arc-sprayed steels are also often applied for top coatings. Steffens *et al.* (1986) arc-sprayed a steel wire of composition (in wt%) of Fe + 2.2Cr + 1.8Mn + 1C + 0.2Ti. The hardness of the deposits was about  $HV_3 = 400$  and increased up to 450 when 25 vol% of methane was added to the atomizing gas. Milewski and Sartowski (1986) used the same spray technique to deposit a stainless steel of composition (in wt%) of Fe + 12Cr + 9Ni + 2Mn. The coatings had a hardness of about  $HV_1 = 420$ . Khatri *et al.* (1994) plasma-sprayed a high-nitrogen-bearing steel of composition (in wt%) of Fe + 16Cr + 19Mn in air, under vacuum and in a nitrogen atmosphere. The hardness of air-plasma sprayed deposits increased with the volume fraction of the nitrogen in the working gases to reach a mean value of  $HV_3 = 418$ . Vacuum and nitrogen-atmosphere plasma-sprayed coatings were softer and had hardness in the range  $224 < HV_3 < 314$ .

An alloy of composition (in wt%) of Co + 25Cr + 10Ni + 8W + 0.5C was plasma-sprayed to obtain top coatings having hardnesses varying from  $HV_3 = 330$  (Wolf and Longo, 1980) to  $HV_3 = 350$  (Tucker, 1982). The same powder, plasma-sprayed by Wolf and Longo under vacuum, was slightly harder,  $HV_3 = 430$ . An increase in the hardness correlated well with the increase in density from 7600 to 7800 kg/m<sup>3</sup>.

**Bond coatings** have to be *ductile* in order to absorb stresses, rather than *hard*. Microhardness is a practical indicator of the spray-processing quality. Cross-sections of a few bond coatings are shown in Figure 8.8, with descriptions of the powders used and some properties of the bond coatings presented in Table 8.6.

A bond coating of NiCoCrAlY, used typically in thermal-barrier coatings, was intensively tested by Lin and Berndt (1995) and Valente (1997). The hardnesses of the coatings were equal to  $HV_3 = 196$  in the former case and to  $HV_3 = 122$  in the latter deposits. These authors carried out a great number of Vickers indentation tests and analysed the distributions of the obtained hardnesses. It was revealed that the distributions were not symmetric with regard to the mean value. A *Weibull statistical distribution* was found to match, at best, to the experimentally obtained Vickers numbers. NiAl and an alloy composed of NiAl and 0.044 wt% B were sprayed under vacuum, as free-standing structures, by Chen *et al.* (1993a) and the reported  $HV_5$  microhardnesses values were about 304 and 340, respectively. A 'bio-inert' Ti6Al4V alloy was sprayed under an inert atmosphere by Valente (1997). Its Vickers hardness, measured under a load of  $F = 1, 3$  and 5 N was about 100. Finally, a copper alloy of composition (in wt%) of Cu + 9.8Al + 3.8Ni was flame-sprayed by Iordanova *et al.* (1995) and the resulting coating had a mean microhardness of  $HV_{0.5} = 165$ .

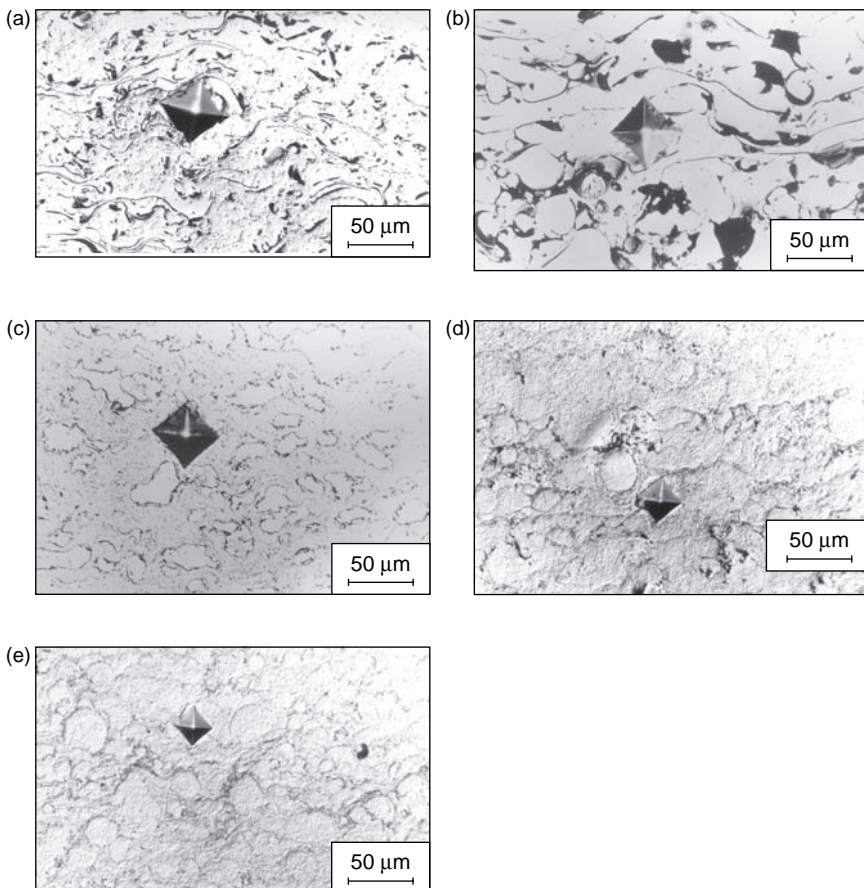


**Figure 8.8** Vickers microhardness indentations in cross-sections of typical bond coatings, plasma-sprayed in air and under vacuum: (a) NiAl by APS,  $HV_3 = 179 \pm 19$ ; (b) NiCrAl by APS,  $HV_3 = 232 \pm 27$ ; (c) NiAl by VPS,  $HV_3 = 258 \pm 10$ ; (d) NiCr by VPS,  $HV_3 = 370 \pm 44$ ; (e) NiCoCrAlY by VPS,  $HV_3 = 543 \pm 23$  (see also Table 8.6)

### 8.2.2 TENSILE ADHESION STRENGTH

The tensile adhesion test using the ASTM 633-01 standard or similar standards describes the bonding of a coating to a substrate. The rupture under stress may occur inside the coating (cohesive rupture) or at the coating-to-substrate interface (adhesive failure), as shown in Chapter, Table 7.6. Tensile adhesion depends on the following parameters, related to the spray process:

- The material used to spray and its thermophysical properties which determine the contact temperature,  $T_c$ , given in Chapter 6,

**Table 8.6** Descriptions of the powders used and some properties of the bond coatings shown in Figure 8.8 (Pawlowski, 1985)

Number	Part number in Figure 8.8	Powder characteristics		Coatings characteristics	
		Grain size ( $\mu\text{m}$ )	Chemical composition (wt%)	Crystalline phases	Density ( $\text{kg}/\text{m}^3$ )
<i>Air-plasma spraying</i>					
1	(a)	-90 + 45	Ni + 5Al	Ni	7200
2	(b)	-100 + 30	Ni+19Cr+6Al	Ni	6900
<i>Vacuum-plasma spraying</i>					
3	(c)	-20 + 5	Ni+5Al	Ni	7800
4	(d)	-20 + 5	Ni+19Cr+0.4Fe	Ni	7700
5	(e)	-36	Ni + 36Co + 21Cr + 8Al + 0.9Si + 0.2Fe	Ni, Co, Cr	7200

Equation (6.12), such as the latent heat of fusion, specific heat, thermal conductivity and diffusivity. The size and external and internal morphologies of the powder influence the contact area between the lamellae and substrate.

- The **spray** parameters and, in particular, those which determine the velocity and temperature of the particles upon impact with the substrate, as well as the ‘splat’ morphology. These parameters are:
  - power input to the working gas;
  - working gas flow rate;
  - injection of particles into the jet or flame.
- **Substrate** properties, such as the thermophysical ones (thermal diffusivity and conductivity). Moreover, the substrate surface morphology, described by the roughness and its temperature upon spraying, plays a role in the coating’s adhesion.

If rupture during the tensile adhesion test has a cohesive character, it means that the bonding is stronger than the cohesion. The latter mainly depends on the material used to spray and the processing technique. Consequently, some reviewed data have been selected from such literature sources in which the above parameters had been specified. Another limitation was set for the substrate material – only the tensile adhesion

strengths for the coatings sprayed on the following substrate materials are discussed:

- steel;
- aluminium;
- nickel alloys;
- titanium and its alloys.

It must be stressed that an increasing number of coatings are sprayed onto non-metallic substrates.

## Carbides

The tensile adhesion strengths of some carbides are collected in Table 8.7. The bond strength, in most cases, is greater than 50 MPa. This value is close to the cohesive rupture in a resin ('test limit') which is in the range of 70 MPa to 100 MPa (see Chapter 7, Table 7.6).

The strong bonding is due to the fact that the matrices in carbide powder particles are metals (Co, Ni) or alloys (NiCr, CoCr) with relatively low melting points or are liquids. For example,  $T_m = 1726\text{ K}$  for Ni and  $T_m = 1766\text{ K}$  for Co. Sprayed particles have a molten matrix at impact and, subsequently, the lamellae can contact the substrate on a greater part of their lower surface area. Post-spray annealing at temperatures of 770–970 K may lead to a substantial decrease in the bond strength of carbide coatings, such as WC–Co (Lim *et al.*, 1996).

Carbides are most frequently sprayed with the use of flames having a low temperature and high-velocity characteristics for a detonation gun or high-velocity combustion spray techniques (entries 1–5 and 8 of Table 8.7). Coatings sprayed using high-temperature jets which occur during plasma spraying (entries 6 and 7 of Table 8.7) are more weakly bonded to the substrate.

## Oxides

The tensile bond strengths of oxide coatings are collected in Table 8.8. The bonding strength to metals is clearly smaller than that of carbides. Oxides adhere to metals mainly by mechanical anchorage (see Chapter 6, Figure 6.11). This is evidenced by an increase in adhesion with substrate roughness (entries 1–4 of Table 8.8). Substrate oxidation resulting from a long period after roughening lowers the bond strength (entries 11 and

Table 8.7 Tensile adhesion of some carbides sprayed using different techniques onto different substrates

Number	Reference	Powder characteristics			Substrate characteristics			Critical tensile stress (MPa)
		Chemical composition (wt%)	Grain size (µm)	Method of manufacturing	Material	Roughness, $R_a$ (µm)	Method of roughening	
<i>High-velocity combustion spraying</i>								
1	Kreye <i>et al.</i> , 1986	WC, 12Co	−45 + 5.6	Fused, sintered, agglomerated and porous clad	Mild steel	—	—	> 100
2	Matsubara and Tomiguchi, 1992	WC, 30NiCr	—	—	Mild steel	Variable up to 20 µm	$\text{Al}_2\text{O}_3$ grit-blasting	100
3	Bezkowiāk <i>et al.</i> , 1993	$\text{Cr}_{13}\text{C}_{2}$ , 25NiCr	$d_{50} \text{ \%} = 2.5$	Agglomerated and sintered	Steel (probably)	—	—	72
4	Bezkowiāk <i>et al.</i> , 1993	WC, 10Co, 4Cr	$d_{50} \text{ \%} = 3.6$	Sintered and crushed	Steel (probably)	—	—	69
5	Bezkowiāk <i>et al.</i> , 1993	WC, 20CrC, 7Ni	$d_{50} \text{ \%} = 20$	Sintered and crushed	Steel (probably)	—	—	68
<i>Air-plasma spraying</i>								
6	Alonso <i>et al.</i> , 1991	SiC, 25Al	—	Blend	Mild steel	—	—	48
7	Lim <i>et al.</i> , 1996	WC, 17Co	—	Amdry 983	Ductile cast iron	—	$\text{Al}_2\text{O}_3$ grit-blasting	55 (tensile strength of adhesive)
<i>D-gum™</i>								
8	Li, 1980	$\text{Cr}_{23}\text{C}_{6}$ , 20NiCr	—	—	Hastelloy X	—	—	79

Table 8.8 Tensile adhesion of some plasma-sprayed oxides onto different substrates

Number	Reference	Powder grain size ( $\mu\text{m}$ )	Substrate characteristics			Critical tensile stress (MPa)
			Material	Roughness, $R_a$ ( $\mu\text{m}$ )	Method of roughening	
$\text{Al}_2\text{O}_3$						
1	Iwamoto <i>et al.</i> , 1983	—	Stainless steel	2.6	$\text{Al}_2\text{O}_3$ grit-blasting	52
2	Iwamoto <i>et al.</i> , 1983	—	Stainless steel	0.6	HCl acid-etch	32
3	Wielage and Drozak, 1990	—	Mild steel	$R_z = 18$	Spheres-blasting (probably metallic)	33
4	Wielage and Dworzak, 1990	—	Mild steel	$R_z = 92$	Sand-blasting	58
$\text{Cr}_2\text{O}_3$						
5	Roseberry and Boulger, 1977	$-74 + 10$	Mild steel	6.3	$\text{Al}_2\text{O}_3$ grit-blasting	31
6	Funk <i>et al.</i> , 1988	$-60 + 15$	CuZn brass	—	—	20

Table 8.8 (Continued)

Number	Reference	Powder grain size ( $\mu\text{m}$ )	Substrate characteristics			Critical tensile stress (MPa)
			Material	Roughness, $R_a$ ( $\mu\text{m}$ )	Method of roughening	
<i>Hydroxyapatite</i>						
7	Heimann <i>et al.</i> , 2001	Amdry 6021™	TiAl6V4 alloy	4	$\text{Al}_2\text{O}_3$ grit blasting	49 maximum
8	Lima <i>et al.</i> , 2004a	$d_{50\%} = 34$	TiAl6V4 alloy	—	—	18
9	Roseberry and Boulger, 1977	—53 + 15	Al	$\text{Al}_2\text{O}_3 + 13\text{wt\% TiO}_2$	7.6	$\text{Al}_2\text{O}_3$ grit-blasting
10	Yang <i>et al.</i> , 1997	—	Low-carbon steel	—	$\text{Al}_2\text{O}_3$ grit-blasting	16.8
<i>ZrO<sub>2</sub> + 8wt% Y<sub>2</sub>O<sub>3</sub></i>						
11	Shankar <i>et al.</i> , 1982	—90 + 40	Mild steel	—	Directly after grit-blasting	34
12	Shankar <i>et al.</i> , 1982	—90 + 40	Mild steel	—	100 h after grit-blasting	18

12 of Table 8.8). The careful study of Funk *et al.* (1988) evidenced the importance of the initial temperature of the substrate prior to spraying. These authors suggested pre-heating the metal substrate to the temperature for which the metal ‘dilates’ to a defined value. This value should be equal to the ‘dilatation’ of a ceramic coating from room temperature to start of some kind of the *plastic deformation*. Their study, made for Cr<sub>2</sub>O<sub>3</sub> coatings, plasma-sprayed on to mild steel, show the following bond strengths:

- 37 MPa, at an initial temperature of  $T_0 = 363$  K;
- 61 MPa, at an initial temperature of  $T_0 = 513$  K.

A high conductivity of the substrate lowers the contact temperature, which results in weak bonding (entries 5 and 6 of Table 8.8). Adhesion of Al<sub>2</sub>O<sub>3</sub> to steel is better than that of Al<sub>2</sub>O<sub>3</sub> + 13 wt% TiO<sub>2</sub> (entries 1–4 and 10 of Table 8.8). This can result from a lower liquidus temperature of alloyed alumina than the melting point of alumina, which, in turn, lowers the contact temperature, given in Chapter 6, Equation (6.12). When spraying onto ‘easy-to-melt’ metals, it is easier for the molten ceramic particles to melt the substrate. This can explain the difference in bond strengths of alumina–titania alloys sprayed on to aluminum and low-carbon steel substrates (entries 9 and 10 of Table 8.8). Similarly, the impacting of ‘low-refractory’ ceramics, such as hydroxyapatite would result in a low value of the contact temperature and relatively low adhesion (entry 8 of Table 8.8). The exceptionally high adhesion of this compound found by Heimann *et al.* (2001), shown in entry 7 of Table 8.8, can be attributed to the very careful optimization of the process using statistical methods.

An improvement in oxide coating adhesion can be achieved by the application of bond coatings such as NiCr or NiCrAl (Yang *et al.*, 1997). Further improvement is achieved by inserting an intermediate cermet coating between the alloy and the ceramic.

## Metals

The tensile bond strengths of some thermally sprayed metals are collected in Table 8.9. In general, the bond strengths of metals to metallic substrates are clearly greater than those of ceramic coatings. A nickel coating, flame-sprayed using a wire, adheres to steel better than that sprayed using a powder (entries 1 and 2 of Table 8.9). An arc-sprayed titanium coatings shows better adhesion to mild steel when

Table 8.9 Tensile adhesion strength of some metals sprayed using different techniques

Number	Reference	Powder/wire characteristics		Substrate characteristics			Remarks	Critical tensile stress (MPa)
		Chemical composition (wt%)	Size ( $\mu\text{m}$ )/diameter (mm)	Material	Roughness, $R_a$ ( $\mu\text{m}$ )	Method of roughening		
1	Wielage <i>et al.</i> , 1990	Ni	-/3.18	Wire flame-spraying Steel	—	Iron grit-blasting	—	51
2	Wielage <i>et al.</i> , 1990	Ni	-75+30	Powder flame-spraying Steel	—	Iron grit-blasting	—	40
3	Müller, 1973	Ti	—	Arc spraying Mild steel	—	—	Reactive N <sub>2</sub> atmosphere	35
4	Müller, 1973	Ti	—	Mild steel	—	—	Inert Ar atmosphere	15
5	Wielage <i>et al.</i> , 1990	Ni	-/1.6	Steel	—	Iron grit-blasting	—	56

6	Wang <i>et al.</i> , 1996	Stainless steel	—	Aluminum	—	Grit-blasting	Classical nozzle, $v_p = 530 \text{ m/s}$
7	Wang <i>et al.</i> , 1996	Stainless steel	—	Aluminum	—	Grit-blasting	Modified nozzle, $v_p = 610 \text{ m/s}$
<i>Air plasma-spraying</i>							
8	Roseberry and Bouger, 1977	Mo	-70 + 30	Mild steel	6.4	$\text{Al}_2\text{O}_3$ grit-blasting	Initial temperature, $T_0 = 340 \text{ K}$
9	McPherson and Cheang, 1989	99Ni	-75 + 45	Mild steel	—	Grit-blasting	—
10	Wielage <i>et al.</i> , 1990	Ni	-75 + 30	Steel	—	Iron grit-blasting	Rupture in resin

sprayed under a argon atmosphere than in nitrogen (entries 3 and 4 of Table 8.9). This might be related to the formation of hard and less ductile nitrides when spraying in nitrogen. Hard nitrides deform less than ductile titanium upon impact with substrates. Consequently, the contact area of the particle with the substrate is greater and the adhesion stronger. Finally, an increase in the particle velocity strongly improves the bond strength of arc-sprayed stainless steel onto aluminium (entries 6 and 7 of Table 8.9). This effect was achieved by modification of the torch nozzle which consisted of the formation of two gas streams:

- the *primary* gas stream which atomizes the molten wire;
- the *secondary* gas stream which protects the spray volume by a conical gas sheath.

## Alloys

The tensile bond strengths of some alloy coatings are shown in Table 8.10. A typical bond coating of NiAl was tested many times and its adhesion to a substrate was proven to strongly depend on the deposition technique. Consequently, arc- and air-plasma spraying results in coatings which adhere better to steel than flame-sprayed ones (entries 1–4 of Table 8.10). Powder manufacturing techniques do seem to play a major role for this alloy (entries 5 and 6 of Table 8.10). Vacuum-plasma spraying is preceded by ‘transferred’ arc pre-treatment of the substrate. This treatment cleans the surface, removes oxides (if the arc is negatively polarized) and heats the substrate prior to spraying. This enhances the bonding by enabling a ‘metallurgical’ interaction between the coating and substrate (entry 7 of Table 8.10).

### 8.2.3 ELASTIC MODULI, STRENGTHS AND FRACTURE TOUGHNESS

Mechanical properties depend strongly on the microstructure and, in particular, on the porosity and interlamellar contacts. A small porosity and large contact area between the lamellae forming the coating would result in the mechanical properties being closer to that of the bulk materials. These features depend, in turn, on the following characteristics:

Table 8.10 Tensile adhesion strength of some alloys sprayed using different techniques

Number	Reference	Powder/wire characteristics			Substrate characteristics		Remarks	Critical tensile strength (MPa)
		Chemical composition (wt%)	Size ( $\mu\text{m}$ )	Method of preparation	Material	Method of roughening		
<i>Wire flame-spraying</i>								
1	Unger, 1987	Ni+20Al	—	Cladded wire	Mild steel	$\text{Al}_2\text{O}_3$ grit-blasting	—	38
<i>Powder flame-spraying</i>								
2	Unger, 1987	Ni+20Al	—	Dense clad	Mild steel	$\text{Al}_2\text{O}_3$ grit-blasting	—	21
<i>Arc spraying</i>								
3	Unger, 1987	Ni+5Al	—	Pre-alloyed wire	Mild steel	$\text{Al}_2\text{O}_3$ grit-blasting	—	63

Table 8.10 (Continued)

Number	Reference	Powder/wire characteristics			Substrate characteristics		Remarks	Critical tensile strength (MPa)
		Chemical composition (wt%)	Size (μm)	Method of preparation	Material	Method of roughening		
<i>Air plasma-spraying</i>								
4	Unger, 1987	Ni+5Al	—	Porous clad	Mild steel	$\text{Al}_2\text{O}_3$ grit-blasting	—	51
5	McPerson and Cheang, 1989	—	—88 + 37	'Pre-alloyed'	Mild steel	Grit-blasting	—	45 maximum
6	McPherson and Cheang, 1989	—	—90 + 44	Dense clad	Mild steel	Grit-blasting	—	40 maximum
<i>Vacuum plasma-spraying</i>								
7	Steffens and Beczkowiak, 1983	NiCoCrAlY	—	—	In 100 alloy	Grit-blasting	Transferred-arc <i>in situ</i> pre-heating	75

- The **spray process** and its parameters. The process determines the kinetics and enthalpy of the particles forming the sprayed coating.
- The **properties of the particles** and especially their morphologies. The latter are determined by the manufacturing methods and the sizes.
- The **microstructure of the coatings** and their anisotropic character. Consequently, the elastic moduli and strengths will depend on the direction of mechanical stress application and it is important to indicate its direction at testing. For example, the stresses 3 at- and 4-point bending act mainly in the in-plane direction of the coatings. This is why the mechanical data in the following sections will be accompanied, if relevant, by the measurement techniques and directions of stress.

## Carbides

The mechanical properties of sprayed carbides are presented in Table 8.11. The properties of typical bulk (sintered) materials are given for comparison:

- $E = 575 \text{ GPa}$  and  $\sigma_f = 6\text{--}8 \text{ GPa}$  for WC + 10 wt% Co (Kelly and McMillan, 1986);
- $E = 410 \text{ GPa}$  and  $\sigma_f = 3.6 \text{ GPa}$  for WC + 12 wt% Co (Kim *et al.*, 1997).

The *Young's moduli* values reach, for carbides sprayed by a detonation gun of similar compositions, a 30 to 80 % fraction of the bulk material modulus (entries 1–3 of Table 8.11). The greatest value was reached for an agglomerated powder having a spherical shape and homogenous distribution of the carbides inside the powder particles. The fracture strengths of these carbides are in the range of 5 to 22 % of the bulk material values. Comparison of elastic moduli and fracture strengths of the coatings sprayed using powders prepared by the same technique (sintering) and having different contents of binder (12, 17 and 20 wt% of Co) shows that, in general, the elastic modulus and fracture strength grows with the content of metal binder (see entries 2, 4 and 5 of Table 8.11). This effect can be interpreted as an improvement of the interlamellar contacts inside such coatings and an increase in the coating overall ductility. A comparison of the detonation gun and high-velocity combustion spray techniques shows that the coatings have relatively similar values for the elastic moduli (see entries 4, 6 and 7 in Table 8.11). The differences could have resulted from the different testing methods (Rybicki *et al.*, 1995). Richard *et al.* (1996) found that post-spray annealing increases the elastic moduli of 'as-sprayed' coatings by 10–20 %.

**Table 8.11** Mechanical properties of some carbides sprayed using different techniques

Number	Reference	Powder characteristics			Coating porosity (%)	Mechanical properties			Method of measurement
		Chemical composition (wt%)	Particles size ( $\mu\text{m}$ )	Method of preparation		$E$ (GPa)	$\sigma_f$ (MPa)	$K_c$ (MPam $^{0.5}$ )	
<i>Detonation-gun spraying</i>									
1	Kim <i>et al.</i> , 1997	WC+12Co	—	Cast and crushed	—	181	415	—	—
2			—	Sintered	—	225	610	—	—
3			—	Agglomerated	—	331	820	—	—
4		WC+17Co	—	Sintered	—	186	630	—	—
5		WC+20Co	—	Sintered	—	422	860	—	—
<i>High-velocity combustion spraying</i>									
6	Rybicki <i>et al.</i> , 1995	WC+17Co	JK 117™	—	180	—	—	0.278	Cantilever beam method
7	Richard <i>et al.</i> , 1996	WC+16Co	Stelcar 117™	—	140	—	—	—	4-point bending test
<i>Air plasma-spraying</i>									
8	Richard <i>et al.</i> , 1996	WC+16Co	Stelcar 117™	—	138	—	—	—	4-point bending test
9	Leigh <i>et al.</i> , 1997	Cr <sub>3</sub> C <sub>2</sub> +25NiCr	—	—	2.3	175	—	—	Indentation test
10	Li <i>et al.</i> , 1998b	Cr <sub>3</sub> C <sub>2</sub> +25NiCr	—	—	10.7	—	—	5.4	—
11		WC+17Co	—	—	10.8	—	—	8.4	—

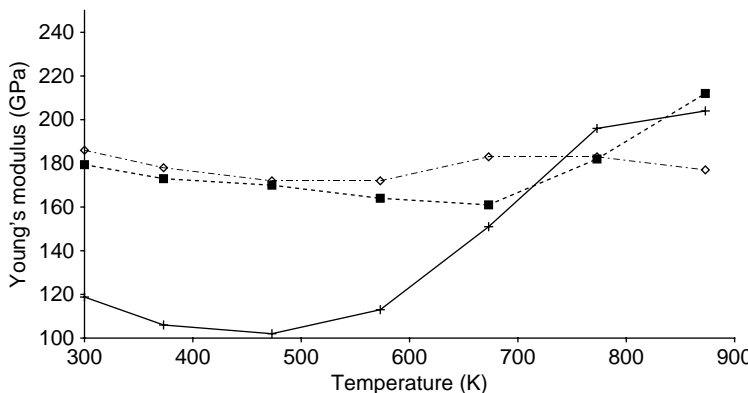


**Figure 8.9** Elastic modulus versus temperature of  $\text{Cr}_2\text{O}_3$  sprayed by APS (■), WC + 20 wt% Co sprayed by APS (+) and WC + 20 wt% Co sprayed by VPS (◊) coatings and tested by using the ultrasonic technique (Tronche, 1986) (further details about the coatings can be found in Table 8.2)

The elastic modulus versus temperature data (Figure 8.9) show a typical decrease up to 500 K, before this value starts to increase. The decrease could have resulted from the generation of thermal stresses which can generate cracks. At higher temperatures, the coatings start to sinter, which improves the interlamellar contacts and increases the elastic modulus.

## Oxides

The mechanical properties of plasma-sprayed oxides are presented in Table 8.12. The elastic moduli of typical sintered oxides are as follows:

- $\text{Al}_2\text{O}_3$ ,  $E = 370 \text{ GPa}$  (Samsonov, 1978);
- $\text{ZrO}_2$  crystallized in the tetragonal phase,  $E = 140\text{--}200 \text{ GPa}$  (Stevens, 1986);
- $\text{Cr}_2\text{O}_3$ ,  $E = 314 \text{ GPa}$  (Richard *et al.*, 1992).

The moduli for sprayed oxides are 20–40 % fractions of those of the bulk materials. The values are slightly greater in compression than in tension (entry 2 of Table 8.12). These also depend on the direction of measurement during the indentation test; the modulus measured on the plane-section is 20–40 % lower than on the cross-section of the deposit (see entry 12 in Table 8.12). This anisotropy can be explained by the voids between the successive lamellae. The Young's modulus versus temperature curve behaves in a similar way to the previously

**Table 8.12** Mechanical properties of air-plasma-sprayed oxides<sup>a</sup>

Number	Reference	Powder characteristics			Coating characteristics			Mechanical properties			Method of measurement
		Chemical composition (wt%)	Size (μm)	Preparation method	Crystalline phase	Density (kg/m <sup>3</sup> )/Porosity (%)	E (GPa)	$\sigma_f$ (MPa)	$K_c$ (MPam <sup>0.5</sup> )	$C_{lc}$ (J/m <sup>2</sup> )	
1	Lutz, 1994	Al <sub>2</sub> O <sub>3</sub>	—192+48	—	—	3120/—	—	8.2   to surface; 25.2 $\perp$ to surface	0.47   to surface; 1.62 $\perp$ to surface	—	$\sigma_f$ – 3-point bending test; $K_c$ – single-edge bend test
2	Kovarik <i>et al.</i> , 2005	Al <sub>2</sub> O <sub>3</sub>	—50+40	Crushed	—	—	57 in compression; 46 in tension	—	—	—	4-point bending test
3	Li <i>et al.</i> , 2004	Al <sub>2</sub> O <sub>3</sub>	—40+20	—	—	—	—	—	—	26.6 maximum	Double-cantilever beam
4	Leigh <i>et al.</i> , 1997	Al <sub>2</sub> O <sub>3</sub>	—	—	$\gamma$ -Al <sub>2</sub> O <sub>3</sub> + 23 % $\alpha$ -Al <sub>2</sub> O <sub>3</sub>	—/5 maximum	126	—	—	—	Knoop indentation test
5	Richard <i>et al.</i> , 1992	Cr <sub>2</sub> O <sub>3</sub>	—25+5	—	—	3500/	138	—	—	—	Ultrasonic test
6	Barbezat <i>et al.</i> , 1993	Cr <sub>2</sub> O <sub>3</sub>	—45+22	—	—	—/2.7	—	—	3	—	Indentation test
7	Li <i>et al.</i> , 1998	Cr <sub>2</sub> O <sub>3</sub>	—	—	—	—/4.7	—	—	3.5	—	3-point bending test

8	Ibrahim <i>et al.</i> , 2005	TiO <sub>2</sub>	TiO <sub>2</sub>	Metco 102	—	—	—	—	1.45 <sup>b</sup>	—	Vickers indentation test
<hr/>											
9	Li <i>et al.</i> , 2005	Ca <sub>10</sub> (PO <sub>4</sub> ) <sub>6</sub> (OH) <sub>2</sub>	Hydroxyapatite	HA, α-TCP, β-TCP, TTCP	—	50	—	—	—	—	Indentation test
<hr/>											
10	Sainte- Catherine <i>et al.</i> , 1991	ZrO <sub>2</sub> +7Y <sub>2</sub> O <sub>3</sub>	d <sub>50</sub> % = 34	Agglomeration t'	ZrO <sub>2</sub> -Y <sub>2</sub> O <sub>3</sub> Monoclinic, tetragonal- t'	—/17	51	—	1.8	—	E – ultrasonic test; K <sub>IC</sub> – indentation test
11	Barbezat <i>et al.</i> , 1993	ZrO <sub>2</sub> +8Y <sub>2</sub> O <sub>3</sub>	—63+16	—	—/6	—	—	—	2.9	—	Indentation test
12	Wallace and Ilavsky, 1997	—96+26	Plasma 'spheroidized'	—	—/10.4	38.5 – cross- section;	—	—	—	—	Indentation with spherical indenter
13	Eaton and Novak, 1986	ZrO <sub>2</sub> +20Y <sub>2</sub> O <sub>3</sub>	—90+10	Agglomeration	—	47 maximum	47 maximum	—	—	—	4-point bending test

Table 8.12 (Continued)

Number	Reference	Powder characteristics			Coating characteristics		Mechanical properties			Method of measurement
		Chemical composition (wt%)	Size (µm)	Preparation method	Crystalline phase	Density (kg/m³)/Porosity (%)	E (GPa)	σ <sub>f</sub> (MPa)	K <sub>IC</sub> (MPam <sup>0.5</sup> )	
<i>Al<sub>2</sub>O<sub>3</sub>-TiO<sub>2</sub></i>										
14	Ostojic and McPerson, 1988	Al <sub>2</sub> O <sub>3</sub> + 3TiO <sub>2</sub>	—	—	—	—	—	—	—	Double-cantilever beam Indentation test
15	Barbezat <i>et al.</i> , 1993	—30+5	—	—	—	-3.7	—	—	3.8	—
<i>Titanate</i>										
16	Cibor <i>et al.</i> , 2000	14TiO <sub>2</sub> , 11MgO, CaO, geikielite-perovskite	-125+63	Sintering and crushing	MgTiO <sub>3</sub> , Mg <sub>2</sub> TiO <sub>4</sub> , MgTi <sub>2</sub> O <sub>5</sub>	3.68/6-7 maximum	22	—	—	4-point bending test

<sup>a</sup> Oxides described in entries 1, 2, 4 and 16 were sprayed using a water-stabilized torch.<sup>b</sup> Reported value was 14.5 MPam<sup>0.5</sup>, but this was probably a printing error.

discussed carbides, namely, it decreases to reach a minimum at about 700 K and increases at higher temperatures (Figure 8.9). The minimum is at a higher temperature than in the carbide because sintering of the chromium oxide starts at a higher temperature than that of the carbide binder–cobalt.

The fracture strengths of sprayed oxides were measured by using 3- or 4-point bending tests. These tests enabled us to visualize the ‘anisotropy of strength’, which is greater in the direction perpendicular to the coatings’ surfaces than in the direction parallel to them (entry 1 in Table 8.12). This effect can be explained by the fact that the lamellae are in contact with the others in their lower and upper parts and hardly on their sides. Application of a tensile stress which acts parallel to the coating surface would not be countered by a resisting force inside the coating as the lamellae can ‘slide’ past each other. The effect of ‘sliding’ has already been mentioned by Berndt (1986) when discussing the extremely low values of the Young’s modulus in YSZ coatings, found by tensile testing. The *pseudoplastic behaviour* of sprayed oxides enables indeed a prediction of the anisotropy in fracture strength. The reported values of fracture toughness are in the range  $K_{Ic} = 0.5\text{--}3.8 \text{ MPam}^{0.5}$  (entries 1, 6–8, 10, 11 and 15 in Table 8.12), independent of the oxide and the testing technique. The toughness values of sprayed yttria-stabilized zirconia (entries 10 and 11 in Table 8.12) are much lower than those of sintered zirconia of a similar composition,  $K_{Ic} = 6.4 \text{ MPam}^{0.5}$  (Stevens, 1986). The low toughness can be attributed to the high porosity of the sprayed coatings.

The fracture mechanism in ‘as-sprayed’ oxides is rather *interlamellar*, i.e. cracks develops along the interfaces between the lamellae. This mechanism was found by Siemers and Mehan (1983) during testing of ‘as-sprayed’ magnesia-stabilized zirconia coatings. On the other hand, post-spray annealing increases the contacts between the lamellae. Consequently, the fracture grows in an *intralamellar* way (LaPierre *et al.*, 1991).

Any crack can grow more easily in the direction along the lamella diameter because this way is relatively straightforward in comparison with the deviations expected if cracks develop in the direction perpendicular to it. This is why the fracture toughness in the direction parallel to the coating’s surface is lower than that in the perpendicular direction (entry 1 in Table 8.12). The fracture toughness found by Lutz (1994) for post-spray annealed alumina is equal to  $K_{Ic} = 4.64$ . This value is close to that of a fine-grained sintered material.

The strain-energy release rate, i.e. the energy it is necessary to apply when the propagating crack was found to be in the range  $G_{lc} = 11\text{--}27 \text{ J/m}^2$  (entries 3 and 14 in Table 8.12). The energy was also estimated for a crack developing at the interface of a vacuum plasma-sprayed alumina coating and mild steel to be in the range of  $G_{lc} = 400\text{--}500 \text{ J/m}^2$ , depending on the coating thickness and its deposition temperature (Itoh and Clyne, 1995)

## Metals

The mechanical properties of thermally sprayed metals are collected in Table 8.13. The elastic moduli and ultimate strengths of some bulk metals are as follows:

- $E = 205 \text{ GPa}$  and  $\sigma_u$  is about 500 MPa for Ni (Fedorczenko, 1977);
- $E = 71 \text{ GPa}$  and  $\sigma_u$  is between 80 and 100 MPa for Al (Fedorczenko, 1977);
- $E = 323 \text{ GPa}$  and  $\sigma_u$  is between 500 and 2500 MPa, depending on the preparation method, for Mo (Fedorczenko, 1977);
- $E$  is about 105 GPa and  $\sigma_u$  is about 500 MPa for Ti (Steffens *et al.*, 1992);
- $E$  is about 365 GPa and  $\sigma_u$  is between 1800 and 4100 MPa, depending on the preparation method, for W (Fedorczenko, 1977);
- $\sigma_u$  is between 230 and 390 MPa, depending on the preparation method, for Cu (Gärtner *et al.*, 2006).

The elastic moduli of sprayed metals are 40–82 % fractions of the bulk materials. The moduli becomes closer to that of the bulk metals for vacuum-plasma spraying (entry 6 in Table 8.13). The  $E$ -values decrease, as expected, with porosity (entry 3 in Table 8.13). Surprisingly, the moduli measured in the directions parallel and perpendicular to the coatings' surface directions do not differ (entry 6. in Table 8.13). This can result from the large quantity of unmelted and partially melted grains present in the tested coating. Such particles preserve the spherical shape, i.e. it is less deformed. Consequently, the structure is more isotropic. The ultimate strength for 'less-refractory' metals (Al, Ni, Ti) is a 50–75 % fraction of the values for bulk materials (see entries 2 and 10 in Table 8.13, plus Figure 8.10) but only a 20 % fraction for the very refractory tungsten ( $T_m = 3670 \text{ K}$ , see entry 11 in Table 8.13). It must be stressed that the ultimate strengths of copper coatings, cold-gas-sprayed

Table 8.13 Mechanical properties of metals sprayed using different techniques

Number	Reference	Powder characteristics		Coating characteristics		Mechanical properties				Remarks	Method of measurements
		Metal	Particles size ( $\mu\text{m}$ )	Density ( $\text{kg}/\text{m}^3$ )	Porosity (%)	$E$ (GPa)	$\sigma_y$ (MPa)	$\sigma_u$ (MPa)	$K_{Ic}$ (MPam $^{0.5}$ )		
<i>Flame spraying</i>											
1.	Brantner <i>et al.</i> , 2003	Mo	—	—	—	—	—	—	—	—	Indentation for individual lamellae; bending test for coatings
<i>Air plasma-spraying</i>											
2	Tucker, 1982	Ni	—	7500	1	97	—	380	—	—	Tensile test
3	Pina <i>et al.</i> , 1991	Mo	—	—	3; 5; 9; 10	131; 110; 79; 78	—	—	—	—	$E$ tested for different porosities
<i>Vacuum plasma-spraying</i>											
4	Howard and Clyne, 1991	Ti	—	—	13	62	—	—	0.79	6.8	—
											3- and 4-point bending tests

Table 8.13 (Continued)

Number	Reference	Powder characteristics	Coating characteristics		Mechanical properties				Remarks	Method of measurements	
			Metal	Particles size ( $\mu\text{m}$ )	Density ( $\text{kg}/\text{m}^3$ )	Porosity (%)	$E$ (GPa)	$\sigma_y$ (MPa)	$\sigma_u$ (MPa)	$K_{ic}$ ( $\text{MPa m}^{0.5}$ )	$G_{ic}$ ( $\text{J}/\text{m}^2$ )
5	Steffens <i>et al.</i> , 1992	—	—	—	5	—	109–115	—	—	—	Tensile test
6	Neiser <i>et al.</i> , 1993	W	—25+5	17500	—	—	298   to surface; 280 $\perp$ to surface	—	—	—	Ultrasonic test
7	Montavon <i>et al.</i> , 1996	Cu	—90+45	—	0.6; 0.8; 4.0	Not measured; 27; 38	—	206; 192; 142	—	—	$E$ and $\sigma_u$ tested for different porosities
<i>Arc spraying</i>											
8	Gartner <i>et al.</i> , 2006	Cu	1.6	—	—	—	65	68	—	—	After annealing at 873 K
											In-plane tensile test

		<i>High-velocity oxy-fuel spraying</i>							
		Cu			Al			In-plane tensile test	
		-88+31	-	-	-	-	125	129	After annealing at 873 K
<i>'Shrouded' plasma spraying</i>									
10	Tucker, 1982	Al	-	86 % bulk	-	-	38.6	-	-
11	Tucker, 1982	W	-75+45; -39+10	90 % bulk; 91 % bulk	-	-	220; 352	-	-
<i>Cold-gas spraying</i>									
12	Gärtner <i>et al.</i> , 2006	Cu	-25+5	-	-	-	403	453	-
13	Gärtner <i>et al.</i> , 2006						165	210	-
									Using He as working gas Using N <sub>2</sub> as working gas and annealed at 873 K after spray

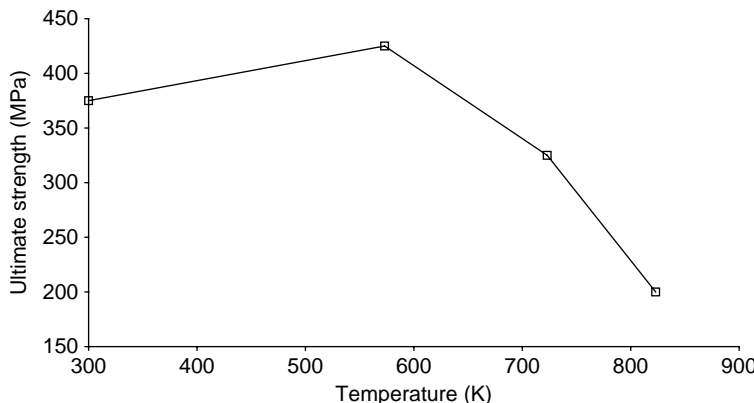


**Figure 8.10** Ultimate strength versus temperature for vacuum-sprayed titanium coatings (descriptions of the coatings are given in Table 8.13)

using helium, is greater than those of the bulk materials (entry 12 in Table 8.13). Cold-gas spraying with helium is expensive but such processing with the less-expensive nitrogen, followed by annealing at 873 K results in a coating having an ultimate strength close to that of the bulk material.

The fracture toughness of a molybdenum coating sprayed by a flame was greater for the overall coating than for the individual lamellae (entry 1 in Table 8.13). This effect can be explained by hampering of the crack progress by deflection and branching. The very low fracture toughness of a vacuum plasma-sprayed titanium coating ( $K_{lc} = 0.79 \text{ MPam}^{0.5}$ ) can be explained by the high porosity of deposits.

## Alloys

The mechanical properties of sprayed alloys should match the coating's specification. Thus, alloys used for bond coatings under an oxide ceramic overlay in high-temperature applications, such as Ni+5 wt% Al or Ni+20 wt% Cr, should be rather ductile and have an elastic modulus as close as possible to that of the substrate. On the other hand, alloys used as 'free-standing' bodies should be strong. This is why the latter are sprayed under vacuum in order to avoid oxidation and are frequently densified by post-spraying treatment (annealing or hot isostatic pressing). The mechanical properties of such materials are

similar to those of ‘wrought’ materials (Schneider and Grünling, 1983; Nguyenat *et al.*, 1992).

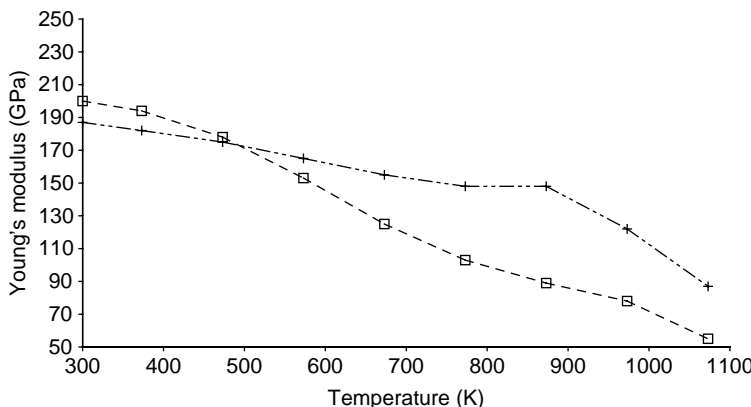


Figure 8.11 Elastic modulus versus temperature of NiCoCrAlTaY (+) and NiCrAlY (□) alloys, plasma-sprayed under vacuum (descriptions of the coatings are given in Table 8.14)

The elastic modulus versus temperature curve (Figure 8.11) of two ‘superalloys’ sprayed under vacuum shows a decrease in modulus at temperatures of about 700–800 K. A similar behaviour was reported by Cook *et al.* (1994) for vacuum-sprayed NiCrAlY alloys with different contents of Cr. The alloy containing 33 wt% of Cr has an elastic modulus 15 % higher than that containing only 15.6 wt% (entries 12–14 in Table 8.14).

The elastic moduli of atmospheric plasma-sprayed nickel alloys are relatively low and seem to be clearly lower from those sprayed under vacuum. The strength and elongation versus temperature curves collected in Figures 8.12–8.14 of nickel and cobalt based coatings show that these parameters are relatively constant up to temperatures in the range 600–900 K. At higher temperatures, the strength starts to decrease and the elongation to increase.

Post-spray annealing results in fine-grained structure of coatings with a matrix composed typically of ‘intermetallics’ (entries 6 and 7 in Table 8.14) which results, most probably, in isotropic properties of the deposits. As-sprayed atmospheric plasma-sprayed NiAl alloy has a considerably anisotropic elastic modulus (entry 4 in Table 8.14). The strain energy release rate measured for typical bond coatings is in the range 200–500 J/m<sup>2</sup> (entries 2 and 3 in Table 8.14).

**Table 8.14** Mechanical properties of alloys sprayed using different techniques

Number	Reference	Powder characteristics			Coatings Characteristics			Mechanical properties				Remarks	Method of testing
		Chemical composition (wt%)	Particle size ( $\mu\text{m}$ )	Method of manufacturing	Density ( $\text{kg}/\text{m}^3$ )	Phase content	$E$ (GPa)	$\sigma_y$ (MPa)	$\sigma_u$ (MPa)	Elongation (%)	$G_{\text{ic}}$ ( $\text{J}/\text{m}^2$ )		
1	Tucker, 1982	Co+ 2.5Cr+ 10Ni+7W	—	—	8000	—	55	—	366	—	—	—	Tensile test
2	Berndt and McPherson, 1980	Ni+4.5Al	—88+45	Porous clad	—	—	—	—	—	—	396-524	—	Double- cantilever beam
3	Ostojic and Ni+20Cr McPherson, 1988	—	—	—	—	—	—	—	—	—	219-239	—	—
4	Leigh <i>et al.</i> , Ni, 5Al 1997	—	—	—	—	—	30 $\parallel$ to surface; 20 $\perp$ to surface	—	—	—	—	Porosity, 2.5 %	Indentation test
5	Siemens and Mehan, 1983	Ni+ 22Cr+	-38	—	—	—	<i>Vacuum plasma-spraying</i>				—	—	Tensile test
6	Smith, 1981	Co+ 29Cr+ 6Al+1Y	-38	Gas atomized	—	Co, NiAl, CoAl, CoCr, Ni <sub>3</sub> Al	—	—	Figure 8.13	Figure 8.14	—	Annealed after spraying	—
7	Veys <i>et al.</i> , 1988	Ni+ 22Co+ 21Cr+ 8Al+ 4Ta+0.5Y	-38	Gas atomized	—	$\beta$ -NiAl, $\gamma$ -NiI	Figure 8.11	Figure 8.12	Figure 8.13	Figure 8.14	—	Annealed after spraying	Tensile test

8	Nguyentat <i>et al.</i> , 1992	Fe+20Ni+	—	—	—	—	—	750	900	11	—
9	Nguyentat <i>et al.</i> , 1992	15Cr + 2Ti+1Mo	—	—	—	—	—	850	1250	20-25	—
10	Nguyentat <i>et al.</i> , 1992	Ni + 19Cr + 17Fe + 3Mo + 5(Nb + Ta)+3Mo	—	—	—	—	—	570	1000	43	—
11	Chen <i>et al.</i> , 1993b	Ni + 22Cr + 10Mo + 2Fe	—	—	—	—	Figure 8.11	—	Figure 8.14	—	Annealed after spraying
12	Cook <i>et al.</i> , 1994	Cu+3Ag + 0.5Zr	—	—	—	—	$\gamma\text{-Ni}-$ CrAl <sub>y</sub> Ni <sub>3</sub> Al	205	—	—	—
13	Cook <i>et al.</i> , 1994	Ni + 15.6Cr + 5.2Al + 0.2Y	—	—	—	—	—	200	—	—	—
14	Cook <i>et al.</i> , 1994	Ni + 17.2Cr + 11.6Al + 0.98Y	—	—	—	—	—	—	—	—	—
		Ni + 33Cr + 6.2Al + 0.95Y	—	—	—	—	—	231	—	—	—
											Tensile test
											Acoustic- resonance method
											Acoustic- resonance method
											Acoustic- resonance method

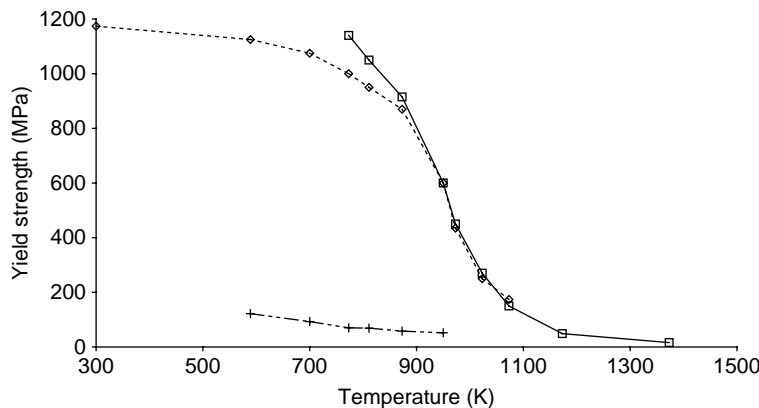


**Figure 8.12** Yield stress versus temperature of NiCoCrAlTaY ( $\diamond$ ), NiCrAlY ( $\square$ ) and CuAgZr (+) alloys, plasma-sprayed under vacuum (descriptions of the coatings are given in Table 8.14)

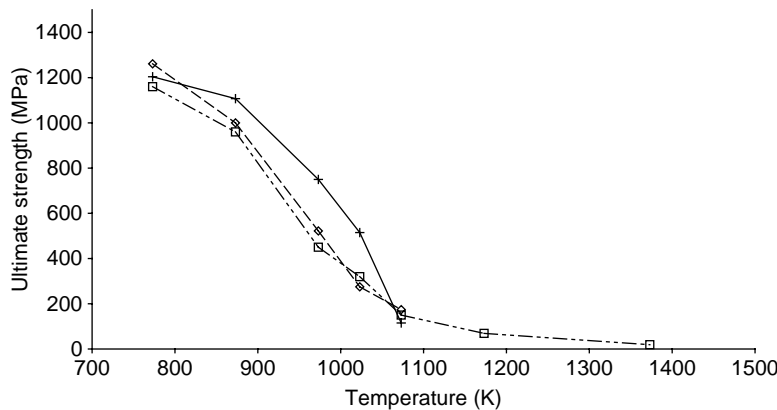


**Figure 8.13** Ultimate strength versus temperature of NiCoCrAlTaY ( $\diamond$ ), NiCrAlY ( $\square$ ) and CoCrAlY (+) alloys, plasma-sprayed under vacuum (descriptions of the coatings are given in Table 8.14)

## Composites

Thermally sprayed composites usually fulfill the following functions:

- **Intermediate coatings** between the bond and top deposits with different properties. A multi-coating system, specified to be in service at higher temperatures, should include neighbouring coatings having a thermal expansion and elastic modulus as low as possible. Otherwise,

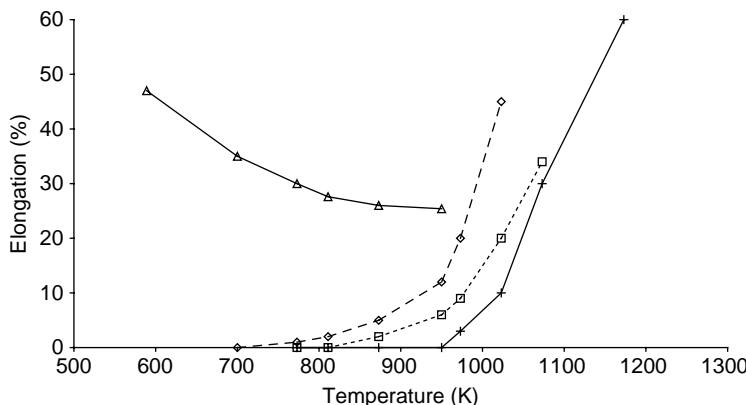


**Figure 8.14** Elongation versus temperature of NiCoCrAlTaY ( $\diamond$ ), NiCrAlY ( $\square$ ), CoCrAlY (+) and CuAgZr ( $\Delta$ ) alloys, plasma-sprayed under vacuum (descriptions of the coatings are given in Table 8.14)

the generated thermal stresses would be greater than the resistance of the coating, which results in cracking. In particular, the elastic modulus of the intermediate composite should be between that of the bond and top coating. An example of such a design, in which yttria-stabilized zirconia was part of the particulate composite with NiCr and magnesia-stabilized zirconia with NiAl, was reported by Gault *et al.* (1988) for a thermal-barrier coating. The Young's moduli of these composites are indeed intermediate between those of the alloys and ceramics at room temperature (Figure 8.15) and at higher temperatures (Figure 8.16) – the mechanical properties of these composites are presented in Table 8.15.

- Near-'net-shape' structures have been studied extensively for use in many applications. Such structures should be as strong as possible. The strengths of such composites are enhanced by the type and morphology of the reinforcement (Table 8.16). 'Whiskers-reinforced' coatings were studied by, e.g. Tsunekawa *et al.* (1987). These authors used the FS-wire technique for aluminium–SiC composites forged after spraying. The ultimate strength of the resulting material (shown as entry 1 in Table 8.15) was about two times greater than that of the aluminum. Fibre-reinforced composites can be obtained by the use of long or short fibres. Long fibres, being in fact 'wires', are easier to process than short ones. The difficulties with stable feeding of the latter were described by, e.g. Berndt and Yi (1987). The technology of long-fibre composites has been demonstrated by Steffens

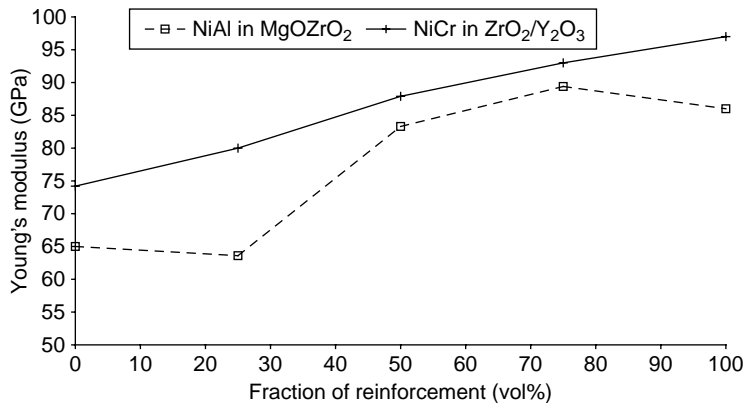


Figure 8.15 Young's modulus versus volume fraction of reinforcement in composites of  $\text{ZrO}_2 + 7 \text{ wt\% } \text{Y}_2\text{O}_3$  reinforced with  $\text{Ni} + 20 \text{ wt\% Cr}$  (+) and  $\text{ZrO}_2 + 24 \text{ wt\% MgO}$  reinforced with  $\text{Ni} + 5 \text{ wt\% Al}$  (□) (see also Table 8.15)

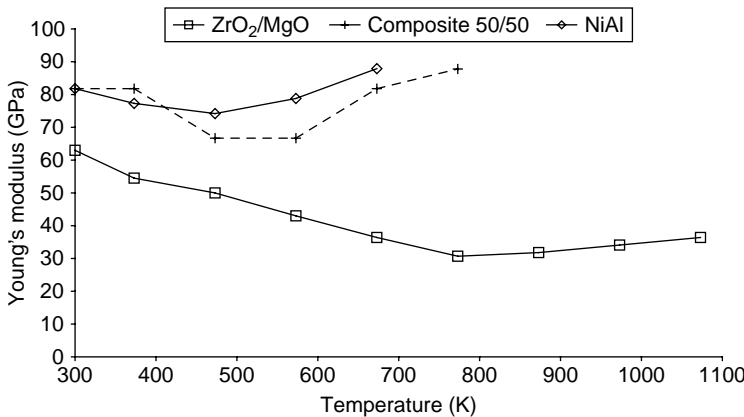


Figure 8.16 Young's modulus versus temperature of the alloy  $\text{ZrO}_2 + 7 \text{ wt\% MgO}$  (□), the reinforcement  $\text{Ni} + 5 \text{ wt\% Al}$  (◊) and a 50/50 (volume/volume) composite of these materials (+), sprayed using the APS technique (see also Table 8.15)

and Kaczmarek (1991). Particulate-reinforced composites are easy to manufacture with existing thermal-spray hardware. However, the strength of an 'as-sprayed' material, with the use of an SiC reinforcement in an  $\text{Al}_2\text{O}_3$  matrix composite, can be lower than that of the ceramic itself due to the weak bonding between the carbide and oxide (LaPierre *et al.*, 1991).

Table 8.15 Mechanical properties of composites obtained using different spray techniques

Number	Reference	Matrix	Reinforcement			Mechanical properties		Remarks	Method of testing		
			Chemical composition (wt%)	Size/Diameter (µm/mm)	Chemical composition (wt%)	Type	Fraction (vol%)	E (GPa)	$\sigma_y$ (MPa)	$\sigma_u$ (MPa)	
1	Tsunekawa <i>et al.</i> , 1987	Al	/3.18	SiC	Flame spraying Whiskers	14	—	—	188	Post-spray forging	Tensile test
2	Westfall, 1987	Fe + 15Cr + 4Al + 0.5Y	/1.6	W	Arc spraying under argon atmosphere	30	—	—	666	—	Tensile test
3	Gault <i>et al.</i> , 1988	ZrO <sub>2</sub> + 24MgO	—	Ni, 5Al	Atmospheric plasma-spraying Particulates	0-100	Figure 8.15 and 8.16	—	—	—	Ultrasonic test
4	Gault <i>et al.</i> , 1988	ZrO <sub>2</sub> + 8Y <sub>2</sub> O <sub>3</sub>	—	Ni, 20Cr	Atmospheric plasma-spraying	Figure 8.15	—	—	—	—	—
5	Hoffmann <i>et al.</i> , 1993	Al	—	C	—	40	—	—	460	—	—

**Table 8.16** Properties of typical reinforcements used in thermally sprayed composites (after Kudinov (1977) and Berndt and Yi (1989))

Number	Material	Form	E (GPa)	$\sigma_u$ (GPa)	$T_m$ (K)
1	SiC	Short fibre	186–407	—	2973
2	$Si_3N_4$	Short fibre	310	—	2173
3	Carbon	Fibre	590	8	—
4	Steel	Wire	210	4.2	1803
5	W	Wire	410	3.8	3673

### 8.2.4 FRICTION AND WEAR

The basic mechanisms of wear and methods for their characterization are explained in Chapter 7, Section 7.2.5. In general, the methods vary from author to author and it is hard to compare the wear-resistance data of coatings characterized in different papers. Wear of a coating depends mainly on:

- the coating material (hard materials and composites are generally used);
- the residual stress in the worn zone knowing that compressive stresses are probably more advantageous in reducing wear;
- the spray techniques, where it must be stressed that highly energetic spray techniques are generally used.

#### Friction and Adhesive (Sliding) Wear

**Ceramics** Sliding-wear resistance has been mainly tested for oxides and carbides (composites with metals or alloys). A selection of the literature data is shown in Table 8.17.

Among the oxides,  $Cr_2O_3$  and its alloys with  $SiO_2$  and  $TiO_2$ , and  $Al_2O_3$  and its alloys with  $TiO_2$  and  $ZrO_2$  have been frequently tested. The friction coefficient depends on the used ‘counter-body’, initial roughness of the coating and lubrication of the contacting surfaces. The coefficient and wear increase when dry surfaces are tested (entry 3 in Table 8.17) and the main mechanisms of wear are (Jin and Yang, 1996):

- plastic ‘smearing’ at low friction and wear;
- adhesive tearing at higher friction and low wear.

Table 8.17 Sliding wear and friction of ceramics thermally sprayed using different methods

Number	Reference	Coating composition (wt%)	'Counter-body' composition (wt%)	Lubrication, Yes/No	Friction coefficient	Wear ( $\text{m}^3/\text{N}$ )	Remarks	Testing method
<i>Atmospheric plasma-spraying</i>								
1	Bull <i>et al.</i> , 1996	$\text{Al}_2\text{O}_3$	$\text{Al}_2\text{O}_3$ , monolithic sphere	No	—	$3.5\text{--}5.1 \times 10^{-13}$ under load of 1–6 N	Weak or no sphere wear	Pin-on-disc test, with 3 mm diameter $\text{Al}_2\text{O}_3$ sphere
2	Li <i>et al.</i> , 1998b	$\text{Cr}_2\text{O}_3$	Similar coating	Yes – water	0.23–0.3	$6.4\text{--}8.5 \times 10^{-16}$ under load of 400 N	Wear on block and on ring	Block-on-disc test
3	Jin and Yang, 1996	$\text{Al}_2\text{O}_3 + 20\text{TiO}_2$	Similar coating	No	0.75	$5.3\text{--}8.1 \times 10^{-13}$ , upper –lower specimen	At room temperature	Roller-on-disc test
4	Wu <i>et al.</i> , 1994	$\text{Al}_2\text{O}_3 + 40\text{ZrO}_2$	Cast iron	Yes – engine oil	About 0.1	$1.6\text{--}3.2 \times 10^{-16}$ , cast-iron specimen	At 473 K, changing load	Roller-on-disc test

Table 8.17 (Continued)

Number	Reference	Coating composition (wt%)	'Counter-body' composition (wt%)	Lubrication, Yes/No	Friction coefficient	Wear ( $\text{m}^3/\text{N}$ )	Remarks	Testing method
<i>High-velocity oxy-fuel spraying</i>								
5	Qiao <i>et al.</i> , 2001	WC+10Co	Si <sub>3</sub> N <sub>4</sub> monolithic sphere	No	—	$1.5 \times 10^{-16}$ under load of 10 N	WC content, 97.7 wt%	Pin-on-disc test
6		WC+15Co				$6 \times 10^{-16}$ under load of 10 N	WC content, 31 wt%	
<i>Vacuum plasma-spraying</i>								
7	Bull <i>et al.</i> , 1996	Al <sub>2</sub> O <sub>3</sub>	Al <sub>2</sub> O <sub>3</sub> monolithic sphere	No	—	$4.9 - 92 \times 10^{-13}$ under load of 1–6 N	Sphere was worn ten times less	Pin-on-disc test, with 3 mm diameter Al <sub>2</sub> O <sub>3</sub> sphere
8	Leblanc, 2003	Cr <sub>2</sub> O <sub>3</sub> + 5SiO <sub>2</sub> + 3 TiO <sub>2</sub>	Si <sub>3</sub> N <sub>4</sub> monolithic sphere	No	—	$1.6 \times 10^{-15}$ for conventional powder; $1 \times 10^{-15}$ for 'nano-structured' powder	Under load of 10 N at room temperature	Pin-on-disc test after ASTM G99

Spray techniques play a role in sliding-wear resistance by:

- influencing the stress patterns and generation of the compressive stresses act in favour of wear resistance<sup>5</sup> (Bull *et al.*, 1996);
- less or more intensive in-flight sintering of nanostructured powders (entry 8 in Table 8.17).

Tungsten carbide with cobalt seems to be the most frequently used and tested carbide. A direct comparison of chromium carbide,  $\text{Cr}_3\text{C}_2 + 25 \text{ wt\% NiCr}$ , with tungsten carbide, WC+12 wt% Co, shows a nearly two-orders-of-magnitude better wear resistance for the latter (Jin and Yang, 1996). The high wear resistance of tungsten carbide correlates strongly with (Qiao *et al.*, 2001):

- high hardness of the deposits;
- high content<sup>6</sup> of the WC phase and small content of the hard but brittle  $\text{W}_2\text{C}$  phase (entries 5 and 6 in Table 8.17).

Another way of reducing wear is the application of self-lubricating coatings or lubricating additives to hard coatings.  $\text{TiO}_2$  has been tested as a possible candidate for such a coating (see, e.g. Buchmann and Gadow, 2001). On the other hand,  $\text{CaF}_2$  was agglomerated with  $\text{Cr}_2\text{O}_3$  to obtain a powder useful in spraying a wear-resistant coating with a relatively low friction coefficient of  $\mu = 0.25$  (Vos *et al.*, 1998)

**Metals and Alloys** Molybdenum, bronzes, nickel-based, iron-based and copper-based coatings have been most frequently tested to protect against adhesive wear.

Molybdenum is frequently agglomerated with its oxide for plasma spraying in order to obtain coatings with low friction coefficients against cast iron or steel (Houck and Whisenant, 1987; Habig *et al.*, 1985).

Bronzes (alloys of copper with aluminium) were plasma- and arc-sprayed and used with and without lubricant against steel by Tucker (1982) and Wen *et al.* (1988). *Quasi-crystals*, being alloys of the forbidden five-fold symmetry of aluminium, copper and iron (among others), were plasma-sprayed by De Palo *et al.* (1997) and Lugscheider

<sup>5</sup> Direct comparison of wear resistance of alumina, plasma-sprayed in air and under vacuum, show a slightly better resistance of air-processed material (entries 1 and 7 in Table 8.17).

<sup>6</sup> In other words, decarburation during spraying is to be avoided in order to reach a high sliding-wear resistance of tungsten carbide coatings.

*et al.* (2000). The authors obtained coatings having friction coefficients in the range  $\mu = 0.1\text{--}0.6$ .

Flame-sprayed nickel-chromium alloy of a composition (in wt%) of Ni + 18Cr + 8Fe + 1Si was tested against an AlSn alloy without lubricant by Kretschmar (1986), while plasma- and high-velocity-flame sprayed self-fluxing alloys of a composition (in wt%) of Fe + (27–43)Ni + 10Cr + (3–5)B + (0.1–2)Mn + (0.1–5)Si + (0.2–1.5)C was tested against hardened bearing steel in dry conditions (Smith *et al.*, 1992).

**Composites** Flame spraying of *self-fluxing* alloy matrixes and particulate reinforcement of carbides or oxides, followed by fusion after spraying, is the simplest and cheapest way of adhesive wear-resistant coatings' manufacturing. An example of such a matrix is an alloy having the composition (in wt%) of Ni + 15Cr + 4B + 4Si + 4Fe + 0.5C and examples of reinforcements are Cr<sub>2</sub>O<sub>3</sub>, Al<sub>2</sub>O<sub>3</sub> or TiC (Sandt and Krey, 1984, 1985). Another way of manufacturing particulate composites of such composition can be the simultaneous use of a plasma torch to spray the refractory reinforcement and a flame torch to spray the self-fluxing matrix (Lugscheider, 1987). This approach renders an easier optimization of the spray parameters. A particulate composite of aluminium bronze as the matrix and Al<sub>2</sub>O<sub>3</sub> as the reinforcement, manufactured by plasma spraying, was successfully tested in contact with SAE 4640 steel by Tucker (1982). The volume content of the alumina resulting in the smallest wear losses was found to be about 10 %. An interesting composite of molybdenum with molybdenum carbide was proposed by Sampath and Wayne (1994). Molybdenum was thought to provide a low friction coefficient and its carbide to enhance the wear resistance, and the composite was manufactured by powder agglomeration. The kinetic friction coefficient of the sprayed coatings varied from  $\mu = 0.2$  to 0.4 as a function of the carbide content (15–55 vol%). The mechanism of wear of metal matrix–ceramic composites is fracture and removal of reinforcement particles, followed by plastic deformation of the denuded matrix (Lira Olivares and Grigorescu, 1987).

## Two-Body-Abrasive Wear

**Ceramic Coatings** The following oxides were sprayed by plasmas in air and under vacuum and tested against two-body-abrasion:

- $\text{Al}_2\text{O}_3$  and its alloys with  $\text{ZrO}_2$  and/or  $\text{TiO}_2$ ;
- $\text{Cr}_2\text{O}_3$  and its alloy with  $\text{TiO}_2$ ;
- $\text{TiO}_2$ .

The study of Barbezat *et al.* (1993) enabled us to find out that a better two-body-abrasion resistance against SiC paper for an oxide coating sprayed under vacuum was achieved when compared to that sprayed in air. The most abrasion-resistant coating, among the tested  $\text{Al}_2\text{O}_3$ ,  $\text{Al}_2\text{O}_3 + 40$  wt%  $\text{TiO}_2$ ,  $\text{TiO}_2$  and  $\text{Cr}_2\text{O}_3$ , was  $\text{Cr}_2\text{O}_3$  among those sprayed under vacuum and  $\text{Al}_2\text{O}_3$  among those sprayed in air. Lugscheider *et al.* (1995) agglomerated fine  $\text{Al}_2\text{O}_3$ ,  $\text{ZrO}_2 + 7$  wt%  $\text{Y}_2\text{O}_3$  and monoclinic  $\text{ZrO}_2$  using the spray-drying method to obtain powders used for atmospheric plasma-spraying of coatings. Two-body-wear losses against SiC paper depended on the  $\text{ZrO}_2$  fraction in the agglomerated powder (Figure 8.17).

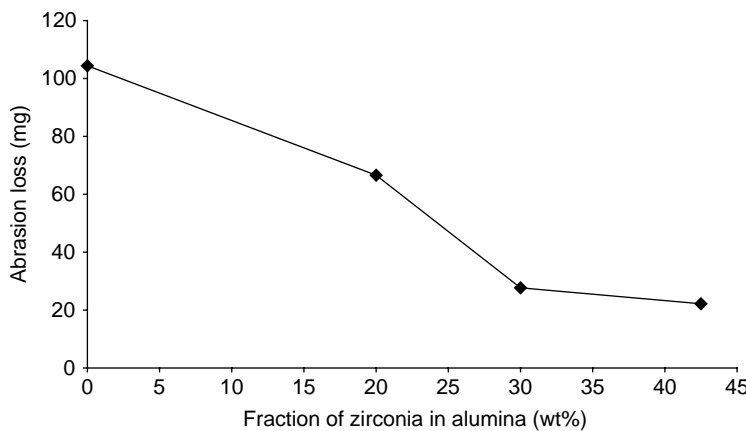


**Figure 8.17** Two-body-abrasion wear losses measured using ‘pin-on-disc’ equipment against 400 grit SiC paper under a load of 5 N and using water as the lubricant for atmospheric plasma-sprayed coatings using agglomerated powders having different contents of  $\text{ZrO}_2 + 7$  wt%  $\text{Y}_2\text{O}_3$  in  $\text{Al}_2\text{O}_3$  (after Lugscheider *et al.*, 1995). Reproduced by permission of the High Temperature Society of Japan from Lugscheider *et al.*, 1995, ‘Influence of various oxide additions on the wear resistance of plasma sprayed alumina coatings’, in *Thermal Spraying: Current Status and Future Trends*, A. Ohmori (Ed.), High Temperature Society of Japan, Osaka, Japan, pp. 833–838

The highest abrasion-wear resistance was obtained for a coating with a composition which correspond and to the eutectic one in the alumina-zirconia system.

**Metals and Alloys** Mo coatings sprayed by a plasma in air were tested for protection against two-body abrasion by Cheney *et al.* (1978). These authors analysed the influence of the molybdenum powder characteristics on the two-body-abrasion plasma-sprayed coatings. The powder was prepared initially by agglomeration of 4- $\mu\text{m}$  precursors and was subjected to high-temperature oven densification. Abrasion testing showed that the finest powder densified after agglomeration and having the greatest apparent density of  $5860 \text{ kg/m}^3$ , resulted in coatings with the best abrasion resistance.

**Composites**<sup>7</sup> Particulate composites with an alloy matrix reinforced with carbides and oxides have been most often tested against two-body-abrasive wear. The microscopic effects of the particulate-reinforced composites' parameters, i.e. volume of reinforcement and its size on the abrasive grain behaviour, are shown in Figure 8.18.

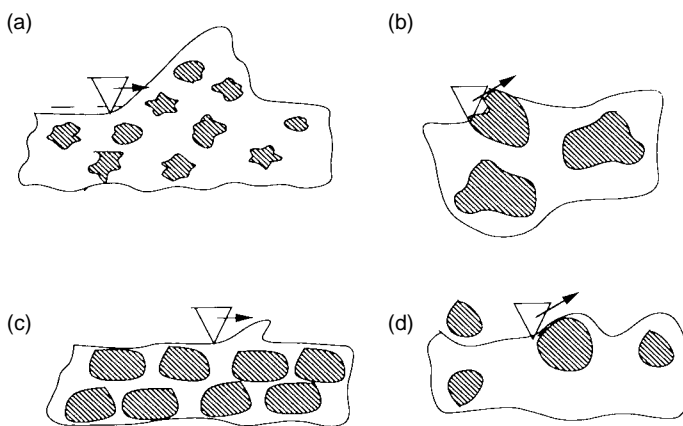


Figure 8.18 Microscopic effects upon two-body-abrasion of particulate composites of: (a) small reinforcement volume and small size; (b) large reinforcement volume and large size; (c) large reinforcement volume and 'intermediate' size; (d) small reinforcement volume and large size (after Barbezat *et al.*, 1991)

Theoretically, a coating with the best two-body-abrasion resistance should have a particulate reinforcement of a size comparable to that of the abrasive grain (Figure 8.18(c)). Composite coatings with a low

<sup>7</sup>In this section, the carbides–metal/alloy composites are discussed together with other composites.

reinforcement density would lead to the matrix becoming easily worn. Experimental information for this model was brought by Usmani *et al.* (1997). These authors studied coatings, HVOF-sprayed using spray-dried powders of WC + 17 wt% Co with the following sizes of carbide reinforcement:

- fine, of a mean size of about 1.2  $\mu\text{m}$ ;
- medium, of a mean size of about 3.8  $\mu\text{m}$ ;
- ‘coarse 1’, of a mean size of about 7.9  $\mu\text{m}$ ;
- ‘coarse 2’, of a mean size between 5 and 7  $\mu\text{m}$ .

The abrasion rate of sprayed coatings was correlated with the content of decomposition product (W<sub>2</sub>C and W) and the sizes of the carbide particles and their densities in the coatings (found on ‘metallographic’ sections), as shown in Figure 8.19.

The experimental data indicate that the best two-body-abrasion resistance is shown by coatings with the greatest reinforcement size and lowest density (Figure 8.18(b)). This result is probably related to the fact that smaller carbide particles decompose more easily during processing (Figure 8.19(b)). Usmani *et al.* (1997) suggested a correlation of abrasion resistance with coating toughness. In contrast, Ishikawa *et al.* (2005) suggested a correlation of the abrasion resistance of WC + 20 wt% Cr<sub>3</sub>C<sub>2</sub> + 7 wt% Ni powder deposited using the ‘shrouded’ HVOF technique with the coating’s microhardness. A similar carbide, Cr<sub>3</sub>C<sub>2</sub> + 25 wt% NiCr, obtained by detonation spraying, was successfully tested against abrasion and against hot-gas corrosion by Wang *et al.* (2002). The particulate composite, having a matrix of  $\tau$ -borides of composition (in wt%) of Ni + 10Cr + 5Ti + 3.5B, was prepared by the agglomeration route with a reinforcement of TiC and sprayed by the SPS technique (Lugscheider *et al.*, 1992). The two-body-abrasion test revealed that the coatings are of similar resistance to the WC-Co deposits prepared by the HVOF technique. A similar route of powder preparation was used to prepare a composite of Mo + (2–12) wt% Mo<sub>2</sub>C, which was used in plasma spraying of coatings and tested against a resin-bonded diamond surface (Sampath and Wayne, 1994). The greatest abrasion resistance was shown by the composite obtained with 12 wt% of Mo<sub>2</sub>C.

Finally, a number of blends of self-fluxing alloys of composition (in wt%) of Ni + 15Cr + 4B + 4Si + 4Fe + 0.5C, with reinforcements of up to 50 vol% of ceramics such as Cr<sub>3</sub>C<sub>2</sub>, TiC, W<sub>2</sub>C, Al<sub>2</sub>O<sub>3</sub> and Cr<sub>2</sub>O<sub>3</sub>, were applied by flame spraying and fused after processing by Sandt and

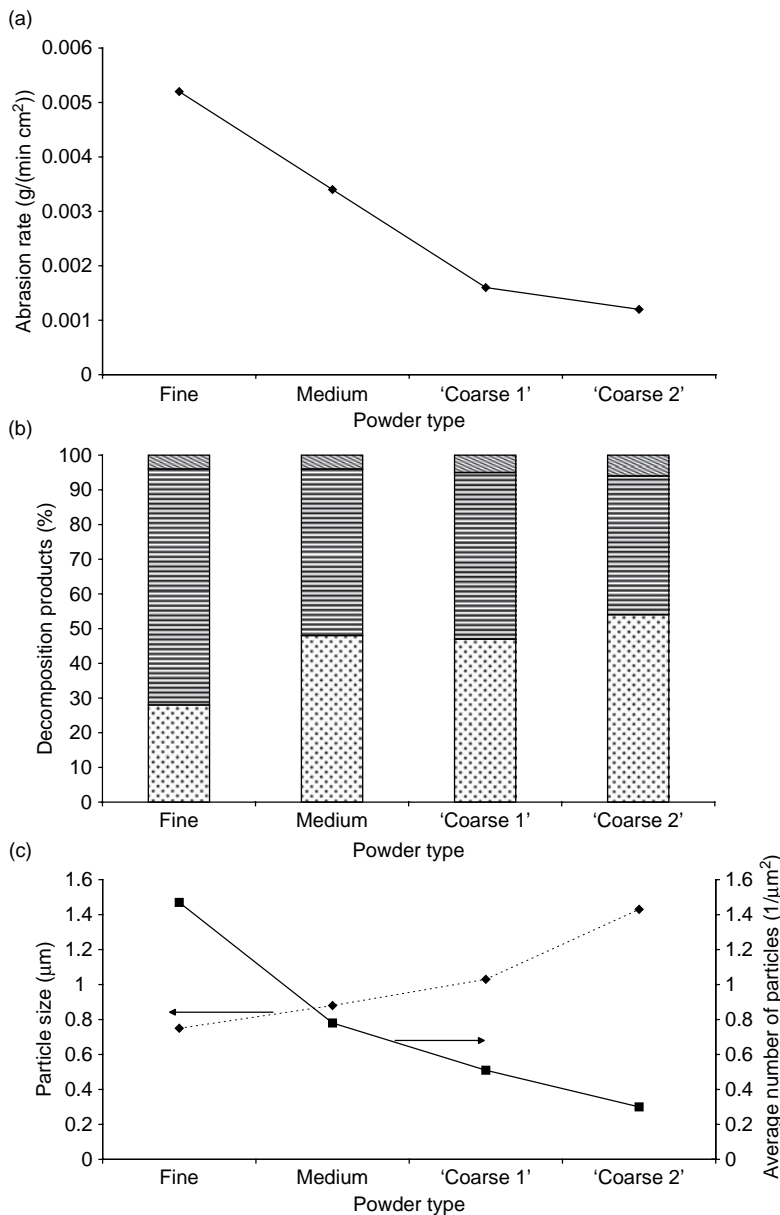


**Figure 8.19** (a) Two-body-abrasion rates, for various SiC 120 grits, of HVOF sprayed coatings from different WC + 17 wt% Co powders, (b) content of crystal phases in carbide reinforcements ([■], WC; [■], W<sub>2</sub>C; [■], W) and (c) mean carbide reinforcement size (◆) and average number of particles ('density') (■) found 'metallographically' in the deposits (after Usmani *et al.*, 1997). Reproduced by permission of the Society of Tribologists and Lubrication Engineers from S. Usmani *et al.*, 1997, 'Effect of carbide grain size on sliding and abrasive wear behavior of thermally sprayed WC-Co coatings', *Tribology Trans.*, 40, 470–478

Krey (1985). The greatest resistance against an SiC abrasive paper of grade 220 was shown by the composite containing 25 vol% W<sub>2</sub>C.

### Three-Body-Abrasive Wear

**Ceramic and Composite Coatings** Tungsten, chromium and titanium carbide-reinforced composite coatings have been most frequently used against three-body abrasion. Some studies have been made for coatings of chromia and its alloys with titania and silica, and alumina and its alloys with zirconia and titania. Abrasion-resistant coatings were sprayed by the use of 'major' spray techniques and tested mainly with the standardized ASTM G 65 procedure.

The mechanism of abrasion of metal-ceramic composite coatings was found, by Khan and Clyne (1996), to be via 'excavating' of the ceramic particles by a 'ploughing' action without any fracturing of the latter, as shown in Figure 8.18(d). Consequently, the content of metal/alloy should be rather small in order to enhance the abrasion resistance. For example, the composition of WC + 9 wt% Co was proved by the authors to be more resistant than that of WC + 17 wt% Co. Vacuum-plasma spraying was found by these authors to be better adapted for spraying tungsten carbide composites than atmospheric-plasma spraying. The reason is most probably oxidation of the carbides during processing. Barbezat *et al.* (1993) found that the wear losses were clearly smaller for tungsten carbide composites deposited by high-velocity combustion spraying and the detonation-gun technique rather than with plasma spraying.

Cr<sub>3</sub>C<sub>2</sub> + 20 and 50 wt% NiCr were tested against abrasion by Eronen *et al.* (2005) and Reardon *et al.* (1981), respectively. Gärtner *et al.* (1999) tested composite powders having reinforcements based on TiC, Ti(C,N) and (Ti, Mo) (C,N) and metal matrices of Ni and its alloys with Mo, Co, or Mn, prepared by spray-drying and sintering. Ti (C,N) was chosen as the phase which 'grows less' than TiC during sintering. The greatest three-body-abrasion resistance was found for coatings plasma-sprayed under vacuum with a composition of (Ti,Mo) (C, N) + 35 wt% NiCo. Processing under vacuum was proved to produce more abrasion-resistant coatings than high-velocity combustion spraying because of the atmosphere which protected the titanium compounds against oxidation. The bimodal distributions of reinforcement sizes, with maximums at about 2 and 0.1 µm were optimal to guarantee high abrasion resistance.

$\text{Al}_2\text{O}_3$ , plasma-sprayed in air using axial injection (Axial III<sup>TM</sup> torch) was tested against abrasion by Hawthorne *et al.* (1997). An  $\text{Al}_2\text{O}_3 + 3$  wt%  $\text{TiO}_2$  powder was sprayed by a plasma in air and by the detonation-gun technique (Niemi *et al.*, 1993). The abrasion resistance of a coating having this composition was superior to that of a composition with 40 wt%  $\text{TiO}_2$  and even to that of sintered alumina. Finally, an  $\text{Al}_2\text{O}_3 + 40$  wt%  $\text{ZrO}_2$  coating obtained by high-velocity combustion spraying was tested to have a superior three-body-abrasion resistance against quartz sand than a coating of  $\text{TiO}_2$  (by HVOF) and than that of plasma-sprayed  $\text{Cr}_2\text{O}_3$  coatings alloyed with  $\text{SiO}_2$  and/or  $\text{TiO}_2$  (Niemi *et al.*, 2003). ‘Nano-structured’  $\text{TiO}_2$  coatings, processed using vacuum-plasma spraying and high-velocity combustion spraying, had the best three-body-abrasion resistance of all 14 types of powders and 4 types of spraying. The resistance values obtained correlated strongly with the crack-propagation resistance values of the coatings, rather than with their microhardness values (Lima *et al.*, 2004b).

**Alloy Coatings** Chrome- and iron-based alloy coatings were tested against three-body abrasion resistance. An alloy of composition (in wt%) of  $\text{Cr} + 16\text{Mn} + 3\text{Si} + 1\text{V}$  was recommended by Kretschmar (1986) for the flame spraying of ‘cheap coatings’. A ‘high-chromium’ alloy was sprayed simultaneously with stainless steel by an arc and favourably tested by the ASTM-65 test (Lima *et al.*, 2005). Finally, the alloy, Fe17Cr10Mn6VMo, was plasma-sprayed under vacuum using nitrogen as the secondary working gas and tested against ‘slurry-abrasion’ following the ASTM-75 procedure. Reactive spraying allowed dissolution of nitrogen in the coatings and the formation of fine-structured vanadium nitrides which resulted in the production of abrasion-resistant metal matrix composites (Siegmann *et al.*, 2004).

## Erosive Wear

The choice of a coating which is resistant against erosion should take into account the following factors:

- nature of the erodent, i.e. mainly hardness, size and morphology;
- velocity of the erodent upon impact and the angle of impact;
- medium in which the erodent is suspended – a special case of erosion in water is called *hydroerosion*;
- temperature of the coating upon erosion.

A simplified guide for the selection of a coating material, depending on erodent speed and impact angle, is presented in Figure 8.20.

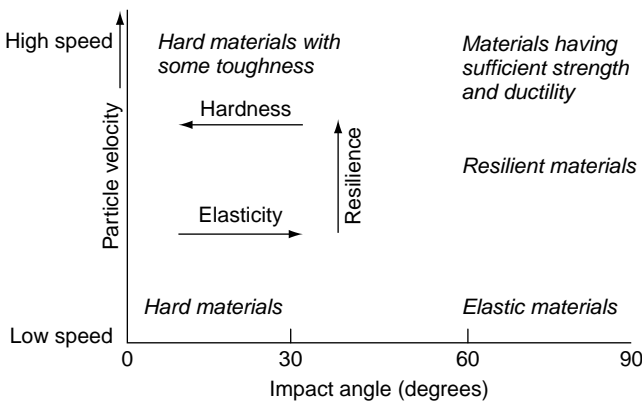


**Figure 8.20** Simplified guide for selecting materials which resist erosion by particles having different speeds and impact angles (after Lansdown and Price, 1986 – see also Dallaire and Levert, 1997). Reproduced by permission of Pergamon Press/Elsevier from A.R. Lansdown and A.L. Price, 1986, *Materials to Resist Wear – A Guide to their Selection and Use*, Pergamon Press, Oxford, UK

Materials subjected to erosion have different mechanisms of wear, depending on the impact angle (Figure 8.21).

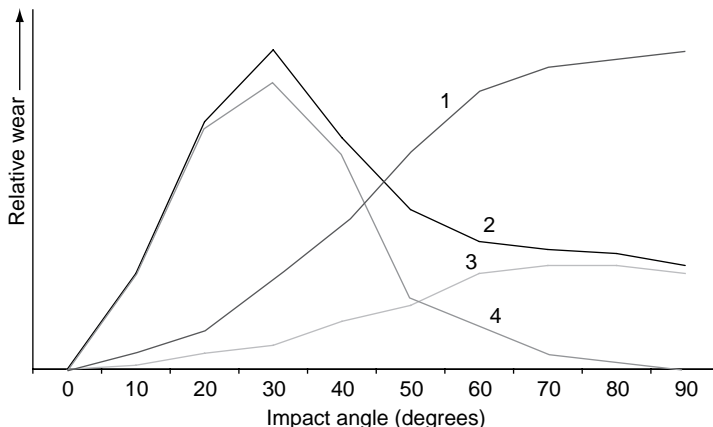


**Figure 8.21** Mechanisms of erosion for different coating materials as a function of impact angle: 1, brittle, hard; 2, ductile; 3, fatigue; 4, cutting (after Verpoort and Baumann, 1992). Reproduced by permission of Dr. Clemens M. Verpoort from C. Verpoort and R. Baumann, 1992, 'Verschleissmechanismen untersuchen, verstehen und einschränken', *Zeit. Metall. Oberfläche*, 46(9)

Hard and brittle materials as ceramics become worn more intensively at high angles of impact and better resist erosion at low angles. Ductile materials, such as metals and alloys, are subjected to the most intensive abrasion at impact angles ranging from 20 to 40°, with the mechanism of wear due to ‘cutting’ of pieces of the material at its surface. At higher angles, abrasion of the surface drops and the main mechanism of wear becomes *fatigue*. As thermally sprayed coatings have many ‘particularities’, such as porosity and lamellar structure, and, on the other hand, ‘hard-ductile’ composites are frequently sprayed, the materials’ selection rules must be more specific. A tentative presentation of such rules was made by Kulu and Pihl (2002). These authors recommended the following as being suitable for coatings to be resistant against erosion:

- **Minimum porosity** – high-velocity spray processes should be used and the porosity should be kept lower than 3 %.
- **Optimal hardness of coatings** – the hardness depends on the erosion conditions. At small impact angles, the hardness must be high and indeed higher than that of the erodent. At higher angles, the hardness should be optimized.
- **Optimal microstructure** – at ‘oblique impact’, the cermet structure seems to be optimal. At ‘normal impact’, dispersion strengthened the metal or composite with such a matrix.
- **Hardness of abradant** – the erosion resistance is guaranteed if the hardness of the erodent is lower than the hardness of the coating.

**Ceramic and Composite Coatings** Composite coatings of tungsten and chromium carbide with a metal and/or alloy matrix and ceramic coatings of Cr<sub>2</sub>O<sub>3</sub> and Al<sub>2</sub>O<sub>3</sub> were tested for protection against erosive wear. A selection of the coatings tested against erosion wear is shown in Table 8.18. The results of the tests are expressed as mass or volume of the coating with regard to mass of the erodent.

Tungsten carbide is a reinforcement for metal–matrix composites useful against abrasion at room temperature (entries 1, 3 and 5 in Table 8.18). The choice of matrix depends on the erosion conditions. Upon erosion by a slurry (*hydroerosion*), the matrix should resist well against wet corrosion. For example, a CoCr alloy has a more positive corrosion potential than Co and was proved to resist better against *hydroerosion* (Arsenault *et al.*, 1998). For erosion at high temperatures, the composite coatings with chromium carbide reinforcement are more practical (entry 4 in Table 8.18). The mechanism of erosion of composite coatings is rather brittle than ductile and wear is greater at 90° than

Table 8.18 Erosion wear of some ceramics and composites thermally sprayed using different methods

Number	Reference	Coating		Erosion	Remarks			
		Chemical composition (wt%)	Post-spray treatment					
<i>High-velocity oxy-fuel spraying</i>								
1	Karimi <i>et al.</i> , 1995	WC+14CoCr	No	1269	Sand in water	90	RT/small test	1.4 mm <sup>3</sup> after 55 min
2	Yoshida <i>et al.</i> , 2002	Cr <sub>3</sub> C <sub>2</sub> +20NiCr	No	808	Alumina angular; silica	42	RT/15	89 mg
3	Arsenault <i>et al.</i> , 1998	WC+36Ni +8Cr+6Co+2Fe	No	about 1000	angular Alumina in air	84	RT/20; 90	18 mm <sup>3</sup> /kg; 20 mm <sup>3</sup> /kg
<i>Detonation-gun spraying</i>								
4	Tucker and Ashari, 1998	Cr <sub>3</sub> C <sub>2</sub> +NiCoCrAlY	Annealed at 823 for 72 h	—	Chromite in air	70	305	823/90; 30 0.6; 0.3
<i>Atmospheric plasma-spraying</i>								
5	Guo <i>et al.</i> , 1995	WC+17Co	Laser re-melting	—	Angular quartz in air	+150 less than 80 mesh	RT/30	0.9 × 10 <sup>-4</sup> g/g
6	Li <i>et al.</i> , 2006	Al <sub>2</sub> O <sub>3</sub>	No	—	Angular alumina	330	RT/90	0.25 mm <sup>3</sup> /g
								Using P = 31.5 kW of electric power

at lower angles (entries 3 and 4 in Table 8.18). Post-spray processing as annealing (entry 4 in Table 8.18) or laser treatment (entry 5 in Table 8.18 and Bardal *et al.*, 1995) seal the coatings and improve their erosion wear resistance with regard to their as-spray characteristics.

Ceramic coatings of alumina and chromia obtained by plasma spraying were successfully tested against erosion wear (entry 6 in Table 8.18 and Karimi *et al.*, 1995), respectively. Erosion of sprayed alumina occurred through 'spalling' of the lamellae at the exposed surface and results from interlamellar cracking.

An  $\text{Al}_2\text{O}_3$  reinforcement was blended with CoNi-based of alloy composition (in wt%) of  $\text{Co} + 34\text{Ni} + 22\text{Cr} + 7.7\text{Al} + 0.7\text{Y}$  in different proportions by Gudmundsson *et al.* (1988). The powders were plasma-sprayed in vacuum and tested against erosion at 970 K by 'flying-ash'. The optimal composition of the particulate composite contained 40–60 vol% of reinforcement. The results of the study made by Wang *et al.* (1992) stressed the importance of matching the elastic moduli of the reinforcement and matrix. In fact, the relatively 'less-hard' niobium carbide with an *E*-modulus similar to that of a CoCr alloy made it possible to obtain particulate composite coatings with an outstanding hot-erosion resistance.<sup>8</sup>

***Coatings of Metals and Alloys*** Alloys based on nickel, cobalt and iron, sprayed by an arc, are most frequently used against erosion wear. These alloys have a lower abrasion wear resistance than ceramics or composites, especially at low-angle abrasion. Examples of such alloys with compositions expressed in wt% include the following arc-sprayed coatings:

- $\text{Ni} + 17\text{W} + 15\text{Cr} + 4\text{Si} + 3.5\text{Fe} + 3\text{B} + 0.8\text{C}$  and  $\text{Co} + 24\text{Cr} + 8.8\text{Ni} + 4.8\text{Mo} + 2.9\text{Fe} + 2\text{W} + 0.06\text{C}$ , tested against slurry *hydroerosion* using alumina by Arsenault *et al.* (1997).
- $\text{Fe} + 28\text{Cr} + 5\text{Ni} + 3.5\text{B} + 2.5\text{Mn}$ , tested against low-angle and high-temperature (773 and 973 K) erosion using angular alumina by Yoshida *et al.* (2002).
- $\text{Fe} + 25\text{Cr} + 3\text{B} + 2\text{Si}$ , tested for elevated-temperature (573 and 723 K) erosion using 'bed-and-fly' ashes by Wang (1997).

<sup>8</sup> Abrasion tests were made at temperatures of 573 and 723 K using an  $\text{SiO}_2$  erodent under angles of 30 and 90°.

### Other Kinds of Wear

**Fretting Wear** Cobalt alloys, particulate composites with oxides, carbides and nitrides reinforcements have been applied against fretting wear. *Abradable coatings*, i.e. deposits that become worn until the desired state is achieved and should keep in intimate contact with a ‘counter-body’ based on nickel and cobalt alloys, were also tested.

Co-based alloys and oxides ( $\text{Al}_2\text{O}_3$  and  $\text{Cr}_2\text{O}_3$ )-reinforced composites sprayed by the detonation-gun technique were tested against high-temperature (between 600 and 1366 K) fretting (25 cycles of 8 mm amplitude, under a load of 7 MPa) by Wolfla and Tucker (1978). The overall best behaviour (results from hot-corrosion and fretting-wear tests) revealed the composite with a cobalt-based alloy matrix of a composition (in wt%) of Co + 30Cr + 10Ta + 1Y and 10 vol%  $\text{Al}_2\text{O}_3$  reinforcement. Beczkowiak (1991) recommended a particulate mixture of a self-fluxing NiCrSiB matrix with a Mo additive by flame spraying followed by fusion to be useful against fretting wear.

Composites realized by the help of powder agglomeration enabled De Bonte *et al.* (1993) to find two compositions (in wt%) as follows:

- $\text{ZrN} + 50(\text{Cr}_2\text{O}_3 + 3\text{TiO}_2 + \text{SiO}_2)$ ;
- $\text{B}_4\text{C} + 70(\text{Cr}_2\text{O}_3 + 40\text{TiO}_2)$ .

Coatings, plasma-sprayed using powders of these compositions, resisted particularly well against fretting wear.

An Ni alloy having a composition (in wt%) of Co + (31–33)Ni + (20–22)Cr + (7–9)Al was plasma-sprayed under argon by Li *et al.* (1998a). The coatings were tested under fretting conditions (displacement amplitude of 20–100  $\mu\text{m}$  at a frequency of 5 Hz under a normal load of  $F = 10\text{--}70\text{ daN}$ ). Fretting induced recrystallization of the surfaces of the coatings which became harder than the initial ones. This transformation occurred at low temperatures.

**Cavitation Wear** Cavitation describes the process of formation and rapid collapse of bubbles caused by fluctuations in the local pressure. Bubbles are formed when the static pressure of the liquid is lower than the vapour pressure of the fluid or below the partial pressure of the gas dissolved in the fluid. The bubbles ‘implode’ when the pressure increases again below the pressure values and their collapse can produce a maximum pressure of about 100 MPa (Schwetze and Kreye, 1996).

The cavitation process of a coating can be represented by the following stages (Figure 8.22):

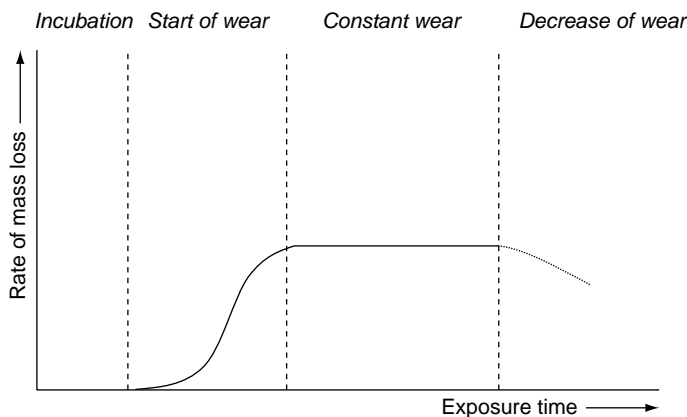


**Figure 8.22** Cavitation wear versus exposure time (Schwetzke and Kreye, 1996). Reproduced by permission of ASM International from R. Schwetzke and H. Kreye, 1996, 'Cavitation erosion of HVOF coatings', in *Thermal Spray: Practical Solutions for Engineering Problems*, C.C. Berndt (Ed.), ASM International, Materials Park, OH, USA, pp. 153–158

- an incubation period associated with hardening of the material and formation of micro-cracks;
- propagation of cracks and the start of material removal;
- steady rate of wear;
- decrease of wear resulting from modification of the local flow conditions.

Some coatings tested against cavitation wear are collected in Table 8.19. A cobalt-based alloy, 'Stellite', is frequently used as a coating deposited by high-velocity combustion (entry 1 in Table 8.19) or vacuum plasma-spraying (entries 5 and 6 in Table 8.19). The 'Stellite' coating is most probably 'work-hardened' during the cavitation test and its hardness is greater than before it. Other high-velocity combustion-sprayed materials recommended by Kreye *et al.* (1998) for better resistance against cavitation wear than a bulk sample of 316 L stainless-steel include among others:

- an NiCrSiB alloy (see also entry 4 in Table 8.19);
- WC + 17 wt% Co;
- Cr<sub>3</sub>C<sub>2</sub> + 25 wt% NiCr (see also entry 3 in Table 8.19).

Table 8.19 Cavitation wear of some coatings sprayed using different methods

Number	Reference	Coating		Cavitation wear		Remarks
		Chemical composition (wt%)	Post-spray treatment	Microhardness	Wear rate (mg/h)	
<i>High-velocity oxy-fuel spraying</i>						
1	Kumar <i>et al.</i> , 1997	Stellite 6 <sup>TM</sup> , Co + 29Cr + 4.4W + 1.5Si + 1.15C	Enamel sealing	—	11.7	Submerged cavitating jet under a pressure of 27.6 MPa 3.6 times smaller wear rate
<i>Vibratory cavitation test (ASTM G 32)</i>						
2	Schwertke and Kregel, 1996	Cr <sub>2</sub> O <sub>3</sub>	—	1210	2.9	—
3		Cr <sub>3</sub> C <sub>2</sub> + 25 NiCr	—	1220	3.8	
4		NiCrFeSiB, type 60	—	674	4.4	
<i>Vacuum plasma-spraying</i>						
5	Adachi <i>et al.</i> , 2001	Stellite 6 <sup>TM</sup> , Co + 29Cr + 4.4W + 1.5Si + 1.15C	—	586	4.2	Microhardness after test, $HV = 714$
6		Heat-treated	—	610	4.9	Microhardness after test, $HV = 773$

Atmospheric plasma-spraying produces coatings having a cavitation-wear resistance considerably worse than that of more energetic, high-velocity combustion or vacuum plasma-spraying. Moreover, post-spray treatment improves the resistance (entries 1 and 6 in Table 8.19).

**Impact Wear** Coatings resistant against impact wear must be, to a degree, ductile. The self-fluxing NiCrSiB alloy, sprayed by flame and subsequently melted, was tested for impact wear<sup>9</sup> by Föhl *et al.* (1988). The wear resistance was about four orders of magnitude smaller than that of the bulk hard-bearing steel 100 Cr 6 H. The porosities of the coatings act favourably upon the impact-wear resistance. Consequently, more porous oxide coatings plasma-sprayed in air were tested to have a greater resistance against impact than the dense, vacuum plasma-sprayed ones (Takeuchi *et. al.*, 1991). These authors found that the modified alumina  $\text{Al}_2\text{O}_3 + 40 \text{ wt\% TiO}_2$  has the best impact-wear resistance.<sup>10</sup> A blend of a conventional agglomerated and sintered powder having a composition of WC+20 wt%  $\text{Cr}_2\text{C}_3 + (7-10) \text{ wt\% Ni}$  with an atomized powder of Ni or Ni + 20 wt% Cr was sprayed by the high-velocity combustion technique. The obtained coatings were tested with an impact tester using steel balls (diameter of 9.5 mm and mass of 3.3 g) falling from a height of 1 m on to the coating. The coatings sprayed using blended powders withstood more than 60 impacts before failure, while the number was only 20 impacts for a conventional WC + 12 wt% Co coating. An increase in the impact resistance was attributed to the ductility of the metal component of the cermet.

### 8.3 THERMOPHYSICAL PROPERTIES

The thermophysical properties, discussed in this section, are as follows:

- thermal conductivity and, closely related to it, thermal diffusivity;
- specific heat;
- thermal expansion;

<sup>9</sup> One cycle of the test consisted of the impacting of a 3 kg metal load onto the coatings with a kinetic energy of 1.5 J.

<sup>10</sup> One cycle of the test consisted of dropping a steel ball (of diameter 40 mm) onto the coating surface.

- emissivity;
- thermal shock resistance, i.e. the resistance of a brittle material against rapid temperature variations.

Thermal conductivity and diffusivity have been measured mainly for thermal-isolating oxide ceramics in view of applications such as thermal-barriers coatings. Similarly, measurements of the conductivity and diffusivity of bond coatings, as well as the determination of thermal contact resistance between the coatings, are related to this important application. Thermal conductivity describes the capacity of a material to transport energy and is a more fundamental material property than thermal diffusivity. This is why the latter will be shown only if no conductivity data are available.

Specific-heat measurements enable the determination of thermal conductivity from diffusivity and density data, as shown in Chapter 7, Equation (7.18). On the other hand, measurements of  $c_p$  might be used, thanks to the *Kopp–Neumann* law,<sup>11</sup> for the detection of oxidation in sprayed metals or alloys. This is particularly valid for small quantities of oxides which are below the detection threshold of X-ray diffraction.

Thermal expansion data are used in the calculation of thermal conductivity. On the other hand, thermal expansion coefficients and elastic moduli are the material properties which determine the cooling and quenching stresses generated during the coating process (see Chapter 6, Equation (6.18)). The coefficient should be intermediate between those of the substrate and top coating for the application of coatings at high temperatures in order to keep the thermal stresses low.<sup>12</sup> This can be achieved by spraying of particulate composites containing materials of the substrate (or bond coating) and the top coating. It must be stressed that the thermal expansion coefficient is *anisotropic* because of the lamellar microstructure of the coatings.

Emissivity data of coatings are useful in pyrometric measurements of temperature. Additionally, emissivity plays a role when the radiative heat transfer between the coatings and surroundings is of importance, i.e. at high temperatures.

The thermal shock resistance determines the behaviour of the coatings subjected to cyclic and/or sudden temperature variations.

---

<sup>11</sup> The Kopp–Neumann law states that the specific heat of an alloy is equal to the sum of the specific heats of its components, multiplied by their atomic fractions.

<sup>12</sup> A precise discussion, made, e.g. by Kokini and Takeuchi (1994), should include the status of stresses in as-sprayed coatings.

### 8.3.1 THERMAL CONDUCTIVITY AND DIFFUSIVITY

#### Oxides

Among the thermally sprayed oxides, the thermophysical properties of zirconia have been tested most frequently. The motivation of this research was its application as the top layer of thermal barrier coatings used at high temperatures. Zirconia transforms with temperature (see Chapter 6, Figure 6.22) and has to be stabilized with yttria or other oxides.

**ZrO<sub>2</sub> Stabilized with Y<sub>2</sub>O<sub>3</sub>** This is a very frequently tested oxide and there is a wealth of experimental data available. The thermal conductivity of thermal-sprayed zirconia depends on the microstructure of coatings, which is determined, in this particular case, by:

- porosity, which is reduced by sintering for high-temperature measurements;
- phase composition (monoclinic, ‘tetragonal-transformable’ and ‘non-transformable’, and cubic);
- crystal grain size;
- shape and size of the defects of the microstructure, such as voids and cracks, that depend, in turn, on the processing conditions and, in particular, on the coating thickness.

The sintering effect was observed during measurements of thermal diffusivity up to 1500 K for 2 mm-thick, 8 wt% yttria-stabilized zirconia coatings (Schwingel *et al.*, 1998). The number of defects, such as horizontal and vertical cracks or pores, is particularly important in thick coatings. The diffusivity values measured during heating were smaller than those measured during cooling. The differences in the ‘second runs’ of the measurements were much smaller and the diffusivity becomes close to that for the cooling cycle of the ‘first run’. The models of heat conduction in yttria-stabilized zirconia were developed based mainly on the assumption that the voids or cracks are filled with gas (see Chapter 7, Equation (7.17)). The thermal conductivity of yttria-stabilized zirconia, tested by different authors, is shown in Figure 8.23, while descriptions of the coatings are presented in Table 8.20.

The shape of the thermal conductivity curves indicates a phonon-conduction mechanism up to 1000–1100 K with conductivity being

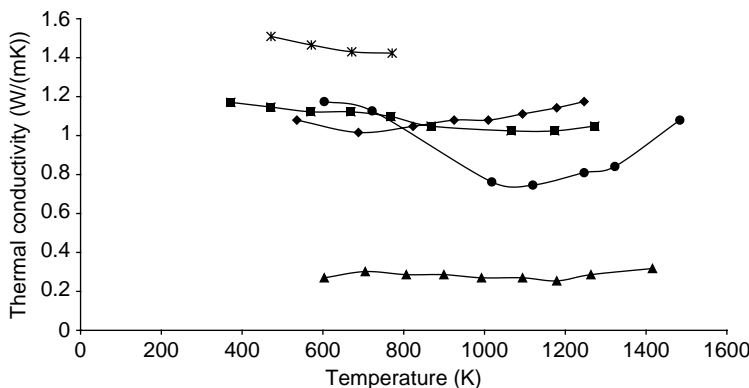


**Figure 8.23** Thermal conductivity versus temperature curves of air-plasma-sprayed zirconia coatings stabilized with 7.25 wt%  $\text{Y}_2\text{O}_3$  ( $\blacklozenge$ ), 8.00 wt%  $\text{Y}_2\text{O}_3$  ( $\bullet$ ) and 20.00 wt%  $\text{Y}_2\text{O}_3$  ( $\blacktriangle$ ) tested under vacuum, a suspension-precursor plasma-sprayed zirconia coating stabilized with 7 wt%  $\text{Y}_2\text{O}_3$  ( $\blacksquare$ ) tested under vacuum and an air-plasma-sprayed zirconia coating stabilized with (7–8) wt%  $\text{Y}_2\text{O}_3$  (\*) tested under a pressure of  $p = 0.1 \text{ MPa}$  of nitrogen (descriptions of the coatings are given in Table 8.20)

inversely proportional to temperature (Pawlowski and Fauchais, 1992). At higher temperatures, the thermal conductivity increases with the temperature which is probably due to the photon conduction mechanism following a relationship in which the conductivity is proportional to  $T^3$  and, on the other hand, to the samples sintering during the measurements. The ‘effect-quantities’ of yttria and, consequently, of the phases in dense sintered zirconia (96–98 % of the theoretical density), at temperatures ranging from 300 to 1400 K on the thermal conductivity is as follows (Raghavan *et al.*, 1998):

- pure zirconia is monoclinic and its conductivity decreases from about 6 to 3.5 W/(mK);
- zirconia stabilized with 5.8 wt% of yttria is tetragonal and its conductivity is nearly constant and equal to 2.7–2.8 W/(mK);
- zirconia stabilized with 8 wt% yttria is tetragonal (77 wt%) and cubic (23 wt%) and its conductivity rises slightly from about 2 to 2.2 W/(mK);
- zirconia stabilized with 15 wt% yttria is cubic and its conductivity is similar to that stabilized with 8 wt% of yttria.

The crystal phases in thermally sprayed coatings are different to those of sintered samples due to the rapid solidification of the particles (see

**Table 8.20** Thermal conductivity of yttria-stabilized zirconia coatings sprayed using different methods and tested under vacuum and in nitrogen (see also Figure 8.23)

Number	Reference	Coating			Remarks	Testing method
		Chemical composition (wt. %)	Porosity (%)	Density (kg/m <sup>3</sup> )		
<i>Air plasma-spraying</i>						
1	Pawlowski <i>et al.</i> , 1985	ZrO <sub>2</sub> + 7.25Y <sub>2</sub> O <sub>3</sub>	—	5550	Tetragonal and tetragonal 'non-transformable'	Laser flash method under vacuum for diffusivity, specific heat, density and thermal expansion
2		ZrO <sub>2</sub> +8Y <sub>2</sub> O <sub>3</sub>	14	5190	Tetragonal and a small fraction of monoclinic Cubic	—
3	Pawlowski, 1985	ZrO <sub>2</sub> +20Y <sub>2</sub> O <sub>3</sub>	20	4700	—	As above but laser flash measurements were made under a pressure of $p = 0.1$ MPa of nitrogen
4	Mogro-Campero <i>et al.</i> , 1997	ZrO <sub>2</sub> + (7-8)Y <sub>2</sub> O <sub>3</sub>	12	5330	—	Vertical and horizontal cracks
<i>Solution plasma-spraying</i>						
5	Jadhav <i>et al.</i> , 2006	ZrO <sub>2</sub> +7Y <sub>2</sub> O <sub>3</sub>	15	5160	—	Spherical and disc-shaped pores engineered with spray parameters

Chapter 6, Section 6.3.1) but the values of the conductivities probably correspond to their contents in a similar way. The conductivities of sprayed yttria-stabilized zirconia samples are considerably smaller than that of the dense material (see Figure 8.23). This difference can be explained by the porosity, which should be divided into the following categories (see Chapter 6, Figure 6.32):

- large horizontal and vertical cracks occurring in air plasma-sprayed deposits (see also Chapter 6, Figure 6.16);
- spherical and disc-shaped pores occurring in solution plasma-sprayed deposits

If the pores contain gas under normal (and higher) pressures, its thermal conductivity contributes to the total value of the conductivity of the coating. The contribution is described in Chapter 7, Equation (7.17), which was successfully verified by Mogro-Campero *et al.* (1997) for the data presented in Figure 8.23. The size of the crystallites does not influence the thermal conductivity of yttria-stabilized zirconia down to 50 nm (Raghavan *et al.*, 1998). The porosity plays an important role. A numerical model developed for the digitized microstructures of coatings by Jadhav *et al.* (2006) takes into account both spherical and disc-shaped pores and enabled them to predict, fairly precisely, the thermal conductivity of the suspension-precursor plasma-sprayed yttria-stabilized zirconia shown in Figure 8.23. Laser treatment, associated with the plasma-spraying process, generates vertical pores and densifies the coatings (see Chapter 4, Figure 4.14). The thermal conductivity of a laser re-melted<sup>13</sup> 7YSZ coating was about 15 % lower than that of the as-sprayed samples (Antou *et al.*, 2006).

**ZrO<sub>2</sub> stabilized with Other Oxides** The thermal conductivities of two calcia-stabilized zirconia are showed in Figure 8.24 and the details of the tested samples are shown in Table 8.21.

The thermal diffusivity values used for the conductivity calculations were greater on cooling than on heating. The effect could have been caused by, as discussed earlier, sintering of the samples during the measurements but also to destabilization of zirconia resulting from the losses of calcia during processing (Pawlowski *et al.*, 1984). Calcia is less refractory than yttria and its selective evaporation in the plasma

<sup>13</sup> The process was *in situ* laser re-melting, i.e. plasma spraying and simultaneous laser treatment.

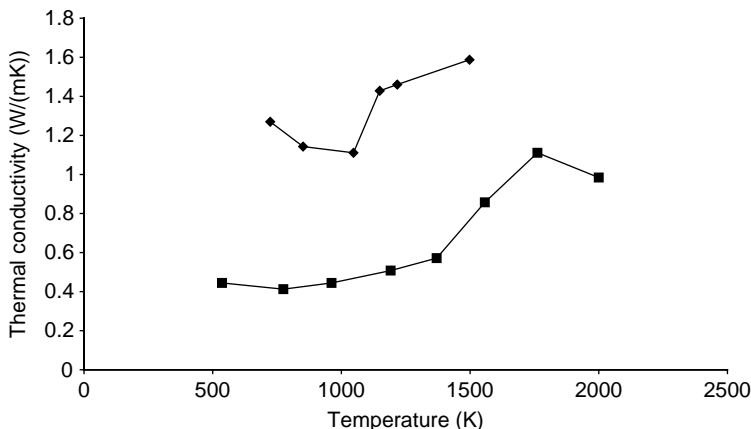


**Figure 8.24** Thermal conductivity versus temperature of coatings of air-plasma-sprayed zirconia stabilized with 4.6 wt% CaO (■) and 7.5 wt% CaO (◆). More information about the samples can be found in Table 8.21

jet could have happened. The shapes of the thermal diffusivity and thermal conductivity curves indicate phonon-conduction mechanisms. The thermal conductivities of zirconia stabilized with magnesia and a compound of zirconia and silica,  $\text{ZrSiO}_4$ , are presented in Figure 8.25.

The very low thermal conductivity of rod-flame-sprayed  $\text{ZrSiO}_4$  (Figure 8.25) is related to the deposition process. The density of the coating was low and the particles of the powder were most probably not fully melted which must have resulted in poor contact between the lamellae. The thermal diffusivity of ceria-stabilized zirconia is shown in Figure 8.26.

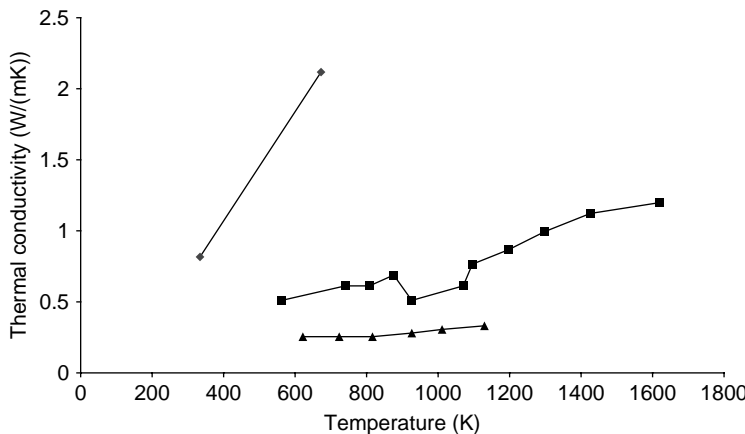
The thermal diffusivities of ceria- and yttria-stabilized zirconia are quite similar (Rudajevova, 1993). The phase content of CeSZ stabilized with more than 20 wt% of  $\text{CeO}_2$  is metastable teragonal, which resembles the  $t'$  phase in YSZ coatings. Rudajevova stressed that CeSZ is more transparent to IR radiation than YSZ.

**Other Oxides** The thermal conductivities of thermally sprayed alumina are showed in Figure 8.27. Detailed data about the tested samples are collected in Table 8.22.

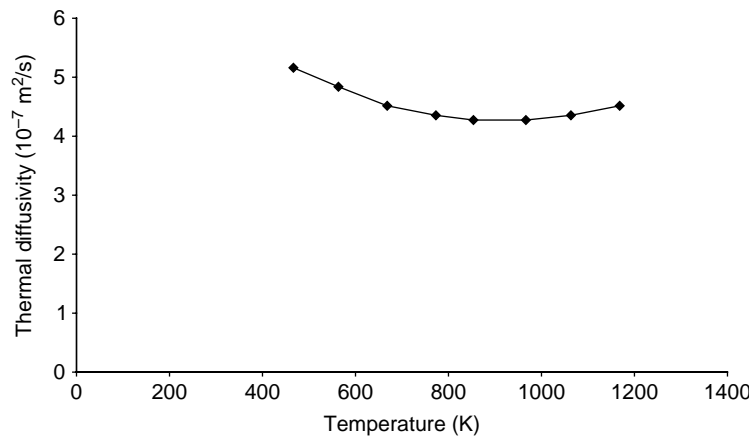
Fiedler (1984) found that the thermal conductivity of  $\alpha\text{-Al}_2\text{O}_3$  is about  $\lambda = 27 \text{ W/(mK)}$  which is ten times more than that of  $\gamma\text{-Al}_2\text{O}_3$ . Correctly optimized processing parameters result in melting of the particles and formation of  $\gamma\text{-Al}_2\text{O}_3$  or other metastable phases ( $\delta$ ,  $\theta$ ). An important quantity of  $\alpha\text{-Al}_2\text{O}_3$  in sprayed coatings can be obtained by:

Table 8.21 Thermal conductivity and diffusivity of coatings of zirconia stabilized with different oxides sprayed by different methods and tested under vacuum and in nitrogen (see also Figures 8.24–8.26)

Number	Reference	Coating			Remarks	Testing method
		Chemical composition (wt%)	Porosity (%)	Density (kg/m <sup>3</sup> )		
<i>Air plasma-spraying</i>						
1	Pawlowski, 1985	ZrO <sub>2</sub> + 7.25CaO	—	5120	Cubic – major; monoclinic – minor	Figure 8.24
2	Wilkes and Lagedrost, 1973	ZrO <sub>2</sub> + 4.8CaO	—	4420	—	—
3	Desplanches, 1988	ZrO <sub>2</sub> + 24MgO	7.6 (open)	5010	Cubic – major; monoclinic – traces, magnesia	Figure 8.25
4	Daniault, 1981	ZrSiO <sub>4</sub>	—	—	—	—
5	Rudajevova, 1993	ZrO <sub>2</sub> + 25CeO <sub>2</sub>	—	—	Tetragonal	Figure 8.26; grinding of sample surfaces influences diffusivity values
<i>Rod flame-spraying</i>						
6	Bogdanov <i>et al.</i> , 1965	ZrSiO <sub>4</sub>	—	3440	—	Figure 8.25
						'Home-made' device



**Figure 8.25** Thermal conductivity versus temperature of coatings of air-plasma sprayed zirconia stabilized with 24 wt% MgO ( $\blacklozenge$ ) and of ZrSiO<sub>4</sub> (■, air-plasma sprayed; ▲, flame-sprayed). More information about the samples can be found in Table 8.21



**Figure 8.26** Thermal diffusivity versus temperature of a coating of air-plasma sprayed zirconia stabilized with 25 wt% CeO<sub>2</sub>. More information about the tested sample can be found in Table 8.21

- heating the substrate upon spraying above the temperature of the  $\gamma$ -to- $\alpha$  transformation;
- post-spray annealing.

The high thermal conductivities of thermally sprayed Al<sub>2</sub>O<sub>3</sub> coatings found by Mackay and Muller (1967) and shown in Figure 8.27 could

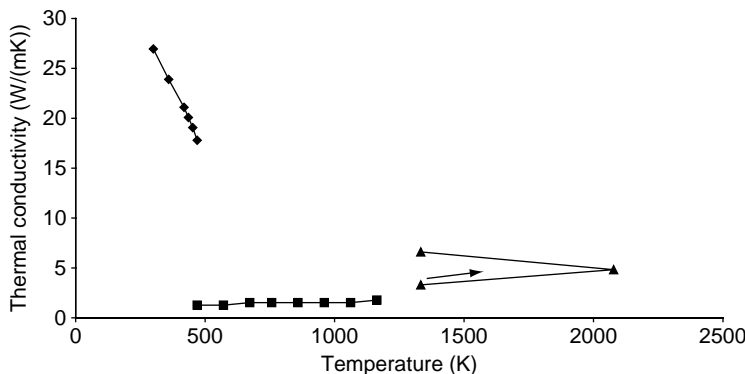


**Figure 8.27** Thermal conductivity versus temperature of coatings of air-plasma and flame-sprayed alumina, as reported by various authors: ♦, Mackay and Muller, 1967; ■, Buzovkina *et al.*, 1972; ▲, Wilkes and Lagedrost, 1973). More information about the tested samples can be found in Table 8.22

therefore be explained by the formation of  $\alpha\text{-Al}_2\text{O}_3$  in their coatings (the authors did not carry out any XRD analysis).

The thermal diffusivities of plasma-sprayed chromia coatings are shown in Figure 8.28 with detailed descriptions of the samples collected in Table 8.22.

The high thermal conductivity of chromia is desirable in many mechanical applications of this oxide. In fact, the energy generated at friction is more easily ‘evacuated’ when the coating is a good heat conductor. On the other hand, wollastonite (see Figure 8.28) is tested for biomedical applications and a knowledge of its thermophysical properties is useful in controlling thermal and residual stresses in the coatings.

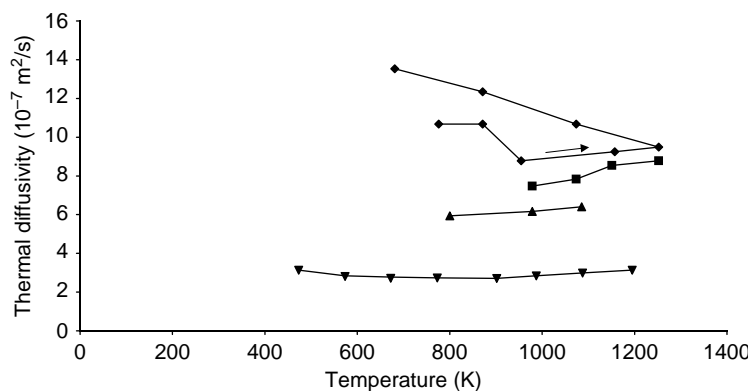
## Metals and Alloys

The thermal conductivities of plasma-sprayed molybdenum coatings are shown in Figure 8.29. Details of the samples’ preparation are collected in Table 8.23.

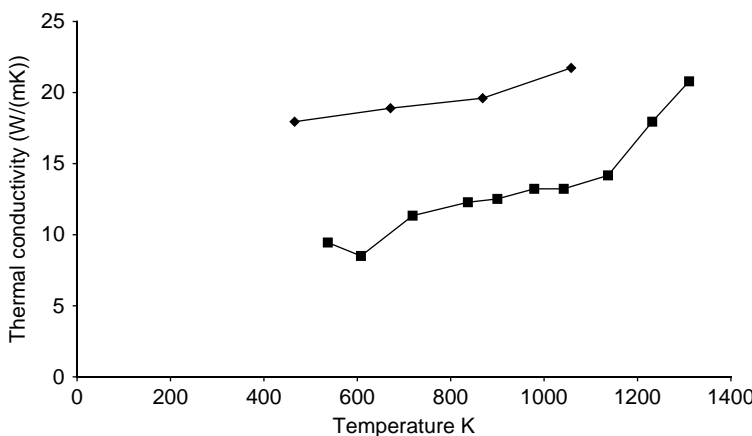
Brandt *et al.* (1979) found the thermal conductivity of molybdenum to be in the range of  $\lambda = 10\text{--}20 \text{ W}/(\text{mK})$ , while Wilkes and Lagedrost (1973) found values of  $18\text{--}22 \text{ W}/(\text{mK})$ . The material of Brandt and his colleagues was densified during thermal-diffusivity testing. The differences in the thermal conductivity of molybdenum could have originated from different levels of oxidation of the used samples. The thermal diffusivity of tungsten was tested at room temperature by Boire-Lavigne

Table 8.22 Thermal conductivity of alumina and thermal diffusivity of chromia and wollastonite coatings sprayed by a plasma in air  
(see also Figures 8.27 and 8.28)

Number	Reference	Coating			Remarks	Testing method
		Chemical composition (wt%)	Porosity (%)	Density (kg/m <sup>3</sup> )		
1	Mackay and Muller, 1967	96 Al <sub>2</sub> O <sub>3</sub>	—	3400	—	Resistivity at 285 K equal to 10 <sup>12</sup> Ω cm
2	Buzovkina <i>et al.</i> , 1972	Al <sub>2</sub> O <sub>3</sub> , ‘very pure’	13.3	—	γ-Al <sub>2</sub> O <sub>3</sub>	—
3	Wilkes and Lagedrost, 1973	99.67 Al <sub>2</sub> O <sub>3</sub>	—	3350	—	Laser-flash method under H <sub>2</sub> ( <i>p</i> = 3.55) for diffusivity, specific heat, density and thermal expansion
4	Tronche, 1986	Cr <sub>2</sub> O <sub>3</sub>	2	—	—	HV <sub>2</sub> = 1400
5	Chuanxian and Bingran, 1988	Cr <sub>2</sub> O <sub>3</sub>	5–8	4400–4700	—	HV <sub>2</sub> = 900–1100
6	Chuanxian <i>et al.</i> , 1984	Cr <sub>2</sub> O <sub>3</sub>	—	—	—	HV <sub>2</sub> = 900–1100
7	Liu and Ding, 2002	Wollastonite, CaSiO <sub>3</sub>	—	—	Wollastonite, calcia (CaO) and tridymite (SiO <sub>2</sub> )	Sprayed onto Ti-6Al-4V for biomedical applications



**Figure 8.28** Thermal diffusivity versus temperature of coatings of air-plasma sprayed chromia and wollastonite, as reported by various authors:  $\diamond$ , chromia (Tronche, 1986);  $\blacksquare$ , chromia (Chuanxian *et al.*, 1984);  $\blacktriangle$ , chromia (Chuanxian and Bingtan, 1988);  $\blacktriangledown$ , wollastonite (Liu and Ding, 2002). More information about the tested samples can be found in Table 8.22



**Figure 8.29** Thermal conductivity versus temperature of coatings of air-plasma sprayed molybdenum, as reported by various authors:  $\diamond$ , Wilkes and Lagedrost, 1973;  $\blacksquare$ , Brandt *et al.*, 1979. More information about the tested samples can be found in Table 8.23

Table 8.23 Thermal conductivity of air plasma-sprayed molybdenum coatings (see also Figure 8.29)

Number	Reference	Coating			Remarks	Testing method
		Chemical composition (wt. %)	Density (kg/m <sup>3</sup> )	Phase composition		
1	Brandt <i>et al.</i> , 1979	Mo	7900	Mo	Large spraying distance that could have resulted in a number of unmelted grains and some oxidation	Modulated-beam method under vacuum for diffusivity, specific heat, density and thermal expansion
2	Wilkes and Lagedrost, 1973	—	7710	—	—	Laser-flash method under vacuum for diffusivity, specific heat, density and thermal expansion

*et al.* (1995). The obtained values were  $a = 34 \times 10^{-7} \text{ m}^2/\text{s}$  for an air-plasma-sprayed sample and  $a = 88 \times 10^{-7} \text{ m}^2/\text{s}$  for argon-atmosphere-plasma-sprayed ones. The difference in the thermal diffusivity values was attributed to better contacts between the lamellae of the particles in argon-atmosphere-sprayed samples.

Thermal conductivity data of plasma-sprayed *self-bonding* NiAl coatings are shown in Figure 8.30. The thermal conductivities of NiAl coatings sprayed in vacuum are two to three times greater than the conductivities of open-air-sprayed coatings.

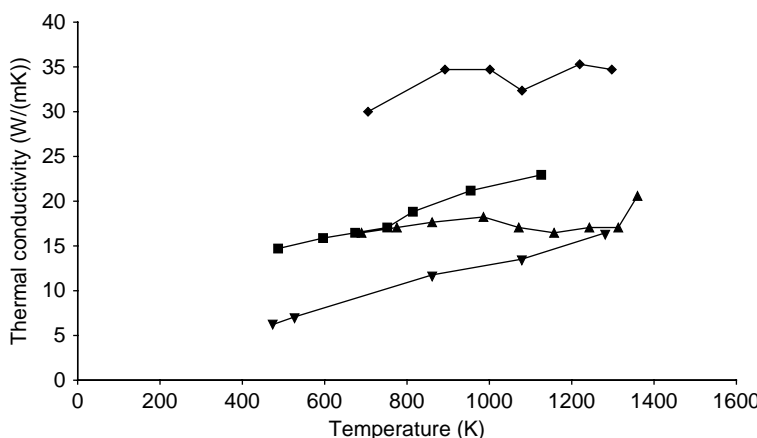


Figure 8.30 Thermal conductivity versus temperature of coatings of NiAl alloys, plasma-sprayed in air (APS) and under vacuum (VPS), as reported by various authors:  $\blacklozenge$ , VPS (Brandt *et al.*, 1986);  $\blacksquare$ , APS (Daniault, 1981);  $\blacktriangle$ , APS (Brandt *et al.*, 1986);  $\blacktriangledown$ , APS (Wilkes and Lagedrost, 1973). More information about the tested samples can be found in Table 8.24

Differences in the conductivities result from oxidation during air-plasma spraying. As shown in Table 8.24, the density of vacuum-plasma-sprayed NiAl is greater than the open-air-sprayed material. The vacuum-sprayed coatings are very homogenous and do not show any porosity (see Figure 8.8(c)).

The thermal conductivities of some NiCr-based alloys are shown in Figure 8.31, with further details about the tested samples presented in Table 8.25.

An important influence on the thermal conductivity is again the spray atmosphere. Vacuum-plasma-sprayed coatings have a thermal conductivity nearly three times greater than the NiCr ones sprayed in air. To

Table 8.24 Thermal conductivity of NiAl coatings sprayed using different methods (see also Figure 8.30)

Number	Reference	Coating			Remarks	Testing method
		Chemical composition (wt.%)	Density (kg/m <sup>3</sup> )	Phase composition		
<i>Air plasma-spraying</i>						
1	Daniault, 1981 Brandt <i>et al.</i> , 1986	Ni + 5Al	—	—	—	—
2			7200	Ni – cubic	—	Laser-flash method under vacuum for diffusivity, specific heat, density and thermal expansion
3	Wilkes and Lagedrost, 1973		7400	—	—	—
4	Brandt <i>et al.</i> , 1986	Ni + 5Al + 0.3Fe	7800	Ni – cubic	Microstructure in Figure 8.8(c)	Laser-flash method under vacuum for diffusivity, specific heat, density and thermal expansion

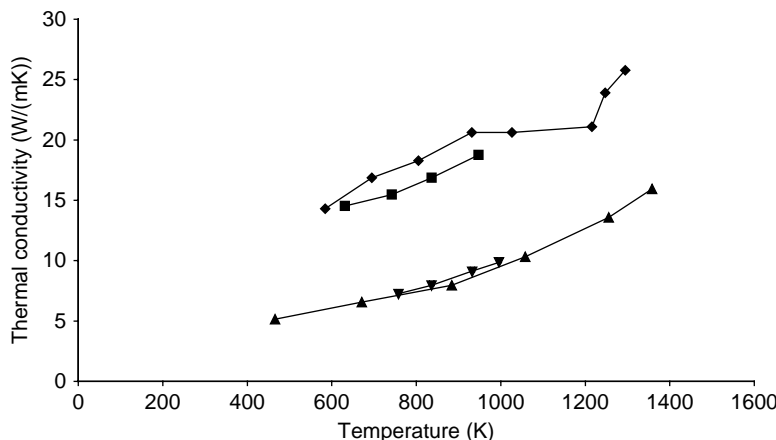


**Figure 8.31** Thermal conductivity versus temperature of coatings of NiCr-based alloys, plasma-sprayed in air (APS) and under vacuum (VPS): ♦, NiCr by VPS; ■, NiCoCrAlY by VPS; ▲, NiCr by APS; ▼, NiCrAl by APS. More information about the tested samples can be found in Table 8.25

take as an example, the microstructure of an air-plasma-sprayed NiCrAl coating is shown above in Figure 8.8(b). The contacts between the lamellae in the coating are very poor which indicate ‘in-flight’ oxidation in the plasma jet. The thermal conductivity of the coatings increases with temperature. Knowing that the electronic conductivity does not depend on temperature in this temperatures range (see Chapter 7, Section 7.3.2), this evolution can be attributed to the coatings’ densification and to the growth of crystal grains during testing.

### Composites and Duplex Coatings

Particulate composites should have a thermal expansion coefficient and an elastic modulus between that of the ceramic overlay and the bond coating in order to reduce thermal stresses. The composites usually contain ceramics from the overlay coating and alloys (metals) from the bonding one. Typical compositions include (in wt%) 25, 50 or 75 of one component with the other component corresponding to a total of 100 wt%. Thermal conductivities of cermets of molybdenum with  $ZrO_2$  stabilized with CaO, having compositions of (25/75) and (75/25), as well as the cermet NiAl with  $ZrO_2$  (composition 50/50) are

Table 8.25 Thermal conductivity of NiCr-based alloys sprayed using different methods (see also Figure 8.31)

Number	Reference	Coating			Remarks	Testing method
		Chemical composition (wt%)	Density (kg/m <sup>3</sup> )	Phase composition		
1	Brandt <i>et al.</i> , 1986	Ni + 19Cr + 5.6Al	7700	Air plasma-spraying Ni – cubic	Microstructure in Figure 8.8(b)	Laser-flash method under vacuum for diffusivity, specific heat, density and thermal expansion
2	Wilkes and Lagedrost, 1973	Ni + 24.6Cr + 0.6Si	6800	—	—	—
3	Brandt <i>et al.</i> , 1986	Ni + 19.2Cr + 0.4Fe	7700	Vacuum plasma-spraying Ni – cubic	—	Laser-flash method under vacuum for diffusivity, specific heat, density and thermal expansion
4	Wilkes and Lagedrost, 1973	Ni + 36Co + 21Cr + 8.8Al + 1Y + 0.9Si	7200	Ni – cubic; Cr – cubic; Co – cubic	—	—

shown in Figure 8.32, with further details about the tested samples are shown in Table 8.26.

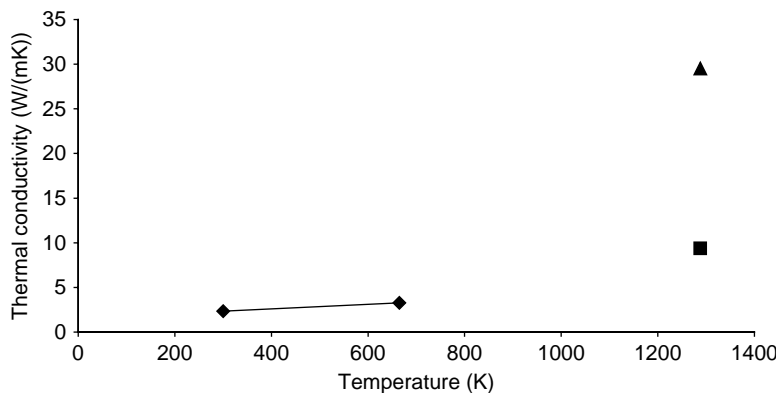


Figure 8.32 Thermal conductivity versus temperature of coatings of cermets: ♦, 50 wt% NiAl and 50 wt% MgSZ; ■, 25 wt% Mo and 75 wt% CaSZ; ▲, 75 wt% Mo and 25 wt% CaSZ. More information about the tested samples can be found in Table 8.26

One of the possible designs for thermal-barrier coatings is known as *duplex*. The duplex configuration is composed of a top zirconia coating and a bond coating which is usually an alloy. Heat, coming from a combustion engine, flows from the surface of the top coating down to the substrate. This flow can be hampered by an interface between the components of the duplex. The parameter that describes this effect is the *thermal contact resistance*. The thermal contact resistances of two duplex configurations, namely Mo with YSZ and NiAl with YSZ at different temperatures, are shown in Figure 8.33.

The resistance can vary with temperature. The resistance values of a thermal contact between steel and a molybdenum coating were found by Wilkes and Lagedrost (1973) to be in the range  $2 \times 10^{-6}$  to  $5 \times 10^{-6} \text{ m}^2\text{K/W}$ . The values presented in Figure 8.33 are two orders of magnitude greater. This may result from the total surface of the contact at the interface between two coatings in a duplex which is smaller than that between a metallic coating and a substrate. Similarly, the adhesion of two coatings must be smaller than that of a coating to its substrate. Gitzhofer *et al.* (1985) followed this idea and tried to find a correlation between the thermal contact resistance and the adhesion of a coating to its substrate.

Table 8.26 Thermal conductivity versus temperature data for composites (see also Figure 8.32) and thermal contact resistance versus temperature data inside the coatings sprayed by a plasma in air (see also Figure 8.33)

Number	Reference	Coating			Remarks	Testing method
		Chemical composition (wt%)	Porosity (%)	Density (kg/m <sup>3</sup> )		
1	Wilkes and Lagedrost, 1973	Mo + 25(ZrO <sub>2</sub> + 5CaO)	4.1	—	—	Figure 8.32 Laser-flash method under H <sub>2</sub> ( $p = 3.5$ MPa) for diffusivity, specific heat, density and thermal expansion
2		Mo + 75 (ZrO <sub>2</sub> + 5CaO)	16.2	7360	—	Figure 8.32 Laser-flash method under H <sub>2</sub> ( $p = 3.55$ MPa) for diffusivity, specific heat, density and thermal expansion
3	Daniault, 1981	(Ni + 5Al) + 50(ZrO <sub>2</sub> + 24MgO)	—	—	—	—
4	Gitzhofer <i>et al.</i> , 1985	Mo/ZrO <sub>2</sub> + 8Y <sub>2</sub> O <sub>3</sub>	8–9	7900/5600	$\tau'$	Figure 8.33 Laser-flash method under vacuum
5		(Ni + 5Al + 0.3Fe)/ZrO <sub>2</sub> + 7Y <sub>2</sub> O <sub>3</sub>	9–10	7200/5500	—	—

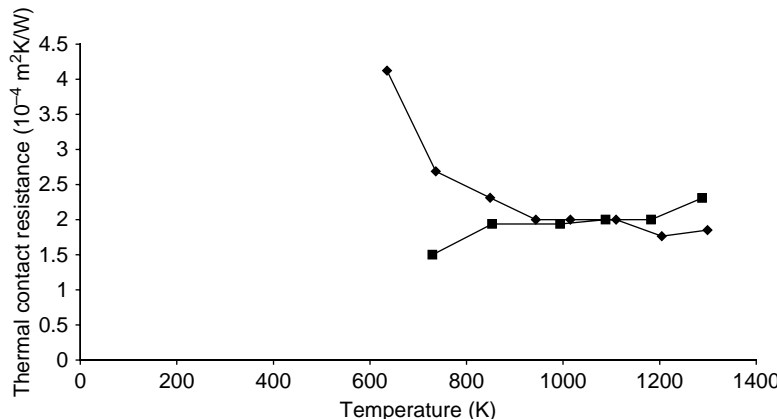


Figure 8.33 Thermal-contact resistance versus temperature between the components of *duplex* coatings: ♦, Mo and 8YSZ; ■, NiAl and 7YSZ. More details about the coatings can be found in Table 8.26

### 8.3.2 SPECIFIC HEAT

Specific heat is a fundamental property of a material which depends on its chemical composition. It does not depend on other elements of the coating's microstructure, such as porosity, contact between particles, etc. Measurement of  $c_p$  can indicate transformations of the initial material at processing. For example, Figure 8.34 shows the specific heats of NiAl samples plasma-sprayed in air and in vacuum.

The curves are clearly different for air- and vacuum-sprayed deposits, as well as that of pure nickel – shown for comparison sake. The vacuum-sprayed coating shows a magnetic transformation for nickel at 631 K, while the air-sprayed ones do not exhibit this peak. The changes in specific heat in the sample deposited in air must have resulted from oxidation during spraying although the presence of oxides has not been detected by X-ray diffraction. A comparison of the specific heats of the powders used to spray and the obtained coatings, calculated the following *Kopp-Neumann law* and presented in Table 8.27, indicates that the:

- the vacuum-sprayed sample has a  $c_p$  value which coincides reasonably well with that of the initial powder and the relative difference is not larger than 3.6 % at any temperature;
- the air sprayed sample has a  $c_p$  value which diverges from that of the initial powder by about 12 % at temperatures close to the magnetic transformation.

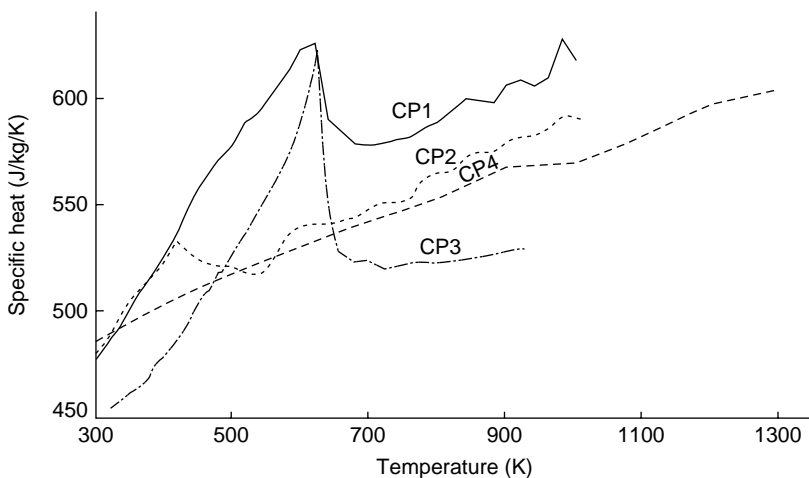


**Figure 8.34** Specific heat versus temperature for pure nickel (CP1) and for NiAl coatings plasma-sprayed in air (CP2 and CP4 – described in entries 2 and 3, respectively, of Table 8.24) and in vacuum (CP3 – described in entry 4 of Table 8.24)

Consequently, vacuum deposition did not introduce many changes into the processed material.

### 8.3.3 THERMAL EXPANSION

Thermal expansion is an important property which influences the integrity of a coating in service by being responsible for the generation of different kinds of stresses:

- quenching and cooling stresses, which are generated during low-temperature-applications (see Chapter 6, Section 6.2.3);
- thermal stresses, which are generated during high-temperature applications and frequently provoke cracking and ‘spalling’ of the coatings.

Neither porosity nor the lamellar structure influence the thermal expansion and their values are similar to that of the bulk materials (Kuroda and Clyne, 1991). Only the phase composition has an influence. On the other hand, the thermal expansion, measured in the longitudinal direction (parallel to the coating’s surface), is similar to that of the bulk material but its measurement in the transverse (perpendicular to the surface) direction sometimes gives unexpectedly high values. This

Table 8.27 Verification of the Kopp–Neumann law for NiAl coatings plasma-sprayed in air and under vacuum – shown in Figure 8.34 as CP2 and CP3 (Pawlowski, 1985).

Number	T (K)	Vacuum-sprayed coating (CP3)			Air-sprayed coating (CP2)				
		Chemical composition of powder (wt%)	$c_p$ calculated for powder ( $J/(kgK)$ ) <sup>a</sup>	$c_p$ measured for coating ( $J/(kgK)$ )	Relative difference in $c_p$ (%)	Chemical composition of powder (wt%)	$c_p$ calculated for powder ( $J/(kgK)$ )	$c_p$ measured for coating ( $J/(kgK)$ )	Relative difference in $c_p$ (%)
1	373	Ni + 5Al + 0.3Fe	516.0	517.1	0.22	Ni + 5Al	515.8	512.9	-0.56
2	473		555.2	569.4	2.50		557.1	521.3	-6.87
3	573		593.3	615.5	3.60		593.1	529.6	-11.99
4	673		569.0	579.9	1.88		568.3	543.9	-4.48
5	773		576.5	584.5	1.37		575.9	558.5	-3.12
6	873		583.8	598.7	2.49		583.0	574.4	-1.50

<sup>a</sup> Specific data for the elements have been taken from Touloukian and Buyco (1970).

phenomenon, studied by Berndt and Herman (1983) and Wang and Berndt (1991), can be explained by relaxation of the residual stresses in the tested samples. This relaxation results in deflection of the coating in the transverse direction. Finally, the thermal expansion permits us to find the density at high temperatures (see Chapter 7, Equation (7.22)) which is, in turn, necessary for calculating the thermal conductivity (see Chapter 7, Equation (7.18)). As the thermal expansion may not be linear, its values should be given with the temperature limits.

## Ceramics

The thermal expansion data for some thermally sprayed ceramics are shown in Table 8.28. The tested samples shrink, in general, during measurements of the thermal expansion. Some of them modify the crystal structure after high-temperature testing. For example, the 8YSZ coating, which crystallizes in the t'-phase after spraying (see entry 1 in Table 8.28), retains this structure after annealing at temperatures up to 1573 K. The coating becomes destabilized after annealing at 1670 K for 100 h and the t'-phase transforms into the monoclinic phase at about 600 K (Brandon and Taylor, 1991a). This destabilization is associated with a dramatic change in the thermal expansion behaviour. Similarly,  $\text{ZrO}_2$  alloyed with 20 wt%  $\text{CeO}_2$  (or less), crystallizes in the tetragonal and monoclinic phases. The coatings transform upon annealing at temperatures above 1473 K into the monoclinic phase. This transformation results in an important modification of the thermal expansion at temperatures of about 423 and 673 K (Brandon and Taylor, 1991b). Such a modification can be detrimental for the coatings' integrity. Only stabilizing with 25 wt% ceria (or more) enables retaining of the tetragonal structure at all temperatures and keeping the thermal expansion relatively constant.

Typical metal substrates for high-temperature applications have thermal expansion values in the range,  $TEC = 15\text{--}18 \times 10^{-6}$  1/K. Examples include the following:

- mild steel has a thermal expansion coefficient in the temperature range  $T = 300$  to 1300 K, equal to  $TEC = 16.6 \times 10^{-6}$  1/K;
- Inconel 600 has a thermal expansion coefficient in the temperature range  $T = 300$  to 1300 K, equal to  $TEC = 16.4 \times 10^{-6}$  1/K;
- aluminium has a thermal expansion coefficient in the temperature range  $T = 300$  to 1300 K, equal to  $TEC = 24.3 \times 10^{-6}$  1/K.

Table 8.28 Thermal expansion of some ceramics thermally sprayed using different techniques

Number	Reference	Chemical composition (wt%)	Coating characteristics			Remarks
			Crystal phase 'as-sprayed'	Longitudinal thermal expansion ( $10^{-6}$ 1/K)	Transversal thermal expansion ( $10^{-6}$ 1/K)	
Air plasma-spraying						
1	Berndt and Herman, 1983	ZrO <sub>2</sub> + 8Y <sub>2</sub> O <sub>3</sub>	t' – major, monoclinic and cubic – minor	9.5	4–20	300–1300
2	Rangaswamy <i>et al.</i> , 1980	ZrO <sub>2</sub> + 20Y <sub>2</sub> O <sub>3</sub>	Cubic	10.6	—	
3	Wang and Berndt, 1991	Al <sub>2</sub> O <sub>3</sub>	—	7.6	—	
4	Rangaswamy <i>et al.</i> , 1980	TiO <sub>2</sub>	γ-Al <sub>2</sub> O <sub>3</sub>	7.0	5.2–7.6	
5	Tronche and Fauchais, 1987	Cr <sub>2</sub> O <sub>3</sub>	—	9.8	—	
6	Wang and Herman, 1990	Forsterite, 2MgO·SiO <sub>2</sub>	Cr <sub>2</sub> O <sub>3</sub>	7.5	—	300–900
7		Spinel, MgO·Al <sub>2</sub> O <sub>3</sub>	—	11	—	300–1100
8	Suzuki <i>et al.</i> , 2000	Zircon, ZrO <sub>2</sub> ·SiO <sub>2</sub>	Forsterite, 2MgO·SiO <sub>2</sub>	7.7	—	300–1300
9	Wang and Herman, 1990	Corderite, 2MgO·2Al <sub>2</sub> O <sub>3</sub> · 5SiO <sub>2</sub>	Tetragonal – ZrO <sub>2</sub> , ZrSiO <sub>4</sub>	5.1	—	'As-sprayed'
10			—	1.7	—	300–1100

Table 8.28 (Continued)

Number	Reference	Chemical composition (wt%)	Coating characteristics				Remarks
			Crystal phase 'as-sprayed'	Longitudinal thermal expansion ( $10^{-6}$ 1/K)	Transversal thermal expansion ( $10^{-6}$ 1/K)	Temperature range (K)	
<i>Air plasma-spraying</i>							
11	Weaver <i>et al.</i> , 2000	Indialite/ quartz/glass (amorphous)	1.2/2/4.5	—	—	—	Thermal expansion increased when adding titania
<i>Air plasma-spraying (water-stabilized plasma torch)</i>							
12	Tronche and Fauchais, 1987	WC+20Co	—	7.4	—	300–900	—
13	Rudajevova, 1994	Zircon, $\text{ZrO}_2\text{-SiO}_2$	Tetragonal – $\text{ZrO}_2$ – major; monoclinic – $\text{ZrO}_2$ – minor	6.4 – 6.8	—	473–973	'As-sprayed'
14	Suzuki <i>et al.</i> , 2000	Zircon, $\text{ZrO}_2\text{-SiO}_2$	Tetragonal – $\text{ZrO}_2$ – major; monoclinic – $\text{ZrO}_2$ – minor; $\text{ZrSiO}_4$ – minor	5.5	—	300–1300	Spray distance of 125 mm and substrate temperature of 1473 K

The differences in the thermal expansion coefficients between the ceramic coatings and the metal substrates might be as high as  $\Delta TEC = 22.6 \times 10^{-6} \text{ } 1/\text{K}$  in the case of *cordierite* sprayed onto an aluminium substrate (entry 10 in Table 8.28). Such a large difference leads to the generation of residual stresses (at the deposition process) and thermal stresses ('at service'). Relaxation of such stresses is likely to detach the coating from its substrate. This is the main reason for applications of either bond coatings or particulate composites containing materials of the top and bond coatings.

### Metals and Alloys

Thermal expansion data for thermally sprayed metals and various alloys are shown in Table 8.29. These parameters for metals and alloys, usually applied as bond coatings, should be intermediate between that of the

**Table 8.29** Thermal expansion of some metals and alloys sprayed using different techniques

Number	Reference	Chemical composition (wt%)	Coating characteristics		Remarks
			Longitudinal thermal expansion ( $10^{-6} \text{ } 1/\text{K}$ )	Temperature range (K)	
<i>Flame spraying</i>					
1	Rangaswamy <i>et al.</i> , 1980	Mo	6.8	300–1300	Probably wire-spraying
2		Ni + 20Al	12.5		
<i>Air plasma-spraying</i>					
3	Rangaswamy <i>et al.</i> , 1980	Ni + 5Al	14.9	300–1300	—
4	Pawlowski, 1985	Ni + 5Al	13.5		
<i>Vacuum plasma-spraying</i>					
5	Pawlowski, 1985	Ni + 5.6Al + 19Cr	15.5	300–1200	—
6		Ni + 19.2Cr + 1.1Si + 0.4Fe.	17.3		
7	Siemers and Mehan, 1983	Ni + 22Cr + 10Al + 1Y	18.3	300–1470	

metal substrate and the ceramic top coating. The spray technique does not influence the thermal expansion of similar materials (entries 3 and 4 in Table 8.29).

## Composites

Particulate composites, including zirconia, were prepared by blending and applied by air plasma-spraying by Gault *et al.* (1988). The resulting coatings have thermal expansion values which are intermediate between the NiAl and NiCr bond coatings and the top coatings (Figure 8.35).

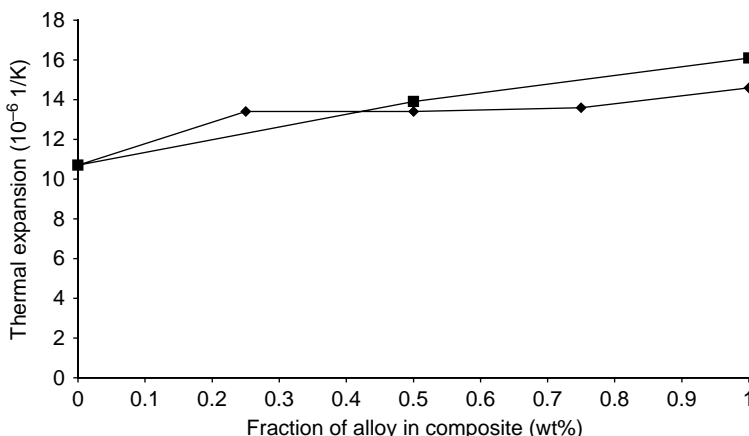


Figure 8.35 Thermal expansion versus mass fraction of alloys in composites: ♦, NiAl alloy in NiAl-24MgYSZ composite; ■, NiCr alloy in NiCr-8YSZ composite. More details about the samples are given in entries 3 and 4 of Table 8.15, respectively

The mass fraction of one component with regard to the other is not a *controlled* parameter upon deposition of a composite. In order to precisely control its composition, it is rather recommended to correlate it with the powder feed rate. The latter is a *controlled* parameter of the process. This approach was applied by Pawlowski (1991). Al and  $\text{Al}_2\text{O}_3$  powders were introduced through separate injectors to the jet issuing from the plasma torch. The relative content of metal in the composite

( $\theta$ ) was defined, starting from the aluminum ( $q_{\text{Al}}$ ) and alumina ( $q_{\text{Al}_2\text{O}_3}$ ) feed rates, from the following equation:

$$\theta = \frac{q_{\text{Al}}}{q_{\text{Al}} + q_{\text{Al}_2\text{O}_3}} \quad (8.3)$$

Thermal expansion data for Al-Al<sub>2</sub>O<sub>3</sub> composites are shown in Figure 8.36, with the corresponding microstructures of the coatings shown in Figure 8.37.

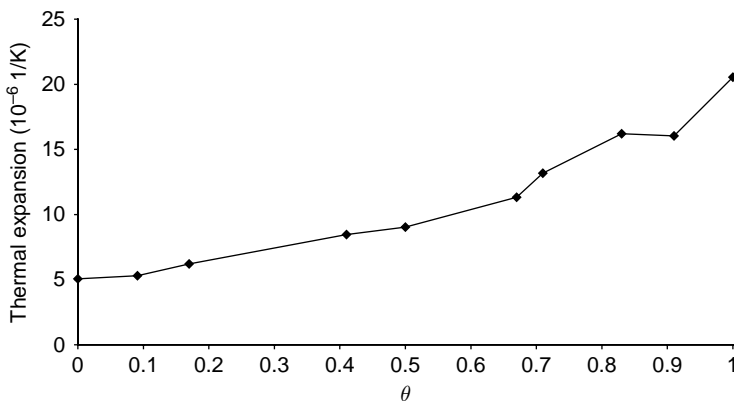


Figure 8.36 Thermal expansion versus relative Al content (expressed by the parameter  $\theta$  – defined in Equation (8.3)) of a particulate composite of Al-Al<sub>2</sub>O<sub>3</sub> (Pawlowski, 1991). The grain sizes of the Al powder and the Al<sub>2</sub>O<sub>3</sub> powder were  $-90 + 45 \mu\text{m}$  and  $-45 + 22.5 \mu\text{m}$ , respectively. The cermets were plasma-sprayed in air and the electric power was varied from 28 to 43 kW. The powders were introduced through two separate injectors into the plasma jet

### 8.3.4 EMISSIVITY

The emissivities of some samples are shown in Figure 8.38 with details of their preparation shown in Table 8.30.

Chromia coatings have the highest emissivity values but it is difficult to say whether the data obtained for plasma- and flame-sprayed coatings are similar. Further studies on emissivity should include characterization of the coating's surface, such as 'rugosity', which may influence the emissivity data.

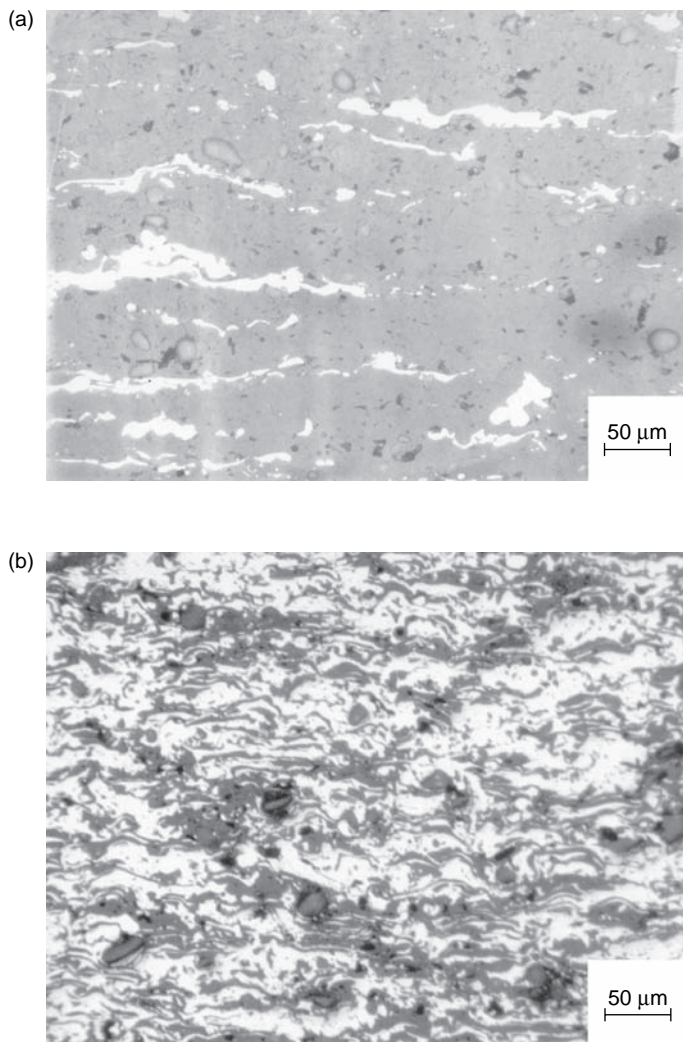


Figure 8.37 Optical micrographs (in bright field) of polished cross-sections of Al-Al<sub>2</sub>O<sub>3</sub> particulate composites with the parameter  $\theta$  – defined in Equation (8.3): (a)  $\theta = 0.1$ ; (b)  $\theta = 0.67$

### 8.3.5 THERMAL SHOCK RESISTANCE

The thermal shock resistance values of ceramics depend on their thermo-mechanical properties (elastic modulus, thermal expansion), as shown in Chapter 7, Equation (7.25). Low-thermal-expansion cermics are expected to resist well against thermal shock. This was confirmed

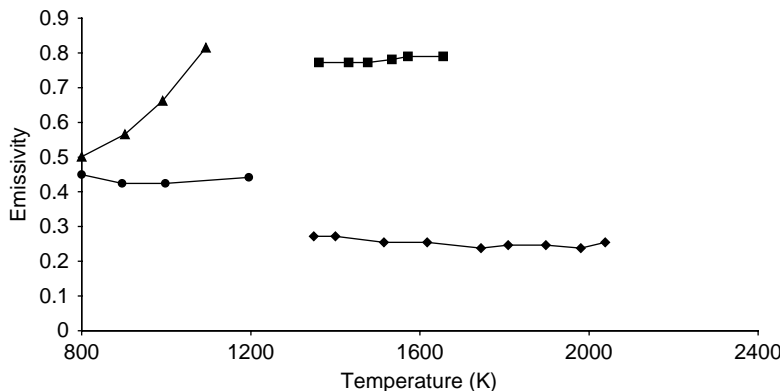


Figure 8.38 Total emissivity versus temperature for different thermally sprayed ceramic oxide coatings, plasma-sprayed in air (APS) and flame-sprayed (FS): ♦,  $\text{Al}_2\text{O}_3$  by APS; ■,  $\text{Cr}_2\text{O}_3$  by APS; ▲,  $\text{Cr}_2\text{O}_3$  by FS; ●,  $\text{ZrO}_2$  by FS

indeed for plasma-sprayed *cordierite* ( $2\text{MgO} \cdot 2\text{Al}_2\text{O}_3 \cdot 5\text{SiO}_2$ ), which has a very small thermal expansion,  $TEC = 1.7 \times 10^{-6}$  1/K (see entry 10 in Table 8.28). In fact, the coefficient of thermal shock resistance was as high as  $TSR = 1110$  K (Wang and Herman, 1990). ‘Free-standing’  $\text{Al}_2\text{O}_3$ , of a greater thermal expansion ( $TEC = 7 - 7.6 \times 10^{-6}$  1/K – entries 3 and 4 in Table 8.28) was tested by Lutz (1995). Tested ‘free-standing’ ‘cylinders’ have coefficients which are definitely smaller, i.e.  $TSR = 230 - 720$  K. The latter mainly depend on the thicknesses of the cylinder walls (ranging from 1.5 to 3 mm) and less on the cylinder dimensions. The thermal shock resistance is influenced by the microstructures of the samples, mainly their porosities. The cracks generated by thermal shock can be arrested by the pores. Experimental evidence for such behaviour in plasma-sprayed  $5\text{CaSZ}$  coatings was provided by Rangaswamy *et al.* (1980). These authors found that the thermal-shock resistance increases with the coating’s porosity and that coatings having 20 % porosity did not fail at all.

Ceramic coatings are often applied for overlays in thermal-barrier coatings, together with bond layers onto the metal substrate. The barriers are applied under conditions of thermal cycling and in a corrosive atmosphere. These include low-thermal-conductivity stabilized-zirconia as the top layer and a superalloy having a composition of MCrAlY (M = Ni, Co, NiCo) as the bonding one and are tested using ‘burner-rigs’ (see Chapter 7, Figure 7.23) and radiation-heat sources (Kokini and Takeuchi, 1994). The tested coatings are subjected to cyclic temperature fields which results in thermal ‘dilatation’ on

Table 8.30 Total normal emissivity of ceramic coatings sprayed using different techniques

Number	Reference	Coatings characteristics			Emissivity	Temperature range (K)	Remarks	Testing method
		Chemical composition (wt%)	Density (kg/m <sup>3</sup> )	Porosity (%)				
<i>Flame spraying (rod)</i>								
1	Bogdanov <i>et al.</i> , 1965	ZrO <sub>2</sub>	4970	12	See Figure 8.38	800–1200	HV <sub>3</sub> = 673	'Home-made' device
2		Cr <sub>2</sub> O <sub>3</sub>	4200	5.5		800–1100	—	
<i>Air plasma-spraying</i>								
3	Brandt <i>et al.</i> , 1979	Cr <sub>2</sub> O <sub>3</sub> +5Cr	—	—	See Figure 8.38	1350–1650	—	—
4	Pawlowski <i>et al.</i> , 1983	Al <sub>2</sub> O <sub>3</sub> ZrO <sub>2</sub> +30CaO	—	—	0.994–5.05 × 10 <sup>-4</sup> × T, correlation= 0.963	1350–2050 300–1300	In the wavelength range 2–5.6 μm, regression equation temperature T expressed in °C	IR camera

6



0.901-4.09 ×  
 $10^{-4} \times T$ ,  
correlation = 0.915  
0.928-3.31 ×  
 $10^{-4} \times T$ ,  
correlation = 0.752  
1.0-3.43 × $10^{-4} \times T$ ,  
correlation = 0.961  
0.901-4.88 ×  
 $10^{-4} \times T$ ,  
correlation = 0.925

---

7



8



9



heating and shrinkage while cooling. The required coating property is ‘strain-tolerance’. An ideal strain-tolerant microstructure would contain columns which are closely attached to the bond coating and independent of the adjacent columns (Sheffler *et al.*, 1982). Such a structure can be obtained in zirconia coatings by electron-beam physical vapour deposition. Some studies have been made to obtain similar structures by application of cryogenic cooling while plasma-spraying, by, e.g. Cosack *et al.* (1992) or Bartlett and Dal Maschio (1995). Other possible strain-tolerant microstructures could be (Grot and Martyn (1981)):

- segmented (see, e.g. Chapter 4, Figures 4.13 and 4.14);
- microcracked;
- controlled porosity micostructure.

The thermal expansion ‘mis-match’ between the substrate and the top coating is another important parameter influencing the thermal shock resistance. The highest resistance relates to the lowest ‘mis-match’. On the other hand, reduction in the top-coating thickness acts in favour of increasing resistance (Joshi and Srivastava, 1993; Kokini and Takeuchi, 1994) even if the heat-insulating effect if considered, i.e. the temperature drop on the barrier is lower. In fact, all of the factors enabling the keeping compressive (instead of tensile) stresses on the top coating at thermal testing increase the capacity to resist against the formation of cracks and increases the thermal-shock resistance.

## 8.4 ELECTRIC PROPERTIES

The electric and magnetic properties of thermally sprayed coatings are now being tested more and more frequently. In fact, applications, such as copper conductors sprayed by the cold-spray technique for ‘heat-sinks’ (Gärtner *et al.*, 2005) or solid oxide fuel cells (SOFCs) with ionic conductors (Lang *et al.*, 2001), related to these properties are emerging and continue to grow considerably.

### 8.4.1 PROPERTIES OF CONDUCTORS

Electrically conducting materials can be categorized as a function of the species carrying the charge:

- electrons;
- ions;
- mixed (electrons and holes).

## Electronic Conductors

Electronic conductors that have been thermally sprayed are mainly metals such as Cu, Ta, Au, Mo, Nb and Cr. Ceramics such as silicides and borides have also been tested for high-temperature applications.

Braguier *et al.* (1973) sprayed Cu coatings with a plasma in air. ‘As-sprayed’ coatings (20 µm thick) had a resistivity of about  $\rho = 14 \mu\Omega \text{ cm}$  but after annealing in hydrogen at 800 °C the resistivity decreased to  $\rho = 7 \mu\Omega \text{ cm}$ . Plasma spraying in a vacuum was applied by Pawlowski (1978) to deposit Cu and Ta coatings. The Cu ‘as-sprayed’ coatings had a resistivity of  $\rho = 2\text{--}5 \mu\Omega \text{ cm}$  and their thermal coefficient of resistivity was in the range of  $TCR = 2.6\text{--}3.1 \times 10^{-3} \text{ 1/K}$ . Copper is nowadays sprayed using the cold-gas spray technique and its ‘as-sprayed’ resistivity is close to that of the bulk material,  $\rho = 2.24 \mu\Omega \text{ cm}$  (Xiong *et al.*, 2005). Tantalum deposits revealed a resistivity of  $\rho = 170\text{--}320 \mu\Omega \text{ cm}$  and the  $TCR = 190\text{--}1300 \times 10^{-6} \text{ 1/K}$ . Harris and Janowiecki (1970) reported the successful air-plasma spraying of Au, Mo, Al and MoSi<sub>2</sub> conductors (the latter for a high-temperature, oxidizing atmosphere). Conductors such as Nb, Ta and Al were air-plasma and flame-sprayed by Raideren (1967). These metals were subsequently used as electrodes for electrolytic capacitors. For this application, the technology of spraying was optimized in order to obtain porous coatings having rough and developed surfaces. Another conducting metal, namely chromium, was used to plasma-spray electrodes for high-temperature heaters with working temperatures of 1000 K (Ositinski and Basko, 1977). Smyth and Anderson (1976) studied the resistivities of typical electronic conductors obtained by air-plasma spraying (Table 8.31). The resistivities of the following borides have been tested:

- TiB<sub>2</sub>, sprayed by a plasma in air had a resistivity of  $\rho = 10\text{--}70 \text{ m}\Omega \text{ cm}$  (Ananthapadmanabhan *et al.*, 1993). The resistivity is considerably higher than that of the sintered material ( $\rho = 30 \mu\Omega \text{ cm}$ ), which resulted from oxidation during processing.
- ZrB<sub>2</sub>, sprayed by a plasma under an inert atmosphere had a resistivity of  $\rho = 320 \mu\Omega \text{ cm}$  (Tului *et al.*, 2002). The use of an inert atmosphere during spraying hampered oxidation of the powder.

**Table 8.31** Resistivities of some electronic conductors (Smyth and Anderson, 1976). Reproduced by permission of the American Welding Society from R.T. Smyth and J.C. Anderson, 1976, 'Electronic circuit production by arc plasma spraying', in *Proceedings of the 8th International Thermal Spray Conference*, American Welding Society, Miami, FL, USA, pp. 456–463

Material	Resistivity of bulk material ( $\mu\Omega \text{ cm}$ )	Resistivity of air-plasma sprayed coating ( $\mu\Omega \text{ cm}$ )
Aluminium	2.8	25
Copper	1.7	20
Chromium	2.6	180
Nickel	7.8	40
Stainless-steel	40	80
Tantalum	14	200
Tin	11.5	70
Titanium	3.2	170

### Ionic Conductors

One important application of sprayed coatings is in the area of solid oxide fuel cells. This application requires a solid electrolyte which can be a ceramic that does not conduct electrons but conducts ions at temperatures between 1073 and 1273 K. Historically, the 'first-chosen' ceramic was  $\text{ZrO}_2$  with the  $\text{Zr}^{4+}$  cation stabilized with oxides that have cations of lower valences, such as  $\text{Ca}^{2+}$ ,  $\text{Sc}^{3+}$  and  $\text{Y}^{3+}$ . The process stabilizes zirconia but also creates vacancies (Boivin and Mairesse, 1998). The vacancies make it possible for the oxygen anions ( $\text{O}^{2-}$ ) to traverse across the solid electrolyte and generate an electromotive force in the cell. Ionic conduction also occurs in oxides such as  $\text{Bi}_2\text{O}_3$  and bismuth mixed oxides, although zirconia is the material studied most frequently by thermal spraying. Electric conductivity data for some zirconia coatings at high temperatures are shown in Figure 8.39, with further details about the tested samples given in Table 8.32.

### Semiconductors

Semiconducting materials transport electric charges by electrons and vacancies (holes). Studies of 'classic' semiconducting materials were started as early as the 1960s. Janowiecki *et al.* (1968) used air-plasma spraying to deposit p- and n-doped silicon–germanium alloys for use as thermoelectric materials in the temperature range  $T = 673\text{--}1173\text{ K}$ . A careful optimization of the spray parameters enabled the finding of

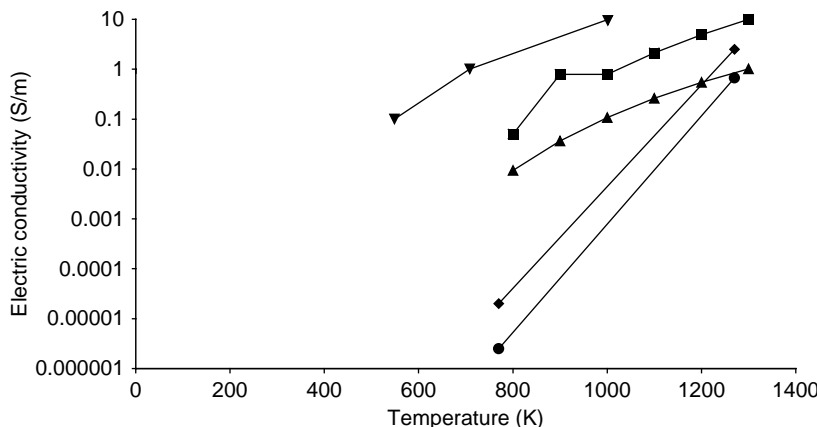


**Figure 8.39** Electrical conductivity versus temperature of coatings of zirconia stabilized using different oxides, plasma-sprayed in air (APS) and under vacuum (VPS), as reported by various authors: ◆, 12 YSZ by APS (Scagliotti *et al.*, 1988); ■, 12 YSZ by VPS (Renouard-Vallet *et al.*, 2004); ▲, 12 YSZ by APS (Renouard-Vallet *et al.*, 2004); ▽, 10 ScZ by VPS (Lang *et al.*, 2004); ●, 19 YSZ by APS (Scagliotti *et al.*, 1988) More information about the tested samples can be found in Table 8.32

the electrical resistivity of the deposits as  $\rho = 4.15 \text{ m}\Omega \text{ cm}$  and a *Seebeck coefficient*<sup>14</sup> equal to  $126 \mu\text{V/K}$ . Air-plasma spraying of p- and n-doped silicon has been extensively studied in the CNRS Laboratory in Meudon, France by Suryanarayanan and Zribi (1982), Suryanarayanan *et al.* (1984, 1986, 1987), Akani *et al.* (1987a,b) and Kayali *et al.* (1991). The ‘as-sprayed’ material had a resistivity of  $\rho = 0.8 \Omega \text{ cm}$  and the *carrier mobility*<sup>15</sup> was equal to  $6 \text{ cm}^2/(\text{Vs})$ . After heat-treatment in vacuum at  $T = 1273\text{--}1523 \text{ K}$  for times ranging from 2 to 12 h, the mobility increased to  $25\text{--}40 \text{ cm}^2/(\text{Vs})$ . The ‘e-beam glazing’ of the ‘as-sprayed’ material leads to an increase in the carrier mobility up to  $320 \text{ cm}^2/(\text{Vs})$  and a decrease in the resistivity down to  $\rho = 0.02 \Omega \text{ cm}$ . Microstructural studies, using the XRD, XPS and AES techniques, of plasma-sprayed silicon were made by Alaee *et al.* (1983) and Alaee (1989). Parent *et al.* (1987) studied plasma-sprayed  $\alpha\text{-Fe}_2\text{O}_3$ , doped with Si, In or Mg, onto Ti substrates. The oxide was, in part, reduced to  $\text{Fe}_3\text{O}_4$  during processing. The photocurrents in the coatings,  $J$ , have been tested

<sup>14</sup> This effect consists of the diffusion of electrons from the ‘hot’ regions in a semiconductor to the ‘colder’ regions, resulting in the generation of an electromagnetic force.

<sup>15</sup> Defined as ‘acceleration of a carrier in an electric field’.

**Table 8.32** Electric conductivity of zirconia stabilized with different oxides and plasma sprayed in air and under vacuum (see also Figure 8.39)

Number	Reference	Coatings characteristics			Remarks
		Chemical composition	Porosity (%)	Density (kg/m <sup>3</sup> )	
1	Scagliotti <i>et al.</i> , 1988	ZrO <sub>2</sub> + 12 wt% Y <sub>2</sub> O <sub>3</sub>	—	—	Post-spray treatment
2	Renouard-Vallet <i>et al.</i> , 2004	Up to 10	—	—	—
3	Scagliotti <i>et al.</i> , 1988	ZrO <sub>2</sub> + 19 wt% Y <sub>2</sub> O <sub>3</sub>	—	5800	Cubic Post-spray treatment
5	Lang <i>et al.</i> , 2001	ZrO <sub>2</sub> + 10 mol% Sc <sub>2</sub> O <sub>3</sub>	Vacuum plasma-spraying 1.5–2.5	—	—
6	Renouard-Vallet <i>et al.</i> , 2004	ZrO <sub>2</sub> + 12 wt% Y <sub>2</sub> O <sub>3</sub>	—	—	—

and found to be proportional to the light intensity,  $q$ , following the relationship:

$$J \propto q^\gamma \quad (8.4)$$

The coefficient was in the range  $\gamma = 0.86\text{--}1$ . Another semiconducting material is thermally sprayed  $\text{TiO}_2$ . The electrical properties of  $\text{TiO}_2$  were discussed, e.g. by Ohmori *et al.* (1991) and Tomaszek *et al.* (2006). Ramachandran *et al.* (1998) studied the properties of  $\text{TiO}_2$  alloys with  $\text{Al}_2\text{O}_3$  at different temperatures. The DC resistivity of such coatings decreases with the oxygen loss in the sprayed coatings. This loss of oxygen creates vacancies which contribute to the conduction. Addition of hydrogen to the plasma or flame-forming gases would enhance the oxygen loss. The DC resistivity of air-plasma sprayed rutile was reported by Ohmori *et al.* (1991) to be in the range  $\rho = 0.1\text{--}1 \Omega \text{ cm}$ , depending mainly on the  $\text{Ti}_2\text{O}_3$  content in the sprayed coatings. The AC impedance of suspension-plasma sprayed rutile, described in Chapter 6, Section 6.3.1, and having the phase composition shown in Chapter 6, Figure 6.21(b), corresponds to the *equivalent circuit* shown in Figure 8.40.

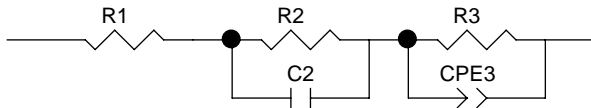


Figure 8.40 Equivalent circuit describing the AC impedance of suspension-plasma sprayed rutile (Tomaszek *et al.*, 2006)

The electrical equivalent circuit is typical for composite materials having well-crystallised grains, which are dielectric rutile and anatase, immersed in a disordered/amorphous electrically conducting matrix, the latter being highly disordered Magnéli-phases and impurities. The resistance  $R_1$  represents the matrix, close to the electrode region of the substrate (Au screen-printed electrodes were used). The overall impedance of the conductive matrix is represented by the branch identified by  $R_2$  and  $C_2$ . The branch  $R_3$  and  $\text{CPE}_3$  represents the grain (rutile and anatase) bulk. The element  $\text{CPE}_3$  has the character of a ‘loss-less’ capacitor. The current in the sample structure flows through the matrix (Magnéli-phases). The conductance, which is an inverse of the sum of

all resistances of the equivalent circuit shown in Figure 8.40, measured at different frequencies and temperature is shown in Figure 8.41.

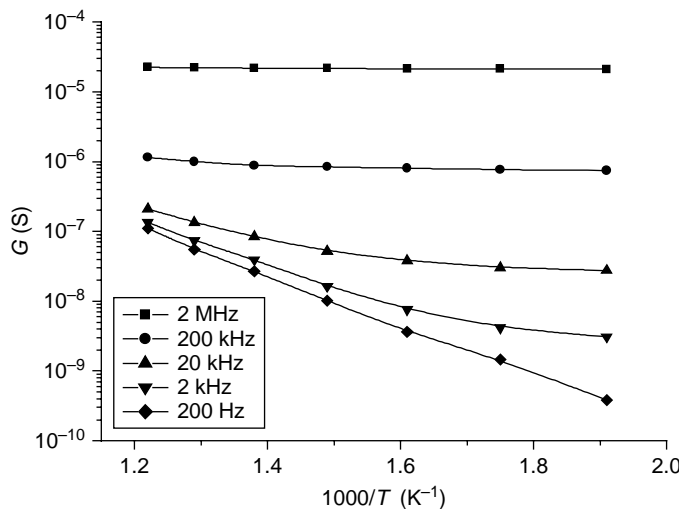


Figure 8.41 Arrhenius plots of the conductances at different frequencies and temperatures for coatings of suspension-plasma sprayed  $\text{TiO}_2$  (Tomaszek *et al.*, 2006)

The temperature dependence of the resistivity for all tested samples was characteristic for semiconductors, i.e. the resistance decreased with temperature. Alumina samples alloyed with 13 and 40 wt% titania are also semiconductors in the temperature range from RT to 650 K. In this temperature range, the resistivity of the coatings decreases, as shown in Figure 8.42. The resistivity starts to increase at higher temperatures which is typical for metals.

The evolution of resistivity can be explained by the ‘picking-up’ of oxygen from the surroundings by ‘under-stoichiometric’  $\text{TiO}_2$  observed in the coatings at temperatures above 650 K (Ramachandran *et al.*, 1998). Consequently, the oxygen atoms fill the vacancies and titania becomes crystallized in the rutile phase which is a ‘high-resistivity’ dielectric. The evolution of resistivity with time at 673 K confirms this explanation (Figure 8.43).

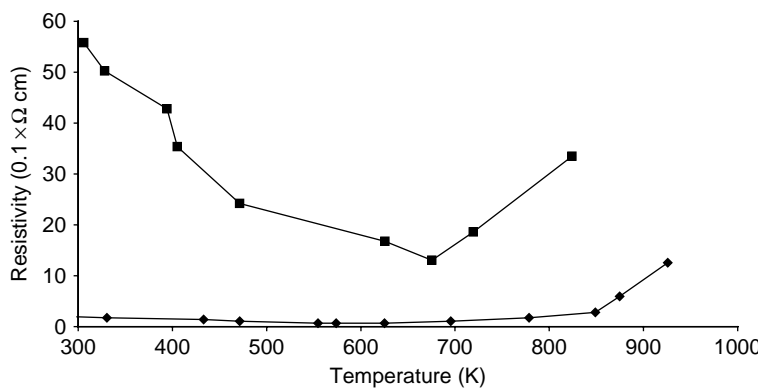


Figure 8.42 Electrical resistivity versus temperature of alloy coatings of atmospheric-plasma sprayed  $\text{Al}_2\text{O}_3 + 13 \text{ wt\% TiO}_2$  (■) and  $\text{Al}_2\text{O}_3 + 40 \text{ wt\% TiO}_2$  (◆) (Ramachandran *et al.*, 1998). This article was published in *Thin Solid Films*, 315, K. Ramachandran, V. Selvarajan, P.V. Ananthapadmanabhan and K.P. Sreekumar, ‘Microstructure, adhesion, microhardness, abrasive wear resistance and electrical resistivity of plasma-sprayed alumina and alumina–titania coatings’, 144–152, Copyright Elsevier (1998)

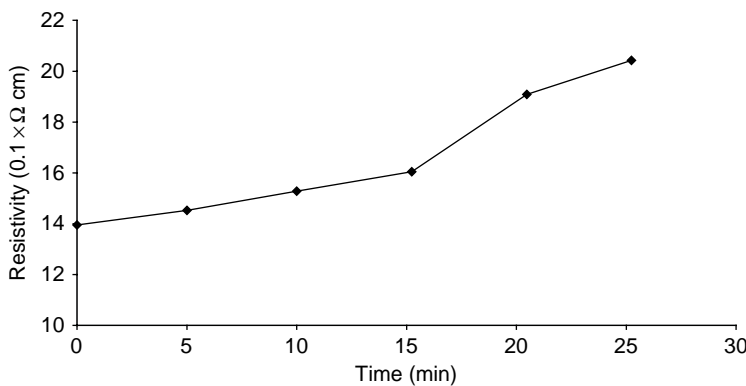


Figure 8.43 Evolution of the electrical resistivity with time of annealing at 673 K for a plasma-sprayed  $\text{Al}_2\text{O}_3 + 13 \text{ wt\% TiO}_2$  coating (Ramachandran *et al.*, 1998). This article was published in *Thin Solid Films*, 315, K. Ramachandran, V. Selvarajan, P.V. Ananthapadmanabhan and K.P. Sreekumar, ‘Microstructure, adhesion, microhardness, abrasive wear resistance and electrical resistivity of plasma-sprayed alumina and alumina–titania coatings’, 144–152, Copyright Elsevier (1998)

The activation energies of titania and its alloys in the semiconducting range were calculated by:

- Tomaszek *et al.* (2006) in the low-temperature region for suspension-plasma sprayed  $\text{TiO}_2$  to be in the range 0.46–0.66 eV at a frequency of  $f = 100 \text{ Hz}$ .
- Ramachandran *et al.* (1998) for air-plasma sprayed  $\text{Al}_2\text{O}_3 + 13 \text{ wt\% TiO}_2$  and  $\text{Al}_2\text{O}_3 + 40 \text{ wt\% TiO}_2$  to be in the range  $1.38 - 1.62 \times 10^{-3} \text{ eV}$  or  $0.90 - 1.23 \times 10^{-3} \text{ eV}$ , respectively, under DC conditions.

#### 8.4.2 PROPERTIES OF RESISTORS

Smyth and Anderson (1975) carried out a detailed study on an air-plasma sprayed mixture of  $\text{NiO}$  with  $\text{Fe}_3\text{O}_4$  powder. The sprayed coatings had resistivities in the range  $\rho = 10^3 - 10^5 \Omega \text{ cm}$ , depending on the operational spraying parameters and the composition of the powder used for spraying. The optimal composition was found to be  $\text{NiO} + 45 \text{ wt\% Fe}_3\text{O}_4$ . The thermal coefficient of resistance of these resistors varied from  $TCR = -8$  to  $+20 \text{ } 1/\text{K}$  and the resistance change after 10 000 h of the test at  $T = 423 \text{ K}$  was about  $\Delta R/R = -5\%$ . The authors summarized the best resolutions achieved during manufacturing of these resistors with the use of photolithography (see Chapter 2, Section 2.5):

- minimum width of conducting path— $50 \mu\text{m}$ ;
- minimum separation for parallel paths— $80 \mu\text{m}$ .

A comparison of ‘quality’ plasma-sprayed resistors with printed resistors has been carried out by Anderson *et al.* (1973) by testing the generated electrical noise. These measurements revealed that sprayed resistors generated more noise than the printed and ‘fired’ ones. The idea of application of plasma-sprayed particulate composites, such as  $\text{W} + \text{Al}_2\text{O}_3$ , to manufacture resistors was initiated by Pawlowski (1974) and, later on, developed by Taylor *et al.* (1989). These authors tested composites based on:

- $\text{Al}_2\text{O}_3$  with  $\text{W}$ ,  $\text{Mo}$ ,  $\text{Cu}$  or  $\text{Ni}$ ;
- $\text{ZrO}_2 + 13 \text{ wt\% Y}_2\text{O}_3$  with  $\text{Ni}$  or  $\text{W}$ .

All of the composites were sprayed by the use of ‘double-powder feeders’ for the simultaneous delivery of ceramic and metal component. The

tested coatings indicated a similar behaviour for the curve of resistivity versus volume of metal, namely for:

- a small concentration of the metal, the resistivity was close to that of the ceramic;
- a slightly greater metal content, the resistivity slowly decreases until the metallic particles in the coating start to become interconnected;
- such a concentration at which the metallic particles become interconnected, the resistivity is close to that of the metal component.

The composite coatings were designed for hot-water-tank heaters and could withstand electric loads up to  $q = 80 \text{ kW/m}^2$  and temperature up to  $T = 770 \text{ K}$ . Finally, Borisov *et al.* (1998) tested the resistivity of magnetic alloys based on iron and nickel. For example, plasma-sprayed Ni + 10 wt% P alloy coatings were found to indicate resistivities of  $\rho = 135$  to  $250 \mu\Omega \text{ cm}$ . The alloys were mainly amorphous and their resistivities mainly depended on the coatings' resistivities.

#### 8.4.3 PROPERTIES OF DIELECTRICS

##### $\text{Al}_2\text{O}_3$

The dielectric properties of thermally sprayed alumina are collected in Table 8.33. The sprayed material crystallizes in the  $\gamma$ -phase. Müller and Kreye (2001) tried to spray alumina alloyed with chromia, expecting to obtain a coating crystallizing in the  $\alpha$ -phase (entries 4 and 5 in Table 8.33). Unfortunately, they did not succeed. The  $\gamma$ -phase is highly hygroscopic which may lead to an increase in the dielectric constant of alumina coatings<sup>16</sup> and thus the dielectric constant and loss factor of such a material might be high. The resistivities of the alumina coatings also depend on their microstructures, operational processing parameters and morphology of the initial powder (Pawlowski, 1988). For practical applications, alumina coatings should be sealed with e.g. silicone or epoxy resins. The dielectric strength mostly depends on the porosity of the sprayed alumina and on the size of the pores. Sintered alumina has a dielectric strength as high as  $700 \text{ kV/cm}$ , while the air entrapped in

<sup>16</sup> Sintered alumina is characterized by  $\varepsilon_r = 9$  at 1 kHz and 300 K, which is generally lower than 10, while water has a dielectric constant of  $\varepsilon_r = 78$  at 1 kHz and 300 K.

Table 8.33 Electrical properties of alumina and alumina–chromia coatings thermally sprayed using different techniques

Number	Reference	Coating characteristics						
		Chemical composition (wt%)	Temperature range (K)	Frequency range (Hz)	Resistivity ( $\Omega$ cm)	Dielectric constant	Loss factor	Dielectric strength (kV/cm)
<i>Atmospheric plasma-spraying</i>								
1	Pawlowski, 1988	Al <sub>2</sub> O <sub>3</sub>	300	0–10 <sup>3</sup>	10 <sup>10</sup> –10 <sup>15</sup>	5–8	0.01–0.5	100–175
2	Brown <i>et al.</i> , 1986			10 <sup>2</sup> –10 <sup>6</sup>	—	9–37	0.01–0.1	—
3	Smyth and Anderson, 1976			0–10 <sup>3</sup>	—	60–120	80	—
4	Müller and Kreye, 2001	Al <sub>2</sub> O <sub>3</sub> +8Cr <sub>2</sub> O <sub>3</sub>		0 and 2 × 10 <sup>4</sup>	2 × 10 <sup>11</sup> and 2 × 10 <sup>8</sup>	at AC 14	at AC 0.03	At DC 25
5		Al <sub>2</sub> O <sub>3</sub> +20Cr <sub>2</sub> O <sub>3</sub>			2 × 10 <sup>11</sup> and 2 × 10 <sup>8</sup>	At AC 13	at AC 0.28	At DC 25
<i>Flame-spraying</i>								
6	Pirogov <i>et al.</i> , 1966	Al <sub>2</sub> O <sub>3</sub>	300–1000	0–10 <sup>5</sup>	10 <sup>12</sup> –10 <sup>6</sup>	5–24	—	—
<i>High-velocity oxy-fuel spraying</i>								
7	Müller and Kreye, 2001	Al <sub>2</sub> O <sub>3</sub>	300	0 and 2 × 10 <sup>4</sup>	3 × 10 <sup>9</sup> and 3.5 × 10 <sup>8</sup>	at AC 13	At AC 0.0175	At DC 125

the pores has a strength as low as 30 kV/cm (Pawlowski, 1988). Consequently, small pores in less-porous materials promote high dielectric strength.

### Titanates

Two titanates have been extensively tested, i.e. barium titanate and lead-zirconate titanate, known as *PZT* and having the general formula  $\text{Pb}(\text{Zr}_x\text{Ti}_{1-x})\text{O}_3$ , where  $x$  is in the range 0.48–0.66. The titanates are ferroelectric and are characterized by a very high dielectric constant and a phase transformation at the *Curie temperature*. Some selected properties of thermally sprayed titanate coatings are collected in Table 8.34.  $\text{BaTiO}_3$  reportedly lost  $\text{BaO}$ , depending on the plasma-spray conditions (entry 2 in Table 8.34). The phase transition at the Curie temperature did not occur in ‘as-sprayed’ deposits, but annealing at a temperature of 873 K restored this effect (Figure 8.44).

The loss factors of the coatings depend on the porosities of the barium titanate coatings. Porous deposits, plasma-sprayed using coarse powders having particle sizes ranging from 56 to 116  $\mu\text{m}$  and shown in Figure 8.45, have loss factors as high as 1.8 (entry 3 in Table 8.34).

Dense deposits, obtained by high-velocity oxy-fuel spraying using fine powders (particle sizes in the range  $-30 + 5 \mu\text{m}$ ), have loss factors lower by two or even three orders of magnitude (entry 4 in Table 8.34). Lead-zirconate titanate was reported to loose  $\text{PbO}$  upon plasma spraying (entry 5 in Table 8.34). Annealing at temperatures higher than 1074 K in a lead-oxide atmosphere (generated by  $\text{PbO}-\text{PbZrO}_3$  pellets) was reported to partly compensate this deficiency. Again, ‘as-sprayed’ coatings did reveal a phase transition at the Curie temperature and after annealing at temperatures above 823 K, the transition peak appears.

### Other Dielectrics

The dielectric properties of silicates and yttria-stabilized zirconia are collected in Table 8.35. Silicates coatings were sprayed by using a water-stabilized plasma torch by Ctibor *et al.* (2002). These authors observed discrepancies between the dielectric data measured for sprayed coatings and those for sintered ceramics. These were explained by absorption of humidity in the pores and voids and, on the other hand, by the presence of amorphous phases in the coatings. Zirconia, stabilized with

Table 8.34 Electrical properties of titanate coatings thermally sprayed using different techniques

Number	Reference	Spray technique	'As-sprayed' or annealed (conditions)	Coating characteristics				Remarks
				Temperature range (K)	Frequency range (Hz)	Dielectric constant	Loss factor	
<i>Barium titanate (<math>BaTiO_3</math>)</i>								
1	Braguier <i>et al.</i> , 1973	Air-plasma spraying	'As-sprayed'	RT	—	400–600	0.06–0.09	100–150
2	Elyard <i>et al.</i> , 1975	Annealed at 1473 K for 16 h in air			1080	—	—	$T_s = 973\text{--}1173\text{ K}$ 2–3 % of barium was lost by evaporation during processing
3	Malewski and Pawłowski, 1981	—	'As-sprayed' and annealed at 873 K for 4 h in air	RT–410	$10^3$	Figure 8.44 'as-sprayed': 0.32–1.8; annealed: 0.5–1.0	At RT, —	Microstructure shown in Figure 8.45

4	Dent <i>et al.</i> , 2000	High-velocity combustion spraying	'As-sprayed'	RT	$10^4$	24–115
5	Häßter <i>et al.</i> , 1993	Air-plasma spraying	Annealed at $T = 973\text{--}1273\text{ K}$ in PbO-rich atmosphere	RT	$10^3$	'As-sprayed'; 180; annealed: 230–420
6	Häßler <i>et al.</i> , 1995			—	'As-sprayed'; 225–325; annealed: 475–850	— — —

*Lead-zirconate-titanate ( $\text{Pb}(Zr_x\text{Ti}_{1-x})\text{O}_3$ ,  $x = 0.48\text{--}0.66$ )*

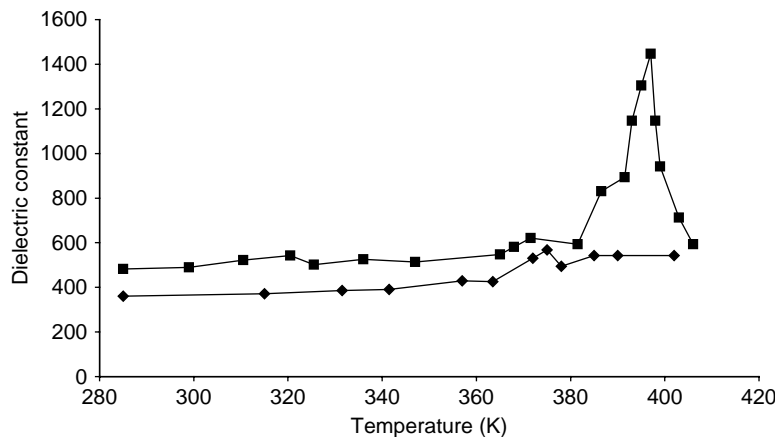


Figure 8.44 Dielectric constant versus temperature of an air-plasma sprayed  $\text{BaTiO}_3$  coating, 'as-sprayed' (◆) and after annealing at 873 K for 4 h in air (■) (Malewski and Pawlowski, 1981)

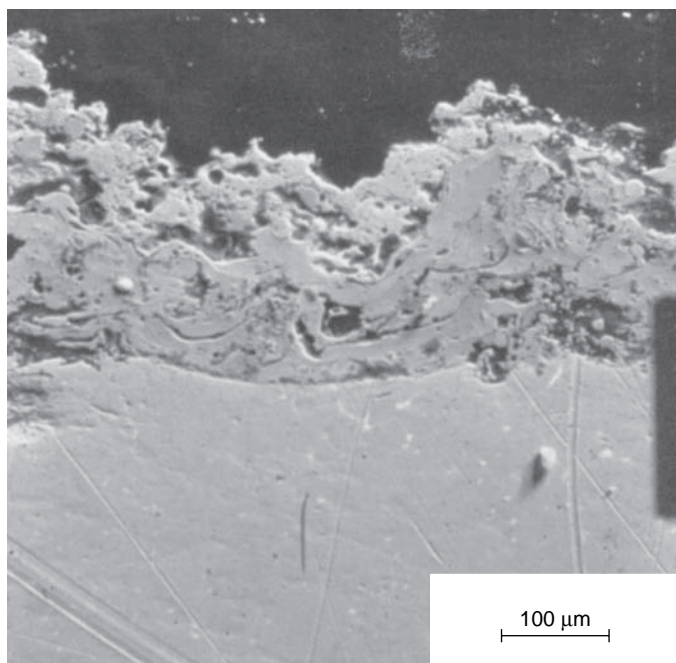


Figure 8.45 Scanning electron micrograph (secondary electrons) of a cross-section of the  $\text{BaTiO}_3$  coating described in Table 8.34 (entry 3), sprayed onto an NiAl intermediate coating and a *kovar* alloy substrate (the latter is an alloy composed of Fe + 26–29.2 wt% Ni + 17.3–23 wt% Co + 0.04 wt% Mn, having a small thermal expansion coefficient)

Table 8.35 Dielectric properties at room temperature of air-plasma sprayed silicates and yttria-stabilized zirconia

Number	Reference	Chemical formula or composition (wt%)	Coating properties				Remarks
			Frequency range (Hz)	Resistivity ( $\Omega$ cm)	Dielectric constant	Loss factor	
<i>Silicates</i>							
1	Cribor <i>et al.</i> , 2002	3Al <sub>2</sub> O <sub>3</sub> .3SiO <sub>2</sub> (Mullite) Mullite + 15 glass (mechanical mixture)	10 <sup>6</sup>	5.34 × 10 <sup>8</sup>	6.7	2.6 × 10 <sup>-3</sup>	7.8
2		Mg <sub>2</sub> SiO <sub>4</sub> (Olivine–Forsterite)	2.28 × 10 <sup>8</sup>	10.2	5 × 10 <sup>-3</sup> at 7 × 10 <sup>4</sup> Hz	4.2	Electric field applied perpendicular to the coating surface
3		MgO.SiO <sub>2</sub> (Steatite) mineral, having a composition close to that given	3.87 × 10 <sup>7</sup>	14.7	1.6 × 10 <sup>-2</sup>	4.4	
4		Li <sub>2</sub> O.Al <sub>2</sub> O <sub>3</sub> . 4SiO <sub>2</sub> (Spodumene)	1.99 × 10 <sup>7</sup>	6.0	3 × 10 <sup>-3</sup>	—	
5		MgO.SiO <sub>2</sub> (Steatite)	8.08 × 10 <sup>4</sup>	10.3	8.3 × 10 <sup>-3</sup>	3.7	
<i>Yttria-stabilized zirconia</i>							
6	Chiadelli <i>et al.</i> , 1988	ZrO <sub>2</sub> + (12–19)Y <sub>2</sub> O <sub>3</sub>	10 <sup>6</sup>	See Figure 8.39	30–34	—	—

12–19 wt%  $\text{Y}_2\text{O}_3$ , was deposited by air-plasma spraying by Chiodelli *et al.* (1988) and its properties are shown in entry 6 of Table 8.35.

#### 8.4.4 ELECTRIC FIELD EMITTERS

A macroscopic electric field, acting between the electrodes (the cathode is the electron emitter), is enhanced in the neighbourhood of the protrusions or irregularities on the emitting surface and/or around small conducting grains inside the dielectric. The field which extracts the electrons is often called the *local field*,  $E$  (Znamirowski *et al.*, 2004). The relationship between the local and macroscopic fields is given in Chapter 7, Equation (7.31), while *Fowler–Nordheim* relationship describes the relation between the field-electron-current density and the field:

$$j = A \frac{E^2}{\Phi} \exp\left(B \frac{\Phi^{1.5}}{E}\right) \quad (8.5)$$

In the above,  $A$  and  $B$  are constants and  $\Phi$  is the work function of the electrons. A few technologies and materials have been tested by the research groups of Dr Znamirowski at the Wrocław University of Technology, Poland and Professor Pawłowski at the Ecole Nationale Supérieure de Chimie de Lille, France to realize electron-emitting coatings:

- Plasma-sprayed and laser-engraved  $\text{Cr}_2\text{O}_3$  covered by a titanium thin layer obtained by PVD (Znamirowski *et al.*, 2003a,b). The radius of the emitting sites was estimated to be in the range of 6 to 9 nm. The sites were tentatively attributed to small chromia crystals, ‘resolidified’ from the laser-generated melt.
- Plasma-sprayed and laser-engraved  $\text{TiO}_2$ , as well as  $\text{Al}_2\text{O}_3 + 13$  wt%  $\text{TiO}_2$  and  $\text{Al}_2\text{O}_3 + 13$  wt%  $\text{TiO}_2$  alloys (Znamirowski *et al.*, 2004). The greatest emission current of  $25 \mu\text{A}$  was measured for a plasma-sprayed  $\text{TiO}_2$  coating, laser-engraved with a linear cell density of  $LD = 60 \text{ cm}^{-1}$  (see Chapter 4, Section 4.1.1). The emitting sites were hypothetically attributed to electrically conducting grains (Magnéli-phases) inside the dielectric matrix.
- Suspension-plasma sprayed  $\text{TiO}_2$  coatings (Tomaszek *et al.*, 2005, 2006). Typical curves of electron emission versus macroscopic electric field show slight increases in the current with time (Figure 8.46). The

emitting sites were, again, conducting grains of ‘sub-stoichiometric’ Magnéli-phases inside the dielectric matrix of stoichiometric TiO<sub>2</sub> (see Section 8.4.1).

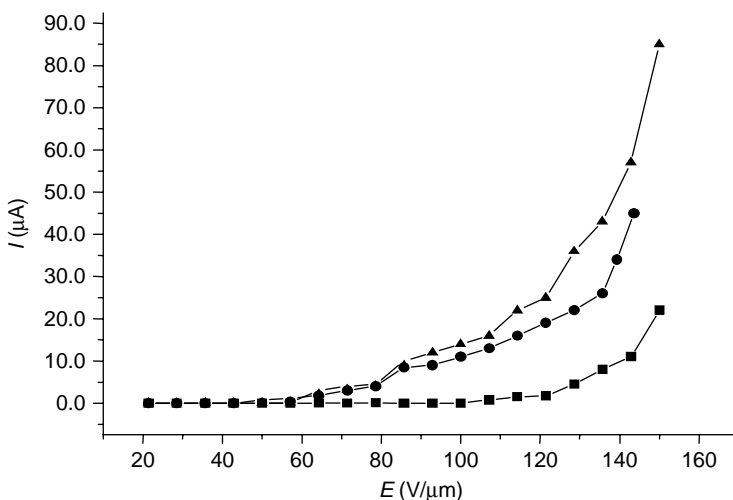


**Figure 8.46** Electron emission versus macroscopic electric field with time for suspension-plasma sprayed TiO<sub>2</sub> coatings: ■, initial; ●, after 3 h; ▲, after 4 h (Tomaszek *et al.*, 2005)

#### 8.4.5 PROPERTIES OF SUPERCONDUCTORS

Our description of thermally sprayed superconductors will be limited to two characteristic high- $T_c$  superconductors, namely  $\text{YBa}_2\text{Cu}_3\text{O}_x$  and  $\text{Bi}-\text{Sr}-\text{Ca}-\text{Cu}-\text{O}$  (having stoichiometries of 2-2-1-2-8 and 2-2-2-3-10, respectively). An excellent introduction to high-temperature superconductors has been provided by Almond (1989).

YBa<sub>2</sub>Cu<sub>3</sub>O<sub>7-x</sub>

'As-sprayed' coatings from orthorhombic  $\text{YBa}_2\text{Cu}_3\text{O}_{7-x}$  powders have a simple cubic phase with a lattice constant of  $a = 0.2982 \text{ nm}$  found by Pawłowski *et al.* (1990) or  $a = 0.701 \text{ nm}$  reported by Neiser *et al.* (1989). Heintze and McPherson (1988) and Pawłowski *et al.* (1991) reported on the loss of copper during spraying and reduction of the oxide (from 7 to 5.8 oxygen atoms per molecule). As superconductivity

occurs only at a composition of  $\text{YBa}_2\text{Cu}_3\text{O}_{7-x}$  with  $x < 0.37$  and with the othorhombic phase (O'Bryan and Gallagher, 1987) it is necessary to anneal the 'as-sprayed' coatings at temperatures of  $T = 900\text{--}1200\text{ K}$  in air or oxygen. Microstructures of the coatings, before and after heat treatment, are shown in Chapter 6, Figure 6.26. The greatest critical current density values, measured at  $T = 77\text{ K}$ , without an external magnetic field, were reported to be:

- $j_c = 690 \text{ A/cm}^2$  in vacuum-plasma sprayed deposits, obtained by Tachikawa *et al.* (1988);
- $J_c = 460 \text{ A/cm}^2$  in air-plasma sprayed coatings, obtained by Pawlowski *et al.* (1990).

### Bi–Sr–Ca–Cu–O

The Bi–Sr–Ca–Cu–O high-temperature superconductor has been sprayed in air (Asthana *et al.*, 1988) and under vacuum (Lugscheider and Weber, 1989). The 'as-sprayed' material was *not* a superconductor. Heat treatment at a temperature of at least 1053 K proved necessary to restore the superconductivity. Optimal heat treatment temperatures, enabling restoration of the 2–2–2–3–10 phase (with a  $T_c$  of about 110 K), seems to be 1123–1133 K. Stabilization of this phase might be achieved with 'Pb doping' (Chandler, 1989). However, this element was reported by Lugscheider and Weber (1990) to evaporate during spraying. These authors found that the critical current density at 55 K was about  $j_c = 50 \text{ A/cm}^2$ .

As the critical current density necessary for most of the applications of superconductors (magnets, large machines, etc.) must be at least  $10^4 \text{ A/cm}^2$ , the thermal spray technology of high-temperature superconductors has not yet proved successful enough to be considered as a viable approach.

## 8.5 MAGNETIC PROPERTIES

### 8.5.1 SOFT MAGNETS

The following thermally sprayed 'soft magnets' have been tested.

*Ferrites*, which have a general chemical formula of  $\text{MeFe}_2\text{O}_4$  in which Me can be a single metal, such as Ni, Li and Fe, or 'metal pairs', as such

$\text{Ni}_x\text{Zn}_{1-x}$  or  $\text{Mg}_x\text{Mn}_{1-x}$ . Different types of thermally sprayed ferrites have been tested over more than the last 30 years. Harris *et al.* (1969) tested APS-deposited MgMn ferrites. After annealing, the coercivity of the ferrites was in the range  $H_c = 1.2\text{--}1.8$  Oe and was the same as for the bulk material. Belt and Florio (1972) reported on the flame-sprayed ferrite,  $\text{Ni}_{0.52}\text{Zn}_{0.48}\text{Fe}_2\text{O}_4$ . This material was prepared by spraying a methanol solution of the ferrite and subsequent ‘hot-pressing’ at temperatures of 1300–1500 K. These authors found permeability values of  $\mu_r = 20\text{--}100$ . In the early 1970s, suspension-plasma sprayed ferrites were studied intensively at the Wolfson Centre for Magnetic Technology, Cardiff, UK and presented in the following papers: Andrews and Preece (1973), Preece and Andrews (1973), Andrews and Fuller (1974, 1975) and Andrews *et al.* (1974). The tested ferrites were Ni and NiZn. These authors reported on the Zn loss during spraying. Consequently, in order to obtain sprayed coating having a composition of  $\text{Ni}_{0.5}\text{Zn}_{0.5}\text{Fe}_2\text{O}_4$ , the powders used to spray were richer in zinc ( $\text{Ni}_{0.5}\text{Zn}_{0.64}\text{Fe}_2\text{O}_4$ ). As oxygen was also lost during processing, post-spray annealing at  $T = 1500$  K for 1 h was used to restore oxygen stoichiometry. The permeability of the NiZn ferrite after annealing was  $\mu_r = 33$  and of the Ni ferrite,  $\mu_r = 7\text{--}11$ . The coercivity,  $H_c$ , of the sprayed and annealed nickel ferrite was  $H_c = 17\text{--}36$  Oe. Babbit (1976) tested air-plasma sprayed and annealed Li-ferrite. The reported coercivity was in the range  $H_c = 1.6\text{--}2.1$  Oe. Bamberskij *et al.* (1978) reported the losses of Zn while plasma-spraying NiZn ferrites. The initial powder-weight ratio of  $\text{ZnO}/\text{NiO}$  of 2.3 decreased to 1.6 in the sprayed coating. The oxygen loss of the intial oxides resulted in a very small resistivity of the ‘as-sprayed’ material and the tested sample had a resistance of only a few ohms. Annealing in air 1560 K proved necessary. After annealing, the ferrites had a coercivity of 1.8 Oe and a resistance in the megaohms range. Dooling and Cook (1991) used XRD and Mössbauer spectroscopy to investigate the phase changes in plasma-sprayed NiZn ferrites. They discovered that nearly 40 % of the total iron in the coating reduces to  $\text{Fe}^{+2}$  and annealing at a temperature of 950 K enabled oxidization of the iron back to  $\text{Fe}^{+3}$ , thus restoring the magnetic properties of the sprayed ferrite.

**Iron alloys with silicon, boron and niobium** have been tested more recently. Borisov *et al.* (1998) found that air-plasma sprayed coatings of composition Fe + 46 wt% Ni + 5.1 wt% B had slightly lower values of the coercivity and of the relative magnetic permeability than those of the bulk amorphous material. Post-spray annealing (presumably in air) at temperature of  $T = 620$  K and higher made it possible to obtain similar magnetic properties. The ‘voluminous’ PhD thesis of Cherigui (2005)

describes, among other aspects, the technology and magnetic properties of FeSi and FeNb alloys sprayed using microcrystalline powders. The obtained values of coercivity for air-plasma sprayed FeSi alloys were as follows:

- $H_c = 4$  Oe for the initial powder;
- $H_c = 6$  Oe for ‘as-sprayed’ deposits.

The coercivity of an HVOF-sprayed FeNb alloy, after post-spray annealing at  $T = 1073$  K for 20 min, enabled the obtaining of a coercivity of  $H_c = 137$  Oe.

### 8.5.2 HARD MAGNETS

Thermally sprayed SmCo<sub>5</sub> magnets have been extensively studied at The Charles Stark Draper Laboratory in Cambridge, MA, USA by Kumar and Das (1979, 1980, 1986, 1987). This material was sprayed by the use of plasma spraying in an argon atmosphere. The post-spraying heat treatment usually included annealing in an argon atmosphere at  $T = 1273$  K for 2 h, followed by a  $T = 1173$  K treatment for 4 h and then aging at  $T = 923\text{--}1073$  K for 6–90 h. The coercivity was found to be in the range,  $H_c = 28\text{--}54$  kOe. These authors discovered that the magnetization increases when the annealing was carried out in hydrogen. Finally, the coatings, when sprayed onto hot substrates, enabled formation of the aligned structure, which allowed the obtaining of a maximum energy product of  $HB_{\max} = 9.3$  MG Oe.

An Fe<sub>76</sub>Nd<sub>16</sub>B<sub>8</sub> alloy was deposited using vacuum-plasma spraying by Overfelt *et al.* (1986). These authors found coercivity values in the range  $H_c = 5.8\text{--}10.9$  kOe.

## 8.6 OPTICAL PROPERTIES

Thermally sprayed coatings have a granular microstructure and include an intrinsic porosity. Their surfaces are generally rough. Such a microstructure does not match well to any optical applications and atomistic deposition techniques, such as PVD, are mainly used to obtain optically functional coatings (Pawlowski, 2003). On the other hand, sprayed coatings are attractive because of the easy deposition of any material on large surfaces. They can be easily used for decorative purposes.

### 8.6.1 DECORATIVE COATINGS

Many sprayed oxides are wear-resistant and, on the other hand, have ‘interesting colours’. Some examples of materials and processes include the following:

- **Copper oxide** was applied by flame spraying onto a glass substrate by Eerola (1993). This process enabled the author to obtain red ( $\text{Cu}_2\text{O}$ ) and black ( $\text{CuO}$ ) deposits.
- **Different oxides** were applied by air-plasma spraying by Douglas (1993) in order to obtain coating having the following colours:
  - $\text{Al}_2\text{O}_3$ , – white;
  - $\text{TiO}_2$  – grey;
  - $\text{Al}_2\text{O}_3$  alloyed with  $\text{TiO}_2$  – blue;
  - $\text{Cr}_2\text{O}_3$  – black;
  - $\text{ZrO}_2$  – yellow.

### 8.6.2 OPTICALLY FUNCTIONAL COATINGS

A number of studies on optically functional coatings have been made recently at the Centro Siluppo Materiali, Rome, Italy by research group of Dr Tului on optically selective coatings. The motivation to this work was the development of coatings having a high absorption (and emission) at wavelengths ranging from  $\lambda = 0.3\text{--}2.0 \mu\text{m}$  and low absorption (and emission) in the infrared region of  $\lambda = 2\text{--}25 \mu\text{m}$ . The following materials and technologies have been tested:

- a **zirconium diboride**,  $\text{ZrB}_2$ , powder was prepared by agglomeration of fine ( $2 \mu\text{m}$ ) precursors by the spray-drying method and then plasma-sprayed in air in an argon atmosphere (Tului *et al.*, 2002). The obtained coatings absorbed well in the visible and ir regions of the spectrum and *did not* meet the necessary specifications.
- an **indium tin oxide** (ITO),  $\text{In}_2\text{O}_3 + 10 \text{ wt \% } \text{SnO}_2$ , fine ( $0.5 \mu\text{m}$ ) ‘pre-alloyed’ precursor were agglomerated using spray-drying and plasma-sprayed in air and argon atmospheres (Tului, 2003; Tului *et al.*, 2004). Microstructure analysis of the coatings by X-ray diffraction and electron-dispersive spectroscopy revealed the presence of  $\text{In}_2\text{O}_3$  (feature ‘A’ in Figure 8.47) and metallic In (probably feature ‘B’ in Figure 8.47).

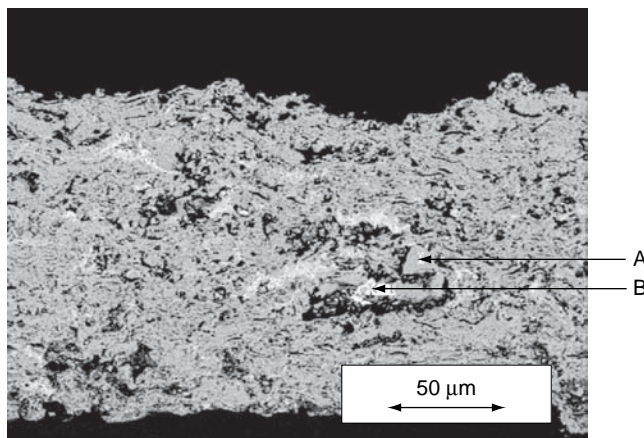


Figure 8.47 Scanning electron micrograph (backscattered electrons) of the cross-section of an indium tin oxide (ITO) coating plasma-sprayed under an argon atmosphere (Tului, 2003)

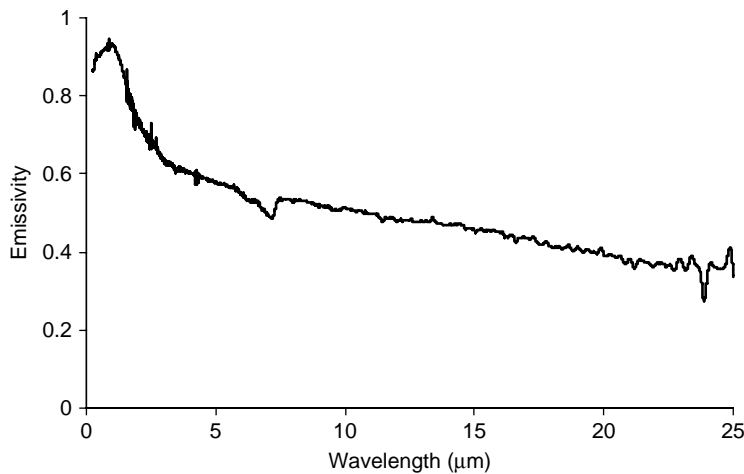


Figure 8.48 Emissivity as a function of wavelength of an inert-atmosphere sprayed indium tin oxide (ITO) coating (Tului, 2003)

The optical behaviour of a sprayed coating (Figure 8.48) revealed emission (close to the optical absorption) close to that specified.

- Aluminum zinc oxide (AZO), i.e. ZnO alloyed with 3 and 22 wt%  $\text{Al}_2\text{O}_3$  fine ( $0.5 \mu\text{m}$ ) precursors agglomerated by spray-drying

and heat-treated in air at 1523 K for 2 h (Tului, 2003). The argon-atmosphere-sprayed coatings revealed the presence of ZnO and  $ZnAl_2O_4$  phases and their optical behaviours were close to that specified.

## 8.7 CORROSION RESISTANCE

'Corrosion' is a generic term that usually describes the oxidation of a metal. This can be understood as the loss of a material in a chemical or electrochemical fashion. In the real conditions of 'coating service', corrosion is usually associated with mechanical wear, such as erosion or abrasion. This is sometimes called *tribocorrosion*. A discussion of corrosion-protective thermally sprayed coatings is easy to consider if one categorizes corrosion as follows:

- **Aqueous corrosion** which describes material loss in an aqueous environment. This corrosion occurs at temperatures close to RT. Coating(s) and substrate(s) form one of the different types of galvanic cells described in Chapter 7, Section 7.6.1.
- **Hot-medium corrosion** which is related to material loss by chemical reactions of the coating or a substrate with gases or liquids at high temperatures (Chapter 7, Section 7.6.2).

### 8.7.1 AQUEOUS CORROSION

Metals and alloys have traditionally been used to protect steel against such a type of corrosion. Increasingly, however, composite coatings are being used. The composites include:

- particulate composites that include a hard phase (carbides, oxides) which renders the coating resistant against wear and a metal (alloy) matrix which assures wet-corrosion resistance;
- multilayer composites, such as bi-layer *duplex* composites which include two (or more) coatings having different functions.

Ceramic coatings have been tested for protection against wet corrosion, especially biomedical coatings tested in *simulated body fluids* (SBFs) which have compositions similar to those of human-body blood plasma.

## Metals

Titanium, aluminium, tantalum and niobium are the metals which have been most frequently tested against wet corrosion. The results from anodic polarization tests are summarized in Table 8.36. Some coatings were tested for resistance against salt-water corrosion, e.g. aluminium, sprayed using a flame, arc and high-velocity combustion (see entries 1, 2 and 6 in Table 8.36), and titanium, flame-sprayed using a wire and an epoxy resin sealed after deposition (Ishikawa *et al.*, 1997). Niobium and tantalum, plasma-sprayed in vacuum, titanium, plasma-sprayed under a 'shroud' (entries 3–5 in Table 8.36) and titanium, sprayed using the high-velocity combustion method (Wank *et al.*, 2005) were tested against corrosion by condensed acids. Many authors have realized comparative tests of sprayed coatings and bulk metal sheets of the same metal. The sprayed deposits typically have much greater corrosion 'currents' and sometimes do not exhibit a passivation zone. The reason for this behaviour is mainly 'open porosity'. Open pores can be easily penetrated by an electrolyte. The developed surface of the sprayed deposits (roughness) was tested and found to not influence the corrosion behaviour (Schwarz *et al.*, 1997). Penetration of the electrolyte was confirmed by evolution of an open corrosion potential with time, as tested for aluminium coatings sprayed using different techniques (Figure 8.49).

The corrosion potential is related to interaction of the corroding material with the electrolyte (formation of a corrosion-protecting oxide). It took about 200 h to reach a 'steady-state' of this interaction. There are differences in the corrosion potentials of coatings sprayed using different techniques. In fact, aluminium, sprayed using a flame, was less porous than that sprayed using an arc and its corrosion potential was closer to that of an St37 steel substrate ( $U_{corr} = -675\text{ mV}$  under test conditions).

In order to 'densify' the coatings, the following post-spray treatment methods have been used:

- epoxy-resin sealing, by Ishikawa *et al.* (1997);
- e-beam fusion, by Kinos *et al.* (1995).

**Table 8.36** Thermally sprayed metals tested against wet corrosion

Number	Reference	Process	Coating characteristics			Anodic polarization test results (see Chapter 7, Figure 7.33)				Remarks
			Post-spray treatment	Substrate	Chemical composition (wt%)	Porosity (%)	Thickness ( $\mu\text{m}$ )	Water solution	Temperature (K)	
<i>Flame spraying using a wire</i>										
1	Schaeffler <i>et al.</i> , 2003	No	Low-carbon steel, St37	Al, 99.5	3	235	1 mol/l NaCl	303	SCE	$U_{\text{corr}} = -680 \text{ mV}$ for substrate
<i>Arc spraying</i>										
2	Schaeffler <i>et al.</i> , 2003	No	Low-carbon steel, St37	Al, 99.5	11	200	1 mol/l NaCl	303	SCE	$U_{\text{corr}} = -680 \text{ mV}$ for substrate
<i>Vacuum plasma-spraying</i>										
3	Lugscheider <i>et al.</i> , 1985	No	—	Nb	—	250	10 % aqua regia <sup>b</sup>	294	SCE	About 1000
4	Schwarz <i>et al.</i> , 1997	No	St37	Ta	—	600–1500	Mixture, vol% of 50H <sub>2</sub> O + 33HCl + 16.5HNO <sub>3</sub>	293	SCE	About 750
<i>'Shrouded' plasma-spraying</i>										
5	Kinos <i>et al.</i> , 1995	No/ e-beam- fused	Low-alloy steel, AlSi4130	Ti, 99.5	—	—	1N H <sub>2</sub> SO <sub>4</sub> RT (presumably)	Ag/AgCl	About −350	About 1000/1–1
<i>High-velocity oxy-fuel spraying using a wire</i>										
6	Schaeffler <i>et al.</i> , 2003	No	St37	Al, 99.5	2	610	1 mol/l NaCl	303	SCE	$U_{\text{corr}} = -680 \text{ mV}$ for substrate

<sup>a</sup> SCE, saturated calomel electrode.

<sup>b</sup> Mixture of nitric acid and hydrochloric acid.

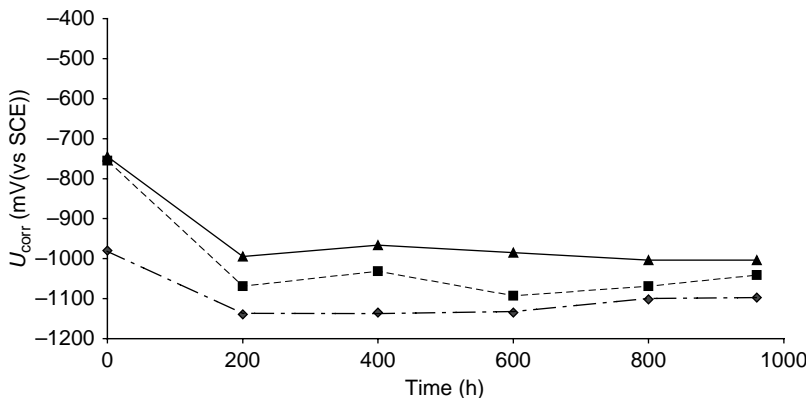


**Figure 8.49** Corrosion potential evolution with time of aluminium coatings thermally sprayed using different techniques, as reported by Schiefler *et al.*, 2003:  $\diamond$ , flame spraying;  $\blacksquare$ , arc spraying;  $\blacktriangle$ , high-velocity oxy-fuel spraying using a wire; SCE, saturated calomel electrode. Further details of the anodic polarization tests are given in Table 8.36. Reproduced by permission of ASM International from M.F.O. Schiefler *et al.*, 2003, ‘Protection of steel components against marine corrosion by thermally sprayed anodic coatings’, in *Thermal Spray 2003: Advancing the Science, Applying the Technology*, C. Moreau and B. Maple (Eds), ASM International, Materials Park, OH, USA, pp. 361–370

## Alloys

Alloyed steels and nickel alloys have been mainly tested against wet corrosion. The results of the polarization tests are summarized in Table 8.37. The most frequently applied method is high-velocity oxy-fuel spraying (entries 2–6 in Table 8.37). The same alloyed-steel coating sprayed using this technique has a more positive corrosion potential than that sprayed using an air plasma (compare entries 1 and 3 in Table 8.37). In contrast, vacuum-plasma sprayed deposits of stainless steel 316L have more positive  $U_{\text{corr}}$  values and smaller passivation currents than that of coatings which are two times thicker, sprayed using the HVOF technique (see entries 6 and 7 in Table 8.37). Consequently, the small porosity of such coatings seems to be a major factor in enhancing the corrosion resistance. This can be achieved by optimization of the spray parameters in such a way that the particles are ‘well-melted’ on impact (Normand *et al.*, 1998). A modern way for such optimization is the use of ‘*in-flight* velocimetry and pyrometry to characterize the particle velocities and temperatures (Lister *et al.*, 2002). Finally, thermally sprayed coatings are less corrosion-resistant than the bulk materials (see entries 6 and 7 in Table 8.37). Their densification by the use of a laser should improve the corrosion behaviour.

**Table 8.37** Thermally sprayed alloys tested against wet corrosion

Number	Reference	Substrate	Coating characteristics			Anodic polarization test results (see Figure 7.33)					Remarks
			Chemical composition (wt%)	Porosity (%)	Thickness (μm)	Water solution	Temperature (K)	Standard electrode <sup>a</sup>	$U_{corr}$ (mV)	$j_{pass}$ ( $\mu\text{A}/\text{cm}^2$ )	
<i>Air plasma-spraying</i>											
1	Orsubo <i>et al.</i> , 2004	—	Fe + 16.2Cr + 30.6Mo + 3.66C + 2B + 0.74Si	—	300–500	1N HCl	303	SCE	−400	About 1000	Amorphous microstructure
<i>High-velocity oxy-fuel spraying</i>											
2	Dorfmann and DeBarro, 1995	Stainless- steel 316L or mild steel	Fe + 17Cr + 11Ni + 2.4Mo + 0.03C	—	—	10 wt% HCl (presumably)	RT	SCE	−398; −403	163; 9 for stainless- steel 316L substrate; −557 for mild-steel substrate −250	— for stainless- steel 316L substrate; 266 for mild steel substrate About 1000 Amorphous microstructure
3	Orsubo <i>et al.</i> , 2004	—	Fe + 16.2Cr + 30.6Mo + 3.66C + 2B + 0.74Si	—	300–500	1N HCl	303	SCE	—	—	—
4	Normand <i>et al.</i> , 1998	Steel	Ni + (27.31)Cr + 9.2Fe + 0.5Si + 0.5Mn + 0.5Cu + 0.1Co	—	—	1N $\text{H}_2\text{SO}_4$	296	Mercurous sulfate electrode	−700	30	Hardness, $HV = 368$

Table 8.37 (Continued)

Number	Reference	Substrate	Coating characteristics			Anodic polarization test results (see Figure 7.33)				Remarks
			Chemical composition (wt%)	Porosity (%)	Thickness (μm)	Water solution	Temperature (K)	Standard electrode <sup>a</sup>	$U_{corr}$ (mV)	
5	Lister <i>et al.</i> , 2002	Stainless-steel 316L	Hastelloy C-22, Ni+13.7Mo+21.1Cr+5.2Fe+3.0W+0.54Si	0.7–2.1	—	10 wt% HCl	RT (presumably)	SCE	About -300	60; 1 for wrought C-22 alloy
6	Siemard and Arsenault, 2003	Stainless-steel 316L	Stainless-steel 316L	—	300	3.5 wt% NaCl	RT (presumably)	SCE	-0.486; -0.189 for stainless-steel 316L substrate	5; 0.8 for stainless-steel 316L substrate
7	Siemard and Arsenault, 2003	Stainless-steel 316L	Stainless-steel 316L	—	150	3.5 wt% NaCl	RT (presumably)	SCE	0.0	0.9

<sup>a</sup> SCE, standard calomel electrode.

## Ceramics

Sprayed ceramic coatings can hardly be used to protect against wet corrosion in the ‘as-sprayed’ state. Intrinsically, ionic oxides, such as alumina, are inert and could provide good protection. Sprayed ceramic coatings have, however, high values of open porosity which considerably reduces the corrosion-protection capacity. This porosity can be reduced by the appropriate post-spray treatment. An example of such a treatment is impregnation with a polymer, as applied by Dianran *et al.* (1997) for air-plasma sprayed 300–400 µm thick alumina coatings onto a steel-type Q235 substrate (Figure 8.50).

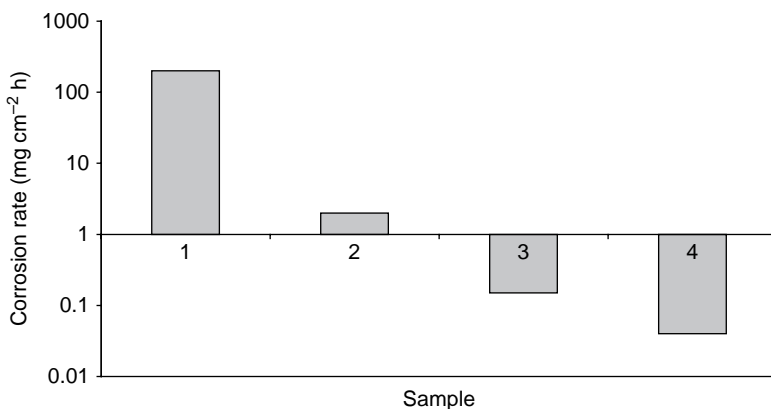


**Figure 8.50** Corrosion rates of steel, with and without an atmospheric-plasma sprayed deposit of alumina ( $\text{Al}_2\text{O}_3$ ), in a boiling solution of 5 % HCl: 1, steel substrate; 2, substrate with an ‘as-sprayed’  $\text{Al}_2\text{O}_3$  coating; 3, substrate with a polymer-impregnated  $\text{Al}_2\text{O}_3$  coating; 4, an  $\text{Al}_2\text{O}_3$  coating without any substrate (Dianran *et al.*, 1997). This article was published in *Surf. Coat. Technol.*, 89, Y. Dianran, H. Jining, W. Jiahjun, Q. Wanqui and M. Jing, ‘The corrosion behaviour of a plasma-sprayed  $\text{Al}_2\text{O}_3$  coating in dilute HCl solution’, 191–195, Copyright Elsevier (1997)

Another important topic related to the interaction between a specific ceramic coating and a liquid concerns biomedical coatings, such as hydroxyapatite, zirconia, titania or *wollastonite*, with a simulated body fluid (SBF). Two liquids are used at present:

- The *Kokubo solution*, as proposed by Kokubo *et al.* (1990), which has a composition close to that of human blood plasma;
- the *Hank’s balanced salt solution* (HBSS), as reported by, e.g. Heiman *et al.* (1998).

The compositions of the solutions used in most papers is collected in Table 8.38, while studies of the interactions of different ceramic coatings immersed in such solutions are reported in Table 8.39. The phenomena occurring in sprayed hydroxyapatite coatings can be summarized in the following way:

- Dissolution of an amorphous phase (ACP) and phases of decomposition, such as TTCP,  $\alpha$ -TCP,  $\beta$ -TCP (entries 1, 2 and 4 in Table 8.39) and CaO (Figure 8.51). The tested coatings and powders treated in a plasma lead to more crystalline hydroxyapatite.
- The precipitation of calcia and carbonates from solution onto the coatings (see entries 3 and 4 in Table 8.39) was observed by using XRD and FTIR spectroscopy. The latter was able to establish ‘dehydroxylation’ of  $\text{OH}^-$  ions into the solution (Haman *et al.*, 1995).

**Table 8.38** Compositions of simulated body fluids

Number	Kokubo solution (after Ohtsuki <sup>a</sup> ), pH = 7.4		Hank's balanced salt solution, pH = 7.0	
	Reactant <sup>b</sup>	Quantity	Reactant <sup>b</sup>	Quantity
1	Ultra-pure water	0.751	Deionized water	1 l
2	NaCl	7.996 g	NaCl	8.0 g
3	NaHCO <sub>3</sub>	0.35 g	MgSO <sub>4</sub>	1.0 g
4	KCl	0.224 g	KCl	0.4 g
5	K <sub>2</sub> HPO <sub>4</sub> .3H <sub>2</sub> O	0.228 g	CaCl <sub>2</sub>	0.14 g
6	MgCl <sub>2</sub> .6H <sub>2</sub> O	0.305 g	MgCl <sub>2</sub>	0.10 g
7	1 kmol/m <sup>3</sup> HCl	40 cm <sup>3</sup>	Na <sub>2</sub> HPO <sub>4</sub>	0.06 g
8	CaCl <sub>2</sub>	0.278 g	K <sub>2</sub> HPO <sub>4</sub>	0.06 g
7	Na <sub>2</sub> SO <sub>4</sub>	0.071 g	—	—
8	(CH <sub>2</sub> OH) <sub>3</sub> CNH <sub>2</sub>	6.057 g	—	—
9	1 kmol/m <sup>3</sup> HCl	To adjust to pH = 7.25 at <i>T</i> = 36.5 °C	—	—

<sup>a</sup> C. Ohtsuki: internet page [<http://mswebs.naist.jp/LABs/tanihara/ohtsuki/SBF/index.html>].

<sup>b</sup> Presented in chronological order of preparation.

Plasma-sprayed ceramic mixtures, including *wollastonite* and titania and zirconia immersed in a simulated body fluid (SBF), showed, after 12 days of test, a precipitation of apatite (see entry 5 in Table 8.39).

**Table 8.39** Interactions of thermally sprayed ceramics with simulated body fluids

Number	Reference	Initial powder		Sprayed coating		Interaction with SBF		Remarks
		Chemical composition (wt%)	Size ( $\mu\text{m}$ )	Spray technique	Crystal phase of 'as-sprayed' coating	Fluid	Duration of soaking	
<i>Hydroxyapatite<sup>a</sup></i>								
1	Kwah <i>et al.</i> , 2002	HA	+20 – 45	Air-plasma spraying	HA, TTCP, CaO, $\beta$ -TCP, $\text{CaCO}_3$ , ACP	Kokubo solution	2, 4, 6, 8, 10 weeks	See Figure 8.51
2	Sun <i>et al.</i> , 2005	—	+10 – 20 and +60 – 80	—	HA, TTCP, $\alpha$ -TCP, ACP	—	1, 2 weeks	Dissolution of ACP, decrease of TTCP and $\alpha$ -TCP
3	Heimann <i>et al.</i> , 1998	—	—	Plasma spraying in air and in vacuum	—	HBSS	1, 2, 4 weeks	Precipitation of calcium phosphates from solution
4	Haman <i>et al.</i> , 1995	—	+15 – 118	High-velocity combustion spraying	HA, $\alpha$ -TCP, $\beta$ -TCP	—	3 h, 3 days, 6 days, 9 days, 12 days, 2 weeks, 3 weeks, 4 weeks, 8 weeks, 12 weeks	XRD and FTIR studies
<i>Wollastonite with titania</i>								
5	Ding <i>et al.</i> , 2004	Wollastonite+ $\text{TiO}_2$	—	Air-plasma spraying	Wollastonite, $\text{TiO}_2$ minor phase	Kokubo solution	12, 14 days	Precipitation of carbonate-containing HA

<sup>a</sup> Crystal phases in sprayed calcium phosphates are discussed in Chapter 6, Section 6.3.1.

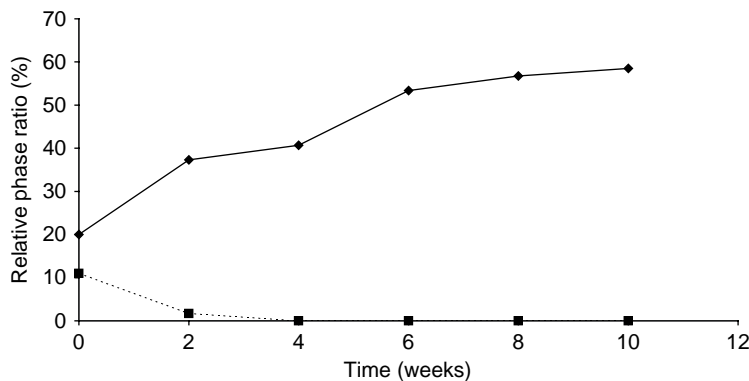


**Figure 8.51** Relative phase ratios of hydroxyapatite ( $\blacklozenge$ ) and calcium oxide ( $\blacksquare$ ) in a calcium phosphate coating in a simulated body fluid (SBF) – a ‘Kokubo solution’ – versus immersion time (Kweh *et al.*, 2002). This article was published in *Biomaterials*, 23, S.W.K. Kweh, K.A. Khor and P. Cheang, ‘An *in vitro* investigation of plasma-sprayed hydroxyapatite (HA) coatings produced with flame-spheroidized feedstock’, 775–785, Copyright Elsevier (2002)

## Composite Coatings

Two types of composite coatings were considered in tests against wet corrosion:

- **Multilayer composites** with two or more layers having different functions. Ishikawa *et al.* (1998) applied a top coating of Al onto a bottom coating of Ni<sub>20</sub>Cr by flame-spraying onto a carbon steel substrate. The coatings were tested against a solution simulating vegetable oil and showed excellent corrosion resistance. The top coating was an anodic and ‘sacrificial’ one, while the bottom coating’s role was to reduce the area to be protected and to enhance adhesion of the entire deposit. Another *duplex* was air-plasma-sprayed onto an S45C steel substrate using a WC + 12 wt% Co (top coating) and an Al + 2 wt% Zn (bottom coating) by Tokaji *et al.* (1996). The configuration was tested against ‘rotating-bending fatigue’ in 3 % NaCl solution and was effective at lower levels of stress (up to 200 MPa).
- **Particulate composite** coatings, namely mixtures of two or more different materials. Cermets with carbides and metal or alloy binders have been most frequently tested against wet corrosion. Some results of these tests are shown in Table 8.40. The particulate composites have to be dense and this is why they are sprayed by using the high-velocity combustion technique. Usually, wet-corrosion resistance is

Table 8.40 High-velocity combustion-sprayed composite coatings tested against wet corrosion

Number	Reference	Substrate	Coating characteristics		Anodic polarization test (see Figure 7.33)			Remarks	
			Chemical composition (wt%)	Thickness (μm)	Water solution	Temperature (K)	Standard electrode <sup>a</sup>		
1	Inaba <i>et al.</i> , 1995	Mild-steel, JIS-SS400	Cr <sub>3</sub> C <sub>2</sub> + 16Ni + 4Cr WC + 20Cr + 7Ni	200	1M NaOH	323	Ag/AgCl	-270	No passivation zone $U_{corr} = -500$ mV for substrate
2								-750	Less than 10 <sup>3</sup>
3	Neville and Hoghness, 1996	Stainless-steel UNS32760 i.e., 3.4C + 2.2Si + 1.3B WC+10Co+4Cr	WC + 50NiCrSiB, Ni + 4.5W + 7Cr + WC+10Co+4Cr	300	Seawater	291/323	SCE	About -400	Very small passivation current, $U_{pirt} = 840$ mV/100 mV
4								-600	Small current/about 80
5	Kirsten <i>et al.</i> , 2005	Low-carbon steel S235RJ	WC+45Cr + 18 (Cr, Ni, Co)	—	1M NaCl	Presumably RT	-233; -266; (-748)	—	$HV_3 = 1260 - 1370$ $U_{corr}$ after 2 h; after 12 h in electrolyte; ( $U_{corr}$ ) for substrate after 2 h in electrolyte
6					0.5M H <sub>2</sub> SO <sub>4</sub>			-236; -255; (-467)	
7					1M NaOH			-307; -281; (-417)	

<sup>a</sup> SCE, standard calomel electrode.

assured by the metal or alloy matrix of the composite. The metals involved are Ni, Cr and Co (entries 1–4, 6 and 7 in Table 8.40) and the alloy NiCrSiB (entry 2 in Table 8.40). The tested electrolytes include basic or acidic water solutions or seawater. A suitable composition which resists all of these media must be an optimized alloy (see entries 5–7 in Table 8.40). A carbide reinforcement is useful in adding wear or abrasion resistance to the ‘corrosion component’ (Guilemany *et al.*, 1998). These types of composites are in ‘competition’ with galvanic chromium coatings (Kirsten *et al.*, 2005).

### 8.7.2 HOT-MEDIUM CORROSION

Studies related to the high-corrosion resistance of coatings have been related to the following applications:

- thermal-barrier coatings used in aeroengines and land-based turbines;
- liquid-metal containers;
- waste incineration plants.

**Thermal-barrier coatings** are usually designed in a duplex configuration with a top layer which is usually yttria-stabilized zirconia and the bottom layer an alloy of MCrAlY ( $M = Ni, Co, Fe$ ). The bottom layer has to be resistant against hot-gas corrosion by oxidation or ‘sulfuration’. The top layer interacts with fuel impurities, such as Na, S, V, pb and P, plus NaCl (salt) from the ‘sea environment’ (Jones, 1997). Degradation of thermal barriers is associated with the following factors:

- Thermal fatigue which results from thermal stresses generated by the thermal fluxes on the components of the barrier which have different thermal expansion coefficients and lead to coating delamination (entry 1 in Table 8.41).
- Oxidation of the bottom alloy coating and formation of simple oxides, such as  $Al_2O_3$ ,  $Y_2O_3$  and  $NiO$ , or ‘double-oxides’, such as  $NiO.Al_2O_3$  and  $Al_5Y_3O_{12}$  (entries 3 and 4 in Table 8.41).
- Oxidation has a *parabolic character* (see Chapter 7, Figure 7.34) in isothermal tests.
- Oxidation results in ‘spallation’ of the coatings in cyclic tests (Figure 8.52).

Cyclic oxidation of thermal-barrier coating leads initially to formation of oxide scales (cycles 1–5 in Figure 8.52) and then to their delamination,

Table 8.41 Hot-medium corrosion behaviour of thermally sprayed coatings

Number	Reference	Coating				Hot-corrosion test				Remarks
		Spray technique	Post-spray	Chemical composition (wt%)	Thickness (μm)	Substrate	Type	Temperature (K)	Atmosphere	
1	Haynes <i>et al.</i> , 1996	VPS	No	Ni + 22Cr + 10Al + 1Y	150	Rene N5	1 cycle: 1420 over 15 min followed by cooling at 360 over 30 min	Air	Delamination after 349 cycles	Duplex TBC
2	Brandl <i>et al.</i> , 1996	APS	Yes	ZrO <sub>2</sub> + 7.5Y <sub>2</sub> O <sub>3</sub>	250	Steel	Isothermal 1323	Air	3 after 350	Formation of oxide 'scales'
3	Brandl <i>et al.</i> , 1997	VPS	No	NiCoCrAlY, including 12Al	—	—	—	He + 10 vol% air	0.7 after 1500	
4	Brandl <i>et al.</i> , 1997	HVOF	No	NiCoCrAlYRe, including 12Al and 3Re	—	—	—	Air	3 after 350	Formation of oxide 'scales'
5	Tsai and Tsai, 1995	APS	No	Ni + 22Cr + 10Al + 1Y	60	Hastelloy-X	Cyclic	1 cycle: 1370 over 1 h followed by cooling at RT over 10 min	Figure 8.52	Duplex TBC
6		Laser treatment		ZrO <sub>2</sub> + 12Y <sub>2</sub> O <sub>3</sub>	220					

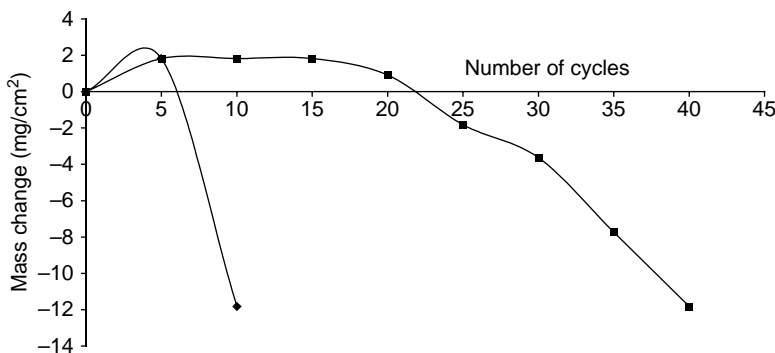


**Figure 8.52** Kinetics of cyclic oxidation for hot-corrosion tests on ‘as-sprayed’ (◆) and sprayed and laser-treated (■) duplex thermal-barrier coatings composed of a YSZ top layer and an NiCrAlY bottom layer (Tsai and Tsai, 1995). This article was published in *Surf. Coat. Technol.*, 71, H.L. Tsai and P.C. Tsai, ‘Performance of laser-glazed plasma sprayed ( $\text{ZrO}_2$ –12 wt %  $\text{Y}_2\text{O}_3$ )/(Ni–22 wt % Cr–10 wt % Al–1 wt % Y) thermal barrier coatings in cyclic oxidation test’, 53–59, Copyright Elsevier (1995)

which decreases their masses (cycles more than 6 for ‘as-sprayed’ coating and cycles more than 27 for sprayed and laser-glazed coatings in this figure). The densification of the top coating by a laser gives a better protection against oxidation of the bottom layer and retards coating delamination.

MCrAlY alloys used for hot-corrosion-resistant coatings should be dense and are usually obtained by using vacuum-plasma spraying (entries 1 and 3 in Table 8.41) or high-velocity oxy-fuel spraying (entry 4 in Table 8.41) (Serghini and Dallaire, 2000). TBCs used in turbines are in contact with corrosive additives which are formed during the combustion of fuel. The additives can be formed from the fuel impurities in the following reactions (Jones, 1997):



These two products are salts and can penetrate, in the molten state, inside the barrier to become in contact with the bottom alloy layer. Longa-Nava *et al.* (1995) tested the corrosion resistance of a CrNiMoSiB alloy against the attack of a molten film mixture of  $\text{V}_2\text{O}_5$ – $\text{Na}_2\text{SO}_4$  at 1173 K. These authors proved that the best corrosion resistance was

shown by coatings plasma-sprayed under vacuum and then post-sprayed by CO<sub>2</sub>-laser treatment.

**Corrosion against liquid metals** was tested by, e.g. Stavros (1996). This author used the D-gun™ and high-velocity oxy-fuel techniques to spray composite coatings with tungsten carbide reinforcements to obtain coatings resistant against molten zinc, held at temperatures of 723–753 K, and a molten Al-Zn alloy, held at temperatures of 863–973 K, for 1000 h. Tungsten-carbide composites with cobalt, sprayed by the detonation-gun technique, were found to resist well against the molten metals.

**Corrosion against molten ashes** was tested by Hidaka *et al.* (1995). These authors tested different alloys coatings with Ni as the major component and Mo, B, Mn, Cu and Si as the minor one. The 300 µm coatings were sprayed by using a plasma in air and the high-velocity oxy-fuel technique onto a stainless-steel substrate and tested in a waste incinerator at temperatures of 1173–1223 K for times ranging from 10 min to 20 days. The coating, sprayed using the alloy (in wt%) of composition Cr + 38Ni + 2.5 Mo + 1Si + 0.5B using the HVOF technique, had the best corrosion resistance among all of the tested samples.

## REFERENCES

- Adachi, M., Tani, K., Harada, Y. and Ogino, K. (2001). Cavitation erosion resistance of Co-based alloy thermally sprayed coatings, in *Thermal Spray 2001: New Surfaces for a New Millennium*, C.C. Berndt, K.A. Khor and E. Lugscheider (Eds), ASM International, Materials Park, OH, USA, pp. 1085–1088.
- Adam, P. (1977). Merkmale thermischer Spritzverfahren und Ihr Einfluß auf die Eigenschaften der Schichten-Verfahrenstechnische Gesichtspunkten, *VDI Ber.*, 333, 97–103.
- Akani, M., Bouree, J.E., Suryanarayanan, R., Rodot, M., Brun, G. and Caymax, M. (1987a). Diffusion length measurements on plasma sprayed polycrystalline silicon substrates and on silicon grown on them by CVD, *Solar Cells*, 22, 97–101.
- Akani, M., Suryanarayanan, R. and Brun, G. (1987b). Resistivity and photoconductivity of plasma sprayed polycrystalline silicon. *Thin Solid Films*, 151, 343–353.
- Alaei, M.S. (1989). Investigation of the oxidation behaviour of plasma sprayed silicon layers, in *Proceedings of the 12th International Thermal Spray Conference*, The Welding Institute, Cambridge, UK, Paper 7.
- Alaei, M.S., Hashemi, T. and Hogarth, C.A. (1983). Plasma sprayed silicon as a possible base material of low cost solar cells, *J. Mater. Sci. Lett.*, 2, 490–494.
- Almond, D.P. (1989). Introduction to high temperature superconductors and the prospects of plasma spraying, in *Proceedings of the 12th International Thermal Spray Conference* The Welding Institute, Cambridge, UK, Paper 101.

- Alonso, F., Fagoaga, I., Liceaga, F. and Oregui, P. (1991). Characterization of plasma sprayed SiC cermets, in *2nd Plasma Technik Symposium*, Vol. 2, S. Blum-Sandmaier, H. Eschnauer, P. Huber, and A.R. Nicoll (Eds), Plasma Technik AG, Wohlen, Switzerland, pp. 175–181.
- Ananthapagmanabhan, P.V., Sreekumar, K.P., Ravidran, P.V. and Venkatramani, N. (1993). Effect of oxygen pick-up on the properties of plasma sprayed diboride coatings. *Thin Solid Films*, **224**, 148–152.
- Anderson, J.C., Smyth, R.T. and Weidmann, E.J. (1973). Third harmonic index measurements on printed and sprayed thick films, in *Proceedings of the Conference on Hybrid Microelectronics*, Canterbury, UK, 25–27 September, pp. 251–258.
- Andrews, C.W.D. and Fuller, B.A. (1974). The deposition of ferrites by arc plasma spraying, *Surf. J.*, **4**, 1–4.
- Andrews, C.W.D. and Fuller, B.A. (1975). The effect of substrate materials and powder type on the properties of plasma sprayed ferrite, *J. Mater. Sci.*, **10**, 1771–1778.
- Andrews, C.W.D. and Preece, I. (1973). Plasma sprayed nickel-zinc ferrites, in *Proceedings of the Conference on Video and Data Recording IERE*, Birmingham, UK, pp. 295–302.
- Andrews, C.W.D., Fuller, B.A. and Preece, I. (1974). Observation of arc-plasma sprayed ferrite films on alumina substrates, *J. Mater. Sci. Lett.*, **9**, 856–858.
- Antou, G., Hlawka, F., Cornet, A., Becker, C., Ruch, D. and Riche, A. (2006). *In situ* laser remelted thermal barrier coatings: thermophysical properties, *Surf. Coat. Technol.*, **200**, 6062–6072.
- Arsenault, B., Immarigeon, J.P., Parameswaran, V.R., Hawthorne, H. and Legoux, J.G. (1998). Slurry and dry erosion of high velocity oxy-fuel thermal spray coatings, in *Thermal Spray, Meeting the Challenges of the 21st Century*, C. Coddet (Ed.) ASM International, Materials Park, OH, USA, pp. 231–236.
- Asthana, A., Han, P.D., Falter, L.M., Payne, D.A., Hilto, G.C. and Van Harlingen, D.J. (1988). Superconducting coatings in the system Bi–Ca–Sr–Cu–O prepared by plasma spraying, *Appl. Phys. Lett.*, **53**, 799–801.
- Babbitt, R.W. (1976). Arc plasma fabrication of ferrite-dielectric composites, *Ceram. Bull.*, **55**, 566–571.
- Bamberskij, M.V., Granik, V.A., Poluszczenko, O.L., Virnik, A.M., Roszczin, B.V., Uspenskij, M.N. and Artemev, N.A. (1978). On transformations of the ferrites by APS, *Fiz. Chim. Obrab. Mater.*, **4**, 49–54 (in Russian).
- Barbezat, G., Hochstrasser, J. and Nicoll, A.R. (1991). Caractérisation et contrôle des revêtements déposés par projection thermique, Plasma Technik, AG, Wohlen, Switzerland, unpublished results.
- Barbezat, G., Nicoll, A. and Sickinger, A. (1993). Abrasion, erosion and scuffing resistance of carbide and oxide ceramic thermal sprayed coatings for different applications, *Wear*, **162–164**, 529–537.
- Bardal, E., Molde, P. and Eggen, T.G. (1973). Arc and flame sprayed aluminium and zinc coatings on mild steel, *Br. Corr. J.*, **8**, 15–19.
- Bardal, E., Eggen, T.G., Rogne, T. and Solem, T. (1995). The erosion and corrosion properties of thermal spray and other coatings, in *Thermal Spraying: Current Status and Future Trends*, A. Ohmori (Ed.), High Temperature Society of Japan, Osaka, Japan, pp. 645–650.
- Bartlett, A.H. and Dal Maschio, R. (1995). Failure mechanism of a zirconia-8 wt% yttria thermal barrier coating, *J. Am. Ceram. Soc.*, **78**, 1018–1024.

- Beczkowiak, J. (1991). Characterization and selection of powders for thermal spraying, in *2nd Plasma Technik Symposium*, Vol. 2, S. Blum-Sandmaier, H. Eschnauer, P. Huber and A.R. Nicoll (Eds), Plasma Technik AG, Wohlen, Switzerland, pp. 323–331.
- Beczkowiak, J., Fischer, J. and Schwier, G. (1993). Cermets für das Hochgeschwindigkeits-Flammspritzen, in *Proceedings of Thermal Spray'93 Conference*, Vol. 152, DVS, Düsseldorf, Germany, pp. 32–36.
- Belt, R.F. and Florio, G.C. (1972). Permeability and temperature coefficient changes in hot pressed flame sprayed NiZn ferrites, *Ceram. Bull.*, **51**, 523–526.
- Berndt, C.C. (1986). Determination of material properties of ceramic coatings, in *Advances in Thermal Spraying*, Pergamon Press, New York, NY, USA, pp. 149–158.
- Berndt, C.C. and Herman, H. (1983). Properties and phase studies of plasma sprayed Y-stabilized zirconia thermal barrier coatings, in *Proceedings of the 10th International Thermal Spray Conference Essen*, Vol. 80, DVS-Berichte, DVS, Düsseldorf, Germany, pp. 175–179.
- Berndt, C.C. and McPherson, R. (1980). A fracture mechanics approach to the adhesion of flame and plasma sprayed coatings, in *Proceedings of the 9th International Thermal Spray Conference*, Nederlands Instituut voor Lastechniek, The Hague, The Netherlands, pp. 310–316.
- Berndt, C.C. and Yi, P. (1987). Strength enhancement of plasma sprayed coatings, in *Thermal Spray: Advances in Coatings Technology*, D.L. Houck (Ed.), ASM International, Materials Park, OH, USA, pp. 297–309.
- Berndt, C.C. and Yi, J.H. (1989). Composite plasma sprayed coatings, in *Proceedings of the 12th International Thermal Spray Conference*, The Welding Institute, Cambridge, UK, Paper 2.
- Bogdanov, A.G., Pirogov, Yu.A. and Makarov, L.P. (1965). Investigation of the effective thermal conductivity and total emissivity of heat resistant ceramic coatings, *Teplofiz. Vys. Temper.*, **3**, 64–69 (in Russian).
- Boire-Lavigne, S., Moreau, C. and Saint-Jacques, R.G. (1995). The relationship between the microstructure and thermal diffusivity of plasma-sprayed tungsten coatings, *J. Therm. Spray Technol.*, **4**, 261–267.
- Boivin, J.C. and Mairesse, G. (1998). Recent material development in fast oxide ion conductors, *Chem. Mater.*, **10**, 2870–2888.
- Borisov, Y., Korzhik, V. and Revo, S. (1998). Electric and magnetic properties of thermal spray coatings with an amorphous structure, in *Thermal Spray: Meeting the Challenges of the 21st Century*, C. Coddet (Ed.), ASM International Materials Park, OH, USA, pp. 687–691.
- Box, G.E.P and Draper, N.R.D. (1987). *Empirical Model Building and Response Surface Methodology*, John Wiley & Sons, Inc., New York, NY, USA.
- Braguier, M., Bejat, J., Tueta, R., Verna, M., Aubin, G. and Naturel, C. (1973). Improvements of plasma spraying processes for hybrid microelectronics, in *Proceedings of Conference on Hybrid Microelectronics*, Canterbury, UK, 25–27 September, pp. 15–37.
- Brandl, W., Grabke, H.J., Toma, D. and Krüger, J. (1996). The oxidation behaviour of sprayed MCrAlY coatings, *Surf. Coat. Technol.*, **86–87**, 41–47.
- Brandl, W., Toma, D., Krüger, J., Grabke, H.J. and Matthäus, G. (1997). The oxidation behaviour of HVOF thermal-sprayed MCrAlY coatings, *Surf. Coat. Technol.*, **94–95**, 21–26.
- Brandon, J.R. and Taylor, R. (1991a). Phase stability of zirconia based thermal barrier coatings, Part I. Zirconia-yttria alloys, *Surf. Coat. Technol.*, **46**, 75–90.

- Brandon, J.R. and Taylor, R. (1991b). Phase stability of zirconia based thermal barrier coatings. Part II. zirconia–ceria alloys, *Surf. Coat. Technol.*, **46**, 81–101.
- Brandt, R., Neuer, G. and Wörner, B. (1979). Thermophysical properties of plasma sprayed materials, *Rev. Int. Hautes Tempér. Réfract.*, **16**, 309–316.
- Brandt, R., Pawłowski, L., Neuer, G. and Fauchais, P. (1986). Specific heat and thermal conductivity of plasma stabilized yttria-stabilized zirconia and NiAl, NiCrAl, NiCrAlY, NiCoCrAlY coatings, *High Temp. High Press.*, **18**, 65–67.
- Brantner, H.P. Pippan, R. and Prantl, W. (2003). Local and global fracture toughness of flame sprayed molybdenum coatings, *J. Therm. Spray Technol.*, **12**, 560–571.
- Brown, L., Herman, H. and MacCrone, R.K. (1986). Plasma sprayed insulated metal substrates, in *Advances in Thermal Spraying*, Pergamon Press, New York, NY, USA, pp. 507–512.
- Buchmann, M. and Gadow, R. (2001). Mechanical and tribological characterization of APS and HVOF sprayed TiO<sub>2</sub> coatings on light metals, in *Thermal Spray 2001: New Surfaces for a New Millennium*, C.C. Berndt, K.A. Khor and E. Lugscheider (Eds), ASM International, Materials Park, OH, USA, pp. 1003–1008.
- Bull, S.J., Kingswell, R. and Scott, K.T. (1996). The sliding wear of plasma sprayed alumina, *Surf. Coat. Technol.*, **82**, 218–225.
- Buzovkina, T.B., Sokolova, T.V., Obuchov, A.N., Vspenska, P.I. and Degen, M.G. (1972). Influence of microstructure and temperature on effective thermal conductivity in plasma sprayed alumina, *Teplof. Vys. Temper.*, **10**, 395–399 (in Russian).
- Chandler, P.E. (1989). High  $T_c$  superconductors – the role of plasma spraying, in *Proceedings of the 12th International Thermal Spray Conference*, The Welding Institute, Cambridge, UK, Paper 93.
- Chen, Z.J., Herman, H. and Safai, S. (1993a). The structure and properties of VPS NiAl and NiAl–B, in *Thermal Spray Coatings: Research, Design and Applications*, C.C. Berndt and T.F. Bernecki (Eds), ASM International, Materials Park, OH, USA, pp. 525–530.
- Chen, P.S., Sanders, J.H., Zimmerman, F.R. and Liaw, Y.K. (1993b). Mechanical properties and microstructure of vacuum plasma sprayed NARloy-Z, in *Thermal Spray Coatings: Research, Design and Applications*, C.C. Berndt and T.F. Bernecki (Eds), ASM International, Materials Park, OH, USA, pp. 549–553.
- Cheney, R.F., Port, D.J. and Lafferty, W.D. (1978). Plasma sprayed coatings, *Eng. Mater. Des.*, March, 25–27.
- Cherigui, M. (2005). Réalisation par projection thermique de revêtements amorphes et nanocristallines destinés au blindage magnétique, *PhD Thesis*, Belfort-Montbéliard University of Technology, Belfort, France.
- Chiodelli, G., Magistris, A., Scagliotti, M. and Parmigiani, F. (1988). Electrical properties of plasma sprayed yttria stabilized zirconia coatings, *J. Mater. Sci.*, **23**, 1159–1163.
- Chuanxian, D. and Bingtang, H. (1988). Structure and properties of chromium oxide coatings, in *Proceedings of the International Symposium on Advanced Thermal Spraying Technology and Allied Coatings*, Osaka, Japan, 13–15 May, pp. 341–345.
- Chuanxian, D., Bingtang, H. and Huiling, L. (1984). Plasma sprayed wear resistant and cermet coating materials, *Thin Solid Films*, **118**, 485–493.
- Cliche, G. and Dallaire, S. (1991). Synthesis and deposition of TiC–Fe coatings by plasma spraying, *Surf. Coat. Technol.*, **46**, 199–206.
- Cook, L.S., Wolfenden, A. and Brindley, W.J. (1994). Temperature dependence of dynamic Young's modulus and internal friction in LPPS NiCrAlY, *J. Mater. Sci.*, **29**, 5104–5108.

- Cosack, T., Pawlowski, L., Schneiderbanger, S. and Sturlese, S. (1992). Thermal barrier coatings on turbine blades by plasma spraying with improved cooling, in *Proceedings of the 37th ASME International Gas Turbine and Aeroengineering Congress and Exposition*, Cologne, Germany, 1–4 June Paper 92-GT-319.
- Ctibor, P., Rohan, P., Neufuss, K., Kolman, B., Dubsky, J. and Chraska, P. (2000). Plasma spraying of titanates, in *Thermal Spray: Surface Engineering via Applied Research*, C.C. Berndt (Ed.), ASM International, Materials Park, OH, USA, pp. 945–950.
- Ctibor, P., Sedlacek, J., Neufuss, K., Dubsky, J. and Chraska, P. (2002). Study of dielectric properties of plasma sprayed silicates at low voltage, in *Proceedings of the International Thermal Spray Conference 2002*, E. Lugscheider and C.C. Berndt (Eds), DVS Verlag, Düsseldorf, Germany, pp. 617–621.
- Dallaire, S. and Levert, H. (1997). Erosion resistance of arc sprayed coatings to iron ore at 25°C and 330°C, in *Thermal Spray: A United Forum for Scientific and Technological Advances*, C.C. Berndt (Ed.), ASM International, Materials Park, OH, USA, pp. 65–73.
- Daniault, J. (1981). Réfractaires projetés au plasma, in *Proceedings of Journées d'Etudes Industrielles*, Versailles, France, 6–7 May, Comité Français d'Electrothermie, Paris, France, pp. 1–16.
- De Bonte, M., Economou, S.N., Celis, J.P., Roos, J.R., Lugscheider, E., Limbach, R. and Smith, R.W. (1993). Wear behaviour of plasma sprayed ceramic coatings: laboratory ball-on-disk testing, in *Thermische Spritzkonferenz TS93*, Vol. 152, DVS, Düsseldorf, Germany, pp. 447–449.
- Dent, A.H., Patel, A.S., Guteleber, J., Sampath, S., Herman, H. and Tormey, E. (2000). Structure-dielectric behaviour in HVOF sprayed BaTiO<sub>3</sub>, in *Thermal Spray: Surface Engineering via Applied Research*, C.C. Berndt (Ed.), ASM International, Materials Park, OH, USA, pp. 495–500.
- De Palo, S., Usmani, S., Sampath, S., Sordelet, D.J., and Besser, M. (1997). Friction and wear behaviour of thermally sprayed Al–Cu–Fe quasicrystal coatings, in *Thermal Spray. A United Forum for Scientific and Technological Advances*, C.C. Berndt (Ed.), ASM International, Materials Park, OH, USA, pp. 135–139.
- Desplanches, G. (1988). A study of plasma sprayed coatings for use in internal combustion alternative engines, in *Proceedings of the 1st Plasma Technik Symposium*, Vol. 1, Eschnauer, P. Huber, A.R. Nicoll and S. Sandmeier (Eds), Plasma-Technik AG, Wohlen, Switzerland, pp. 193–203.
- Dianran Y., Jining, H., Jianjun, W., Wanqui, Q. and Jing, M. (1997). The corrosion behaviour of a plasma spraying Al<sub>2</sub>O<sub>3</sub> coating in dilute HCl solution, *Surf. Coat. Technol.*, **89**, 191–195.
- Ding, C., Liu, X. and Zheng, X. (2004). Bioactivity and biocompatibility of plasma sprayed ceramic coatings, in *Proceedings of International Thermal Spray Conference'04*, CD-Rom, ISBN-3-87155-792-7, DVS-Verlag, Düsseldorf, Germany.
- Dooling, T.A. and Cook, D.C. (1991). Phase changes in plasma sprayed zinc-nickel ferrites, *J. Appl. Phys.*, **69**, 5355–5357.
- Dorfman, M.R. and De Barro, J.A. (1995). Development and applications of corrosion resistant thermal sprayed coatings, in *Thermal Spraying: Current Status and Future Trends*, A. Ohmori (Ed.), High Temperature Society of Japan, Osaka, Japan, pp. 567–572.
- Douglas, R. (1993). Coded-colour ceramic coatings, *Adv. Mater. Process.*, **142**, 4.

- Dyshlovenko, S., Pawłowski, L., Roussel, P., Murano, D. and Le Maguer, A. (2006). Relationship between plasma spray operational parameters and microstructure of hydroxyapatite coatings and powder sprayed into water, *Surf. Coat. Technol.*, 200, 3845–3855.
- Eaton, H.E. and Novak, R.C. (1986). Sintering studies of plasma-sprayed zirconia, *Surf. Coat. Technol.*, 32, 227–236.
- Eerola, M. (1993). Flame spraying copper on glass, *Am. Ceram. Soc. Bull.*, 72, 48–52.
- Eronen, V., Ahmanniemi, S., Niemi, K. and Vuoristo, P. (2005). Microwear in thermally sprayed hard coatings by different abrasives, in *Proceedings of the International Thermal Spray Conference '05*, E. Lugscheider (Ed.), CD-Rom, ISBN 3-87155-793-5, DVS-Verlag, Düsseldorf, Germany.
- Elyard, C.A., Connolly, D.J. and Lambert, R. (1975). The properties of polycrystalline barium titanate fabricated by arc plasma spraying, *Spec. Ceram.*, 6, 79–90.
- Fedorchenko, I.M. (Ed.) (1977). *Encyclopedia of Inorganic Materials*, Principal Redaction of Ukrainian Soviet Encyclopedia, Kiev, Ukraine (in Russian).
- Fiedler, H.C. (1984). The effect of structure on the thermal conductivity of plasma sprayed alumina, *Mater. Res. Soc. Symp. Proc.*, 30, 173–180.
- Föhl, J., Weißenberg, T. and Wiedemeyer, J. (1988). General aspects for tribological applications of hard particle coatings, in *1st Plasma Technik Symposium*, Vol. 3, H. Eschnauer, P. Huber, A.R. Nicoll and S. Sandmeier (Eds), Plasma-Technik AG, Wohlen, Switzerland, pp. 23–34.
- Funk, W., Goebe, F. and Mauz, M. (1988). The influence of substrate temperature on the bond strength of plasma sprayed oxide ceramics, in *1st Plasma Technik Symposium*, Vol. 1, H. Eschnauer, P. Huber, A.R. Nicoll and S. Sandmeier (Eds), Plasma-Technik AG, Wohlen, Switzerland, pp. 59–66.
- Gansert, D., Lugscheider, E., and Müller, U. (1990). High power plasma spraying of oxide ceramics, in *Thermal Spray Research and Applications*, T.F. Bernecki (Ed.), ASM International, Materials Park, OH, USA, pp. 517–520.
- Gärtner, F., Kreye, H., Klassen, T. and Bormann, R. (1999). Titanium carbide based cermets for thermal spray applications, in *Euromat 99*, Vol. 12, Wiley-VCH, Weinheim, Germany, pp. 213–218 (Published 2000).
- Gärtner, F., Kreye, H., Borck, V. and Krömer, W. (2000). The effect of oxidation on microstructure and properties of TiC based cermet coatings, in *Thermal Spray: Surface Engineering via Applied Research*, C.C. Berndt (Ed.), ASM International, Materials Park, OH, USA, pp. 463–469.
- Gärtner, F., Stoltenhoff, T., Schmidt, T. and Kreye, H. (2005). The cold spray process and its potential for industrial applications, in *Proceedings of the International Thermal Spray Conference' 05*, E. Lugscheider (Ed.), CD-Rom, ISBN 3-87155-793-5, DVS-Verlag, Düsseldorf, Germany.
- Gärtner, F., Stoltenhoff, T., Voyer, J., Kreye, H., Riekehr, S. and Koçak, M. (2006). Mechanical properties of cold-sprayed and thermally sprayed copper coatings, *Surf. Coat. Technol.*, 200, 6770–6782.
- Gault, C., Boilevin, S. and Desplanches, G. (1988). Elastic properties of ceramic and ceramic metal composite thermal barrier coatings, *Sci. Ceram.*, 14, 389–394.
- Gitzhofer, F., Pawłowski, L., Lombard, D., Martin, C., Kaczmarek, R. and Boulos, M. (1985). The apparent thermal diffusivity and thermal contact resistance in plasma sprayed multicoatings, *High Temp. High Press.*, 18, 563–573.
- Grot, A.S. and Martyn, J.K. (1981). Behaviour of plasma sprayed ceramic thermal barrier coatings for gas turbine applications, *Am. Ceram. Soc. Bull.*, 60, 807–811.

- Gudmundsson, B., Jacobson, B.E., Berglin, L., L'Estrade, L. and Gruner, H. (1988). Microstructure and erosion resistance of vacuum plasma sprayed CoNiCrAlY/Al<sub>2</sub>O<sub>3</sub> composite coatings, in *1st Plasma Technik Symposium*, Vol. 2, H. Eschnauer, P. Huber, A.R. Nicoll and S. Sandmeier (Eds), Plasma-Technik AG, Wohlen, Switzerland, pp. 105–114.
- Guessasma, S., Montavon, G. and Coddet, C. (2002). On the neuronal network concept to describe the thermal spray deposition process: an introduction, in *Proceedings of the International Thermal Spray Conference'2002*, E. Lugscheider and C.C. Berndt (Eds), DVS Verlag, Düsseldorf, Germany, pp. 435–439.
- Guilemany, J.M., De Paco, J.M., Miguel, J.R., Sanchez, J. and Smith P. (1998). Corrosion resistance HVOF coatings based upon TiC + NiTi and (Ti, W)C + Ni, in *Thermal Spray, Meeting the Challenges of the 21st Century*, C. Coddet (Ed.), ASM International, Materials Park, OH, USA, pp. 57–61.
- Guo, D.Z., Li, F.L., Wang, J.Y. and Sun, J.S. (1995). Effects of post-coating processing on structure and erosive wear characteristics of flame and plasma spray coatings, *Surf. Coat. Technol.*, **73**, 73–78.
- Habig, K.-H., Liedtke, D., Münz, W.-D., Röser, K. and Wahl, G. (1985). Eigenschaften von Verschleiß-Schutzschichten auf Stählen, in *41 Härterei-Kolloquium*, Wiesbaden, Germany, 9–11 October, pp. 1–10.
- Häßler, W., Fischer, K., Eckart, G. and Oswald, A. (1993). Herstellung und Eigenschaften von plasmagespritzten PZT-Schichten, in *Proceedings of Thermal Spray'93 Conference*, Vol. 192, DVS, Düsseldorf, Germany, pp. 421–423.
- Häßler, W., Thielsch, R. and Mattern, N. (1995). Structure and electrical properties of PZT thick films produced by plasma spraying, *Mater. Lett.*, **24**, 387–391.
- Haman, J.D., Lucas, L.C. and Crawmer, D. (1995). Characterization of high velocity oxy-fuel combustion sprayed hydroxyapatite, *Biomaterials*, **16**, 229–237.
- Harris, D.H. and Janowiecki, R.J. (1970). Arc plasma deposits may yield some big microwave dividends, *Electronics*, **2**, 108–115.
- Harris, D.H., Janowiecki, R., Wilson, M.C., Semler, C.E., Cheng, J.T. and Cohen, J. (1969). Arc plasma deposition of magnesium manganese ferrites, in *Proceedings of the Fall Meeting of the Electronics Division of the American Ceramic Society*, Boston, MA, USA, 17 September, pp. 1–19.
- Hawthorne, H.M., Erickson, L.C., Ross, D., Tai, H. and Troczynski, T. (1997). The microstructure dependence of wear and indentation behaviour of some plasma-sprayed alumina coatings, *Wear*, **203–204**, 709–714.
- Haynes, J.A., Rigney, E.D., Ferber, M.K. and Porter, W.D. (1996). Oxidation and degradation of a plasma-sprayed thermal barrier coating system, *Surf. Coat. Technol.*, **86–87**, 102–108.
- Heimann, R.B., Kurzweg, H., Ivey, G.G. and Wayman, M.L. (1998). Microstructural and *in vitro* chemical investigations into plasma-sprayed bioceramic coatings, *J. Biomed. Mater. Res.*, **43**, 441–450.
- Heimann, R.B., Graßmann, O., Zumbrink, T. and Jennissen, H.P. (2001). Biometric processes during *in vitro* leaching of plasma-sprayed hydroxyapatite coatings for endoprosthetic applications, *Mat.-wiss. u. Werkstofftech.*, **32**, 913–921.
- Heintze, G. and McPherson, R. (1988). Thermally sprayed Y–Ba–Cu–O superconductor, *Mater. Sci. Forum*, **34–36**, 345–349.

- Hidaka, K., Tanaka, K., Nishimura, S. and Kawarada, K. (1995). Hot corrosion resistance of a chromium-based alloy coating, in *Thermal Spraying: Current Status and Future Trends*, A. Ohmori (Ed.), High Temperature Society of Japan, Osaka, Japan, pp. 609–614.
- Hoffmann, K., Hausdorf, L. and Süß, T. (1993). Plasmaspritzen von C/Al-Verbundwerkstoffen-Herstellung und Eigenschaften, in *Thermische Spritzkonferenz TS90*, Vol. 152, DVS, Düsseldorf, Germany, pp. 440–441.
- Houck, D.L. and Whisenant, W. (1987). Wear resistance of five molybdenum-containing plasma sprayed coatings, in *Thermal Spray: Advances in Coatings Technology*, D.L. Houck (Ed.), ASM International, Materials Park, OH, USA, pp. 55–61.
- Howard, S.J. and Clyne, T.W. (1991). Interfacial fracture toughness of vacuum plasma sprayed coatings, *Surf. Coat. Technol.*, **45**, 333–342.
- Ibrahim, A., Lima, R.S., Marple, B.R. and Berndt, C.C. (2005). Fatigue and mechanical properties of nanostructured vs. conventional titania coatings, in *Proceedings of the International Thermal Spray Conference'2005*, E. Lugscheider (Ed.), CD-Rom, ISBN 3-87155-793-5, DVS-Verlag, Düsseldorf, Germany.
- Inaba, M., Tani, K., Harada, Y., Nakahira, A., Tomita, T. and Takatani, Y. (1995). Corrosion behaviour of carbide cermet sprayed coating in alkaline aqueous solution, in *Thermal Spraying: Current Status and Future Trends*, A. Ohmori (Ed.), High Temperature Society of Japan, Osaka, Japan, pp. 791–796.
- Iordanova, I., Forcey, K.S., Gergov, B. and Bojinov, V. (1995). Characterization of flame-sprayed and plasma-sprayed pure metallic and alloyed coatings, *Surf. Coat. Technol.*, **72**, 23–29.
- Ishikawa, K., Suzuki, T., Kitamura, Y. and Tobe, S. (1997). Corrosion resistance of thermal sprayd titanium oxide with resin seal in chloride solution, in *Thermal Spray: A United Forum for Scientific and Technological Advances*, ASM International, Materials Park, OH, USA, pp. 203–208.
- Ishikawa, K., Suzuki, T., Tobe, S. and Kitamura, Y. (1998). Resistance of thermally sprayed duplex coatings composed of Al and NiCr alloy against aqueous corrosion, in *Thermal Spray, Meeting the Challenges of the 21st Century*, C. Coddet (Ed.), ASM International, Materials Park, OH, USA, pp. 31–35.
- Ishikawa, Y., Kawakita, J., Osawa, S., Itsukaichi, T., Sakamoto, Y., Takaya, M. and Kuroda, S. (2005). Evaluation of corrosion and wear resistance of hard cermet coatings sprayed using an improved HVOF process, *J. Therm. Spray Technol.*, **14**, 384–390.
- Itoh, A. and Clyne T.W. (1995). Initiation and propagation of interfacial cracks during spontaneous debonding of thermally sprayed coatings, in *Advances in Thermal Spray Science and Technology*, C.C. Berndt and C. Coddet (Eds), ASM International, Materials Park, OH, USA, pp. 425–431.
- Iwamoto, N., Makino, Y., Umesaki, N., Endo, S. and Kobayashi, H. (1983). The effect of pretreatments of metals on bond adhesion, in *Proceedings of the 10th International Thermal Spray Conference*, Vol. 80, DVS, Düsseldorf, Germany, pp. 18–20.
- Jadhav, A.D., Padture, N.P., Jordan, E.H., Gell, M., Miranzo, P. and Fuller Jr, E.R. (2006). Low thermal conductivity plasma-sprayed thermal barrier coatings with engineered microstructures, *Acta Mater.*, **54**, 3343–3349.
- Janowiecki, R.J., Wilson, M.C. and Harris, D.H. (1968). Plasma sprayed thermo-electric materials research, Technical Report AFAPL-TR-68-29, Monsanto Research Corporation, Dayton, Ohio, USA, (March).

- Jarosinski, W.J., Gruninger, M.F. and Londry, C.H. (1993). Characterization of tungsten carbide cobalt powders and HVOF coatings, in *Thermal Spray Coatings: Research, Design and Applications*, C.C. Berndt and T.F. Bernecki (Eds), ASM International, Materials Park, OH, pp. 153–157.
- Jin, Y. and Yang, Y. (1996). Tribological behavior of various plasma-sprayed ceramic coatings, *Surf. Coat. Technol.*, **88**, 248–254.
- Jones, R.L. (1997). Some aspects of the hot corrosion of thermal barrier coatings, *J. Therm. Spray Technol.*, **6**, 77–84.
- Joshi, S.V. and Srivastava, M.P. (1993). On the thermal cycling life of plasma-sprayed yttria-stabilized zirconia coatings, *Surf. Coat. Technol.*, **56**, 215–224.
- Karimi, A., Verdon, Ch., Martin, J.L. and Schmid, R.K. (1995). Slurry erosion behaviour of thermally sprayed WC-M coatings, *Wear*, **186–187**, 480–486.
- Kayali, B., Suryanarayanan, R., Rodot, M., Vardelle, M., Vardelle, A. and Amri, A. (1991). Growth of silicon ribbons from powder using a plasma spray torch, *Thin Solid Films*, **202**, 359–372.
- Kelly, A. and Macmillan, N.H. (1986). *Strong Solids*, Clarendon Press, Oxford, UK.
- Khan, M.S.A. and Clyne, T.W. (1996). Microstructure and abrasion resistance of plasma sprayed cermet coatings, in *Thermal Spray: Practical Solutions for Engineering Problems*, C.C. Berndt (Ed.), ASM International, Materials Park, OH, USA, pp. 113–122.
- Khatri, S., Smith, R., Jokiel, P., Lugscheider, E. and Bohley, M. (1994). Plasma spraying of high-nitrogen-bearing steels for wear-resistant coatings and structural applications, *J. Mater. Eng. Per.*, **3**, 476–483.
- Kim, M.C., Kim, S.B. and Hong, J.W. (1997). Effect of powder types on mechanical properties of D-gun coatings, in *Thermal Spray: A United Forum for Scientific and Technological Advances*, C.C. Berndt (Ed.), ASM International, Materials Park, OH, USA, pp. 791–795.
- Kinos, T., Chen, S.L., Siitonens, P. and Kettunen, P. (1995). Corrosion properties of shrouded plasma sprayed titanium coatings, in *Thermal Spraying: Current Status and Future Trends*, A. Ohmori (Ed.), High Temperature Society of Japan, Osaka, Japan, pp. 573–576.
- Kirner, K. (1980). Plasma spraying of free standing bodies, in *Proceedings of the 9th International Thermal Spray Conference*, Nederlands Instituut voor Lastechniek, The Hague, The Netherlands, pp. 14–19.
- Kirsten, A., Oechsle, M. and Moll, R.F. (2005). Carbide containing materials for hard chromium replacement by HVOF spraying, in *Proceedings of International Thermal Spray Conference '05*, E. Lugscheider (Ed.), CD-Rom, ISBN 3-87155-793-5, DVS-Verlag, Düsseldorf, Germany.
- Kokini, K. and Takeuchi, Y.R. (1994). Initiation of surface cracks in multilayer ceramic thermal barrier coatings under thermal loads, *Mater. Sci. Eng. A*, **189**, 301–309.
- Kokubo, T., Kushitani, H., Sakka, S., Kitsugi, T. and Yamamuro, T. (1990). Solution able to reproduce *in vivo* surface-structure changes in bioactive glass-ceramic A-W, *J. Biomed. Mater. Res.*, **24**, 331–343.
- Kovarik, O., Siegl, J., Nohava, J. and Chraska, P. (2005). Young modulus and fatigue behavior of plasma-sprayed alumina coatings, *J. Therm. Spray Technol.*, **14**, 231–238.
- Kretzschmar, E. (1980). Low vacuum plasma arc coating, in *Proceedings of the 9th International Thermal Spray Conference*, Nederlands Instituut voor Lastechniek, The Hague, The Netherlands, pp. 181–186.
- Kretzschmar, E. (1986). Protection against wear by powder flame spraying, in *Advances in Thermal Spraying*, Pergamon Press, New York, NY, USA, pp. 367–375.

- Kreye, H. (1991). High velocity flame spraying-process and coating characteristics, in *2nd Plasma Technik Symposium*, Vol. 1, S. Blum-Sandmaier, H. Eschnauer, P. Huber and A.R. Nicoll, Plasma Technik AG, Wohlen, Switzerland, pp. 39–47.
- Kreye, H., Fandrich, D., Müller, H.-H. and Reiners, G. (1986). Microstructure and bond strength of WC–Co coatings deposited by hypersonic flame spraying (Jet-Kote process), in *Advances in Thermal Spraying*, Pergamon Press, New York, NY, USA, pp. 121–128.
- Kreye, H., Schwetzke, R., Buschinelli, A. and Bocanera, L. (1998). Cavitation erosion resistant coatings produced by thermal spraying and weld cladding, in *Thermal Spray: Meeting the Challenges of the 21st Century*, C. Coddet (Ed.), ASM International, Materials Park, OH, USA, pp. 269–273.
- Kudinov, V.V. (1977). *Plasma Coatings*, Izdatelstvo Nauka, Moscow, USSR (in Russian).
- Kulu, P. and Pihl, T. (2002). Selection criteria for wear resistant powder coatings under extreme erosive wear conditions, *J. Therm. Spray Technol.*, **11**, 517–522.
- Kumar, K. and Das, D. (1979). Magnetic properties and microstructure of sprayed SmCo<sub>5</sub> magnets exposed to intermediate temperatures, *J. Appl. Phys.*, **50**, 2940–2944.
- Kumar, K. and Das, D. (1980). Role of atmosphere in the crystallization of amorphous plasma sprayed SmCo deposits, *J. Appl. Phys.*, **51**, 1031–1035.
- Kumar, K. and Das, D. (1986). Aligned, plasma sprayed SmCo<sub>5</sub> deposits. *J. Appl. Phys.*, **60**, 3779–3781.
- Kumar, K. and Das, D. (1987). Equilibrium and metastable samarium–cobalt deposits produced by arc plasma spraying, *Thin Solid Films*, **54**, 263–269.
- Kumar, A., Boy, J., Zatorski, R. and March, P. (1997). Cavitation resistance of thermal spray coatings, in *Thermal Spray: A United Forum for Scientific and Technological Advances*, C.C. Berndt (Ed.), ASM International, Materials Park, OH, USA, pp. 83–90.
- Kuroda, S. and Clyne, T.W. (1991). The quenching stresses in thermally sprayed coatings, *Thin Solid Films*, **200**, 49–66.
- Kweh, S.W.K., Khor, K.A. and Cheang, P. (2002). An *in vitro* investigation of plasma sprayed hydroxyapatite (HA) coatings produced with flame-spheroidized feedstock, *Biomaterials*, **23**, 775–785.
- Lang, M., Henne, R., Schaper, S. and Schiller, G. (2001). Development and characterization of vacuum plasma sprayed thin film solid oxide fuel cells, *J. Therm. Spray Technol.*, **10**, 618–625.
- Lansdown, A.R. and Price, A.L. (1986). *Materials to Resist Wear – A Guide to Their Selection and Use*, Pergamon Press, Oxford, UK.
- LaPierre, K., Herman, H. and Tobin, A.G. (1991). The microstructure and properties of plasma sprayed ceramic composites, *Ceram. Eng. Sci. Proc.*, **12**, 1201–1221.
- Leblanc, L. (2003). Abrasion and sliding wear of nanostructured ceramic coatings, in *Advancing Science and Applying the Technology*, C. Moreau and B. Marple (Eds), ASM International, Materials Park, OH, USA, pp. 291–299.
- Leigh, S.-H., Lin, C.-K. and C.C. Berndt (1997). Elastic response of thermal spray deposits under indentation test, *J. Am. Ceram. Soc.*, **80**, 2093–2099.
- Li, C.C. (1980). Characterization of thermally sprayed coatings for high temperature wear protection applications, *Thin Solid Films*, **73**, 59–77.
- Li, S., Langlade-Bomba, C., Treheux, D., Crabos, F. and Monge-Cadet, P. (1998a). Wear mechanism of MCrAlY abradable plasma-sprayed coatings, in *Thermal Spray: Meeting the Challenges of the 21st Century*, C. Coddet (Ed.), ASM International, Materials Park, OH, USA, pp. 293–298.

- Li, J., Zhang, Y., Huang, J. and Ding, C. (1998b). Mechanical and tribological properties of plasma-sprayed Cr<sub>3</sub>C<sub>2</sub>-NiCr, WC-Co, and Cr<sub>2</sub>O<sub>3</sub> coatings, *J. Therm. Spray Technol.*, **7**, 242–246.
- Li, C.-J., Wang, W.-Z. and He, Y. (2004). Dependency of fracture toughness of plasma sprayed Al<sub>2</sub>O<sub>3</sub> coatings on lamellar structure, *J. Therm Spray Technol.*, **13**, 425–431.
- Li, H., Khor, K.A. and Cheang, P. (2005). Nanostructures in thermally sprayed hydroxyapatite (HA) and HA/nano-zirconia coatings and their influence on coating properties, in *International Thermal Spray Conference '05*, E. Lugscheider (Ed.), CD-Rom, ISBN 3-87155-793-5, DVS-Verlag, Düsseldorf, Germany.
- Li, C.-J., Yang, G.-J. and Ohmori, A. (2006). Relationship between particle erosion and lamellar microstructure for plasma-sprayed alumina coatings, *Wear*, **260**, 1166–1172.
- Lim, L.C., Lim, S.C., Lai, M.O., Chong, S.F and Alli, S. (1996). Annealing of plasma sprayed WC-Co coating, *Surf. Coat. Technol.*, **79**, 151–161.
- Lima, R.S. and Marple, B.R. (2003). High Weibull modulus HVOF titania coatings, *J. Therm. Spray Technol.*, **12**, 240–249.
- Lima, R.S., Marple, B.R., Khor, K.A., Li, H. and Cheang, P. (2004a). Mechanical properties, microstructural characteristics and *in-vitro* behavior of APS-sprayed nanostructured and conventional hydroxyapatite coatings, in *International Thermal Spray Conference'04*, CD-Rom, ISBN-3-87155-792-7, DVS-Verlag, Düsseldorf, Germany.
- Lima, R.S., Leblanc, L. and Marple, B.R. (2004b). Abrasion behavior of nanostructured and conventional coatings thermally sprayed via APS, VPS and HVOF, in *International Thermal Spray Conference'04*, CD-Rom, ISBN-3-87155-792-7, DVS-Verlag, Düsseldorf, Germany.
- Lima, C.R.C., Barrera, R. and Camargo, F. (2005). Comparative study of wear and corrosion resistance of electric arc thermally sprayed coatings, in *International Thermal Spray Conference '05*, E. Lugscheider (Ed.), CD-Rom, ISBN 3-87155-793-5, DVS-Verlag, Düsseldorf, Germany.
- Lin, C.K. and Berndt, C.C. (1995). Statistical analysis of microhardness variation in thermal spray coatings, *J. Mater. Sci.*, **30**, 111–117.
- Lira Olivares, J. and Grigorescu, I.C. (1987). Friction and wear behaviour of thermally sprayed nichrome-WC coatings, *Thin Films and Metallurgical Coatings, Surf. Coat. Technol.*, **33**, 183–190.
- Lister, T.E., Wright, R.N., Pinhero, P.J. and Swank, W.D. (2002). Corrosion of thermal spray Hastelloy C-22 coatings in dilute HCl, *J. Therm. Spray Technol.*, **11**, 530–535.
- Liu, X. and Ding, C. (2002). Thermal properties and microstructure of plasma sprayed wollastonite coatings, *J. Therm. Spray Technol.*, **11**, 375–379.
- Longa-Nava, Y., Takemoto, M. and Hidaka, K. (1995). High-temperature corrosion performance of plasma-sprayed CrNiMoSiB coatings, *J. Therm. Spray Technol.*, **4**, 169–174.
- Lugscheider, E. (1987). Plasma spraying for wear applications, in *Thermal Spray: Advances in Coatings Technology*, D.L. Houck (Ed.), ASM International, Materials Park, OH, USA, 105–122.
- Lugscheider, E. and Weber, T. (1989). Plasma spraying of Bi-Sr-Ca-Cu-O high temperature superconductors, in *Thermal Spray: Research and Applications*, T.F. Bernecki (Ed.), ASM International, Materials Park, OH, USA, pp. 635–640.
- Lugscheider, E., Eschnauer, H., Häuser, B. and Jäger, D. (1985). Vacuum plasma spraying of tantalum and niobium, *J. Vac. Sci. Technol. A*, **3**, 2469–2474.

- Lugscheider, E., Jungklaus, H., Limbach, R. and Smith, R.W. (1991). Process structure relationship in TiC reinforced thermal spray wear coatings, in *2nd Plasma Technik Symposium*, Vol. 1, S. Blum-Sandmaier, H. Eschnauer, P. Huber and A.R. Nicoll (Eds), Plasma Technik AG, Wohlen, Switzerland, pp. 217–225.
- Lugscheider, E., Jokiel, P., Pursche, G., Roman, O. and Yushchenko, K. (1992). Particles reinforced material containing titanium- $\tau$ -boride for wear protection, in *Thermal Spray: International Advances in Coatings Technology*, C.C. Berndt (Eds), ASM International, Materials Park, OH, USA, pp. 647–651.
- Lugscheider, E., Jungklaus, H., Remer, P. and Knuuttila, J. (1995). Influence of various oxide additions on the wear resistance of plasma sprayed alumina coatings, in *Thermal Spraying: Current Status and Future Trends*, A. Ohmori (Ed.), High Temperature Society of Japan, Osaka, Japan, pp. 833–838.
- Lugscheider, E., Herbst-Dederichs, C. and Reimann, H. (2000). Thermally sprayed quasicrystal composite coatings for bearings and other friction threaded applications, in *Thermal Spray: Surface Engineering via Applied Research*, C.C. Berndt (Ed.), ASM International, Materials Park, OH, USA, pp. 843–849.
- Lutz, E. (1994). Crack resistance anisotropy in plasma sprayed ceramic composites, LWK Plasmakeramik, Gummersbach, Germany, unpublished results.
- Lutz, E.H. (1995). Size sensitivity to thermal shock of plasma-sprayed ceramics and factors affecting the size effect, *J. Am. Ceram. Soc.*, **78**, 2700–2704.
- Lyonnet, P. (1999). *La Qualité: Outils et Méthodes*, Technique et Documentation, Paris, France.
- Mackay, T.L. and Muller, A.N. (1967). Plasma sprayed dielectric coatings for heat sinks in electronic packaging, *Ceram. Bull.*, **46**, 833–836.
- Malewski, B. and Pawlowski, L. (1981). Wroclaw University of Technology, Wroclaw, Poland, unpublished results.
- Matsubara, Y. and Tomiguchi, A. (1992). Surface texture and adhesive strength of high velocity oxy-fuel sprayed coatings for rolls of steel mills, in *Thermal Spray International Advances in Coatings Technology*, C.C. Berndt (Eds), ASM International, Materials Park, OH, USA, 637–641.
- McPherson, R. and Cheang, P. (1989). Microstructural analysis of Ni-Al plasma sprayed coatings, in *Proceedings of the 12th International Thermal Spray Conference*, The Welding Institute, Cambridge, UK, Paper 17.
- Milewski, W. and Milewski, P. (1980). Some properties of molybdenum coatings produced by electric arc process, in *Proceedings of the 9th International Thermal Spray Conference*, Nederlands Instituut voor Lastechniek, The Hague, The Netherlands, pp. 290–298.
- Milewski, W. and Sartowski, M. (1986). Some properties of coatings arc-sprayed in nitrogen and argon atmosphere, in *Advances in Thermal Spraying*, Pergamon Press, New York, NY, USA pp. 467–475.
- Mogro-Campero, A., Johnson, C.A., Bednarczyk, P.J., Dinwiddie, R.B. and Wang, H. (1997). Effect of gas pressure on thermal conductivity of zirconia thermal barrier coatings, *Surf. Coat. Technol.*, **94–95**, 102–105.
- Montavon, G., Robert, B., Verdy, C., Monin, V., Atcholi, K.E. and Coddet, C. (1996). Characterization of the tensile properties of vacuum plasma spray copper deposits, in *Thermal Spray: Practical Solutions for Engineering Problems*, C.C. Berndt (Ed.), ASM International, Materials Park, OH, USA, pp. 827–833.
- Müller, K.N. (1973). Structure and properties of arc-sprayed titanium coatings, in *Proceedings of the 7th International Metal Spraying Conference*, The Welding Institute, Cambridge, UK, pp. 165–172.

- Müller, J.-H. and Kreye, H. (2001). Microstructure and properties of thermally sprayed alumina coatings, *Weld. Cut.*, **53**(6), 122–127.
- Neiser, R.A., Zhu, Y.M., Herman, H. and Gudmundsson, B. (1989). The morphology and crystal structure of as-deposited  $\text{YB}_2\text{Cu}_3\text{O}_x$  produced by air plasma spraying, in *Proceedings of the 12th International Thermal Spray Conference*, The Welding Institute, Cambridge, UK, Paper 55.
- Neiser, R.A., Smolik, G.R., Hollis, K.J. and Watson, R.D. (1993). Evaluation of plasma sprayed tungsten for fusion reactors, *J. Therm. Spray Technol.*, **2**, 393–399.
- Neville, A. and Hodgkiss, T. (1996). Corrosion behaviour and microstructure of two thermal spray coatings, *Surf. Eng.* **12**, 303–312.
- Nguyentat, T., Dommer, K.T. and Bowen, K.T. (1992). Metallurgical evaluation of plasma sprayed structural materials for rocket engines, in *Thermal Spray: International Advances in Coatings Technology*, C.C. Berndt (Ed.), ASM International, Materials Park, OH, USA, pp. 321–325.
- Niemi, K.J., Vuoristo, P.M.J. and Mäntylä, T.A. (1991). Chromium oxide coatings deposited by plasma spraying and detonation gun spraying, in *2nd Plasma Technik Symposium*, Vol. 2, S. Blum-Sandmaier, H. Eschnauer, P. Huber and A.R. Nicoll (Eds), Plasma Technik AG, Wohlen, Switzerland, pp. 311–322.
- Niemi, K., Vuoristo, P. and Mäntylä, T. (1993). On the wear resistance of thermally sprayed alumina based coatings, in *TS93*, Vol. 152, DVS, Düsseldorf, Germany, pp. 307–309.
- Niemi, K.J., Rekola, S., Vuoristo, P., Laurila, J., Vippola, M. and Mäntylä, T. (2003). Advanced oxide ceramic coatings for applications demanding high wear resistance, in *Thermal Spray 2003: Advancing the Science and Applying the Technology*, C. Moreau and B. Marple (Eds), ASM International, Materials Park, OH, USA, pp. 233–236.
- Normand, B., Liao, H., Landemarre, O., Coddet, C. and Pagetti, J. (1998). Corrosion resistance of thermal spray Inconel 690 coatings, in *Thermal Spray: Meeting the Challenges of the 21st Century*, C. Coddet (Ed.), ASM International, Materials Park, OH, USA, pp. 69–73.
- O'Bryan, H.M. and Gallagher, P.K. (1987). Characterization of  $\text{YBa}_2\text{Cu}_3\text{O}_x$  as a function of oxygen partial pressure, *Adv. Ceram. Mater.*, **2**, 640–648.
- Ohmori, A., Park, K.C., Inuzuka, M., Arata, Y., Inoue, K. and Iwamoto, N. (1991). Electrical conductivity of plasma sprayed titanium oxide (rutile) coatings, *Thin Solid Films*, **201**, 1–8.
- Ositinski, B.L. and Basko, V.P. (1977). Application of plasma spraying for preparation of contact fields in cermet heaters, *Poroshk. Metall.*, **169**, 51–54 (in Russian).
- Ostojic, P. and McPherson, R. (1988). Toughness: its characteristics in thermally sprayed coatings, in *Ceramic Development*, Materials Science Forum, Vol. 34–36, C.C. Sorrell and B. Ben-Nissan (Eds), pp. 451–455.
- Otsubo, F., Shimoda, A., Era, H. and Kishitake, K. (2004). Corrosion resistance of Fe–Cr–Mo–(C, B, P) amorphous coatings thermal sprayed by HVOF and APS processes, in *International Thermal Spray Conference'04*, CD-Rom, ISBN-3-87155-792-7, DVS-Verlag, Düsseldorf, Germany.
- Overfelt, R.A., Anderson, C.D. and Flanagan, W.F. (1986). Plasma sprayed  $\text{Fe}_{76}\text{Nd}_{16}\text{B}_8$  permanent magnets, *Appl. Phys. Lett.*, **49**, 1799–1801.
- Overs, M.P., Harris, S.J. and Waterhouse, R.B. (1980). The effect of oxygen content on the microstructure and fretting wear properties of flame sprayed molybdenum, in *Proceedings of the 9th International Thermal Spray Conference*, Nederlands Instituut voor Lasttechniek, The Hague, The Netherlands, pp. 345–352.

- Parent, L., Dodelet, J.P. and Dallaire, S. (1987). Plasma sprayed semiconductor electrodes, *J. Electrochem. Soc.*, **134**, 2226–2233.
- Pawlowski, L. (1974). A study of electrical and structural properties of plasma sprayed  $\text{Al}_2\text{O}_3 + \text{W}$  coatings, in *Proceedings of the 2nd Polish Symposium on Plasma Chemistry*, Czestochowa, Poland, October, pp. 278–284.
- Pawlowski, L. (1978). Analysis of the applications possibility of plasma spraying process in microelectronic basing onto research on the VPS copper and tantalum coatings, *PhD Thesis*, Wroclaw University of Technology, Wroclaw, Poland (in Polish).
- Pawlowski, L. (1985). Optimisation des paramètres de projection des céramiques par plasma d'arc. Etude des propriétés physiques et thermophysiques des couches projetées—exemple d'application: substrats pour la microélectronique hybride, *DSc Thesis*, University of Limoges, Limoges France.
- Pawlowski, L. (1988). The relationship between structure and dielectric properties in plasma sprayed alumina coatings, *Surf. Coat. Technol.*, **35**, 285–298.
- Pawlowski, L. (1991). The properties of plasma sprayed aluminium–aluminium oxide cermets, *Surf. Coat. Technol.*, **48**, 219–224.
- Pawlowski, L. (2003). *Dépôts Physiques. Techniques, Microstructures et Propriétés*, Presse Polytechnique et Universitaire Romande, Lausanne, Switzerland.
- Pawlowski, L. and Fauchais, P. (1992). Thermal transport properties of thermally sprayed coatings, *Int. Mater. Rev.*, **37**, 271–289.
- Pawlowski, L., Martin, C. and Fauchais, P. (1983). The application of infrared thermography in testing the coatings and optimizing the plasma spraying process, in *Proceedings of 10th International Thermal Spray Conference Essen*, Vol. 80, DVS, Düsseldorf, Germany, pp. 31–36.
- Pawlowski, L., Lombard, D., Mahlia, A., Martin, C. and Fauchais, P. (1984). Thermal diffusivity of arc plasma sprayed zirconia coatings, *High Temp. High Press.*, **16**, 347–359.
- Pawlowski, L., Lombard, D. and Fauchais, P. (1985). Structure–thermal properties relationship in plasma sprayed zirconia coatings, *J. Vac. Sci. Technol.*, **A**, **3**, 2494–2500.
- Pawlowski, L., Hill, A., McPherson, R., Garvie, D., Przelozny, Z. and Finlayson, T. (1990). Properties of plasma sprayed  $\text{YBa}_2\text{Cu}_3\text{O}_x$  high temperature superconductors, in *Thermal Spray: Research and Applications*, T.F. Bernecki (Ed.), ASM International, Materials Park, OH, USA, pp. 641–646.
- Pawlowski, L., Gross, A. and McPherson, R. (1991). Microstructure of plasma sprayed  $\text{YBa}_2\text{Cu}_3\text{O}_x$  high-temperature superconductor, *J. Mater. Sci.*, **26**, 3803–3808.
- Pawlowski, L., Zacchino, R., Dal Maschio, R., Sglavo, V.M., Andresen, J. and Driller, F.J. (1993). Structure–properties relationship in plasma sprayed chromium oxide coatings in *Thermische Spritzkonferenz*, Vol. 152, DVS, Düsseldorf, Germany, pp. 132–138.
- Perrin, R. and Scharff, J.P. (1999). *Chimie Industrielle*, Dunod, Paris, France.
- Pina, J., Dias, A.M., Costa, V., Gonsalves, A., Zaouali, M. and Lebrun, S.L. (1991). Residual stresses in plasma sprayed coatings, in *2nd Plasma Technik Symposium*, Vol. 2, S. Blum-Sandmeier, H. Eschnauer, P. Huber, and A.R. Nicoll (Eds), Plasma Technik AG, Wohlen, Switzerland, pp. 99–108.
- Pirogov, J.S., Brown, R.M. and Friedberg, A.L. (1966). Electrical properties of  $\text{Al}_2\text{O}_3$ –nickel metal multilayer flame sprayed coatings, *Ceram. Bull.*, **45**, 1071–1074.
- Preece, I. and Andrews, C.W.D. (1973). Plasma spraying of ferrites, *J. Mater. Sci.*, **8**, 964–967.
- Qiao, Y., Liu, Y.R. and Fischer, T.E. (2001). Sliding and abrasive wear resistance of thermal-sprayed WC–Co coatings, *J. Therm. Spray Technol.*, **10**, 118–25.

- Raghavan, S., Wang, H., Dinwiddie, R.B., Porter, W.D. and Mayo, M.J. (1998). The effect of grain size and yttria content on the thermal conductivity of nanocrystalline zirconia, *Scripta Mater.*, **39**, 1119–1125.
- Rairden, J.R. (1967). Porous bodies of Ta, Nb, Al fabricated by metal spray processes, *Electrochem. Technol.*, July–August, 407–408.
- Rajamäki, E., Varis, T., Kulkami, A., Gutleber, J., Vaidya, A., Karadge, M., Sampath, S. and Herman, H. (2002). Parameter optimization of HVOF sprayed alumina and effect of the spray parameters on the electrical properties of the coatings, in *Proceedings of The International Thermal Spray Conference 2002 Essen*, E. Lugscheider and C.C. Berndt (Eds), DVS Verlag, Düsseldorf, Germany, pp. 622–626.
- Ramachandran, K., Selvarajan, V., Ananthapadmanabhan, P.V. and Sreekumar, K.P. (1998). Microstructure, adhesion, microhardness, abrasive wear resistance and electrical resistivity of the plasma sprayed alumina and alumina–titania coating, *Thin Solid Films*, **315**, 144–152.
- Rangaswamy, S., Herman, H. and Safai, S. (1980). Thermal expansion study of plasma sprayed coatings, *Thin Solid Films*, **73**, 43–52.
- Reardon, J.D., Mignogna, R. and Longo, F.N. (1981). Plasma- and vacuum-plasma-sprayed Cr<sub>3</sub>C<sub>2</sub> composite coatings, *Thin Solid Films*, **83**, 345–351.
- Renouard-Vallet, G., Bianchi, L., Sauvet, A.L., Fauchais, P., Vardelle, M., Boulos, M. and Gitzhofer, F. (2004). Elaboration of SOFCs electrolytes by air plasma spraying and vacuum plasma spraying – comparison of electrolytes' properties, in *International Thermal Spray Conference'04*, CD-Rom, ISBN 3-87155-792-7, DVS-Verlag, Düsseldorf, Germany.
- Richard, C., Lu, J., Flavenot, J.F., Beranger, G. and Decamps, F. (1992). Study of Cr<sub>2</sub>O<sub>3</sub> coating materials and characterization by an interfacial test of coating/substrate adherence, in *Thermal Spray Coatings: Research, Design and Applications*, C.C. Berndt and T.F. Bernecki (Eds), ASM International, Materials Park, OH, USA, pp. 11–16.
- Richard, C.S., Béranger, G., Lu, J., Flavenot, J.F. and Grégoire, T. (1996). Four-point bending test of thermally produced WC-Co coatings, *Surf. Coat. Technol.*, **78**, 284–294.
- Riley, M.A. and Sturgeon, A.J. (2005). Influence of spraying parameters on the properties of HVOF alumina coatings, in *International Thermal Spray Conference '05*, E. Lugscheider (Ed.), CD-Rom, ISBN 3-87155-793-5, DVS-Verlag, Düsseldorf, Germany.
- Roseberry, T.J. and Boulger, F.W. (1977). *A Plasma Flame Spray Handbook*, Report No. MT-043, US, Department of Commerce, National Technical Information Service, Springfield, VA, USA.
- Rudajevova, A. (1993). Thermal diffusivity of plasma-sprayed coatings of ZrO<sub>2</sub> with 8 wt% Y<sub>2</sub>O<sub>3</sub> and ZrO<sub>2</sub> with 25 wt% CeO<sub>2</sub>, *Thin Solid Films*, **223**, 248–252.
- Rudajevova, A. (1994). Thermal properties of plasma-sprayed ZrSiO<sub>4</sub> material, *Surf. Coat. Technol.*, **64**, 47–51.
- Rybicki, E.E., Shadley, J.R., Xiong, Y. and Greving, D.J. (1995). A cantilever beam method for evaluating Young's modulus and Poisson's ratio of thermal spray coatings, *J. Therm. Spray Technol.*, **4**, 377–383.
- Sainte-Catherine, M.C., Derep, J.L. and Lumet, J.P. (1991). Zirconia–alumina plasma sprayed coatings: correlation between microstructure and properties, in *2nd Plasma Technik Symposium*, Vol. 2, S. Blum-Sandmeier, H. Eschnauer, P. Huber and A.R. Nicoll (Eds), Plasma-Technik AG, Wohlen, Switzerland, pp. 131–141.
- Sampath, S. and Wayne, S.F. (1994). Microstructure and properties of plasma-sprayed Mo–Mo<sub>2</sub>C composite, *J. Therm. Spray Technol.*, **3**, 282–288.

- Samonov, G.V. (1978). *Physicochemical Properties of Oxides*, Metallurgija, Moscow, USSR (in Russian).
- Sandt, A. and Krey, J. (1984). NiCrBSi-Schichten mit Hartstoff-Beimischungen, Teil I: Herstellung und Charakterisierung der Schichten, *Metall*, 38, 1171–1176.
- Sandt, A. and Krey, J. (1985). NiCrBSi-Schichten mit Hartstoff-Beimischungen, Teil II: Verhalten bei gleitender und abrasiver Verschleißbeanspruchung, *Metall*, 39, 15–19.
- Scagliotti, M., Parmigiani, F., Chiodelle, G., Magistris, A., Samoggia, G. and Lanzi, G. (1988). Plasma sprayed zirconia electrolytes, *Solid State Ionics*, 28–30, 1766–1769.
- Schiefler, M.F.O., Gärtner, F., Voyer, J., Kirsten, A., Kreye, H. and Buschinelli, A.J.A. (2003). Protection of steel components against marine corrosion by thermally sprayed anodic coatings, in *Thermal Spray 2003: Advancing the Science, Applying the Technology*, C. Moreau and B. Marple (Eds), ASM International, Materials Park, OH, USA, pp. 361–370.
- Schneider, K. and Grünling, W.H. (1983). Mechanical aspects of high temperature coatings, *Thin Solid Films*, 107, 395–416.
- Schwarz, K., Kunert, W. and Paul, M. (1997). Investigation of tantalum on steel by vacuum plasma spraying, *Mater. Corros.*, 48, 237–242.
- Schwetzkre, R. and Kreye, H. (1996). Cavitation erosion of HVOF coatings, in *Thermal Spray: Practical Solutions for Engineering Problems*, C.C. Berndt (Ed.), ASM International, Materials Park, OH, USA, pp. 153–158.
- Schwingel, D., Taylor, R., Haubold, T., Wigren, J., Gualco, C., Ladru, F., Lugscheider, E. and Gourlaouen, V. (1998). Thermophysical and mechanical properties of PYSZ thick thermal barrier coatings, in *Thermal Spray: Meeting the Challenges of the 21st Century*, C. Coddet (Ed.), ASM International, Materials Park, OH, USA,
- Serghini, S. and Dallaire, S. (2000). Cyclic and isothermal oxidation at 1200°C of HFOF NiCrAlY sprayed coatings, in *Thermal Spray: Surface Engineering via Applied Research*, C.C. Berndt (Ed.), ASM International, Materials Park, OH, USA, pp. 1005–1009.
- Shankar, N.R., Berndt, C.C. and Herman, H. (1982). Failure and acoustic emission response of plasma sprayed ZrO<sub>2</sub>–8 wt% Y<sub>2</sub>O<sub>3</sub> coatings, *Ceram. Eng. Sci. Proc.*, 3, 772–792.
- Sheffler, K.D., Graziani, R.A. and Sinko, G.C. (1982). *JT9D thermal barrier coated vanes*, NASA Report No. CR-16964, NASA, Lewis Research Center, Cleveland, OH, USA.
- Siegmund, S., Brandt, O. and Dvorak, M. (2004). Thermally sprayed wear resistant coatings with nanostructured hard phases, *J. Therm. Spray Technol.*, 13, 37–43.
- Siemard, S. and Arsenault, B. (2003). Influence of thermal spray process on corrosion behavior of high-density 316L stainless steel coating on simulated marine environment, in *Thermal Spray 2003: Advancing the Science and Applying the Technology*, C. Moreau and B. Marple (Eds), ASM International, Materials Park, OH, USA, pp. 323–327.
- Siemers, P. and Mehan, R.L. (1983). Mechanical and physical properties of plasma sprayed stabilized zirconia, *Ceram. Eng. Sci. Proc.*, 3, 828–840.
- Smith, R.W. (1981). Mechanical properties of a low pressure plasma applied CoCrAlY coating, *Thin Solid Films*, 84, 59–72.
- Smith, R.W., Mutasim, Z.Z., Kangutkar, P.B., Mohanty, M., Krepski, R.P. and Drossman, R.O. (1992). A new iron-based thermal spray coating for wear resistance, in *Thermal Spray: International Advances in Coatings Technology*, C.C. Berndt (Ed.), ASM International, Materials Park, OH, USA, pp. 653–659.

- Smyth, R.T. and Anderson, J.C. (1975). Production of resistors by arc plasma spraying, *Electrocomp. Sci. Technol.*, **2**, 135–145.
- Smyth, R.T. and Anderson, J.C. (1976). Electronic circuit production by arc plasma spraying, in *Proceedings of the 8th International Thermal Spray Conference*, American Welding Society, Miami, FL, USA, pp. 456–463.
- Stavros, A.J. (1996). Behavior of some tungsten carbide coatings in molten zinc, in *Thermal Spray: Practical Solutions for Engineering Problems*, C.C. Berndt (Ed.), ASM International, Materials Park, OH, USA, pp. 141–146.
- Steffens, H.-D. and Beczkowiak, J. (1983). Adhesion by low pressure plasma spraying, in *Proceedings of the 10th International Spray Conference*, Vol. 80, DVS, Düsseldorf, Germany, pp. 218–221.
- Steffens, H.-D. and Kaczmarek, R. (1991). Metal matrix composites made by thermal spraying, *Powder Metall. Int.*, **23**, 105–107.
- Steffens, H.-D., Höhle, H.-M. and Ertürk, E. (1980). Low pressure plasma spraying of reactive materials, *Thin Solid Films*, **73**, 19–29.
- Steffens, H.-D., Busse, K.-H. and Matthäus, G. (1986). Arc spraying of steel and cored wires, in *Advances in Thermal Spraying*, Pergamon Press, New York, NY, USA, pp. 457–466.
- Steffens, H.-D., Dvorak, M. and Nassenstein, K. (1992). Mechanical properties of vacuum plasma sprayed titanium and titanium alloys, in *Thermal Spray: International Advances in Coatings Technology*, C.C. Berndt (Ed.), ASM International, Materials Park, OH, USA, pp. 369–374.
- Stevens, R. (1986). *Zirconia and zirconia ceramics*, Magnesium Elektron Ltd, Twickenham, UK.
- Sun, R.-X., Lu, Y.-P., Li, M.-S., Li, S.-T. and Zhu, R.-F. (2005). Characterization of hydroxyapatite particles plasma-sprayed into water, *Surf. Coat. Technol.*, **190**, 281–286.
- Suryanarayanan, R. and Zribi, G. (1982). Microstructure and electrical properties of plasma sprayed polycrystalline silicon, *J. Phys. Coll.*, **C1**, **43**, 375–380.
- Suryanarayanan, R., Brun, G. and Akani, M. (1984). Growth and electrical properties of plasma sprayed silicon, *Thin Solid Films*, **119**, 67–73.
- Suryanarayanan, R., Akani, M. and Brun, G. (1986). Electrical properties of plasma sprayed silicon, in *Advances in Thermal Spraying*, Pergamon Press, New York, NY, USA, pp. 507–512.
- Suryanarayanan, R., Akani, M., Gauthier, R., M'Ghaieith, R. and Pinard, P. (1987). Electron beam recrystallization of plasma sprayed silicon, *Appl. Phys. Lett.*, **51**, 259–260.
- Suzuki, M., Sodeoka, S., Inoue, T., Shimosaka, K. and Oki, S. (2000). Structure and properties of plasma-sprayed zircon coating, in *Thermal Spray: Surface Engineering via Applied Research*, C.C. Berndt (Ed.), ASM International, Materials Park, OH, USA, pp. 333–339.
- Tachikawa, K., Watanabe, I., Kosuge, S., Kobasawa, M., Suzuki, T., Matsuda, Y. and Shinbo, Y. (1988). High  $T_c$  superconducting films of Y–Ba–Cu oxides prepared by low-pressure plasma spraying, *Appl. Phys. Lett.*, **52**, 1011–1013.
- Takeuchi, J., Nakahira, H. and Nagai, J. (1991). Physical properties of some oxide coatings by low pressure plasma spraying, in *2nd Plasma Technik Symposium*, Vol. 2, S. Blum-Sandmeier, H. Eschnauer, P. Huber and A.R. Nicoll (Eds), Plasma Technik AG, Wohlen, Switzerland, pp. 141–151.

- Taylor, A.J., Parker, N.J. and Wellhofer, F. (1989). Plasma sprayed cermets, in *Proceedings of the 12th International Thermal Spray Conference*, The Welding Institute, Cambridge, UK, Paper 29.
- Tokaji, K., Ogawa, T., Hwang, J.U., Kobayashi Y. and Harada, Y. (1996). Corrosion fatigue behavior of a steel with sprayed coatings, *J. Therm. Spray Technol.*, 5, 269–276.
- Tomaszek, R., Znamirowski, Z., Brylak, M., Pawlowski, L. and Sokolowski, A. (2005). Comparative study of the TiO<sub>2</sub> deposits obtained by plasma spraying of powders and suspensions, in *Neue Materialien und Verfahren in der Beschichtungstechnik*, Vol. 22, B. Wielage (Ed.), TU Chemnitz, Allemagne, France ISBN:3-00-016841-9, pp. 333–341.
- Tomaszek, R., Nitsch, K., Pawlowski, L., Znamirowski, Z. and Brylak, M. (2006). Impedance spectroscopy of suspension plasma sprayed titania coatings, *Surf. Coat. Technol.*, 201, 1930–1934.
- Touloukian, Y.S. and Buyco, E.H. (1970). *Specific Heat, Metallic Elements and Alloys, Thermophysical Properties of Matter*, Vol. 4, IFI Plenum, New York, NY, USA.
- Troczyński, T. and Plamondon, M. (1992). Response surface methodology for optimization of plasma spraying, *J. Therm. Spray Technol.*, 1, 293–300.
- Tronche, A. (1986). Contribution à l'étude de dépôts durs projetés par plasma, *PhD Thesis*, ENSCI Limoges, Limoges, France.
- Tronche, A. and Fauchais, P. (1987). Hard coatings (Cr<sub>2</sub>O<sub>3</sub>, WC-Co) properties on aluminum or steel substrates, *Mater. Sci. Eng. A*, 92, 133–144.
- Tsai, H.L. and Tsai P.C. (1995). Performance of laser-glazed plasma sprayed ZrO<sub>2</sub>–12 wt% Y<sub>2</sub>O<sub>3</sub>)/(Ni–22 wt% Cr–10 wt% Al–1 wt% Y) thermal barrier coatings in cyclic oxidation test, *Surf. Coat. Technol.*, 71, 53–59.
- Tsunekawa, Y., Okumiya, M., Niimi, I. and Okumura, K. (1987). Flame spraying fabrication of silicon carbide whisker-reinforced aluminium, *J. Mater. Sci Lett.*, 6, 191–193.
- Tucker Jr, R.C. (1982). Plasma and detonation gun deposition techniques and coating properties, in *Deposition Technologies for Films and Coatings*, R.F. Bunshah (Ed.), Noyes Publications, Park Ridge, NJ, USA, pp. 454–489.
- Tucker, Jr, R.C. and Ashari, A.A. (1998). The structure–property relationship of erosion resistant thermal spray coatings, in *Thermal Spray: Meeting the Challenges of the 21st Century*, C. Coddet (Ed.), ASM International, Materials Park, OH, USA, pp. 259–262.
- Tului, M. (2003). Propriétés optiques d'oxydes et de borures obtenus par projection plasma sous différentes pressions, *PhD Thesis*, Ecole Nationale Supérieure de Chimie de Lille, Lille, France.
- Tului, M., Ruffini, F., Arezzo, F., Lasisz, S., Znamirowski, Z. and Pawlowski, L. (2002). Some properties of atmospheric air and inert gas high-pressure plasma sprayed ZrB<sub>2</sub> coatings, *Surf. Coat. Technol.*, 151–152, 483–489.
- Tului, M., Arezzo, F. and Pawlowski, L. (2004). Optical properties of plasma sprayed semiconducting oxides, in *Proceedings of the International Thermal Spray Conference'04*, CD-Rom, ISBN 3-87155-792-7, DVS-Verlag, Düsseldorf, Germany.
- Unger, R.H. (1987). Comparison of thermal spray bond coats, in *Thermal Spray: Advances in Coatings Technology*, D.L. Houck (Ed.), ASM International, Materials Park, OH, USA, pp. 365–370.
- Usmani, S., Sampath, S., Houck, D.L. and Lee, D. (1997). Effect of carbide grain size on sliding and abrasive wear behavior of thermally sprayed WC–Co coatings, *Tribol. Trans.*, 40, 470–478.

- Valente, T. (1997). Statistical evaluation of Vicker's indentation test results for thermally sprayed materials, *Surf. Coat. Technol.*, **90**, 14–20.
- Varacalle, Jr, D.J., Lundberg, L.B., Herman, H., Bancke, G. and Riggs II, W.L. (1994). Vacuum plasma sprayed zirconium carbide coatings, *Surf. Coat. Technol.*, **68–69**, 86–91.
- Varacalle, Jr, D.J., Lundberg, L.B., Crawmer, D.E. and Didier, P.A. (1995). An experimental study of the air plasma spraying of aluminum powder, in *Thermal Spray: Science and Technology*, C.C. Berndt and S. Sampath (Eds), ASM International, Materials Park, OH, USA, pp. 381–386.
- Verpoort, C. and Baumann, R. (1992). Verschleissmechanismen untersuchen, verstehen und einschränken, *Zeits. Metall. Oberfläche*, **46**(9).
- Veys, J.M., Riviere, A. and Mevrel, R. (1988). Mechanical properties of LPPS NiCoCrAlTa alloy, in *1st Plasma Technik Symposium*, Vol. 2, H. Eschnauer, P. Huber, A.R. Nicoll and S. Sandmeier (Eds), Plasma Technik AG, Wohlen, Switzerland, pp. 115–123.
- Vinayo, M.E., Gaide, L., Kassabji, F. and Fauchais, P. (1985). Optimization of some spraying parameters under low pressure and controlled atmosphere, in *Proceedings of the 7th International Symposium on Plasma Chemistry*, C.J. Timmermans (Ed.), IUPAC, University of Technology, Eindhoven, The Netherlands, 1–5 July, pp. 1161–1166.
- Vos, F., Delaey, L., De Bonte, M. and Froyen, L. (1998). Plasma sprayed self-lubricating Cr<sub>2</sub>O<sub>3</sub>–CaF<sub>2</sub> coatings: friction and wear properties, in *Thermal Spray: Meeting the Challenges of the 21st Century*, C. Coddet (Ed.), ASM International, Materials Park, OH, USA, pp. 117–122.
- Voyer, J. and Marple, B.R. (2000). Thermal spray processing of WC–Co nanomaterials, in *Thermal Spray: Surface Engineering via Applied Research*, C.C. Berndt (Ed.), ASM International, Materials Park, OH, USA, pp. 895–904.
- Wallace, J.S. and Ilavsky, J. (1997). Elastic modulus measurements in plasma sprayed deposits, in *Thermal Spray: A United Forum for Scientific and Technological Advances*, C.C. Berndt (Ed.), ASM International, Materials Park, OH, USA, pp. 757–762.
- Wang, B. (1997). The erosion–corrosion behaviour of thermal sprayed coatings in fluidized combustor systems, in *Surface Modification Technology*, X, T.S. Sudarshan, K.A. Khor and M. Jeandin (Eds), The Institute of Materials, London, UK, pp. 265–279.
- Wang, D. and Berndt, C.C. (1991). Anisotropic thermal expansion bahaviour of thermally sprayed coatings, in *2nd Plasma Technik Symposium*, Vol. 2, S. Blum-Sandmeier, H. Eschnauer, P. Huber and A.R. Nicoll (Eds), Plasma Technik AG, Wohlen, Switzerland, pp. 295–304.
- Wang, H.G. and Herman, H. (1990). Thermomechanical properties of plasma sprayed oxides in the MgO–Al<sub>2</sub>O<sub>3</sub>–SiO<sub>2</sub> system, *Surf. Coat. Technol.*, **42**, 203–216.
- Wang, B.Q., Geng, G.Q., Levy, A.V. and Buchanan, E.R. (1992). Elevated temperature erosion of carbide–metal composite coatings, in *Thermal Spray: International Advances in Coatings Technology*, C.C. Berndt (Ed.), ASM International, Materials Park, OH, USA, pp. 735–742.
- Wang, X., Heberlein, J., Pfender, E. and Gerberich, W. (1996). Effect of gas velocity and particle velocity on coating adhesion in wire-arc spraying, in *Thermal Spray: Practical Solutions for Engineering Problems*, C.C. Berndt (Ed.), ASM International, Materials Park, OH, USA, pp. 807–811.
- Wang, J., Sun, B., Guo, Q., Nishio, M. and Ogawa, H. (2002). Wear resistance of a Cr<sub>3</sub>C<sub>2</sub>–NiCr detonation spray coating, *J. Therm. Spray Technol.*, **11**, 261–265.

- Wank, A., Wielage, B., Jansen, F., Wieczorek, D. and Höhle, H.-M. (2005). Corrosion properties of X-HVOF corrosion protective coatings, in *Proceedings of the International Thermal Spray Conference '05*, E. Lugscheider (Ed.), CD-Rom, ISBN 3-87155-793-5, DVS-Verlag, Düsseldorf, Germany.
- Weaver, D.T., Miller, F.S., Van Aken, D.C. and Smith, J.D. (2000). Development of cordierite coatings for low temperature thermal expansion refractory concretes, in *Thermal Spray: Surface Engineering via Applied Research*, C.C. Berndt (Ed.), ASM International, Materials Park, OH, USA, pp. 829–835.
- Weirich, G. and Wilwerding, A. (1983). Economical hard surfacing by flame spraying and flame fusing of metal powders, in *Proceedings of the 10th International Thermal Spray Conference Essen*, Vol. 80, DVS, Düsseldorf, Germany, pp. 129–132.
- Wen, J., Zhang, Z. and Liu, X. (1988). Wear resistance of arc sprayed aluminium bronze coatings, in *International Symposium on Advanced Thermal Spraying Technology and Allied Coatings*, Osaka, Japan, 13–15 May, pp. 405–409.
- Westfall, L.J. (1987). Composite monolayer fabrication by an arc spray process, in *Thermal Spray: Advances in Coatings Technology*, ASM International, Materials Park, OH, USA, pp. 417–426.
- Wielage, B. and Drozak, J. (1990). Haftungsprobleme bei APS-gespritztem Verbundwerkstoffen, in *TS90*, Vol. 130, DVS, Düsseldorf, Germany, pp. 243–246.
- Wielage, B., Milewski, W. and Drozak, J. (1990). Einfluß der Spritzverfahren auf die Eigenschaften von Nickelschichten, in *TS90*, Vol. 130, DVS, Düsseldorf, Germany, pp. 206–209.
- Wilkes, K.E. and Lagedrost, J.F. (1973). *Thermophysical properties of plasma sprayed coatings*, NASA Report, CR-121144, Lewis Research Center, Cleveland, Ohio, USA.
- Wolf, P.C. and Longo, F.N. (1980). Vacuum plasma spray process and coatings, in *Proceedings of the 9th International Thermal Spray Conference*, Nederlands Instituut voor Lastchniek, The Hague, The Netherlands, pp. 187–96.
- Wolfila, T.A. and Tucker, Jr, R.C. (1978). High temperature wear-resistant coatings, *Thin Solid Films*, **53**, 353–364.
- Wu, H., Jin, Y., Nicoll, A.R. and Barbezat, G. (1994). Friction and wear of a plasma sprayed  $\text{Al}_2\text{O}_3$ –40 %  $\text{ZrO}_2$ -cast iron system, *Wear*, **176**, 49–60.
- Xiong, T., Bao, Z., Li, T. and Li, Z. (2005). Study on cold-sprayed copper coating's properties and optimizing parameters for the spraying process, in *Proceedings of the International Spray Thermal Conference '05*, E. Lugscheider (Ed.), CD-Rom, ISBN 3-87155-793-5, DVS-Verlag, Düsseldorf, Germany.
- Yang, Y., Liu, Z., Luo, C. and Chuang, Y. (1997). Measurements of residual stress and bond strength of plasma sprayed laminated coatings, *Surf. Coat. Technol.*, **89**, 97–100.
- Yoshida, M. and Tani, K. (2004). Erosion mechanism of thermally sprayed coatings depending on shape and hardness of particles, in *Proceedings of the International Thermal Spray Conference'04*, CD-Rom, ISBN-3-87155-792-7, DVS-Verlag, Düsseldorf, Germany.
- Yoshida, M., Yomogizawa, M. and Endo, N. (2002). Particulate erosion resistance of thermally sprayed coatings at elevated temperature, in *Proceedings of International Thermal Spray Conference 2002 Essen*, E. Lugscheider and C.C. Berndt (Eds), DVS, Düsseldorf, Germany, pp. 408–413.
- Znamirowski, Z., Czarczynski, W., Pawlowski, L. and Le Maguer, A. (2003a). Field emission from the laser engraved surface, *Vacuum*, **70**, 397–402.

- Znamirowski, Z., Czarczynski, W., Le Maguer, A. and Pawlowski, L. (2003b). Plasma sprayed and laser engraved field electron emitters, *Surf. Coat. Technol.*, **165**, 211–215.
- Znamirowski, Z., Pawlowski, L., Cichy, T. and Czarczynski, W. (2004). Low macroscopic field emission from surface of plasma sprayed and laser engraved  $\text{TiO}_2$ ,  $\text{Al}_2\text{O}_3 + 13\text{TiO}_2$  and  $\text{Al}_2\text{O}_3 + 40\text{TiO}_2$  coatings, *Surf. Coat. Technol.*, **187**, 37–46.

# 9

## Applications of Coatings

Thermal spraying is a part of the coatings' industry. The businesses, which are clearly related to thermal spraying, are as follows (Walser, 1996):

- manufacturing of equipment, such as spray installations and their infrastructure;
- production of consumables, such as spray feedstocks and spray gases;
- coating deposition services.

Annual values of the entire market can be estimated<sup>1</sup> by adding the reported values of the national and regional markets, namely:

- 800 M Euros in Europe in the year 2000 (Ducos and Durand, 2001);
- 220 M Euros in Japan in the year 2001 (Tani and Nakahira, 2004);
- 110 M Euros in China in the year 2002 (Xiaouou and Yufen, 2004).

The North and South American market can be supposed to be equal to the European one, which gives a world market for thermal spraying which is worth about 2 billion Euros at the present time.<sup>2</sup> The coating deposition service is a major part of the thermal-spray market, e.g. 77 % of the European market following the study of Ducos and Durand (2001). The typical industrial sectors in which thermal spray coatings are used in different countries are collected in Table 9.1. The number

---

<sup>1</sup> This estimation is rough because economic statistics differ from country to country.

<sup>2</sup> Supposing an annual production of one person in a year of 100 000 Euros, this corresponds to the number of employees in the thermal spraying industry equal to 20 000.

Table 9.1 Principal industrial sectors in selected countries/regions using thermal spray coatings

Reference	Country/ region	Greatest sectors in order of decreasing part of the market (%)					Remarks
		1	2	3	4	5	
Xiaouo and Yufen, 2004	China	Corrosion protection (25)	Steel (20)	Textiles (10)	Automobile and engines (10)	Process industries (10)	—
Ducos and Durand, 2001	European Union	Aeronautical (28)	Automobiles (15)	Process industries (13)	Machine building (heavy wear) (11)	Corrosion protection (10)	Corrosion protection, including chemical industry and civil engineering
Tani and Nakahira, 2004	Japan	Machine building (24)	Printing and paper industries	Steel structures, bridges (15)	Steel (14)	Semiconductors, liquid crystal displays (10)	Steel structures and bridges, corresponding to part of corrosion protection

of different applications of sprayed coatings is growing steadily. The available hardware and consumables, many trained development engineers, the technical maturity of many spray techniques and, last but not least, new methods of spraying, such as the cold-gas spray technique, are significant factors in this growth. The applications described in this chapter are intended to be typical. On the other hand, emerging applications, e.g. solid-oxide fuel cells in the energy sector, are described with further details and perspectives of development. Descriptions of case-studies, i.e. practical solutions for particular problems follow, if possible, the pattern of:

- identification of problems, such as scuffing wear, abrasion, etc.;
- specification of coating properties;
- proposed solutions, namely:
  - coating processes and materials;
  - pre-/post-spray techniques;
- evaluation of the conformity of coatings' properties with specifications.

A similar procedure is used by research and development engineers during development of a new coating (see, e.g. Chapter 7, Figure 7.1).

Finally, it should be stressed that many successful applications of coatings have occurred by 'technology transfer' from one industrial sector to another.

## 9.1 AERONAUTICAL AND SPACE INDUSTRIES

### 9.1.1 AERO-ENGINES

The design of an aero-engine is subject to the principle of a high power-to-weight ratio and demands the highest possible performance of each component (Anon, 1986). The materials used to manufacture engines are high-tensile steel, titanium, high-temperature nickel and cobalt alloys. The methods of machining the engine components include:

- grinding;
- turning;
- drilling;
- boring.

More demanding materials are machined by the following treatments:

- electrodischarge;
- electrochemical;
- laser hole drilling;
- chemical size reduction.

Thermal spraying is one of many manufacturing methods used on partly finished or finished components, including:

- heat treatment;
- electroplating;
- anodizing;
- chemical and mechanical cleaning.

Today, applications in the aero-engine industry represent an important part of the market for thermal spray coatings (Longo, 1992). The coatings applied in aero-engines have the functions presented in Figure 9.1.

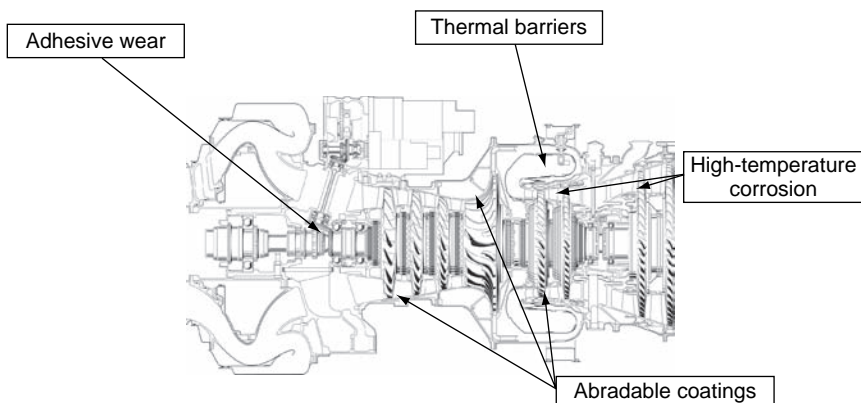
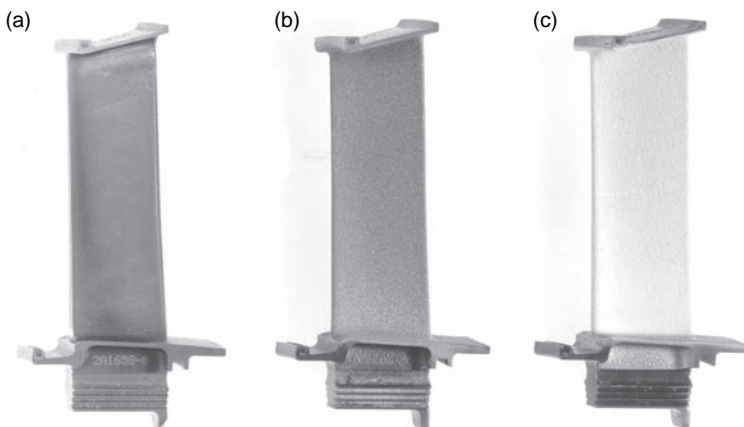


Figure 9.1 Section of an aero-engine showing the families of thermally sprayed coatings and their places of application (Crabos, 2003). Reproduced by permission of Tuboméca, Bordes, France

Typical materials and processes used to realize the functions are as follows (Crabos, 2003):

- Adhesive wear:
  - WC–Co and Cr<sub>3</sub>C<sub>2</sub>–NiCrAlY by high-velocity combustion spraying and detonation-gun spraying;
  - Al<sub>2</sub>O<sub>3</sub> or Cr<sub>2</sub>O<sub>3</sub> by air-plasma spraying.
- The duplex thermal barrier is usually ZrO<sub>2</sub> stabilized with 8 wt % Y<sub>2</sub>O<sub>3</sub> by air-plasma spraying onto an NiCrAlY bond coating applied by a plasma under vacuum (see Figure 9.2).



**Figure 9.2** Turbine blades coated with duplex barrier coatings at different stages of preparation: (a) uncoated blade; (b) blade with bond coating; (c) blade with bond and top coatings. Reproduced by permission of MTU Aero Engines, Munich, Germany

- High-temperature corrosion resistant coatings, such as those sprayed by a plasma under vacuum:
  - NiCrAlY;
  - NiCoCrAlYTa.
- Abradable coatings, such as:
  - Al + 6 wt % Si sprayed by a flame;
  - a composite of Al–Si + polyester by air-plasma spraying;
  - a composite of CoNiCrAlY with BN and a polyester by air-plasma spraying;
  - CoNiCrAlY by vacuum-plasma spraying.

Some examples of parts on which thermally sprayed coatings are applied in aero-engines include (Rhys-Jones, 1990; Crabos, 2003):

- Adhesive wear:
  - *fan blade clappers*;
  - *stator blades*;
  - *flame tube locations*.
- Duplex thermal barriers:
  - *combustion cans*;
  - *combustion vanes*;
  - *turbine blades* (see Figure 9.2).
- Corrosion-resistant coatings:
  - *turbine vanes*;
  - *turbine blades*.
- Abradable coatings:
  - *sectors of turbine rings*.

Adhesive-wear-resistant coatings have to withstand temperatures of up to 850 K. The corrosion that occurs in aero-engines can be influenced by a ‘salt environment’. Such an environment is experienced when the aircraft approaches the sea surface (Meetham, 1985). This author reports the application of such coatings in the Pegasus engine of the Harrier military aircraft. The temperature of the gas in the *combustors* of commercial aircraft exceeds 1640 K. The parts of the combustor must be made of ‘super-alloys’ with melting points of about 1500–1590 K (Manning Meier *et al.*, 1991). Without the protection provided by the thermal barrier coatings, such alloys would fail by melting, creeping or oxidation.

Thermal barriers have a typically duplex configuration, as proposed for the first time by Stecura (1977). Such a duplex is specified for the *platforms of turbine stator blades* in the RB211-534E4 aero-engine of Rolls-Royce (Meetham, 1985). The barriers are also applied in the ‘first-stage’ *vane platforms* in the *high-pressure turbine* of the JT9D-70/59 turbofan aero-engine made by Pratt and Whitney (Sumner and Ruckle, 1980). Application of a sprayed thermal barrier was reported to enable a reduction in the cooling-air requirements.

Abradable coatings are used to ensure that the engine ‘working-fluids’ (air in the compressor and fuel-combustion products with air in the turbine) flow over the blade and not between the blade and a *casing liner* (Rhys-Jones, 1990). This can be achieved by coating the *casing liner* with an abradable coating and the blade tip with an abrasive one. Each coating adapt to its ‘partner’ and forms an optimal seal. In the *turbine*, the typical abradable coatings are thermal barriers and the abrasive ones are M–Cr–Al–X alloys with some additives (e.g. alumina) to enhance abrasivity (Rhys-Jones, 1990). A review of abradable coatings for high-temperature applications has been made recently (Schmid *et al.*, 2000). These authors suggested a composite coating of CoNiCrAlY–BN–polymer deposited by air-plasma spraying for all applications in which the operating temperature does not exceed 870 K, such as jet engines, land-based gas turbines, industrial *compressors*, and *turbochargers*.

Finally, in the modern RB211 aero-engine, which powers the Boeing 747 aircraft and is manufactured by Rolls-Royce, about 50 % of all of the parts are coated (Meetham, 1985; Anon, 1986). The contribution of thermal spraying, among the coating methods used in aero-engines, increases and those of the galvanic coating methods decreases. In particular, electrolytically deposited chromium coatings are associated with hexavalent chrome emission<sup>3</sup> and are replaced by high-velocity combustion-sprayed tungsten carbide–tungsten composites (Grasset, 2003). Such coatings have replaced galvanic chrome in the TF 33 aero-engines produced by Pratt and Whitney in the following components (Froning *et al.*, 2004):

- *low-pressure turbine shafts;*
- *high-pressure turbine shafts;*
- *bearing housings;*
- *rear-compressor rear-hubs;*
- *front-compressor rear hubs.*

### 9.1.2 LANDING-GEAR COMPONENTS

*Landing-gear* components, which include *inner cylinders*, *drag braces*, *struts* and *brake torque tubes*, are made from low-alloy steels and are

---

<sup>3</sup> Hexavalent chrome is known to be carcinogenic to humans.

chromium-plated. At present, this type of coating is being replaced by high-velocity combustion-sprayed carbide coatings. For example, Delta Air Lines have sprayed WC–Co–Cr deposits for replacing chromium by using this technique (Randolph, 2004). The procedures of cleaning, old coating removal and non-destructive testing were also reportedly adapted to the sprayed coatings.

### 9.1.3 ROCKET THRUST-CHAMBER LINERS

The requirements of materials for *thrust chambers* in *rocket nozzles* include the following:

- a low thermal conductivity;
- a smooth exterior surface;
- a strain-relief mechanism.

The technology of production of *ceramic rocket thrust-chambers* using thermally sprayed materials was developed to meet these requirements (Quantmeyer *et al.*, 1985). This *spray forming* technology includes two plasma sprayed coatings:

- $\text{ZrO}_2 + 8 \text{ wt\% Y}_2\text{O}_3$ , 80 to 130  $\mu\text{m}$  thick, or  $\text{ZrO}_2 + 8 \text{ wt\% CaO}$ , 200  $\mu\text{m}$  thick;
- Ni + 20 wt% Cr, 130–380  $\mu\text{m}$  thick.

The complete technology includes the following steps:

- preparation of a stainless-steel mandrel;
- plasma spraying of a zirconia coating and subsequently an NiCr coating;
- electrodeposition of a copper deposit of 2 mm thickness and milling grooves in the copper for ‘coolant passage’;
- filling the grooves with a wax and forming ‘close-outs’ on unprotected areas by the electroplating of copper with a thickness of about 5 mm.
- removing the wax and final machining.

The *liners* prepared with this technology show a ten-fold increase in the thrust chamber lifetime when compared to the standard uncoated copper thrust chambers. Nguyentat *et al.* (1992) applied the vacuum-spray technique to prepare components for the combustion chamber of the

*Advanced Launch System.* The tested coating materials included alloys, such as IN-718, IN-625 and JBK-75, sprayed onto copper tubes. The authors concluded that vacuum-sprayed coatings can be applied to form a ‘structural jacket’ supporting the combustion chamber liner. A *circular aerospike plug*, a part of a ‘supersonic aircraft’, is also manufactured with the help of thermal spraying (Vlcek *et al.*, 1999). In fact a *pressure-jacket* was realized by the use of high-velocity combustion spraying of a 316L stainless-steel. The *spray-forming* technology of this piece also includes spraying of a water soluble, AlSn-based alloy, known as *Aqualloy*. These authors underlined the cost-effectiveness of the process resulting from avoiding welding during manufacturing of the pressure-jacket.

## 9.2 AGROALIMENTARY INDUSTRY

Many agroalimentary liquids, also containing solid components (fruits, etc.) are transported by using *twin-screw machines*. The machines often need ‘run-in coatings’ (abradable), which may assure optimal clearance between a rotor and a stator. The requirements for such run-in coatings in these machines are as follows (Bach *et al.*, 2000):

- fast run-in effect;
- suitable abradability for sliding velocities up to 150 m/s;
- sufficient corrosion and erosion resistance;
- sufficient lifetime;
- high-temperature resistance up to 673 K;
- satisfactory adhesion;
- thicknesses up to 500 µm;
- low price.

The authors proposed  $\text{ZrO}_2 + 8 \text{ wt\% Y}_2\text{O}_3$  coatings obtained by air-plasma spraying with a controlled porosity, achieved by an unusually large spray distance and a low electric power input to the plasma torch.

## 9.3 AUTOMOBILE INDUSTRY

Automobile manufacturing is an increasing market for thermal spraying and the number of coating applications grows steadily. Typical examples of applications are collected in Table 9.2. One of the most important

Table 9.2 Typical applications of thermally sprayed coating in automobiles (Barbezat, 2005, 2006)

Group of applications	Component	Coating material	Coating function and requirements	Coating process
Motor (diesel, gasoline, gas)	Cylinder bores	Composite of steel with iron oxides	High scuffing and wear resistance	Air plasma spraying with a RotaPlasma™ torch
	Piston ring (gasoline engine)	Mo + NiCrBSi		Air-plasma spraying
	Piston ring (diesel engine)	Cr <sub>3</sub> C <sub>2</sub> + NiCr		
	Piston head (diesel engine)	Duplex: MCrAlY and ZrO <sub>2</sub> + Y <sub>2</sub> O <sub>3</sub>	Seizure, wear and abrasion resistance	High-velocity combustion-spraying
	Oxygen detector (lambda sensor)	Al <sub>2</sub> O <sub>3</sub> , MgO	Thermal-barrier and corrosion resistance	Air-plasma spraying
	Nozzle of injection (diesel engine)	Mo	Erosion resistance and thermal-shock resistance	
	Synchron ring	Mo	Corrosion and erosion resistance	Flame spraying using a powder or wire
	Gear-shift fork	Mo	Constant friction coefficient and seizure resistance	Flame spraying using a wire
	Power train	Steel	Weight reduction and lifetime prolongation	Air-plasma spraying or high-velocity combustion-spraying
	Various	Copper based alloys (CuPbSn)	Adhesion wear and seizure resistance	High-velocity combustion-spraying

applications in this sector is the development of coatings inside the cylinders of motor blocks. The following spray techniques have been considered for coatings in cylinder bores made of light AlSi alloys (Barbezat *et al.*, 1999; Barbezat, 2005):

- the plasma-transferred arc process (wire-arc process);
- high-velocity combustion-spraying (wire or powder);
- rotating plasma using a powder (RotaPlasma<sup>TM</sup>).

The specifications with regard to the coating deposited onto cylinder walls result from the balance in the tribological system, which includes the cylinder wall, piston ring and lubrication in an internal-combustion engine. These can be summarized as follows (Barbezat *et al.*, 1999):

- low coefficient of friction and low wear against the piston ring under lubrication conditions;
- lower wear rate than that of the cast-iron liner under similar tribological conditions;
- good resistance against thermal shocks;
- consistent properties after surface finishing;
- ‘strategic materials’, such as nickel or cobalt, should be excluded;
- porosity should be adequate in order to retain oil and provide the necessary lubrication conditions.

The materials tested for the coatings using the RotaPlasma<sup>TM</sup> technique were, among others:

- Carbon steel with the solid lubricants *wüstite* ( $\text{FeO}$ ) and *magnetite* ( $\text{Fe}_3\text{O}_4$ ), having the ferritic structure and an  $HV_{0.3}$  of 400, of adhering to the AlSi cast alloy with a bond strength of 40–60 MPa, a 2 % porosity, typical thicknesses after machining and finishing ('smooth honing') of 70–170  $\mu\text{m}$  and a friction coefficient against 'nitrided steel' of  $\mu \approx 0.09$ .
- A carbon tool steel composite with molybdenum, having the ferritic structure, including iron carbides and molybdenum as isolated phases, and an  $HV_{0.3}$  of 400.
- Corrosion-resistant steel alloyed with chromium and molybdenum, with the  $\alpha$ -Fe structure, including fine carbides and oxides, and an  $HV_{0.3}$  of 350.

An estimation of the costs via the use of four rotating plasma torches was based on a price of 1.65 €/bore and some examples of coatings for industrial applications are shown in Table 9.3.

**Table 9.3** Examples of combustion engines using plasma-sprayed coatings in cylinder bores (Barbezat, 2005) Reproduced by permission of Sulzer Metco AG, Wohlen, Switzerland from G. Barbezat, 'Application of thermal spraying in the automobile industry', in *Proceedings of the 2nd Recontres Internationales sur la Projection Thermique*, L. Pawlowski (Ed.), 1–2 December, 2005, Lille, France, Sulzer Metco AG, Wohlen, Switzerland, pp. 231–235

Number	Engine	Number of cylinders	Vehicle
<i>Gasoline engines</i>			
1	Lupo FSI 1.4 l	4	VW Lupo
2	Bugatti W 16	16	'Exclusive' car
<i>Diesel engines</i>			
3	V 10 TDI	10	VW Touareg, Phaeton
4	L 5EA 115	5	VW Touareg, Van T5

## 9.4 CERAMICS INDUSTRY

The ceramics industry is more traditional and changes in the manufacturing technologies have not been very rapid.

### 9.4.1 FREE-STANDING SAMPLES

Ceramic rolls are one of the most frequently used products of the ceramics industry. Rolls and cone-shaped pieces of different ceramics, obtained by air-plasma spraying, were reported a long time ago by Kirner (1980). These ceramics were prepared as *free-standing samples* (see Chapter 7, Section 7.2.3.). Lutz (1993) used a water stabilized plasma torch to prepare rolls of 79 mm diameter and a wall thickness of  $3.2 \pm 0.2$  mm. These rolls were applied as *band rollers* in contact with zinc and aluminium melts (Figure 9.3).

Another application, reported by Holcombe (1978), concerns an  $\text{Y}_2\text{O}_3$  tube of an external diameter of 59 mm, a length of 178 mm and a wall thickness of 0.8 mm. Holcombe reports applications of sprayed



Figure 9.3 Ceramic tubes prepared by a water-stabilized plasma torch. Reproduced by permission of Dr. T. Vilics, LWK Plasmakeramik GmbH, Gummersbach, Germany

ceramic tubes for ‘thermocouple sheats’. Comparison of free-standing samples with a tube of porous ceramic the Sillimantin 60<sup>TM4</sup>, prepared by a ‘classical’ sintering technique, shows that the mechanical properties ( $E$ ,  $\sigma_f$ ) of sprayed (and post-spray treated) ceramics are comparable to the sintered ones (Table 9.4). The sprayed ceramics can be reportedly welded via the use of a CO<sub>2</sub> laser (Lutz and Florian, 1993).

#### 9.4.2 BRICK-CLAY EXTRUDERS

These *extruders* are of a mild-steel casting with replaceable mild-steel wear plates (Hoffman, 1980). The air-plasma-sprayed WC-17Co coatings on the wear plates were successfully tested.

<sup>4</sup> Sillimantin 60 is a tradename used by W Haldenwanger GmbH, Berlin, Germany.

Table 9.4 Properties of ceramic rolls prepared by thermal spraying

Number Reference	Powder	Process		Microstructure		Properties		
		Grain size ( $\mu\text{m}$ )	Chemical composition (wt%)	Technique	Post-spray $\rho$ ( $\text{kg}/\text{m}^3$ )	Phases	$E$ (GPa)	$\sigma_f$ (MPa)
1 Holcombe, 1978	—	Y <sub>2</sub> O <sub>3</sub>	APS	—	4450	—	—	8
2 Lutz, 1993	-180	Al <sub>2</sub> O <sub>3</sub> + 0.02SiO <sub>2</sub>	WSP	1823 K for 4 h in air	3580	$\alpha$ -Al <sub>2</sub> O <sub>3</sub>	165	79.4 ± 9.9 7.4–9.0
3 Lutz, 1993	-200	Al <sub>2</sub> O <sub>3</sub> + 22.3ZrO <sub>2</sub>			3373	$\alpha$ -Al <sub>2</sub> O <sub>3</sub> , (T+M) ZrO <sub>2</sub>	95	76 ± 4.6 7–9
4 Lutz, 1993	—	Sillimanite 60 <sup>rm</sup> ; Al <sub>2</sub> O <sub>3</sub> + (25–27)SiO <sub>2</sub>	Sintering	—	—	56 ± 12	37.2 ± 2.1	4.6–5.7

### 9.4.3 CRUCIBLES TO MELT OXIDE CERAMICS

*Graphite crucibles* are used to melt oxide ceramics such as  $\text{Al}_2\text{O}_3$ ,  $\text{Al}_2\text{O}_3\cdot\text{ZrO}_2$  and  $\text{Al}_2\text{O}_3\cdot\text{Y}_2\text{O}_3$ . To avoid carbon contamination of the oxides, the refractory metal coatings were evaluated to deposit onto graphite (Sordelet and Ellis, 1993). The air-plasma-sprayed coatings were tested at temperatures greater than 2370 K. The most promising results were achieved with a tungsten coating of 630  $\mu\text{m}$  and duplex coatings of tantalum on tungsten and rhenium on tungsten with similar total thicknesses. The major problem was the penetration of the liquid ceramic into the coating. Application of denser coatings obtained by the cold-spray method are expected to give better results.

### 9.4.4 CERAMIC MEMBRANES

Brozek *et al.* (1993) proposed use of a water-stabilized plasma torch to produce ceramic membranes. The tested ceramics included  $\text{TiB}_2$ ,  $\text{B}_4\text{C}$ ,  $\text{MoSi}_2$ ,  $\text{SiC}$ ,  $\text{Ti-TiN-TiO}_2$ ,  $\text{ZrSiO}_4$ ,  $\text{Al}_2\text{O}_3$ ,  $\text{Al}_2\text{O}_3 + 13 \text{ wt\% TiO}_2$  and *mullite*. It was possible to modify the porosities of the membranes by using different powder grain sizes. The coatings were sprayed onto an Mo substrate that was later oxidized at 1240 K.

## 9.5 CHEMICAL INDUSTRY

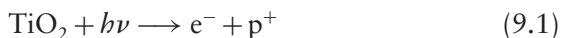
Among many applications of thermal spraying in the chemical industry, the development of photocatalytic surfaces seems to be the most promising and many laboratories around the world have tested different materials and spray methods in this regard. Thermally sprayed coatings are used in many branches of the chemical industry to protect against different form of wear and corrosion.

### 9.5.1 PHOTOCATALYTIC SURFACES

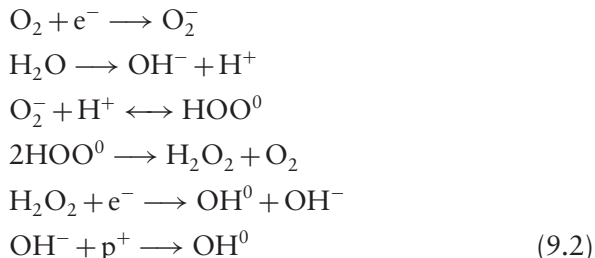
The degradation and destruction of organic pollutants is an important issue in the chemical industry today. Thermally sprayed coatings of semiconducting oxides, such as  $\text{TiO}_2$ ,  $\text{ZnO}$  or  $\text{SnO}_2$ , pure or doped, are studied in order to provide a solution to this problem. Photocatalysis

was ‘discovered’ by Fujishima and Honda (1972) in the presence of  $\text{TiO}_2$ , water and air. These authors tested the original titanium oxide electrodes in water. The mechanism seems to also concern humid air, as discussed in the paper of Herrmann and Guillard (2000). The authors explain the mechanism of photocatalysis as follows:

- Initially, an electron–hole pair is generated on the semiconductor’s surface by a quantum of light:



- Subsequently, two reactions, including electrons, holes, anions and cations in water and oxygen molecules in air, can take place until the formation of the free radical  $\text{OH}^0$ :



The free radical may react with a pollutant by degrading it until a stable compound is formed. Examples of such pollutants are, after Herrmann and Guillard (2000) and Ye and Ohmori (2002), as follows:

- pesticides;
- detergents;
- dyes;
- herbicides.

Titanium oxide is recognized as an excellent photocatalyst. Among three  $\text{TiO}_2$  phases, namely *rutile*, *anatase* and *brookite*, anatase seems to be more photocatalytically active (Berger, 2004). The forbidden gap of anatase is about 3.2 eV, which makes necessary the application of UV radiation to generate electron–hole pairs. Photocatalytic coatings are being produced using different methods in laboratories around the world:

- The research group of Professor Ohmori (Osaka, Japan) used atmospheric-plasma spraying of coarse powders having the following

compositions:  $\text{TiO}_2$  (Ohmori *et al.*, 2002),  $\text{TiO}_2$  doped with  $\text{Fe}_3\text{O}_4$  (Ye and Ohmori, 2001, 2002a, Ye *et al.*, 2003) and  $\text{TiO}_2$  doped with  $\text{ZnO}$  (Ye and Ohmori, 2002b). The titanium oxide feedstock was anatase of a 0.2  $\mu\text{m}$  size and was agglomerated by spray drying up to the final size of about 30  $\mu\text{m}$ . These authors tested the photodegradation of acetaldehyde by the use of UV light of wavelength,  $\lambda = 360$  nm and an intensity of 1 mW/cm<sup>2</sup>. The photolytic efficiency was the best for coatings sprayed using powders of chemical composition  $\text{TiO}_2 + 10 \text{ wt\% Fe}_3\text{O}_4$ .

- The group of Dr Bertrand (Belfort, France) initially used a similar spray technique to that described above, i.e. atmospheric-plasma spraying of a coarse spray-dried anatase powder (Toma *et al.*, 2004). Later, the researchers used atmospheric-plasma spraying of fine (25–50 nm)  $\text{TiO}_2$  powders composed mainly (80 vol %) of anatase. The fine powders were formulated in a solution including water and ethanol (Toma *et al.*, 2005, 2006). These authors tested photolytic activity by a decrease in  $\text{NO}_x$  in a reactor illuminated by UV radiation. The activity was lowered when an ethanol-based suspension was used.
- A similar technique of suspension-plasma spraying was applied in the group of Professor Pawlowski (Lille, France). These authors used rutile precursors having a size of about 0.33  $\mu\text{m}$  and found a transformation of rutile into anatase (Tomaszek *et al.*, 2006). The transformation rate increased with spray distance (Jaworski *et al.*, 2008).
- A liquid flame spray technique, using a torch supplied with  $\text{O}_2$ ,  $\text{N}_2$  and  $\text{H}_2$  and a liquid suspension of  $\text{Ti}(\text{OC}_2\text{H}_5)_4$  in ethanol, injected into a generated flame was used by Mäkelä *et al.* (2006) to form a  $\text{TiO}_2$  ‘nanometric’ soot onto a steel substrate. The fraction of anatase increased with the distance from the torch (up to 80 %). More anatase was also formed when the temperature of the substrate was lower. The powder generation method is not thermal spraying but rather chemical vapour deposition.

### 9.5.2 TOOLS IN PETROL SEARCH INSTALLATIONS

The tools used in petroleum mining fail due to two- and three-body abrasion, erosion and corrosion (Keshavan and Kembalyan, 1993). As the modifications of the tools’ design are limited, improvement in their

characteristics can be reached by the use of coatings. The following components were reportedly coated:

- *drill bit cones*, by the use of a WC-15 wt % Co powder by the Super D-gun™ technique;
- a *polycrystalline diamond cutter*, using a self-fluxing alloy having a composition (in wt%) of Ni, 43.5W, 6Cr, 1.35B, 1.9Fe, 6.25Co, 1.8Si and 3.1C, and flame spraying followed by post-spraying fusion in a furnace;
- *rotors*, using a powder having a composition (in wt%) of W, 20Cr, 7Ni and 6C by the Super D-gun™ technique.

### 9.5.3 VESSELS IN CHEMICAL REFINERIES

One of the vessels used in a refinery is made of 0.5Mo steel and has a diameter of 3 m and a length of 12 m. This vessel was designed with a wall thickness of 127 mm because of the expected corrosion by the high-temperature sulfur and ammonia environment (Moskowitz, 1992). Instead of replacing all vessels, which should cost about 600 000 US\$, coatings of stainless-steel 316L were sprayed instead by using a high-velocity oxy-fuel torch. The coatings were 760 µm thick. The entire cost of the coating operation was about 120 000 US\$ and the coatings protected the vessels against corrosion for 2 years.

### 9.5.4 GAS-WELL TUBING

The ends of gas-well tubing used in drilling research of gases are attacked by cavitation wear and by corrosion. Pipes of a 9 m length are connected to each other to reach a depth of 3000 m. These are subjected to H<sub>2</sub>S corrosion and to cavitation wear due to the gas velocity and poor contacts between the pipes (Moskowitz, 1992). To improve the contacts, a Hastelloy C-276 coating was applied by using high-velocity combustion spraying onto the pipe ends. An exposure test over three months showed satisfactory results.

### 9.5.5 POLYMERIC COATINGS ON PIPELINE COMPONENTS

Steel pipes are used in the construction of pipelines to transport pressurized natural gas from the sources (e.g. the northern territories of Russia)

to the final industrial users of the gas. The pipelines are buried underground and need corrosion-protection. Usually, three-layer polyethylene coatings, applied by electrostatic spray guns and extrusion are used and give entire satisfaction. The extrusion method is not suitable for coating more complicated elements of pipelines, such as *T-joints*, *bends* and *valves* (Vuoristo *et al.* 2003). The flame-spraying technique was tested by the use of polyethylene powders to reach thicknesses ranging from 1 to 3 mm. The bond coating was a fusion-bonded epoxy or a liquid-bonded epoxy having a thickness of about 200 µm. Different coatings were tested and a practical demonstration of deposition onto a real *valve* was carried out.

### 9.5.6 OZONIZER TUBES

Ozone is a chemically active gas which can be used as an oxidant in the treatment of water, bleaching and other processes that need intensive oxidation (Friedrich *et al.*, 1999a). The ozone can be produced in ozonizer tubes, as studied intensively at The University of Stuttgart in the group of Professor Gadow. The tubes are about 1–1.5 m long and have a diameter ranging from 30 to 70 mm. A cross-section of a tube including sprayed coatings is shown in Figure 9.4.

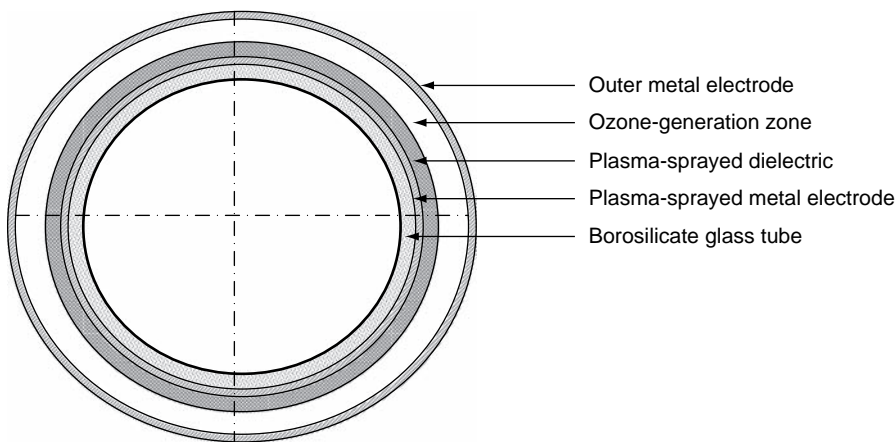


Figure 9.4 Cross-section of an ozonizer tube with thermally sprayed coatings, as studied at the University of Stuttgart

The electrodes are supplied with an AC high voltage (up to 12 kV) of low frequency,  $\nu = 50 - 625$  Hz. The voltage results in a discharge in the

flowing oxygen which leads to the formation of ozone. The efficiency of ozone production increases with the capacity of the tube, which, in turn, can be achieved by the use of thin dielectric films having high dielectric constant. The technology of ozonizers includes the following two air-plasma sprayed coatings (Friedrich *et al.*, 1998, 1999b): (i) an Al + 12 wt % Si alloy electrode deposited directly onto a borosilicate tube; (ii) a dielectric coating of  $\text{Al}_2\text{O}_3$ ,  $\text{Al}_2\text{O}_3 + 3$  wt %  $\text{TiO}_2$ ,  $\text{ZrO}_2$ ,  $\text{ZrO}_2 + 5$  or 30 wt %  $\text{CaO}$  and  $\text{ZrO}_2 + \text{Y}_2\text{O}_3$ . Among these ceramics, the zirconia-based ceramic gave the highest ozone production efficiency.

## 9.6 CIVIL ENGINEERING

Steel and concrete *bridges*, especially in regions close to sea, are subjected to humid air containing salt and to chemicals from the atmosphere (Klinge, 1973). Protection of the steel construction with zinc or aluminium by use of the arc-spraying technique is an application which permits the constructions to be protected for many years. These metals are less ‘noble’ than iron (see Chapter 7, Table 7.8). Thermal spray is in competition with painting as far as bridges in the USA are concerned (Herman, 1992). The following bridges have been reportedly protected by sprayed metal coatings (mainly Zn):

- the *Rombak Bridge* in Norway (Klinge, 1973);
- the *Pierre Laport bridge* (Quebec, Canada) over the St. Lawrence River of about 1 km length (Jadoin and Nadeau, 1980);
- the *Cape Creek Bridge* on coastal Highway 101 (California, USA) (Wixson, 1993);
- the *Kanmon Bridge* of about 1 km length between Honshu and Kyushu Islands (Japan) (Ishikawa *et al.*, 1993; Kobe, 1998);
- the *Howard Frankland Bridge* (Florida, USA) described by Kobe (1998).

The technology of the *Kanmon Bridge* protection includes a thermally spray Zn (75 µm thick) deposited onto all surfaces during the bridge construction. Subsequently, the bridge has been repainted every eight years with the use of the following polymers (Kobe, 1998):

- three layers of an ‘undercoating’ of epoxy resin;
- one layer of an intermediate coating of polyurethane resin;
- one layer of a top coating of polyurethane resin.

## 9.7 DECORATIVE COATINGS

Eerola (1993) reported on copper coatings deposited onto glass artware by flame spraying. Different-colour coatings were achieved thanks to regulation of the copper oxidation level ( $\text{Cu}_2\text{O}$  is red and  $\text{CuO}$  is black). Coating took place at the glass-blowing stage at temperatures of about 1000–1300 K. A black coating is reached if the sprayed deposit is left to oxidize in air. To achieve the red colour, the coating has to be covered with additional glass, which eliminates further oxidation. The ceramic oxide coatings might also be used for decorative purposes. Air-plasma spraying enables the obtaining of the following colours of deposits:

- white (alumina);
- grey (titania);
- blue (alumina–titania);
- black (chromia);
- yellow (zirconia).

Small additions of cobalt oxide or copper oxides to other oxides produce blue colours (Douglas, 1992). In cases of application of decorative coatings onto products which are in contact with food (dishes, etc.), care must be paid to *biocompatibility*. Moreover, the coatings are generally porous and absorb water and dirt which may result in loss of their original colour. This is why sealing might prove necessary.

## 9.8 ELECTRONICS INDUSTRY

The electronics industry is very innovative and accustomed to rapid introduction of new technologies. Thermal spraying belongs, from the point of view of an electronics technologist, to very thick-film technology. The usual thickness in thermal spraying is greater than 50  $\mu\text{m}$ , which is more than that in thick-film technology (up to 10  $\mu\text{m}$ ) and much more than that of PVD or CVD technologies (generally up to a few micrometres). The recent development of intermediate thick coatings (10–20  $\mu\text{m}$ ) obtained by vacuum-plasma spraying of fine metallic feedstocks (Loch and Barbezat, 2000) or suspension-plasma sprayed ceramic ‘multi-coatings’ (e.g. Tomaszek *et al.*, 2007) open new possibilities for electronics applications.

### 9.8.1 HEATERS

Heaters, thermally sprayed onto rolls or plates, have been described by Shibata *et al.* (1988) and, more recently, by Prudenziati *et al.* (2006) by the use of air-plasma spraying. Shibata and his colleagues realized a multilayer onto a steel cylinder, including a bond coating (NiAlMo alloy), an electrical insulator ( $\text{MgAl}_2\text{O}_4$ ) and heating coatings of:

- Cu-Zn ferrite;
- $\text{TiO}_2 + 10 \text{ wt\% NiCr}$  cermet;
- $\text{Al}_2\text{O}_3 + 10 \text{ wt\% NiCr}$  cermet.

Prudenziati *et al.* (2006) describes plate and cylindrical heaters for high-temperature applications (up to 873 K). The design of the heater includes the following coatings sprayed onto a metal substrate:

- a 100  $\mu\text{m}$  alumina insulating coating;
- a 30  $\mu\text{m}$  heating element in a form of a ‘meander’ produced by spraying of Ni, Ni20Cr or Ni5Al with the masks;
- a 100  $\mu\text{m}$  protecting top coating.

The heaters have a relatively small size (a few cm width and length for the plates) and will soon be applied in high-temperature operating sensors. An example of an industrial application of a heater sprayed onto the ‘cooking recipient’ of glass is shown in Figure 9.5.

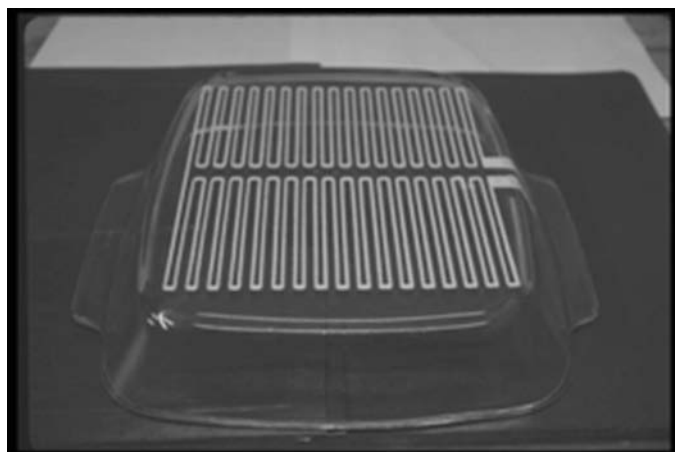


Figure 9.5 Electric heater coatings deposited onto a ‘cooking recipient’ of glass.  
Reproduced by permission of Terolabservices, Villeneuve-Le-Roi, France

### 9.8.2 SOURCES FOR SPUTTERING

Air-plasma sprayed *sputtering sources* of tantalum–hafnium mixtures have been fabricated by Locker and Malm (1971). These authors discovered that plasma spraying introduces slightly more non-metallic impurities than hot-pressed sources but the sources were still acceptable for use. Another example of an application of thermal spraying to fabricate sputtering sources comes from the study of Lugscheider and Weber (1989). These authors mentioned  $\text{YBa}_2\text{Cu}_2\text{O}_{7-x}$  ‘targets’ produced by using atmospheric-plasma spraying which resulted in high-quality PVD films having a critical current density of  $j_c = 10^5 - 10^6 \text{ A/cm}^2$ . RF spraying was applied by Müller *et al.* (2000) to obtain ‘targets’ of Cr onto Cu substrates. These authors optimized substrate cooling in order to obtain satisfactory adhesion of the coatings.

### 9.8.3 SUBSTRATES FOR HYBRID MICROELECTRONICS

The idea of *metal–ceramic substrates* for hybrid microelectronics was reported as early as 1978 by Smyth *et al.* (1978). Later on, other authors have considered this idea, e.g. Braguier and Tueta (1980), Golonka and Pawłowski (1983), Gorecka-Drzazga *et al.* (1984), Brown *et al.* (1986), Palmer (1992) and Prudenziati *et al.* (2006). The substrate is composed of a metal plate, made of *Kovar*, copper, aluminium, or steel and of a thermally sprayed electrically insulating ceramic layer, which is usually alumina. The metal has a high thermal conductivity ( $\lambda_m$ ), enabling the dissipation of heat generated by the high-power electronic circuits. The total heat conductivity of the substrate ( $\lambda_{tot}$ ) is given by the following expression (Golonka and Pawłowski, 1983):

$$\lambda_{tot} = \frac{\lambda_c(l+d)}{\left[ d \left( \frac{\lambda_c}{\lambda_m} + l \right) \right]} \quad (9.3)$$

In Equation (9.3),  $\lambda_c$  is the heat conductivity of the dielectric layer,  $d$  is the metal plate thickness and  $l$  is the sprayed coating thickness. We can take, for example, the following data:

- an  $l = 100 \mu\text{m}$  alumina layer, having a heat conductivity of  $\lambda_c = 6 \text{ W/(mK)}$  at 423 K;
- a  $d = 500 \mu\text{m}$  copper base, having a conductivity of  $\lambda_m = 400 \text{ W/(mK)}$ .

One can calculate the total thermal conductivity of a metal ceramic substrate to be equal to about  $\lambda_{\text{tot}} = 33 \text{ W}/(\text{mK})$ . This value is five times greater than that of sprayed ceramics and even greater than the heat conductivity of sintered alumina. The latter is equal to  $\lambda_c = 17\text{--}29 \text{ W}/(\text{mK})$  for sintered 96 wt%  $\text{Al}_2\text{O}_3$  applied for substrates in microelectronics, after Maissel and Glang (1970). Smyth *et al.* (1978) estimated that the cost of one substrate having dimensions of  $25 \times 25 \text{ mm}^2$  and an alumina dielectric deposit obtained by air-plasma spraying onto *Kovar*, for production of 50 000 pieces, is around 0.02 US\$.

#### 9.8.4 CAPACITOR ELECTRODES

Ikeda *et al.* (1988) applied air-plasma sprayed aluminium in a small-size, double-layer capacitor. Such a capacitor has electrodes of an activated carbon fibre and sprayed aluminium is used to decrease their resistances. The same application was realized by Rairden (1967) by the use of Al, Ta and Nb coatings. More recently, van Rodijnen and Knepper (2002) modified an arc-spray installation in order to enable spraying of zinc electrodes onto polycarbonate films without any thermal damage.

#### 9.8.5 CONDUCTOR PATHS FOR HYBRID ELECTRONICS

Copper coatings can be applied as *conductor paths* on sintered  $\text{Al}_2\text{O}_3$  substrates. The advantage of such paths is a low sheet resistance,  $R_s$  (see Chapter 7, Equation 7.28) and thus a possibility to carry high currents, so making a possible application in high-power circuits used, e.g. in cars. Copper coatings were obtained by the use of vacuum-plasma spraying (Braguier and Tueta, 1980; Pawlowski, 1980). Copper can easily be sprayed by using the cold-spray technique and this is a probable way of producing low-resistance coatings in the future.

#### 9.8.6 MICROWAVE INTEGRATED CIRCUITS

Brigginshaw and Riches (1975) described *circulators* designed by using an air-plasma sprayed ferrite insert into an alumina substrate. Annealing proved necessary to improve the properties of the integrated circuit, including an Mg–Mn ferrite. The circuit achieved a 20 dB bandwidth

of 800 MHz for a 7 GHz *circulator*. Similarly, Harris and Janowiecki (1970) described microwave *circulators* made with a thermally sprayed Mg–Mn ferrite, as well as *striplines* with sprayed ferrites and dielectrics.

## 9.9 ENERGY GENERATION AND TRANSPORT

Thermal spraying offers a possibility of obtaining coatings and massive pieces of any refractory material. This is why the technology is extensively used in energy generation and transport facilities. An important development concerns solid-oxide fuel cells (SOFCs), which work over the temperature range 1000–1300 K, and in other types of cells. Thermal spraying make it possible to obtain three elements of an SOFC cell:

- anode;
- cathode;
- solid-electrolyte.

On the other hand, thermally sprayed coatings are also applied in other types of electric generators, gas turbines and boilers.

### 9.9.1 SOLID-OXIDE FUEL CELL (SOFCS)

The principles of a *solid-oxide fuel cell* (SOFC) are shown in Figure 9.6. Only two phases exist in the cell:

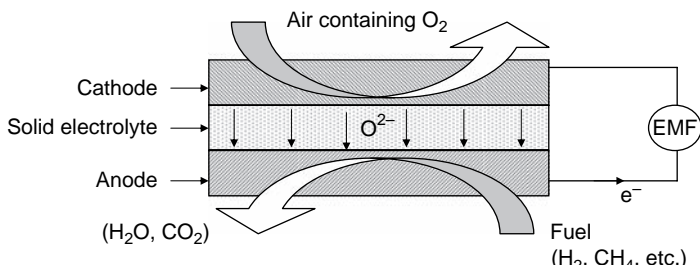


Figure 9.6 Principles of a solid-oxide fuel cell

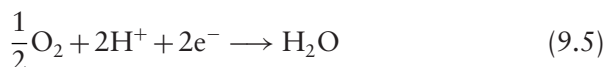
- solid of a cathode, electrolyte and anode;
- gas, i.e. oxygen on the cathode side and a reducing gas, such as hydrogen or methane, on the anode side.

In the case of the hydrogen–oxygen cell, the following reactions occur:<sup>5</sup>

- at the anode:



- at the cathode;



The electrons produce an electric current which flows from the anode to the cathode and the electromotive force (EMF) is generated by the products of the electrochemical reactions on each electrode. There are three types of SOFC geometries (Hathiramani *et al.*, 2005):

- cylindrical-tube, cathode-supported;
- planar, electrolyte-supported;
- planar, anode-supported.

The electrodes of an SOFC should be:

- porous with an open porosity greater than 25 %;
- electronic and ionic conductive;
- having a thermal expansion matching to that of the electrolyte;
- stable in an oxidizing/reducing atmosphere up to 1100 K.

The specifications with regard to the electrolyte are as follows:

- a thickness not greater than 50  $\mu\text{m}$ ;
- gas-tight;
- ionic-conductive (no electronic conductivity);
- stable at operating temperatures;
- compatible with the electrodes.

---

<sup>5</sup> Website: [www.annso.freesurf.fr/index.html].

Table 9.5 shows some examples of the realization of SOFCs, partly or entirely by thermal spraying. The electrolyte is mainly  $\text{ZrO}_2$  stabilized with  $\text{Y}_2\text{O}_3$  or  $\text{Sc}_2\text{O}_3$ . Zirconia is an ionic conductor whose electrical conductivity data are shown in Chapter 8, Figure 8.39. The electrolyte should be also dense and thin. This is why the processed coatings are often sprayed under vacuum (entries 1 and 4 in Table 9.5) or by using a high-energy spray torch, Triplex II<sup>TM</sup> (entry 5 in Table 9.5) and, in some studies, sintered after spraying (entry 3 in Table 9.5). The anode is also processed by using-thermal-spraying techniques. Mainly, YSZ is used as a cermet with Ni or an oxide mixture with NiO. As the electrode should be porous, the spray parameters are selected in such a way that the particles are only partly molten. Another solution, shown in Table 9.5 (entry 2) was to use a low-energetic flame-spraying technique. Finally, the cathodes of the SOFC are mainly *perovskites*, deposited by thermal spraying but also by other deposition techniques, such as:

- ‘dip-coating’ (entry 2 in Table 9.5);
- sintering of a layer pre-deposited by ‘screen-printing’ (entry 5 in Table 9.5).

### 9.9.2 THERMOPILE DEVICES FOR THERMOELECTRIC GENERATORS

Batalov *et al.* (2005) reported on the thermal spraying of thermopiles of *chromel* ( $\text{NiCr}$ )/*constantan* ( $\text{NiCu}$ ). These authors developed a ‘multi-wire’ high-velocity combustion spray/arc spray gun. The chromel/constantan thermopiles generate electricity by the *Seebeck effect* at high temperatures. The authors designed tubular thermocouples for fixing onto a hot-temperature gas exhaust produced by waste burning. Forty of these thermocouples were able to generate a voltage of about  $V = 800$  mV at 673 K. Okuno *et al.* (2004) reported on the development of sulfidation-resistant  $\text{Fe} + 75$  wt% Cr coatings to protect the aluminium walls of a sodium-sulfur battery cell. As the inner surface of the aluminium container had to be protected, a new torch, similar to the RotaPlasma<sup>TM</sup> device used to coat automobile cylinder bores, had to be developed. The production rate of the coated containers was reportedly 1300/day.

**Table 9.5** Summary of recent studies on thermally sprayed SOFCs

Number	Reference	Electrolyte			Anode			Cathode			Open circuit voltage (V)	Remarks
		Material (wt %)	Spray technique	Characteristics	Material (wt %)	Spray technique	Characteristics	Material (wt %)	Spray technique	Characteristics		
1	Mallener <i>et al.</i> , 1992	8YSZ	Vacuum-plasma spraying	Dense coating	Ni + 8YSZ	Vacuum-plasma spraying	Very porous	<i>Peroxybite</i> , $\text{La}_{0.84}\text{Sr}_{0.16}$ $\text{MnO}_3$	Vacuum-plasma spraying	Porosity up to 25%	$U = 0.8$	Planar type
2	Takenoiri <i>et al.</i> , 2000	8YSZ	Air-plasma spraying	—	NiO + 8YSZ	Flame spraying	—	—	Dip-coating	—	$U = 2.7$ (open)	Planar type, Ni substrate
3	Okumura, <i>et al.</i> , 2000	8YSZ (same samples with MnO <sub>2</sub> )	Air-plasma spraying + sintering	Cubic phase, $TEC = 9.9 - 10.4 \times 10^{-6}$ $1/K, 60 \mu\text{m}$ thick	Ni + YSZ	—	—	<i>Lanthanum chromite</i> , $\text{La}_{0.8}\text{Ca}_{0.2}$ $\text{Cr}_{0.95-1.15}$ $\text{O}_{3-x}$	Air-plasma spraying + sintering	$TEC = 9.7 - 10.0$	$U = 1.1$	Planar type
4	Lang <i>et al.</i> , 2001	ZrO <sub>2</sub> +10 mol % Sc <sub>2</sub> O <sub>3</sub>	Vacuum-plasma spraying	Porosity 1.5–3.5 %, 23–30 μm thick	NiO + ScSZ	Vacuum-plasma spraying	30–40 μm thick	$(\text{La}_{0.8}\text{Sr}_{0.2})_{0.98}$ $\text{MnO}_3$	Vacuum-plasma spraying	20–30 μm thick	$U = 1.1$	Planar type, Cr-based alloy
5	Stöver <i>et al.</i> , 2006	8YSZ	Air-plasma spraying, Triplex II™ torch	50 μm thick	NiO + YSZ	Air-plasma spraying, Triplex II™ torch	—	(La, Sr) (Co, Fe)O <sub>3</sub>	Sintering of screen-printed layer	—	$U = 0.9 - 1$	Planar-type ferritic Fe/Cr alloy substrate

### 9.9.3 BOILERS IN POWER-GENERATION PLANTS

*Boilers* are used to burn pulverized coal, biomass and/or waste. Inside the boiler, there is a tubing system, including water and steam. The tubing is heated by the flame of the burning material. The tubes, with an outer diameter of about 50 mm, carry the steam under high pressure ( $p \geq 17$  MPa) and are subjected from the outside to erosive and hot-corrosive wear resulting from ash and all products of burning (Kay, 1987). The tubes could be coated with stainless-steel type 310 by air-plasma spraying (Bennett and Quigley, 1990) or high-velocity combustion spraying (Kay, 1987). Spraying can be carried out in a workshop or *in situ*.

More, recently Langer *et al.* (2005a) proposed the application of *self-fluxing* alloys (see Chapter 4, Section 4.1.4) to be deposited via any thermal spray method and then post-sprayed treated. Finally, Kobayashi and Yamaguchi (2004) have carefully optimized the composition and morphologies of powders to be applied via high-velocity combustion spraying on boiler tubes. The best properties were revealed by a commercial cermet,  $\text{Cr}_3\text{C}_2 + 25$  wt% NiCr, taken for comparison and two, developed by the authors, spray-dried and sintered powders where the particles included an  $\text{Ni}_3\text{Al}$  matrix and borides such as  $\text{ZrB}_2$ , WB, CrB and MoB as reinforcements.

### 9.9.4 STATIONARY GAS TURBINES

The technology transferred from the aero-engine turbine area may be successful for *stationary gas turbines*. Taking an example, coatings vacuum-plasma sprayed with an NiCrAlY powder were compared with those deposited by chromium electroplating and by ‘pack-cementation’ (Schmitz *et al.*, 1984). The coatings were deposited onto Udimet 520<sup>TM</sup> alloy blades and tested in a *stationary gas turbine* generating 125 MW of electrical power. The electroplated chromium coatings revealed the best corrosion resistance while the vacuum-sprayed ones were only slightly worse. The steam turbine parts and especially the blades are subjected to erosion by water drops which results in their accelerated wear (Storch and Bick, 1993). The high-velocity combustion spraying of a *Stellite 6* coating of thickness 150–200  $\mu\text{m}$  was successfully applied to protect the outlet zones of turbine blades. A review of the state of the art with regard to the coatings applied in different parts of stationary gas turbines was given recently by Dorfman *et al.* (2004). The following components of the turbines were coated:

- the *combustor* with thermal barrier coatings, including an MCrAlY bond coating and a YSZ top deposit obtained mainly by air-plasma spraying;
- the *transition duct*, also with thermal barrier coatings;
- the *inlet nozzle guide vanes* with MCrAlY obtained by high-velocity combustion spraying and YSZ by air-plasma spraying;
- the *first-stage rotating airfoils* with MCrAlY obtained by vacuum-plasma spraying or, more recently, by high-velocity combustion spraying.

### 9.9.5 HYDROPOWER STATIONS

Erosion and cavitation are the two main mechanisms of wear in hydropower plants. The components of such a plant are made of the martensitic steel X5CrNi13.4 (Gustafsson *et al.*, 1999). The *Lavey* turbine plant in Lausanne (Switzerland) was successfully coated with a CoCr–WC powder using high-velocity combustion spraying. This plant can expect important savings due to fewer maintenance services.

### 9.9.6 MHD GENERATORS

*MHD generators* are used to convert the thermal energy of a plasma (temperature of 2800 K, velocity of 800–900 m/s) into electricity. Due to the high temperature, velocity and the influence of potassium added to increase the thermal conductivity of the plasma, the channels of MHD generators become quickly eroded. An initial part of the *plasma channel*, namely, the water-cooled nozzle at the exit from the *main combustor*, made of carbon steel and having an id ranging from 532 to about 70 mm and a length of 200 mm, was reportedly protected with air-plasma-sprayed thermal barrier coatings, an NiCrAl bond coating and yttria-stabilized zirconia (Thiagarajan, 1990).

## 9.10 IRON AND STEEL INDUSTRIES

One of the major applications of thermally sprayed coatings are in the continuous annealing lines (CALs) used for the production of sheets. These lines are nowadays of the horizontal and vertical types (Fukubayashi, 2004). As the industrial sector is traditional, the older examples are also considered in this present section.

### 9.10.1 CONTINUOUS ANNEALING LINE (CAL)

The *continuous annealing line* is a continuous heat-treatment process which involves heating, cooling and aging processes, enabling the thermal treatment of steel sheets having outstanding properties and surface quality (Namba *et al.*, 1988; Fukobayashi, 2004). The initial sheets come from a cleaning process, while the next step after the CAL process is *galvanizing*. The major technical problems related to the rolls are:

- pickup, i.e. mass transfer from sheet to roll;
- high-temperature corrosion in the annealing zone of the line;
- loss of roughness of the coating by a roll which results in ‘meandering’ of the sheet in horizontal annealing lines.

The rolls in the high-temprtature annealing zone are coated by  $\text{Cr}_2\text{C}_3 + \text{NiCr}$  cermets using detonation or high-velocity combustion spraying. The air-plasma spraying process can also be applied (Figure 9.7) but the coatings processed in this way are less hard.



Figure 9.7 A continuous annealing line roll during deposition of  $\text{Cr}_3\text{C}_2$  cermets using atmospheric-plasma spraying (external diameter of about 800 mm and a length of about 4500 mm). Reproduced by permission of Tocalo Company, Ltd, Kobe Japan

Cermets, including MCrAlY as the metallic part (15–60 vol%) and oxides ( $\text{Cr}_2\text{O}_3$ ,  $\text{Al}_2\text{O}_3$ ) and/or  $\text{Cr}_3\text{C}_2$  carbide as reinforcements are used also (Fukubayashi, 2004). The cooling rolls are the parts of the continuous annealing line in which the steel sheets are cooled by quenching. The application of  $\text{Al}_2\text{O}_3 + 25\%$   $\text{ZrO}_2$  coatings by air-plasma spraying was reported by Namba *et al.*, 1988). The lifetime of the sprayed rolls was reported to be 2 years in comparison with 3 months for the rolls electroplated with a Cr coating.

### 9.10.2 CONTINUOUS GALVANIZING SECTION

The next stage after the continuous annealing line is the *galvanizing section* which includes *sink rolls*. The rolls are made of stainless-steel type 314L and are coated with WC–Co coatings but also with oxide coatings such as  $\text{Al}_2\text{O}_3$ ,  $\text{Al}_2\text{O}_3 + \text{TiO}_2$  and  $\text{Al}_2\text{O}_3 + \text{ZrO}_2$  (Fukubayashi, 2004). The recommended deposition technique is detonation spraying. The surfaces of the rolls are usually grooved with 2–5 mm spiral pitches and a grooving angle of 120° for WC–CO coatings.

### 9.10.3 STAVE COOLING PIPES

*Stave cooling* of *blast furnace shells* is used in many blast furnaces (Hoffman, 1980). The pipes are 2000 mm in length and about 50 mm in diameter and in service are subjected to carburization during casting of the blocks. Application of a 300- $\mu\text{m}$  coating of alumina–titania by APS protects against carburization. As many as a few thousand pipes per furnace were reportedly coated.

## 9.11 MACHINE BUILDING INDUSTRY

The potential of thermal spraying in machine building for different industries such as, among others, (i) textile and (ii) pump construction, was recognized very early and many of the parts subjected to different kinds of wear in the machines are coated. *Textile machine* parts fail by sliding adhesive wear due to the moving fibre. Kirner (1978) reported on the air-plasma sprayed chromium oxide protection of the *rotating drum* of steel changing the direction of the fibre in the textile machine. Appli-

cation of the coating allowed a replacement of steel by aluminum as the drum material. Consequently, the fibre velocity and overall productivity of the machine increased. Another application is an air-plasma-sprayed alumina-titania coating on the fibre guides (Figure 9.8).



Figure 9.8 Elements for guiding textile fibres coated with ceramics. Reproduced by permission of Terolabservices, Villeneuve-Le-Roi, France

*Agroalimentary pumps* used to transport the liquids (such as yoghurt, chocolate, etc.) in agroalimentary machines have sliding and rotating pistons which are easily worn by three-body abrasion (due to the particulates in the liquid). The surfaces of both the piston and piston liners should be protected by a *biocompatible* ceramic coating from air-plasma spraying. *Vacuum pumps* have piston and piston liners that are subjected to sliding-adhesive wear. The surfaces of the pistons and the piston liners can be protected by chromium oxide coatings obtained by air-plasma spraying.

## 9.12 MEDICINE

The primary application of thermally sprayed coatings in medicine concerns coatings on prostheses. The prostheses are made of 'bio-inert' materials, such as stainless steel, CoCrMo alloy or TiAlV alloy. These coatings began to be used extensively from about 1990 to replace the cements used previously in order to ensure a reliable contact between

the implant surface and the living bone tissue. The prostheses, which are coated today, are those of (Tourenne, 2004):

- the hip;
- the knee;
- the arm;
- the tooth.

At present, about 1 million knee and hip prostheses are implanted yearly (Heimann, 2006). Bio-inert coatings should fulfil the following requirements (Winkler-Gniewek *et al.*, 1988):

- a large porosity,  $P = 20 - 40 \%$ , in order to enlarge the surface of the prosthesis;
- biocompatibility and stability in the body;
- reasonably good adhesion to the prosthesis;
- the coating must not become detached after 'in-growth' of the bone.

An example of such a coating is the titanium one obtained by vacuum-plasma spraying. A much greater market is represented by bioactive coatings. These coatings, usually made of hydroxyapatite, accelerate the implantation of the prosthesis in the bone. Although other bioactive ceramics have been tested, such as calcium carbonate  $\text{CaCO}_3$  (Langer *et al.*, 2002), plasma-sprayed hydroxyapatite coatings have become a standard in the medical industry. A stem of a typical hip prosthesis is shown in Figure 9.9.

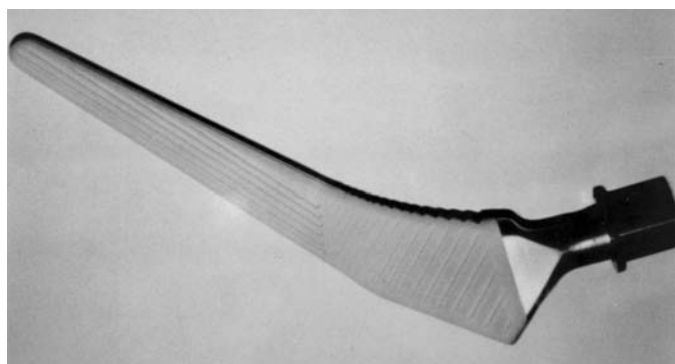


Figure 9.9 A *femoral stem* of a hip prosthesis with a part coated with bioactive hydroxyapatite ceramics

Biocompatible coatings dissolve in the bone and the dissolution rate depends on the crystallinity. In fact, amorphous calcium phosphates dissolve most rapidly and different phases dissolve at different rates (see Chapter 8, Figure 8.51). Bonding between the bioactive, hydroxyapatite coating and the metallic prosthesis is not very good. This results from the method of spraying, which results from the fact that the particles are only partly molten (see Chapter 5, Figure 5.24). The bonding can be improved by application of  $\text{TiO}_2$  intermediate coatings (Heimann, 2006) from 5–20 MPa to more than 50 MPa (using the ASTM 633-01 test). Another possible way of improvement of hydroxyapatite adhesion is the use of a bio-inert titanium intermediate coating by vacuum-plasma spraying. This is a solution proposed by the society *Medicoat* (Niederrohrdorf, Switzerland).

## 9.13 MINING INDUSTRY

*Hydraulic props* used in coal mines are subjected to corrosion by aggressive mine water (Matejka *et al.*, 1988). The coating deposited on the internal parts of the props has bronze as the ‘mating surface’ and should be:

- corrosion-resistant;
- wear-resistant;
- having suitable friction properties against bronze.

An air-plasma-sprayed particulate composite coating of 400  $\mu\text{m}$  thickness has been designed for this purpose. The composition of the powder blend was (in vol%) self-fluxing  $\text{NiCrSiB}$ , 35CuSn10 and 5 $\text{MoS}_2$ . The coatings were deposited onto the walls of the internal part of 250 mm diameter. The application of sprayed coatings increased the lifetime in service of the steel props by a factor of three.

## 9.14 NON-FERROUS METAL INDUSTRY

### 9.14.1 HOT-EXTRUSION DIES

A *hot extrusion technique* is used to manufacture *seamless tubes* of brass or copper. The extruded material is in the ‘plastic state’ (temperature of 1070 K) and is squeezed through the *die* to achieve the desired

external diameter (Modi *et al.*, 1986). An uncoated die of a steel having a composition (in wt%) of Fe + 5Cr + 1C + 0.4V + 0.2Mo cannot be used for more than 22 extrusions. The coated die, produced by air-plasma spraying, has the following graded composite coatings:

- 50  $\mu\text{m}$  NiCr bond coat;
- 100  $\mu\text{m}$  top coat of alumina;
- three 100  $\mu\text{m}$  particulate composite coatings sprayed using NiCr and  $\text{Al}_2\text{O}_3$  powders blended in the proportions – 25:75, 50:50 and 75:25.

The protected dies could be used 58 times which brings an annual cost savings of 7800 US\$.

### 9.14.2 PROTECTIVE COATINGS AGAINST LIQUID COPPER

Bialucki (1988) tested  $\text{Cr}_2\text{O}_3$  particulate composites, plasma-sprayed using blends of  $\text{Cr}_2\text{O}_3 + (25, 50, 75)$  wt% TiC and of  $\text{MgO} + 50$  wt%  $\text{ZrSiO}_3$  coatings deposited on a mild-steel substrate with an NiCrAl bond coat. The coatings were subjected to a thermal-shock resistance test and to a liquid-copper resistance test at 1470 K. The chromia-titanium carbide composite revealed better thermal-shock resistance. Protection by the chromia–titanium carbide composite coating in the open atmosphere was limited to 5 h. Thereafter, the coating dissolved in the liquid copper and slag.

### 9.14.3 PROTECTIVE COATINGS AGAINST LIQUID ZIRCONIUM

The melting of such a reactive metal as zirconium is usually carried out in a *graphite crucible* under vacuum. The crucible must be coated in order to avoid carbon contamination (Bird and Holcombe, 1992). The coating specification is as follows:

- be able to withstand a temperature of more than 2000 K (the melting point of Zr is 2125 K) without cracking;
- does not dissolve in liquid zirconium.

These specifications were fulfilled by the following ‘multi-coating’:

- 400  $\mu\text{m}$  Mo bond coat sprayed under an argon atmosphere;
- 200  $\mu\text{m}$  particulate composite of Mo + 50 wt% CaSZ as the intermediate coating;
- 400  $\mu\text{m}$  CaSZ as the top coating.

## 9.15 NUCLEAR INDUSTRY

Nuclear devices generate an important fraction of the energy used in many countries.<sup>6</sup> The increasing price of petrol has triggered research on a new generation of nuclear devices, including magnetic confined-fusion devices such as the International Thermonuclear Experimental Reactor (ITER) and others. The devices include elements that are in contact with a high-temperature plasma and should be protected against the important thermal flux.

### 9.15.1 COMPONENTS OF TOKAMAK DEVICE

The coatings protecting the *limiter* and *armor* components in *Tokamak*, which is a fusion device from an ‘older generation’, should resist thermal fatigue, be refractory and of low or moderate atomic number (Mullendore *et al.*, 1981). The coatings must be thick in order to resist the severe ion erosion. Air-plasma sprayed coatings of TiC, VC, TiB<sub>2</sub> and their composite with V and with B, were applied onto pure copper, 316 stainless-steel, pure Ta and POCO graphite for this purpose. Post-spraying hot-isostatic pressing was also applied. The results were not conclusive but such coatings as, e.g. TiC on Cu or VC on Ta, performed reasonably well in thermal fatigue tests at 1000 and 1770 K.

### 9.15.2 MAGNETIC-FUSION ENERGY DEVICE

Smith *et al.* (1991) plasma-sprayed, under vacuum, pure Cu coatings of high-purity copper onto copper composites.<sup>7</sup> The coatings were sprayed

---

<sup>6</sup> For example, the fraction of electrical energy generated in nuclear devices in France is about 75 %

<sup>7</sup> Dr Mark Smith’s laboratory is also working at present on cold-gas spraying which could be used for this application.

onto Glidcop™ tubes and were used as intermediate layers which made possible the brazing of a graphite armor to the tubes. The assembly was successfully tested under a surface-heat flux of up to  $q = 2 \text{ kW/cm}^2$  by the electron-beam test. Inert plasma spraying was used by the same authors to spray Be coatings onto stainless steel. The spraying resulted in *in situ* repair to coat the damaged walls in the fusion devices. The beryllium first-wall component for the ITER reactor was intensively tested by Hollis *et al.* (2005). The vacuum-plasma-sprayed Be coating onto a copper alloy (Cu–0.65Cr–0.1Zr) had to fulfil the following specifications:

- the thickness must be in the range 5–10 mm;
- the temperature at coating deposition has to be lower than 923 K in order to avoid metallurgical transformation of the substrate;
- cost reduction, i.e. the intermediate coatings and post-spray treatment should be excluded;
- reduction of worker-exposure to hazardous beryllium.

The authors developed a technology of vacuum-plasma-sprayed Be coatings having a low porosity (< 2 %) avoiding metallurgical transformation of the substrate. Finally, W coatings sprayed under vacuum can be used for the protection of surfaces interacting with the plasma in advanced fusion devices. This was tested by Malléner (2001) on *divertor wings* made of copper or copper alloy and successfully tested in a high-intensity electron beam. This material is of high atomic number and can also be applied as an *armor*.

## 9.16 PAPER INDUSTRY

### 9.16.1 DRYERS

Drying is the process which uses most of the energy in the papermaking industry. Consequently, even a modest improvement in drying efficiency gives a substantial yield in cost savings (Lenling *et al.*, 1992). The so-called *yankee dryers* are used for drying the tissue paper and the dryer is a cast-iron cylinder of typically 6000 mm od and 7000 mm length (Melkert and Renner, 1987). Drying occurs by superheated steam under a pressure of 1 MPa. The continuous tissue web is ‘glued’ to the dryer surface, dried and later scraped (‘doctored’) off the dryer. The ‘doctoring’ wears the dryer’s surface. As its transport is expensive, the coating is usually carried out *in situ* (Figure 9.10).



**Figure 9.10** A yankee dryer coated, *in situ*, with an Mo coating, applied by air-plasma spraying. Reproduced by permission of Tocalo Company, Ltd, Kobe Japan

The technologies used to increase the wear resistance of dryers include:

- arc spraying of AISI 420 stainless-steel (Ritchie, 1983);
- air-plasma spraying of Mo (see Figure 9.10);
- air-plasma spraying of Ni base coatings containing Mo (Melkert and Renner, 1987).

The spray process lasts up to 40 h and during this time more than 1000 kg of consumables could be used. An increase in the coating growth rate can be achieved by the application of many torches in the spray process. *Impulse drying* is used to process wet paper by the simultaneous action of heat ( $T = 473\text{--}673\text{ K}$ ) and pressure ( $p = 3\text{--}6\text{ MPa}$ ). The research reported by Lenling *et al.* (1992) has shown the usefulness of air-plasma-sprayed multi-coatings in avoiding delamination of the paper. The multi-coating is composed of:

- a NiAlMo alloy bond coat, 80–130  $\mu\text{m}$  thick;
- $\text{ZrO}_2 + 8\text{ wt\% Y}_2\text{O}_3$  doped with an  $\text{HfO}_2$  porous coating ( $P = 17\text{ \%}$ ), 380  $\mu\text{m}$  thick;
- a similar dense coating ( $P = 5\text{--}7\text{ \%}$ ), 50  $\mu\text{m}$  thick.

In fact, the coated roll had a better drying efficiency and enabled the production of a good quality paper.

### 9.16.2 GLOSS CALENDER ROLLS

A *gloss calender roll* has a typical od of 1300 mm and a length of about 3500 mm. The roll works in contact with a *doctor blade*, which wears its surface. The standard surfacing technology consists of chromium plating and results in three to six months service lifetime. The application of wear-resistant coatings of 100  $\mu\text{m}$ -thick WC–NiCr or WC–Co by high-velocity combustion spraying and a post-spray finishing treatment achieved an  $R_a$  of 0.01–0.03  $\mu\text{m}$  and increased the lifetime up to 2 years of service (Figure 9.11).

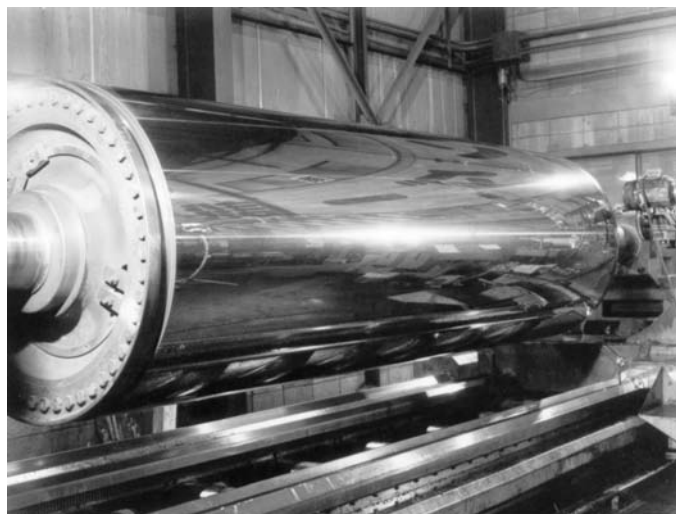


Figure 9.11 A gloss calendar roll coated with WC–Co, sprayed by the high-velocity technique, followed by post-spray ‘finishing’. Reproduced by permission of Tocalo Company, Ltd, Kobe Japan

### 9.16.3 TUBING IN BOILERS

Boilers are used in the pulp industry to fire ‘black liquor’ and inorganic compounds (Gustaffson, 1986). The boiler is a chemical reactor in which the organic part of the fuel is burned and the inorganic part is reduced to sodium sulfide. The tubes inside the boiler are made of steel and are subjected to chemical corrosion associated with erosion. Protective

coatings of *Kanthal M*™, an alloy of Fe, Cr and Al, are applied by wire-flame spraying. Gustaffson reported the deposition of the coatings in a workshop or *in situ*. Verification after 9 months did not reveal any traces of corrosion attack.

## 9.17 PRINTING AND PACKAGING INDUSTRIES

### 9.17.1 CORONA ROLLS

The corona-discharge treatment of polyethylene is a well-established method of surface activation which improves the ability of adhesion of the printing ink, i.e. decreases the angle of wetting (Sonkin, 1977; Hansmann, 1981). The corona roll can have a typical od of 250–500 mm and can be as long as 5000 mm. One of the key elements of a ‘corona treater’ is a dielectric-covered treater roll (very often called the *corona roll*). Traditionally, the rolls were coated with silicone (Gilbertson, 2004). Since the middle of the 1980s, the rolls have been coated by using air-plasma spraying. The dielectric coatings have to fulfil the following specifications:

- resistance against the wear of the polyethylene ‘web’;
- a breakdown voltage greater than 20 kV;
- a dielectric constant in the range  $\varepsilon_r = 6\text{--}9$ , i.e. not very different from that of the silicone;
- the dielectric constant should have the same value throughout the whole service time.

Air-plasma sprayed alumina is sufficiently wear-resistant but efforts had to be undertaken in order to fulfil the other requirements. The dielectric strengths of sprayed alumina coatings are in the range 100–175 kV/cm (entry 1 in Table 8.33, Chapter 8). Consequently, in order to achieve the breakdown voltage of 20 kV it is necessary to have 2 mm thick coatings and to carefully optimize the operational spray parameters (Pawlowski, 1987). ‘Thick’ alumina must be deposited onto the intermediate coatings which must have a thermal expansion coefficient between that of the alumina and the roll metal. This enables reducing the thermal stresses generated after deposition. Such stresses can lead to the formation of cracks and decrease the dielectric breakdown voltage (see Chapter 7, Figure 7.7). The ‘breakdown’ interrupts the treatment of the polyethylene, so making necessary an ‘exchange’ of the roll. Such an operation

is easier if the roll is not heavy – this is why the rolls have recently been made of aluminium. The successful development of aluminium corona rolls coated with alumina required a very careful study of the aluminium–alumina cermets (see Chapter 8, Figures 8.36 and 8.37). The ‘as-sprayed’ alumina coatings are crystallized in the hygroscopic  $\gamma\text{-Al}_2\text{O}_3$  phase. The dielectric constant depends on the water content in the coatings. Thus, in order to preserve the *constant properties* of the dielectric upon corona treatment, the coatings must be ‘post-spray sealed’ with a silicone resin. Depending on the polarization of the generator, the ceramic coatings on a the corona rolls are applied by air-plasma spraying using electrically insulating  $\text{Al}_2\text{O}_3$  (Figure 9.12) or electrically conducting  $\text{Al}_2\text{O}_3\text{-TiO}_2$  (Figure 9.13).



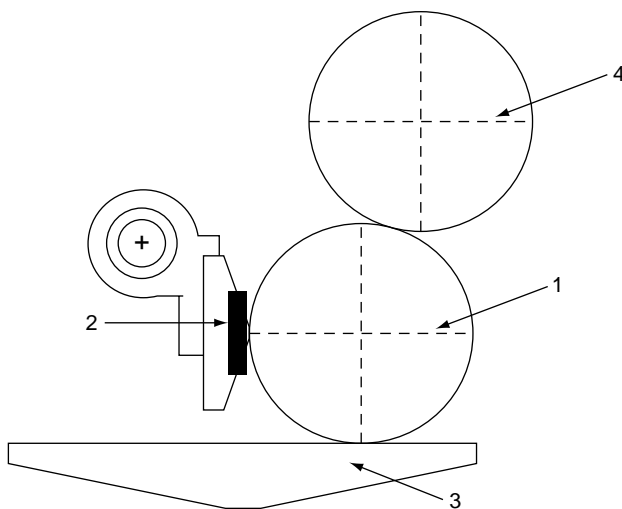
Figure 9.12 A corona ‘treater’ with a roll coated with electrically conducting alumina. Reproduced by permission of Softal Electronic GmbH, Hamburg, Germany



Figure 9.13 A corona ‘treater’ with a roll coated with electrically conducting alumina–titania. Reproduced by permission of Softal Electronic GmbH, Hamburg, Germany

### 9.17.2 ANILOX ROLLS

The anilox rolls are used in printing machines working with the flexographic system (Figure 9.14)



**Figure 9.14** Schematic of part of a flexographic printing machine: (1) anilox roll; (2) 'doctor blade'; (3) ink container; (4) printing roll

The roll (1) is used to transport a precisely defined quantity of ink from the ink container (3) onto the printing roll (4). The ink quantity is determined by the depth and density of the 'cell' engraved on the roll surface. The excessive ink is removed by the doctor blade (2). The rolls have dimensions which depend on the printing machine. A typical roll is shown in Figure 9.15.

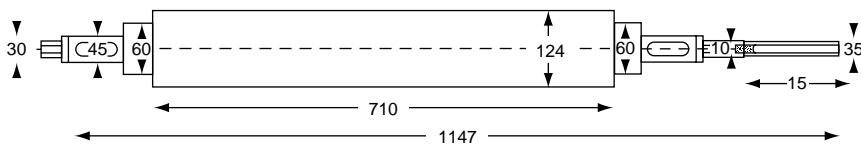


**Figure 9.15** Schematic of a typical anilox roll (all dimensions in mm)

The earlier conventional technology of the rolls includes the galvanic deposition of a copper-nickel bond coating, followed by mechanical

engraving with diamond indenters and finally, galvanic deposition of a wear-resistant chromium top coating. Modern rolls consist of a ceramic with a plasma-sprayed chromium oxide top coating deposited onto an alloy bond coat. The air-plasma spray technique has been used since the beginning of 1980, initially by Union Carbide in Indianapolis, IN, USA, which later Praxair ST, followed by many companies, including W Haldenwanger, Berlin, Germany. The sprayed coatings are ground and polished with a diamond wheel, engraved with a CO<sub>2</sub> laser (see Chapter 4, Figure 4.21) and then again 'post-laser polished'. The properties of some ceramic coatings are specified in Table 9.6. These specifications can be fulfilled by alumina, although alumina becomes translucent after laser engraving, which makes impossible microscopical measurement of depths. On the other hand, alumina-titania alloys have been tested on the laboratory scale and will be discussed later, although these ceramics can interact some inks (Douglas, 1992). At present, chromium oxide coatings are mainly applied. Air-plasma spraying enables the easy realization of Cr<sub>2</sub>O<sub>3</sub> coatings, having the properties specified in entries 1–4 of Table 9.6. More difficult is reduction of the metallic inclusions,

**Table 9.6** Top-coating specifications for the production of anilox rolls

Number	Coating properties	Property specification	Remarks
1	Open and interconnected porosity	Low (< 5 %)	To prevent ink penetration from the bond coat to the metallic roll
2	Pore sizes	Small, say less than half of the cell diameter, i.e. 15 µm for ruling 300 lines/cm	To prevent ink accumulation inside the 'cells'
3	Hardness	HV > 1000	To promote wear resistance
4	Cohesion	High Young's modulus and high toughness	To promote coating integrity
5	Metallic impurities	No impurities	To promote corrosion-resistance
6	Light-absorption	High light-absorption	For wavelengths, $\lambda = 10.6\mu\text{m}$ (CO <sub>2</sub> laser) and 1.06 µm (Nd:YAG laser)

which result from reduction of Cr<sup>+3</sup> to Cr<sup>0</sup>. To avoid this reduction the following can be applied:

- the use of oxygen as a carrier gas;
- elimination of the sub-oxides in the Cr<sub>2</sub>O<sub>3</sub> powders used to spray by acid washing;
- the use of spray-dried powders (see Chapter 1, Figure 1.8) which necessitate, however, a greater electric power input for spraying (Bartnik *et al.* 1992) and consequently should be densified (see Chapter 1, Figures 1.10 and 1.11);
- the use of crystallized powders, as discussed by Pawlowski (1996).

The 6th entry in the specification list (Table 9.6) is achieved by proper grinding and polishing procedures. The small roughness is necessary in order to achieve the same focus of the laser by engraving. On the other hand, the surface can act as a ‘mirror’ and only a small fraction of the laser light would be used to ‘burn-out’ the cells. The values of  $R_{\max}$  in the range 1 to 3 µm seem to be optimal. The surfaces of engraved cells is shown in Chapter 4, Figure 4.18. The market for ceramic anilox rolls covers the following:

- rolls for new printing machines;
- replacements of galvanically plated rolls with ceramic ones;
- replacement of used ceramic anilox rolls.

Progress in this technology should be first related to the replacement of chromium oxide by more environmental-and worker-friendly-titania and alumina-titania alloys (Tomaszek *et al.*, 2004) or tungsten carbides (Langer *et al.*, 2005b). Air-plasma sprayed Al<sub>2</sub>O<sub>3</sub> + 40 wt % TiO<sub>2</sub> had a relatively low porosity ( $P = 1.9\%$ ), acceptable hardness,  $HV_{0,3} = 1083$ , was relatively homogeneously composed of alumina-titania spinel (see Chapter 4, Figure 4.21), ‘absorbed-well’ CO<sub>2</sub> laser radiation and generates less of the liquid phase which results in the so-called *overflow effect* (Pawlowski, 1999). On the other hand, high-velocity combustion spraying of WC-Co cermets is a possible solution, although the coating is not homogeneous and should be tested against ‘ink corrosion’. Progress in engraving technology is application of the solid-state Nd:YAG laser (Meiners, 1996). Finally, the roll bodies can be made from ‘height-weight’ materials, such as carbon or a glass-reinforced composite (Langer *et al.*, 2005b).

## 9.18 SHIPBUILDING AND NAVAL INDUSTRIES

### 9.18.1 MARINE GAS-TURBINE ENGINES

Coatings developed for aero-engines have proved useful in *marine gas turbines*, with some minor adjustments. Thus, a powder of composition Co + 25 wt % Cr + 10.5 wt % Al + 2.5 wt % Hf + 5 wt % Pt was sprayed by the use of a plasma in a ‘shrouded’ atmosphere or under vacuum onto the blades of the *second-stage high pressure turbine* of the LM2500 *marine engine* in a US Navy ‘test-ship’ (Wortman 1985). Thermally sprayed coatings were favourably compared with PVD coatings of a similar composition by the use of hot-corrosion burner rig test. Streeter and Sampson (2000) reported on the application of an NiCrB (1.5 mm thick) coating sprayed using high-velocity combustion spraying in the *power stage of gas turbine shafts* and many other applications of thermal spraying in connection with the Chilean Navy.

### 9.18.2 STEAM VALVE STEMS

Air-plasma sprayed coatings were applied onto the *stems of craft-carrier ships* of the US Navy (Travis *et al.*, 1992). The stems were originally of stainless steel 410 and were coated with an NiCrAlMoFe bond coat and a top coating of composition (in wt %) of ZrO<sub>2</sub> + 18TiO<sub>2</sub> + 10Y<sub>2</sub>O<sub>3</sub>. The coatings were sealed after deposition. Metallographic observations and thermal wave analysis, carried out after 4 years of service, did not indicate any structural changes or ‘de-bonding’. The savings brought about by application of thermal spraying in refurbishment are of the order of 880\$ per stem.

### 9.18.3 NON-SKID HELICOPTER FLIGHT DECK

Arc-sprayed aluminium coatings were successfully applied to coat flight decks with a non-skid coating (Sulit *et al.*, 1980). Such coatings had to resist corrosion for at least three years. This application proved to be successful in some ships of the US Navy.

## REFERENCES

- Anon (1986). *The Jet Engine*, Rolls-Royce plc, Derby, UK.  
Bach, F.W., Duda, T., Unterberg, W. and Josefiak, L.A. (2000). Atmospheric plasma spraying of run-in-coatings for twin-screw-compressors, in *Thermal Spray: Surface*

- Engineering via Applied Research*, C.C. Berndt (Ed.), ASM International, Materials Park, OH, USA, pp. 1155–1158.
- Barbezat, G. (2005). Application of thermal spraying in the automobile industry, in *Proceedings of the 2nd Rencontres Internationales sur la Projection Thermique*, L. Pawlowski (Ed.), 1–2 December, Lille, France, Sulzer Metco AG, Wohlen, Switzerland, pp. 231–235.
- Barbezat, G. (2006). Application of thermal spraying in automobile industry, *Surf. Coat. Technol.*, 201, 2028–2031.
- Barbezat, G., Keller, S. and Wuest, G. (1999). The advantage of the plasma spray process for the coating of cylinder bores on AlSi cast alloy in the automotive industry, in *Proceedings of the United Thermal Spray Conference*, E. Lugscheider and P.A. Kammer (Eds), DVS, Düsseldorf, Germany, pp. 10–14.
- Bartnik, Z., Bialucki, P., Kozerski, S., Bork, P., Schrader, B., Clinton, G., Davies, K., Guglielmi, F. and Pawlowski, L. (1992). Improvements in manufacturing technology of wear resistant plasma sprayed Cr<sub>2</sub>O<sub>3</sub> coatings, in *Thermal Spray: International Advances in Coatings Technology*, C.C. Berndt (Ed.), ASM International, Materials Park, OH, USA, pp. 983–995.
- Batalov, M., Kosikowski, D. and Mohanty, P.S. (2005). Design, fabrication and characterization of sprayed thermopiles, in *Proceedings of the International Thermal Spray Conference '05*, CD-Rom, ISBN 3-87155-793-5, DVS-Verlag, Düsseldorf, Germany.
- Bennett, A.P. and Quigley, M.B.C. (1990). The spraying of boiler tubing in power stations, *Weld. Met. Fabri.*, November, 485–489.
- Berger, L.-M. (2004). Titanium oxide – new opportunities for an established coating material, in *Proceedings of the International Thermal Spray Conference '04*, CD-Rom, ISBN 3-87155-792-7, DVS-Verlag, Düsseldorf, Germany.
- Bialucki, P. (1988). The development of plasma sprayed layer for contact with liquid copper and slag, in *1st Plasma Technik Symposium*, Vol. 1, H. Eschnauer, P. Huber, A.R. Nicoll and S. Sandmeier (Eds), Plasma Technik AG, Wohlen, Switzerland, pp. 263–271.
- Bird, E.L. and Holcombe, Jr, C.E. (1992). Investigation of plasma-sprayed laminates for high temperature melting operations, in *Thermal Spray: International Advances in Coatings Technology*, C.C. Berndt (Ed.), ASM International, Materials Park, OH, USA, pp. 625–629.
- Braguier, M. and Tueta, R. (1980). Supersonic and vacuum arc plasma spraying apparatus characteristics and application to metallic coatings, in *Proceedings of the 9th International Thermal Spray Conference*, Nederlands Instituut voor Lastechniek, The Hague, The Netherlands, pp. 167–172.
- Brigginshaw, P.M. and Riches, E.E. (1975). Developments of MIC circulators from 1 to 40 GHz, *IEEE Trans. Mag.*, Mag-11, 1273–1275.
- Brown, L., Herman, H. and MacCrone, R.K. (1986). Plasma sprayed insulated metal substrates, in *Advances in Thermal Spraying*, Pergamon Press, New York, NY, USA, pp. 507–512.
- Brozek, V., Buzek, V., Kolman, B. and Chraska, P. (1993). Ceramic membranes produced by APS technology, in *Thermal Spray Coatings: Research, Design and Applications*, C.C. Berndt and T.F. Bernecki (Eds), ASM International, Materials Park, OH, USA, pp. 649–654.

- Crabos, F. (2003). Application de la projection thermique contre l'oxydation/corrosion haute température, in *Proceedings of the 1st Rencontres Internationales sur la Projection Thermique*, L. Pawlowski (Ed.), 4–5 December, Lille, France, Sulzer Metco AG, Wohlen, Switzerland, pp. 86–96.
- Dorfman, M.R., Nonni, M., Mallon, J., Woodard, W. and Meyer, P. (2004). Thermal spray technology growth in gas turbine coatings, in *Proceedings of the International Thermal Spray Conference '04*, CD-Rom, ISBN 3-87155-792-7, DVS-Verlag, Düsseldorf, Germany.
- Douglas, R. (1992). Colour-coded ceramic coatings, *Adv. Mater. Proc.*, **142**, 4.
- Ducos, M. and Durand, J.-P. (2001). Thermal coatings in Europe: a business perspective, *J. Therm. Spray Technol.*, **10**, 407–411.
- Eerola, M. (1993). Flame spraying copper on glass artware, *Am. Ceram. Soc. Bull.*, **72**, 48–52.
- Friedrich, C., Gadow, R., Killinger, A. and Voss, A. (1998). Combined metallurgical and ceramic coating in the development of tubular ozone generators, in *Thermal Spray: Meeting the Challenges of the 21st Century*, C. Coddet (Ed.), ASM International, Materials Park, OH, USA, pp. 1083–1091.
- Friedrich, C., Gadow, R. and Killinger, A. (1999a). Thermally sprayed multilayer coatings as electrodes and dielectrics in high efficiency ozonizer tubes, in *Proceedings of the United Thermal Spray Conference 99*, H. Lugscheider and P.A. Kammer (Eds), DVS-Verlag, Düsseldorf, Germany, pp. 676–683.
- Friedrich, C., Gadow, R., and Killinger, A. (1999b). Atmospheric plasma sprayed dielectric ceramic coatings for ozonizer tubes, in *American Ceramic Society 101 Annual Meeting*, 25–28 April, Indianapolis, IN, USA, Symposium E: Dielectric Materials and Devices.
- Froning, M., Ruggiero, P., Tsiao, J., Marnix, J., Alford, C. and Shubert, G. (2004). Transition of a world class HVOF thermal spray capability into a US engine overhaul facility, in *Proceedings of the International Thermal Spray Conference '04*, CD-Rom, ISBN 3-87155-792-7, DVS-Verlag, Düsseldorf, Germany.
- Fujishima, A. and Honda, K. (1972). Electrochemical photolysis of water at a semiconductor electrode, *Nature*, **238**, 37–39.
- Fukabayashi, H.H. (2004). Present furnace and pot roll coating and future development, in *Proceedings of the International Thermal Spray Conference '04*, CD-Rom, ISBN 3-87155-792-7, DVS-Verlag, Düsseldorf, Germany.
- Gilbertson, T. (2004) Corona-treating rolls, *J. Therm. Spray Technol.*, **13**, 488–489.
- Golonka, L. and Pawlowski, L. (1983). Ceramic on metal substrates produced by plasma spraying for thick film technology, *Electrocomp. Sci. Technol.*, **10**, 143–150.
- Gorecka-Drzazga, A., Golonka, L., Pawlowski, L. and Fauchais, P. (1984). Application of the plasma spraying process to the production of metal-ceramics substrates for hybrid microelectronics, *Rev. Int. Hautes Tempér. Refract.*, **21**, 153–165.
- Grasset, G. (2003). Solutions de remplacement du chrome revêtements par projection thermique et par codéposition électrolytique, in *Proceedings of the 1st Rencontres Internationales sur la Projection Thermique*, L. Pawlowski (Ed.), 4–5 December, Lille, France, Sulzer Metco AG, Wohlen, Switzerland, pp. 197–202.
- Gustafsson, S. (1986). Thermal coating as corrosion protection in boilers, in *Advances in Thermal Spraying*, Pergamon Press, New York, NY, USA, pp. 19–28.
- Gustaffson, S., Wasserman, C. and Chapuis, L. (1999). Surface protection of components for hydro power stations, in *Proceedings of the United Thermal Spray Conference '99*, H. Lugscheider and P.A. Kammer (Eds), DVS-Verlag, Düsseldorf, Germany, pp. 82–85.

- Hansmann, J. (1981). Oberflächebehandlungsmethoden zur Haftverbesserung, *Papier Kunstoff-Verarb.*, (7), 1–8.
- Harris, D.H. and Janowiecki, R.J. (1970). Arc plasma deposits may yield some big microwave dividends, *Electronics*, 2, 108–115.
- Hathiramani, D., Vassen, R., Stöver, D. and Damani, R.J. (2005). Plasma sprayed components for SOFC applications, *2nd Rencontres Internationales sur la Projection Thermique*, 1–2 December 2005, Lille, France, invited presentation.
- Heimann, R.B. (2006). Thermal spraying of biomaterials, *Surf. Coat. Technol.*, 201, 2012–2019.
- Herman, H. (1992). American bridges falling down: Guest commentary, *J. Therm. Spray Technol.*, 1, 195–196.
- Herrmann, J.-M. and Guillard, C. (2000). Photocatalytic degradation of pesticides in agriculturals used waters, *C.R. Acad. Sci. Paris, Série II c, Chimie/Chem.*, 3, 417–422.
- Hoffman, J.W. (1980) Thermal spraying in Australian mining and secondary industries, in *Proceedings of the 9th International Thermal Spray Conference*, Nederlands Instituut voor Lastechniek, The Hague, The Netherlands, pp. 58–61.
- Holcombe, Jr, C.E. (1978). Fabrication of thin walled ceramic structures, *Ceram. Bull.*, 57, 610.
- Hollis, K.J., Bartram, B.D. and Rödig, M. (2005) Plasma sprayed beryllium for high heat flux components, in *Proceedings of the International Thermal Spray Conference '05*, CD-Rom, ISBN 3-87155-793-5, DVS-Verlag, Düsseldorf, Germany.
- Ikeda, M., Nishino, A. and Yshida, A. (1988). Application of plasma sprayed Al coatings to electronic components and housing product, in *International Symposium on Advanced Thermal Spraying Technology and Allied Coatings*, High Temperature Society of Japan, Osaka, Japan, pp. 223–227.
- Ishikawa, K., Seki, M. and Tobe, S. (1993). Application of thermal spray coatings to prevent corrosion of construction in Japan, in *Thermal Spray Coatings: Research, Design and Applications*, C.C. Berndt and T.F. Bernecki (Eds), ASM International, Materials Park, OH, USA, pp. 679–684.
- Jaworski, R., Pawlowski, L., Roudet, F., Kozerski, and Le Maguer, A. (2008). Influence of suspension plasma spraying process on TiO<sub>2</sub> coatings microstructure, *J. Therm. Spray. Technol.*, doi: 10.1007/s11666-007-9147-z.
- Jodoin, N. and Nadeau, M. (1980). The biggest on-site metallizing project Pierre-Laporte bridge, in *Proceedings of the 9th International Thermal Spray Conference*, Nederlands Instituut voor Lastechniek, The Hague, The Netherlands, pp. 53–57.
- Kay, A. (1987). Jet Kote application for corrosion protection, in *Thermal Spray: Advances in Coatings Technology*, D.L. Houck (Ed.), ASM International, Materials Park, OH, USA, pp. 393–397.
- Keshavan, M.K. and Kembalyan, K.T. (1993). Wear characterization and practical applications of thermal spray coatings in drilling applications, in *Thermal Spray Coatings: Research, Design and Applications*, C.C. Berndt and T.F. Bernecki (Eds), ASM International, Materials Park, OH, USA, pp. 635–641.
- Kirner, K. (1978). Plasmaspritzen in der Mengenfertigung, *WT Zeit. Indust. Fertig.*, 68, 465–470.
- Kirner, K. (1980). Plasma spraying of free standing ceramic bodies, in *Proceedings of the 9th International Thermal Spray Conference*, Nederlands Instituut voor Lastechniek, The Hague, The Netherlands, pp. 14–19.

- Klinge, R. (1973). Metal spraying on bridge work in Norway, in *Proceedings of the 7th International Metal Spraying Conference*, The Welding Institute, Cambridge, UK, pp. 224–231.
- Kobayashi, Y. and Yamaguchi, S. (2004) Development of thermal spray coating applied for boiler tube, in *Proceedings of the International Thermal Spray Conference '04*, CD-Rom, ISBN 3-87155-792-7, DVS-Verlag, Düsseldorf, Germany.
- Kobe, S. (1998). A review on protection against corrosion, oxidation and hot corrosion by thermal spray coatings, in *Thermal Spray: Meeting the Challenges of the 21st Century*, C. Coddet (Ed.), ASM International, Materials Park, OH, USA, pp. 3–11.
- Lang, M., Henne, R., Schaper, S. and Schiller, G. (2001). Development and characterization of vacuum plasma sprayed thin films solid oxide fuel cells *J. Therm. Spray Technol.*, **10**, 618–625.
- Langer, G., Kwo, J. and Murano, D. (2002). New coating solutions for biomedical applications, in *Proceedings of the International Thermal Spray Conference '02*, E. Lugscheider and C.C. Berndt (Eds), DVS, Düsseldorf, Germany, pp. 192–195.
- Langer, G., Kremsner, A. and Polak, R. (2005a). TeroComposite™ – coating solutions against high-temperature corrosion and erosion in boiler applications, in *Proceedings of the International Thermal Spray Conference '05*, CD-Rom, ISBN 3-87155-793-5, DVS-Verlag, Düsseldorf, Germany.
- Langer, G., Wewel, M. and Wand, R. (2005b). Carbide coatings on fibre-reinforced anilox rollers using TeroStar™ process, in *Proceedings of the International Thermal Spray Conference '05*, CD-Rom, ISBN 3-87155-793-5, DVS-Verlag, Düsseldorf, Germany.
- Lenling, W.L., Smith.M.F. and Orloff, D.I. (1992). Thermal coating development for impulse drying, in *Thermal Spray: International Advances in Coatings Technology*, C.C. Berndt (Ed.), ASM International, Materials Park, OH, USA, pp. 619–624.
- Loch, M. and Barbezat, G. (2000). Characteristics and potential application of thermally sprayed thin film coatings, in *Thermal Spray: Surface Engineering via Applied Research*, C.C. Berndt (Ed.), ASM International, Materials Park, OH, USA, pp. 1141–1144.
- Locke, L.D. and Malm, D.L. (1971). Fabrication of sputtering sources by plasma spraying: tantalum–hafnium mixtures, *Rev. Sci. Instr.*, **42**, 1696–1698.
- Longo, F.N. (1992). Thermal spray coatings markets, trends and forecasts, in *Proceedings of the 1st Gorham's International Thermal Spray Coatings Conference*, Cambridge, MA, USA, 8–10 November.
- Lugscheider, E. and Weber, T. (1989). Plasma spraying of Bi–Sr–Ca–Cu–O high temperature superconductors, in *Thermal Spray: Research and Applications*, ed. T. Bernecki (Ed.), ASM International, Materials Park, OH, USA, pp. 635–640.
- Lutz, E.H. (1993). Plasma ceramics, *Powder Met. Int.*, **25**, 131–137.
- Lutz, E.H. and Florian, R. (1993). Schweißen von Plasmakeramik, *Keram. Zeit.*, **45**, 458–460.
- Maissel, L.I. and Glang, R. (1970). *Handbook of Thin Film Technology*, McGraw Hill, New York, NY, USA.
- Mäkelä, J.M., Hellstén, S., Silvonen, J., Vippola, M., Levänen, E. and Mantylä, T. (2006). Collection of liquid flame generated TiO<sub>2</sub> nanoparticles on stainless steel surface, *Mater. Lett.*, **60**, 530–534.
- Malléner, W. (2001). Tungsten coatings for divertor wings, in *Thermal Spray: New Surfaces for a New Millennium*, C.C. Berndt, K.A. Khor and E. Lugscheider (Eds), ASM International, Materials Park, OH, USA, pp. 55–60.

- Malléner, W., Wippermann, K., Jansen, H., Li, Z. and Stöver, D. (1992). VPS fabrication of electroactive solid oxide fuel cell membranes, in *Thermal Spray: International Advances in Coatings Technology*, C.C. Berndt (Ed.), ASM International, Materials Park, OH, USA, pp. 835–838.
- Manning-Meier, S., Gupta, D.K. and Sheffler, K.D. (1991). Ceramic thermal barrier coatings for commercial gas turbine engines, *J. Met.*, March, 50–53.
- Matejka, D., Berezovsky, M., Palka, V., Kolenciak, V. and Ivan, L. (1988). The development of plasma sprayed coatings for use in the production and repair of hydraulic steel mine props, in *1st Plasma Technik Symposium*, Vol.1, H. Eschnauer, P. Huber, A.R. Nicoll and S. Sandmeier (Eds), Plasma Technik AG, Wohlen, Switzerland, pp. 247–257.
- Meetham, G.W. (1985). Coating requirements in gas turbine engines, *J. Vac. Sci. Technol.*, A, 3, 2509–2515.
- Meiners, E. (1996). Mikrostrukturierung von Makrooberflächen–Laserwendungen in der Druckformenherstellung, in *Proceedings of the 6th European Conference on Laser Treatment of Materials*, F. Dausinger, H.W. Bermann and J. Sigel (Eds), AWT, Stuttgart, Germany, pp. 663–674.
- Melkert, S. and Renner, G. (1987). Wear and temperature characteristics of thermal sprayed yankee dryers, in *Thermal Spray: Advances in Coatings Technology*, D.L. Houck (Ed.), ASM International, Materials Park, OH, USA, pp. 227–232.
- Modi, M.D., Modi, S.C. and Mayuram, M.M. (1986). A case study on the use of plasma sprayed oxide ceramic coatings in hot extrusion dies for non-ferrous metals, in *Advances in Thermal Spraying*, Pergamon Press, New York, NY, USA, pp. 359–366.
- Moskowitz, L.N. (1992). Can HVOF coatings solve the economic and technical corrosion problems in refineries and chemical plants?, in *Proceedings of the 1st Gorham's International Thermal Spray Coatings Conference*, Cambridge, MA, USA, 8–10 November.
- Müller, M., Heimann, R.B., Gitzhofer, F., Boulos, M.I. and Schwarz, K (2000). Radio frequency plasma processing to produce chromium sputter targets, *J. Therm. Spray Technol.*, 9, 488–493.
- Mullendore, A.W., Whitley, J.B. and Mattox, D.M. (1981). Thermal fatigue properties of coated materials for fusion device applications, *J. Nucl. Mater.*, 103–104, 251–256.
- Namba, Y., Itoh, S., Okura, M., Takatsuka, K. and Kawata, S. (1988). The application of plasma sprayed coatings for cooling rolls in continuous annealing lines, in *International Symposium on Advanced Thermal Spraying Technology and Allied Coatings*, High Temperature Society of Japan, Osaka, Japan, pp. 229–234.
- Nguyentat, T., Dommer, K.T. and Bowen, K.T. (1992). Metallurgical evaluation of plasma sprayed structural materials for rocket engines, in *Thermal Spray: International Advances in Coatings Technology*, C.C. Berndt (Ed.), ASM International, Materials Park, OH, USA, pp. 321–325.
- Ohmori, A., Ye, F. and Li, C.-J. (2002). The effects of the additives on photocatalytic performance of plasma sprayed titanium oxide coatings, in *Proceedings of the International Thermal Spray Conference '02*, E. Lugscheider and C.C. Berndt (Eds), DVS, Düsseldorf, Germany, pp. 165–169.
- Okumura, K., Aihara, S., Ito, S. and Kawasaki, S. (2000). Development of thermal spraying-sintering technology for SOFC, *J. Therm. Spray Technol.*, 9, 354–359.
- Okuno, A., Harada, Y. and Ando, T. (2004). Development of plasma sprayed corrosion protection coatings for sodium sulfur battery cell containers, in *Proceedings of the International Thermal Spray Conference '04*, CD-Rom, ISBN 3-87155-792-7, DVS-Verlag, Düsseldorf, Germany.

- Palmer, R.H. (1992). Using a plasma sprayed alumina coating as an electrical insulator with semiconductor device packages, in *Thermal Spray: International Advances in Coatings Technology*, C.C. Berndt (Ed.), ASM International, Materials Park, OH, USA, pp. 825–828.
- Pawlowski, L. (1980). The vacuum plasma sprayed copper and tantalum coatings, in *Proceedings of the 9th International Thermal Spray Conference*, Nederlands Instituut voor Lastchniek, The Hague, The Netherlands, pp. 299–305.
- Pawlowski, L. (1987). Microstructural study of plasma sprayed alumina and nickel chromium coatings, *Surf. Coat. Technol.*, **31**, 103–16.
- Pawlowski, L. (1996). Technology of thermally sprayed anilox rolls, state of art, problems, and perspectives, *J. Therm. Spray Technol.*, **8**, 317–334.
- Pawlowski, L. (1999). Thick laser coatings: a review, *J. Therm. Spray Technol.*, **5**, 279–295.
- Prudenziati, M., Cirri, G. and Dal Bo, P. (2006). Novel high-temperature reliable heaters in plasma spray technology, *J. Therm. Spray Technol.*, **15**, 329–331.
- Quentmeyer, R.J., McDonald, G. and Hendricks, R.C. (1985). Fabrication of ceramic substrate-reinforced and free forms by mandrel plasma spraying metal-ceramic composites, *J. Vac. Sci. Technol.*, **A**, **3**, 2450–2455.
- Rairden, J.R. (1967). Porous bodies of Ta, Nb, Al fabricated by metal spray processes, *Electrochem. Technol.*, July–August, 407–408.
- Randolph, J. (2004). HVOF facility qualification at an airline – importance and benefits for landing gear applications, in *Proceedings of the International Thermal Spray Conference '04*, CD-Rom, ISBN 3-87155-792-7, DVS-Verlag, Düsseldorf, Germany.
- Rhys-Jones, T.T. (1990). The use of thermally sprayed coatings for compressor and turbine applications in aero engines, *Surf. Coat. Technol.*, **42**, 1–11.
- Ritchie, J. (1983). Advancements in thermal spraying of yankee dryers utilizing the plasma process, in *Proceedings of the 10th International Thermal Spray Conference*, Vol. 80, DVS, Düsseldorf, Germany, Band 80 (added paper).
- Schmid, R.K., Ghasripor, F., Dorfman, M. and Wei, X. (2000). An overview of compressor abdardables, in *Thermal Spray: Surface Engineering via Applied Research*, C.C. Berndt (Ed.), ASM International, Materials Park, OH, USA, pp. 1087–1093.
- Schmitz, F., Slotty, W. and Thien, V. (1984). Oberflächenschutzschichten gegen Hochtemperaturkorrosion von Schaufelwerkstoffen stationärer Gasturbinen, *Metall*, **38**, 204–212.
- Shibata, R., Kasakoshi, T., Iimura, T. and Harada, H. (1988). Surface heating fuser roll made by arc plasma spraying, in *Proceedings of the International Symposium on Advances in Thermal Spray Technologies and Allied Coatings*, (Eds), High Temperature Society of Japan, Osaka, Japan, pp. 235–241.
- Smith, M.F., Croessmann, C.D., Hosking, F.M., Watson, R.D. and Koski, J.A. (1991). Plasma sprayed materials for magnetic fusion energy devices, in *2nd Plasma Technik Symposium*, Vol. 3, S. Blum-Sandmeier, H. Eschnauer, P. Huber and A.R. Nicoll (Eds), Plasma Technik AG, Wohlen, Switzerland, pp. 43–52.
- Smyth, R.T., Dittrich, F.J. and Weir, J.D. (1978). Thermal spraying – a new approach to thick film circuit manufacture, in *Proceedings of the International Conference on Advances in Surface Coating Technology*, London, UK, 13–15 February, pp. 233–236.
- Sonkin, R.M. (1977). Corona discharge treatment of polyolefin films, *Plas. Eng.*, February, 50–52.

- Sordelet, D.J. and Ellis, T.W. (1993). Evaluation of plasma arc sprayed refractory metal coatings for crucible containing molten ceramic oxides, in *Thermal Spray Coatings: Research, Design and Applications*, C.C. Berndt and T.F. Bernecki, (Eds), ASM International, Materials Park, OH, USA, pp. 643–648.
- Stecura, S. (1977). Two-layer thermal barrier coating for high temperature components, *Ceram. Bull.*, **56**, 1082–1089.
- Storch, W. and Bick, H. (1993). Erosionschutz für Dampfturbinenschaufeln mittels Stellitieren, in *Proceedings of Thermal Spray '93*, Vol. 152, DVS, Düsseldorf, Germany, pp. 184–187.
- Stöver, D., Hathimarani, D., Vaßen, R. and Damani, R.J. (2006). Plasma-sprayed components for SOFC applications, *Surf. Coat. Technol.*, **201**, 2002–2005.
- Streeter, J. and Sampson, E.R. (2000). Hard chrome replacement and other thermal spray application in the Chilean Navy, in *Thermal Spray: Surface Engineering via Applied Research*, C.C. Berndt (Ed.), ASM International, Materials Park, OH, USA, pp. 1145–1148.
- Sulit, R.A., Vanderveldt, H.H.J. and Schaper, V.D. (1980). Corrosion control using wire sprayed aluminium in the US Navy, in *Proceedings of the 9th International Thermal Spray Conference*, Nederlands Instituut voor Lastechniek, The Hague, The Netherlands, pp. 49–52.
- Sumner, I.E. and Ruckle, D.L. (1980). Development of improved durability plasma sprayed ceramic sprayed coatings for gas turbine engines, in *Proceedings of the 16th AIAA/SAE/ASME Joint Propulsion Conference*, Hartford, CT, USA, 30 June–2 July, Paper AIAA-80-1193.
- Takenori, S., Kadokawa, N. and Koseki, K. (2000). Development of metallic substrate planar SOFC fabricated by APS, *J. Therm. Spray Technol.*, **9**, 360–363.
- Tani, K. and Nakahira, A. (2004). Latest study and subject of thermal spraying in Japan, in *Proceedings of the International Thermal Spray Conference '04*, CD-Rom, ISBN 3-87155-792-7, DVS-Verlag, Düsseldorf, Germany.
- Thiagarajan, K. (1990). Applications of plasma spray ceramic coatings for MHD components, *Tool Alloy Steels*, October, 351–354.
- Toma, F.-L., Bertrand, G., Chwa, S.O., Coddet, C. and Klein, D. (2004). Studies of the photocatalytic efficiency of titanium dioxide powders and coatings obtained by plasma spraying, in *Proceedings of the International Thermal Spray Conference '04*, CD-Rom, ISBN 3-87155-792-7, DVS-Verlag, Düsseldorf, Germany.
- Toma, F.-L., Bertrand, G., Klein, D., Coddet, C. and Meunier, C. (2005). Photocatalytic decomposition of nitrogen over  $\text{TiO}_2$  elaborated by liquid feedstick plasma spraying, in *Proceedings of the International Thermal Spray Conference '05*, CD-Rom, ISBN 3-87155-793-5, DVS-Verlag, Düsseldorf, Germany.
- Toma, F.-L., Bertrand, G., Begin, S., Meunier, C., Barres, O., Klein, D. and Coddet, C. (2006). Microstructure and environmental functionalities of  $\text{TiO}_2$  supported photocatalysis obtained by suspension plasma spraying, *Appl. Catal., B: Environ.*, **68**, 74–84.
- Tomaszek, R., Pawłowski, L., Zdanowski, J., Grimbolt, J. and Lureyns, J. (2004). Microstructure transformations of  $\text{TiO}_2$ ,  $\text{Al}_2\text{O}_3 + 13\text{TiO}_2$  and  $\text{Al}_2\text{O}_3 + 40\text{TiO}_2$  at plasma spraying and laser engraving, *Surf. Coat. Technol.*, **185**, 137–149.
- Tomaszek, R., Pawłowski, L., Gengembre, L., Laureyns, J., Znamirowski, Z. and Zdanowski, J. (2006). Microstructural characterization of plasma sprayed  $\text{TiO}_2$  functional coatings with gradient of crystal size, *Surf. Coat. Technol.*, **201**, 45–56.

- Tomaszek, R., Pawlowski, L., Gengembre, L., Laureyns and Le Maguer, A. (2007). Microstructure of suspension plasma sprayed multilayer coatings of hydroxyapatite and titanium oxide, *Surf. Coat. Technol.*, 201, 7432–7440.
- Tourenne, F. (2004). Application des dépôts projetés dans l'industrie biomédicale, in *Journée Spécialisée MS12*, Paris, 21–22 October, CNAM CACEMI, Paris, France.
- Travis, R., Herbstritt, J., Blackburn, J. and McCaw, R.L. (1992). Thermal sprayed coatings for shipboard steam valve stems, in *Thermal Spray: International Advances in Coatings Technology*, C.C. Berndt (Ed.), ASM International, Materials Park, OH, USA, pp. 601–603.
- van Rodijnen, F. and Knepper, M. (2002). Low energy arc spraying in the capacitor industry, in *Proceedings of the International Thermal Spray Conference '02*, E. Lugscheider and C.C. Berndt (Eds), DVS, Düsseldorf, Germany, pp. 170–174.
- Vlcek, J., Huber, H., Kretschmer, Schenkel, T. and Voggenreiter, H. (1999). Spray forming composite combustion chamber, in *Proceedings of the United Thermal Spray Conference' 99*, H. Lugscheider and P.A. Kammer (Eds), DVS-Verlag, Düsseldorf, pp. 15–19.
- Vuoristo, P., Leivo, E., Turunen, E., Leino, M., Järvelä and Mäntylä, T. (2003). Evaluation of thermally sprayed and other polymeric coatings for use in natural gas pipeline components, in *Thermal Spray 2003: Advancing the Science and Applying the Technology*, C. Moreau and B. Marple (Eds), ASM International, Materials Park, OH, USA, pp. 1693–1702.
- Walser, B. (1996). Our thermal spray industry, *J. Therm. Spray Technol.*, 5, 235–238.
- Winkler-Gniewek, W., Stallforth, H., Ungethüm, M. and Gruner, H. (1988). Structure and properties of VPS coatings in medical technology, in *1st Plasma Technik Symposium*, vol. 3, H. Eschnauer, P. Huber, A.R. Nicoll and S. Sandmeier (Eds), Plasma Technik AG, Wohlen, Switzerland, pp. 95–102.
- Wixson, M.S. (1993). Arc sprayed zinc coatings for cathodic protection of steel rebar in concrete, in *Thermal Spray Coatings: Research, Design and Applications*, C.C. Berndt and T.F. Bernecki (Eds), ASM International, Materials Park, OH, USA, pp. 673–678.
- Wortman, D.J. (1985). Performance comparison of plasma spray and physical vapour deposition BC23 coatings in the LM2500, *J. Vac. Sci. Technol.*, A, 3, 2532–2536.
- Xiaouo, H. and Yufen, L. (2004). The current situation and future of thermal spraying industry in China, in *Proceedings of the International Thermal Spray Conference '04*, CD-Rom, ISBN 3-87155-792-7, DVS-Verlag, Düsseldorf, Germany.
- Ye, F. and Ohmori, A. (2001). Photocatalytic activity and photo-absorption of plasma sprayed  $\text{TiO}_2$ –10 %  $\text{Fe}_3\text{O}_4$  coatings, *Trans. JWRI*, 30, 73–78.
- Ye, F. and Ohmori, A. (2002a). The photocatalytic activity and photo-absorption of plasma sprayed  $\text{TiO}_2$ – $\text{Fe}_3\text{O}_4$  binary oxide coatings, *Surf. Coat. Technol.*, 160, 62–67.
- Ye, F. and Ohmori, A. (2002b). Microstructure and photoelectrochemical characteristics of  $\text{TiO}_2$ –ZnO electrodes prepared by plasma spraying technique, *Trans. JWRI*, 31, 201–205.
- Ye, F., Ohmori, A., and Li, C.-J. (2003). Investigation of the photocatalytic efficiencies of plasma sprayed  $\text{TiO}_2$ – $\text{Fe}_3\text{O}_4$  coatings, in *Thermal Spray 2003: Advancing the Science and Applying the Technology*, B.R. Marple and C. Moreau (Eds), ASM International, Materials Park, OH, USA, pp. 169–175.

# Index

Note: Figures and Tables are indicated by *italic page numbers*, footnotes by suffix ‘n’.

- Abel inversion* 178  
Ability of heating factor (AHF) 197  
    plot *vs* pressure 198  
Abradable coatings 449  
    applications  
        aero-engines 546, 547, 549  
        food industry 551  
Abrasive grit blasting 53, 56–63  
    laboratory installation 56, 57  
    *see also* Grit blasting  
Abrasive wear 337–8  
Abrasive wear resistance  
    ceramic coatings 438–9, 443–4  
    composites 440–4  
    metals and alloys 440, 444  
Absorption bands 298  
Acoustic emission analysis (AEA)  
    367–8  
Acoustical methods, quality  
    determination by 365–8  
Active zone in electrochemical cell  
    361, 362  
Active zones (splat on substrate) 246  
    adhesion mechanisms 247–9  
        metallurgical interactions 248–9  
        physical interactions 248  
    factors affecting 246–7  
Adhesion  
    determination of 317–18, 318–24  
        double-cantilever beam (DCB)  
        method 322  
    four-point bending test 322  
    fracture mechanics based tests  
        318, 322–3  
    tensile adhesion test (TAT) 317,  
        318, 319–22  
        statistical models 387  
Adhesion mechanisms  
    coating-to-substrate 246–9, 315,  
        317  
    in wear mechanisms 336–7  
Adhesion strength of coating  
    meaning of term 319  
    *see also* Tensile adhesion strength  
Adhesive wear 336–7  
Adhesive-wear-resistance  
    factors affecting 337  
    *see also* Sliding-wear resistance  
Adhesive-wear-resistant coatings  
    applications, aero-engines 546,  
        547, 548  
        ceramics 143, 434–7, 547  
        composites 438  
        laser-glazed coatings 137, 143  
        metals and alloys 137, 437–8

- Aero-engines 545–9  
 coatings used 546, 547–9  
 abradable coatings 546, 547,  
 549  
 adhesive-wear-resistant coatings  
 546, 547, 548  
 duplex thermal barriers 546,  
 547, 548  
 high-temperature corrosion  
 resistant coatings 546,  
 547, 549  
 machining processes 545–6  
 materials used 545
- Aeronautical and space industries,  
 applications 545–51
- Agglomerate, meaning of term 4n3
- Agglomeration  
 of sprayed particles 194, 196  
*see also* Spray drying of powders
- Agroalimentary/agrofoods industry,  
 applications 551, 575
- Air plasma spraying, *see* Atmospheric  
 plasma spraying (APS)
- Aircraft landing-gear components  
 549–50
- Alloy coatings  
 abrasive wear resistance 444  
 adhesive/sliding-wear resistance  
 437–8  
 aqueous corrosion resistance 510,  
 511–12  
 erosive wear resistance 444  
 fretting wear resistance 449  
 hardness 401–2, 403  
 mechanical properties 426–30  
 thermal conductivity 465–7  
 thermal expansion 477–8
- Alloy powders, manufacture of  
 4, 5–8, 26–8
- Alloying, of coating with substrate  
 120, 129
- Alumina 268  
 elastic modulus (bulk material)  
 417
- Alumina coatings  
 abrasive wear resistance 439  
 applications 547, 565, 566,  
 583, 584  
 aqueous corrosion resistance 513  
 crystal size 245  
 as decorative coatings 505, 563  
 dielectric properties 354, 493, 494  
 emissivity 481, 482, 483
- erosive wear resistance 447, 448  
 friction and wear properties  
 435, 436  
 growth 249–50  
 hardness 395, 397, 398  
 mechanical properties 418, 421  
 metallographic preparation (for  
 microscopy) 310  
 phase compositions 268  
 post-spray treatment of 118, 119,  
 138, 153, 155  
 tensile adhesion strength 84, 407  
 thermal breakdown in 355  
 thermal conductivity 458,  
 460–1, 461  
 thermal expansion coefficients 475
- Alumina particles  
 modelling of temperatures and  
 velocities 207  
 temperature affected by load  
 effect 195
- Alumina sand, in grit blasting 59
- Alumina–chromia coatings, electrical  
 properties 494
- Alumina–NiCr coatings 564
- Alumina–titania alloy coatings  
 abrasive wear resistance 439, 444  
 applications 574, 575, 584,  
 586, 587  
 as decorative coatings 505, 563  
 electrical properties 490–2  
 emissivity 483  
 friction and wear properties 435  
 hardness 395, 398  
 impact-wear resistance 452  
 mechanical properties 420  
 tensile adhesion strength 407, 409
- Alumina–zirconia alloy coatings  
 abrasive wear resistance 439  
 applications 574  
 friction and wear properties 435  
 hardness 395
- Aluminium  
 electrical properties of bulk  
 metal 486  
 mechanical properties of bulk metal  
 422
- Aluminium bronzes  
 adhesive wear resistance 437  
 alumina-reinforced composite,  
 adhesive-wear resistance 438
- Aluminium-coated nickel powder 25,  
 248, 266

- Aluminium coatings  
  applications 562, 566, 588  
  aqueous corrosion resistance 508,  
    509, 510  
  electrical properties 486  
  hardness 401  
  mechanical properties 422, 425  
Aluminium oxide, *see* Alumina  
Aluminium phosphate, impregnation  
  of coating surface using 155–6  
Aluminium–alumina composite  
  coatings 478–9  
  applications 584  
  microstructures 480  
  thermal expansion 479  
Aluminium–SiC composite coating,  
  mechanical properties 431, 433  
Aluminium–tin alloy coating,  
  applications 551  
Aluminum zinc oxide (AZO) coatings  
  506–7  
Amdry powders 8, 11, 406  
Amorphous grain microstructure 244  
Amorphous phase fraction, statistical  
  models 387, 388–9  
Amperit powders 8, 11, 25  
Anatase ( $TiO_2$ ) 269, 271, 489, 558  
*Anilox rolls* 585–7  
  cleaning of 54  
  fine-pattern 146  
  grit blasting of 58  
  laser engraving of 129, 143, 144,  
    145–7  
Anisotropic mechanical properties  
  331  
  metal and alloy coatings 427, 428  
  oxide coatings 417, 418, 421  
Anisotropic thermal expansion  
  coefficients 345, 453  
'Anisotropy of strength' 421  
Anodic coating 361  
*Anticathode* 302, 306  
Applications of coatings 543–96  
  aerospace industries 545–51  
  agroalimentary/agrofoods industry  
    551, 575  
  automobile industry 551–4  
  ceramics industry 554–7  
  chemical industry 557–62  
  civil engineering industry 562  
  decorative coatings 563  
  electronics industry 563–7  
  energy generation industry 567–72  
  food industry 551, 575  
  iron and steel industries 572–5  
  machine building industry 574–5  
  medicine 575–7  
  mining industry 577  
  nonferrous industry 577–9  
  nuclear industry 579–80  
  paper industry 580–3  
  printing and packaging industries  
    583–7  
  shipbuilding and naval  
    industries 588  
Aqueous corrosion 359–63, 507  
Aqueous corrosion-resistant coatings  
  361, 507–18  
Arc plasma densified powders 18, 19  
Arc root fluctuations (in plasma  
  jet) 168  
Arc sprayed coatings  
  applications 553, 562, 566,  
    581, 588  
  aqueous corrosion resistance 509  
  inhomogeneities 278  
  mechanical properties 424  
  physical properties 81–2  
  tensile adhesion strength 81–2,  
    412, 413  
Arc-sprayed steels, as top  
  coatings 402  
Arc spraying (AS) 1, 2, 68, 79–82  
  combined with HVOF process 81  
  contact temperature of sprayed  
    particle 237  
  heat transfer in 196  
  morphology of lamellae 233  
  principles 79–80  
  process parameters 80–1  
    electric arc 80  
    principal parameters 81  
    wires 81  
Archimedean force 181  
Archimedean method (for density  
  determination) 344, 348  
Argon-atmosphere plasma sprayed  
  coatings  
  magnetic properties 504  
  optical properties 505, 506, 507  
  thermal conductivity 465  
  wear properties 449  
Arithmetic mean diameter 37  
Arrhenius equation 172–3  
Arrhenius plots 490

- Atmosphere Temperature-Controlled Spraying (ATCS) 93, 94, 95, 95, 96
- Atmospheric plasma sprayed coatings applications  
aero-engines 547, 549  
automobile industry 552, 554, 555, 556, 557  
ceramics industry 554, 555, 556, 557  
decorative coatings 505, 563  
electronics industry 564, 565, 566  
energy generation facilities 570, 571, 572  
food industry 551, 575  
iron and steel industry 573, 574  
mining industry 577  
non-ferrous metal industry 578  
nuclear industry 579  
ozonizers 557, 559, 562  
paper industry 581  
printing and packaging industries 583, 584, 586, 587  
shipbuilding and naval industries 588  
textile industry 574–5
- aqueous corrosion resistance 510, 511, 513, 516  
causes of inhomogeneity 278  
crystal size 245  
dielectric properties 498, 499  
electrical properties 485, 486, 487, 491, 492, 494, 496–7  
friction and wear properties 435, 439, 439, 443, 452  
hardness 390, 392, 394, 395, 396, 403, 404  
hot-corrosion resistance 519, 521  
hydroxyapatite (HA) coatings 272, 419, 515  
interactions with simulated body fluids 515  
magnetic properties 503, 504  
mechanical properties 416, 417, 418–20, 423, 428  
metallographical preparation (for microscopy) 318  
optical properties 505  
phase composition 267, 271–5  
physical properties 79
- post-spray treatment of 117, 131–2, 135–6, 141, 148, 151, 155, 156, 157, 158  
specific heats 472, 473  
tensile adhesion strength 79, 406, 412, 414  
thermal conductivity 455, 458, 460, 463, 465, 467, 469  
thermal expansion 475–6, 477, 479  
yttria-stabilized zirconia (YSZ) coatings 271–2, 419
- Atmospheric plasma spraying (APS) 68, 74–9  
contact temperature of sprayed particle 237  
history 74  
modelling of particles' temperatures and velocities 207  
modelling of plasma jet 177  
morphology of lamellae 233  
particle velocity measurements 190–1  
principles 74, 75  
process parameters 75–9, 385–6  
arc plasma 75–7  
powder characteristics 77  
powder injection 78  
principal parameters 78–9  
temperature and velocity profiles of plasma jet 176
- Atomic force microscopy (AFM) 243, 245, 293, 294, 295
- Atomization  
powders manufactured by 4, 5–8, 266, 267  
factors affecting oxygen content 6–8  
process parameters 6  
in spray drying process 14–15
- Attritor processes 22, 27
- Auger electron spectroscopy (AES)* 321
- Automobile industry, applications 551–4
- Axial III<sup>TM</sup> torch 69, 101, 444
- $\beta$  factor 357
- Backwall echo* (in ultrasonic testing) 366
- Ballistic model* 45, 181
- Band rollers* 554, 555

- Barium titanate coatings  
  dielectric properties 353, 495,  
    496, 498  
  hardness 399  
  microstructure and porosities 498
- Beer-Lambert law* 122–3, 298
- Bending tests  
  adhesion determination 322  
  elasticity determination 327–8  
  *see also* Four-point bending test;  
    Three-point bending test,  
    elasticity determination
- Berkovitch* pyramid 324, 327
- Beryllium coatings 580
- B–H* curve 358  
  determination of 359
- Biocompatibility  
  biomedical coatings 515  
  decorative coatings 563
- Biomedical coatings 117, 130,  
  461, 508  
  *see also* Hydroxyapatite (HA)  
    coatings; Wollastonite, thermal  
    diffusivity
- Biot number 196
- Bi-Sr-Ca-Cu-O (high-temperature  
  superconductor) 502
- Black-body* concept 208
- Blast furnace stave cooling pipes  
  574
- Block-on-disc/cylinder friction/wear  
  test 335, 435
- Bolometer*, in IR spectrometer 299
- Bond coatings  
  characteristics 404  
  hardness 402, 403  
  mechanical properties 426  
  thermal expansion 477–8
- Bond strength  
  arc-sprayed coatings 81–2, 410–1  
  CGSM coatings 100  
  D-gun™ coatings 84, 406  
  flame-sprayed coatings 74, 410  
  HVOF-sprayed coatings 89, 406  
  plasma-sprayed coatings 79, 92–3,  
    96, 406, 407–8, 411
- Bohrde coatings, electrical  
  resistivities 485
- Boundary conditions  
  flames/jets 171–2  
  particles at flight 202–3
- Bragg's law* 298, 304, 306
- Bragg-Brentano* geometry (in X-ray  
  diffraction) 306
- Bremsstrahlung* 297
- 'Brick wall' microstructure 243, 244
- Brick-clay extruders 556
- Bridges, protection of 562
- Brinell* hardness test, metal  
  coatings 401
- Brookite* ( $TiO_2$ ) 269n14, 558
- Brunauer-Emmett-Teller (BET)  
  technique (for porosity  
    evaluation) 343
- Bunsen ice calorimetry* (BIC) 348
- Burner rigs 349, 481
- Calcia-stabilized zirconia coatings  
  applications 579  
  emissivity 482  
  thermal conductivity 458  
    factors affecting 457–8  
  thermal shock resistance 481
- Calcination* 32, 33, 155, 275
- Calcium titanate, hardness 399
- Cantilever beam method, elasticity  
  determination by 330
- Capacitor electrodes 566
- Carbide ceramic coatings  
  erosive wear resistance 446–8  
  friction and wear properties  
    436, 437  
  hardness 389–92, 393  
  mechanical properties 415–17  
  metallographical preparation (for  
    microscopy) 310  
  tensile adhesion strength 405, 406  
  *see also* Tungsten carbide–cobalt  
    cermet coatings
- Carbide powders  
  decarburization during  
    spraying 211  
  manufacture of 4, 8–11
- Carbide-reinforced composites, laser  
  (post-spray) treatment of  
    130, 132–4
- Carbon fibre-reinforced aluminium,  
  mechanical properties 433
- Carbon fibre, properties 434
- Carbon steel–iron oxides composites,  
  applications 552, 553
- Carrier mobility 353, 487
- Cathodic coating* 361
- Cavitation erosion/wear* 339, 449–50
- Cavitation wear resistance 450–2

- Cavitation* 449  
 Centrifugal atomizer 12, 15  
 Ceramic coatings  
   abrasive wear resistance 438–9  
   aqueous corrosion resistance 513–16  
   emissivity 479, 481, 482–3  
   erosive wear resistance 446–8  
   fretting-wear resistance 449  
   hardness 389–92, 393, 395–400  
   interactions with simulated body fluids 513–14, 515, 516  
   mechanical properties 415–22, 556  
   metallographical preparation (for microscopy) 310  
   post-spray treatment of 138–41, 149–50, 151, 152, 153  
   tensile adhesion strength 405, 406, 407–8, 409  
   thermal conductivity 454–61  
   thermal expansion 474–7, 556  
   *see also* Carbide ceramic coatings; Oxide ceramic coatings  
 Ceramic membranes 557  
 Ceramic rods, use in spraying 2  
 Ceramic rolls 554–5, 556  
 Ceramics industry, applications 554–7  
 Ceria-stabilized zirconia coatings  
   phase composition 458, 459  
   thermal conductivity 460  
 Cermet agglomerates 4  
 Cermet clads 4, 20–6  
 Cermet powders, manufacture of 4, 8–26, 28–30  
 Cermet, meaning of term 4n1  
 Characterization of coatings 291  
   methods 291–380  
     chemical properties 359–64  
     electrical properties 292, 350–7  
     magnetic properties 292, 357–9  
     mechanical properties 291, 317–40  
     microstructural investigations 291, 292–317  
     physical properties 340–2  
     thermophysical properties 291–2, 342–50  
     non-destructive techniques 364–70  
 Charge effect 184  
 Chemical analysis  
   of jets and flames 180  
   of powders 38–9  
 techniques used in characterization of coatings 294, 295, 296, 297–303, 314  
 Chemical etching, in microstructure investigations 311  
 Chemical industry, applications 557–62  
 Chemical precipitation, cladded powders manufactured by 22–3, 24  
 Chemical properties of coatings 359–64  
 Chemical reactions, lamella/substrate 248–9  
 Chemical refinery vessels 560  
 Chemical treatment, surface cleaning by 54  
 Chemical vapour deposition (CVD)  
   cladding of powders by 25–6  
   compared with thermal spraying 563  
 Chromel/constantan thermopiles 569  
 Chromia coatings  
   alternative coatings for anilox rolls 146–7, 587  
   applications 143, 547, 574, 575, 586–7  
   as decorative coatings 505, 563  
   electrical properties 500  
   emissivity 481, 483  
   friction and wear properties 435, 439, 448  
   hardness 106, 392, 395, 395, 397, 397, 398  
   laser engraving of 143, 144  
   mechanical properties 418  
   post-spray treatment of 156  
   tensile adhesion strength 407, 409  
   thermal diffusivity 463  
   thermal expansion coefficient 475  
   *see also* Alumina–chromia coatings, electrical properties  
 Chromia–silica powder 18, 19  
   apparent density 42  
 Chromia–titanium carbide composite coatings, applications 578  
 Chromium-based alloy coatings, abrasive-wear resistance 444  
 Chromium carbide coatings 391, 393, 394  
   alloyed with NiCr  
   applications 571, 573

- friction and wear properties 437, 447, 451  
mechanical properties 416  
hardness 389, 391–2  
mechanical properties 417
- Chromium coatings  
applications 485  
electrical properties 486
- Chromium diffusion, post-spray treatment using 156–7
- Chromium oxide  
elastic modulus (bulk material) 417  
*see also* Chromia coatings
- Chromium oxide powder 8–9  
reduction during spraying 211
- Civil engineering industry, applications 562
- Clad, meaning of term 4n2
- Cladding  
coating on substrate 120, 129  
powders manufactured by 4, 20–6, 266, 267  
gas-phase cladding 25–6  
liquid-phase cladding 22–5  
solid-phase cladding 22
- Clausius–Clapeyron equation 201
- Cleaning process 53, 54–5
- Co-current airflow dryers 16
- Coating build-up 221–90  
coating growth 249–64  
coating surface 264  
impact of particles 222–49  
mechanisms 249–51  
overview 221–2  
temperature of coatings at spraying 251–5  
thermal stresses 255–64
- Coating properties  
arc-sprayed coatings 81–2  
CGSM coatings 100  
D-gun™ coatings 84  
flame-sprayed coatings 74  
HVOF-sprayed coatings 89  
plasma-sprayed coatings 79, 92–3, 96
- Coating surface 264
- Coating thickness  
arc-sprayed coatings 82  
CGSM coatings 100  
D-gun™ coatings 84  
flame-sprayed coatings 74  
HVOF-sprayed coatings 89
- measurement of 340, 341  
plasma-sprayed coatings 79, 93, 96
- Coatings  
phase composition 275–6  
post-spray treatment of 276  
properties 501–2  
selective evaporation phenomena 211
- Cobalt alloy powders 8
- Cobalt-based alloys, wear properties 449, 450, 451
- Cobalt chromium–tungsten carbide coating, applications 572
- Cohesive strength of coating, meaning of term 319
- Cold-gas sprayed coatings  
applications 557, 566  
electrical properties 485  
mechanical properties 425, 426  
physical properties 100
- Cold-gas spraying method (CGSM)  
68, 96–100  
history 96–7  
materials suitable for 99, 150  
modelling of gas flow 177  
principles 97  
process parameters 97–100  
nozzle characteristics 98  
powder characteristics 98–9  
principal parameters 100  
substrate 99  
working gases 97–8, 426
- Columnar microstructure, laser-treated coatings 139, 140
- Combustion flame re-melting 152
- Combustion reaction 87, 172
- Composite clads 4, 20–6
- Composite coatings 281–3  
abrasive wear resistance 440–4  
aqueous-corrosion resistance 507, 516–18  
classification 282  
erosive wear resistance 446–8  
fretting-wear resistance 449  
friction and wear properties 438  
as intermediate coatings 430–1  
manufacturing methods 282–3  
mechanical properties 430–4  
near-‘net-shape’ structures 431–2  
thermal conductivity 467, 469
- Composite powders, manufacture of 4, 20–6, 30–1
- Composite, meaning of term 4n4

- Compression test, Young's modulus determination 329
- Computational domain 171, 172
- Computational fluid dynamics (CFD) software 175–6
- Concentration cells 360
- Conduction band 351
- Conduction, heat transfer by 194
- Conductivity, *see* Electrical conductivity; Thermal conductivity
- Conductors, electrical properties 484–92
- Conservation of energy 170
- Conservation of mass 169
- Conservation of momentum 169
- Constantan, in thermopiles 569
- Contact temperature of sprayed particle impacting on substrate 222 factors affecting 248, 409 listed for various spraying techniques 237
- Controlled-atmosphere plasma sprayed coatings, hardness 401
- Controlled-atmosphere plasma spraying (CAPS) 68, 93–6 history 93 principles 93–4 process parameters 94–6 arc plasma 94 powder characteristics 95 principal parameters 95–6
- Controlled parameter, in deposition of composite coatings 478–9
- Convection, heat transfer by 193
- Convective thermal fluxes (during spraying) 253, 253, 254
- Cooling stress 257, 258, 472
- Cooper pairs (of electrons) 350
- Copper alloy coatings applications 552, 579 hardness 402
- Copper coatings applications 566 electrical properties 485, 486 mechanical properties 422, 424, 425, 426
- Copper oxide decorative coatings 505, 563
- Copper, mechanical properties (bulk metal) 422
- Copper–zinc ferrite coating 564
- Cordierite coatings thermal expansion coefficient 475, 477, 481 thermal shock resistance 481
- Core zone, temperature measurement in 178
- Corona (on splat/lamella) 232, 239
- Corona rolls 583–4 alumina coating 262, 269, 312 grit blasting of 58 impregnation with silicone resin 158, 584 plasma spraying of 77 surface cleaning of 54
- Corrosion aqueous corrosion 359–63, 507 hot-gas/hot-medium corrosion 363–4, 507
- Corrosion-resistant coatings 89, 359, 361 aqueous corrosion-resistant 361, 507–18 hot corrosion-resistant 89, 359, 518–21 post-spray treatment of 135, 137
- Corrosive wear 339
- Counter-current airflow* dryers 17
- Covalent bonds 3
- Crevice corrosion 363
- Critical current density, values for superconductors 502
- Crucibles, molten ceramics 557
- 'Cryo-blasting' 63
- Crystal growth 244
- Crystal phase composition 264–77
- Crystallographic techniques characterization of coatings using 294, 295, 296, 303–7
- see also* Neutron diffraction; Selected-area diffraction (SAD); X-ray diffraction (XRD) technique
- Curie temperature 495
- Curvature-monitoring method* 340
- Cylinder bores, spraying inside 100, 104, 552, 553–4
- Cylinders spraying of 249–51 rotation and traverse speeds calculated for 251

- D-gun<sup>TM</sup> process, *see* Detonation-gun spraying (D-gun<sup>TM</sup> process)  
*De Broglie* hypothesis 293  
Decarburization of carbides at spraying 211, 391  
Decorative coatings 505, 563  
Defects in coating microstructure 280 detection of 365  
*Deflocculating agents* (in spray-drying slurry) 14  
Deformation of particles on impact 223–35  
    Madejski's theory 226–8  
Dense cladding 21, 266  
Density determination of 344, 348 factors affecting 348 slurry for spray drying 14  
Deposition process, phase composition affected by 265, 267–77  
Design of experiments (DOE) 383, 384–9  
Detonation-gun sprayed coatings applications  
    aero-engines 547  
    iron and steel industry 573, 574  
    petroleum exploration 560  
    hardness 390, 393, 395, 396  
    mechanical properties 415, 416  
    physical properties 84  
    tensile adhesion strength 84, 406  
    wear properties 443, 447, 449  
Detonation-gun spraying (D-gun<sup>TM</sup> process) 68, 82–4  
    detonation cycle 83, 168  
    history 82  
    modelling of jet 177  
    modelling of particles' temperatures and velocities 207  
    principles 82–3  
    process parameters  
        detonation wave 83–4  
        powder injection 84  
        powder properties 84  
        principal parameters 84  
    compared with HVOF process 85  
Development of new product 292  
Dielectric coatings, properties 493–500  
    Dielectric constant 353  
    determination of 354  
    oxide ceramic coatings 354, 494, 499  
    silicate coatings 499  
    titantate coatings 496–7, 498  
Dielectric strength 354 determination of 356  
Dielectrics  
    breakdown mechanisms 354–6  
        electronic breakdown 355  
        thermal breakdown 355–6  
    properties 353–7, 493–500  
        alumina coatings 493–5  
        alumina–chromia coatings 494  
        determination of 354, 356  
        silicates 495, 499  
        titantate coatings 495, 496–7, 498  
        yttria-stabilized zirconia coatings 499  
Differential aeration cell 360  
Differential interference contrast (DIC) technique 311  
Differential scanning calorimetry (DSC) 41, 348  
Differential temperature analysis (DTA) 42  
Differential temperature cells 360  
Difficulty of melting factor (DMF) 197 listed for various materials 198  
Diffraction techniques, characterization of coatings using 294, 295, 296, 303–7  
Diode lasers 126, 127  
Dissimilar electrode cells 360  
Doppler effect 188  
    *see also laser Doppler velocimeter (LDV) technique*  
Double-cantilever beam (DCB) method adhesion test 322 fracture toughness determination 333–4  
Double torsion (DT) method, fracture toughness determination 333, 334  
DPV-2000<sup>TM</sup> particle temperature and velocity measurement system 190, 209  
Drag coefficient 181–2 correction factors 183  
Drag force on particle 45, 181  
Dripping anode, in vacuum plasma spraying 91–2  
'Dry sand–rubber' abrasion test 338

- Dryers (in papermaking industry) 581–2
- Ductility, determination of 331
- Duplex thermal barrier coatings 136, 138, 139, 140, 150, 151, 469
- applications
- aero-engines 546, 547, 548
- automobiles 552
- aqueous corrosion resistance 516
- hot corrosion resistance 518, 519
- thermal contact resistance 469, 471
- ultrasonic testing of 366
- Dye-penetration methods, quality determination using 365
- Dynamic friction 334
- Dynamic viscosity 174
- Effective strain energy release rate 333
- Elastic modulus
- bulk carbides 415
  - bulk metals 422
  - bulk oxides 417
  - carbide coatings 416
    - variation with temperature 417
  - determination of 325–31
    - destructive methods 326–30
    - nondestructive methods 326, 330–1
  - metal coatings 422, 423–5
  - oxide coatings 418–20
- Elastic strength
- carbide coatings 416
  - determination of 325–31
  - oxide coatings 418–19
- Electric arc treatment 54–5
- Electric field emitters 500–1
- Electric heater coatings 564
- Electric insulation coatings 104
- Electrical conductivity 350
- relation to thermal conductivity 350
- Electrical properties of coatings 292, 350–7, 484–502
- conductors 484–92
- dielectrics 493–500
- electric field emitters 500–1
- resistors 492–3
- superconductors 501–2
- Electrical resistivity
- meaning of term 351n19
  - measurement of 351
  - variation with temperature 351
- Electrochemical cell 362
- Electrochemical methods, porosity determination using 344
- Electrolytic cladding of powders 24–5
- Electromagnetic heating (post-spray treatment) 116–49
- electron beam treatment 148–9
  - laser treatment 119–47
  - microwave sintering 118, 119
  - spark plasma sintering 116–17
- Electromagnetical methods, quality determination using 365
- Electron beam treatment 148–9
- drawbacks 148
  - process parameter 148
  - properties affected by 149, 487
  - types of coatings treated by 148–9
- Electron emission 357
- measurement of 358
- Electron emitting coatings 500–1
- Electron energy-loss spectroscopy (EELS) 295, 314
- applications 316
- Electron microprobe analysis (EMPA) 39, 129, 293, 294, 295, 297
- Electron spectroscopy for chemical analysis (ESCA), *see* X-ray photoelectron spectroscopy (XPS)
- Electronic conductors 485
- resistivities listed 486
- Electronic thermal conduction 342
- Electronics industry, applications 563–7
- Elemental distribution
- powders 39
  - sprayed coatings 297, 298
- Elongation, alloy coatings, variation with temperature 430
- Emissivity 453
- ceramic coatings 479, 481, 482–3
  - measurement of 348, 369
- Energy balance equation 226
- Energy-dispersive spectroscopy (EDS) 293, 294, 295, 297
- applications 297, 505
- Energy generation industry, applications 567–72
- Energy, conservation of 170
- Epitaxy 247
- Equivalent circuit, AC impedance of sprayed rutile 489

- Erosive wear 338–9  
mechanisms as function of impact angle 445, 446
- Erosive wear resistance  
ceramics and composites 446–8  
factors affecting 444  
hardness of abradant 446  
hardness of coatings 446  
microstructure 446  
porosity 446  
guide to selecting materials 445, 446  
metals and alloys 448
- Excimer laser 126
- Extended X-ray absorption fine structure (EXAFS) technique 315
- Factorial design (of experiments) 285
- Fatigue wear 339, 446
- Feeding of powders 42, 43–4
- Ferrites 502–3
- Ferroelectrics* 353, 495
- Ferromagnetics* 357
- Fibre-reinforced composites 283, 431  
mechanical properties 431, 433
- Fine-pattern anilox rolls* 146
- Finishing processes 154–9  
grinding 158  
lapping 159  
polishing 159
- Flame sprayed coatings  
applications 547, 552, 559, 560, 561, 569, 570, 583  
aqueous corrosion resistance 509, 516  
electrical properties 494  
hardness 401  
magnetic properties 503  
mechanical properties 423  
physical properties 74  
thermal expansion 477
- Flame sprayed coatings, tensile adhesion strength 74, 412, 413
- Flame spraying (FS) 68, 69–74  
history 69–70  
modelling of flame 177  
morphology of lamellae 233  
process parameters 71–4  
flame characteristics 71–2  
powder injection 73  
powder properties 72  
principal parameters 73–4
- rod properties 73  
wire properties 73
- using powder 70, 71, 413
- using rods 2, 70–1, 72
- using wires 1, 2, 70–1, 72  
*see also* Wire flame spraying (FS-wire)
- Flames  
meaning of term 168n1  
*see also* Jets and flames
- Flexographic printing machines 143, 585  
*see also* Anilox rolls
- Flower morphology (of lamella/splat) 228, 231, 232, 234, 239–40
- Fluorescence 302  
*see also* X-ray fluorescence (XRF) spectroscopy
- ‘Flyingash’, erosion by 448
- Foam content, spray-drying slurry 14
- Food industry, applications 551, 575
- ‘Forbidden band/gap/zone’ 351, 558
- Forsterite coatings, thermal expansion coefficient 475
- Fountain atomizer 12, 15, 17
- Four-point bending test  
adhesion determination 322  
elasticity determination 327, 328
- Fourier equation 199, 203
- Fracture mechanics  
adhesion tests based on 318, 322–3  
properties related to 332–4
- Fracture mechanism  
oxide coatings 421  
in wear mechanisms 337
- Fracture strength, brittle materials 325, 326
- Fracture toughness 332  
carbide coatings 416  
determination of 333–4, 421  
metal coatings 423–5, 426  
oxide coatings 418–20, 421
- Free fall of sprayed particles 232–3
- Free-standing alumina ‘cylinders’, Thermal shock resistance (TSR) 481
- Free-standing bodies/samples  
elasticity determination 328–30  
manufacture of 150, 328, 554–5
- Fretting wear 339
- Fretting wear resistance 449

- Friction coefficient 334  
 determination of 335–6
- Frictional wear 336
- Froud number* 44
- Fuel cell solid electrolytes 117, 157,  
 484, 486, 568–9
- Furnace treatment (post-spray  
 treatment) 149–50, 151  
 metal and alloy coatings 150, 151  
 oxide coatings 149–50, 151
- Fusion/sintering, powders  
 manufactured by 4, 8–11
- Galvanic cells 360
- Galvanic corrosion 363
- Galvanizing section (in steel sheet  
 production) 574
- Gas-atomized powders 7, 8, 266
- Gas flow, differential equations  
 169–75
- Gas-phase cladding of powders 25–6  
 by chemical vapour deposition  
 25–6  
 by physical vapour deposition 26
- Gas-phase methods  
 post-spray treatment by lasers  
 143–7  
 powders manufactured by 34
- Gas turbine components 549,  
 571, 588  
*see also* Aero-engines
- Gas-well tubing 560
- Generalized conservation principle  
 170
- Gerdien-type plasma generator* 74
- Glass artware, decorative coatings  
 505, 563
- Gloss calender rolls (in papermaking)  
 582
- Grain size analysis 35–8  
 conversion of equivalent  
 diameters 38  
 mean diameters used 37
- Grey-body* 208–9
- Griffith equation 332
- Grinding  
 as post-spray treatment 158  
 specimen preparation for  
 microscopy 309, 310  
 porous coatings 308–9
- Grit blasting 53, 56–63  
 effect of blasting angles 60–1
- factors affecting choice of grit  
 size 59
- mechanical stresses caused by 255
- process parameters 57
- surface contamination caused by  
 62–3
- surface roughness and 59–62
- Hank's balanced salt solution (HBSS)  
 513, 514
- interactions with ceramic coatings  
 513, 515
- 'Hard' magnets 358, 359  
 examples 504
- Hard-phase dispersion* (in coating)  
 120, 129
- Hardness  
 determination of 324–5  
 for various coatings 389–403  
 alloys 401–2, 403  
 carbides 389–92  
 metals 400–1  
 oxides 392, 394–400
- Hastelloycoatings 512, 560
- Heat conduction equation  
 Fourier equation 199, 236  
 thermal fluxes as boundary  
 conditions 255  
 one-dimensional 346
- Heat insulation coatings 104
- Heat transfer  
 by conduction 194  
 by convection 193  
 by radiation 194  
 from jets/flames to sprayed particles  
 192–210  
 particles with one temperature  
 197–9  
 particles with temperature  
 gradient 199–203
- Heat treatment 115–53  
 combustion flame re-melting 152  
 electromagnetic heating 116–49  
 furnace treatment 149–50, 151  
 hot isostatic pressing 150,  
 152, 153
- Helicopter flight deck, non-skid  
 coatings 588
- Hertz-Knudsen equation* 211
- High body drying chamber (in spray  
 drying process) 15

- High-energy/high-power plasma spraying 69, 106  
chromium oxide coatings 106, 395
- High-temperature behaviour, powders 41–2
- High-temperature corrosion-resistant coatings 89, 359, 518–21  
applications, aero-engines 518, 546, 547, 549
- High-temperature densification, spray-dried powders 18–20
- High-temperature superconductors, properties 501–2
- High-velocity air fuel (HVAF) spraying 68
- High-velocity oxy-fuel (HVOF) spraying 68, 85–9  
combined with arc spraying 81  
history 85  
modelling of flame 177  
modelling of particles' temperatures and velocities 207  
particle velocity measurements 192, 193  
principles 85–6  
process parameters 86–8, 386  
flame 86–8  
powder characteristics 88  
powder injection 88  
principal parameters 88  
compared with D-gun<sup>TM</sup> process 85
- High-velocity oxy-fuel sprayed coatings  
applications  
aeronautical industry 547, 549, 550  
automobile industry 552, 553  
chemical industry 560  
energy generation industry 569, 571, 572  
iron and steel industry 573  
printing and packaging industries 587  
shipbuilding and naval industries 588  
aqueous corrosion resistance 509, 510, 510, 511–12, 517  
electrical properties 494  
friction and wear properties 436, 441, 442, 443, 444, 447, 450, 451, 452
- hardness 390, 391, 392, 393, 395, 396
- hot-corrosion resistance 519, 520, 521
- interactions with simulated body fluids 515
- magnetic properties 504
- mechanical properties 415, 416, 425
- physical properties 89
- post-spray treatment of 132, 149
- tensile adhesion strength 89, 406
- High-velocity spray techniques transformation of kinetic energy into heat on impact 185
- see also* Cold-gas spraying method (CGSM); Detonation-gun spraying (D-gun<sup>TM</sup> process); High-velocity oxy-fuel (HVOF) spraying
- Hole-drilling method* (for determination of residual stresses) 259–60, 340
- Homogenous oven spherical powders* (HOSPs) 18
- Hot-corrosion resistance, determination of 364
- Hot-extrusion dies 577–8
- Hot-gas/hot-medium corrosion 363–4, 507
- Hot-isostatic pressing (HIP) 150, 152, 153  
of alloy coatings 152, 153  
of ceramic and cermet coatings 152, 153
- Hot-wire method, thermal conductivity determination by 346
- Hybrid electronics, conductor paths for 566
- Hybrid microelectronics, substrates for 565–6
- Hydraulic props* (in coal mines) 577
- Hydroerosion 446
- Hydrogen-pressure-reducing powder-coating* (HYPREPOC) process 22, 23
- Hydropower plant 572
- Hydroxyapatite (HA) coatings biomedical applications 129, 130, 576–7

- Hydroxyapatite (HA) coatings  
*(Continued)*  
 hardness 399–400  
 interactions with simulated body fluids 514, 515, 516  
 lamellae/splats 225, 231  
 mechanical properties 419  
 phase composition 129–30, 272–5, 301, 388  
 plasma spraying of 77n7  
 porous coating 280, 281  
 post-spray treatment of 117, 129–30, 131, 132, 136  
 simulation of coating growth 251, 252  
 XRD diagrams 142
- Hydroxyapatite (HA) powder 20, 36  
 agglomeration of 36, 37, 194, 196  
 analysis of water content 299  
 modelling of particles' temperatures and velocities 207  
 particle size distribution 37  
 physical data for porous powder 203, 204  
 temperature field inside HA particle at flight 203  
 velocity plots 182
- Hydroxyapatite (HA),  
 high-temperature decomposition of 129, 272–3
- Image analysis 36, 269, 311  
 porosity determination using 311–12, 344
- Impact of particles 222–49  
 adhesion mechanisms 222, 246–9  
 deformation of particles 222, 223–35  
 different situations described 240, 242  
 solidification, nucleation and crystal growth 241–5  
 temperature at impact 222, 236–41
- Impact wear 339
- Impact wear resistance 452
- Impedance spectroscopy 356–7
- Impregnation (to seal porosities) 154–8  
 by inorganic sealants 154–7  
   aluminium phosphate 155–6  
   chemical treatment 157  
   chromium diffusion 156–7
- molten metals 156  
 sol-gel method 155  
 by organic sealants 157–8
- Impulse drying (in papermaking industry) 582
- Indentation tests  
 adhesion determination 322–3  
 fracture toughness determination 334  
 hardness determination 324–5  
 loading–unloading curves 327  
*see also* Micro-indentation test, elasticity determination by
- Indium tin oxide (ITO) coating 505  
 microstructure 506  
 optical properties 506
- Inductively coupled plasma emission spectroscopy (ICPES) 38
- Inert coating 361
- Inert plasma sprayed coatings  
 applications 580  
 electrical properties 485
- Inert Plasma Spraying (IPS) 68, 93, 95  
 heat transfer in 198–9  
 splat adhesion affected by 247  
*see also* Argon-atmosphere plasma sprayed coatings
- Infrared spectroscopy (IRS) 293, 294, 295, 298–9  
 applications 299
- Infrared thermography 368–9
- Inhibitive coating 361
- Inhomogeneity of coatings 278–80, 345
- Injection of powders 44–7  
 in D-gun™ process 84  
 in flame spraying 73  
 in HVOF process 88  
 in plasma spraying 78, 92  
 trajectory in jets/flames 184–5
- Intentionally porous coatings 280, 281, 399  
 bond strength determination 323–4
- Interface echo (in ultrasonic testing) 366
- Interfacial indentation test, adhesion determination using 322–3
- Interference-layer technique (in optical microscopy) 311
- Intergranular corrosion 363
- Interlamellar fracture mechanism 421

- Intermediate coatings 430–1  
Intermetallic compounds/phases  
  between sprayed particles and  
  substrate 248–9  
  coatings 427  
  powders, manufacture of 7  
Intralamellar fracture mechanism  
  421  
*Ionic bonds* 3  
Ionic conductors 486  
Iron and steel industries, applications  
  572–5  
Iron-based alloy coatings,  
  abrasive-wear resistance 444  
Iron–boron alloys, magnetic properties  
  503  
Iron–niobium alloys, magnetic  
  properties 504  
Iron–silicon alloys, magnetic properties  
  504  
Isopleths (response surfaces) 388
- Jets and flames  
  experimental determination of  
    properties 176, 178–80  
  gas flow properties 169–75  
  heat transfer to sprayed particles  
    192–214  
  mathematical modelling methods  
    175–6, 177  
  meaning of terms 168n1  
  momentum transfer to sprayed  
    particles 180–92  
  temperature measurement 178–9  
  temperature profiles 176  
  velocity measurement 179–80  
  velocity profiles 176
- JK powders 20  
*Joule heating* 116–17  
  dielectrics affected by 355
- Kaleidoscope* (in laser  
  treatment) 122  
*Kanthal M<sup>TM</sup>* coatings 583  
Kerosene, in HVOF process 86  
Knoop hardness test 324, 325  
*Knudsen effect* 183, 191, 194  
*Kokubo solution* 513, 514  
  interactions with ceramic coatings  
    513, 515, 516  
*Kopp–Neumann law* 453  
  verification of 471, 473  
Kovar alloy 138, 565, 566
- Lagrangian approach* 181  
Lamellae  
  factors affecting shape 228, 230–1  
  flower shape 228, 231, 232, 234  
  morphologies 232  
  *pancake shape* 228, 230–1,  
    232, 234  
  thermal fluxes during cooling 253  
  thicknesses 234–5  
Lamellar microstructure 27, 223  
Lapping 159  
Laser ablation  
  post-spray treatment by 124  
  surface activation by 63–4  
Laser (post-spray) treatment 119–47  
  gas phase 143–7  
  liquid phase 134–43  
  process parameters 127  
  solid phase 129–34  
  technology 120–6  
  two-step laser deposition (2SLD)  
    process 128
- Laser acoustic method, elasticity  
  determination by 330–1
- Laser Doppler Velocimeter (LDV)  
  technique  
    flame/jet velocity measurement 179  
    particle velocity measurement  
      188–9
- Laser engraving 143–7, 586  
  alternative coatings 146–7  
  drop and pitch of engraved lines  
    145  
  mathematical modelling 147  
  principal parameters 145
- Laser-flash (LF) method, thermal  
  diffusivity determination by  
    346–7
- Laser glazing 134
- Laser induced fluorescence* 179
- Laser re-melting 134
- Laser shock processing (LSP) 124–6  
  carbide-reinforced composite treated  
    by 132–4  
  confined treatment method 124–5  
  direct ablation method 124
- Laser ‘sizers’ 35, 36, 37
- Laser technology 120–6  
  comparison of various lasers 126  
  optical absorption depth 123  
  listed for various metals and  
    oxides 123

- Laser technology (*Continued*)  
 power density 121–2  
   listed for various types of treatment 122  
 reflectivity 123  
 temperature distribution 123–4, 125
- Laser Two Focus (L2F) method, velocity measurement 179, 189
- Laser velocimetry techniques 179, 188–9
- ‘Laser-shock’ adhesion test 324
- Lattice thermal conduction 342
- Laval (convergent–divergent) nozzle 87, 98, 106
- Layer (in coating build-up), meaning of term 221n1
- Lead-zirconate titanate (PZT) coatings, dielectric properties 495, 497
- Linear elastic fracture mechanics 332
- Linear velocity 250  
   for cylinders 250–1
- Linear wear 336
- Liquid copper, protective coatings against 578
- Liquid metals, corrosion by 521
- Liquid-phase cladding of powders 22–5  
   by chemical precipitation 22–3, 24  
   by electrolytic cladding 24–5  
   by painting 25
- Liquid-phase methods  
   post-spray treatment by lasers 134–43  
   powders manufactured by 32–3
- Liquid plasma spraying 101, 103–4
- Liquid zirconium, protective coatings against 578–9
- Load effect 184, 194, 195
- Local thermodynamical equilibrium* (LTE) 172
- Long-fibre-reinforced composites 431
- Longitudinal thermal expansion  
   ceramic coatings 475–6  
   metals and alloys 477
- Loss factor (in dielectrics) 353  
   alumina and alumina–chromia coatings 494  
   titanate coatings 495, 496–7
- Low-Pressure Plasma Spraying (LPPS) 68, 89  
   splat adhesion affected by 247
- see also* Vacuum plasma spraying (VPS)
- Low-temperature plasma* 26
- Madejski splat formation model/theory 226–8
- Madejski, Professor Jan 226
- Magnesia-stabilized zirconia coatings composite with NiAl, mechanical properties 431, 432, 433  
   fracture mechanism in 421  
   thermal conductivity 460
- Magnesium–manganese ferrite coatings 566, 567
- Magnetic-fusion energy device components 579–80
- Magnetic properties of coatings 292, 357–9, 502–4
- Magnetite* ( $\text{Fe}_3\text{O}_4$ ) 553  
   *see also* NiO– $\text{Fe}_3\text{O}_4$  coatings
- Magnetohydrodynamic (MHD) generators 572
- Marine engine* valve stems 588
- Marine gas-turbine engines 588
- Marine turbine shaft coatings, testing of 370
- Market for thermal spraying  
   industrial sectors 544  
   regional share(s) 543
- Masking of substrates 64–5
- Mass spectrometry* 180
- Mass, conservation of 169
- Materials, spraying 1–51
- Maxwell equation* 203
- McPherson thermal conductivity model 345
- McPherson, Professor Reginald 318
- Mechanical alloying 4, 26–8  
   *see also* Mechanofusion (MF)
- Mechanical anchorage (of coating to substrate) 246, 405
- Mechanical properties 291, 317–40  
   bulk carbides 415  
   bulk metals 422  
   bulk oxides 417  
   parameters affecting  
    coating microstructure 415  
    particle properties 415  
    spray process 415  
   tests (listed) 318
- for various coatings 415–34  
   alloys 426–30  
   carbides 415–17

- composites 430–4  
metals 422–6  
oxides 417–22  
*see also* Elastic modulus; Elastic strength; Fracture toughness; Tensile adhesion strength
- Mechanical-sieve analysis, powder grain size determined by 35
- Mechanofusion (MF)  
factors affecting morphology 28  
parameters for new powders 28  
powders manufactured using 4, 26–8
- Median diameter 37
- Medical applications 575–7  
*see also* Biomedical coatings
- Menstruum process* 10
- Mercury intrusion porosimetry (MIP) 343
- Metal coatings  
abrasive-wear resistance 440  
adhesive/sliding-wear resistance 437  
aqueous-corrosion resistance 508–10  
electrical properties 485, 486  
hardness 400–1  
mechanical properties 422–6  
thermal conductivity/thermal diffusivity 461, 463, 465  
thermal expansion 477
- Metal matrix composites (MMCs), laser treatment of 141
- Metal powders, manufacture of 4, 5–8
- Metal-ceramic composites  
abrasion mechanisms 440, 443  
wear mechanism 438
- Metal-ceramic substrates*, for hybrid microelectronics 565
- Metallic bonds 3
- Metallurgical interactions, adhesion affected by 248–9
- Metals, resistivities (listed) 486
- MHD generators 572
- Micro-indentation test, elasticity determination by 326–7
- Microhardness  
critical load 397  
determination of 325  
effect of heat treatment on coatings 399, 400
- for various coatings 389–403  
alloys 401–2, 403  
carbides 389–92  
metals 400–1  
oxides 392, 394–400
- Microplasma spray torches 100, 104
- Micropores 342
- Microstructural investigational techniques 294, 295, 296, 307–15
- Microstructure of coatings 264–80  
defects 280  
meaning of term 293  
methods of characterization 291, 292–317
- Microwave circulators 566, 567
- Microwave integrated circuits 566–7
- Microwave sintering 118, 119
- Mild wear 336–7
- Mining industry, applications 577
- Mixed airflow dryers* 17
- Mobility of electric charges 353
- Modelling  
jets and flames 175–6, 177, 206, 207  
particle temperatures and velocities 206, 207  
spray parameters 394
- Modulated-beam (MB) method, thermal diffusivity determination by 347
- Molten ash, corrosion by 521
- Molybdenum coatings  
abrasive wear resistance 440  
applications 552, 579, 581  
friction characteristics 437, 438  
hardness 400  
mechanical properties 423, 426  
thermal conductivity 463  
thermal expansion 477
- Molybdenum, mechanical properties of bulk metal 422
- Molybdenum–molybdenum carbide composite coatings  
abrasive wear resistance 441  
friction and wear properties 438
- Momentum  
conservation of 169–70  
transfer from jets/flames to sprayed particles 180–92
- Monte Carlo* method, coating microstructure predicted using 251

- Morphology  
powders 39–41  
effect of various manufacturing methods 40–1
- Mössbauer spectroscopy 315, 503
- Most frequent diameter 37
- Mullite* 399, 557
- Multi-coatings, applications 563, 564, 579, 581
- Multilayer composites 507, 516  
aqueous corrosion resistance 516  
*see also* Duplex thermal barrier coatings
- Nanocomposites* 2
- Nanostructure, meaning of term 4n5, 293n1, 391n4
- Nanostructured coatings 4, 12  
spraying of 69, 104
- Naval engines and flight-deck components 588
- Navier–Stokes equation* 169
- Neural network method 384–5
- Neutron diffraction 293, 294
- New Anilox Technology* 146
- Nickel  
electrical properties of bulk metal 486  
mechanical properties of bulk metal 422  
specific heat, variation with temperature 472
- Nickel alloy powders 8
- Nickel-based alloys  
applications 581  
fretting-wear resistance 449  
hot-corrosion resistance 521
- Nickel-coated aluminium powder 21, 24, 248, 266
- Nickel coatings  
electrical properties 486  
hardness 401  
mechanical properties 422, 423  
tensile adhesion strength 409, 410, 411
- Nickel-aluminium alloy coatings  
hardness 402, 403  
phase compositions 267, 466  
specific heats 472, 473  
tensile adhesion strength 74, 412, 413–14
- thermal conductivity 465
- thermal expansion 477
- Nickel–aluminium powders 25, 28  
exothermic reactions 21, 248  
manufacturing methods 21, 25, 266
- Nickel-chromium coatings  
applications, aerospace industries 550  
friction and wear properties 438  
hardness 402, 403  
hot-corrosion behaviour 519  
IR thermography 369  
tensile adhesion strength 414  
thermal conductivity 467
- Niobium coatings, aqueous-corrosion resistance 508, 509
- $\text{NiO}-\text{Fe}_3\text{O}_4$  coatings  
electrical properties 492  
emissivity 483
- Nomarski interference contrast (NIC) technique 311
- Non-destructive methods, elastic modulus determination 326, 330–1
- Non-destructive testing (NDT)  
techniques 364–70  
acoustical methods 365–8  
thermal methods 365, 368–70
- Noncontinuum effect* 183, 195
- Nonferrous industry, applications 577–9
- Normal emissivity 348
- Nuclear industry, applications 579–80
- Nucleation of crystals (in coating)  
241–2  
factors affecting 242–4
- Nusselt number 194
- ‘Off-normal’ spraying 230
- One-colour pyrometry 208
- One-torch-pass thermal stresses 258
- Open porosity 342  
corrosion resistance affected by 508  
measurement of 343
- Optical methods  
particles’ temperature measurement 208–10  
particles’ velocity measurement 189–90  
quality determination using 365
- Optical microscopy (OM) 293, 294, 295, 307–12

- applications/images  
  coatings 131, 137, 143, 269,  
    278, 307, 310, 480  
  powders 16, 19, 33, 36, 39, 196
- differential interference contrast  
(DIC) technique 311
- interference-layer technique 311
- Nomarski interference contrast  
(NIC) technique 311
- specimen preparation 307–9, 310
- Optical properties 504–7
- Optically functional coatings 505–7  
  spray-dried powders 17, 20, 505,  
    506
- Optimization of spray parameters  
  434, 478–9, 510, 583
- Oscillating wear 339
- Oscillating wear resistance, effect of  
laser (post-spray) treatment 134
- Oseen's regime 182
- Overcooling effect (in solidification)  
  270
- Overflow effect (in laser engraving)  
  147, 587
- Oxidation  
  of lamellae/splats 230  
  of powders during spraying 213–14
- Oxidation potentials, listed for  
  various, metals 360
- Oxide alloy powders 4, 11
- Oxide ceramic coatings  
  abrasive wear resistance 438–9  
  dielectric properties 493–5, 499  
  electrical properties 487, 490, 491,  
    494, 500–1  
  emissivity 479, 481, 482–3  
  friction and wear properties 434,  
    435, 436, 437, 446–8, 449  
  hardness 392, 395–400  
  mechanical properties 417–22  
  metallographical preparation (for  
    microscopy) 310  
  post-spray treatment of 138–41,  
    149–50, 151, 152, 153  
  tensile adhesion strength 405,  
    407–8, 409  
  thermal properties 454–61, 475–6
- Oxide ceramics, molten, crucibles for  
  557
- Oxide powders  
  manufacture of 4, 4, 8–20  
  reduction during spraying 211
- Ozonizer tubes 561–2
- Painting (porous-cladding) process  
  25
- Pancake morphology (of lamella/splat)  
  228, 230–1, 232, 234, 239
- Paper pulp industry, boiler tubing  
  582–3
- Papermaking industry  
  applications 580–3  
  dryers 581–2  
  gloss calender rolls 582
- Parabolic oxidation behaviour 363,  
  364, 518
- Particle deformation 223–35
- Particle evaporation, Knight model  
  200
- Particle impact 222–49
- Particle size of powders  
  in cold-gas spraying 96  
  in D-gun™ process 84  
  in flame spraying 72  
  in HVOF process 88  
  measurement of 35–8  
  in plasma spraying 77, 92
- Particle temperature measurement  
  208–10  
  one-colour pyrometry 208  
  two-colour pyrometry 208–10,  
    238
- Particle velocity measurement  
  examples 190–2  
  experimental methods 186–90  
    laser methods 188–9  
    mechanical methods 186–8  
    optical methods 189–90
- Particulate composite coatings  
  aqueous corrosion resistance 507,  
    516–18  
  friction and wear properties 438,  
    440  
  mechanical properties 431, 432,  
    433  
  thermal conductivity 467,  
    469
- Particulate-reinforced composites  
  283  
  microscopic effects upon two-body  
    abrasion 440
- Passive zone in electrochemical cell  
  361, 362
- Peel adhesion test 324
- Permeability of magnets 359  
  typical values for soft magnets 503

- Perovskites* 569  
 Petroleum exploration tools 559–60  
 Phase analysis  
   heat-treated coatings 141, 142,  
   144, 304, 314  
   powders 39, 41, 42  
 Phase composition  
   coatings 268–77  
   factors affecting 265, 267–8  
   particle in plasma/flame 200  
 Phase diagrams  
   CaO-P<sub>2</sub>O<sub>5</sub> 273  
   limited usefulness 264–5  
   W-C 277  
   YO<sub>1.5</sub>-BaO-CuO 276  
   yttria-stabilized zirconia 272  
 Phase transformation stress 262–4  
 Phonon-conduction mechanisms  
   454–5, 458  
 Phonons 350  
 Photoacoustical methods, quality  
   determination using 365  
 Photocatalysts 557–9  
 Photoelectric cell, in IR spectrometer  
   299  
 Photographic streak technique (for  
   velocity measurements) 179–80,  
   186  
 Photolithography 65, 492  
 Photon conduction 342  
 Photoresist 65  
 Physical interactions, adhesion affected  
   by 248  
 Physical vapour deposition (PVD)  
   cladding of powders by 26  
   compared with thermal spraying  
   563, 588  
 Pin-on-disc abrasion/wear test 338  
   results 435, 436, 439  
 Pipelines, polymeric coatings 560–1  
 Pit-props (in coal mines) 577  
*Pitot tube* 179  
 Pitting corrosion 363  
 Pitting potential 361  
 Plasma-enhanced chemical vapour  
   deposition (PECVD) 2  
   cladding of powders by 25–6  
 Plasma generator 74, 75  
*Plasma spheroidization* method 30  
 Plasma spraying 68, 74–9, 93–6  
   high-energy/high-power 69, 106  
   particle residence times 168  
   periodic variations in jet 168–9  
   pulsed 107  
   underwater 68–9, 106–7  
   water-stabilized 69, 75, 76, 77,  
   105  
   *see also* Atmospheric plasma  
   spraying (APS);  
   Controlled-atmosphere plasma  
   spraying (CAPS); Vacuum  
   plasma spraying (VPS)  
 Plasma torches 76  
   electric power 77  
   electrode geometry 77  
   gas composition 75  
   temperature and velocity of plasma  
   76–7  
 Plasmas  
   thermal conductivity 174–5  
   variation with temperature 175  
*Plasticizers* (in slurry for spray drying)  
   14  
 Plumes, temperature measurement in  
   178  
 Poisson modulus/ratio, determination  
   of 330–1  
 Polarization test 361, 362  
 Polishing  
   as post-spray treatment 159  
   specimen preparation for  
     microscopy 309, 310  
 Polyethylene coatings 561  
 Polyethylene, corona-discharge  
   treatment of 583  
 Polymer spraying 72, 561  
 Polymer surface treatment, by laser  
   126  
 Polymeric coatings 72, 560–1  
 Pore sizes in coatings 279, 341, 342  
 Porosity 341, 342  
   arc-sprayed coatings 82  
   CGSM coatings 100  
   D-gun™ coatings 84  
   flame-sprayed coatings 74  
   HVOF-sprayed coatings 89  
   statistical models 387  
   measurement of 311–12, 343–4  
   plasma-sprayed coatings 79,  
    93, 96, 416, 418–20, 423–4,  
    456  
   yttria-stabilized zirconia coatings  
    456  
 Porous cladding 25, 266  
 Porous coatings, intentional 280,  
   281

- Post-spray treatment 115–65  
arc-sprayed coatings 81  
by inorganic sealants 154–7  
by organic sealants 157–8, 508,  
513, 584  
cracks induced by 262  
finishing processes 158–9  
grinding 158  
lapping 159  
polishing 159  
flame-sprayed coatings 74  
heat treatment 115–53  
combustion flame re-melting  
152  
electromagnetic treatment  
116–49  
electron beam treatment 148–9,  
508  
furnace treatment 149–50, 151  
hot isostatic pressing 150, 152,  
153  
laser treatment 119–47  
microwave sintering 118, 119  
spark plasma sintering 116–17  
impregnation (to seal porosities)  
154–8  
phase formation affected by 265  
plasma-sprayed coatings 78–9, 117  
Postcritical flow regime 224–5  
Powder feed rate 78  
Powder feeders 42, 43–4  
Powder flame spraying (FS-powder)  
70, 71  
Powder 32, 33, 275  
synthesis 32  
Powders  
in atmospheric plasma spraying 77  
characterization methods 35–42  
apparent density measurement  
42  
chemical analysis 38–9  
element distribution 39  
flowability measurement 42  
grain size analysis 35–8  
high-temperature behaviour  
41–2  
morphology determination  
39–41  
particle-size measurement 35–8  
phase analysis 39  
chemical properties 3  
in cold-gas spraying 96–7  
in D-gun<sup>TM</sup> process 84  
feeding of 42, 43–4  
and inhomogeneity of coatings  
278  
in flame spraying 72  
in HVOF process 88  
injection of 44–7  
in D-gun<sup>TM</sup> process 84  
in flame spraying 73  
in HVOF process 88  
in plasma spraying 78, 92  
manufacturing methods 4–34  
atomization 4, 5–8, 266  
cladding 4, 20–6, 266  
effect on morphology 40–1  
fusion/sintering 4, 8–11  
gas-phase method 34  
liquid-phase method 32–3  
mechanofusion 4, 26–8  
self-propagating high-temperature  
synthesis (SHS) 4, 28–31  
solid-phase method 32  
spray drying 4, 5, 11–20  
particle size measurement 35–8  
physical characteristics 3  
in plasma spraying 77, 92, 95  
transport of 44  
types 3–4  
Power-generation plants, boilers 571  
Power law 171  
Prandtl number 194  
Pratt & Whitney aero-engines 548,  
549  
Praxair powders 25  
Pre-spray treatment 53–66  
mechanical stresses caused by  
255–6  
substrate shaping 55, 55–6  
surface activation 56–64  
surface cleaning 54–5  
Pressure nozzle atomizer 12, 15, 17  
Printing and packaging industries  
applications 583–7  
*see also Anilox rolls; Corona rolls*  
PROTAL<sup>TM</sup> process 64  
laser treatment/plasma spraying  
technique similar to 134  
Prostheses  
bio-inert coatings 576  
bioactive coatings 576–7  
'Pseudo-alloy' coating 80  
*Pseudoplastic behaviour*, oxide  
coatings 421

- Pulsed laser process, surface activation by 64  
 Pulsed plasma spraying 107
- Quality determination 364–70  
*Quasi-crystals*, friction characteristics 437–8  
 Quenching stress 257–8, 472
- Radiation thermometry 208  
 Radiation, heat transfer by 194  
 Radiative thermal fluxes (from plasma jets) 253, 254  
 Raman effect 299–300  
 Raman spectroscopy (RS) 293, 294, 295, 299–302  
     applications 269, 300–1  
 Rapid prototyping 120  
*Recalcescence effect* 239, 243  
 Reduction of powders during spraying 211  
 Regression equation(s) 386  
     listed for various coatings' properties 387  
 Reinforcement in composite coatings 282–3  
 Residual stresses, determination of 259–60, 339–40  
 Resistivities  
     electronic conductors 486  
     temperature dependence, semiconductors 491  
 Resistors, electrical properties 492–3  
 Response surfaces (in statistical modelling) 388–9  
 Reynolds number 182  
 RF plasma spraying 68, 105–6  
 Rocket thrust chamber liners 550–1  
 Rockwell hardness test 325  
     metal and alloy coatings 400, 401  
 Rod flame spraying 2, 70–1, 72  
     coatings, thermal conductivity 460  
 Rokide<sup>TM</sup> process 2  
 Roller-on-disc friction/wear test 435  
 Rolls-Royce aero-engine 548, 549  
 RotaPlasma<sup>TM</sup> technique 100, 104  
     applications 552, 553, 569  
 Rotary atomizer 12, 15  
 Rotating mirror method, particle velocity measurement using 186–7
- Rotating-substrate method, particle velocity measurement using 187–8  
 Roughening of substrate surfaces 53, 56–63  
 Roughness of substrate, splat flattening affected by 229  
 Roughness parameters 58  
 Rutile (TiO<sub>2</sub>) 245, 268, 269, 271, 489, 558
- Sacrificial coating 361  
 Salt-water corrosion, *see Aqueous corrosion*  
 Samarium–cobalt magnets 504  
*Sample-integrity stage*, in metallographical preparation 309  
 Sampling of powders 35  
*Sauter mean diameter* 37  
 Scandia-stabilized zirconia coatings  
     applications 569, 570  
     electrical conductivity 487  
 Scanning electron microscopy (SEM) 293, 294, 296, 312–14  
     back-scattered electrons (BSE)  
         emission 313  
         images 138, 140, 147, 312, 313–14, 506  
     powder grain size determined by 36  
     powder morphology studied by 16, 19, 39  
 secondary electrons (SE) emission 313  
     images 7, 9, 11, 16, 19, 36, 133, 144, 225, 231, 249, 264, 276, 281, 312, 313, 341, 498  
     shadow effect in 312, 313  
     specimen preparation for 313  
 Scanning tunnelling microscopy (STM) 293, 294, 296  
 Scratch test 323–4  
 Scuffing wear 337  
 Scuffing wear resistance, factors affecting 337  
*Secondary-ion mass spectrometry (SIMS)* technique 315  
*Seebeck coefficient* 487  
*Seebeck effect* 487n14, 569  
 Segments, laser-treated thermally sprayed coatings 139, 140, 140

- Selected-area diffraction (SAD) 293, 294, 295, 304–5, 314  
applications 305, 316
- Selective evaporation phenomena 211
- Self-bonding coatings* 2  
thermal conductivity 465
- Self-fluxing alloy powders 3, 7
- Self-fluxing alloy wires 73
- Self-fluxing alloys  
adhesive wear resistance 438  
applications 560, 571, 577  
flame spraying of 73  
impact-wear resistance 452  
post-spray treatment of 74, 116, 134, 135, 137–8, 152  
in top coatings 401
- Self-fluxing coatings 73, 74
- Self-lubricating coatings 437
- Self-propagating high-temperature synthesis (SHS) 4, 28–31  
compounds suitable for 29–30
- Semiconductors 486–7, 489–92
- Severe wear 337
- Shear test, adhesion determination using 324
- Sheet resistance 352
- Shipbuilding and naval industries, applications 588
- 'Shot peening with laser, *see* Laser shock processing (LSP)
- Shrouded plasma sprayed coatings  
aqueous corrosion resistance 509  
mechanical properties 425
- Shrouded plasma spraying (SPS) 68, 93, 95, 96
- Signification test 386
- Silica sand, in grit blasting 59
- Silicate coatings, dielectric properties 495, 499
- Silicon carbide-reinforced alumina 432
- Silicon carbide-reinforced aluminium, mechanical properties 433
- Silicon carbide reinforcement, properties 434
- Silicon nitride coating 26
- Silicon nitride reinforcement, properties 434
- Silicone resin, impregnation of coatings with 158, 584
- Silicon–germanium alloys 486–7
- Sillimantin 60<sup>TM</sup> 555, 556
- Simulated body fluids (SBFs) 508, 513, 514  
interactions with ceramic coatings 513, 515, 516  
*see also* Hank's balanced salt solution (HBSS); Kokubo solution
- 'Sin<sup>2</sup>ψ' method, residual stress determination using 340
- Sintering  
porous powders 18, 203–4  
powders manufactured by 4, 8–11
- Sliding wear 336
- Sliding-wear resistance  
ceramics 434–7  
composites 438  
factors affecting 437  
metals and alloys 437–8  
*see also* Adhesive-wear-resistance
- 'Slurry abrasion' 444
- Slurry erosion 446
- Smearing effect (of porous coatings in metallographic preparation) 308–9
- 'Soft' magnets 358  
examples 502–4
- Sol-gel method  
impregnation of coating surface using 155  
powders produced using 32–3
- Solid-oxide fuel cells 117, 157, 484, 486, 567–9
- Solid-phase cladding of powders 22  
*see also* Mechanical alloying
- Solid-phase methods  
post-spray treatment by lasers 129–34  
powders manufactured by 32
- Solidification of sprayed particles 236, 241
- Solidification time  
calculations 237  
listed for various spraying techniques 237
- Sonarc<sup>TM</sup> process 81
- Spark plasma sintering 116–17
- Specific heat 347, 471–2  
measurement of 348, 453
- Spectral emissivity 348
- Spheroidization* 8
- Spinel coatings  
hardness 399  
thermal expansion coefficient 475

- 'Splashing' of particles on impact 223–4, 231, 234
- Splats 225
- analysis of formation 226–30
  - experimental observations 230–5
  - flattening parameter 226, 227
  - flower shape 228, 231, 232, 234, 239–40
  - pancake shape 228, 230–1, 232, 234, 239
  - temperature at impact 236–41
  - experimental determination 237–41
  - thermal fluxes on solidification 253
- Spray drying of powders 4, 5, 11–20
- atomization process 14–15
  - composites 282, 283
  - densification of particles 18–20
  - droplet-air contact 15–17
  - drying of sprays (evaporation of moisture) 18
  - constant-rate period* 18
  - falling-rate period* 18
  - principles 12–13
  - slurry preparation for 13–14
- Spray-forming technology* 550, 551
- Sprayed particles
- chemical modification of 210–4
  - temperature measurement of 208–10
  - velocity measurement of 186–92
  - see also* Particle temperature measurement; Particle velocity measurement
- Spraying techniques 67–113
- see also* Thermal spraying techniques
- SprayWatch<sup>TM</sup> particle temperature and velocity measurement system 190, 209
- Sputtering sources 565
- Stainless steel coatings
- applications 551, 560, 571, 581
  - aqueous corrosion resistance 512
  - electrical properties 486
  - hardness 402
  - tensile adhesion strength 411, 412
- Static friction 334
- Stationary gas turbines 549, 571–2
- Statistical design of experiments 383, 384–9
- Steel coatings, hardness 402
- Steel sheet production
- continuous annealing line 573–4
  - galvanizing section 574
- Steel wire reinforcement, properties 434
- Stefan problem* 236
- Stellite<sup>TM</sup> coatings
- applications 571
  - cavitation wear resistance 450, 451
- Stoichiometric reaction(s), in HVOF process 87
- Stokes regime 182, 197
- Strain energy release rate 332
- alloy bond coatings 427, 428
  - effective 333
  - oxide coatings 418, 420, 422
- Strain-tolerant microstructures 484
- Stress-strain curves
- brittle materials 326
  - ductile materials 326
- Subcritical flow regime* 224
- Substrate shaping 53, 55, 55–6
- Substrate surface temperature
- in flame spraying 73
  - in plasma spraying 78
- Superalloy coatings
- applications 547, 571, 588
  - in duplex thermal-barrier coatings 136, 138, 139, 140, 150, 151, 481, 518, 547, 572
  - hot-medium corrosion behaviour 519, 520
  - mechanical properties 427, 428, 429, 430, 431
- Superconductors 350
- parameters for 352
  - determination of 352
  - properties 501–2
  - see also* YBa<sub>2</sub>Cu<sub>3</sub>O<sub>x</sub> (high-temperature superconductor)
- Supersaturation effect* 392
- Supersonic flow 175
- in cold-gas spraying 96, 97
  - in HVOF flame 87
- Surface acoustic wave (SAW) methods
- elasticity determination 331
  - porosity determination 343
- Surface activation 53, 56–64
- Surface cleaning 53, 54–5
- Surface contamination, and grit blasting 62–3

- Surface echo* (in ultrasonic testing) 366  
Surface roughness, factors affecting 59–62  
*Suspending agents* (in spray-drying slurry) 14  
Suspension plasma sprayed coatings 223, 230  
  applications 559, 563  
  crystal size 245  
  nickel-zinc ferrites 503  
  titania 271, 341, 500–1, 559  
  yttria-stabilized zirconia 455, 456, 457  
Suspension plasma spraying 101, 103–4
- $\tau$ -borides 441  
Tan  $\delta$  factor 353  
  factors affecting 354  
Tantalum coatings  
  aqueous corrosion resistance 508, 509  
  electrical properties 485, 486  
Tantalum–hafnium mixtures 565  
Temperature  
  coatings at spraying 251, 253–5  
  analytical models 255  
  experimental determination 255, 256  
  measurement of  
    coatings on deposition 255, 256  
    jets and flames 178–9  
    sprayed particles 208–10  
Temperature coefficient of resistivity (TCR)  
  ionic conductors 485  
  resistors 492  
Temperature profiles  
  chromia particles 205–6  
  hydroxyapatite particle at flight 203  
Tensile adhesion  
  parameters affecting 403–4  
  materials used to spray 403–4  
  spray parameter 404  
  substrate properties 404  
Tensile adhesion strength  
  alloys 412, 413–14  
  carbides 405, 406  
  metals 409–12  
  oxides 405, 407–8, 409
- Tensile adhesion test (TAT) 317, 318, 319–22, 403  
adhesive rupture in 321, 403  
cohesive rupture in 321, 322, 403, 404, 405  
limitations 321, 324  
specimen requirements 319, 321
- Tensile strength, meaning of term 319
- Textile machine parts 574–5
- Texture, in coatings 244
- Thermal-barrier coatings (TBCs)  
  applications  
    aero-engines 546, 547, 548  
    turbines 520, 547  
  duplex configuration 469, 518, 520  
  factors affecting degradation 518, 520  
  post-spray treatment of 138–41, 150, 151, 399  
  removal from surface 54  
  spraying of 93, 104  
  *see also* Duplex thermal barrier coatings
- Thermal coefficient of resistance (TCR) 351  
  conductors 485  
  resistors 492
- Thermal conduction  
  factors affecting 345  
  mechanisms 342
- Thermal conductivity 453  
  coatings  
    composites 467, 469  
    factors affecting 345  
    McPherson model 345  
    measurement of 346, 369, 453  
    metals and alloys 461, 463–7  
    oxides 454–61  
    steady-state methods of  
      determination 346  
    time-dependent methods of  
      determination 346  
  jets/flames 174–5, 194  
  relation to electrical conductivity 350
- Thermal contact resistance 229, 241  
  determination of 347, 453  
  duplex coatings 469, 471  
  solidification affected by 243
- Thermal CVD process, cladded powders manufactured by 26

- Thermal diffusivity 453  
 determination of 346–7  
   by laser-flash (LF) method 346–7  
   by modulated-beam (MB) method 347  
 plasma-sprayed coatings 463, 465
- Thermal expansion coefficients (TECs)  
 ceramic coatings 475–6  
 composite coatings 478, 479  
 definition 348  
 metal substrates 474  
 metals and alloys coatings 477
- Thermal expansion 472, 474–7  
 anisotropy 345, 453  
 ceramic coatings 474–7  
 composite coatings 478–9  
 factors affecting 345  
 metal/alloy coatings 477–8  
 mismatch between coating and substrate  
 stresses caused by 258, 260–2, 340, 477  
 thermal shock resistance affected by 484
- Thermal fluxes, in various spraying techniques 253, 254
- Thermal shock resistance (TSR)  
 348–50, 453  
 ceramic coatings 480–1, 484  
 determination of 349–50  
 factors affecting 348, 480, 481, 484
- Thermal spraying techniques 67–113  
 arc spraying (AS) 1, 2, 68, 79–82  
 atmospheric plasma spraying (APS) 68, 74–9  
 classification  
   controlled-atmosphere techniques 68–9, 89–96, 106–7  
   high kinetic energy techniques 68, 82–9, 96–100  
   high productivity techniques 69, 69–82, 101–5  
   nanostructured coating spraying 69  
 cold-gas spraying method (CGSM) 68, 96–100  
 controlled-atmosphere plasma spraying (CAPS) 68, 93–6  
 detonation-gun spraying 68, 82–4  
 effect on particle deformation 233–5
- flame spraying (FS) 68, 69–74  
 high-velocity oxy-fuel (HVOF) process 68, 85–9  
 new developments 100–7  
 one-step laser deposition (1SLD) technique 119–20  
 vacuum plasma spraying (VPS) 68, 89–93
- Thermal stress resistance 348
- Thermal stresses  
 effect of post-spray treatment 149  
 in high-temperature applications 472  
 spraying-induced 255–64
- Thermal-Wave Interferometry 369–70
- Thermally grown oxide (TGO) 54, 150
- Thermally sprayed coatings  
 laser treatment of 129–47  
   gas phase 143–7  
   liquid phase 134–43  
   solid phase 129–34
- Thermally sprayed composite coatings 281–3
- Thermite reaction* 10
- Thermodynamic data, species in jets/flames 172–4
- Thermoelectric generators 569
- Thermoelectric materials 486–7
- Thermogravimetric analysis (TGA) 39, 40, 42
- Thermonuclear reactor components 579
- Thermophysical properties of coatings 291–2, 340, 342, 345–8, 452–84  
*see also* Emissivity; Specific heat;  
   Thermal conductivity; Thermal diffusivity; Thermal expansion;  
   Thermal shock resistance
- Thermopiles 569
- Thick thermal-barrier coatings* (TTBCs) 156
- Thickness, *see* Coating thickness
- Three-body abrasion test 338
- Three-body abrasion 337
- Three-cathode plasma spraying torch 69, 101
- Three-point bending test, elasticity determination 327, 328
- Tin coatings, electrical properties 486

- Titanate coatings  
  dielectric properties 495, 496–7, 498  
  hardness 399  
  mechanical properties 420  
  *see also* Barium titanate coatings; Lead-zirconate titanate (PZT) coatings
- Titania coatings  
  abrasive wear resistance 439  
  alloyed with other oxides, hardness 395, 398  
  applications 558–9  
  crystal size 245  
  as decorative coatings 505  
  electrical properties 489, 490, 500–1  
  fracture toughness 419  
  hardness 395, 398–9, 398  
  phase compositions 268–71, 300–1  
  tensile adhesion test 321–2  
  thermal expansion coefficient 475  
  thickness 341  
  uses 268  
  X-ray diffraction diagrams 270
- Titania–NiCr coatings 564
- Titanium  
  electrical properties of bulk metal 486  
  mechanical properties of bulk metal 422
- Titanium alloy coatings, hardness 402
- Titanium carbide composite coatings 392, 393  
  hardness 389, 392
- Titanium coatings  
  aqueous corrosion resistance 508, 509  
  electrical properties 486  
  hardness 401  
  mechanical properties 422, 423–4, 426, 426  
  tensile adhesion strength 409, 410, 412
- Titanium diboride coatings, electrical properties 485
- Titanium dioxide powder, reduction during spraying 211, 212
- Titanium dioxide 268  
  *see also* Titania coatings
- Titanium nitride coatings 134, 135, 401, 412
- Titanium–molybdenum coatings,  
  post-spray treatment of 156
- Tokamak device components 579
- Top coatings, hardness 401–2
- Total emissivity 348
- Transformation toughening effect 399
- Transmission electron microscopy (TEM) 293, 294, 296, 314–15  
  applications 314, 316, 342  
  specimen preparation 314–15  
  *see also* Electron energy-loss spectroscopy (EELS); Selected-area diffraction (SAD)
- Transport of powders 44
- Transport properties of gases 174–5
- Transversal porosity 342  
  measurement of 344
- Transversal thermal expansion, ceramic coatings 475–6
- Tribocorrosion* 507
- Tribological tests, coating parameters affecting 335–6
- Tribometers 335
- Triplex<sup>TM</sup> torch 69, 101  
  applications 569, 570
- Tungsten carbide composite coatings 390, 393  
  erosive wear resistance 446, 447  
  hardness 389  
  hot-corrosion resistance 521  
  tensile adhesion strength 406  
  *see also* Tungsten carbide–cobalt cermet coatings
- Tungsten carbide 276–7
- Tungsten carbide–cobalt cermet coatings  
  abrasive wear resistance 441  
  applications 547, 574, 582, 587  
  erosive wear resistance 447  
  friction and wear properties 436, 437  
  hardness 389, 391, 393, 394  
  factors affecting 390  
  mechanical properties 416, 417  
  phase composition 277, 393  
  physical properties 84, 96, 393, 394  
  post-spray treatment of 118  
  tensile adhesion strength 84, 96, 405, 406  
  thermal expansion coefficient 476

- Tungsten carbide–cobalt cermet, mechanical properties of bulk material 415
- Tungsten carbide–cobalt powder manufacture of 10, 11, 20, 390 modelling of particles' temperatures and velocities 207
- Tungsten carbide–cobalt–chromium coatings, applications 550
- Tungsten carbide–NiCr coatings, applications 582
- Tungsten carbide–tungsten composite coatings, applications 549
- Tungsten coatings applications 557, 580 mechanical properties 424, 425
- Tungsten wire reinforcement, properties 434
- Tungsten, mechanical properties of bulk metal 422
- Turbine blade coatings 547, 549 thermal shock testing of 349
- Turbulent flows, conservation equations for 170
- Twin-screw machines*, 'run-in' (abradable) coatings 551
- Two-body abrasion test 338
- Two-body abrasion 337
- Two-body abrasive wear resistance ceramic coatings 438–9 composites 440–3 metals and alloys 440
- Two-colour pyrometry 208–10, 238
- Two-fluid nozzle atomizer* 15
- Two-step laser deposition (2SLD) process 120, 128, 137
- Ultimate stress/strength bulk metals 422 determination of 325, 326 metal and alloy coatings 422, 423–5 variation with temperature 430
- Ultrasonic methods, elasticity determination by 331
- Ultrasonic testing 365–7 limitations 367
- Umklapp process* 342
- Undercooling effect (nucleation of crystals) 242, 244
- Underwater plasma spraying (UPS) 68–9, 106–7 dry methods 106 wet methods 107
- Vacu-blast nozzle* 58
- Vacuum electric arc treatment 54–5
- Vacuum plasma sprayed coatings applications aerospace industry 547, 550–1 electronics industry 563, 566 energy generation facilities 569, 570, 571, 572 medical applications 577 nuclear industry 579, 580 aqueous corrosion resistance 509, 510, 512 causes of inhomogeneity 278 crystal size 245 electrical properties 485, 487 friction and wear properties 435, 439, 443, 444, 450, 451, 452 hardness 390, 392, 394, 397–8, 398, 403 hot-corrosion resistance 519, 520 interactions with simulated body fluids 515 magnetic properties 504 mechanical properties 417, 422, 423–4, 426, 427, 428–9, 430, 431 metallographical preparation (for microscopy) 318 phase composition 267 physical properties 93 post-spray treatment of 117, 135, 149, 151, 157 specific heats 472, 473 tensile adhesion strength 92, 412, 414 thermal properties 465, 467, 476, 477
- Vacuum plasma spraying (VPS) 68, 89–93 history 89 modelling of particles' temperatures and velocities 207 modelling of plasma jet 177 particle velocity measurements 191–2 principles 89–90 process parameters 91–2 arc plasma 91–2

- powder characteristics 92  
powder injection 92  
principal parameters 92  
temperature measurement of plasma jet 179  
Vacuum pump components 575  
Valence band 351  
*Van der Waals forces* 248  
Velocity measurement  
  jets and flames 179–80  
  sprayed particles 186–92  
Vickers indentation test  
  adhesion determination 322–3  
  fracture toughness determination 334  
  hardness determination 324–5  
Vickers microhardness  
  alloy coatings 402, 403  
  carbide coatings 389, 391, 392  
  metal coatings 400–1  
  oxide coatings 395, 397, 398, 399, 400  
Vickers number 324–5  
Viscosity, spray-drying slurry 14  
Viscous conditions, velocity of gas moving in 174  
*Volume-surface mean diameter* 37  
*Volumic wear* 336
- Water atomized powders 7, 8, 266  
Water-jet blasting 54, 63  
Water-stabilized plasma (WSP) torches 69, 75, 76, 77, 105, 476  
  applications 554, 556, 557  
Wavelength-dispersion spectroscopy (WDS) 293, 294, 296, 297–8  
  applications 274, 298  
Wavenumber, meaning of term 298n2  
Wear  
  factors affecting 317  
  mechanisms 336, 434  
  *see also* Abrasive wear; Adhesive wear; *Cavitation erosion/wear*; Erosive wear; Fretting wear  
Wear of coatings, factors affecting 434  
Wear-resistant coatings  
  post-spray treatment of 134, 135–6, 137  
  spray-dried powders 17, 18, 19  
*Weibull statistical distribution* 402  
Weight percent solids, spray-drying slurry 14  
'Weld surfacing' 119  
Welding points (splat on substrate) 246  
Wet corrosion, *see* Aqueous corrosion  
Wetting agents (in spray-drying slurry) 14  
Wetting of substrate by splat 228–9  
Whiskers 282  
'Whiskers-reinforced' composites 282–3  
  mechanical properties 431, 433  
Wide body drying chamber (in spray drying process) 15  
*Wiedemann–Franz–Lorenz law* 350  
Wien relationship 208  
*Williamson and Hall diagram* 307  
Wire flame sprayed coatings  
  applications 583  
  hardness 400  
  inhomogeneity 278  
  tensile adhesion strength 412, 413  
Wire flame spraying (FS-wire) 70–1, 72  
  feeding of wires 42  
Wires 1–2  
  *in* arc spraying 81  
  *in* flame spraying 70–1, 72  
Wollastonite, thermal diffusivity 463  
Wollastonite–titania mixtures, interactions with simulated body fluids 514, 515  
World market for thermal spraying 543  
Wüstite (FeO) 553
- X-ray diffraction (XRD) technique 294, 296, 305–7  
Debye–Scherer method 306  
phase analysis using 39, 41, 42, 141, 142, 144, 270, 305, 503, 505  
residual stress determination 260, 340  
X-ray fluorescence (XRF) spectroscopy 294, 296, 302  
  applications 38, 302  
X-ray photoelectron spectroscopy (XPS) 294, 296, 301–2  
  applications 38–9, 302, 303

- Yankee dryers* (in papermaking industry) 581, 582
- $\text{YBa}_2\text{Cu}_3\text{O}_x$  (high-temperature superconductor)
- Yield stress/strength  
determination of 325, 326  
metal and alloy coatings 423–5  
variation with temperature 430
- Young's modulus  
carbide coatings 415, 416  
variation with temperature 417  
determination of 329, 330–1  
oxide coatings 418–20  
variation with temperature 417, 421
- Young's modulus in compression  
alumina coatings 418  
determination of 329
- Young's modulus in tension  
alumina coatings 418  
determination of 329, 330
- Yttria ceramic rolls 554, 556
- Yttria-stabilized zirconia (YSZ)  
coatings  
adhesion checking of 324  
applications  
aerospace industry 547, 550  
food industry 551  
papermaking industry 581  
solid-oxide fuel cells 117, 157, 486, 569, 570  
composite with NiCr, mechanical properties 431, 432, 433  
electrical properties 487, 499  
hardness 395, 400  
hot-medium corrosion behaviour 519  
IR thermography 369  
mechanical properties 419, 421  
phase compositions 271–2, 455, 456  
phase transformation 474  
porosity 456, 457  
post-spray treatment of 117, 136, 138, 140, 152, 153, 156, 157
- tensile adhesion strength 408  
thermal conductivity 454–7  
factors affecting 454  
thermal expansion coefficients 475  
thermal stresses in 258, 259, 261
- Zinc coatings  
applications 562  
hardness 401
- Zircon, thermal expansion coefficient 475, 476
- Zirconia coatings  
as decorative coatings 505, 563  
emissivity 481  
mechanical properties 421
- Zirconia 271  
in duplex coatings 136, 138, 139, 140, 151, 469, 547, 572  
elastic modulus (bulk material) 417  
modelling of particles' temperatures and velocities 207  
reduction during spraying 211  
stabilized with other oxides  
applications 117, 157, 486, 569, 570  
electrical conductivity 487  
thermal conductivity 454–8, 460  
*see also* Calcia-stabilized zirconia  
coatings; Ceria-stabilized  
zirconia coatings;  
Magnesia-stabilized zirconia  
coatings; Scandia-stabilized  
zirconia coatings;  
yttria-stabilized zirconia (YSZ) coatings  
thermal conductivity 455
- Zirconium carbide composite coatings 394  
hardness 389, 392
- Zirconium diboride coatings  
electrical properties 485  
optical properties 505
- Zirconium silicate, thermal conductivity 460